Università degli Studi di Ferrara

DOCTORAL COURSE IN

"ADVANCED THERAPIES AND EXPERIMENTAL PHARMACOLOGY "

CYCLE *XXXVI*

COORDINATOR Prof. Varani Katia

In vitro and in vivo pharmaco-toxicological characterization of Novel Psychoactive Substances (NPS): focus on Novel Synthetic Opioids (NSOs)

Scientific/Disciplinary Sector (SDS) MED/43

Candidate	**Supervisor**
Dr. Bilel Sabrine	Prof. Marti Matteo

Years 2020/2023

In loving memory of my dear Dad Ismail

my hero, my best friend, and now

my guardian angel

I know you would be so proud of me

Acknowledgements

Abstract

The rapid emergence of novel psychoactive substances (NPS) in the global drug market poses a significant threat to public health and presents a challenge to drug policy. Often, there is insufficient information about the adverse clinical effects and social hazards linked to NPS, hindering the development of effective preventive measures and treatment strategies. The widespread dissemination and diversity of New Synthetic Opioids (NSOs) have introduced complexity into recreational NPS markets globally. Given the limited understanding of the pharmaco-toxicological properties of NSOs, my research project seeks to address the gaps in this area. It is a component of a multicenter research project affiliated with the Anti-Drug Policy Department (DPA) of the Presidency of the Council of Ministers. The University of Ferrara's Forensic Toxicology and Translational Medicine Laboratory is a national coordinator for this initiative. The aim of this multidisciplinary project is to investigate the effects of the emerging NSOs in a large spectrum calling different disciplinaries. In particular, the characterization of NSOs in this project involved *in silico* (Absorption, Distribution, Metabolism, Excretion and Toxicity-ADMET prediction), *in vitro* (receptor binding and Gi/β-arrestin 2 interaction tests, genotoxicity tests), *in vivo* (mouse model, zebrafish model) and *ex-vivo* (histological analysis) approaches. Sex differences in the pharmaco-toxicology of some NSOs was also evaluated. The in silico ADMET and zebrafish model were used to find rapid alternative methods for NSOs screening. As a last approach of my research project is the development of potential therapeutic interventions, I applied Naloxone (opioid receptor antagonist) alone or with Antalarmin (CRF-1 antagonist) to reverse the toxic effects of the studied opioids (particular focus on cardiorespiratory alteration) and evaluate the potential role played by stress in their toxic action.

The extensive results obtained through the multidisciplinary approach applied in my PhD project have unveiled substantial pharmaco-toxicological insights and novel mechanisms attributed to NSOs toxicity. Moreover, these findings suggest new rapid screening tools of NSOs. A part of these findings is published in significant scientific journals. Disseminating this data aims to increase awareness of the risks linked to NSOs and facilitate the development of more effective therapeutic strategies for managing NSO-related intoxications.

Statement of authorship

I, Sabrine Bilel, affirm that this thesis and the content presented within it are the product of my independent and original research. I verify that this work was conducted entirely during my enrollment in a research degree program at the University of Ferrara. When referencing the published work of others, I have consistently provided clear attribution, and in cases of direct quotation, the source has been explicitly cited. I have duly acknowledged all primary sources of assistance received. In instances where the thesis is based on collaborative efforts with others, I have transparently delineated the contributions made by co-researchers and my individual contributions. My thesis is partially based on cumulative publications obtained before submission. Recent submitted articles have also been included in my thesis (keeping the same formatting of journals submissions). Additionally, more data was included in a separate part in my thesis concluding my final contributions. I further declare that I have not submitted this thesis to any other institution in order to obtain a degree.

Table of Contents

List of Figures

List of Tables

xi

List of Abbreviations

4F-FUF	4-Fluoro-Furanylfentanyl
ADMET	Absorption, Distribution, Metabolism and Toxicity
ANNE	Artificial Neural Network Ensemble
BUF	Butyrlfentanyl
4F-BUF	4-Fluoro-Butyrylfentanyl
CBN	Contraction Band Necrosis
CNS	Central Nervous System
DCSA	Central Directorate for Anti-Drug Services
DEA	Drug Enforcement Administration
DMPK	Drug Metabolism and Pharmacokinetics
DOR	Delta Opioid Receptor
DPA	Antidrug Policy Department
DUID	Driving Under the Influence of Drugs
EMCDDA	European Monitoring Centre for Drugs and Drug Addiction
EWS	Warning System
FAs	Fentanyl Analogs
FDA	Food and Drug Administration
Fu	Fraction unbound
GIT	GastroIntestinal Tract
GPCRs	G Protein-Coupled Receptors
HBA	Hydrogen Bond Acceptors
hERG	Ether-a-go-go Related Gene
IBF	Isobutyrylfentanyl
IP	Intraperitoneal injection
KOR	Kappa Opioid Receptor
MOR	Mu Opioid Receptor
NLX	Naloxone

NOR	Nociceptin/Orphanin FQ peptide Receptor
NPF	Non Pharmaceutical Fentanyl
NPS	Novel Psychoactive substances
NSOs	Novel Synthetic Opioids
PDSP	Psychoactive Drug Screening Program
PM	Post-Mortem
RIS	Department of Scientific Investigation (Carabinieri)
SCRAs	Synthetic Cannabinoid Receptor Agonists
UNODC	United Nations Office for Drugs and Crime
WDI	World Drug Index
ZOR	Zeta Opioid Receptor

Chapter 1 Introduction

1.1 Research Background

Over the past 5 years, Novel Synthetic Opioids (NSOs) have evolved into one of the fastest-growing groups of new psychoactive substances (NPS) worldwide. While these substances constitute a lesser proportion of the overall array of NPS, their notably potent characteristics present a significant risk of poisoning. Moreover, as with many NPS, the opioid market is continuously diversifying, witnessing the (re) appearance of high-potency opioids. Due to the lack of knowledge on the pharmaco-toxicological properties of the highly potent NSOs my research project is aimed to fill the gaps in this field. My research project is a component of a multicenter research project affiliated with the Anti-Drug Policy Department (DPA) of the Presidency of the Council of Ministers. The University of Ferrara's Forensic Toxicology and Translational Medicine Laboratory is a national coordinator for this initiative. Since 2020, I have been focusing on the pharmaco-toxicological characterization of the most recent NSOs (Tramadol, fentanyl, and fentanyl analogs, Brorphine) in animal models. Sex differences in the pharmaco-toxicology of some NSOs was also evaluated. In addition, I have used other screening models including silico ADMET (Absorption, Distribution, Metabolism, Excretion and Toxicity) and zebrafish model to find rapid alternative methods of screening for NPS and particularly NSOs. As a last approach of my research project is the development of potential therapeutic interventions, I have been focusing on using Naloxone alone or with other antagonist (Antalarmin) to revert the toxic effects of the studied opioids (particular focus on cardiorespiratory alteration). The results obtained during the three years of my PhD research regarding the pharmaco-toxicology of NSOs are mostly published in important scientific journals addressing relevant and novel insights on the pharmacological aspects of the most dangerous class of NPS.

1.2 Novel Psychoactive Substances phenomenon

The term NPS refers to *'a new narcotic or psychotropic drug, in pure form or in preparation, that is not controlled by the United Nations drug conventions, but which may pose a public health threat comparable to that posed by substances listed in these conventions'* (European Monitoring Center for Drugs and Drug Addiction, EMCDDA website). The EMCDDA plays

an active role in the monitoring, assessment, and control of new and potentially threatening NPS (natural and synthetic alike) as they appear on the European drug markets (EMCDDA. 2009). Europe was one of the regions in the world first affected by the rapid emergence of NPS. Since 1997, the early warning and risk-assessment system has been recognized in Europe to identify and respond to the emergence of new drugs. Highlighting emerging and enduring NPS patterns has thus become a key focus for incorporation into the EMCDDA's yearly reports. The EMCDDA's annual reporting began to shine a spotlight on NPS and the activities of the EU Early Warning System (EWS) in 2007, where the emergence of piperazines, such as benzodiazepines, was discussed, as was the sale and aggressive marketing of these drugs through specialized shops and the internet. In 2009, there was a significant surge in the annual reporting of newly identified NPS, leading to a subsequent rise in the prominence of this subject in the following years' reports (EMCDDA. 25 YEARS FINAL. 2020). At the end of 2022, the EMCDDA was monitoring approximately 930 new psychoactive substances (**Figure 1.1**), with 41 of them having their initial reports in Europe during the same year (EMCDDA. 2023).
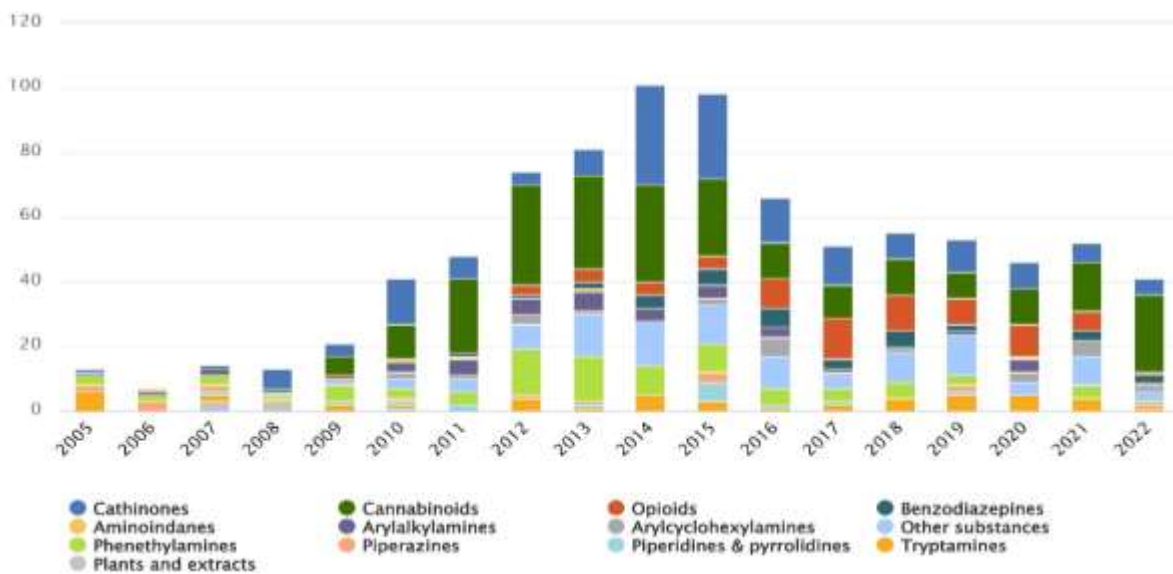
Figure 1.1. *Number of new psychoactive substances reported each year following their first detection in the European Union, by category, 2005–2021 (EMCDDA.2023).*

In Italy, over 200 NPS were registered in Early Warning Advisory in 2022 (EMCDDA. 2022). The NPS market is characterized by a large number and diversities of the substances seized each year (EMCDDA.2023). Additionally, the United Nations on Drugs and Crime (UNDOC) is currently monitoring 1230 NPS in 141 countries and territories (UNDOC EWA).

The intricate task of classifying NPS is exacerbated by the extensive diversity in pharmacological profiles and chemical structures exhibited by this group of substances. According to UNDOC, the NPS can be classified based on their pharmacological effects into six classes: stimulants, synthetic cannabinoid receptor agonists (SCRAs), classic hallucinogens, synthetic opioids, sedatives/hypnotics and dissociative (**Figure 1.2**).
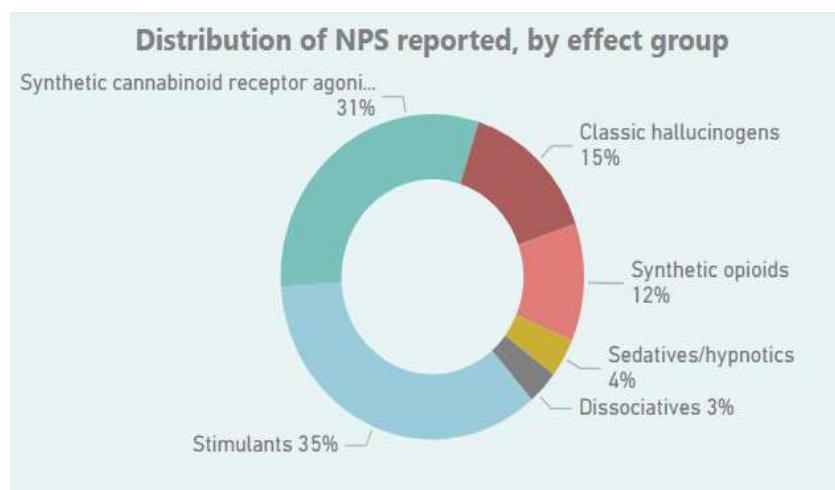
Figure 1.2. Effect group classification of NPS (UNDOC EWA. 2023).

The categorization of NPS based on their pharmacological effects can pose a significant challenge, particularly for newly identified substances, as there is usually a lack of information regarding their pharmacological and toxicological profiles. Hence, the UNDOC and EMCDDA adopted another categorization based on chemical structure similarities. Fourteen groups identified by UNODC are subsequently reported in alphabetic order: Aminoindanes, Benzodiazepines, Fentanyl analogues, Lysergamides, Nitazenes, Other substances, Phencyclidine, Phenethylamines, Phenidates, Phenmetrazines, Piperazines, Plant-based substances, Synthetic cannabinoids, and Tryptamines (UNDOC EWA. 2023). In difference to UNDOC, the EMCDDA identified thirteen groups (**Figure 1.1**) of which some classes are not identified by UNDOC and vice-versa. The distinct methods of categorizing NPS substances by these two international agencies could be seen as an outcome of their significantly independent efforts.

From 2021 to October 2022, there were 1200 reported cases of NPS poisoning involving 63 distinct substances. The most frequently encountered substances included benzodiazepine

analogues, SCRAs, and synthetic opioids, according to the UNODC (UNDOC. 2022). The data primarily originates from three sources: post-mortem (PM) cases, instances of driving under the influence of drugs (DUID), and hospital admissions (**Figure 1.3**).
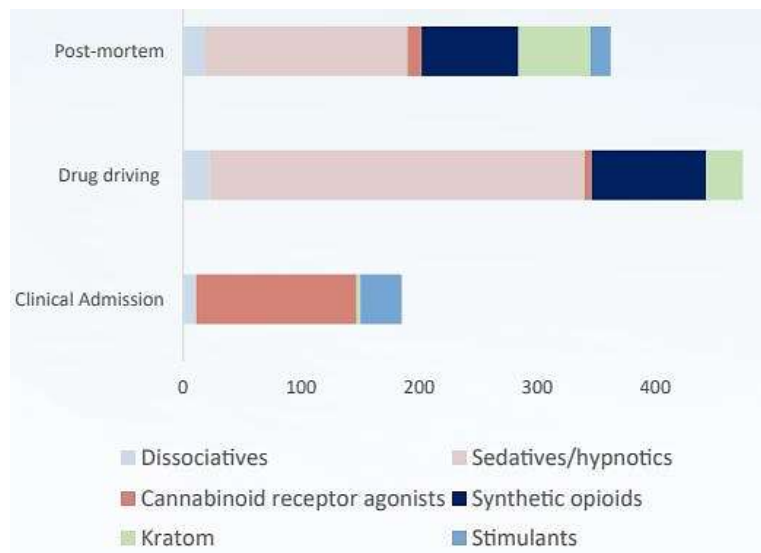
Figure 1.3. NPS classes involved in main toxicological cases (UNDOC. 2022).

It can be seen from **Figure 1.3** that most reported hospitalizations (74%) concern SCRAs, while synthetic opioids are the second class of substances involved in cases of DUID and PM (UNODC. 2022).

1.2.1 Novel Synthetic Opioids (NPS class investigated by present study)

Novel synthetic opioids (NSOs) is a subclass of NPS, which emerged on the illicit drug market in the second half of 2000's (Zawilska et al., 2023). From 2009 to 2022, a cumulative total of 74 new opioids have been identified on the European drug market (**Figure 1.4**), with one substance reported in 2022 (10 in 2020 and 6 in 2021; EMCDDA. 2023).
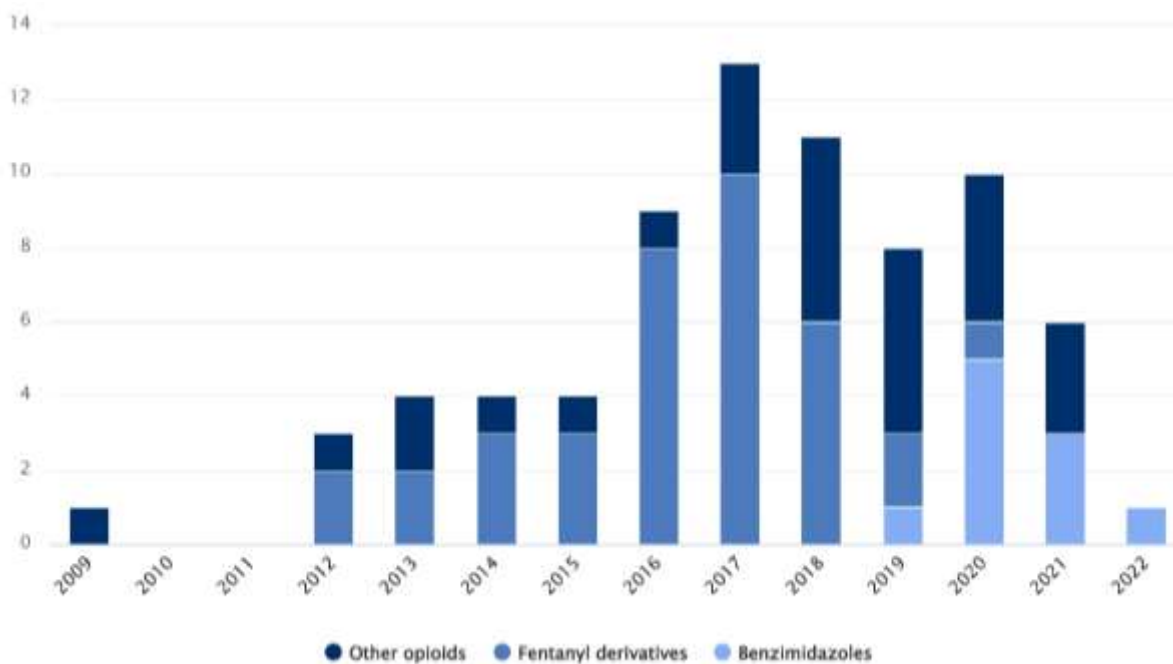
Figure 1.4. *Number of opioids reported for the first time to the EU Early Warning System, 2009–2022 (EMCDDA.2023).*

Novel synthetic opioids are basically categorized into fentanyl and its analogs used in medical therapy (i.g. Sufentanil, Alfentanil and Remifentanil), novel non-pharmaceutical fentanyl analogs (e.g. Ocfentanil, Furanylfentanyl, Acetylfentanyl, Carfentanyl, Acrylfentanyl, Tetrahydrofuranylfentanyl, etc.), non-fentanyl structured compounds including diphenylethylpiperazines (MT-45), cinnamylpiperazines (2-methyl AP-237), cyclohexylbenzamides (U-47700 and AH-7921), 2-benzylbenzimidazoles (nitazenes), benzimidazolones (brorphine), atypical opioid agonists (mitragynine) and others (Zawilska et al., 2023).

1.2.1.1 Fentanyl

In 1960, Paul Janssen synthesized Fentanyl in Belgium, initially marketing it as a pain treatment. It is the prototype of 4-anilinopiperidine carrying a propionylamide moiety linked to the aniline-nitrogen (**Figure 1.5**). It activates the mu opioid receptors as agonist, exerting the typical opioids effects on the central nervous system (CNS) like sedation, euphoria, pain relief, unconsciousness and anesthesia, confusion, drowsiness, dizziness, fatigue, nausea and vomiting, urinary retention, pupillary constriction, bradycardia, and respiratory depression (Di Trana & Del Rio, 2020).

5
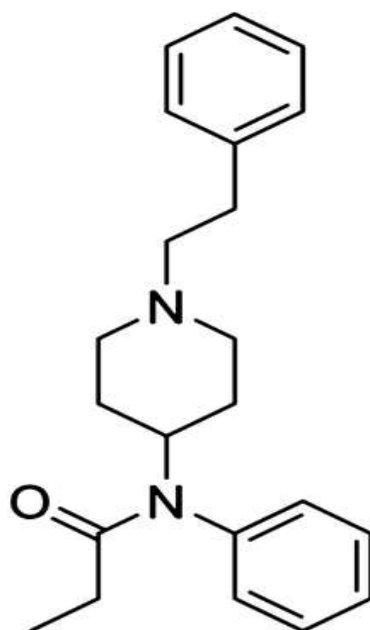
Figure 1.5. *Chemical Structure of fentanyl $C_{22}H_{28}N_2O$ (Burns et al., 2018).*

The United States Food and Drug Administration (US FDA) approved fentanyl as an intravenous anesthetic in 1972, sold under the trade name Sublimaze®. A year after its patent expiration in 1981, Fentanyl sales surged tenfold. Reports of misuse and illicit use emerged among clinicians, predominantly anesthesiologists and surgeons with access to the drug, starting in the 1980s and persisting into the early 2000s (Armenian et al., 2018). During the 1990s, fentanyl transdermal patches were introduced for broader palliative care, expanding access from clinicians to patients. Consequently, reports of overdoses stemming from the misuse of fentanyl transdermal patches surfaced in the 1990s and persisted into the early 2000s (Velagapudi & Sethi, 2023). There was a notable increase in overdose fatalities attributed to illicitly produced nonpharmaceutical fentanyl (NPF) in the mid-2000s (Armenian et al., 2018).

In May 2006, the Centers for Disease Control (CDC) and the US Drug Enforcement Agency (DEA) introduced a surveillance system that detected 1013 deaths related to NPF (CDC. 2008). The majority of the implicated NPF stemmed from adulterated heroin or cocaine sold as a street drug and administered through injection. Since 2013, a dramatic increase of fentanyl seizures has been seen. Subsequently unprecedented surge in fentanyl overdose deaths has been also reported in the US with illicitly produced fentanyl and/or fentanyl analogs labeled as heroin (Jannetto et al., 2019). The CDC and US DEA both issued nationwide alerts regarding fentanyl and its analogs in 2015 (CDC. 2017).

The appearance of fentanyl on the illegal drug market within the European Union (EU) can be traced back to sporadic reports from the mid-1990s (EMCDDA. 2012). During that period, German authorities confiscated the precursors utilized in the production of fentanyl, along with ortho, meta, and para-fluorofentanyl. In 1992, the first case report documenting a fatal overdose attributed to the use of fentanyl–cocaine combination was documented in Italy. However, the origin of the drug remains unclear. Additional evidence comes from a case series documenting 8 fatal overdoses between May 1994 and August 1995 in Sweden, a period during which fentanyl was being distributed on the illicit drug market disguised as heroin or amphetamine (EMCDDA. 2012). Subsequently, reports on fentanyl and its analogs in the European Union were infrequent. In 2008, incidents of fatalities among heroin users linked to fentanyl and analogs were documented in Estonia (Tuusov et al., 2013). A study conducted in 2012 revealed that heroin users in Bulgaria and Slovakia were turning to China white heroin mixed with fentanyl and its analogs (EMCDDA. 2012). Although there has been a decline in the reporting of fentanyl and its analogs to the EMCDDA in recent years, there were still 140 deaths linked to fentanyl reported in EU Member States in 2021 (EMCDDA. 2023).

1.2.1.2 Fentanyl Analogs (FAs)

After the discovery of fentanyl, pharmaceutical industries have developed various structural analogs aimed at enhancing the pharmacological profile of these substances. In particular, Sufentanil, Alfentanil and Remifentanil were used in medical therapy while other NPF including Acetylfentanyl, Ocfentanil and Furanylfentanyl were not approved for human medical treatment (Burns et al., 2018). Carfentanil has been synthesized by Janseen Pharmaceutica in 1974 and used as a general anesthetic for large animals (Armenian et al., 2018). After their appearance on the market, some of fentanyl analogs from therapeutic use have been reported, linked to misuse and illicit use by clinicians (Armenian et al., 2018). In 1979, numerous opioid overdoses were reported in US due to the consumption of 'China White' or synthetic heroin. However, toxicology analyses did not detect heroin or any known opioids. The causative agent was later identified as a fentanyl analog α-methylfentanyl. Another analog, 3-methylfentanyl, emerged in 1984 and was responsible for 16 fatal overdose cases. α-methylfentanyl and 3-methylfentanyl were subsequently included in schedule I narcotics in 1981 and 1986, respectively (Armenian et al., 2018). The popularity of fentanyl and its analogs

among opioid users can be attributed to their increased potency compared to heroin, lower cost, and the euphoric effects they produce (De Trana & Del Rio, 2020).

Para-fluorofentanyl is the first fentanyl analog appearing in EU in 1990s (EMCDDA.2012). 3-methylfentanyl was seized in Finland in 2001 (Jannetto et al., 2019). Since 2013, the number of NPF increased exponentially in Europe, US and many other countries (Armenian et al.,2018). Structural modification on fentanyl scaffold (**Figure 6**) may be theoretically performed on the piperidine ring, the anilinophenyl ring, the 2-phenethyl moiety and the carboxamide group, resulting in a large number of new molecules (Ellis et al., 2018).
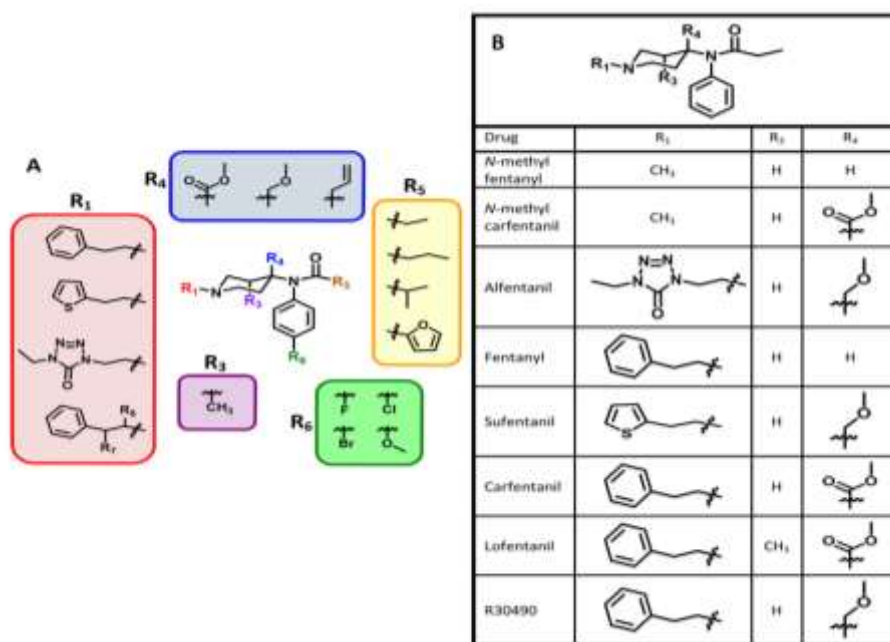
Figure 1.6. *Fentanyl derivatization. Panel A: commonly modified positions along the 4-anilidopiperidine core of fentanyl A. Panel B: chemical structure modifications of some of its emerging analogs (Ellis et al., 2018).*

Generally, fentanyl analogs recently seized as NSOs are usually generated by replacement of the ethylphenyl moiety (Isofentanyl, β-hydroxythiofentanyl) or modification of fentanyl propionyl chain (Acrylfentanyl, Ocfentanyl, Acetylfentanyl, Furanylfentanyl, Butyrylfentanyl and Isobutyrylfentanyl), (Burns et al., 2018). Despite the increasing legislative controls and prohibition of many fentanyl analogs, some of them continue to appear in the NPS market such as Carfentanil (EMCDDA. 2023). Despite variations in illicit markets at the national level, the misuse of fentanyl analogs remains a significant public health concern that spans across multiple countries worldwide (De Trana & Del Rio. 2020).

1.2.1.3 Non-fentanyl NSOs

Since 2010, a new generation of synthetic opioids, distinct in structure from fentanyl, has surfaced in the drug market. Their chemical structures fall into categories such as benzamide (U-47700, U-48800, or AH-7921), acetamide (U-50488, U-51754), or piperazine (MT-45) (Armenian et al., 2018). The potency of these synthetic opioids is frequently measured in comparison to morphine or, less commonly, fentanyl (Zawilska et al., 2023).

These NSOs have not been detected as contaminants in heroin batches; instead, users report purchasing them directly, as evidenced by published case reports (Zawilska et al., 2023). While no systematic studies have been conducted to comprehensively understand the procurement and distribution of these NSOs, they are easily accessible through the internet. AH-7921 and U-47700 are structural isomers synthesized in the 1970s by Allen and Hanburys Ltd (referred to as 'AH' synthetic opioids) and Upjohn Pharmaceutical (referred to as 'U' synthetic opioids), respectively. These compounds did not progress to further stages of development owing to their addictive properties (Armenian et al., 2018). In 2013, AH-7921 was found in synthetic cannabis products in Japan (Uchiyama et al., 2013). It has then been identified in various overdose cases across Europe and the US (Coppola & Mondola, 2015; Fels et al., 2017). Likewise, the DEA documented at least 46 confirmed fatalities in 2015/2016 linked to the use of U-47700 (Armenian et al., 2018). MT-45 was initially identified as NPS through the EMCDDA in December 2013. Subsequently, reports of abuse and overdose have emerged in both Europe and US (Helander et al., 2014; Papsun et al., 2016). A fluorinated derivative, 2F-MT-45, has been also identified in the United Kingdom. Nevertheless, there is no indication that the substance is accessible on vendor sites, likely attributed to the lack of popularity of MT-45 (along with its documented side effects) among users (Sharma et al., 2019). Many U-compounds continue to appear started to appear on user discussion fora in early 2016/2017 such as U-51754, U-77891. In 2017, the EMCDDA EWA reported a seizure of U-50488 in Sweden. In the same year, a new U-analogue (U-47931E/bromadoline) known as "bromadoline" started to be sold on web vendor sites and was identified for the first time in Europea (Sharma et al., 2019). Since 2018, U-44700 analogs appeared in Europe and US. Isopropyl-U47700 has been reported in toxicological samples from two cases submitted in March 2018 in the United States in which 3,4-methylenedioxy-U-47700 was also detected (Zawilska et al., 2023). In Europe, 3,4-Methylenedioxy-U-47700 was reported in single seizure in Poland (Sharma et al., 2018). In 2019 and 2020, 2-methyl-AP-237 was notified in Europe and in the US (Vandeputte et al., 2020). Another derivative in this series, para-methyl-AP-237,

was identified in the US in 2020 (Krotulski et al., 2020). Bromadol (trans-4-(p-bromophenyl)-4-(dimethylamino)-1-phenethylcyclohexanol), also referred to as "BDPC" is another synthetic opioid that has been discussed on online user forum since 2013 in Canada and has reportedly continued to be available on the designer illicit drug market internationally (Sharma et al., 2019). The legislative measures implemented in various countries, including China, concerning U-47700 and its analogs have had a significant impact, substantially reducing the global availability of these substances (Sharma et al et al., 2019).

In response to the changes in international control measures aimed at fentanyl analogs and some non-fentanyl opioids, a new generation of NSOs have been surfacing on the recreational drug market such as the "Nitazenes" and "Brorphine" (Vandeputte et al., 2020).

1.2.1.4 2-Benzylbenzimidazole NSOs "Nitazene"

In the mid-1950s, the pharmaceutical research laboratories of the Swiss chemical company CIBA Aktiengesellschaft discovered a group of 2-benzylbenzimidazole compounds referred to as "Nitazene" which exhibit analgesic potency levels several times higher than morphine (Ujváry et al., 2021). This group of structurally distinct analgesics was invented in order to enhance the efficacy and safety of opioid analgesics. Several of these compounds demonstrated potent opioid (heroin-like) effects, yet none were subsequently marketed for human or veterinary use (Ujváry et al., 2021). Both etonitazene and clonitazene are regulated under the United Nations Single Convention on Narcotic Drugs of 1961 due to the potential risks they present to public health (Pergolizzi et al., 2023). Specifically, this is attributed to their capacity to induce morphine-like adverse effects, suppress withdrawal symptoms in established morphine addiction, and perpetuate morphine addiction in experimental models. Internationally, 2-benzylbenzimidazole opioids have been previously identified as substances subject to misuse. For instance, etonitazene was linked to the deaths of 10 drug users in Moscow in 1998, and clandestine labs producing this compound have sporadically been discovered since then. In 2003, an American chemist in Utah manufactured etonitazene, placing it in nasal spray bottles, seemingly for personal use. More recently, there have been numerous global reports of severe toxicity associated with 2-benzylbenzimidazole opioids, particularly isotonitazene. As of November 2021, nine of these compounds, namely isotonitazene, 5-aminoisotonitazene, N-pyrrolidino-etonitazene, butonitazene, metonitazene, protonitazene, etodesnitazene (etazene), flunitazene, and metodesnitazene (metazene), had

been reported to the UNODC EWA (**Figure 1.7**, Pergolizzi et al., 2023). In the United States, isotonitazene has been identified in over 250 deaths (Vandeputte et al., 2021).
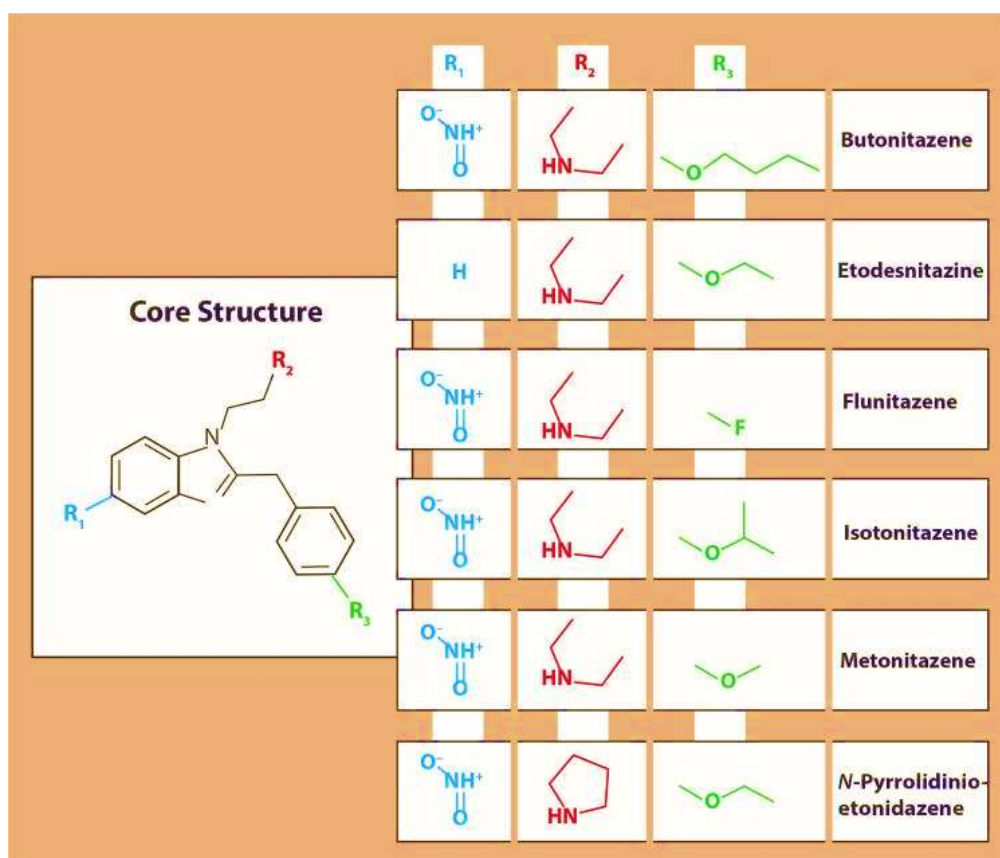
Figure 1.7. Chemical Structures of some main nitazenes emerging in the illicit drug market (Pergolizzi et al., 2023).

In Europe, Isotonitazene was notified to the EMCDDA EWA in 2019 (EMCDDA. Risk assessments Isotonitazene. 2020). In recent years, most of the newly identified opioid substances reported to the EMCDDA EWS have been the highly potent benzimidazole opioids (**Figure 1.4**). These substances have been linked to a rise in overdose deaths in the Baltic countries (EMCDDA. 2023). Nitazenes are found in powder form, counterfeit tablets, or liquids, and they can be blended with inert substances or combined with other drugs, such as heroin, fentanyl, and benzodiazepines. Their incorporation into other drug products may go unnoticed by consumers, and sellers may not disclose such mixtures. When these new clandestine nitazenes entered the illicit market, they were not initially classified as controlled substances. However, in December 2021, the Drug Enforcement Administration (DEA) temporarily placed numerous nitazenes on its Schedule I. Due to the limited availability of

validated methods to detect these substances and a lack of information about the clandestine networking, the geographical distribution of these substances remains unknown (Pergolizzi et al., 2023).

1.2.1.5 Benzimidazolone NSOs

In 2020, Brorphine [1-(1-(1-(4-bromophenyl)ethyl)piperidin-4-yl)-1,3-dihydro-2H-benzo[d]imidazol-2-one], a derivative of piperidine benzimidazolone, emerged in the NPS market. Occasionally referred to as "purple heroin" on the street, it was first identified in the NPS market in the United States in August 2019 and reported to the EMCDDA from Sweden in June 2020 (Grafinger et al., 2021). Structurally related piperidine benzimidazolones (not including Brorphine itself) can be traced back to early patents by Jansen in early 1967 (Vandeputte et al., 2022). Brorphine was first synthesized in 2018 together with a series of mu opioid receptor agonists with reported high G protein signaling bias (Kennedy et al., 2018). The chemical structure of Brorphine shares some similarities with Isotonitazene and fentanyl (**Figure 1.8**).
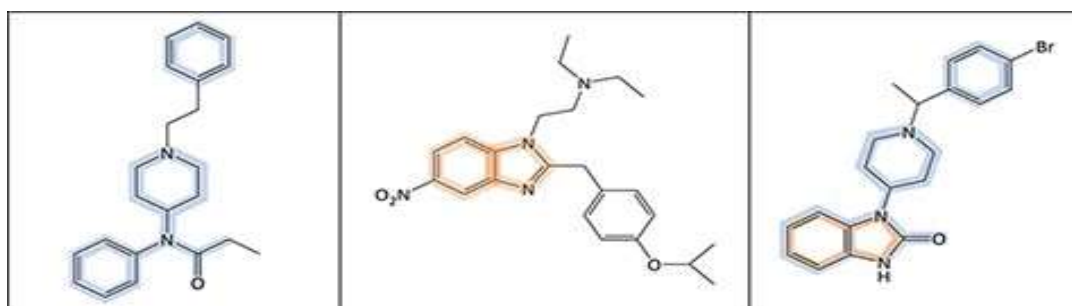
Figure 1.8. *Chemical structures of fentanyl (left), Isotonitazene (middle) and Brorphine (right) (Vandeputte et al.,2022).*

It is widely believed that the introduction of Brorphine as a NSO is associated with its inclusion in a study conducted by Kennedy et al. in 2018 (Kennedy et al., 2018). This indicates the keen awareness of clandestine chemists regarding recent developments in medicinal chemistry widely reported in literature. The first confirmed brorphine case in Europe was reported by *Verougstraete et al.*, where Brorphine was identified at high purity in a powder and in the serum of a patient seeking medical help for detoxification (Verougstraete et al. 2020). In the same year, Brorphine was also identified in Sweden, Slovenia, and Finland (Vandeputte et al., 2022).

Around June 2020, an increasing number of fatalities related to Brorphine were reported in the US (Krotulski et al., 2021). During this period, it appeared that Brorphine had largely replaced Isotonitazene in the recreational opioid market, as detections of Isotonitazene had dwindled to only a few instances each month (**Figure 1.2**). In the course of this transition, some cases were identified in the USA that contained both Isotonitazene and Brorphine (Vandeputte et al., 2022). In March 2021 Brorphine was officially placed in Schedule I of the Controlled Substances Act in December 2020 (Vandeputte et al., 2022) and it was also banned in some European countries including Italy (European Comission. 2021; Gazzetta ufficiale dell'Unione europea. 2022). Around the time of these restrictions, Brorphine cases started declining and only one identification of this substance was reported in US in the first quarter of 2023 (Krotulski et al., 2023). The NSO market is very dynamic, and some opioids' popularity can be transient as shown with Brorphine yet future analogs of this drug could possibly be emerged in the NPS market as seen with fentanyl analogs.

1.2.2 Pharmaco-toxicology of Opioids (a focus on NSOs)

Opioids produce pharmacologic effects that are primarily opioid receptor mediated. The opioid receptors are G protein-coupled receptors (GPCRs) consisting of a C-terminus, 7 transmembrane-spanning helical domains, and a protein binding intracellular N-terminus. To date, five types of opioid receptors (**Table 1.1**) have been discovered namely μ receptor (MOR), δ receptor (DOR), κ receptor (KOR), nociception receptor (NOR) and ζ receptor (ZOR) (Dhaliwal & Gupta. 2023).

Table 1.1. *Opioid receptors, Endogenous ligands, corresponding precursors, distribution, and actions (Dhaliwal & Gupta. 2023).*

	Endogenous Ligand	Ligand Precursor	Organ Distribution	Action
MOR	Endorphin & Edomorphin	Propiomelanocortin (POMC)	CNS including brain &spinal cord, gastrointestinal system (GIT), and peripheral sensory nerves (PNS)	Mu-1 for analgesia &dependance Mu-2 for euphoria, dependance, respiratory depression, miosis & constipation Mu-3 for vasodilation
KOR	Dynorphin	Pro-dynorphin	Central and Peripheral Nervous System (CNS& PNS)	Analgesia, diuresis & disphoria
DOR	Enkephalin	Pro-enkephalin	Brain and Peripheral Nervous System (PNS)	Analgesia & constipation
NOR	Nociceptin/Orphanin	Pre-pronociceptin	Central Nervous System (CNS)	Analgesia & hyperalgesia (concentration dependent)
ZOR	-	-	Hear, liver, muscle, brain, pancreas & kidney	Development regulation in normal & tumor cells

The complexity of the endogenous opioid system is heightened by the discovery of μ, κ and δ opioid heteroreceptors and gene splice variants of the μ-opioid receptor. The different opioid receptors subtypes discovered are mu-1, mu-2, mu-3, kappa-1, kappa-2, kappa-3, delta-1, and delta-2 (Dhaliwal & Gupta. 2023). The utilization of absolute quantitative real-time reverse transcriptase PCR (AQ rt RT-PCR) for precise opioid receptor mRNA expression measurement, coupled with numerous immunohistochemistry studies, has unveiled a broad distribution of opioid receptors (**Table 1.1**) within the CNS (Sobczuk et al., 2014). Notably, the cerebellum, caudate nucleus, and nucleus accumbens exhibited the highest expression of MOR. DOR were identified in the hippocampus, cerebral cortex, putamen, caudate nucleus, nucleus accumbens, and temporal lobe. The most significant expression of KOR was observed in the caudate nucleus, nucleus accumbens, hypothalamic nuclei, and putamen (Sobczuk et al., 2014). Opioid receptors exhibit a broad distribution in both neuronal and non-neuronal tissues in the periphery, encompassing neuroendocrine, immune, and ectodermal cells (Tubia & Khalife. 2019). Within the gastrointestinal tract (GIT), these receptors are found in smooth muscle cells and at the terminals of both sympathetic and sensory peripheral neurons (Sobczuk et al., 2014). Preclinical studies have demonstrated the synthesis of opioid receptors in the dorsal root ganglion, with subsequent central and peripheral transportation to nerve terminals (Wood et al., 2004). Interestingly, opioid receptors were also found in high amounts on lymphocytes and macrophages (Peng et al., 2012).

The selectivity of opioid receptors plays a crucial role in the clinical effects of opioid drugs (summarized in **Table 1.1**). Despite the complexity of the endogenous opioid system, various lines of evidence, including studies involving opioid receptor knockout mice, confirm that the

primary pharmacologic effects of morphine, such as euphoria, analgesia, respiratory depression, and dependence, are primarily attributed to agonist actions at the μ-opioid receptor (Williams et al., 2013; Charbogne et al., 2014). Morphine is the prototypical opioid receptor agonist, and the standard to which all other opioid analgesics are compared. Taking morphine as an opioid ligand, the mechanism of action of opioids is presented in **Figure 1.8**. Following the binding of the ligand (morphine) to the opioid receptor, a three-dimensional conformational change takes place in the receptor. This alteration leads to the ligand-receptor complex attaining a state of high affinity for intracellular Gα/Gbγ heterotrimeric G proteins. Subsequently, this facilitates guanosine diphosphate (GDP)/ guanosine triphosphate (GTP) exchange, causing the receptor to bind with the Gα subunit and releasing the Gbγ subunit. Gα GTP and Gbγ then target intracellular effectors, including adenylate cyclases and $Ca2^+/K^+$ ion channels. Gα GTP and Gbγ selectively target intracellular effectors, such as adenylate cyclases and $Ca2^+/K^+$ ion channels. Notably, inhibitory Gαi/o subunits exhibit a preference for opioid receptors, leading to a decrease in intracellular cAMP levels, inhibition of $Ca2^+$ current, and an elevation in extracellular K^+ current. Ultimately, this sequence of events results in the reduction of neuronal excitation and the inhibition of neurotransmitter and/or neuropeptide release. The hydrolysis of GTP to GDP restores the receptor bound Gα subunit to its inactive state, leading to subsequent dissociation. The binding of Gα subunit on the intracellular side of the opioid receptor is primarily facilitated by the third intracellular loop and the carboxy terminal. Additionally, as there are multiple putative phosphorylation sites susceptible to various intracellular kinases, the phosphorylation of the opioid receptor disrupts its effective coupling with G-proteins (Schäfer. 2011).
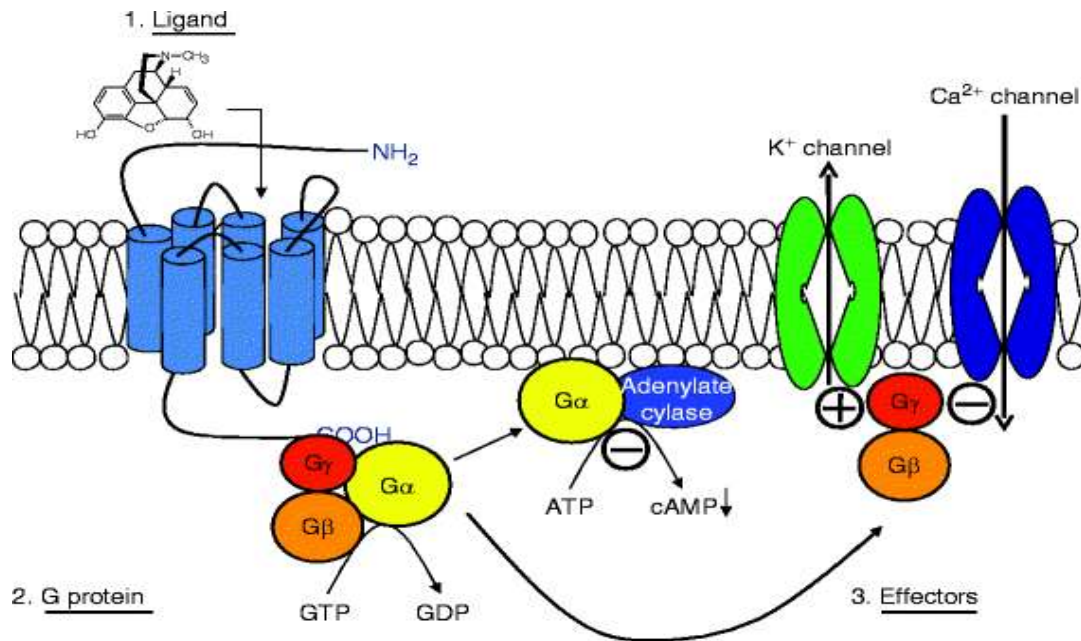
Figure 1.9. *Mechanisms underlying opioid receptor ligand-induced G-protein activation. The binding of a ligand (exp. morphine) to the opioid receptor induces a conformational change, increasing the receptor's affinity for intracellular G proteins, specifically Gαi. The activation of these proteins leads to the inhibition of downstream effectors like adenylate cyclase and Ca2+ channels or the stimulation of K+ channels. Consequently, intracellular concentrations of cAMP, K+, and Ca2+ decrease, preventing the release of neurotransmitters/neuropeptides and the excitation of the neuron (Schäfer. 2011.)*

Based on their ability to initiate G-protein coupling with opioid receptors, ligands are categorized into full opioid agonists, partial agonists, antagonists, and inverse agonists (**Figure 1.10**). Opioid agonists induce typical opioid effects through reversible receptor G-protein coupling. Full opioid agonists, such as fentanyl and sufentanil, exhibit high potency and necessitate minimal receptor occupancy for maximal response. On the other hand, partial opioid agonists, such as buprenorphine, require a higher receptor occupancy for maximal efficacy, typically lower than that of full agonists. Conversely, an opioid inverse agonist produces an effect opposite to that of an agonist, and inverse agonists can also be "full" or "partial". An antagonist produces no effect on its own but blocks the effects of both opioid agonists and inverse agonists (Azzam et al., 2019).
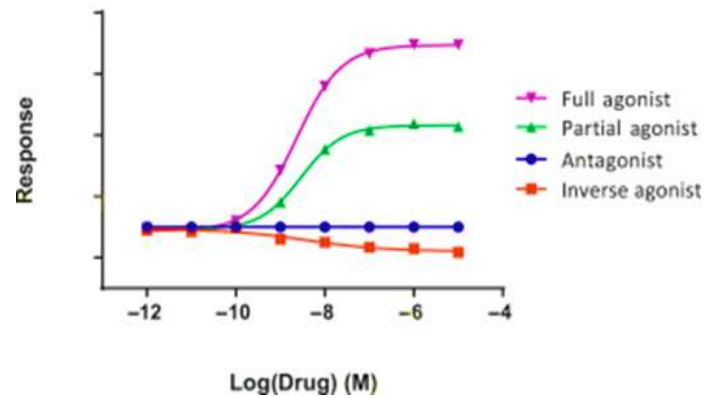
Figure 1.10. *Graphical representation depicting typical pharmacological behaviors. A full agonist generates the maximal possible response (loosely corresponding to efficacy) on the y-axis, measured in arbitrary units. The green curve represents a partial agonist with a lower maximum efficacy. A neutral antagonist, when administered alone, does not produce any response but can reverse the effects of an agonist. An inverse agonist reduces basal activity, often referred to as tone, and is represented by an inverse sigmoid curve. Drug potency is illustrated on the x-axis (Log [Drug]), with a standard measure being the concentration or dose required to produce 50% of the maximal response (EC_{50} or ED_{50}); (Azzam et al., 2019).*

An additional aspect influencing functional activity of GPCRs is ligand bias. Biased agonism, also known as functional selectivity, refers to the capability of a specific ligand to favorably influence one signaling pathway over another (bias). Opioid receptors engage with multiple signaling pathways, resulting in what is termed 'pluridimensional efficacy' (Azzam et al., 2019) and positioning them as targets for the development of biased ligands (**Figure 1.11**). The concept of targeting specific signaling transduction pathways in opioid receptors emerged from a significant 1999 study by Bohn and colleagues (Bohn et al., 1999). In this study, they disrupted the function of the β-arrestin 2 protein in mice through gene deletion, leading to an enhancement in the analgesic effect of morphine and reduced tolerance compared to wild-type animals. This was attributed to the effective blockade of the β-arrestin desensitization process. Administering naloxone to both groups attenuated the analgesic effect of morphine, while the administration of naltrindole and nor-binaltorphimine, acting at DOR and KOR receptors, respectively, proved ineffective. Additionally, these β-arrestin 2 knockout animals exhibited diminished morphine-induced constipation (in animal models of GI transit) and ventilatory depression. The bias in favor of G-protein signaling at the expense of β-arrestin signaling holds the potential to yield analgesic effects with reduced side effects (exp respiratory depression) (Azzam et al., 2019), however this has been questioned (Azevedo Neto et al., 2020).
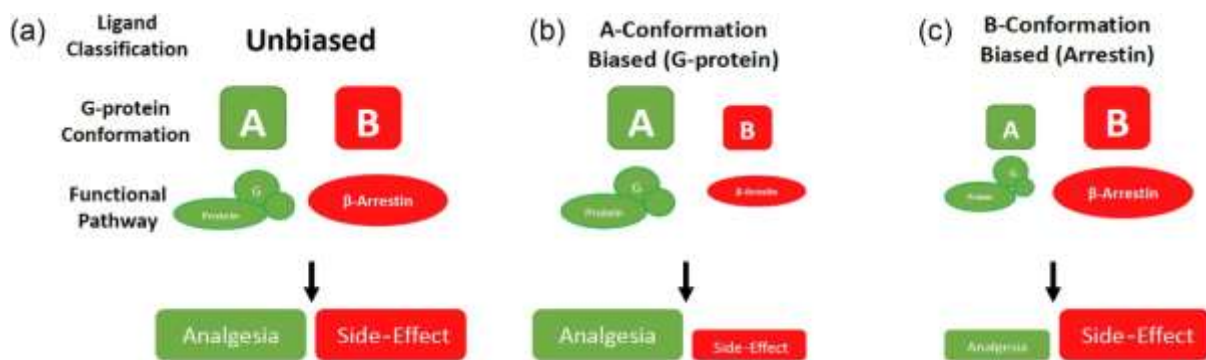
Figure 1.11. *A schematic illustration of biased agonism at the mu receptor. Three scenarios depict coupling to either G-protein or β-arrestin. (a) Represents an unbiased agonist, interacting equally with both pathways, and is predicted to generate both analgesic effects and side effects. (b) Demonstrates bias towards G-protein signaling, predicting analgesia with fewer side effects. (c) Depicts the opposite bias, favoring β-arrestin, which is predicted to result in more side effects and a diminished analgesic profile (Azzam et al., 2019).*

Following their emergence in the NPS market, many NSOs from different classes were implicated in many cases of intoxication and death worldwide (Frisoni et al., 2019). NSOs that are structurally unrelated to morphine, share analgesic and CNS depressant properties similar to it, including respiratory depression (Papsun et al., 2016). They are also associated with adverse effects including dizziness, nausea, vomiting, anxiety, sweating, and disorientation (Frisoni et al., 2019). Given the limited available information on the pharmacology and toxicology of NSOs in abuse settings, many research topics were addressed to fill gap in this field. In particular, many studies evaluated *in silico* (molecular docking; Vasudevan et al., 2020), *in vitro* (opioid receptor affinity and their interaction with Gαi/β-arrestin 2 proteins; Vandeputte et al., 2022) and *in vivo* (physiology, behavior and metabolites) pharmacological profiling of many NSOs belonging to the different classes mentioned above (Baumann et al., 2020, Bilel et al., 2020, 2021, 2022, 2023).

Due to the high potency of NSOs and their epidemiological aspects (in particular with fentanyl), scientific topics have been focused on drug interactions with NSOs through pharmacokinetic and pharmacodynamic mechanisms and discussed the role of naloxone (an opioid receptor antagonist) as an antidote to the NSO toxidrome (Pérez-Mañá et al., 2018; Frisoni et al, 2019; Burns et al., 2018; Edinoff et al., 2023). These studies have helped the development of public safety protocols. In particular, measures such as Overdose Education and Naloxone Distribution programs (OEND), prescription drug monitoring programs, and prescription drug take-back programs have been implemented to mitigate overdose occurrences

and curb the misuse of opioids, particularly fentanyl and nitazenes (Edinoff et al., 2023; Pergolizzi).

Sex differences in Opioids side effects is another issue that have concerned the scientific community. Notably, despite the extensive utilization of opioids, previous research has highlighted significant individual variations in the response to opioid analgesics. Specifically, the reactions to opioids, encompassing adverse effects, can differ between males and females. Discrepancies in the rates of adverse reactions have been noted in adults, children, tobacco smokers, individuals with opioid use disorder, and postoperative patients. Moreover, these variations have been observed across different NSOs, including morphine and fentanyl (Lopes et al., 2021).

In 2021, approximately 39.5 million individuals globally were grappling with drug use disorders, yet only one in five of those affected received proper drug treatment. The treatment gap has been exacerbated by the COVID-19 pandemic. Women who use drugs tend to progress to drug use disorders faster than men (UNDOC. 2023). The proportion of women who abuse non-pharmaceutical opioids (47%) was higher than opiates users (25%) (**Figure 1.12**). However, the proportion of women in treatment is very low and that was explained by decline among women for drug treatment due to sociocultural barriers (UNDOC. 2023)
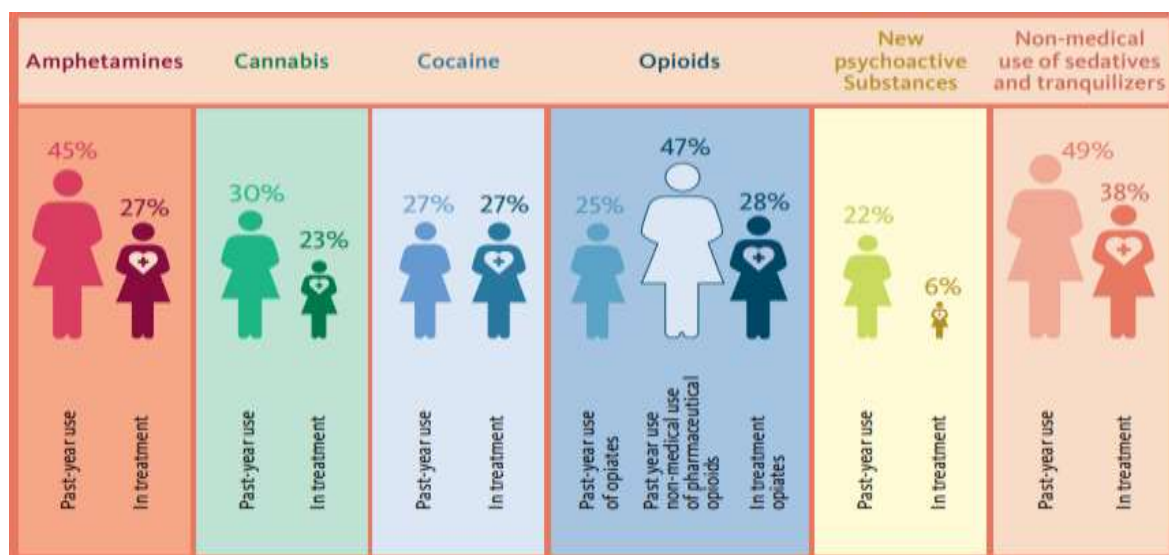
Figure 1.12. Proportion of women among drug users and in people in drug treatment (UNDOC, 2023).

While men in the US exhibit higher rates of illicit drug use and opioid-related deaths compared to women (Wightman et al., 2021), recent years have seen a similar rate of increase in overdose deaths for both genders. Between 1999 and 2019, the age-adjusted drug overdose death rates surged by over 350% for both men and women (Wightman et al., 2021). Notably, among women aged 30–64 years in the US from 1999 to 2018, there was a significant rise in deaths involving synthetic opioids (1643%), heroin (915%), and benzodiazepines (830%) (VanHouten et al., 2019). Although variations in all aspects of drug dependence, such as drug acquisition, escalation of use, withdrawal, recurrence of use, and treatment response, have been well-documented, the majority of national and local initiatives aimed at tackling the opioid overdose crisis tend to overlook these important sex and gender differences (VanHouten et al., 2019). Indeed, research on sex-based treatment differences in opioids use disorders has increased (Lopes et al., 2021), however, the studies focusing on sex-dependent differences in the pharmaco-toxicology induced by NSOs have not yet been established (Fattore et al., 2020).

Chapter 2 Aims and objectives

In Europe, the mortality rate due to overdoses in 2021 is estimated at 18.3 deaths per million population aged 15 to 64. Only in 2021, it is estimated that at least 6 166 overdose deaths involving illicit drugs occurred in the European Union (EMCDDA. 2023). Opioids frequently appear in approximately three-quarters (74%) of reported fatal overdoses within the European Union. Tramadol, an opioid medicine used to treat moderate to severe pain, was involved in 42 % of the deaths reported by the French registry of medicine misuse-related deaths (EMCDDA, 2023). Fentanyl and fentanyl analogs were linked to about 137 deaths in 2021 in Europe (including Germany). Preliminary data from Estonia indicate that the number of drug-induced deaths involving new synthetic opioids (of benzimidazoles class "Nitazenes") doubled to 79 deaths. (EMCDDA. 2023). Globally, since the early 2010s, NSOs have significantly contributed to overall opioid-related overdose mortalities (Edinoff et al., 2023). It is important to highlight that toxicology reports for opioid-induced deaths often reveal the presence of multiple substances (EMCDDA. 2023). An examination of 36 studies spanning 13 EU countries and Norway projected that individuals involved in high-risk drug use face an elevated risk of death, ranging from three to more than twenty times that of individuals of similar age and gender in the general population. This heightened risk isn't solely linked to overdoses; other causes of death, where drug use might play a role, are significant but challenging to quantify at the EU level. These encompass accidents, violence, cardiovascular and respiratory diseases, cancer, infections like HIV and viral hepatitis, as well as suicide (EMCDDA. 2023). The evolving demographics of individuals engaging in opioid injection, coupled with shifts in the substances they use, pose new and intensified challenges for interventions aimed at mitigating overdose deaths. To face such challenges, it is of great interest to understand the pharmaco-toxicology and the physiopathology of these emerging NSOs. To fill gap in this void, my research project was developed during these three years as a multidisciplinary approach involving national and international research units with different expertise (*in vitro* pharmacodynamics, zebrafish model, cytotoxicity and drug metabolism and pharmacokinetics (DMPK) laboratories) to provide a comprehensive characterization of NSOs from a panoramic perspective (**Figure 2.1**).
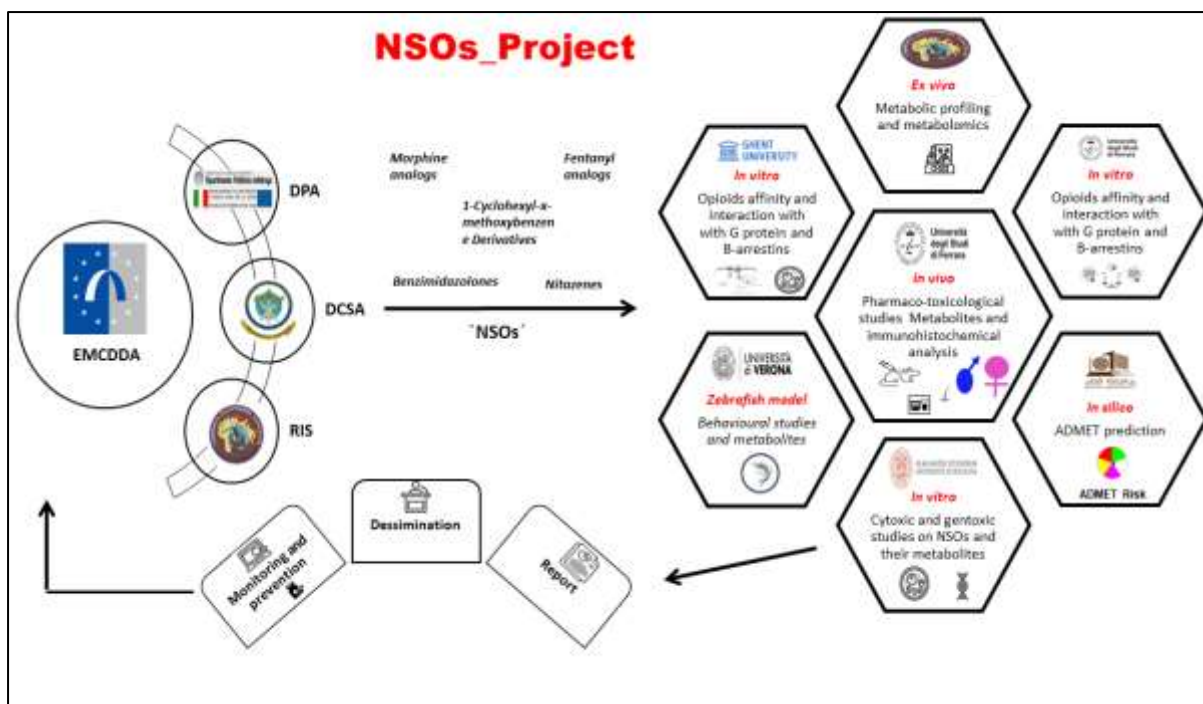
Figure 2.1. *The multidisciplinary approach used in my research project to characterize rapidly and efficiently the NSOs. NSOs are selected based on signaling and alerts coming from national governmental units such as Anti-drug policy department (DPA), Central Directorate for Anti-Drug Services (DCSA), Carabinieri Scientific Investigation Departments (RIS) and international units such as the EMCDDA. Based on the lack of knowledge on each NSO pharmacology and physiopathology the different collaborations are aimed at evaluating a specific characteristic of these substances. By conducting in vitro studies at the University of Ferrara and the University of Ghent, in vivo studies at the University of Ferrara ,metabolic profiling by Carabinieri Scientific Investigations Department (RIS), employing alternative screening models through in silico ADMET prediction at Qatar University and zebrafish model at the University of Verona, and exploring the long-term effects of NSOs on genetic material at the University of Bologna, scientific reports will be disseminated to both the scientific community, policymakers, and the public. This dissemination aims to contribute to the development of integrated strategies for prevention, screening, and the facilitation of linkages to drug abuse treatment programs. The broader community stands to gain from enhanced control over the global NSOs crisis.*

Chapter 3 Publications on NSOs

3.1 List of published articles

1. **Bilel, S.**, Tirri, M., Arfè, R., Sturaro, C., Fantinati, A., Cristofori, V., Bernardi, T., Boccuto, F., Cavallo, M., Cavalli, A., De-Giorgio, F., Calò, G., & Marti, M. (2021). *In Vitro* and In Vivo Pharmaco-Toxicological Characterization of 1-Cyclohexyl-x-methoxybenzene Derivatives in Mice: Comparison with Tramadol and PCP. *International journal of molecular sciences, 22*(14), 7659. https://doi.org/10.3390/ijms22147659

2. Montesano, C., Vincenti, F., Fanti, F., Marti, M., **Bilel, S.**, Togna, A. R., Gregori, A., Di Rosa, F., & Sergi, M. (2021). Untargeted Metabolic Profiling of 4-Fluoro-Furanylfentanyl and Isobutyrylfentanyl in Mouse Hepatocytes and Urine by Means of LC-HRMS. *Metabolites*, *11*(2), 97. https://doi.org/10.3390/metabo11020097

3. **Bilel, S.**, Azevedo Neto, J., Arfè, R., Tirri, M., Gaudio, R. M., Fantinati, A., Bernardi, T., Boccuto, F., Marchetti, B., Corli, G., Serpelloni, G., De-Giorgio, F., Malfacini, D., Trapella, C., Calo', G., & Marti, M. (2022). *In vitro* and in vivo pharmaco-dynamic study of the novel fentanyl derivatives: Acrylfentanyl, Ocfentanyl and Furanylfentanyl. *Neuropharmacology, 209*, 109020. https://doi.org/10.1016/j.neuropharm.2022.109020

4. **Bilel, S.**, Giorgetti, A., Tirri, M., Arfè, R., Cristofori, V., Marchetti, B., Corli, G., Caruso, L., Zauli, G., Giorgetti, R., & Marti, M. (2023). Sensorimotor Alterations Induced by Novel Fentanyl Analogs in Mice: Possible Impact on Human Driving Performances. *Current neuropharmacology, 21*(1), 87–104. https://doi.org/10.2174/1570159X21666221116160032

5. Gasperini, S., **Bilel, S.**, Cocchi, V., Marti, M., Lenzi, M., & Hrelia, P. (2022). The Genotoxicity of Acrylfentanyl, Ocfentanyl and Furanylfentanyl Raises the Concern of Long-Term Consequences. *International journal of molecular sciences, 23*(22), 14406. https://doi.org/10.3390/ijms232214406

6. Pesavento, S., **Bilel, S**., Murari, M., Gottardo, R., Arfè, R., Tirri, M., Panato, A., Tagliaro, F., & Marti, M. (2022). Zebrafish larvae: A new model to study behavioural effects and metabolism of fentanyl, in comparison to a traditional mice model. *Medicine, science, and the law*, *62*(3), 188–198. https://doi.org/10.1177/00258024221074568

7. **Bilel, S.**, Murari, M., Pesavento, S., Arfè, R., Tirri, M., Torroni, L., Marti, M., Tagliaro, F., & Gottardo, R. (2023). Toxicity and behavioural effects of ocfentanil and 2-furanylfentanyl in zebrafish larvae and mice. *Neurotoxicology*, *95*, 83–93. https://doi.org/10.1016/j.neuro.2023.01.003

3.2 Copies of published articles

Article

In Vitro and In Vivo Pharmaco-Toxicological Characterization of 1-Cyclohexyl-x-methoxybenzene Derivatives in Mice: Comparison with Tramadol and PCP

Sabrine Bilel [1,†], Micaela Tirri [1,†], Raffaella Arfè [1], Chiara Sturaro [2], Anna Fantinati [3], Virginia Cristofori [3], Tatiana Bernardi [3], Federica Boccuto [3], Marco Cavallo [4], Alessandro Cavalli [4], Fabio De-Giorgio [5,6,*], Girolamo Calò [7] and Matteo Marti [1,8,*]

[1] Section of Legal Medicine and LTTA Centre, Department of Translational Medicine, University of Ferrara, 44121 Ferrara, Italy; sabrine.bilel@unife.it (S.B.); micaela.tirri@unife.it (M.T.); raffaella.arfe@unife.it (R.A.)
[2] Section of Pharmacology, Department of Neuroscience and Rehabilitation, University of Ferrara, 44121 Ferrara, Italy; chiara.sturaro@unife.it
[3] Department of Chemistry and Pharmaceutical Sciences, University of Ferrara, 44121 Ferrara, Italy; anna.fantinati@unife.it (A.F.); virginia.cristofori@unife.it (V.C.); tatiana.bernardi@unife.it (T.B.); federicaboccuto@gmail.com (F.B.)
[4] NPS Section and Synthetic Drugs, Central Directorate for Anti-Drug Services (DCSA), 00173 Rome, Italy; marco.cavallo@interno.it (M.C.); cavalli.alessandro2@gdf.it (A.C.)
[5] Section of Legal Medicine, Department of Health Care Surveillance and Bioethics, Università Cattolica del Sacro Cuore, 00168 Rome, Italy
[6] Fondazione Policlinico Universitario A. Gemelli IRCCS, 00168 Rome, Italy
[7] Department of Pharmaceutical and Pharmacological Sciences, University of Padua, 35122 Padua, Italy; girolamo.calo@unipd.it
[8] Collaborative Center for the Italian National Early Warning System, Department of Anti-Drug Policies, Presidency of the Council of Ministers, 00186 Roma, Italy
* Correspondence: fabio.degiorgio@unicatt.it (F.D.-G.); matteo.marti@unife.it (M.M.); Tel.: +39-0532-455781 (M.M.)
† Authors equally contributed to this work.

Abstract: 1-cyclohexyl-x-methoxybenzene is a novel psychoactive substance (NPS), first discovered in Europe in 2012 as unknown racemic mixture of its three stereoisomers: ortho, meta and para. Each of these has structural similarities with the analgesic tramadol and the dissociative anesthetic phencyclidine. In light of these structural analogies, and based on the fact that both tramadol and phencyclidine are substances that cause toxic effects in humans, the aim of this study was to investigate the in vitro and in vivo pharmacodynamic profile of these molecules, and to compare them with those caused by tramadol and phencyclidine. In vitro studies demonstrated that tramadol, ortho, meta and para were inactive at mu, kappa and delta opioid receptors. Systemic administration of the three stereoisomers impairs sensorimotor responses, modulates spontaneous motor activity, induces modest analgesia, and alters thermoregulation and cardiorespiratory responses in the mouse in some cases, with a similar profile to that of tramadol and phencyclidine. Naloxone partially prevents only the visual sensorimotor impairments caused by three stereoisomers, without preventing other effects. The present data show that 1-cyclohexyl-x-methoxybenzene derivatives cause pharmaco-toxicological effects by activating both opioid and non-opioid mechanisms and suggest that their use could potentially lead to abuse and bodily harm.

Keywords: 1-cyclohexyl-x-methoxybenzene; opioid receptors; tramadol; PCP; behavior; mice; novel psychoactive substances

1. Introduction

Over the last decade, an increasing number of new substances, known as new psychoactive substances (NPS), have been detected on the European market. The increase

in the number of these substances is the result of a significant shift in the way that drugs can now be manufactured, marketed and sold, which was driven by rapid changes in both technology and globalization [1]. This rapidly changing environment has led to confusion for clinicians, psycho-pharmacologists, and the public at large [2]. In addition to the "classical" NPS, which are classified into known classes of compounds (i.e., cathinones, cannabinoids, phenethylamines, opioids, tryptamines, benzodiazepines, and dissociative anesthetics), law enforcement carries out seizures of compounds that are not classified into these groups of molecules, which are labeled as "other substances" [1].

Reviving abandoned drugs by mining old sources (e.g., from chemical journals or patents), or creating new entities with slight or major structural variations, can transform the restricted progenitor drug into an uncertain category of legal status, a "legal gray zone". The allure of NPS is magnified by the current lack of reference materials and the need for sophisticated detection methods which are not routinely available (e.g., mass spectroscopy).

One case, first brought to the attention of EMCDDA and Europol in 2012, under the terms of Council Decision 2005/387/JHA, focuses on 1-cyclohexyl-x-methoxybenzene. This molecule was first identified in Austria on 3 February 2012, in white powder form. It is important to underline that the "street name" of 1-cyclohexyl-x-methoxybenzene has yet to be discovered. This is highly significant to the understanding of the potential impact of this substance on the "gray" market. The drug shares some structural analogies with tramadol and phencyclidine (PCP) (Figure 1; [3–5]). Therefore, these substances could be used as substitutes for tramadol and PCP to avoid clinical-toxicological and forensic identification.
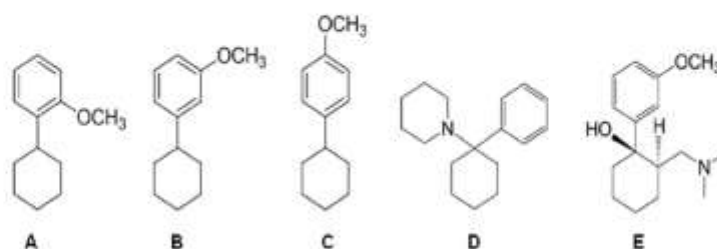
Figure 1. Chemical structures of (**A**) 1-cyclohexyl-2-methoxybenzene (ortho), (**B**) 1-cyclohexyl-3-methoxybenzene (meta), (**C**) 1-cyclohexyl-4-methoxybenzene (para), (**D**) phencyclidine (PCP) and (**E**) tramadol.

In our previous study [5] we synthetized the 1-cyclohexyl-x-methoxybenzene derivatives (ortho, meta and para stereoisomers) and, for the first time, investigated some of the pharmacological effects caused by these stereoisomers. We demonstrated that systemic administration of 1-cyclohexyl-x-methoxybenzene derivatives impairs visual sensorimotor response, thermal analgesia and modulates core temperature, without affecting motor performance on the accelerod test, in CD-1 mice. Therefore, we suggested that the derivatives not only share some structural characteristics with tramadol and PCP, they also could evoke a similar pharmacological profile, thereby potentially representing a similar threat to human health [5]. Tramadol is an atypical, phenylpiperidine, centrally acting synthetic analgesic used to treat moderate to severe pain, with antinociceptive effects that are mediated by a combination of mu-opioid agonist effects and norepinephrine and serotonin reuptake inhibition [6]. Globally, the trafficking and consumption of fake tramadol has been increasing since 2007. Organized crime, armed groups and terrorist organizations were involved in the marketing of tramadol [7], as highlighted by the quantities of tramadol seized in Europe in 2017 [8].

On the other hand, phencyclidine (PCP) is a potent hallucinogenic drug, representing a synthetic arylcyclohexylamine, originally developed as an anesthetic that acts as a

25

glutamatergic N-methyl-D-aspartate (NMDA) antagonist, also showing cholinergic and monoaminergic activity [9]. Both drugs are abused [2,10] and produce severe adverse effects, characterized by sensory changes with dissociative, out-of-body feelings and distorted visual and auditory perception. Cognitive changes, such as memory impairment, altered perception of time and slowness are common, as are affective changes, although these are quite labile, varying between euphoria, anxiety, apathy and irritability. Unpredictable changes in behavior (including aggression) and changes in consciousness are also not uncommon. Moreover, there are considerable risks associated with their use, including pulmonary edema, cerebrovascular accidents, cardiac arrest and death by overdose [2,8,11,12]. Given the large increase in the use and abuse of tramadol and the resurging interest in PCP-type substances [7], 1-cyclohexyl-x-methoxybenzene derivatives could also attract the attention of consumers and be sold in the NPS market as substitutes or alternatives to tramadol and PCP.

1-cyclohexyl-x-methoxybenzene may be sold not as a pure stereoisomer composition but as racemic mixture containing different amounts of the three ortho, meta and para stereoisomers. The 1-cyclohexyl-x-methoxybenzene compound was sequestered and identified, without determination of the composition of the racemic mixture in its three ortho, meta and para strereoisomers. This is of great relevance, as the different replacements of the methoxy group on the benzyl ring may confer different pharmacological and toxicological properties to the molecule [5]. In fact, as reported for other NPS (synthetic cannabinoids), the substitution of a hydroxyl group in the para, meta or ortho position on the benzene ring of the naphthoylindole structure causes a change in the pharmacodynamic properties and biological activity of compounds [13,14].

The aim of this study was to investigate the pharmacodynamic profile of the ortho-, meta-, and para-1-cyclohexyl-x-methoxybenzene derivatives (and tramadol for comparison) at mu, kappa and delta opioid receptors. To this aim, we used a calcium mobilization assay performed in CHO cells co-expressing human recombinant opioid receptors and chimeric G proteins that force Gi receptors to couple with the PLC-IP3-Ca2+ pathway. This assay, previously validated for the nociceptin opioid peptide receptor (NOP) [15] and later extended to classical opioid receptors [16], was used to pharmacologically characterize a large number of novel ligands, obtaining very similar results to those attained with classical assays for Gi-coupled receptors. Moreover, we investigated the effect of acute systemic administration of the single stereoisomers on neurological alterations (i.e., tail elevation, hyperreflexia and convulsions), sensorimotor responses (to visual and acoustic stimulation), body temperature, mechanical and thermal analgesia, akinesia (bar test), motor activity (spontaneous locomotion and accelerod test) and cardio-respiratory (breath rate, SpO2, hearth rate, pulse distension) changes in CD-1 male mice. In order to better characterize the pharmaco-toxicological profile of the derivatives, we compared their effects with those induced by tramadol and PCP. Moreover, to verify if 1-cyclohexyl-x-methoxybenzene derivatives have an opioid action, we studied their effect and, for comparison, that of tramadol and PCP, after administration of naloxone.

2. Results

2.1. In Vitro

In these experiments, we evaluated the ability of the tramadol and ortho-, meta-, and para-1-cyclohexyl-x-methoxybenzene derivatives to activate the mu, kappa and delta human recombinant receptors that were stably transfected in CHO cells. In such cells, the co-expression of a chimeric G protein allows for receptor activation to be measured with an automated calcium mobilization assay. Dermorphin, Dynorphin A and DPDPE were used as standard agonists for mu, kappa and delta receptors, respectively.

In CHOmu cells, the standard agonist Dermorphin evoked a robust concentration-dependent stimulation of calcium release, displaying a pEC50 of 7.76 and maximal effects of $295 \pm 33\%$ over the basal values. Tramadol and the three analogs were completely inactive. The concentration response curves obtained with these ligands are displayed in Figure 2A.

26
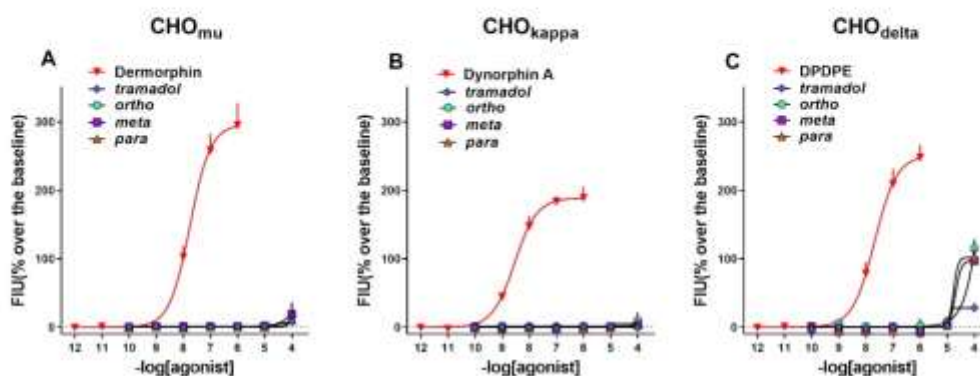
Figure 2. Calcium mobilization assay. Concentration response curves of standard opioid agonists, tramadol, and ortho-, meta- and para-1-cyclohexyl-X-methoxybenzene tested in CHOmu (**A**), CHOkappa (**B**), and CHOdelta cells (**C**). Data are the mean ± sem of 4 separate experiments performed in duplicate.

In CHOkappa cells, the standard agonist Dynorphin A evoked a robust concentration-dependent stimulation of calcium release, displaying a pEC50 of 8.50 and maximal effects of 198 ± 16% over the basal values. Tramadol and its three analogs were completely inactive. The concentration response curves obtained with these ligands are displayed in Figure 2B.

In CHOdelta cells, the standard agonist DPDPE evoked a robust concentration-dependent stimulation of calcium release, displaying high potency (pEC50 of 7.65) and maximal effects of 248 ± 19% over the basal values. Tramadol was completely inactive, while the three analogs displayed a stimulatory effect only at the higher concentration tested. The concentration response curves obtained with these ligands in CHOdelta cells are displayed in Figure 2C.

The results of these experiments are summarized in Table 1.

Table 1. Potencies (pEC50) and maximal effects of tramadol and 1-cyclohexyl-x-methoxybenzene derivatives at mu, kappa and delta opioid receptors. Data are means of 3–4 separate experiments performed in duplicate.

	Mu		Kappa		Delta	
Compounds	pEC$_{50}$ (CL$_{95\%}$)	E$_{max}$ ± Sem %	pEC$_{50}$ (CL$_{95\%}$)	E$_{max}$ ± Sem %	pEC50 (CL95%)	E$_{max}$ ± Sem %
Standard agonists	7.76 (7.53–7.99)	295 ± 33%	8.50 (8.32–8.68)	189 ± 16%	7.65 (7.36–7.94)	248 ± 19%
Tramadol	Inactive		Inactive		Crc incomplete, at 100 mM 102 ± 9%	
Ortho	Inactive		Inactive		Crc incomplete, at 100 mM 115 ± 7%	
Meta	Inactive		Inactive		Crc incomplete, at 100 mM 115 ± 7%	
Para	Inactive		Inactive		Crc incomplete, at 100 mM 97 ± 8%	

The standard agonists for mu, kappa and delta receptors were Dermorphin, Dynorphin A and DPDPE, respectively.

2.2. In Vivo

2.2.1. Major Neurological Changes

Systemic administration of 1-cyclohexyl-x-methoxybenzene derivatives (0.1–100 mg/kg i.p.) and PCP (0.01–10 mg/kg i.p.) did not induce neurological changes, such as convulsions, hyperreflexia, myoclonia and tail elevation. Conversely, tramadol at the highest dose tested (100 mg/kg) caused tail elevation and convulsive episodes. The elevation of the tail preceded the appearance of the first seizure episode and was present in 90% of the tramadol treated animals, with a latency of appearance of 121 ± 24 s and an average duration of 65 ± 24 min. The average score was 3.5 (arbitrary units) and reached the maximum value

(four arbitrary units) in approximately 78% of the treated mice. Pretreatment with naloxone 6 mg/kg did not prevent the elevation of the tail induced by tramadol at 100 mg/kg.

Tramadol induced convulsive episodes (average number of episodes 1.6 ± 0.18) in 90% of the treated animals, with a latency of 236 ± 14 s and a mean duration of 270 ± 30 s. Pretreatment with naloxone 6 mg/kg worsened the seizure effect of tramadol. It reduces the latency time of the first convulsive episode (176 ± 13 s; unpaired t-test: $p = 0.0072$, $t = 3.141$, df = 14) and increases the number of convulsive episodes (average number of episodes 2.7 ± 0.11; unpaired t-test: $p = 0.0103$, $t = 2.964$, df = 14), but did not significantly increase their overall duration (360 ± 39 s; unpaired t-test: $p = 0.0888$, $t = 1.829$, df = 14).

2.2.2. Sensorimotor Studies

Evaluation of the Visual Object Response

Visual object response did not change in vehicle-treated mice over 5 h of observation (Figure 3A), and the effect was similar to that observed in naïve untreated animals (data not shown). Systemic administration of 1-cyclohexyl-x-methoxybenzene derivatives (0.1–100 mg/kg) dose-dependently inhibited visual object responses in mice. Data of 1-cyclohexyl-x-methoxybenzene derivatives (ortho, meta and para) are replicated from [5]. Systemic administration of tramadol (0.1–100 mg/kg, i.p.; Figure 3A) significantly ($p < 0.0001$) and dose-dependently reduced the visual object response in mice ((significant effect of treatment ($F_{4,280} = 129.5$), time ($F_{7,280} = 25.43$) and time x treatment interaction ($F_{28,280} = 4.147$)). Tramadol produced an impairment, especially at the highest dose of 100 mg/kg i.p., which reached the maximum inhibitory effect at 60 min and persisted for up to 5 h. Systemic administration of PCP (0.01–10 mg/kg) dose- dependently inhibited visual object responses in mice. PCP data are replicated from [17]. A comparison of the maximal effect among 1-cyclohexyl-x-methoxybenzene derivatives, tramadol and PCP (Figure 3B) revealed significant differences between the effects of these compounds ((significant effect of treatment ($F_{4,175} = 33.09$; $p < 0.0001$), dose ($F_{4,175} = 103.5$; $p < 0.0001$) and dose x treatment interaction ($F_{16,175} = 4.28$; $p < 0.0001$)). Meta at 0.1 mg/kg was the powerful compound, inducing the maximal inhibitory effect on visual object responses ($p < 0.05$). Moreover, the meta and para at 1 mg/kg were more effective with respect to tramadol and PCP for the object visual impairment ($p < 0.05$). Pretreatment with naloxone 6 mg/kg partially prevented the inhibitory effect induced by ortho, meta, para and tramadol (100 mg/kg), while the effect of PCP 10 mg/kg was naloxone-insensitive (Figure 3C).
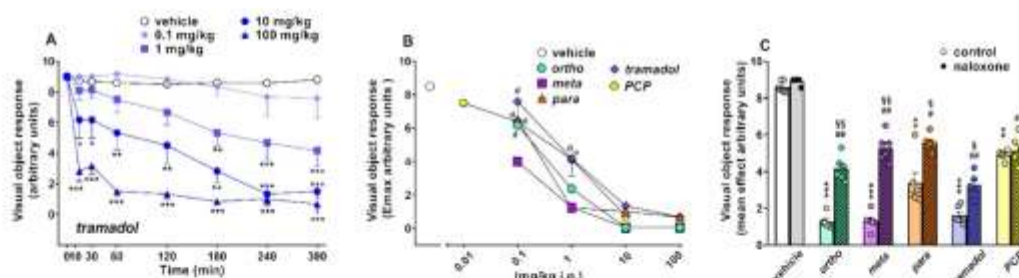
Figure 3. Effect of the systemic administration of tramadol (0.1–100 mg/kg i.p.; (**A**)) on the visual object test in mice. Comparison of the maximal effect of ortho, meta, para, tramadol (0.1–100 mg/kg) and PCP (0.01–10 mg/kg) observed in 5 h (**B**) [1,2]. Interaction of the maximal effective dose of ortho, meta, para, tramadol (100 mg/kg) and PCP (10 mg/kg) with the opioid receptor antagonist naloxone (6 mg/kg, i.p.; (**C**)). Data are expressed as arbitrary units and represent the mean $\pm$ SEM of 6–8 determinations for each treatment. Statistical analysis was performed by two-way ANOVA, followed by the Bonferroni's test for multiple comparisons for the dose–response curve of each compound at different times (**A**), and for the antagonist studies (**C**), while the statistical analysis of (**B**) was performed with one-way ANOVA followed by Bonferroni test for multiple comparisons. * $p < 0.05$, ** $p < 0.01$, *** $p < 0.001$ versus vehicle; [d] $p < 0.05$ versus meta; [e] $p < 0.05$ versus para; [*] $p < 0.05$, [**] $p < 0.01$ versus naloxone; [§] $p < 0.05$, [§§] $p < 0.01$ versus without naloxone. [1] ortho, meta and para data are elaborated from [5]; [2] PCP data are elaborated from [17].

Evaluation of the Visual Placing Response

Visual placing response did not change in vehicle-treated mice over 5 h of observation (Figure 4A–D), and the effect was similar to that observed in naïve untreated animals (data not shown). Systemic administration (0.1–100 mg/kg i.p.) of ortho (Figure 4A; significant effect of treatment ($F_{4,280} = 105.0$, $p < 0.0001$), time ($F_{7,280} = 45.07$, $p < 0.0001$) and time x treatment interaction ($F_{28,280} = 3.433$, $p < 0.0001$)), meta (Figure 4B; significant effect of treatment ($F_{4,280} = 66.29$, $p < 0.0001$), time ($F_{7,280} = 32.83$, $p < 0.0001$) and time x treatment interaction ($F_{28,280} = 2.525$, $p < 0.0001$)), para (Figure 4C; significant effect of treatment ($F_{4,280} = 12.33$, $p < 0.0001$), time ($F_{7,280} = 19.13$, $p < 0.0001$) but not time x treatment interaction ($F_{28,280} = 0.6801$, $p = 0.8897$)) and tramadol (Figure 4D; significant effect of treatment ($F_{4,280} = 190.8$, $p < 0.0001$), time ($F_{7,280} = 38.10$, $p < 0.0001$) and time x treatment interaction ($F_{28,280} = 4.715$, $p < 0.0001$)) reduced the visual placing response in mice in a dose-dependent manner, with the effect persisting for up to 5 h at higher doses. Systemic administration of PCP (0.01–10 mg/kg) dose-dependently inhibited visual placing responses in mice. PCP data are replicated from [17].

A comparison of the maximal effect among 1-cyclohexyl-x-methoxybenzene derivatives, tramadol and PCP (Figure 4E) revealed significant differences between the effects of these compounds ((significant effect of treatment ($F_{4,175} = 3.176$; $p = 0.0156$), dose ($F_{4,175} = 47.92$; $p < 0.0001$) and dose x treatment interaction ($F_{16,175} = 3.889$; $p < 0.0001$)). Notably, PCP at 10 mg/kg was the most powerful compound in inducing the maximal inhibitory effect on the visual placing responses ($p < 0.05$). Moreover, tramadol at 100 mg/kg was more effective with respect to para regarding visual placing impairment ($p < 0.05$). Pretreatment with naloxone 6 mg/kg partially prevented the inhibitory effect induced by ortho, meta and tramadol (100 mg/kg), while the effect of PCP 10 mg/kg was naloxone-insensitive (Figure 4F).

Evaluation of the Acoustic Response

Acoustic response did not change in vehicle-treated mice over 5 h of observation (Figure 5A–D), and the effect was similar to that observed in naïve untreated animals (data not shown). Systemic administration (0.1–100 mg/kg i.p.) of ortho (Figure 5A; significant effect of treatment ($F_{4,280} = 155.5$, $p < 0.0001$), time ($F_{7,280} = 60.48$, $p < 0.0001$) and time × treatment interaction ($F_{28,280} = 7.714$, $p < 0.0001$)), meta (Figure 5B; significant effect of treatment ($F_{4,280} = 85.99$, $p < 0.0001$), time ($F_{7,280} = 36.88$, $p < 0.0001$) and time x treatment interaction ($F_{28,280} = 4.026$, $p < 0.0001$)), para (Figure 5C; significant effect of treatment ($F_{4,280} = 36.98$, $p < 0.0001$), time ($F_{7,280} = 23.45$, $p < 0.0001$) but not time x treatment interaction ($F_{28,280} = 2.946$, $p = 0.8897$)) and tramadol (Figure 5D; significant effect of treatment ($F_{4,280} = 53.86$, $p < 0.0001$), time ($F_{7,280} = 40.41$, $p < 0.0001$) and time x treatment interaction ($F_{28,280} = 3.747$, $p < 0.0001$)) reduced the visual placing response in mice in a dose-dependent manner, with the effect persisting for up to 5 h at higher doses.

Ortho, meta and tramadol inhibited the acoustic responses at a dose of 1 mg/kg, while the para was effective from 10 mg/kg. The inhibitory effect caused by ortho and meta at the 100 mg/kg dosage was significant 10 min after administration of the compounds. Para and tramadol doses of 100 mg/kg were effective 60 min after administration. Systemic administration of PCP (0.01–10 mg/kg) dose-dependently inhibited acoustic responses in mice. PCP data are replicated from [17].

Figure 4. Effects of the systemic administration (0.1–100 mg/kg i.p.) of ortho (**A**), meta (**B**), para (**C**) and tramadol (**D**) on the visual placing test in mice. Comparison of the maximal effect of ortho, meta, para, tramadol (0.1–100 mg/kg) and PCP (0.01–10 mg/kg) observed in 5 h (**E**) [2]. Interaction of the effects of ortho, meta, para, tramadol (100 mg/kg) and PCP (10 mg/kg) with the opioid receptor antagonist naloxone (6 mg/kg, i.p.; (**E**)). Data are expressed as a percentage of baseline and represent the mean ± SEM of 6–8 determinations for each treatment. Statistical analysis was performed by two-way ANOVA, followed by the Bonferroni's test for multiple comparisons for the dose–response curve of each compound at different times (**A–D**), and for the antagonist studies (**F**), while the statistical analysis of (**E**) was performed with one-way ANOVA followed by Bonferroni test for multiple comparisons. * $p < 0.05$, ** $p < 0.01$, *** $p < 0.001$ versus vehicle; [a] $p < 0.05$ versus tramadol; [b] $p < 0.05$ versus PCP; [#] $p < 0.05$, [##] $p < 0.01$ versus naloxone; [§] $p < 0.05$ versus without naloxone. [2] PCP data are elaborated from [17].

Figure 5. Effects of the systemic administration (0.1–100 mg/kg i.p.) of ortho (**A**), meta (**B**), para (**C**) and tramadol (**D**) on the acoustic response in mice. Comparison of the maximal effect of ortho, meta, para, tramadol (0.1–100 mg/kg) and PCP (0.01–10 mg/kg) observed over 5 h (**E**)[2]. Interaction of the effects of ortho, meta, para, tramadol (100 mg/kg) and PCP (10 mg/kg) with the opioid receptor antagonist naloxone (6 mg/kg, i.p.; (**F**)). Data are expressed as arbitrary units and represent the mean ± SEM of 6–8 determinations for each treatment. Statistical analysis was performed by two-way ANOVA, followed by the Bonferroni's test, for multiple comparisons of the dose–response curve of each compound at different times (**A–D**), and for the antagonist studies (**E**), while the statistical analysis of panel F was performed with one-way ANOVA followed by Bonferroni test for multiple comparisons. * $p < 0.05$, ** $p < 0.01$, *** $p < 0.001$ versus vehicle; [d] $p < 0.05$ versus meta; ## $p < 0.01$ versus naloxone; [2] PCP data are elaborated from [17].

A comparison of the maximal effect among 1-cyclohexyl-x-methoxybenzene derivatives, tramadol and PCP (Figure 5E) revealed significant differences between the effects of these compounds ((significant effect of treatment ($F_{4,175} = 40.14$; $p < 0.0001$), dose ($F_{4,175} = 137.4$; $p < 0.0001$) and dose x treatment interaction ($F_{16,175} = 4.959$; $p < 0.0001$)). Notably, ortho, meta and tramadol doses of 1 mg/kg were more effective in inhibiting acoustic responses ($p < 0.05$) in mice. Pretreatment with naloxone 6 mg/kg did not prevent the inhibitory effect induced by ortho, meta, para, tramadol (100 mg/kg) and 10 mg/kg of PCP (Figure 5F).

Evaluation of the Core Body Temperature

Core body temperature did not change in vehicle-treated mice over 5 h of observation (Figure 6A,B) and the effect was similar to that observed in naïve untreated animals (data not shown). Systemic administration of 1-cyclohexyl-x-methoxybenzene derivatives (0.1–100 mg/kg) dose-dependently affected core temperature in mice. Data of 1-cyclohexyl-x-methoxybenzene derivatives (ortho, meta and para) are replicated from [5].

Figure 6. Effects of the systemic administration of tramadol (0.1–100 mg/kg i.p.; (A)) and PCP (0.01–10 mg/kg i.p.; (B)) on the mouse core temperature. Comparison of the maximal effect of ortho, meta, para, tramadol (0.1–100 mg/kg) and PCP (0.01–10 mg/kg) observed in 5 h (C) [1]. Interaction of the effects of ortho, meta, para, tramadol (100 mg/kg) and PCP (10 mg/kg) with the opioid receptor antagonist naloxone (6 mg/kg, i.p.; (D)). Data are expressed as the difference between control temperature (before injection) and temperature following drug administration (Δ°C; see material and methods), and represent the mean ± SEM of 6–8 determinations for each treatment. Statistical analysis was performed by two-way ANOVA followed by the Bonferroni's test for multiple comparisons for the dose–response curve of each compound at different times (A,B), and for the antagonist studies (D), while the statistical analysis of (C) was performed with one-way ANOVA followed by Bonferroni test for multiple comparisons. * $p < 0.05$, ** $p < 0.01$, *** $p < 0.001$ versus vehicle; [b] $p < 0.05$ versus PCP; [c] $p < 0.05$ versus ortho; [*] $p < 0.05$, [**] $p < 0.01$ versus naloxone; [§] $p < 0.05$ versus without naloxone. [1] ortho, meta and para data are elaborated from [5].

32

Systemic administration of tramadol (0.1–100 mg/kg, i.p.; Figure 6A; significant effect of treatment ($F_{4,245}$ = 26.31; p < 0.0001), time x treatment interaction ($F_{28,245}$ = 2.588; p = 0.0001) but not time ($F_{7,245}$ = 1.044; p = 0.3976)) and PCP (0.01–10 mg/kg, i.p.; Figure 6B; significant effect of treatment ($F_{4,245}$ = 10.77; p < 0.0001), time ($F_{7,245}$ = 7.55; p < 0.0001) but not time x treatment interaction ($F_{28,245}$ = 0.4589; p = 0.9871)) transiently reduced the core body temperature in mice. Hypothermia caused by tramadol at 100 mg/kg was evident after 30 min and reached maximum effect at 85 min ($\Delta°C$ = −−3.6 °C; Figure 6A), while the hypothermic effect caused by PCP at 10 mg/kg was significant and reached a maximum after 140 min ($\Delta°C$ = −−2.7 °C; Figure 6B). A comparison of the maximal effect among 1-cyclohexyl-x-methoxybenzene derivatives, tramadol and PCP (Figure 6C) revealed significant differences ((significant effect of dose ($F_{4,175}$ = 47.96; p < 0.0001) but not treatment ($F_{4,175}$ = 1.491; p = 0.2070) and dose x treatment interaction ($F_{16,175}$ = 1.415; p = 0.1393)). Notably, PCP transiently induced hypothermia in mice at both 1 and 10 mg/kg (p < 0.05). Moreover, the meta and tramadol at 100 mg/kg were more effective with respect to ortho regarding the induction of hypothermia in mice (p < 0.05). Pretreatment with naloxone 6 mg/kg did not prevent the reduction in body core temperature induced by ortho, meta, para (100 mg/kg) and PCP 10 mg/kg, while it partially prevented that caused by tramadol 100 mg/kg (Figure 6D).

Evaluation of Pain Induced by Mechanical and Thermal Stimuli

The threshold of mechanical pain did not change in vehicle-treated mice over 5 h of observation (Figure 7A–D), and the effect was similar to that observed in naïve untreated animals (data not shown). Systemic administration (0.1–100 mg/kg i.p.) of ortho (Figure 7A; significant effect of treatment ($F_{4,245}$ = 2.467, p = 0.0455) but not time ($F_{6,245}$ = 0.6174, p = 0.7163) and time x treatment interaction ($F_{24,245}$ = 0.6098, p = 0.9252)), meta (Figure 7B; significant effect of treatment ($F_{4,245}$ = 7.664, p < 0.0001) but not time ($F_{6,245}$ = 1.073, p = 0.3792) and time x treatment interaction ($F_{24,245}$ = 0.9550, p = 0.5270)) and tramadol (Figure 7D; significant effect of treatment ($F_{4,245}$ = 39.08, p < 0.0001), time ($F_{6,245}$ = 6.759, p < 0.0001) and time x treatment interaction ($F_{24,245}$ = 3.762, p < 0.0001)) increased the threshold of mechanical pain in the pinch test in mice. However, the para compound was ineffective (Figure 7C).

Ortho and meta at 10 mg/kg transiently and mildly induced mechanical analgesia after 205 (ortho Emax −18%) and 145 (meta Emax −25%) minutes, respectively, while at the highest dose (100 mg/kg), both compounds were ineffective. However, tramadol induced a rapid increase in mechanical analgesia at 10 mg/kg (Emax −25%) and 100 mg/kg (Emax −56%; Figure 7D), and the effect of tramadol 100 mg/kg persisted for up to 145 min. Systemic administration of PCP (0.01–10 mg/kg) dose-dependently induced mechanical analgesia in mice. PCP data are replicated from [17].
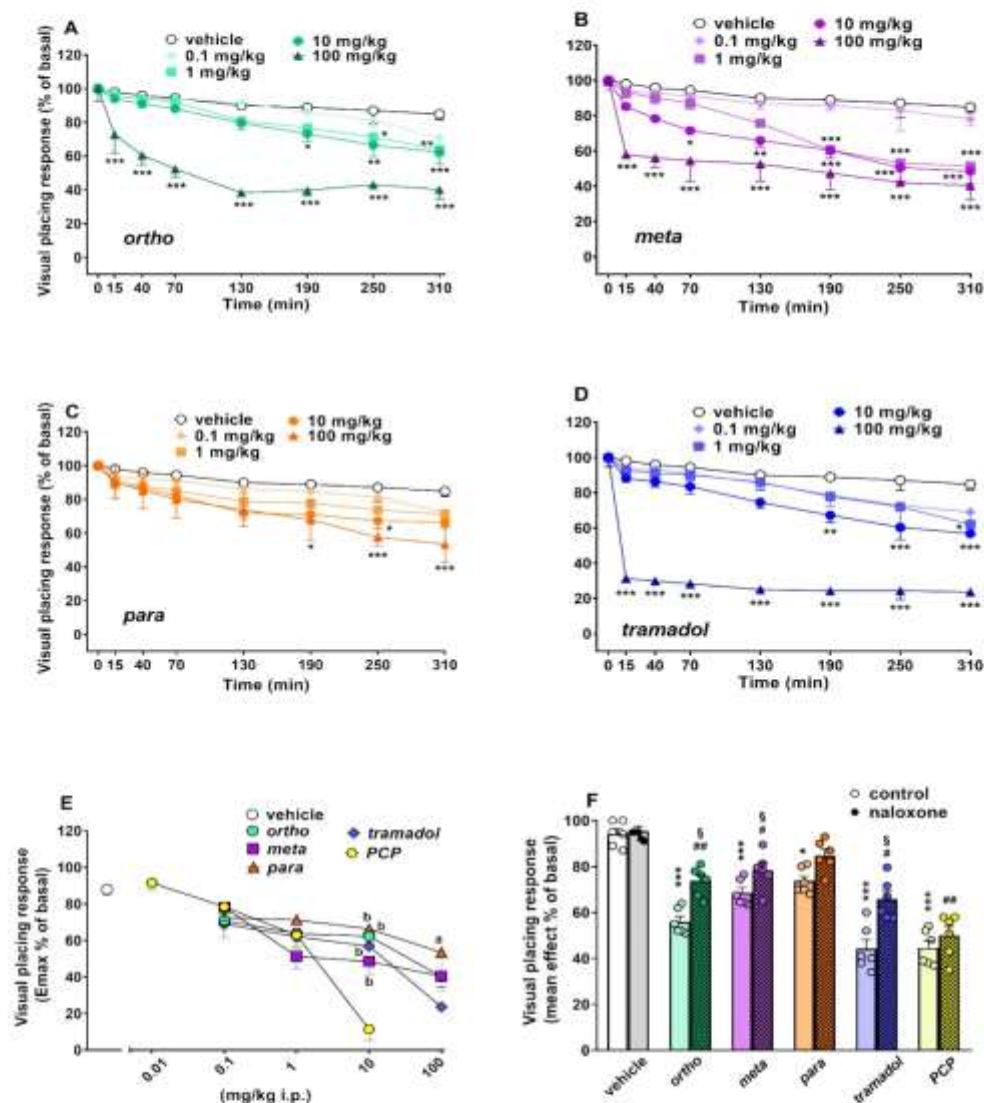
A comparison of the maximal effect among 1-cyclohexyl-x-methoxybenzene derivatives, tramadol and PCP (Figure 7E) revealed significant differences between the effects of these compounds ((significant effect of treatment ($F_{4,175}$ = 10.98; p < 0.0001), dose ($F_{4,175}$ = 21.74; p < 0.0001) and dose x treatment interaction ($F_{16,175}$ = 5.517; p < 0.0001)). PCP was the most potent compound, while tramadol 100 mg/kg was more effective with respect to ortho and meta derivatives. Pretreatment with naloxone 6 mg/kg did not prevent the analgesic effect induced by ortho, meta and PCP (10 mg/kg), while it partially prevented that caused by tramadol 100 mg/kg (Figure 7F).
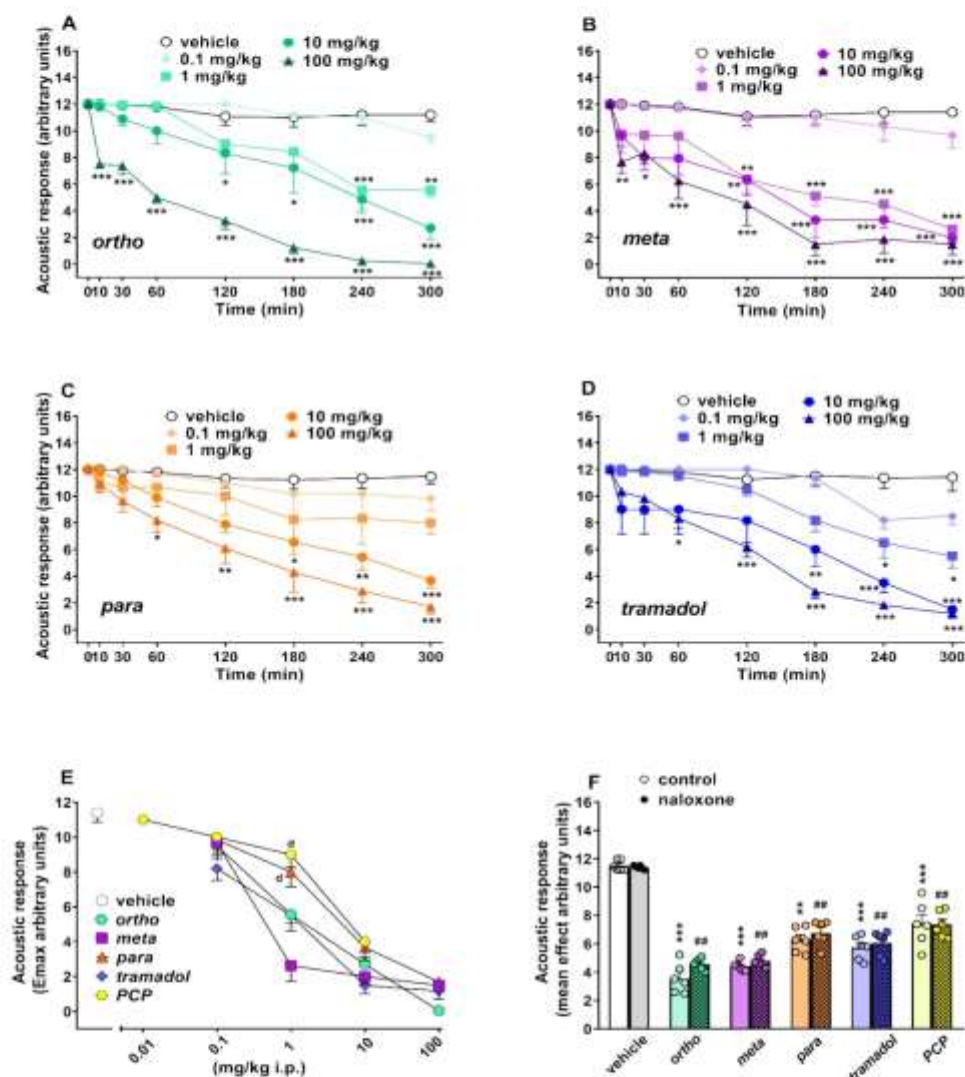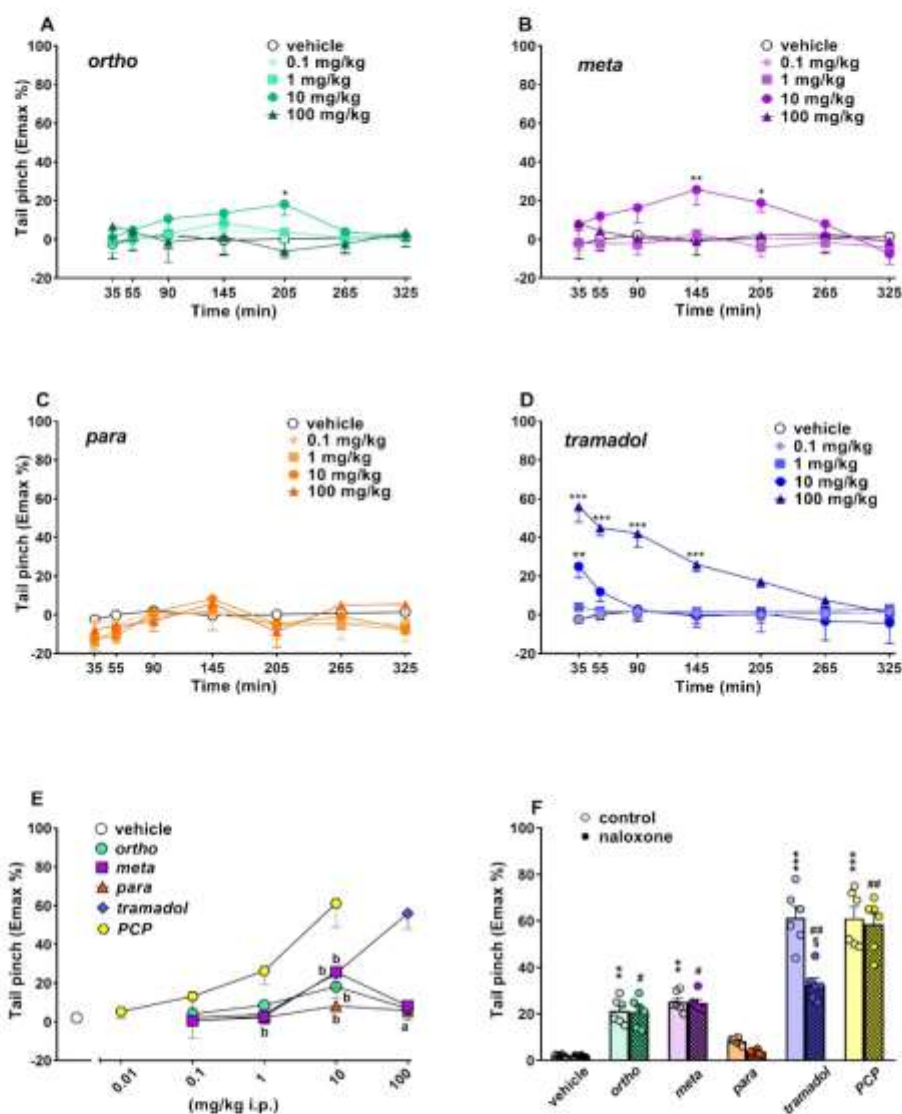
Figure 7. Effects of the systemic administration (0.1-100 mg/kg i.p.) of ortho (**A**), meta (**B**), para (**C**) and tramadol (**D**) on the tail pinch test in mice. Comparison of the maximal effect of ortho, meta, para, tramadol (0.1–100 mg/kg) and PCP (0.01–10 mg/kg) observed in 5 h (**E**) [2]. Interaction of the effects of ortho, meta, para, tramadol (100 mg/kg) and PCP (10 mg/kg) with the opioid receptor antagonist naloxone (6 mg/kg, i.p.; (**F**)). Data are expressed as percentage of maximum effect (Emax%; see material and methods) and represent the mean ± SEM of 6–8 determinations for each treatment. Statistical analysis was performed by two-way ANOVA, followed by the Bonferroni's test for multiple comparisons for the dose–response curve of each compound at different times (**A**–**D**), and for the antagonist studies (**E**), while the statistical analysis of panel F was performed with one-way ANOVA followed by Bonferroni test for multiple comparisons. * $p < 0.05$, ** $p < 0.01$, *** $p < 0.001$ versus vehicle; [a] $p < 0.05$ versus tramadol; [b] $p < 0.05$ versus PCP; [#] $p < 0.05$, [##] $p < 0.01$ versus naloxone; [§] $p < 0.05$ versus without naloxone; [2] PCP data are elaborated from [17].

34

The threshold of thermal pain did not change in vehicle-treated mice over 5 h of observation (Figure 8A) and the effect was similar to that observed in naïve untreated animals (data not shown). Systemic administration of 1-cyclohexyl-x-methoxybenzene derivatives (0.1–100 mg/kg) and PCP (0.1–10 mg/kg) dose-dependently affected the threshold of thermal pain in mice. Data of 1-cyclohexyl-x-methoxybenzene derivatives (ortho, meta and para) are replicated from [5], and PCP data are replicated from [17].
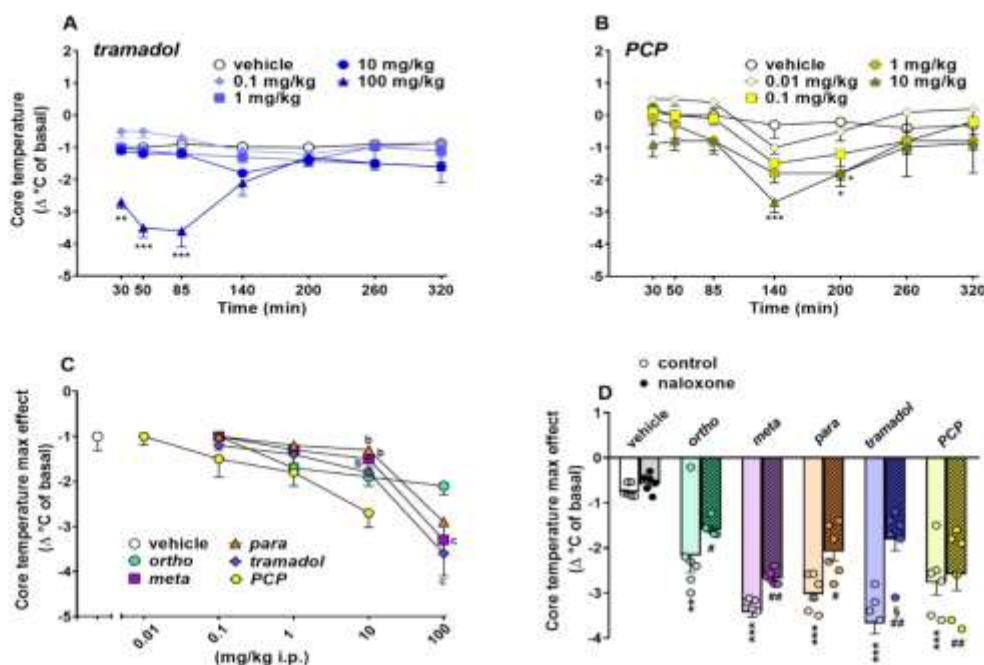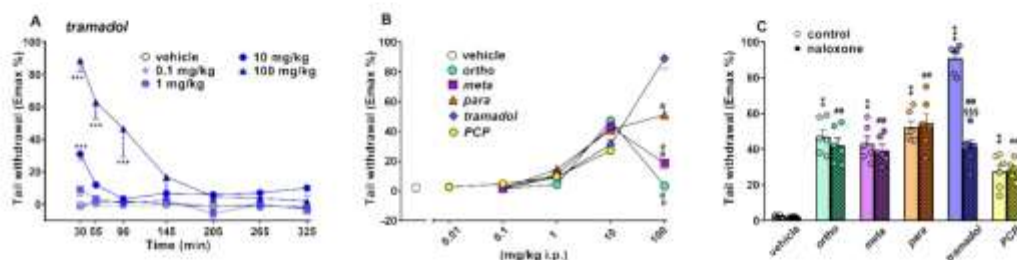

Figure 8. Effect of the systemic administration of tramadol (0.1–100 mg/kg i.p.; (**A**)) on the tail withdrawal test in mice. Comparison of the maximal effect of ortho, meta, para, tramadol (0.1–100 mg/kg) and PCP (0.01–10 mg/kg) observed over 5 h (**B**) [1,2]. Interaction of the maximal effective dose of ortho, meta, para, tramadol (100 mg/kg) and PCP (10 mg/kg) with the opioid receptor antagonist naloxone (6 mg/kg, i.p.; (**C**)). Data are expressed as percentage of maximum effect (Emax%; see material and methods) and represent the mean $\pm$ SEM of 6–8 determinations for each treatment. Statistical analysis was performed by two-way ANOVA, followed by Bonferroni's test for multiple comparisons for the dose–response curve of each compound at different times (**A**), and for the antagonist studies (**C**), while the statistical analysis of (**B**) was performed with one-way ANOVA followed by Bonferroni test for multiple comparisons. ** $p < 0.01$, *** $p < 0.001$ versus vehicle; [a] $p < 0.05$ versus tramadol; [c] $p < 0.05$ versus para; ## $p < 0.01$ versus naloxone; §§§ $p < 0.001$ versus without naloxone; [1] ortho, meta and para data are elaborated from [5]; [2] PCP data are elaborated from [17].

Systemic administration of tramadol (0.1–100 mg/kg i.p.) increased the threshold for thermal pain in the tail withdrawal test in mice (Figure 8A; significant effect of treatment ($F_{4,245} = 57.54$, $p < 0.0001$), time ($F_{6,245} = 17.84$, $p < 0.0001$) and time x treatment interaction ($F_{24,245} = 8.908$, $p < 0.0001$)). Tramadol induced a rapid increase in the thermal analgesia at 10 mg/kg (Emax ~31%) and 100 mg/kg (Emax ~89%; Figure 8A), and the effect of tramadol 100 mg/kg persisted for up to 90 min.

A comparison of the maximal effect among 1-cyclohexyl-x-methoxybenzene derivatives, tramadol and PCP (Figure 8B) revealed significant differences between the effects of these compounds ((significant effect of treatment ($F_{4,175} = 11.36$; $p < 0.0001$), dose ($F_{4,175} = 122.7$; $p < 0.0001$) and dose x treatment interaction ($F_{16,175} = 17.27$; $p < 0.0001$)). Tramadol was the more effective compound with respect to the 1-cyclohexyl-x-methoxybenzene derivatives. Pretreatment with naloxone 6 mg/kg did not prevent the analgesic effect induced by ortho, meta, para and PCP (10 mg/kg), while it partially prevented that caused by tramadol 100 mg/kg (Figure 8C).

Bar Test

The time spent on the bar did not change in vehicle-treated mice over 5 h of observation (data not shown), and the effect was similar to that observed in naïve untreated animals (data not shown). The systemic administration of ortho, meta, para, tramadol (0.1–100 mg/kg i.p.) and PCP (0.01–10 mg/kg i.p.) did not induce akinesia and did not affect the time spent on bar (data not shown).

Accelerod Test

The time spent on the accelerod did not change in vehicle-treated mice over 5 h of observation (Figure 9A,) and the effect was similar to that observed in naïve untreated animals (data not shown). Systemic administration of 1-cyclohexyl-x-methoxybenzene

derivatives (0.1–100 mg/kg; [5]) and PCP (0.1–10 mg/kg; [17]) dose-dependently affected motor activity on the accelerod in mice. Data of 1-cyclohexyl-x-methoxybenzene derivatives (ortho, meta and para) are replicated from [5], and PCP data are replicated from [17].
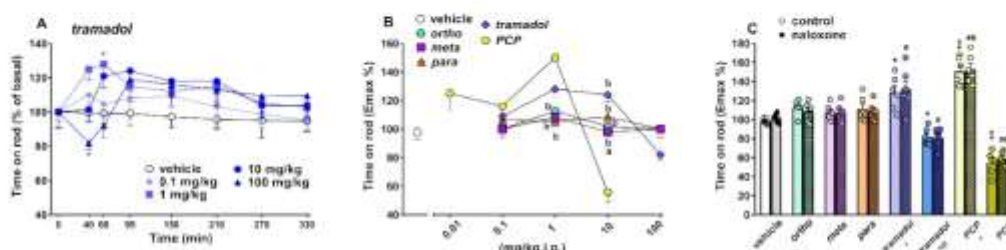
Figure 9. Effect of the systemic administration of tramadol (0.1–100 mg/kg i.p.; (**A**) on the accelerod test in mice. Comparison of the maximal effect of ortho, meta, para, tramadol (0.1–100 mg/kg) and PCP (0.01–10 mg/kg) observed in 5 h (**B**) [1,2]. Interaction of the maximal effective doses of ortho, meta, para (100 mg/kg), tramadol (1 and 100 mg/kg) and PCP (1 and 10 mg/kg) with the opioid receptor antagonist naloxone (6 mg/kg, i.p.; (**C**)). Data are expressed as percentage of basal and represent the mean ± SEM of 6–8 determinations for each treatment. Statistical analysis was performed by two-way ANOVA, followed by the Bonferroni test for multiple comparisons for the dose–response curve of each compound at different times (**A**), and for the antagonist studies (**C**), while the statistical analysis of (**B**) was performed with one-way ANOVA followed by Bonferroni test for multiple comparisons. * $p < 0.05$, ** $p < 0.01$, versus vehicle; [a] $p < 0.05$ versus tramadol; [b] $p < 0.05$ versus PCP; [‡] $p < 0.05$, [‡‡] $p < 0.01$ versus naloxone; [1] ortho, meta and para data are elaborated from [5]; [2] PCP data are elaborated from [17].

Systemic administration of tramadol transiently modulated the motor activity in the accelerod test in mice ((significant effect of treatment ($F_{4,280} = 5.502$; $p = 0.0003$), time ($F_{7,280} = 2.125$; $p = 0.0411$) but not time x treatment interaction ($F_{28,280} = 1.257$; $p = 0.1802$)). In particular, tramadol transiently facilitated the stimulated motor activity of mice on the accelerod at 1 mg/kg (~28% of basal activity at 60 min timepoint) and inhibited it at 100 mg/kg (~20% of basal activity at 40 min timepoint) (Figure 9A).

A comparison of the maximal effect among 1-cyclohexyl-x-methoxybenzene derivatives, tramadol and PCP (Figure 9B) revealed significant differences between the motor effects of these compounds ((significant effect of treatment ($F_{4,175} = 36.18$; $p = 0.0077$), dose ($F_{4,175} = 25.56$; $p < 0.0001$) and dose x treatment interaction ($F_{16,175} = 10.85$; $p < 0.0001$)). Notably, PCP was more effective than tramadol in facilitating (at 1 mg/kg) and inhibiting (10 mg/kg) the motor coordination of mice on the accelerod test. The 1-cyclohexyl-x-methoxybenzene derivatives were inactive in this motor test [5]). Pretreatment with naloxone 6 mg/kg did not prevent the facilitatory and inhibitory motor effects caused by both tramadol (1 and 100 mg/kg, respectively) and PCP 1 and 10 mg/kg, respectively (Figure 9C).

Spontaneous Locomotion Test

Spontaneous locomotion was affected by the systemic administration of ortho (Figure 10A; significant effect of treatment ($F_{4,280} = 15.26$, $p < 0.0001$), time ($F_{7,280} = 152.7$, $p < 0.0001$) and time x treatment interaction ($F_{28,280} = 3.886$, $p < 0.0001$)), meta (Figure 10B; significant effect of treatment ($F_{4,280} = 22.99$, $p < 0.0001$), time ($F_{7,280} = 131.6$, $p < 0.0001$) and time x treatment interaction ($F_{28,280} = 3.599$, $p < 0.0001$)) para (Figure 10C; significant effect of treatment ($F_{4,280} = 3.22$, $p = 0.0132$), time ($F_{7,280} = 55.98$, $p < 0.0001$) and time x treatment interaction ($F_{28,280} = 1.003$, $p = 0.4651$)) and tramadol (Figure 10C; significant effect of treatment ($F_{4,280} = 6.908$, $p < 0.0001$), time ($F_{7,280} = 58.63$, $p < 0.0001$) and time x treatment interaction ($F_{28,280} = 3.377$, $p < 0.0001$)). In particular, 1-cyclohexyl-x-methoxybenzene derivatives differently affected spontaneous motor activity. Ortho (Figure 10A) transiently facilitated spontaneous locomotion in mice at 1 (~+43% at 30 min) and 10 (~+56%) mg/kg,

while, at the highest dose (100 mg/kg), it inhibited (~−30%) mouse motor activity. Meta (Figure 10B) transiently facilitated spontaneous locomotion in mice at 1 (~+38% at 30 min) and 10 (~+70%) mg/kg, while para (Figure 10C) inhibited it at 10 (~−32% at 30 min) and 100 (~−48%) mg/kg. Tramadol (Figure 10D) facilitated spontaneous locomotion in mice at lower doses of 0.1 (~+29% at 30 min) and 1 (~+52%) mg/kg, while at the highest dose (100 mg/kg), it inhibited (~−38%) mouse motor activity. As previously reported, the systemic administration of PCP (0.01–10 mg/kg) facilitated spontaneous locomotion in mice. PCP data are replicated from [17].

A comparison of the overall distance travelled among 1-cyclohexyl-x-methoxybenzene derivatives, tramadol and PCP, analyzed at the same dose range (Figure 10E), revealed significant differences among the motor effects of these compounds. In particular, tramadol and PCP were more potent in facilitating spontaneous locomotion with respect to 1-cyclohexyl-x-methoxybenzene derivatives ($F_{4,45} = 32.06$; $p < 0.0001$), since they were effective at 0.1 mg/kg. Moreover, statistical analysis revealed that PCP is the most effective compound in stimulating locomotion in mice, at both 1 mg/kg ($F_{4,45} = 58.18$; $p < 0.0001$) and 10 mg/kg ($F_{4,45} = 217$; $p < 0.0001$). However, para was the more effective compound in inhibiting spontaneous locomotion at the highest dose tested (100 mg/kg; $F_{3,36} = 596$; $p < 0.0001$).

Pretreatment with naloxone 6 mg/kg did not prevent the motor effects caused by both 1-cyclohexyl-x-methoxybenzene derivatives and PCP (Figure 10F). It is interesting to note that, while the facilitating effect of tramadol at 1 mg/kg is insensitive to naloxone, the facilitating effect induced by tramadol at 100 mg/kg in the time window ranging from 90 to 120 min is prevented by treatment with naloxone.

Cardiorespiratory Analysis

To investigate if treatment with highest doses of the 1-cyclohexyl-x-methoxybenzene derivatives (100 mg/kg), tramadol (100 mg/kg) and PCP (10 mg/kg) can modify the normal cardiorespiratory pattern of mice, we used the MouseOX instrument (see Materials and Methods). Vehicle administration did not affect the basal breath rate (BR, 175 ± 15 brpm; Figure 11A), oxygen saturation (SpO2, $99.5 \pm 1.2\%$; Figure 11C), heart rate (HR, 570 ± 15 bpm; Figure 11E) and pulse distention (Pd, 243 ± 17 μm; Figure 11G) of mice during the 4 h of measuring. Administration of the 1-cyclohexyl-x-methoxybenzene derivatives (100 mg/kg), tramadol (100 mg/kg) and PCP (10 mg/kg) affected the basal BR in mice (Figure 11A; significant effect of treatment ($F_{5,210} = 69.21$, $p < 0.0001$), time ($F_{6,210} = 2.15$, $p = 0.0491$) and time x treatment interaction ($F_{30,210} = 5.773$, $p < 0.0001$)). Notably, BR was transiently increased by ortho (max effect ~ +38% of basal values at 30 min) and meta (max effect ~ +21% of basal values at 15 min), but not para, administration, while BR was transiently reduced by tramadol (max effect ~−40% of basal values at 60 min) and PCP (max effect ~−30% of basal values at 30 min). Pretreatment with naloxone 6 mg/kg completely prevented the bradypnea induced by tramadol, but was ineffective in blocking the effects caused by ortho, meta and PCP administration (Figure 11B).

37
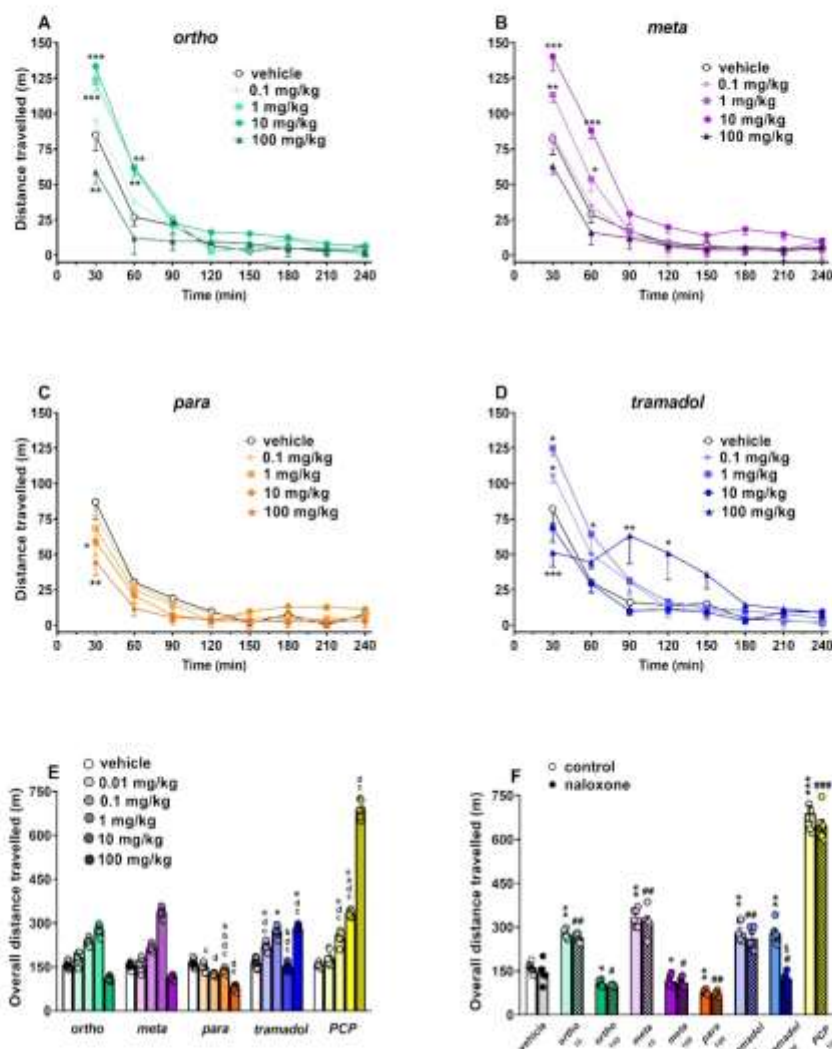
Figure 10. Effects of the systemic administration (0.1–100 mg/kg i.p.) of ortho (**A**), meta (**B**), para (**C**) and tramadol (**D**) on the total distance travelled of the mouse. Representation of the effect induced by ortho, meta, para, tramadol (0.1–100 mg/kg) and PCP (0.01–10 mg/kg) treatments on the overall distance traveled observed in 4 h (**E**) [2]. Interaction of the effective doses of ortho (10 and 100 mg/kg), meta (10 and 100 mg/kg), para (100 mg/kg), tramadol (1 and 100 mg/kg) and PCP (10 mg/kg) with the opioid receptor antagonist naloxone (6 mg/kg, i.p.; (**F**)). Data are expressed as meters travelled (total distance travelled) and represent the mean ± SEM of 8 determinations for each treatment. Statistical analysis was performed by two-way ANOVA, followed by Bonferroni's test for multiple comparisons of the dose–response curve of each compound at different times (**A–D**), and for the antagonist studies (**F**), while the statistical analysis of panel E was performed with one-way ANOVA followed by Bonferroni test for multiple comparisons. * $p < 0.05$, ** $p < 0.01$, *** $p < 0.001$ versus vehicle; [a] $p < 0.05$ versus tramadol; [b] $p < 0.05$ versus PCP; [c] $p < 0.05$ versus ortho; [d] $p < 0.05$ versus meta; [e] $p < 0.05$ versus para; # $p < 0.05$, ## $p < 0.01$, ### $p < 0.001$ versus naloxone; [$] $p < 0.05$ versus without naloxone. [2] PCP data are elaborated from [17].

The administration of tramadol (100 mg/kg) and PCP (10 mg/kg), but not 1-cyclohexyl-x-methoxybenzene derivatives (100 mg/kg), affected the basal SpO2 in mice (Figure 11C; significant effect of treatment ($F_{5,210} = 6.12$, $p < 0.0001$), time ($F_{6,210} = 4.281$, $p = 0.0004$) and time x treatment interaction ($F_{30,210} = 1.452$, $p = 0.0695$)). Notably, SpO2 was transiently reduced by tramadol (max effect $\sim -20\%$ of SpO2 saturation at 30 min) and PCP (max effect $\sim -19\%$ of SpO2 saturation at 30 min), and their inhibitory effects disappeared 60 min after compound administration. Pretreatment with naloxone 6 mg/kg completely prevented the reduction in SpO2 induced by tramadol, but was ineffective in blocking the effects of PCP administration (Figure 10D).

The administration of 1-cyclohexyl-x-methoxybenzene derivatives (100 mg/kg), tramadol (100 mg/kg) and PCP (10 mg/kg) affected the basal HR in mice (Figure 11E; significant effect of treatment ($F_{5,210} = 82.51$, $p < 0.0001$), time ($F_{6,210} = 6.673$, $p < 0.0001$) and time x treatment interaction ($F_{30,210} = 7.413$, $p < 0.0001$)). In particular, HR was transiently but maximally increased at 30 min by ortho (max effect $\sim +25\%$ of basal values), meta (max effect $\sim +37\%$ of basal values) and para (max effect $\sim +15\%$ of basal values), and the effects persisted for up to 120 min. Conversely, HR was mildly and transiently reduced by PCP (max effect $\sim -25\%$ of basal values at 30 min), and was reduced for up to 120 min by tramadol (max effect $\sim -35\%$ of basal values at 60 min). Pretreatment with naloxone 6 mg/kg did not prevent the increase in HR in mice that was induced by 1-cyclohexyl-x-methoxybenzene derivatives, or the inhibition caused by PCP administration, while naloxone prevented the inhibition induced by tramadol (Figure 11F).

The administration of the 1-cyclohexyl-x-methoxybenzene derivatives (100 mg/kg), tramadol (100 mg/kg) and PCP (10 mg/kg) affected the basal Pd in mice (Figure 11G; significant effect of treatment ($F_{5,210} = 61.59$, $p < 0.0001$), time ($F_{6,210} = 4.881$, $p = 0.0001$) and time x treatment interaction ($F_{30,210} = 6.055$, $p < 0.0001$)). Notably, Pd was maximally reduced at 30 min by ortho (max effect $- -35\%$ of basal values at 60 min), meta (max effect $\sim -33\%$ of basal values at 60 min), para (max effect $\sim -25\%$ of basal values at 30 min), and PCP (max effect $\sim -25\%$ of basal values at 30 min). The reduction in the Pd persisted for the ortho and meta for up to 180 min and for para and PCP up to 60 min. Conversely, tramadol increased the Pd in mice (max effect $- +31\%$ of basal values at 60 min), and its effect lasted for up to 120 min. Pretreatment with naloxone 6 mg/kg did not prevent the reduction in Pd in mice induced by 1-cyclohexyl-x-methoxybenzene derivatives and PCP administration, while it prevented the increase induced by tramadol (Figure 11H).

39
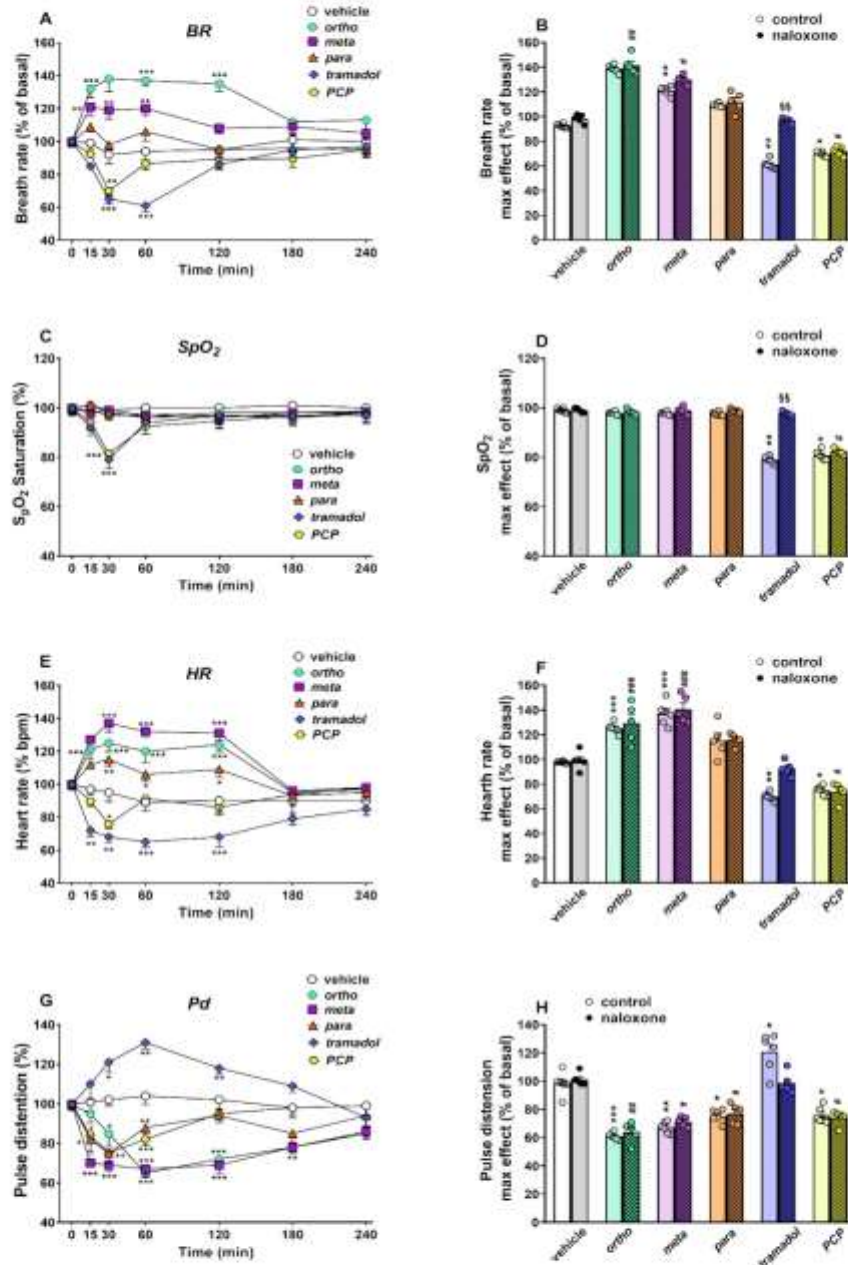
Figure 11. Effect of the systemic administration of ortho, meta, para, tramadol (100 mg/kg i.p.) and PCP (10 mg/kg i.p.) on breath rate (BR; (**A**)), on arterial saturation (SpO2; (**C**)), heart rate (HR; (**E**)) and pulse distention (Pd; (**G**)). Interaction of the effective doses of ortho, meta, para, tramadol (100 mg/kg) and PCP (10 mg/kg) with the opioid receptor antagonist naloxone (6 mg/kg, i.p.) on breath rate (BR; (**B**)), arterial saturation (SpO2; (**D**)), heart rate (HR (**F**)) and pulse distention (Pd; (**H**)). Data

are expressed as percentage of basal value (BR, HR and Pd), while absolute values for oxygen blood saturation (% SpO2 saturation) are represent as the mean ± SEM of 6–5 determinations for each treatment. Statistical analysis was performed by two-way ANOVA followed by Bonferroni's test for multiple comparisons for both the dose–response curve of each compound at different times ((A,C,E,G)) and interactions with naloxone (B,D,F,H). * $p < 0.05$, ** $p < 0.01$, *** $p < 0.001$ versus vehicle; # $p < 0.05$, ## $p < 0.01$ ### $p < 0.001$ versus naloxone; §§ $p < 0.01$ versus without naloxone.

3. Discussion

Our study presents novel results regarding the in vitro and in vivo characterization of the 1-cyclohexyl-x-methoxybenzene stereoisomers. Using the calcium mobilization assay, we demonstrated in vitro that the three stereoisomers, similar to tramadol, were inactive at mu, kappa and delta human recombinant receptors coupled with calcium signaling via chimeric G proteins. Conversely, the in vivo study provides the first direct comparison of the effects of 1-cyclohexyl-x-methoxybenzene stereoisomers and those of the two most similar compounds, tramadol and PCP [3], and demonstrates that ortho, meta and para stereoisomers impair acoustic and visual sensorimotor responses, induce analgesia, modulate motor activity and affect cardiorespiratory functions in mice. The three stereoisomers show a similar profile of action, with slight differences in potency and efficacy, probably due to their different substitution on the benzyl ring of the methoxylic group [5]. The effects caused by 1-cyclohexyl-x-methoxybenzene derivatives are generally qualitatively similar to those induced by tramadol and/or PCP administration, and in some tests, partially blocked by naloxone administration (see Table 2), suggesting the involvement of the opioid receptor system.

Table 2. Summary of the most important effects induced by the molecules, tested using neurological, behavioral and cardiorespiratory tests.

	1-Cyclohexyl-x-Methoxybenzene (0.1–100 mg/kg i.p)			Tramadol (0.1–100 mg/kg i.p)	PCP (0.01–10 mg/kg i.p)
	ortho	meta	para		
Neurological changes	no effect			tail elevation and convulsion NLX insensitive	no effect
Visual object response	dose-dependent inhibition NLX partially sensitive			dose-dependent inhibition NLX partially sensitive	dose-dependent inhibition NLX insensitive
Visual placing response	dose-dependent inhibition NLX partially sensitive	dose-dependent inhibition NLX partially sensitive	dose-dependent inhibition NLX sensitive	dose-dependent inhibition NLX sensitive	dose-dependant inhibition NLX insensitive
Acoustic response	dose-dependent inhibition NLX insensitive			dose-dependent inhibition NLX insensitive	dose-dependent inhibition NLX insensitive
Core body temperature	dose-dependent inhibition NLX insensitive			dose-dependent inhibition NLX partially sensitive	dose-dependent inhibition NLX insensitive
Mechanical analgesia	mild analgesia NLX insensitive	mild analgesia NLX insensitive	no effect	dose-dependent analgesia NLX partially sensitive	dose-dependent analgesia NLX insensitive
Thermal analgesia	dose-dependent inhibition NLX insensitive			dose-dependent analgesia NLX partially sensitive	dose-dependent analgesia NLX insensitive
Bar test	no effect			no effect	no effect
Stimulated locomotion	no effect			biphasic effect NLX insensitive	biphasic effect NLX insensitive
Sponotaneous locomotion	biphasic effect NLX insensitive	biphasic effect NLX insensitive	inhibitory effect NLX insensitive	biphasic effect NLX partially sensitive with low dosage	biphasic effect NLX insensitive
Breath rate	increased NLX insensitive	increased NLX insensitive	no effect	decreased NLX sensitive	decreased NLX insensitive
SpO2 saturation	no effect	no effect	no effect	decreased NLX sensitive	decreased NLX insensitive
Heart rate	increased NLX insensitive	increased NLX insensitive	increased NLX insensitive	decreased NLX sensitive	decreased NLX insensitive
Pulse distention	decreased NLX sensitive	decreased NLX sensitive	decreased NLX sensitive	increased NLX sensitive	decreased NLX insensitive

3.1. Major Neurological Changes

The administration of up to 100 mg/kg of three stereoisomers does not induce major neurological alterations, such as tail elevation, hyperreflexia and convulsions, in mice, highlighting their lower toxicity than tramadol and PCP. In fact, tramadol at 100 mg/kg causes tail elevation and convulsions in 90% of mice, while PCP at 100 mg/kg causes the rapid death of all treated mice.

Convulsions are typically reported in tramadol overdose in both animals and humans and, together with respiratory depression, they represent the most serious and dangerous aspect of acute tramadol poisoning [18–23]. Our data are consistent with previous reports showing that naloxone does not antagonize tail elevation or even augment tramadol-induced seizures in rodents [22,24]. This aspect is very important, as it highlights that incorrect antidotal therapy can worsen the symptoms of intoxication. However, the administration of naloxone is ineffective or only partially effective in preventing the effects of the 1-cyclohexyl-x-methoxybenzene derivatives and, fortunately, it does not worsen their pharmaco-toxicological effects.

3.2. Effect on Sensorimotor Responses

The present study confirms and extends previous evidence showing that 1-cyclohexyl-x-methoxybenzene derivatives impair visual sensorimotor responses in mice [5]. Notably, these compounds impair visual perception under both "static" (visual object response; [5]) and "dynamic" (visual placing response, present data) conditions, and reduce similar acoustic responses to tramadol and PCP [17]. Notably, the meta compound at 1 mg/kg appears to be more effective than PCP and tramadol in reducing visual and acoustic sensorimotor responses, suggesting it may have potential detrimental effect on driving and other human activities that require skill and attention.

The pharmacological response induced by the stereoisomers on sensorimotor responses is more similar to that caused by tramadol than that induced by PCP, having a prolonged effect, characterized by a slow appearance, with a maximum effect at 120 min which lasts up to 5 h. Otherwise, PCP causes a transient, rapid and maximum impairment of the visual and acoustic sensorimotor responses in the first 10–30 min, which reverts quickly and is extinguished in 130–180 min (visual impairments) or 60 min (acoustic alterations) for doses lower than 10 mg/kg [17].

The sensorimotor alteration induced by tramadol (as racemic mixture) could be due to its different opioid and non-opioid pharmacodynamic activity. The opioid component, which is predominant in the (+) enantiomer, has a weak affinity for μ opioid receptors, while its metabolite [(+)-Odesmethyl-tramadol] was about 300-fold more potent at mu opioid receptors [25]. The non-opioid component, predominant in the (−) enantiomer, is related to the inhibition of neuronal serotonin (5-HT) and norepinephrine (NE) reuptake [22], and also to the non-competitive antagonism of NMDA and GABAA receptors [26].

Therefore, these mechanisms could be involved in the visual sensorimotor alterations of tramadol; particularly the opioid component, since visual sensorimotor alterations are partially prevented by blocking opioid receptors with naloxone. In vitro results suggest a very low potency of tramadol at opioid receptors. However, it should be noted that tramadol is metabolized to O-Desmethyltramadol (O-Dt), a more potent mu agonist [25]. In fact, a differential study of the brain uptake of tramadol and its metabolite O-Dt showed that the peak brain levels of the two compounds coincide at higher dosage (40 mg/kg; [27]). Thus, the O-Dt metabolite of tramadol could be responsible for the neurological (particularly tail elevation) and sensorimotor alterations that are, at least in part, sensitive to naloxone.

Accordingly, data from our laboratory showed that stimulation of the opioid receptor by morphine or fentanyl impairs visual object and visual placing responses in mice in a dose-dependent and naloxone-sensitive manner, and this effect is possibly due to the activation of opioid receptors in brain areas controlling both visual and vestibular function [28,29].

An increase in serotonergic and noradrenergic transmission may also contribute to alterations in the visual sensorimotor. In fact, tramadol, by increasing 5-HT levels, may induce visual alterations via the activation of serotonin receptors in the cortico-visual circuits [30,31]. In particular, the inhibition of both visual object and visual placing responses in rodents has been observed after the systemic administration of MDMA [32], DOB [33] or the potent serotoninergic agonist 25I-NBOMe [34].

The increase in the noradrenergic signal could contribute to altering the sensorimotor responses in the visual placing test, and not the visual object test. This differing response is due to the fact that NE does not alter the perception of visual stimuli (i.e., visual object response), but possibly causes an alteration in the vestibular signals involved in the correct execution of the visual placing test (see [35]). Therefore, tramadol, by releasing NE, could change the vestibulo-ocular reflex and the optokinetic response in mice through β- and α2-receptor activation [36], thus impairing visual placing responses.

The antagonism on NMDA receptors exerted by tramadol [26] should also be considered. NMDA-receptor blockade caused inhibitions in visual sensory motor responses in mice, as reported for PCP and other dissociative drugs (i.e., ketamine, methoxetamine [17]).

Therefore, 1-cyclohexyl-x-methoxybenzene derivatives could impair visual object and visual placing responses by recruiting both opioid (naloxone-sensitive) and non-opioid mechanisms such as tramadol and PCP, and be used to alter visual perception.

The three stereoisomers (particularly ortho and meta) induce a significant and long-lasting impairment of the acoustic startle responses in mice, similarly to tramadol (100 mg/kg), but not PCP, which causes a rapid but transient inhibition of acoustic responses (10 mg/kg; [17]). The acoustic impairment was naloxone-resistant for all the tested compounds. Recently, the role of serotonin in modulating auditory brainstem responses has been demonstrated in mice, starting from the cochlear nucleus [37]. Indeed, in the dorsal region of this nucleus, the activation of 5HT2 receptors acts by increasing the electrical activity of neurons, leading to the final suppression of auditory process [38,39]. The exclusion of the possible involvement of opioid receptors in acoustic responses is supported by the fact that, in addition to the naloxone-resistant action reported in this study, morphine or the synthetic opioid MT-45 are ineffective in altering auditory sensorimotor responses, although they reduce visual responses in CD-1 mice [28]. Therefore, the fact that the three stereoisomers alter sensorimotor responses must be well-studied.

3.3. Effect on Spontaneous and Stimulated Motor Activity

The ortho and meta stereoisomers facilitate spontaneous locomotion in mice at low doses (0.1 and 1 mg/kg), and inhibit it at higher doses (100 mg/kg) spontaneous, while the para stereoisomer only inhibits motor activity. These motor effects are independent of opioid receptor stimulation, as they are not prevented by naloxone administration. The facilitation of spontaneous (open field) but not "stimulated" locomotion (rotarod test; [5]) suggests that these stereoisomers probably do not promote DA release in motor brain areas, even if administered at a higher dose (100 mg/kg). In fact, as reported for some typical DA/NEergic psychostimulants, such as methylone, butylone [40], α-PVP, MDPV [41] and methiopropamine [35–42], the robust stimulation of spontaneous motor activity is associated with an improvement in the rotarod test performance, and with the appearance of stereotypies and turning behavior at the highest tested dose, which impairs motor performance in mice [35,41]. It is interesting to note that the inhibition of spontaneous locomotion caused by the highest dose of 1-cyclohexyl-x-methoxybenzene derivatives (100 mg/kg) is not due to akinesia (no effect in the bar test), or the appearance of stereotypies and turning behavior. Therefore, this motor inhibition could possibly be due to either an anxiogenic effect of the molecule (stimulation of the noradrenergic fight-or-flight response) or as a consequence of the impaired visual and acoustic sensorimotor responses. In fact, the systemic administration of hallucinogenic phenethylamines that act as 5-HT receptor agonists, such as DOB, 2C-I and 25I-NBOMe [43], profoundly inhibits

visual and acoustic sensorimotor responses in CD-1 mice, inducing a mild inhibition of spontaneous locomotion [33].

Differently from 1-cyclohexyl-x-methoxybenzene derivatives, tramadol and PCP [17] affect both spontaneous and stimulated motor activity in mice. Notably, low doses (0.1 and 1 mg/kg) of tramadol facilitate spontaneous locomotion and increase mouse performance on the accelerod (1 mg/kg). At the highest dose (100 mg/kg), tramadol biphasically modulated spontaneous locomotion by producing a transient (30 min) inhibition, followed by a long-lasting (>2 h) stimulation.

Conversely, on the accelerod test, tramadol 100 mg/kg transiently inhibited mice motor performance in the first 40 min, as observed for spontaneous locomotion. The facilitation of locomotion at low doses is independent of the stimulation of opioid receptors, while the modulation of motor activity at 100 mg/kg is partially prevented by naloxone. In particular, naloxone prevented the facilitation of spontaneous locomotion observed in the second phase (from 90 min to 130 min), but did not prevent the inhibitory effect observed in the first 30 min. This naloxone-insensitive impaired locomotion is observed on both spontaneous and stimulated locomotion on the accelerod (in line with that reported by [24]) and could be related to the pro-convulsive effect of tramadol at 100 mg/kg.

PCP-induced increases in locomotor activity and repetitive movements, observed at high doses [17], are possibly related to NMDA blockade [44], the stimulation of dopamine transmission [45–48] or the agonistic action at dopamine D2 receptors [47,48]. On the other hand, only the highest dose of PCP (10 mg/kg) induced a transient reduction in the performance on the rod, probably due to the appearance of stereotyped movements [17,49].

3.4. Effect on Core Body Thermoregulation

While the three stereoisomers did not affect the surface temperature (data not shown), they modified the core temperature [5]. We have previously demonstrated that ortho and meta derivatives produced a mild core hyperthermia at the lowest dose (0.1 mg/kg) and a transient hypothermia at the highest dose (100 mg/kg), and the meta derivate seems to be more effective than the ortho compound. Otherwise, the 1-cyclohexyl-para-methoxybenzene induced only transient hypothermia at the higher dose (100 mg/kg), similar to tramadol (earlier at 100 mg/kg) and PCP (later at 1 and 10 mg/kg). The derivatives that affect thermoregulation are insensitive to naloxone, suggesting that opioid receptors are not involved. In the literature, tramadol and PCP produced hyperthermia, hypothermia or a biphasic effects, depending upon the doses used [50] and the ambient temperatures [51]. Our experimental paradigm had a biphasic effect on tramadol and only a hypothermic effect on PCP. The present data are in line with the significant hypothermia caused by tramadol in mice [52]. The hypothermia induced by tramadol was partially prevented by naloxone, suggesting that other mechanisms come into play in the thermoregulation exerted by tramadol. Indeed, tramadol modulates the release of both NE and 5HT, either of which are directly involved in thermoregulation mechanisms [53]. On the other hand, PCP showed no significant alterations in body temperature in the 3 h after the injection, as reported by [54]. Since the effects of stereoisomers are naloxone-independent, we can speculate that ortho, meta and para could affect body temperature in mice through non-opioid mechanisms, and possibly through NE/5-HT-receptor mechanisms.

3.5. Effect on Acute Mechanical and Thermal Analgesia

In the tail pinch test, ortho and meta derivatives evoke a transient mechanical analgesic effect at the dose of 10 mg/kg, while tramadol and PCP demonstrated a larger and faster analgesic effect. In the tail-withdrawal test, the para compound sustains thermal analgesia up to a 100 mg/kg dose, while the ortho and meta derivatives show activity at 10 mg/kg but lose their activity at the highest dose (100 mg/kg; [5]). The acute analgesic effect induced by the derivatives is naloxone-insensitive, suggesting that opioid receptors are not involved in this action. Tramadol- and PCP-induced transient analgesia peaked in the

first hour. Analgesia induced by tramadol was partially prevented by naloxone, while that induced by PCP was naloxone-insensitive.

A pharmacokinetic study on tramadol in B6 mice after IP administration at a dose of 25 mg/kg revealed that tramadol and its metabolite O-Dt reach similar plasma levels one hour after administration. The same study demonstrated that tramadol and O-Dt were quantifiable up to 4 and 2 h after administration, respectively [55]. These results reveal the high metabolism of tramadol compared to its metabolite O-Dt. Therefore, we suggest that the mechanical and thermal analgesic effects seen in the first 2 h of measurements after tramadol administration are mainly induced by O-Dt, which acts as a mu receptor agonist, eliciting naloxone-sensitive analgesic effects [56]. Interestingly, a recent structure–activity study of tramadol and its metabolite proved that O-Dt and morphine share common pharmacophore features with, and have similar binding modes to, the mu opioid receptor [57]. The experimental data suggest that tramadol and its metabolite, O-DT, exert their analgesic effect through the direct activation of mu opioid receptors, but also through the indirect activation of central $\alpha 2$-adrenoceptors [58,59] and descending serotonergic pathways [60]. Therefore, our data suggest that 1-cyclohexyl-x-methoxybenzene derivatives may share some antinociceptive mechanisms with tramadol and PCP, but not their opioidergic component. Further studies are needed to unveil the mechanisms responsible for the analgesic action of three stereoisomers.

3.6. Cardiorespiratory Effects

Ortho, meta and para increase breath rate without modifying SpO2, enhance heart rate and cause vasoconstriction, highlighting an action profile for the cardio-respiratory system similar to that of compounds stimulating the release of catecholamines, such as those recently reported for methiopropamine [42]. Their effects were naloxone-insensitive, suggesting that they are mediated by opioid-independent mechanisms. Conversely, tramadol and PCP reduce breath rate, SpO2 saturation and heart rate, although they use different mechanisms. Tramadol causes vasodilatation, while PCP causes vasoconstriction. Tramadol-induced cardio-respiratory changes were naloxone-sensitive, while those induced by PCP were not. In preclinical studies, a low dose of tramadol induced a slight increase in arterial blood pressure and heart rate in anaesthetized rabbits [61], dogs [62] and rats [63], possibly due to enhancement of the release of NE and/or 5-HT, which may result in peripheral vasoconstriction and/or heart stimulation [63]. While, at high doses, tramadol caused myocardial depression and hypotension in anaesthetized rabbits [64], dogs [65] and rats [66], possibly due to mu opioid receptor activation [66] and vascular relaxation as a result of nitric oxide production, and exerted a direct effect on smooth muscle [67]. These depressive effects are typically reported in human overdoses. In fact, the intravenous administration of tramadol caused orthostatic hypotension [68] and a transient rise in arterial blood pressure [69], while direct cardiotoxicity, characterized by cardiac arrest and severe biventricular failure, was a factor in intoxication [70] and deaths due to tramadol overdose [71,72]. Together with the cardio-depressive effect, tramadol causes respiratory depression in both animal models [73] and humans [11,18,74] possibly due to the stimulation of mu opioid receptors, which are reverted by naloxone. On the other hand, as previously reported, PCP reduced cardiorespiratory functions [17]. PCP has a complex pharmaco-dynamic profile on different receptor targets [75]; therefore, its cardiorespiratory action could be due to its interaction with the cardiac sigma-receptors [76], dopamine D2-receptors [77] and/or modulation of cardiac potassium channels [78]. Our results are consistent with the literature data showing the adverse effect of high doses of tramadol and PCP on cardiorespiratory functions. This outlines the differences observed with the 1-cyclohexyl-x-methoxybenzene derivatives that led to different modulation on the cardiorespiratory system, resembling the effect of stimulant drugs characterized by an increase in heart and breath rate, associated with vasoconstriction [42]. Further studies are needed to better understand the mechanisms underlying these cardiorespiratory effects that can predispose one to cardiac toxicity.

45

4. Materials and Methods

4.1. In Vitro Studies

4.1.1. Drugs and Reagents

Brilliant black, bovine serum albumin (BSA), 4-(2-hydroxyethyl)-1-piperazineethanesulfonic acid (HEPES), and probenecid were from Sigma Aldrich (St. Louis, MO, USA). Pluronic acid and Fluo-4 AM were from Thermo Fisher Scientific (Waltham, MA, USA). All cells culture media and supplements were from Euroclone (Milano, Italy). Tramadol hydrochloride 50 mg/1 mL was purchased from Grünenthal Italia S.r.l and diluted in sterile water at a concentration of 10 mM, while its three analogs were dissolved in dimethyl sulfoxide (DMSO) at a concentration of 10 mM. The stock solutions were kept at −20 °C until use.

4.1.2. Cells

CHO cells lines permanently co-expressing mu and kappa receptor with the C-terminally modified Gαqi5, and delta receptors with the C-terminally modified GαqG66Di5, were used. Details regarding the generation of these cells have been described previously [16,17]. Cells were cultured in culture medium consisting of Dulbecco's modified Eagle's medium (DMEM)/HAMS F12 (1:1), supplemented with 10% fetal bovine serum (FBS), penicillin (100 IU/mL), streptomycin (100 mg/mL), geneticin (G418; 200 µg/mL) and hygromycin B (100 µg/mL). Cell cultures were kept at 37 °C in 5% CO_2/humidified air. When confluence was reached (3–4 days), cells were sub-cultured as required using trypsin/EDTA and used for experimentation. Cells were seeded at a density of 50,000 cells/well into 96-well, black, clear-bottom plates. After 24 h incubation, the cells were loaded with Hank's Balanced Salt Solution (HBSS), supplemented with 2.5 mM probenecid, 3 µM of the calcium-sensitive fluorescent dye Fluo-4 AM, 0.01% pluronic acid and 20 mM HEPES (pH 7.4) for 30 min at 37 °C. Then, the loading solution was aspirated and a washing step with 100 µL/well of HBSS, HEPES (20 mM, pH 7.4), 2.5 mM probenecid and 500 µM Brilliant Black was carried out. Subsequently, 100 µL/well of the same buffer was added. After placing cell culture and compound plates into the FlexStation II (Molecular Devices, Sunnyvale, CA, USA), changes in the fluorescence of the cell-loaded, calcium-sensitive dye Fluor-4 AM were measured. On-line additions were carried out in a volume of 50 µL/well.

4.1.3. Data Analysis and Terminology

All data were analyzed using Graph Pad Prism 6.0 (La Jolla, CA, USA). Data are expressed as mean ± sem of n experiments performed in duplicate. Agonist effects were expressed as maximum change in percent over the baseline fluorescence. Baseline fluorescence was measured in wells treated with vehicle. Agonist potency was expressed as pEC50, which is the negative logarithm to base 10 of the agonist molar concentration that produces 50% of the maximal possible effect of that agonist. The agonist concentration–response curves were fitted with the four-parameter logistic nonlinear regression model:

$$\text{Effect} = \text{Baseline} + \frac{(E_{max} - \text{Baseline})}{\left(1 + 10^{(\text{LogEC}_{50} - \text{Log}_{[compound]})\text{Hillslope}}\right)}$$

4.2. In Vivo Studies

4.2.1. Animals

Four hundred and fifty-four male ICR (CD-1®) mice weighing 30–35 g (Centralized Preclinical Research Laboratory, University of Ferrara, Italy) were group housed (5 mice per cage; floor area per animal was 80 cm^2; minimum enclosure height was 12 cm), exposed to a 12:12-h light–dark cycle (light period from 6:30 AM to 6:30 PM) at a temperature of 20–22 °C and humidity of 45–55%, and were provided with ad libitum access to food (Diet 4RF25 GLP; Mucedola, Settimo Milanese, Milan, Italy) and water. The experimental protocols performed in the present study were in accordance with the U.K. Animals (Scientific

Procedures) Act of 1986 and associated guidelines and the new European Communities Council Directive of September 2010 (2010/63/EU). Experimental protocols were approved by the Italian Ministry of Health (license n. 335/2016-PR) and by the Animal Welfare Body of the University of Ferrara. According to the ARRIVE guidelines, all possible efforts were made to minimise the number of animals used, minimise the animals' pain and discomfort and reduce the number of experimental subjects. For the overall study, 454 mice were used. In the battery of behavioral tests used in the safety pharmacology studies (see material and methods), for each treatment of (vehicle, 4 different 1-cyclohexyl-x-methoxybenzene derivatives or tramadol doses, 0.1, 1, 10 and 100 mg/kg), 8 mice were used (total mice used: 136). In the safety pharmacology studies, performed with naloxone, for each treatment of (naloxone 6 mg/kg, naloxone+1-cyclohexyl-x-methoxybenzene derivatives (100 mg/kg for each compound), naloxone+tramadol 100 mg/kg and naloxone+PCP 10 mg/kg), 6 mice were used (total mice used: 36). In the analysis of spontaneous locomotion in the open-field test, for each treatment of (vehicle or 4 different 1-cyclohexyl-x-methoxybenzene derivatives or tramadol doses, 0.1, 1, 10 and 100 mg/kg), 8 mice were used (total mice used: 160), while, for the antagonism studies with naloxone, for each treatment of (naloxone 6 mg/kg, naloxone+1-cyclohexyl-x-methoxybenzene derivatives (10 and 100 mg/kg for ortho and meta and 100 mg/kg para), naloxone+tramadol 1 and100 mg/kg and naloxone+PCP 10 mg/kg), 6 mice were used (total mice used: 54); in the cardiorespiratory studies, for each treatment of (vehicle, the highest 1-cyclohexyl-x-methoxybenzene derivatives (100 mg/kg) and tramadol (100 mg/kg), 6 mice were used (total mice used: 30) while for the antagonism studies with naloxone, for each treatment of (naloxone 6 mg/kg, naloxone+1-cyclohexyl-x-methoxybenzene derivatives (100 mg/kg for each compound), naloxone+tramadol 100 mg/kg and naloxone+PCP 10 mg/kg) 5 mice were used (total mice used: 30).

4.2.2. Drug Preparation and Dose Selection

Tramadol hydrochloride ((±)cis-2-[(dimethylamino)methyl]-1-(3-methoxyphenyl) cyclohexanol hydrochloride) and phencyclidine hydrochloride (1-(1-phenylcyclohexyl) piperidine hydrochloride) were purchased from LGC standards (LGC Standards S.r.l., Sesto San Giovanni, Milan, Italy), while naloxone was purchased from Sigma Aldrich (St. Louis, MO, USA). 1-cyclohexyl-x-methoxybenzene derivatives (ortho, meta and para) were synthesized and purified as previously reported [5]. Drugs were initially dissolved in absolute ethanol (final concentration was 2%) and Tween 80 (2%) and brought to the final volume with saline (0.9% NaCl). The solution made with ethanol, Tween 80 and saline was also used as the vehicle. Drugs were administered by intraperitoneal injection at a volume of 4 μL/g. Doses of ortho, meta, para, tramadol (0.1–100 mg/kg i.p.) and PCP (0.01–100 mg/kg used in core temperature and naloxone studies) were chosen in previous studies [5,17]. To compare the effects of 1-cyclohexyl-x-methoxybenzene derivatives and tramadol with those of PCP (0.01–10 mg/kg), we carried out preliminary studies ($n = 3$ mice) evaluating the effect 1-cyclohexyl-x-methoxybenzene derivatives and tramadol at a dose of 0.01 mg/kg. Since this dose was ineffective in each experimental paradigm studied, in order to reduce the number of animals used (3-R rule), we did not carry out further experiments with the dose of 0.01 mg/kg, considering it completely ineffective. The dose–response effects of PCP were obtained by [17]. The dose of 100 mg/kg of PCP (for comparison with 1-cyclohexyl-x-methoxybenzene derivatives and tramadol at 100 mg/kg) was only tested in 3 mice, since it causes convulsion and death of the animal 5–15 min after administration. The high dose of naloxone (6 mg/kg) was used to achieve a complete blockade of the mu, delta and kappa opioid receptors [28].

4.3. Behavioral Studies

The effects of 1-cyclohexyl-x-methoxybenzene derivatives, tramadol and PCP were investigated using a battery of behavioural tests that are widely used in pharmacology safety studies for the preclinical characterization of new psychoactive substances in rodents [5,17,32,79–81]. All experiments were performed between 8:30 AM and 2:00 PM.

Experiments were conducted blindly by trained observers working in pairs [82]. Mouse behaviour (sensorimotor responses) was videotaped and analysed offline by a different trained operator, who provided the test scores.

4.3.1. Major Neurological Changes

Neurological changes in the mice, such as tail elevation, hyperreflexia and convulsions, were evaluated as previously described [79–81]. Neurological changes are expressed as frequency (percent of animals that develop symptoms), duration (total time in seconds), latency (time in seconds of symptom onset) and score (degree of tail elevation). Tail elevation was measured during the observation of freely moving mice in a square area (score 0/4 no tail elevation, score 4/4 Straub tail).

4.3.2. Sensorimotor Studies

We studied the voluntary and involuntary sensorimotor responses of the mice, resulting from different reactions to visual, acoustic and tactile stimuli [80].

Evaluation of the Visual Response

Visual response was verified by two behavioral tests, which evaluated the ability of the animal to capture visual information when the animal was either stationary (the visual object response) or moving (the visual placing response).

Visual object response test was used to evaluate the ability of the mouse to see an object approaching from the front (frontal view) or the side (lateral view), which typically induces the animal to shift or turn the head, bring the forelimbs in the position of "defense" or retreat. For the frontal visual response, a white horizontal bar was moved frontally to the mouse head, and the manoeuvre was repeated three times. For the lateral visual response, a small dentist's mirror was moved into the mouse's field of view in a horizontal arc, until the stimulus was between the mouse's eyes. The procedure was conducted bilaterally [17,80] and repeated three times. The assigned score was 1 if there was a reflection in the mouse movement, or 0 if it was not present. The total value was calculated by adding the scores obtained in the frontal to those obtained in the lateral visual object response test (overall score: 9). The visual object response was measured at 0, 10, 30, 60, 120, 180, 240 and 300 min post-injection.

The Visual Placing response test was performed using a tail suspension modified apparatus, able to bring the mouse towards the floor at a constant speed of 10 cm/sec [80]. In brief, CD-1 mice were suspended 20 cm above the floor by an adhesive tape, placed approximately 1 cm from the tip of the tail. The downward movement of the mouse was videotaped by a camera (B/W USB Camera, day and night, with varifocal lens; Ugo Basile, Gemonio, VA, Italy) placed at the base of the tail suspension apparatus. The films were analyzed off-line by a trained operator who was unaware of the drug treatments performed. The frame-by-frame analysis allowed for an evaluation of the beginning of the mouse's reaction, while it was approaching the floor. The first movement of the mouse when it perceives the floor is the extension of the front legs. When the mouse started the reaction, an electronic ruler evaluated the perpendicular distance in millimeters between the eyes of the mice and the floor. Untreated control mice typically perceive the floor and prepare to contact at a distance of about 25 ± 4.8 mm. The visual placing response was measured at 0, 15, 40, 70, 130, 190, 250 and 310 min post-injection.

Evaluation of Acoustic Response

Acoustic response measures the reflexes of the mouse in response to an acoustic stimulus produced behind the animal. In particular, four acoustic stimuli of different intensities and frequencies were tested [80]. Each sound test was repeated three times. A score of 1 was given if there was a response and a score of 0 was given if there was no response, for a total score of 3 for each sound. The acoustic total score was calculated by

48

adding scores obtained in the four tests (overall score of 12). The acoustic response was measured at 0, 10, 30, 60, 120, 180, 240 and 300 min post-injection.

Evaluation of Core Body Temperature

The core temperature was determined using a probe (1 mm diameter) that was gently inserted, after lubrication with liquid Vaseline, into the rectum of the mouse (to about 2 cm), and left in position until the temperature stabilised (about 10 s; [79]). The probe was connected to a Cole Parmer digital thermometer, model 8402. Core body temperature was measured at 0, 30, 50, 85, 140, 200, 260 and 320 min post-injection.

Evaluation of Pain Induced by a Mechanical and a Thermal Stimulus

Acute mechanical nociception was evaluated using the tail pinch test [79]. A special rigid probe connected to a digital dynamometer (ZP-50N, IMADA, Japan) was gently placed on the tail of the mouse (in the distal portion), and progressive pressure was applied. When the mouse flicked its tail, the pressure was stopped and the digital instrument recorded the maximum peak of weight that was supported (g/force). A cut-off (500 g/force) was set to avoid tissue damage. The test was repeated three times, and the final value was calculated by averaging the three obtained scores. Acute thermal nociception was evaluated using the tail withdrawal test [79]. The mouse was restrained in a dark plastic cylinder and half of its tail was dipped in 48 °C water, Then, the length of time (in s) for which the tail was left in the water was recorded. A cut-off (15 s) was set to avoid tissue damage. Acute mechanical and thermal nociception was measured at 0, 35, 55, 90, 145, 205, 265 and 325 min post-injection.

Motor Activity Assessment

Alterations in motor activity were measured using the bar, the accelerod tests and the analysis of spontaneous locomotor activity [28,79]. In the bar test, the mouse's forelimbs were placed on a plastic bar (height 6 cm). The time spent on the bar was measured (immobility cut off: 20 s), and akinesia was calculated as the total time spent on the bar after three consecutive trials (total maximal time of catalepsy: 60 s). The bar test was performed at 0, 20, 40, 70, 140, and 195 min post-injection. In the accelerod test, the animals were placed on a rotating cylinder that automatically increases in velocity in a constant manner (0–60 rotations/min in 5 min). The time spent on the cylinder was measured. The accelerod test was performed at 0, 40, 60, 95, 150, 210, 270 and 330 min post-injection. Spontaneous locomotor activity was measured using the ANY-maze video-tracking system (Ugo Basile, application version 4.99 g Beta). The mouse was placed in a square plastic cage (60 × 60 cm) located in a sound- and light-attenuated room, and motor activity was monitored for 240 min. Four mice were monitored at the same time in each experiment. The spontaneous locomotor activity is measured as the horizontal distance travelled in meters (m). The distance travelled was analysed every 15 min, for a maximum of 240 min. To avoid mice olfactory cues, cages were carefully cleaned with a diluted (5%) ethanol solution and washed with water between animal trials. All experiments were performed between 9:00 AM and 1:00 PM.

4.4. Cardiorespiratory Analysis

To monitor cardiorespiratory parameters in awake and freely moving mice with no invasive instruments and minimal handling, a collar with a sensor was applied to continuously detect breath rate, oxygen saturation, heart rate and pulse distension (vessel diameter changes), with a frequency of 15 Hz [28,83]. During the experiment, the mouse was allowed to freely move in a cage (40 × 40 × 30 cm) with no access to food and water while being monitored by the sensor collar through MouseOx Plus (STARR Life Sciences® Corp. Oakmont, PA, USA) software. In the first hour of acclimation, a fake collar, similar to the real one used in the test but with no sensor, was used to minimize the potential stress during the experiment. Then, the real collar (with sensor) was replaced, and baseline

parameters were monitored for 60 min. Subsequently, 1-cyclohexyl-x-methoxybenzene derivatives, tramadol (100 mg/kg), PCP (10 mg/kg) or vehicle were administered, and data were recorded for up to 240 min. Cardiorespiratory changes were analysed and reported at 0, 15, 30, 60, 120, 180 and 240 min post-injection.

4.5. Data and Statistical Analysis

Core temperature values are expressed as the difference between control temperature (before injection) and temperature following drug administration ($\Delta°C$). Antinociception (tail withdrawal and tail pinch tests) and catalepsy (bar test) are calculated as the percent of maximal possible effect [EMax% = ((test-control latency)/(cut off time-control)) × 100]. Data are expressed in absolute values (seconds (sec) in neurological changes, meters (m) for distance travelled), $\Delta°C$ (core and surface temperature), Emax% (tail withdrawal, tail pinch and bar test) and percentage of basal (accelerod test). In sensorimotor response experiments, data are expressed in arbitrary units (visual objects response and acoustic response) or percentage of baseline (visual placing response). Data are expressed in percentage of basal value (respiratory rate (expressed as respiratory rate per minute (rrpm), SpO2 saturation (oxygen blood saturation expressed as %), heart rate (expressed as heart beats per min (bpm) and pulse distention (vessel diameter changes expressed as μm)). All the numerical data are given as mean ± SEM of 4 independent experimental replications. The statistical analysis of the effects of the individual substances in different concentrations over time, and analysis of the antagonism studies, were performed using a two-way ANOVA, followed by a Bonferroni test for multiple comparisons. The statistical analysis of comparisons of the maximal effects induced by treatments were analyzed by one-way ANOVA, followed by a Bonferroni test for multiple comparisons. Student's t-test was used to determine statistical significance ($p < 0.05$) between two groups (see neurological changes). The statistical analysis was performed using Prism software (GraphPad Prism, San Diego, CA, USA). All analyses were performed using GraphPad Prism software.

5. Conclusions

The present study demonstrates in vitro that the three 1-cyclohexyl-x-methoxybenzene stereoisomers, similar to tramadol, were inactive at mu, kappa and delta receptors. Therefore, their opioid-dependent in vivo effects, such as impairments of visual sensorimotor responses, may be due to metabolic activation, as reported for the O-Dt metabolite of tramadol [25]. Further studies will be undertaken to verify this possibility.

In vivo studies show that three stereoisomers may induce pharmaco-toxicological effects that resemble, in some experimental paradigms, those induced by tramadol and PCP. Notably, they could alter sensorimotor visual responses though mechanisms involving the opioid system and affect, in a naloxone-independent manner, thermoregulation, mechanical and thermal pain threshold, motor activity, and cardiorespiratory functions, highlighting their potentially dangerous effects.

Therefore, further studies on the receptor activity of the 1-cyclohexyl-x-methoxybenzene are recommended, in order to better understand their potential for abuse and the dangers they pose in many daily activities, greatly increasing the risk factors for workplace accidents and traffic injuries.

Author Contributions: M.M., S.B. and G.C. contributed conception and design of the study; M.M., S.B., M.T., R.A., C.S. and V.C. performed in vivo experimental section; C.S., G.C. and A.F. performed in vitro experimental section; M.M., S.B. and G.C. wrote the manuscript; S.B., M.M., M.T., R.A., M.C., F.D.-G. and A.C., edited sections of the manuscript; S.B., M.M., M.T., R.A., T.B. and F.B. performed statistical analysis. All authors contributed to manuscript revision. All authors have read and agreed to the published version of the manuscript.

References

1. European Monitoring Centre for Drugs and Drug Addiction (EMCDDA). EU Drug Markets Report: In-Depth Analysis. 2016. Available online: https://www.emcdda.europa.eu/publications/joint-publications/eu-drug-markets-2016-in-depth-analysis_en (accessed on 31 March 2021).
2. Baumeister, D.; Tojo, L.M.; Tracy, D.K. Legal highs: Staying on top of the flood of novel psychoactive substances. *Ther. Adv. Psychopharmacol.* **2015**, *5*, 97–132. [CrossRef] [PubMed]
3. European Monitoring Centre for Drugs and Drug Addiction (EMCDDA). Annual Report on the State of the Drugs Problem in Europe. 2012. Available online: https://www.emcdda.europa.eu/publications/annual-report/2012_en (accessed on 31 March 2021).
4. Serpelloni, G.; Macchia, T.; Locatelli, C.; Rimondo, C. Seri Nuove Sostanze Psicoattive (NSP): Schede Tecniche Relative alle Molecole Registrate dal Sistema Nazionale di Allerta Precoce. 2013. Available online: http://www.en.npsalert.it/modules/pubbdetails/690/Nuove+Sostanze+Psicoattive+(NSP):+schede+tec.html (accessed on 16 July 2021).
5. Fantinati, A.; Ossato, A.; Bianco, S.; Canazza, I.; de Giorgio, F.; Trapella, C.; Marti, M. 1-cyclohexyl-x-methoxybenzene derivatives, novel psychoactive substances seized on the internet market. Synthesis and in vivo pharmacological studies in mice. *Hum. Psychopharmacol.* **2017**, *32*, e2560. [CrossRef]
6. Lanier, R.K.; Lofwall, M.R.; Mintzer, M.Z.; Bigelow, G.E.; Strain, E.C. Physical dependence potential of daily tramadol dosing in humans. *Psychopharmacology* **2010**, *211*, 457–466. [CrossRef]
7. United Nations Office on Drugs and Crime (UNDOC). Annual Report: Covering Activities during 2017. 2017. Available online: https://www.unodc.org/documents/AnnualReport/Annual-Report_2017.pdf (accessed on 31 March 2021).
8. European Monitoring Centre for Drugs and Drug Addiction (EMCDDA). European Drug Report. 2019. Available online: https://www.emcdda.europa.eu/edr2019_en (accessed on 31 March 2021).
9. Finnegan, K.T.; Kanner, M.I.; Meltzer, H.Y. Phencyclidine-induced rotational behavior in rats with nigrostriatal lesions and its modulation by dopaminergic and cholinergic agents. *Pharmacol. Biochem. Behav.* **1976**, *5*, 651–660. [CrossRef]
10. Simonsen, K.W.; Christoffersen, D.J.; Banner, J.; Linnet, K.; Andersen, L.V. Fatal poisoning among patients with drug addiction. *Dan. Med. J.* **2015**, *62*, A5147.
11. Shadnia, S.; Soltaninejad, K.; Heydari, K.; Sasanian, G.; Abdollahi, M. Tramadol intoxication: A review of 114 cases. *Hum. Exp. Toxicol.* **2008**, *27*, 201–205. [CrossRef]
12. Ryan, N.M.; Isbister, G.K. Tramadol overdose causes seizures and respiratory depression but serotonin toxicity appears unlikely. *Clin. Toxicol.* **2015**, *53*, 545–550. [CrossRef] [PubMed]
13. Brents, L.K.; Gallus-Zawada, A.; Radominska-Pandya, A.; Vasiljevik, T.; Prisinzano, T.E.; Fantegrossi, W.E.; Moran, J.H.; Prather, P.L. Monohydroxylated metabolites of the K2 synthetic cannabinoid JWH-073 retain intermediate to high cannabinoid 1 receptor (CB1R) affinity and exhibit neutral antagonist to partial agonist activity. *Biochem. Pharm.* **2012**, *83*, 952–961. [CrossRef] [PubMed]
14. Wiley, J.L.; Marusich, J.A.; Huffman, J.W. Moving around the molecule: Relationship between chemical structure and in vivo activity of synthetic cannabinoids. *Life Sci.* **2014**, *97*, 55–63. [CrossRef] [PubMed]
15. Camarda, V.; Fischetti, C.; Anzellotti, N.; Molinari, P.; Ambrosio, C.; Kostenis, E.; Regoli, D.; Trapella, C.; Guerrini, R.; Severo, S.; et al. Pharmacological profile of NOP receptors coupled with calcium signaling via the chimeric protein G alpha qi5. *Naunyn-Schmiedeberg's Arch. Pharm.* **2009**, *379*, 599–607. [CrossRef]
16. Camarda, V.; Calo, G. Chimeric G proteins in fluorimetric calcium assays: Experience with opioid receptors. *Methods Mol. Biol.* **2013**, *937*, 293–306. [CrossRef] [PubMed]
17. Ossato, A.; Bilel, S.; Gregori, A.; Talarico, A.; Trapella, C.; Gaudio, R.M.; De-Giorgio, F.; Tagliaro, F.; Neri, M.; Fattore, L.; et al. Neurological, sensorimotor and cardiorespiratory alterations induced by methoxetamine, ketamine and phencyclidine in mice. *Neuropharmacology* **2018**, *141*, 167–180. [CrossRef] [PubMed]
18. Spiller, H.A.; Gorman, S.E.; Villalobos, D.; Benson, B.E.; Ruskosky, D.R.; Stancavage, M.M.; Anderson, D.L. Prospective multicenter evaluation of tramadol exposure. *J. Toxicol. Clin. Toxicol.* **1997**, *35*, 361–364. [CrossRef]

19. Tobias, J.D. Seizure after overdose of tramadol. *South. Med. J.* **1997**, *90*, 826–827. [CrossRef] [PubMed]
20. Matthiesen, T.; Wöhrmann, T.; Coogan, T.P.; Uragg, H. The experimental toxicology of tramadol: An overview. *Toxicol. Lett.* **1998**, *16*, 63–71. [CrossRef]
21. Marquardt, K.A.; Alsop, J.A.; Albertson, T.E. Tramadol exposures reported to statewide poison control system. *Ann. Pharm.* **2005**, *39*, 1039–1044. [CrossRef]
22. Raffa, R.B.; Stone, D.J., Jr. Unexceptional seizure potential of tramadol or its enantiomers or metabolites in mice. *J. Pharmacol. Exp.* **2008**, *325*, 500–506. [CrossRef] [PubMed]
23. Fujimoto, Y.; Funao, T.; Suehiro, K.; Takahashi, R.; Mori, T.; Nishikawa, K. Brain serotonin content regulates the manifestation of tramadol-induced seizures in rats: Disparity between tramadol-induced seizure and serotonin syndrome. *Anesthesiology* **2015**, *122*, 178–189. [CrossRef]
24. Raffa, R.B.; Friderichs, E.; Reimann, W.; Shank, R.P.; Codd, E.E.; Vaught, J.L. Opioid and nonopioid components independently contribute to the mechanism of action of tramadol, an 'atypical' opioid analgesic. *J. Pharmacol. Exp. Ther.* **1992**, *260*, 275–285. [PubMed]
25. Gillen, C.; Haurand, M.; Kobelt, D.J.; Wnendt, S. Affinity, potency and efficacy of tramadol and its metabolites at the cloned human mu-opioid receptor. *Naunyn-Schmiedeberg's Arch. Pharm.* **2000**, *362*, 116–121. [CrossRef] [PubMed]
26. Hara, K.; Minami, K.; Sata, T. The effects of tramadol and its metabolite on glycine, gamma-aminobutyric acidA, and N-methyl-D-aspartate receptors expressed in Xenopus oocytes. *Anesth. Analg.* **2005**, *100*, 1400–1405. [CrossRef]
27. Tao, Q.; Stone, D.J.; Borenstein, M.R.; Codd, E.E.; Coogan, T.P.; Desai-Krieger, D.; Liao, S.; Raffa, R.B. Differential tramadol and O-desmethyl metabolite levels in brain vs. plasma of mice and rats administered tramadol hydrochloride orally. *J. Clin. Pharm. Ther.* **2002**, *27*, 99–106. [CrossRef]
28. Bilel, S.; Azevedo, N.J.; Arfè, R.; Tirri, M.; Gregori, A.; Serpelloni, G.; De-Giorgio, F.; Frisoni, P.; Neri, M.; Calò, G.; et al. In vitro and in vivo pharmacological characterization of the synthetic opioid MT-45. *Neuropharmacology* **2020**, *171*, 108110. [CrossRef]
29. Bilel, S.; Arfè, R.; Tirri, M.; Trapella, C.; Frisoni, P.; Neri, M.; Marti, M. The novel fentanyl-analog "Acrylofentanyl" impairs motor, sensorimotor and cardiovascular functions in mice. *Pharmadvances* **2020**, *2*. [CrossRef]
30. Canal, C.E.; Morgan, D. Head-twitch response in rodents induced by the hallucinogen 2,5-dimethoxy-4-iodoamphetamine: A comprehensive history, a re-evaluation of mechanisms, and its utility as a model. *Drug Test. Anal.* **2012**, *4*, 556–576. [CrossRef] [PubMed]
31. Halberstadt, A.L.; Geyer, M.A. Characterization of the head-twitch response induced by hallucinogens in mice: Detection of the behavior based on the dynamics of head movement. *Psychopharmacology* **2013**, *227*, 727–739. [CrossRef] [PubMed]
32. Bilel, S.; Tirri, M.; Arfè, R.; Stopponi, S.; Soverchia, L.; Ciccocioppo, R.; Frisoni, P.; Strano-Rossi, S.; Miliano, C.; De-Giorgio, F.; et al. Pharmacological and behavioral effects of the synthetic cannabinoid AKB48 in rats. *Front. Neurosci.* **2019**, *13*, 1163. [CrossRef]
33. Tirri, M.; Ponzoni, L.; Bilel, S.; Arfè, R.; Braida, D.; Sala, M.; Marti, M. Acute DOB and PMA administration impairs motor and sensorimotor responses in mice and causes hallucinogenic effects in adult zebrafish. *Brain Sci.* **2020**, *10*, 586. [CrossRef]
34. Miliano, C.; Marti, M.; Pintori, N.; Castelli, M.P.; Tirri, M.; Arfè, R.; de Luca, M.A. Neurochemical and behavioral profiling in male and female rats of the psychedelic agent 25I-NBOMe. *Front. Pharm.* **2019**, *12*, 1406. [CrossRef]
35. Morbiato, E.; Bilel, S.; Tirri, M.; Arfè, R.; Fantinati, A.; Savchuk, S.; Appolonova, S.; Frisoni, P.; Tagliaro, F.; Neri, M.; et al. Potential of the zebrafish model for the forensic toxicology screening of NPS: A comparative study of the effects of APINAC and methiopropamine on the behavior of zebrafish larvae and mice. *Neurotoxicology* **2020**, *78*, 36–46. [CrossRef] [PubMed]
36. Wakita, R.; Tanabe, S.; Tabei, K.; Funaki, A.; Inoshita, T.; Hirano, T. Differential regulations of vestibulo-ocular reflex and optokinetic response by β- and α2-adrenergic receptors in the cerebellar flocculus. *Sci. Rep.* **2017**, *7*, 3944. [CrossRef]
37. Papesh, M.A.; Hurley, L.M. Modulation of auditory brainstem responses by serotonin and specific serotonin receptors. *Hear. Res.* **2016**, *332*, 121–136. [CrossRef] [PubMed]
38. Felix, R.A., 2nd; Elde, C.J.; Nevue, A.A.; Portfors, C.V. Serotonin modulates response properties of neurons in the dorsal cochlear nucleus of the mouse. *Hear. Res.* **2017**, *344*, 13–23. [CrossRef]
39. Tang, Z.Q.; Trussell, L.O. Serotonergic modulation of sensory representation in a central multisensory circuit is pathway specific. *Cell Rep.* **2017**, *20*, 1844–1854. [CrossRef]
40. Baumann, M.H.; Ayestas, M.A., Jr.; Partilla, J.S.; Sink, J.R.; Shulgin, A.T.; Daley, P.F.; Brandt, S.D.; Rothman, R.B.; Ruoho, A.E.; Cozzi, N.V. The designer methcathinone analogs, mephedrone and methylone, are substrates for monoamine transporters in brain tissue. *Neuropsychopharmacology* **2012**, *37*, 1192–1203. [CrossRef]
41. Giannotti, G.; Canazza, I.; Caffino, L.; Bilel, S.; Ossato, A.; Fumagalli, F.; Marti, M. The cathinones MDPV and α-PVP elicit different behavioral and molecular effects following acute exposure. *Neurotox. Res.* **2017**, *32*, 594–602. [CrossRef]
42. De-Giorgio, F.; Bilel, S.; Tirri, M.; Arfè, R.; Trapella, C.; Camuto, C.; Foti, F.; Frisoni, P.; Neri, M.; Botrè, F.; et al. Methiopropamine and its acute behavioral effects in mice: Is there a gray zone in new psychoactive substances users? *Int. J. Leg. Med.* **2020**, *134*, 1695–1711. [CrossRef] [PubMed]
43. Luethi, D.; Liechti, M.E. Designer drugs: Mechanism of action and adverse effects. *Arch. Toxicol.* **2020**, *94*, 1085–1133. [CrossRef]
44. Castañé, A.; Santana, N.; Artigas, F. PCP-based mice models of schizophrenia: Differential behavioral, neurochemical and cellular effects of acute and subchronic treatments. *Psychopharmacology* **2015**, *232*, 4085–4097. [CrossRef] [PubMed]

45. Giannini, A.J.; Nageotte, C.; Loiselle, R.H.; Malone, D.A.; Price, W.A. Comparison of chlorpromazine, haloperidol and pimozide in the treatment of phencyclidine psychosis: DA-2 receptor specificity. *J. Toxicol. Clin. Toxicol.* **1984**, *22*, 573–579. [CrossRef] [PubMed]
46. Ogren, S.O.; Goldstein, M. Phencyclidine- and dizocilpine-induced hyperlocomotion are differentially mediated. *Neuropsychopharmacology* **1994**, *11*, 167–177. [CrossRef]
47. Seeman, P.; Lasaga, M. Dopamine agonist action of phencyclidine. *Synapse* **2005**, *58*, 275–277. [CrossRef] [PubMed]
48. Seeman, P.; Guan, H.C. Phencyclidine and glutamate agonist LY379268 stimulate dopamine D2High receptors: D2 basis for schizophrenia. *Synapse* **2008**, *62*, 819–828. [CrossRef] [PubMed]
49. Jodo, E. The role of the hippocampo-prefrontal cortex system in phencyclidine-induced psychosis: A model for schizophrenia. *J. Physiol.* **2013**, *107*, 434–440. [CrossRef] [PubMed]
50. Hiramatsu, M.; Nabeshima, T.; Kameyama, T. Involvement of opioid receptors in hypo- and hyperthermic effects induced by phencyclidine in mice. *J. Pharm.* **1986**, *9*, 466–472. [CrossRef] [PubMed]
51. Baker, A.K.; Meert, T.F. Functional effects of systemically administered agonists and antagonists of mu, delta, and kappa opioid receptor subtypes on body temperature in mice. *J. Pharmacol. Exp.* **2002**, *302*, 1253–1264. [CrossRef]
52. Wolfe, A.M.; Kennedy, L.H.; Na, J.J.; Nemzek-Hamlin, J.A. Efficacy of tramadol as a sole analgesic for postoperative pain in male and female mice. *J. Am. Assoc. Lab. Anim. Sci.* **2015**, *54*, 411–419.
53. Kiyatkin, E.A. Brain temperature and its role in physiology and pathophysiology: Lessons from 20 years of thermorecording. *Temperature* **2019**, *6*, 271–333. [CrossRef]
54. Itoh, Y.; Oishi, R.; Nishibori, M.; Saeki, K. Comparison of effects of phencyclidine and methamphetamine on body temperature in mice: A possible role for histamine neurons in thermoregulation. *Naunyn-Schmiedeberg's Arch. Pharm.* **1986**, *332*, 293–296. [CrossRef]
55. Evangelista Vaz, R.; Draganov, D.I.; Rapp, C.; Avenel, F.; Steiner, G.; Arras, M.; Bergadano, A. Preliminary pharmacokinetics of tramadol hydrochloride after administration via different routes in male and female B6 mice. *Vet. Anaesth. Analg.* **2018**, *45*, 111–122. [CrossRef]
56. Sevcik, J.; Nieber, K.; Driessen, B.; Illes, P. Effects of the central analgesic tramadol and its main metabolite, O-desmethyltramadol, on rat locus coeruleus neurones. *Br. J. Pharmacol.* **1993**, *110*, 169–176. [CrossRef]
57. Shen, Q.; Qian, Y.Y.; Xu, X.J.; Li, W.; Liu, J.G.; Fu, W. Design, synthesis and biological evaluation of N-phenylalkyl-substituted tramadol derivatives as novel μ opioid receptor ligands. *Acta Pharmacol. Sin.* **2015**, *36*, 887–894. [CrossRef] [PubMed]
58. Ide, S.; Minami, M.; Ishihara, K.; Uhl, G.R.; Sora, I.; Ikeda, K. Mu opioid receptor-dependent and independent components in effects of tramadol. *Neuropharmacology* **2006**, *51*, 651–658. [CrossRef]
59. Aydin, O.N.; Ek, R.O.; Temoçin, S.; Uğur, B.; Alaçam, B.; Şen, S. The antinociceptive effects of systemic administration of tramadol, gabapentin and their combination on mice model of acute pain. *Agri* **2012**, *24*, 49–55. [CrossRef]
60. Yanarates, O.; Dogrul, A.; Yildirim, V.; Sahin, A.; Sizlan, A.; Seyrek, M.; Akgül, O.; Kozak, O.; Kurt, E.; Aypar, U. Spinal 5-HT7 receptors play an important role in the antinociceptive and antihyperalgesic effects of tramadol and its metabolite, O-Desmethyltramadol, via activation of descending serotonergic pathways. *Anesthesiology* **2010**, *112*, 696–710. [CrossRef]
61. Müller, B.; Wilsmann, K. Cardiac and hemodynamic effects of the centrally acting analgesics tramadol and pentazocine in anaesthetized rabbits and isolated guinea-pig atria and papillary muscles. *Arzneimittel-forschung* **1984**, *34*, 430–433.
62. Itami, T.; Tamaru, N.; Kawase, K.; Ishizuka, T.; Tamura, J.; Miyoshi, K.; Umar, M.A.; Inoue, H.; Yamashita, K. Cardiovascular effects of tramadol in dogs anesthetized with sevoflurane. *J. Vet. Med. Sci.* **2011**, *73*, 1603–1609. [CrossRef] [PubMed]
63. Nagaoka, E.; Minami, K.; Shiga, Y.; Uezono, Y.; Shiraishi, M.; Aoyama, K.; Shigematsu, A. Tramadol has no effect on cortical renal blood flow—despite increased serum catecholamine levels—in anesthetized rats: Implications for analgesia in renal insufficiency. *Anesth. Analg.* **2002**, *94*, 619–625. [CrossRef]
64. Egger, C.M.; Souza, M.J.; Greenacre, C.B.; Cox, S.K.; Rohrbach, B.W. Effect of intravenous administration of tramadol hydrochloride on the minimum alveolar concentration of isoflurane in rabbits. *Am. J. Vet. Res.* **2009**, *70*, 945–949. [CrossRef] [PubMed]
65. Nishioka, K. The effect of non-narcotic analgesic, tramadol, on cardiac contractility in dog. *Tohoku J. Exp. Med.* **1979**, *128*, 401–402. [PubMed]
66. Raimundo, J.M.; Sudo, R.T.; Pontes, L.B.; Antunes, F.; Trachez, M.M.; Zapata-Sudo, G. In vitro and in vivo vasodilator activity of racemic tramadol and its enantiomers in Wistar rats. *Eur. J. Pharm.* **2006**, *530*, 117–123. [CrossRef]
67. Kaya, T.; Gursoy, S.; Karadas, B.; Sarac, B.; Fafali, H.; Soydan, A.S. High-concentration tramadol-induced vasodilation in rabbit aorta is mediated by both endothelium-dependent and -independent mechanisms. *Acta Pharmacol. Sin.* **2003**, *24*, 385–389. [PubMed]
68. Close, B.R. Tramadol: Does it have a role in emergency medicine? *Emerg. Med. Australas.* **2005**, *17*, 73–83. [CrossRef] [PubMed]
69. Müller, H.; Stoyanov, M.; Brähler, A.; Hempelmann, G. Hämodynamische und respiratorische effekte von tramadol bei lachgassauerstoff-beatmung und in der postoperativen phase [Hemodynamic and respiratory effects of tramadol during nitrous oxide-oxygen-artificial respiration and in the postoperative period]. *Anaesthesist* **1982**, *31*, 604–610.
70. Elkalioubie, A.; Allorge, D.; Robriquet, L.; Wiart, J.F.; Garat, A.; Broly, F.; Fourrier, F. Near-fatal tramadol cardiotoxicity in a CYP2D6 ultrarapid metabolizer. *Eur. J. Clin. Pharm.* **2011**, *67*, 855–858. [CrossRef] [PubMed]

71. De Decker, K.; Cordonnier, J.; Jacobs, W.; Coucke, V.; Schepens, P.; Jorens, P.G. Fatal intoxication due to tramadol alone: Case report and review of the literature. *Forensic Sci. Int.* **2008**, *175*, 79–82. [CrossRef]
72. Daubin, C.; Quentin, C.; Goullé, J.P.; Guillotin, D.; Lehoux, P.; Lepage, O.; Charbonneau, P. Refractory shock and asystole related to tramadol overdose. *Clin. Toxicol.* **2007**, *45*, 961–964. [CrossRef]
73. Lagard, C.; Malissin, I.; Indja, W.; Risède, P.; Chevillard, L.; Mégarbane, B. Is naloxone the best antidote to reverse tramadol-induced neuro-respiratory toxicity in overdose? An experimental investigation in the rat. *Clin. Toxicol.* **2018**, *56*, 737–743. [CrossRef]
74. Hassanian-Moghaddam, H.; Farajidana, H.; Sarjami, S.; Owliaey, H. Tramadol-induced apnea. *Am. J. Emerg. Med.* **2013**, *31*, 26–31. [CrossRef]
75. Hondebrink, L.; Zwartsen, A.; Westerink, R.H.S. Effect fingerprinting of new psychoactive substances (NPS): What can we learn from in vitro data? *Pharmacology* **2018**, *182*, 193–224. [CrossRef]
76. Zhang, H.; Cuevas, J. Sigma receptor activation blocks potassium channels and depresses neuroexcitability in rat intracardiac neurons. *J. Pharmacol. Exp.* **2005**, *313*, 1387–1396. [CrossRef]
77. Polakowski, J.S.; Segreti, J.A.; Cox, B.F.; Hsieh, G.C.; Kolasa, T.; Moreland, R.B.; Brioni, J.D. Effects of selective dopamine receptor subtype agonists on cardiac contractility and regional haemodynamics in rats. *Clin. Exp. Pharmacol. Physiol.* **2004**, *31*, 837–841. [CrossRef]
78. D'Amico, G.A.; Kline, R.P.; Maayani, S.; Weinstein, H.; Kupersmith, J. Effects of phencyclidine on cardiac action potential: pH dependence and structure-activity relationships. *Eur. J. Pharm.* **1983**, *88*, 283–290. [CrossRef]
79. Vigolo, A.; Ossato, A.; Trapella, C.; Vincenzi, F.; Rimondo, C.; Seri, C.; Varani, K.; Serpelloni, G.; Marti, M. Novel halogenated derivates of JWH-018: Behavioral and binding studies in mice. *Neuropharmacology* **2015**, *95*, 68–82. [CrossRef] [PubMed]
80. Ossato, A.; Vigolo, A.; Trapella, C.; Seri, C.; Rimondo, C.; Serpelloni, G.; Marti, M. JWH-018 impairs sensorimotor functions in mice. *Neuroscience* **2015**, *300*, 174–188. [CrossRef] [PubMed]
81. Canazza, I.; Ossato, A.; Trapella, C.; Fantinati, A.; De Luca, M.A.; Margiani, G.; Vincenzi, F.; Rimondo, C.; di Rosa, F.; Gregori, A.; et al. Effect of the novel synthetic cannabinoids AKB48 and 5F-AKB48 on "tetrad", sensorimotor, neurological and neurochemical responses in mice. In vitro and in vivo pharmacological studies. *Psychopharmacology* **2016**, *233*, 3685–3709. [CrossRef] [PubMed]
82. Ossato, A.; Canazza, I.; Trapella, C.; Vincenzi, F.; de Luca, M.A.; Rimondo, C.; Varani, K.; Borea, P.A.; Serpelloni, G.; Marti, M. Effect of JWH-250, JWH-073 and their interaction on "tetrad", sensorimotor, neurological and neurochemical responses in mice. *Prog. Neuropsychopharmacol. Biol. Psychiatry* **2016**, *67*, 31–50. [CrossRef]
83. Foti, F.; Marti, M.; Ossato, A.; Bilel, S.; Sangiorgi, E.; Botrè, F.; Cerbelli, B.; Baldi, A.; De-Giorgio, F. Phenotypic effects of chronic and acute use of methiopropamine in a mouse model. *Int. J. Leg. Med.* **2019**, *133*, 811–820. [CrossRef] [PubMed]

54

Article

Untargeted Metabolic Profiling of 4-Fluoro-Furanylfentanyl and Isobutyrylfentanyl in Mouse Hepatocytes and Urine by Means of LC-HRMS

Camilla Montesano [1,*], Flaminia Vincenti [1,2], Federico Fanti [3], Matteo Marti [4,5,*], Sabrine Bilel [4], Anna Rita Togna [6], Adolfo Gregori [7], Fabiana Di Rosa [7] and Manuel Sergi [3]

[1] Department of Chemistry, Sapienza University of Rome, 00185 Rome, Italy; flaminia.vincenti@uniroma1.it
[2] Department of Public Health and Infectious Disease, Sapienza University of Rome, 00185 Rome, Italy
[3] Faculty of Bioscience and Technology for Food, Agriculture and Environment, University of Teramo, 64100 Teramo, Italy; ffanti@unite.it (F.F.); msergi@unite.it (M.S.)
[4] Department of Translational Medicine, Section of Legal Medicine and LTTA Centre, University of Ferrara, 44121 Ferrara, Italy; sabrine.bilel@unife.it
[5] Department of Anti-Drug Policies, Collaborative Center for the Italian National Early Warning System, Presidency of the Council of Ministers, University of Ferrara, 44121 Ferrara, Italy
[6] Department of Physiology and Pharmacology Vittorio Erspamer, Sapienza University of Rome, 00185 Rome, Italy; annarita.togna@uniroma1.it
[7] Carabinieri, Department of Scientific Investigation (RIS), 00191 Rome, Italy; adolfo.gregori@carabinieri.it (A.G.); Fabiana.dirosa@carabinieri.it (F.D.R.)
* Correspondence: camilla.montesano@uniroma1.it (C.M.); mto@unife.it (M.M.); Tel.: +39-0649-913-559 (C.M.); +39-0532-455-781 (M.M.)

Abstract: The diffusion of new psychoactive substances (NPS) is highly dynamic and the available substances change over time, resulting in forensic laboratories becoming highly engaged in NPS control. In order to manage NPS diffusion, efficient and innovative legal responses have been provided by several nations. Metabolic profiling is also part of the analytical fight against NPS, since it allows to identify the biomarkers of drug intake which are needed for the development of suitable analytical methods in biological samples. We have recently reported the characterization of two new analogs of fentanyl, i.e., 4-fluoro-furanylfentanyl (4F-FUF) and isobutyrylfentanyl (iBF), which were found for the first time in Italy in 2019; 4F-FUF was identified for the first time in Europe and was notified to the European Early Warning System. The goal of this study was the characterization of the main metabolites of both drugs by in vitro and in vivo experiments. To this end, incubation with mouse hepatocytes and intraperitoneal administration to mice were carried out. Samples were analyzed by means of liquid chromatography-high resolution mass spectrometry (LC–HRMS), followed by untargeted data evaluation using Compound Discoverer software with a specific workflow, designed for the identification of the whole metabolic pattern, including unexpected metabolites. Twenty metabolites were putatively annotated for 4F-FUF, with the dihydrodiol derivative appearing as the most abundant, whereas 22 metabolites were found for iBF, which was mainly excreted as nor-isobutyrylfentanyl. *N*-dealkylation of 4F-FUF dihydrodiol and oxidation to carbonyl metabolites for iBF were also major biotransformations. Despite some differences, in general there was a good agreement between in vitro and in vivo samples.

Keywords: fentanyl analogs; metabolic profile; liquid chromatography-high resolution mass spectrometry; in vitro and in vivo metabolism; new psychoactive substances

1. Introduction

The use of new psychoactive substances (NPSs), introduced as legal alternatives for controlled drugs [1], has become a worldwide phenomenon since the early 90s and it has been exacerbated by the increase in online selling points and sales [2]. To manage NPS

55

issues, efficient and innovative legal responses against the diffusion of new drugs have been provided by several nations. However, the NPS market is highly dynamic and the available substances change over time, resulting in forensic laboratories becoming highly engaged in the fight against NPSs. From an analytical point of view, NPS detection in both seizures and biological samples is a challenge due to the lack of analytical standards, library spectra and pharmacokinetic information. High resolution mass spectrometry (HRMS) is becoming the technique of choice to deal with NPSs and to overcome the limitations of low resolution MS coupled with liquid or gas chromatography (LC or GC), which are usually used in targeted acquisition modes [3,4]. In fact, accurate mass, contrary to nominal masses, may be used to ascertain the molecular formula and putatively annotate a new molecule, when fragmentation spectra are available [5]. Metabolic profiling is also part of the analytical fight against NPSs, since it allows to identify the biomarkers of drug intake, which are needed for the development of suitable analytical methods in biological samples [6]. Characterization of drug metabolites is usually performed using in vitro and/or in vivo studies, which can be assisted by in-silico prediction tools to make LC-HRMS data analysis easier [7]. In vitro studies involve incubation of the drugs with human or animal hepatocyte cultures [8,9], human liver preparations [10] or the fungus *Caenorhabditis elegans* [11], whereas biological samples collected in authentic cases or samples obtained by controlled drug administration to rats, mice and other rodents may be used for in vivo studies. Novel in vivo models such as zebrafish (*Danio rerio*) larvae have been recently reported as a good alternative for NPS metabolism studies [12]. Conversely, controlled human studies would be best suited but are not practicable for ethical reasons and the lack of preclinical safety data.

Metabolic studies have been carried out for a wide range of NPSs from different classes, including synthetic opioids [9,13]. Among this group, fentanyl, also called "synthetic heroin" [14], and its analogues deserve special attention. In the last years these drugs, originally introduced to treat severe pain, and later produced in illegal laboratories, started to appear in the illicit market to replace scheduled related compounds [15–17]. In 2017, about 1300 seizures of new opioids were reported to the EU Early Warning System (EWS) by national law enforcement agencies; 70% of these included fentanyl derivatives, which were often sold as or mixed with heroin [18]. Given the danger of these compounds, a broader knowledge of the metabolic behavior of fentanyl derivatives is mandatory. In recent years, the metabolisms of many of these, including furanylfentanyl [19–21]; butyrylfentanyl [22,23]; 4-fluoro-isobutyrylfentanyl [19] and ortho-, meta- and para-fluorofentanyl [24], have been studied. Similarly, to fentanyl, for most of these drugs the *N*-dealkylated metabolites were shown to be the primary biomarkers; however, it was reported that other biotransformations, including phase I mono- and di-hydroxylation, oxidation to carboxylic acid and phase II glucuronidation and sulfation, dominated metabolite formation [25]. Furanyl fentanyl exhibited a rather different behavior, arising from the heterocyclic furane moiety, with amide hydrolysis and dihydrodiol formation being the principal biotransformations.

We have recently reported the characterization of two new analogs of fentanyl, i.e., 4-fluoro-furanylfentanyl (4F-FUF) and isobutyrylfentanyl (iBF), which were reported for the first time in Italy in 2019 [26]; 4F-FUF was identified for the first time in Europe and a notification to the European Early Warning System (EWS) resulted from the previously cited study. iBF is closely related to fentanyl, with a methyl group linked to the α-carbon in the propionyl group, whereas 4F-FUF differs from fentanyl by a furan-2-carboxamide instead of the propionamide group and a fluorine atom in the para position on the aromatic group. Being two new derivatives, to the best of our knowledge their metabolic profile has not been characterized to date, and the pharmacological effects are also unknown; however, dose-dependent increases in locomotion and antinociception were reported for iBF [27]. For iBF, different isomers of the hydroxylated metabolites were characterized in hepatocyte samples; however, the complete metabolic profile was not investigated [28].

The goal of the present study was the characterization of the main metabolites of both drugs by both in vitro and in vivo experiments. To this end, incubation with mouse hepa-

tocytes and intraperitoneal administration in mice were carried out. In vivo experiments were carried out to confirm the in vitro results, as well as to study pharmacotoxicological effects, which will be presented in a future study. Untargeted analysis of the obtained samples was performed using LC-HRMS, whereas Compound Discoverer software was used for data analysis with an untargeted workflow to putatively identify even unexpected metabolites.

2. Results and Discussion

In this study the main metabolites of iBF and 4F-FUF were studied through in vitro and in vivo studies. All the samples were analyzed using LC-HRMS in data-dependent acquisition mode, which led to the triggering of MS^2 events for the most intense precursor ions. With this setting, semi-quantitative information may be obtained from the MS full scan, while the analysis of the MS^2 spectra may allow one to putatively annotate the detected metabolites. The software Compound Discoverer was selected to automatically extract the metabolic features, using an untargeted approach in order to detect the expected metabolites on the basis of the biotransformations that may occur, as well as the unexpected ones.

Concerning the in vitro study, positive and negative controls served to monitor the incubation. As reported in Section 3. Materials and Methods, diclofenac and testosterone were used as positive controls respectively for phase I and phase II metabolism to ensure that proper incubation conditions were maintained: hydroxydiclofenac was observed in the diclofenac positive control, confirming phase I hepatocyte metabolic activity, whereas testosterone glucuronide and sulphate were detected in the testosterone control, showing that phase II metabolic activity also occurred. On the other hand, all the peaks corresponding to metabolites of iBF and 4F-FUF discussed in the next paragraphs were not detected in the negative controls.

2.1. 4F-FUF Metabolic Profile In Vitro and In Vivo

Overall, 20 metabolites were putatively identified for 4F-FUF, 16 were found in both urine and hepatocytes samples, and four of them were only found in urine. In order to highlight the similarities and differences obtained in vitro and in vivo, the results of the two studies will be presented together. A list of all the metabolites with the proposed metabolic transformation and elemental composition, as well as the retention time, accurate mass of the protonated molecule and mass error, are provided in Table 1. The quantitative results of the in vitro and in vivo studies in terms of peak areas in hepatocyte and urine samples (average) are shown in Table 2. The extracted ion currents of the 20 metabolites are shown in Figure S1.

It is worth noting that 4F-FUF showed a pronounced antidiuretic effect in vivo and no samples could be obtained in the first six hours after administration. Syndrome of inappropriate antidiuretic hormone secretion was previously associated with fentanyl consumption [29]; however, the reduction in urine production was not significant following iBF administration, indicating that the distinct chemical structure of 4F-FUF is responsible for this effect.

The parent drug was found in all the samples; after two hours of drug incubation with hepatocytes, the peak area was reduced by nearly 90%, showing an intense metabolic activity. P_FFUF was also found in urine. In the first samples obtained (6–12 h) the peak area represented ≈7% of the sum of the area of all the metabolites found; this relative amount was reduced to ≈2% at the last time point (24–31 h). Relative quantification is limited by probable differences in ionization efficiency for the different metabolites and the parent compound. Another issue is the matrix effect, which can negatively or, less commonly, positively affect the absolute peak areas, but with the matrices being relatively simple, we did not expect an excessive enhancement or suppression of the signals [30].

Table 1. List of proposed metabolites of 4-fluoro-furanylfentanyl with the main identification parameters and postulated biotransformation. The relatively most intense metabolites are in bold. Rt—retention time.

ID	Biotransformation	Rt (min)	Formula	Measured m/z	Mass Error (PPM)	Diagnostic Ions
M1_FFUF	Oxidative N-dealkylation	4.05	$C_{13}H_{20}NO$	206.1547	1.02	188.1433, 105.0702, 56.0603
M2_FFUF	Amide hydrolysis + oxidative defluorination + glucuronidation	4.08	$C_{25}H_{33}N_2O_7$	473.2289	0.26	188.1433, 297.1960, 105.0702
M3_FFUF	**Dihydrodiol formation + N-dealkylation**	**4.10**	$C_{16}H_{20}FN_2O_4$	**323.1404**	**−0.96**	**84.0814, 194.0810, 166.0863**
M4_FFUF	Oxidative N-dealkylation	5.29	$C_{16}H_{18}FN_2O_2$	299.1346	−2.18	84.0814, 206.0611, 56.0503
M5_FFUF	Oxidation (furanyl ring opened) + oxidation to carboxyl metabolite + taurine conjugation	5.35	$C_{26}H_{33}FN_3O_6S$	534.2060	−0.95	188.1433, 105.0703, 299.1917, 409.1917
M6_FFUF	Dihydrodiol formation + hydroxylation	5.37	$C_{24}H_{28}FN_2O_5$	443.1973	−2.09	121.0650, 204.1382, 323.1401
M7_FFUF	Dihydrodiol formation + hydroxylation	5.64	$C_{24}H_{28}FN_2O_5$	443.1969	−2.99	204.1382, 121.0650, 335.1400
M8_FFUF	Oxidation (furanyl ring opened) + reduction	5.65	$C_{24}H_{32}FN_2O_3$	415.2384	−3.12	188.0702, 105.0702, 299.1918
M9_FFUF	Oxidation (furanyl ring opened + glucuronidation)	5.67	$C_{30}H_{39}FN_2O_9$	589.2552	−1.59	188.1433, 105.0702, 413.2233, 299.1917
M10_FFUF	Oxidation (furanyl ring opened + hydroxylation)	5.80	$C_{24}H_{30}FN_2O_4$	429.2146	−0.84	186.1277, 204.1386, 299.1918
M11_FFUF	Dihydrodiol formation + hydroxylation	5.90	$C_{24}H_{28}FN_2O_5$	443.1976	−1.43	423.1868, 186.1277, 134.0965
M12_FFUF	Oxidation (furanyl ring opened)	6.50	$C_{24}H_{28}FN_2O_3$	411.2078	−1.45	188.1434, 105.0703, 299.1921
M13_FFUF	Oxidation (furanyl ring opened)	6.60	$C_{24}H_{30}FN_2O_3$	413.2237	−0.84	188.1434, 105.0703, 299.1916
M14_FFUF	**Dihydrodiol formation**	**6.77**	$C_{24}H_{28}FN_2O_4$	**427.2027**	**−1.43**	**188.1434, 105.0703, 335.1401**
M15_FFUF	Hydration	6.92	$C_{24}H_{28}FN_2O_3$	411.2085	0.25	188.1434, 105.0703
M16_FFUF	Hydroxylation	7.02	$C_{24}H_{26}FN_2O_3$	409.1915	−3.04	204.1382, 121.0650
M17_FFUF	Hydroxylation	7.35	$C_{24}H_{26}FN_2O_3$	409.1915	−3.04	204.1382, 121.0650
M18_FFUF	Hydroxylation	7.87	$C_{24}H_{26}FN_2O_3$	409.1912	−3.78	204.1385, 186.1278, 391.1817
M19_FFUF	Amide hydrolysis	9.43	$C_{18}H_{24}FN_2$	299.1918	−1.84	105.0703, 204.1385, 186.1277

Table 1. Cont.

ID	Biotransformation	Rt (min)	Formula	Measured m/z	Mass Error (PPM)	Diagnostic Ions
P_FFUF	-	9.62	$C_{24}H_{26}FN_2O_2$	393.1974	−1.10	-
M20_FFUF	N-oxygenation	10.58	$C_{24}H_{26}FN_2O_3$	409.1912	−3.78	186.1277, 204.1386, 349.2273

Table 2. Results of the in vitro and in vivo studies for 4-FUF

ID	Average (n = 3) Peak Area in Hepatocyte Samples				Average Area in Urine Samples (CV%)								
	0.5 h	1 h	2 h	3 h	1 h	2 h	3 h	4 h	5 h	6 h	0–12 h (n = 9)	12–24 h (n = 9)	24–31 h (n = 9)
M1_FFUF	4.35×10^6 (12)	3.86×10^6 (9)	5.52×10^6 (9)	2.30×10^6 (11)	NS	NS	NS	NS	NS	NS	1.18×10^7 (31)	1.35×10^7 (67)	2.28×10^7 (63)
M2_FFUF	2.77×10^6 (11)	1.98×10^6 (8)	2.23×10^6 (36)	3.39×10^6 (16)	NS	NS	NS	NS	NS	NS	4.96×10^6 (51)	4.71×10^6 (41)	5.54×10^7 (48)
M3_FFUF	1.58×10^7 (5)	3.42×10^6 (9)	7.49×10^6 (12)	2.62×10^6 (10)	NS	NS	NS	NS	NS	NS	5.59×10^7 (42)	2.29×10^6 (40)	2.93×10^6 (77)
M4_FFUF	9.34×10^6 (11)	1.66×10^6 (16)	1.66×10^6 (13)	7.12×10^6 (8)	NS	NS	NS	NS	NS	NS	3.06×10^6 (47)	1.35×10^6 (39)	1.02×10^6 (54)
M5_FFUF	NF	7.91×10^6 (16)	5.1×10^6 (11)	NF	NF	NF	NF	NF	NF	NF	7.99×10^6 (51)	6.6×10^6 (44)	4.32×10^6 (64)
M6_FFUF	NF	NF	NF	NF	NS	NS	NS	NS	NS	NS	1.96×10^6 (32)	2.27×10^6 (39)	3.21×10^6 (56)
M7_FFUF	NF	NF	NF	NF	NS	NS	NS	NS	NS	NS	1.15×10^6 (39)	1.45×10^6 (44)	1.54×10^6 (32)
M8_FFUF	5.63×10^6 (9)	1.07×10^6 (11)	9.98×10^6 (11)	9.62×10^6 (12)	NS	NS	NS	NS	NS	NS	3.09×10^6 (93)	1.26×10^6 (14)	1.37×10^6 (96)
M9_FFUF	2.94×10^6 (8)	7.74×10^6 (13)	1.16×10^6 (14)	2.0953 (17)	NS	NS	NS	NS	NS	NS	3.06×10^6 (60)	4.09×10^6 (77)	3.11×10^6 (49)
M10_FFUF	3.06×10^6 (13)	6.57×10^6 (12)	5.55×10^6 (7)	4.02×10^6 (16)	NS	NS	NS	NS	NS	NS	9.69×10^6 (63)	3.94×10^6 (43)	3.70×10^6 (59)
M11_FFUF	3.47×10^6 (6)	8.58×10^6 (15)	1.06×10^6 (38)	3.27×10^6 (18)	NS	NS	NS	NS	NS	NS	7.06×10^6 (44)	9.71×10^6 (21)	2.23×10^6 (41)
M12_FFUF	4.09×10^6 (9)	1.28×10^6 (17)	3.35×10^6 (11)	2.56×10^6 (13)	NS	NS	NS	NS	NS	NS	9.22×10^6 (75)	1.36×10^6 (51)	5.66×10^6 (62)
M13_FFUF	8.02×10^6 (10)	1.4×10^6 (9)	6.68×10^6 (11)	7.87×10^6 (39)	NS	NS	NS	NS	NS	NS	1.35×10^6 (109)	2.54×10^6 (31)	2.44×10^6 (59)
M14_FFUF	3.59×10^6 (4)	6.33×10^6 (16)	7.13×10^6 (12)	1.37×10^6 (12)	NS	NS	NS	NS	NS	NS	1.77×10^{-5} (93)	2.65×10^6 (19)	3.33×10^6 (93)
M15_FFUF	NF	NF	NF	NF	NS	NS	NS	NS	NS	NS	9.11×10^6 (47)	9.89×10^6 (33)	9.44×10^6 (49)
M16_FFUF	5.31×10^6 (16)	1.11×10^6 (5)	4.71×10^6 (7)	8.31×10^6 (17)	NS	NS	NS	NS	NS	NS	8.26×10^6 (75)	5.25×10^6 (59)	1.75×10^6 (72)
M17_FFUF	NF	NF	NF	NF	NS	NS	NS	NS	NS	NS	2.96×10^6 (96)	NF	NF
M18_FFUF	6.80×10^6 (18)	1.20×10^6 (9)	3.75×10^6 (34)	7.37×10^6 (14)	NS	NS	NS	NS	NS	NS	3.27×10^6 (61)	NF	NF
M19_FFUF	7.87×10^6 (11)	4.19×10^6 (16)	1.78×10^6 (7)	5.00×10^6 (9)	NS	NS	NS	NS	NS	NS	1.44×10^6 (31)	1.49×10^6 (41)	2.09×10^6 (79)
P_FFUF	4.09×10^6 (12)	7.47×10^6 (6)	2.55×10^6 (9)	3.91×10^6 (12)	NS	NS	NS	NS	NS	NS	2.04×10^6 (69)	5.95×10^6 (71)	4.62×10^6 (61)
M20_FFUF	1.2×10^6 (9)	8.04×10^6 (19)	3.63×10^6 (21)	1.02×10^6 (12)	NS	NS	NS	NS	NS	NS	5.68×10^6 (81)	4.53×10^6 (79)	1.78×10^6 (95)

NS no sample available, NF not found.

A scheme of the metabolic profile of 4F-FUF is shown in Figure 1. Both in vitro and in vivo, the most intense metabolite, relatively, was M14_FFUF, which corresponded to the dihydrodiol metabolite, resulting from epoxidation of furan, followed by hydration [19]. N-dealkylation of M14_FFUF was shown to be another major biotransformation, producing M3_FFUF, which was the second most relatively intense metabolite in vivo; on the contrary, it was only a minor bio-product in the hepatocyte samples. In vitro, N-dealkylation of the parent compound was predominant, leading to the nor-4F-FUF metabolite (M4_FFUF), which instead showed a low intensity in urine samples. The dihydrodiol metabolite was also further hydroxylated at the piperidine ring to form M11_FFUF and at the phenylethyl moiety to form M6_FFUF and M7_FFUF, which were quite intense in urine but were not detected in hepatocytes.

Amide hydrolysis leading to despropionyl fentanyl, previously identified as the major metabolite of furanyl fentanyl [19–21] which only differs from 4F-FUF for the fluorine atom, appeared to be a minor biotransformation both in vitro and in vivo. This route led to M19_FFUF which was mainly detected in hepatocytes and M2_FFUF which resulted from oxidative defluoruration and glucuronidation of M19_FFUF. The lower prevalence of metabolites deriving from amide hydrolysis in the metabolic profile of 4F-FUF when compared to its defluorinated analogue is not surprising since fluorine substitution can have complex effects on drug metabolism, in terms of route(s) and ex tent; in fact, fluorine substitution even at sites distal to the site of metabolic attack can affect metabolism by either inductive/resonance effects or conformational and electrostatic effects [31]. Hydration of 4F-FUF at the furanyl ring, leading to M15_FFUF, and furanyl ring opening were also observed. Different low-intensity metabolites were formed through this reaction, including M8_FFUF and M13_FFUF, whereas a further hydroxylation or carbonylation led to M10_FFUF and M12_FFUF, respectively. These reactions are typical of furane-containing molecules [32]. Phase II biotransformations were observed for these metabolites: glucuronidation of M13 produced M9_FFUF, whereas an unexpected taurine conjugate of M12_FFUF (M5_FFUF) was found, in a higher amount in urine samples. Hydroxylation at the phenylethyl moiety was a further minor biotransformation. Different isomers (M16_FFUF, M17_FFUF, M18_FFUF), including the N-oxide (M20_FFUF), were observed. These metabolites had a relatively low intensity in both hepatocytes and urine. Finally, oxidative N-dealkylation led to M1_FFUF, which was a minor metabolite.

2.2. Isobutyrylfentanyl Metabolic Profile In Vitro and In Vivo

In total, 22 metabolites of iBF were putatively identified in this study; eight of them were only detected in vivo. iBF exhibited a lower antidiuretic effect compared to 4F-FUF; however, only one sample could be collected one hour after drug administration and two samples were available after two hours. No sample was available after four hours. All the putatively annotated metabolites are listed in Table 3, which also reports the proposed metabolic transformation, the retention time, the accurate mass and elemental composition of the protonated molecule and the mass error. The peak areas in hepatocyte and urine samples (average) are shown in Table 4. Extracted ion currents of the 22 metabolites are shown in Figure S2, whereas a scheme of the metabolic profile of iBF is shown in Figure 2. Similarly, to 4F-FUF, P_iBF was found in all the samples but a pronounced metabolic activity was observed with only 5% of the initial amount found in hepatocytes after 3 h. Nor-iBF (M10_iBF), which was formed by N-dealkylation of iBF, was the most intense metabolite both in hepatocytes and in urine. Another major biotransformation was hydroxylation, which led to four isomers, with the -OH group placed at the isobutyryl moiety (M15_iBF, M16_iBF and M18_iBF), or on the phenylethyl aromatic ring (M20_iBF). The N-oxide was also detected (M22_iBF); this metabolite is characterized by a higher retention time (Rt) than the parent drug, and these data were in accordance with the literature [19,23]. Hydroxylated metabolites, and especially ω-hydroxy-iBF (M16_iBF), were quite intense in hepatocytes, whereas in urine this was an intermediate metabolite which underwent subsequent biotransformations, producing major metabolites. Oxidation

of M16_iBF prevailed in vivo and gave rise to the second and third main metabolites, M17_iBF and M14_iBF respectively. In vitro these metabolites were found in a very low amount, in accordance with the results of Kanamori et al. for butyrylfentanyl [22]; a likely explanation was a low activity of alcohol and aldehyde dehydrogenase in hepatocytes. M17_iBF was ω-carboxy-iBF; further metabolic steps were observed for this metabolite. Hydroxylation produced M6_iBF and M11_iBF, N-dealkylation gave rise to M3_iBF, and M7_iBF and M1_iBF were obtained by glucuronide conjugation of M17_iBF and M2_iBF, respectively. N-dealkylation of M16_iBF was also observed, leading to M2_iBF, which was intense in urine. Finally, phase II glucuronide conjugation was also possible, with the formation of M8_iBF and M12_iBF.

Other minor metabolites were formed by carbonylation (M21_iBF), oxidative N-dealkylation (M4_iBF), dihydroxylation of iBF (M9_iBF and M19_iBF) and subsequent methylation; phase II glucuronidation was observed for these metabolites, producing M5_iBF and M13_iBF respectively.

This is the first report of iBF's complete metabolic profile; however, it should be pointed out that in a study conducted by Wallgren et al. [28] iBF was included among the investigated drugs, and some hydroxylated metabolites isomers were characterized and quantified in hepatocyte samples. In addition, iBF-related fentanyl analogues, i.e., butyrylfentanyl [17,22,23] and 4F-iBF [19], were previously studied by other authors, both in vitro and in vivo. The detected metabolites were similar; in the cited studies for butyrylfentanyl, it was observed that nor-butyrylfentanyl was only intense in vitro, whereas it was a minor metabolite in vivo, with ω-OH-butyrylfentanyl and ω-carboxy-butyrylfentanyl being the relatively most intense. In these studies the available samples were obtained post-mortem and redistribution was deemed responsible for the reduction of the nor-metabolite. For 4F-iBF, the nor-metabolite was the main metabolite both in vivo and in vitro, similarly to what we found; on the other hand, aliphatic hydroxylation was a minor pathway, whereas the piperidine ring and the phenylethyl moiety were the main biotransformation sites. These divergences show that the fluorine atom may have a significant impact on the biotransformation routes, similarly to what was observed for 4F-FUF and FUF.

2.3. Elucidation of Metabolites Structure

For the elucidation of metabolite structures, an in-depth analysis of the corresponding MS/MS spectra was necessary. Initially, characteristic fragments of the parent drugs were taken into account to determine the biotransformation sites. The spectra and the postulated fragmentation patterns of both 4F-FUF and iBF MS/MS core structures are depicted in Figure 3, which shows for both compounds two main fragments: one at mass-to-charge ratio (m/z) 105.0703, corresponding to the phenethyl moiety, and one at m/z 188.1435, resulting from the cleavage between the piperidine and the amide group. When fragmentation occurred at this site, opposite lower fragments at m/z 206.0616 for 4F-FUF and 164.1071 for iBF were observed. In addition, a minor fragment at m/z 134.0965 was observable for both compounds and originated from the phenylethyl moiety attached to the methylamine residue of the piperidine ring after cleavage. Cleavage was possible also in different points of the piperidine ring, leading to the fragments m/z 160.1124 and 272.1085 for 4F-FUF and 230.1542 and 204.1386 for iBF. For 4-FFUF, the unchanged piperidine ring led to fragment m/z 84.0813, whereas the fragment at m/z 281.2017 corresponded to the elimination of isobutyraldehyde through amide cleavage for iBF.
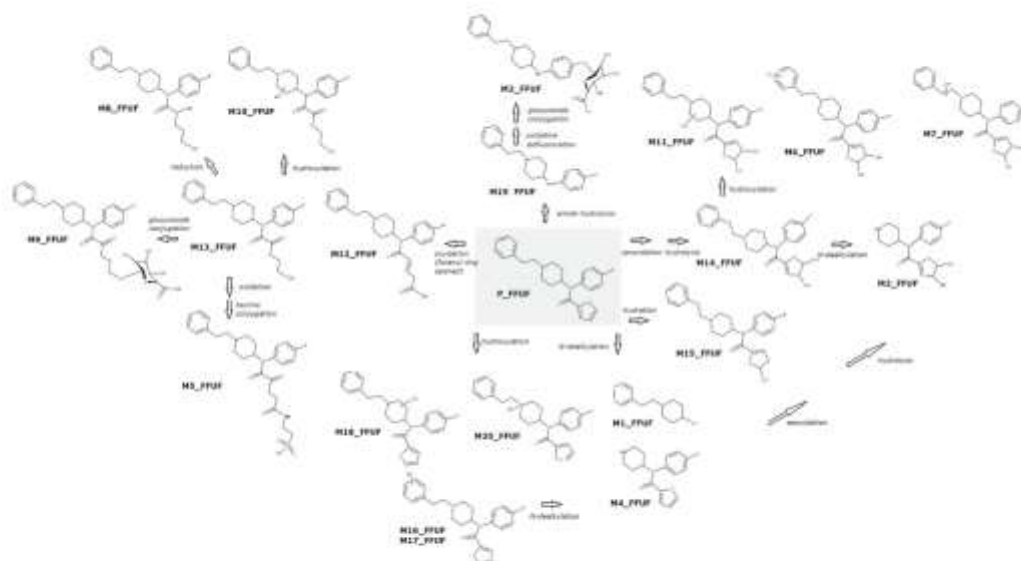
Figure 1. Proposed metabolic pathway of 4-fluoro-furanylfentanyl combining both the in vitro and in vivo studies.

Table 3. List of proposed metabolites of isobutyrylfentanyl with the main identification parameters and postulated biotransformation. The relatively most intense metabolites are in bold.

ID	Biotransformation	Rt (min)	Formula	m/z	Mass Error (PPM)	Diagnostic Ions
M1_iBF	N-dealkylation + hydroxylation + glucuronidation	3.61	$C_{27}H_{33}N_2O_6$	439.2088	1.73	263.1753, 84.0814, 193.1019
M2_iBF	**N-dealkylation + hydroxylation**	**3.86**	$C_{15}H_{23}N_2O_2$	**263.1758**	**−0.58**	84.0814, 245.1648, 177.1387
M3_iBF	N-dealkylation + oxidation	3.89	$C_{16}H_{21}N_2O_2$	277.1546	−2.23	84.0814, 233.1648
M4_iBF	Oxidative N-dealkylation	4.05	$C_{13}H_{20}NO$	206.1542	−1.40	188.1433, 105.0702
M5_iBF	Dihydroxylation + glucuronidation	4.78	$C_{29}H_{38}N_2O_9$	559.2642	−2.42	263.1901, 383.2328, 204.1382, 116.0709
M6_iBF	Oxidation + hydroxylation	4.94	$C_{23}H_{28}N_2O_4$	397.2119	−2.10	204.1384, 121.0651, 353.2221
M7_iBF	Oxidation to carbonyl metabolite + glucuronidation	5.34	$C_{29}H_{37}N_2O_8$	577.2491	−1.63	188.1434, 337.2272, 105.0703
M8_iBF	Hydroxylation + glucuronidation	5.57	$C_{29}H_{36}N_2O_8$	543.2706	−0.08	188.1433, 367.2378, 105.0702
M9_iBF	Dihydroxylation	5.57	$C_{23}H_{31}N_2O_3$	383.2330	−1.22	204.1384, 186.1278, 365.2223
M10_iBF	**Oxidative N-dealkylation**	**5.39**	$C_{15}H_{23}N_2O$	**247.1808**	**−0.96**	84.0813, 177.1386, 164.1073
M11_iBF	Oxidation to carbonyl metabolite + hydroxylation	5.45	$C_{23}H_{28}N_2O_4$	397.2119	−2.10	204.1384, 353.2222, 121.0651
M12_iBF	Hydroxylation + glucuronidation	5.56	$C_{29}H_{36}N_2O_8$	543.2707	0.11	367.2376, 204.1382, 121.0650
M13_iBF	Dihydroxylation + methylation + glucuronidation	5.64	$C_{30}H_{41}N_2O_9$	573.2809	−0.53	397.2534, 410.1813, 234.1488
M14_iBF	**Oxidation + hydroxylation**	**5.77**	$C_{23}H_{29}N_2O_3$	**381.2181**	**0.74**	202.1229, 148.0759, 105.0703
M15_iBF	Hydroxylation	5.87	$C_{23}H_{29}N_2O_2$	365.2225	1.10	188.1436, 105.0704, 244.1332
M16_iBF	Hydroxylation	6.09	$C_{23}H_{31}N_2O_2$	367.2381	−1.23	188.1434, 105.0703, 246.1486
M17_iBF	**Oxidation to carbonyl metabolite**	**6.16**	$C_{23}H_{29}N_2O_3$	**381.2190**	**3.10**	188.1434, 105.0703, 281.2011, 337.2272
M18_iBF	Hydroxylation	6.43	$C_{23}H_{31}N_2O_2$	367.2381	−1.23	188.1434, 105.0703, 281.2013
M19_iBF	Dihydroxylation	7.81	$C_{23}H_{31}N_2O_3$	383.2342	1.91	105.0703, 186.1274, 275.1753
M20_iBF	Hydroxylation	7.84	$C_{23}H_{31}N_2O_2$	367.2381	−1.23	186.1274, 204.1386, 105.0703
M21_iBF	Oxidation	8.80	$C_{23}H_{29}N_2O_2$	365.2226	−0.83	202.1230, 195.1808, 230.1536
P_iBF	-	9.61	$C_{23}H_{31}N_2O$	351.2428	−2.39	-
M22_iBF	N-oxidation	10.54	$C_{23}H_{31}N_2O_2$	367.2381	−1.23	186.1274, 105.0703, 204.1386

Table 4. Results of the in vitro and in vivo studies for isobutyrylfentanyl.

ID	Average (n = 2) Peak Area in Hepatocyte Samples (CV%)							Average Area in Urine Samples (CV%)				
	0.5 h	1 h	2 h	3 h	1 h (n = 1)	2 h (n = 2)	3 h (n = 4)	4 h	5 h (n = 4)	6 h (n = 5)	6–12 h (n = 6)	12–24 h (n = 6)	24–70 h (n = 6)

NS no sample available, NF not found.

Figure 2. Proposed metabolic pathway of isobutyrylfentanyl combining both the in vitro and in vivo studies.
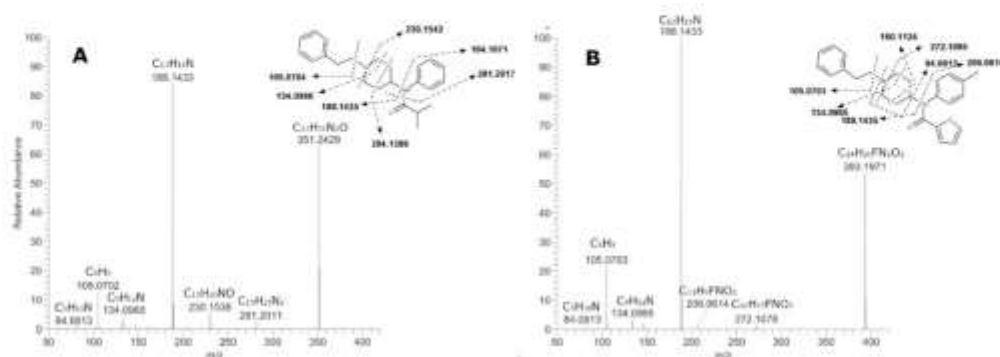
Figure 3. MS/MS fragmentation spectra of isobutyrylfentanyl (**A**) 4-fluoro-furanylfentanyl (**B**) and the postulated fragmentation pattern.

2.3.1. 4F-FUF Metabolites

All the spectra with the postulated fragmentation are reported in Figure S3. The presence of the main fragments m/z 188.1435 and 105.0703 in the metabolite spectra suggested that the phenethylpiperidine structure was unchanged. This was the case for M19_FFUF, which was produced by amide hydrolysis of 4F-FUF and for the most abundant metabolite, M14_FFUF, which was putatively annotated as a dihydrodiol metabolite of 4-FFUF. Based on the fragment 299.1925, it can be hypothesized that the dihydrodiol formation site is the furan ring; even if this structure was postulated on a minor fragment, it must be highlighted that based on the literature data, this was the most probable structure [19]. Based on the fragmentation pattern, the phenetylpiperidine moiety was unchanged also for M2_FFUF and M9_FFUF, which were phase II glucuronide conjugates. In M2_FFUF the glucuronic acid was linked to the aniline ring in the para position subsequently to oxidative defluorination, whereas conjugation occurred at the opened furanyl ring in M9_FFUF. In both metabolites a fragment arising from the loss of the glucuronic acid moiety (loss of 176.0317 u) was observed, reinforcing the hypothesis that they were glucuronides. The fragments m/z 188.1435 and 105.0703 were found also in the spectra of the metabolites arising from furanyl ring scission and subsequent oxidation (M12_FFUF) and taurine conjugation (M5_FFUF) or hydroxylation (M8_FFUF and M13_FFUF) with no biotransformations on the other sites of the molecule. An analogue defluorinated metabolite of M12_FFUF was identified by Watanabe et al. in their work on furanylfentanyl metabolites. For these metabolites the fragment m/z 299.1919, which arose from amide cleavage, was observed in the spectra; this fragmentation pathway was favored by the formation of an α,β-unsaturated carbonyl system consequently to furan ring opening and was rarely observed in the other metabolites and in the parent compound. M15_FFUF is an isomer of M12_FFUF—due to the absence of the fragment 299, we suppose that for this metabolite the furan ring was unopened. Concerning M5_FFUF, to the best of our knowledge this is the first report of the formation of a taurine-conjugated metabolite for fentanyl analogues; the presence of the fragment 409.1918, which corresponded to the loss of the taurine moiety ($C_2H_7NO_3S$) supported the hypothesized structure.

When N-dealkylation occurred (M4_FFUF), the typical phenethylpiperidine fragments were obviously not observed; m/z 84.0815, which corresponded to the elimination of the piperidine, was the base peak. A dihydrodiol N-dealkylated metabolite was also detected (M3_FFUF). The spectrum showed minor fragments, such as m/z 101.0238 ($C_4H_5O_3$), which corresponded to the dihydrodiolfuranyl moiety, suggesting that dihydrodiol formation occurred on the furanyl ring.

Hydroxylation at the phenethylpiperidine moiety was observed for a number of metabolites. This transformation was indicated by the shift of fragment m/z 188.1435 and/or 105.0703 by 16 u. For M6_FFUF, M7_FFUF, M16_FFUF and M17_FFUF, the hydroxylation occurred on the phenylethyl moiety, confirmed by the presence of both m/z 204.1384 and 121.0650, whereas for M10_FFUF, M11_FFUF and M18_FFUF, hydroxylation at the piperidine ring was demonstrated by the phenethyl moiety being left unchanged (the presence of the fragment m/z 105.0703) and the fragments 204.1384 and 186.1278 resulting from H_2O elimination from the former fragment. In the spectrum of M10_FFUF a fragment at m/z 188 was also detected; a likely explanation is that there was the interference of another isomer which was not chromatographically resolved, so that the postulated structure of this metabolite is ambiguous.

2.3.2. iBF Metabolites

All the spectra with the postulated fragmentation are reported in Figure S4.

The same observations made for 4F-FUF can be exploited to elucidate iBF metabolite structures. The unchanged phenetylpiperidine moiety was testified by the presence of the already discussed fragments 188.1435 and 105.0703; these fragments were both detected in the MS/MS spectra of several metabolites, showing that several biotransformations occurred on the isobutyryl moiety or possibly on the aniline ring. The examination of minor fragments in the spectra generally served to determine the exact position of the modifications; for example, for M15_iBF the fragment at m/z 85.0290, corresponding to $C_4H_5O_2$, suggested the elimination of a hydroxylated isobutyryl moiety. Similarly, for M16_iBF, the fragment m/z 337.2278 resulted from elimination of a CH_2O group from the isobutyryl region. Regarding M17_iBF, M18_iBF and M7_iBF, the presence of the fragment 281.2013 indicated that the aniline group was not substituted; thus, the isobutyryl moiety should carry the carboxy, hydroxy and glucuronide groups, respectively. M4_iBF, with m/z 206.1542, which was identical to the 4-FFUF metabolite M1_FFUF, arose from the addition of an -OH to the phenetylpiperidine moiety. This metabolite was produced by an oxidative N-dealkylation reaction, so that the hydroxyl group substituted the amide nitrogen in position 4 of the piperidine ring.

For M8_iBF, no minor fragments indicated the position of the glucuronide conjugation; however, being a phase II metabolite, it probably derives from M16_iBF or M18_iBF, which were putatively annotated as aliphatic hydroxylated metabolites. On the other hand, M12_iBF was an isomer of M8_iBF, with the glucuronide on the aromatic ring of the phenethylpiperidine, indicated by the presence of the fragments m/z 204.1384 and 121.0650. These two fragments were also found in the spectra of M6_iBF and showed that a hydroxylation occurred on the aromatic ring, whereas the aliphatic carboxylation was supported by the fragments 353.2219 ($-CO_2$) and 297.1960, obtained through the elimination of the carboxylated isobutyryl. The isomer M11_iBF had a similar spectrum, but the absence of the fragment 121.0650 suggested that the hydroxylation occurred on the piperidine ring. Hydroxylation at the piperidine ring was hypothesized for other metabolites, including the hydroxylated M20_iBF, the dihydroxylated M9_iBF, M19_iBF and the glucuronide conjugate M5_iBF; however, for all these metabolites the exact position of the -OH groups could not be deduced. For all these metabolites the fragment 186.1280, resulting from hydroxylation followed by H_2O elimination, was detected. Likewise, M22_iBF, which was putatively annotated as a N-oxide metabolite of iBF, also on the basis of the high Rt, showed this fragment. In the spectra of M14_iBF and M21_iBF, the fragment 202.1229 was detected instead of the 204, showing that oxidation to carbonyl metabolites occurred at the piperidine ring and the ethyl, respectively. For the dihydroxylated metabolites, the position of second hydroxylation was the isobutyryl moiety, based on the fragments 279.1855 in the spectrum of M9_iBF and 297.1960 for M19_iBF, which suggested that only one hydroxylation occurred on the phenylethylpiperidine ring and that the aromatic group was also unchanged. Finally, for metabolite M13_iBFm aromatic dihydroxylation followed by methylation and glucuronide conjugation was hypothesized based on the presence of the

fragment *m/z* 151.0755; this fragment differed from fragment 105.0703, which corresponds to the unchanged phenethyl moiety, by 46 u, suggesting that the biotransformation site was the aromatic moiety. For all glucuronides, the typical loss of glucuronic acid (*m/z* 176) was observed.

Concerning the metabolites of iBF which were N-dealkylated, similarly to 4F-FUF metabolites, a main peak at *m/z* 84.0815, which corresponded to the piperazine ring, was detected. M10_iBF was putatively identified as the nor-iBF metabolite, which arose from N-dealkylation of P_iBF; M2_iBF originated from M10_iBF by hydroxylation and was putatively identified on the basis of fragment *m/z* 177.1388, which suggested that the site of the biotransformation was the isobutyryl moiety. M1_iBF was recognized as the corresponding phase II of M2_iBF, which was formed after glucuronidation of the hydroxy group; similarities in the spectra and the typical shift of *m/z* 176 were observed. For M3_iBF, the position of the carboxylic acid could not be deduced from the spectra, but once again carboxylation was only possible on the isobutyryl ring.

3. Materials and Methods

3.1. Chemicals and Reagents

4F-FUF, iBF, diclofenac (sodium salt) and testosterone were purchased from Cayman Chemicals (Ann Arbor, MI, USA). Pooled cryopreserved male mouse hepatocytes, Williams' E Medium (phenol red free), cell maintenance supplement pack (dexamethasone, cocktail B (penicillin-streptomycin, (insulin, transferrin, selenium complex, (ITS) bovine serum albumine (BSA) and linoleic acid), GlutaMAX™ and HEPES), as well as a thawing and plating supplement pack containing prequalified fetal bovine serum (FBS), dexamethasone, Cocktail A (FBS, penicillin, streptomycin human recombinant insulin, GlutaMAX™ and HEPES), were purchased from Life Technologies (Monza, Italy). Formic acid, methanol, acetonitrile and water were obtained from Fisher Scientific (Fair Lawn, NJ, USA). All solvents employed in the incubation and chromatographic system were ultra-performance liquid chromatography (UHPLC) grade.

Ethanol (BioUltra, for molecular biology, ≥99.8%) and TWEEN® 80 for the in vivo study were purchased from Sigma-Aldrich, whereas physiological solution (0.9% *v/v* NaCl) was obtained from Eurospital, S.p.A, (Trieste TS, Italy).

3.2. In Vitro Incubation Using Mouse Hepatocytes

For in vitro experiments, both NPSs, dissolved in acetonitrile, were incubated at 5 μmol L^{-1} and 37 °C with mouse cryopreserved hepatocytes. Cells were thawed in and washed with Williams' E Medium, containing dexamethasone (1 μmol L^{-1}), and cocktail A, which contained penicillin/streptomycin (1%), human recombinant insulin (4 μg mL^{-1}), Glutamax™ (2 mmol L^{-1}), HEPES pH 7.4 (15 mmol L^{-1}) and FBS (5%) and centrifuged at 55× *g* for 3 min at room temperature. After centrifugation and removal of the supernatant, the cell pellet was resuspended in Williams' E Medium, containing dexamethasone (0.1 μmol L^{-1}) and cocktail B, containing penicillin/streptomycin (0.5%), human recombinant insulin (6.25 μg mL^{-1}), human transferrin (6.25 μg mL^{-1}), selenous acid (6.25 ng mL^{-1}), BSA 1.25 mg mL^{-1}, linoleic acid (5.35 μg mL^{-1}), Glutamax™ (2 mmol L^{-1}) and HEPES pH 7.4 (15 mmol L^{-1}). Cell viability was assessed with the Trypan blue 0.4% exclusion method. 4F-FUF and iBF molecules were incubated in duplicate in 800 μL of a 1.10^6 cell mL^{-1} suspension at 37 °C in a water bath under constant gentle shaking. Diclofenac and testosterone were also incubated, as a positive control, to verify metabolic capability under our experimental conditions: diclofenac was used as positive control for phase I metabolism and testosterone was used for phase II metabolism. Negative controls, i.e., hepatocytes without drugs and drugs without hepatocytes, were also included in the experimental study. 200-μL sample aliquots were collected at 0.5, 1, 2 and 3 h; reaction quenching was obtained by the addition of 200 μL acetonitrile. Specimens were stored at −20 °C until analysis. Before injection, samples were centrifuged; the supernatant was

65

removed, diluted 1:4 with water and filtered with Minisart SRP25 4 mm (0.45 μm) syringe filters (Sartorius, Turin, Italy).

3.3. In Vivo Study on Mice

Sixteen-male ICR (CD-1®) mice weighing 30–35 g (Centralized Preclinical Research Laboratory, University of Ferrara, Italy) were group-housed (5 mice per cage; floor area per animal was 80 cm^2; minimum enclosure height was 12 cm), exposed to a 12:12-h light-dark cycle (light period from 6:30 AM to 6:30 PM) at a temperature of 20 °C–22 °C and humidity of 45–55% and were provided with ad libitum access to food (Diet 4RF25 GLP; Mucedola, Settimo Milanese, Milan, Italy) and water. The experimental protocols performed in the present study were in accordance with the U.K. Animals (Scientific Procedures) Act of 1986 and associated guidelines and the new European Communities Council Directive of September 2010 (2010/63/EU). Experimental protocols were approved by the Italian Ministry of Health (license No. 335/2016-PR) and by the Animal Welfare Body of the University of Ferrara. According to the ARRIVE guidelines, all possible efforts were made to minimize the number of animals used, to minimize the animals' pain and discomfort and to reduce the number of experimental subjects. For the overall study, 16 mice were used. In the analysis of urine excretion studies for vehicle (blank control) 4 mice were used, whereas for each treatment (4F-FUF and iBF both at 5 mg/kg) 6 mice were used (total: 12).

For the studies, mice were administered with 4F-FUF or iBF dissolved in absolute ethanol (final concentration of 2% v/v) and Tween 80 (2% v/v) and brought to its final volume with saline (0.9% NaCl v/v). The solution made with ethanol, Tween 80 and saline was also used as the vehicle (blank control). The drugs were administered by intraperitoneal injection at a volume of 4 μL/g; the final concentration of 4F-FUF or iBF was 5 mg/kg. The control group of 4 mice was administered only with vehicle solution. The mice were single-housed (one mouse per metabolic cage, with free access to food and water) in a colony room under constant temperature (23 °C–24 °C) and humidity (45–55%). Urine samples were collected in 2-mL tubes before drug injections (control), and every hour for 6 consecutive hours from the administration of the treatments [9,33] After 6 h, urine was collected cumulatively in the 6–12, 12–24 and 24–36 h time interval and stored at −20 °C until analysis.

Before LC-HRMS analysis, urine samples were diluted 1:4 with water and filtered with Minisart SRP25 4 mm (0.45 μm) syringe filters (Sartorius, Turin, Italy).

3.4. LC-HRMS Analysis

A Thermo Scientific Ultimate 3000 RSLC system coupled with a Thermo Scientific Q-Exactive Mass spectrometer (Thermo Fisher Scientific, Bremen, Germany) was used for analysis.

Chromatographic separation was carried out with an Excel 2 C18-PFP (100 × 2.1 mm ID) column from Ace (Aberdeen, Scotland) packed with particles of 2 μm, maintained at 35 °C at a flow rate of 0.5 mL min^{-1}.

Mobile phases consisted of 0.1% (v/v) formic acid + 10 mM ammonium formate in water (Phase A) and 0.1% formic acid in acetonitrile (Phase B). The gradient started with 0% B and these conditions were maintained for one min; phase B was then increased to 25% in two min, to 35% in the following two min and held for three min. Phase B was then ramped to 50% over 1.5 min and to 100% in 0.5 min; it was kept stable for one min and then equilibrated to the initial conditions, yielding a total runtime of 12.5 min. Injection volume was 6 μL.

The Q-Exactive mass spectrometer was equipped with a heated electrospray ionization source (HESI-II) operated in positive mode; mass spectra were acquired in full scan/data dependent in the range 50–800 m/z. The operating parameters of the ion source were set as follows: spray voltage 3.5 kV, capillary temperature 350 °C, heater temperature 300 °C, S-lens RF level 60, sheath gas flow rate 55, auxiliary gas flow rate 20. Nitrogen was used

66

for spray stabilization, for collision-induced dissociation experiments in the high energy collision dissociation (HCD) cell and as the damping gas in the C-trap.

The instrument was calibrated in the positive and negative mode every working day. For full scan, resolution was 70,000 (FWHM at m/z 200), whereas automatic gain control (AGC) and maximum injection time were set at 1×10^5 and 100 ms, respectively. In MS/MS mode, resolution was 35,000 (FWHM at m/z 200) and three different collision energies, i.e., 10, 30, 50, were applied.

3.5. Data Analysis

The raw files obtained from the in vitro and in vivo studies were processed separately using Compound Discoverer™ 2.0 (Thermo Scientific™, Waltham, MA, USA) with a specific workflow for metabolite identification which encompassed all the common biotransformation reactions, as well as untargeted nodes. For each study an output table including m/z versus retention time versus raw peak intensity for all the analyzed samples was generated. Potential metabolites detected in the negative control, 0 h samples or in the degradation controls were excluded. The different features were evaluated individually and only compounds with a reasonable elemental composition ($1 < N < 3$; $C < 30$; $0 < 10$), an acceptable peak shape and area above 10,000 were considered as potential metabolites. MS/MS fragmentation spectra associated with the precursor ions were then evaluated for structure annotation. Given that no standards were available, only putative identification was possible [34].

4. Conclusions

The metabolic profiles of iBF and 4F-FUF were investigated in this study. For the first compound the N-dealkylated metabolite (nor-isobutyrylfentanyl) was the relatively most intense but hydroxylation and subsequent carbonylation of the parent compound was also a main transformation, leading to two different isomers; all these metabolites can be considered good biomarkers for iBF consumption in biological samples. For 4F-FUF, the main metabolite was the dihydrodiol derivative, which was further N-dealkylated to produce the second most relatively intense metabolites in vivo, whereas N-dealkylation of the parent compound prevailed in vitro. Despite these differences, in general there was a good agreement between in vitro and in vivo samples; in fact, the main metabolites were found in both studies, confirming that hepatocyte incubation is a good approach for metabolite profiling and for the identification of suitable biomarkers for analytical methods. However, it must be taken into account that the relative abundance of metabolites may be different in authentic biological samples.

A limitation of our in vivo study was that it was based on an animal model and no real samples from human consumers were analyzed. On the other hand, controlled administration of drugs to animals has the advantage of providing several samples at different time points to obtain pharmacokinetic parameters analogously to preclinical studies. Analysis of real human samples is desirable; however, in NPS metabolism studies these are often collected from autopsies and scarce or no information about dosage and time of intake is provided. In these cases, post-mortem redistribution may be responsible for unclear results.

Supplementary Materials: The following are available online at https://www.mdpi.com/2218-1989/11/2/97/s1, Figure S1: extracted ion currents of the putatively identified metabolites for 4-fluoro-furanylfentanyl, Figure S2: extracted ion currents of the putatively identified metabolites for isobutyrylfentanyl, Figure S3: MS/MS fragmentation spectra of 4-fluoro-furanylfentanyl metabolites and postulated fragmentation pattern, Figure S4: MS/MS fragmentation spectra of isobutyrylfentanyl metabolites and postulated fragmentation pattern.

References

1. King, L.A.; Kicman, A.T. A brief history of "new psychoactive substances". *Drug Test. Anal.* **2011**, *3*, 401–403. [CrossRef]
2. Van Hout, M.C.; Hearne, E. New psychoactive substances (NPS) on cryptomarket fora: An exploratory study of characteristics of forum activity between NPS buyers and vendors. *Int. J. Drug Policy* **2017**, *40*, 102–110. [CrossRef] [PubMed]
3. Favretto, D.; Pascali, J.P.; Tagliaro, F. New challenges and innovation in forensic toxicology: Focus on the "New Psychoactive Substances". *J. Chromatogr. A* **2013**, *1287*, 84–95. [CrossRef]
4. Vincenti, F.; Montesano, C.; Cellucci, L.; Gregori, A.; Fanti, F.; Compagnone, D.; Curini, R.; Sergi, M. Combination of pressurized liquid extraction with dispersive liquid liquid micro extraction for the determination of sixty drugs of abuse in hair. *J. Chromatogr. A* **2019**, *1605*, 360348. [CrossRef]
5. Montesano, C.; Vannutelli, G.; Gregori, A.; Ripani, L.; Compagnone, D.; Curini, R.; Sergi, M. Broad screening and identification of novel psychoactive substances in plasma by high-performance liquid chromatography-high-resolution mass spectrometry and post-run library matching. *J. Anal. Toxicol.* **2016**, *40*, 519–528. [CrossRef] [PubMed]
6. Richeval, C.; Gaulier, J.-M.; Romeuf, L.; Allorge, D.; Gaillard, Y. Case report: Relevance of metabolite identification to detect new synthetic opioid intoxications illustrated by U-47700. *Int. J. Legal Med.* **2019**, *133*, 133–142. [CrossRef] [PubMed]
7. Zhu, M.; Zhang, H.; Humphreys, W.G. Drug metabolite profiling and identification by high-resolution mass spectrometry. *J. Biol. Chem.* **2011**, *286*, 25419–25425. [CrossRef]
8. Swortwood, M.J.; Ellefsen, K.N.; Wohlfarth, A.; Diao, X.; Concheiro-Guisan, M.; Kronstrand, R.; Huestis, M.A. First metabolic profile of PV8, a novel synthetic cathinone, in human hepatocytes and urine by high-resolution mass spectrometry. *Anal. Bioanal. Chem.* **2016**, *408*, 4845–4856. [CrossRef] [PubMed]
9. Montesano, C.; Vannutelli, G.; Fanti, F.; Vincenti, F.; Gregori, A.; Togna, A.R.; Canazza, I.; Marti, M.; Sergi, M. Identification of MT-45 metabolites: In silico prediction, in vitro incubation with rat hepatocytes and in vivo confirmation. *J. Anal. Toxicol.* **2017**, *41*, 688–697. [CrossRef] [PubMed]
10. Wagmann, L.; Frankenfeld, F.; Park, Y.M.; Herrmann, J.; Fischmann, S.; Westphal, F.; Müller, R.; Flockerzi, V.; Meyer, M.R. How to Study the Metabolism of New Psychoactive Substances for the Purpose of Toxicological Screenings—A Follow-Up Study Comparing Pooled Human Liver S9, HepaRG Cells, and Zebrafish Larvae. *Front. Chem.* **2020**, *8*, 539. [CrossRef] [PubMed]
11. Grafinger, K.E.; Wilke, A.; König, S.; Weinmann, W. Investigating the ability of the microbial model Cunninghamella elegans for the metabolism of synthetic tryptamines. *Drug Test. Anal.* **2019**, *11*, 721–729. [CrossRef]
12. Richter, L.H.J.; Herrmann, J.; Andreas, A.; Park, Y.M.; Wagmann, L.; Flockerzi, V.; Müller, R.; Meyer, M.R. Tools for studying the metabolism of new psychoactive substances for toxicological screening purposes—A comparative study using pooled human liver S9, HepaRG cells, and zebrafish larvae. *Toxicol. Lett.* **2019**, *305*, 73–80. [CrossRef]
13. Wohlfarth, A.; Scheidweiler, K.B.; Pang, S.; Zhu, M.; Castaneto, M.; Kronstrand, R.; Huestis, M.A. Metabolic characterization of AH-7921, a synthetic opioid designer drug: In vitro metabolic stability assessment and metabolite identification, evaluation of in silico prediction, and in vivo confirmation. *Drug Test. Anal.* **2016**, *8*, 779–781. [CrossRef]
14. EMCDDA Trendspotter Study on Fentanyl in Europe Report from an EMCDDA Expert Meeting. 2012. Available online: https://www.emcdda.europa.eu/system/files/publications/748/TD3112230ENN_Fentanyl_400350.pdf (accessed on 28 December 2020).
15. Shoff, E.N.; Zaney, M.E.; Kahl, J.H.; Hime, G.W.; Boland, D.M. Qualitative identification of fentanyl analogs and other opioids in postmortem cases by UHPLC-Ion Trap-MSn. *J. Anal. Toxicol.* **2017**, *41*, 484–492. [CrossRef] [PubMed]

16. Manral, L.; Gupta, P.K.; Ganesan, K.; Malhotra, R.C. Gas chromatographic retention indices of fentanyl and analogues. *J. Chromatogr. Sci.* **2008**, *46*, 551–555. [CrossRef]

17. Staeheli, S.N.; Baumgartner, M.R.; Gauthier, S.; Gascho, D.; Jarmer, J.; Kraemer, T.; Steuer, A.E. Time-dependent postmortem redistribution of butyrfentanyl and its metabolites in blood and alternative matrices in a case of butyrfentanyl intoxication. *Forensic Sci. Int.* **2016**, *266*, 170–177. [CrossRef] [PubMed]

18. *European Monitoring Centre for Drugs European Drug Report*; European Union: Brussels, Belgium, 2019; ISBN 9789291686926.

19. Watanabe, S.; Vikingsson, S.; Roman, M.; Green, H.; Kronstrand, R.; Wohlfarth, A. In Vitro and In Vivo Metabolite Identification Studies for the New Synthetic Opioids Acetylfentanyl, Acrylfentanyl, Furanylfentanyl, and 4-Fluoro-Isobutyrylfentanyl. *AAPS J.* **2017**, *19*, 1102–1122. [CrossRef]

20. Goggin, M.M.; Nguyen, A.; Janis, G.C. Identification of unique metabolites of the designer opioid furanyl fentanyl. *J. Anal. Toxicol.* **2017**, *41*, 367–375. [CrossRef] [PubMed]

21. Gaulier, J.; Richeval, C.; Gicquel, T.; Hugbart, C.; Le Dare, B.; Allorge, D.; Morel, I. In vitro characterization of NPS metabolites produced by human liver microsomes and the HepaRG cell line using liquid chromatography-high resolution mass spectrometry (LC-HRMS) analysis: Application to furanyl fentanyl. *Curr. Pharm. Biotechnol.* **2017**, *18*, 806–814. [CrossRef]

22. Kanamori, T.; Iwata, Y.T.; Segawa, H.; Yamamuro, T.; Kuwayama, K.; Tsujikawa, K.; Inoue, H. Metabolism of butyrylfentanyl in fresh human hepatocytes: Chemical synthesis of authentic metabolite standards for definitive identification. *Biol. Pharm. Bull.* **2019**, *42*, 623–630. [CrossRef]

23. Steuer, A.E.; Williner, E.; Staeheli, S.N.; Kraemer, T. Studies on the metabolism of the fentanyl-derived designer drug butyrfentanyl in human in vitro liver preparations and authentic human samples using liquid chromatography-high resolution mass spectrometry (LC-HRMS). *Drug Test. Anal.* **2017**, *9*, 1085–1092. [CrossRef]

24. Gundersen, P.O.M.; Åstrand, A.; Gréen, H.; Josefsson, M.; Spigset, O.; Vikingsson, S. Metabolite Profiling of Ortho-, Meta- And Para-Fluorofentanyl by Hepatocytes and High-Resolution Mass Spectrometry. *J. Anal. Toxicol.* **2019**, *44*, 144–148. [CrossRef] [PubMed]

25. Armenian, P.; Vo, K.T.; Barr-Walker, J.; Lynch, K.L. Fentanyl, fentanyl analogs and novel synthetic opioids: A comprehensive review. *Neuropharmacology* **2018**, *134*, 121–132. [CrossRef] [PubMed]

26. Vincenti, F.; Pagano, F.; Montesano, C.; Sciubba, F.; Di Cocco, M.E.; Gregori, A.; Rosa, F.D.; Lombardi, L.; Sergi, M.; Curini, R. Multi-analytical characterization of 4-fluoro-furanyl fentanyl in a drug seizure. *Forensic Chem.* **2020**, *21*, 100283. [CrossRef]

27. Varshneya, N.B.; Walentiny, D.M.; Moisa, L.T.; Walker, T.D.; Akinfiresoye, L.R.; Beardsley, P.M. Opioid-like antinociceptive and locomotor effects of emerging fentanyl-related substances. *Neuropharmacology* **2019**, *151*, 171–179. [CrossRef]

28. Wallgren, J.; Vikingsson, S.; Rautio, T.; Nasr, E.; Åstrand, A.; Watanabe, S.; Kronstrand, R.; Gréen, H.; Dahlén, J.; Wu, X.; et al. Structure Elucidation of Urinary Metabolites of Fentanyl and Five Fentanyl Analogs using LC-QTOF-MS, Hepatocyte Incubations and Synthesized Reference Standards. *J. Anal. Toxicol.* **2020**, *21*, 993–1003. [CrossRef]

29. Kokko, H.; Hall, P.D.; Afrin, L.B. Fentanyl-associated syndrome of inappropriate antidiuretic hormone secretion. *Pharmacotherapy* **2002**, *22*, 1188–1192. [CrossRef] [PubMed]

30. Chamberlain, C.A.; Rubio, V.Y.; Garrett, T.J. Impact of matrix effects and ionization efficiency in non-quantitative untargeted metabolomics. *Metabolomics* **2019**, *15*, 135. [CrossRef] [PubMed]

31. Park, B.K.; Kitteringham, N.R.; O'Neill, P.M. Metabolism of fluorine-containing drugs. *Annu. Rev. Pharmacol. Toxicol.* **2001**, *41*, 443–470. [CrossRef] [PubMed]

32. Peterson, L.A. Reactive metabolites in the biotransformation of molecules containing a furan ring. *Chem. Res. Toxicol.* **2013**, *26*, 6–25. [CrossRef] [PubMed]

33. Chieffi, C.; Camuto, C.; De-Giorgio, F.; de la Torre, X.; Diamanti, F.; Mazzarino, M.; Trapella, C.; Marti, M.; Botrè, F. Metabolic profile of the synthetic drug 4,4'-dimethylaminorex in urine by LC–MS-based techniques: Selection of the most suitable markers of its intake. *Forensic Toxicol.* **2020**. [CrossRef]

34. Sumner, L.W.; Amberg, A.; Barrett, D.; Beale, M.H.; Beger, R.; Daykin, C.A.; Fan, T.W.-M.; Fiehn, O.; Goodacre, R.; Griffin, J.L.; et al. Proposed minimum reporting standards for chemical analysis. *Metabolomics* **2007**, *3*, 211–221. [CrossRef] [PubMed]

In vitro and in vivo pharmaco-dynamic study of the novel fentanyl derivatives: Acrylfentanyl, Ocfentanyl and Furanylfentanyl

Sabrine Bilel [a], Joaquim Azevedo Neto [b], Raffaella Arfè [a], Micaela Tirri [a], Rosa Maria Gaudio [a,c], Anna Fantinati [d], Tatiana Bernardi [d], Federica Boccuto [d], Beatrice Marchetti [a], Giorgia Corli [a], Giovanni Serpelloni [e], Fabio De-Giorgio [f,g], Davide Malfacini [h], Claudio Trapella [d], Girolamo Calo' [h], Matteo Marti [a,c,i,*]

[a] Department of Translational Medicine, Section of Legal Medicine and LTTA Centre, University of Ferrara, Italy
[b] Department of Neuroscience and Rehabilitation, Section of Pharmacology, University of Ferrara, Via Fossato di Mortara 17/19, 44121, Ferrara, Italy
[c] Center of Gender Medicine, University of Ferrara, Italy
[d] Department of Chemistry and Pharmaceutical Sciences, University of Ferrara, Italy
[e] Neuroscience Clinical Center & TMS Unit Verona, Italy and Department of Psychiatry in the College of Medicine, Drug Policy Institute, University of Florida, Gainesville, FL, United States
[f] Institute of Public Health, Section of Legal Medicine, Università Cattolica Del Sacro Cuore, Rome, Italy
[g] Fondazione Policlinico Universitario A. Gemelli IRCCS, Rome, Italy
[h] Department of Pharmaceutical and Pharmacological Sciences, University of Padua, Italy
[i] Collaborative Center of the National Early Warning System, Department for Anti Drug Policies, Presidency of the Council of Ministers, Italy

ARTICLE INFO

ABSTRACT

Fentanyl derivatives (FENS) belongs to the class of Novel Synthetic Opioids that emerged in the illegal drug market of New Psychoactive Substances (NPS). These substances have been implicated in many cases of intoxication and death with overdose worldwide. Therefore, the aim of this study is to investigate the pharmacodynamic profiles of three fentanyl (FENT) analogues: Acrylfentanyl (ACRYLF), Ocfentanyl (OCF) and Furanylfentanyl (FUF). In vitro, we measured FENS opioid receptor efficacy, potency, and selectivity in calcium mobilization studies performed in cells coexpressing opioid receptors and chimeric G proteins and their capability to promote the interaction of the mu receptor with G protein and β-arrestin 2 in bioluminescence resonance energy transfer (BRET) studies. In vivo, we investigated the acute effects of the systemic administration of ACRYLF, OCF and FUF (0.01–15 mg/kg i.p.) on mechanical and thermal analgesia, motor impairment, grip strength and cardiorespiratory changes in CD-1 male mice. Opioid receptor specificity was investigated in vivo using naloxone (NLX; 6 mg/kg i.p) pre-treatment. In vitro, the three FENS were able to activate the mu opioid receptor in a concentration dependent manner with following rank order potency: FUF > FENT~OCF > ACRYLF. All compounds were able to elicit maximal effects similar to that of dermorphin, with the exception of FUF which displayed lower maximal effects thus behaving as a partial agonist. In the BRET G-protein assay, all compounds behaved as partial agonists for the β-arrestin 2 pathway in comparison with dermorphin, whereas FUF did not promote β-arrestin 2 recruitment, behaving as an antagonist. In vivo, all the compounds increased mechanical and thermal analgesia with following rank order potency ACRYLF ~ FENT > FUF > OCF and impaired motor and cardiorespiratory parameters. Among the substances tested, FUF showed lower potency for cardiorespiratory and motor effects. These findings reveal the risks associated with the use of FENS and the importance of studying the pharmaco-dynamic properties of these drugs to better understand possible therapeutic interventions in the case of toxicity.

* Corresponding author. Department of Translational Medicine, Section of Legal Medicine, University of Ferrara, via Fossato di Mortara 70, 44121, Ferrara, Italy.
E-mail address: matteo.marti@unife.it (M. Marti).

70

1. Introduction

Novel Synthetic Opioids (NSO) are a growing class of new psychoactive substances (NPS) mostly consisting of analogues of fentanyl (FENT) linked to numerous overdose and fatalities worldwide. NSO accounted for just 2% of NPS identified in 2014; this rose to 9% by 2018 (United Nations Office on Drugs and Crime UNDOC, 2020). Overall, 49 NSOs have been detected on Europe's drug market since 2009 (EMCDDA, 2019), including FENT, its analogues used in medical therapy (e.g. Sufentanyl, Alfentanyl and Remifentanyl; Lemmens, 1995), novel non-pharmaceutical FENT derivatives (e.g. Ocfentanyl, Furanylfentanyl, Acetylfentanyl, Carfentanyl, Acrylfentanyl, Tetrahydrofuranylfentanyl, etc.) and other molecules. FENS recently seized as NSOs are usually generated by replacement of the ethylphenyl moiety (Isofentanyl, β-hydroxythiofentanyl) or modification of FENT propionyl chain (Acrylfentanyl (ACRYLF), Ocfentanyl (OCF), Acetylfentanyl, Furanylfentanyl (FUF), Butyrylfentanyl and Isobutyrylfentanyl). An estimated 58 million people used opioids in 2018, this number is considered lower in respect to cannabis users (192 millions). However, the number of deaths reflects the toxicity of opioids. Yet, opioid use has been involved in 66% of the estimated 167,000 deaths related to drug use disorders in 2017. FENT is a synthetic opioid agonist with analgesic and anaesthetic properties and is approximately 100 times more potent than morphine. New FENS are structurally similar to FENT and therefore often have comparable biological effects (Solimini et al., 2018). The severe adverse effects of FENS include euphoria, drowsiness, dizziness, confusion, miosis, nausea, vomiting, confusion, constipation, sedation, skin rash, respiratory depression, unconsciousness, coma, and death. In 2018, synthetic FENS were implicated in two thirds of the 67,367 overdose deaths registered in the United States. Similar findings have been also reported in Canada, Australia and Europe, but with lower numbers. Novel FENS are frequently sold as heroin adulterant. The overdose death related to these substances is mainly driven by the unpredictability of their potency. Moreover, in some deaths related to FENS such as ACRYLF, OCF and FUF (Fig. 1), no heroin was found. The high availability, the low price and the high potency of these compounds could explain the trends of their abuse. ACRYLF was first developed as an analogue of FENT in 1981 (Zhu et al., 1981). It is an acrylamide derivative of 4-anilinopiperidine and is an unsaturated analogue of FENT. In the last few years it has appeared online as a research chemical. In 2016, the European Monitoring Centre for Drugs and Drug Addiction (EMCDDA) has reported a total of 130 deaths caused by ACRYLF in United States and Europe (EMCDDA, 2016). OCF had been studied clinically for its analgesic activity during the early 1990s (Huang et al., 1986). It was found to have a relative potency 200 times greater than that of morphine and it is more potent than FENT with fewer adverse effects, regarding respiratory depression and bradycardia (Huang et al., 1986). OCF is among the 14 FENT derivatives that have been reported in Europe within 2012–2016. It has been associated with some intoxication cases and deaths in Belgium and Switzerland (Zwalska, 2017). FUF is a FENT derivative that differs from FENT in that it has a furanyl ring in place of the methyl group adjacent to the carbonyl bridge. The first report of a FUF-related intoxication was recorded in 2015 in the USA. In 2016, a total of 494 forensic cases of FUF, including 128 confirmed fatalities, were reported to the DEA. In 2017, the EMCDDA reported a total of 29 serious adverse events (10 acute intoxications and 19 deaths) associated with FUF in Estonia, Germany, United Kingdom, Sweden and Norway (EMCDDA, 2017). Data on the pharmacology of these compounds are limited. Therefore, the aim of this study was to investigate the pharmaco-dynamic profile of the ACRYLF, OCF and FUF compared with FENT. To evaluate the in vitro basic pharmacological profile of these compounds, a calcium mobilization assay was performed using cells expressing opioid receptors and chimeric G-proteins (Camarda and Calo', 2013). Moreover, a bioluminescence resonance energy transfer (BRET) assay was also used to investigate the ability of the compounds to promote mu receptor interaction with G-protein and β-arrestin 2 (Molinari et al., 2010). We investigated the acute effects of the three
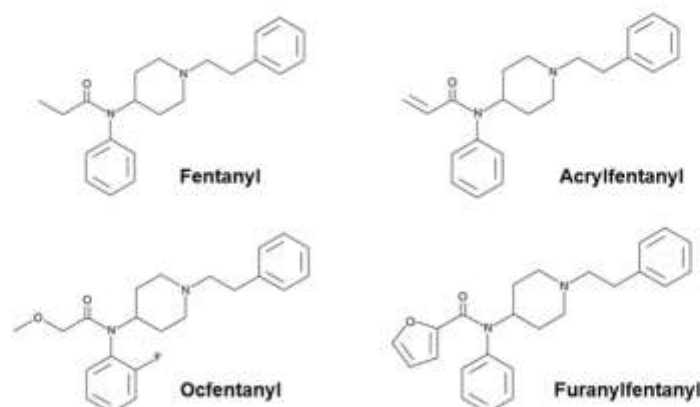

Fig. 1. Chemical structures of Fentanyl; Acrylfentanyl; Ocfentanyl and Furanylfentanyl.

2

G protein
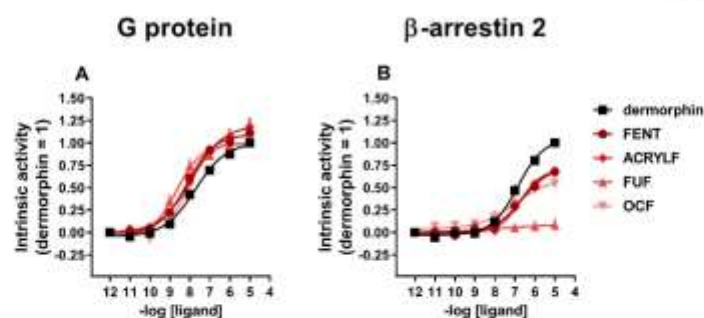
β-arrestin 2

Fig. 2. BRET assay. Concentration response curve to dermorphin, FENT, ACRYLF, FUF, and OCF for mu/G protein (panel A) and mu/β-arrestin 2 (panel B) interaction. Data are the mean ± s.e.m. of 5 separate experiments made in duplicate.

FENS in comparison to FENT, in vivo, on acute mechanical and thermal analgesia, motor impairment, muscle strength and cardiorespiratory changes (heart rate, respiratory rate, SpO2 saturation and pulse distention) in CD-1 male mice. Opioid receptor specificity was investigated in vivo using NLX pre-treatment in all the tests.

2. Materials and methods

2.1. In vitro studies

2.1.1. Drugs and reagents

All cell culture media and supplements were from Invitrogen (Thermo Fisher Scientific Inc. MA, USA). Dermorphin, DPDPE, and Dynorphin A were synthetized in the laboratory of Prof Remo Guerrini (University of Ferrara). FENT was from Bio-Techne (UK) (authorization SP/168 November 04, 2019 to MM). The FENT derivatives, ACRYLF, OCF and FUF were purchased from LGC standards (LGC Standards S.r.l., Sesto San Giovanni, Milan, Italy) (authorization SP/168 November 04, 2019 to MM) while naloxone was purchased from Sigma Aldrich (St. Louis, MO, USA). Opioid peptides were solubilized in bidistilled water, whereas all other compounds were solubilized in DMSO at a final concentration of 10 mM. Stock solutions of ligands were stored at −20 °C. Serial dilutions were made in each assay buffer.

2.1.2. Calcium mobilization assay

CHO cells stably coexpressing the human recombinant mu or kappa receptors with the C-terminally modified $G\alpha_{qi5}$ and CHO cells coexpressing the delta receptor and the $G\alpha_{qGi5o6n5}$ chimeric protein were generated as previously described (Camarda and Calo, 2013). Cells were cultured in medium consisting of Dulbecco's modified Eagle's medium (DMEM)/HAMS F12 (1:1) supplemented with 10% fetal bovine serum (FBS), penicillin (100 IU/ml), streptomycin (100 mg/ml), geneticin (G418; 200 µg/ml) and hygromycin B (100 µg/ml). Cell cultures were kept at 37 °C in 5% CO2/humidified air. When confluence was reached (3–4 days), cells were sub-cultured as required using trypsin/EDTA and used for experimentation. Cells were seeded at a density of 50,000 cells/well into 96-well black, clear-bottom plates. After 24 h incubation the cells were incubated with Hank's Balanced Salt Solution (HBSS) supplemented with 2.5 mM probenecid, 3 µM of the calcium sensitive fluorescent dye Fluo-4 AM, 0.01% pluronic acid and 20 mM HEPES (pH 7.4) for 30 min at 37 °C. Afterwards the loading solution was aspirated followed by a washing step with 100 µl/well of HBSS, HEPES (20 mM, pH 7.4), 2.5 mM probenecid and 500 µM Brilliant Black. Subsequently 100 µl/well of the same buffer was added. After placing cell culture and compound plates into the FlexStation II (Molecular Devices, Sunnyvale, CA, USA), the changes in fluorescence of the cell-loaded calcium sensitive dye Fluo-4 AM were measured.

2.1.3. BRET assay

SH-SY5Y Cells stably co-expressing the different pairs of fusion proteins i.e. mu-RLuc/Gβ1-RGFP and mu-RLuc/β-arrestin 2-RGFP were prepared using a pantropic retroviral expression system as described previously (Molinari et al., 2010; Malfacini et al., 2015). Cells were grown in Dulbecco's modified Eagle's medium (DMEM)/HAMS F12 (1:1) supplemented with 10% fetal bovine serum, penicillin G (100 units/ml), streptomycin (100 µg/ml), L-glutamine (2 mM), fungizone (1 µg/ml), geneticin (G418; 400 µg/ml) and hygromycin B (100 µg/ml) in a humidified atmosphere of 5% CO2 at 37 °C. For G-protein experiments, enriched plasma membrane aliquots from mu-RLuc/Gβ1-RGFP cells were prepared by differential centrifugation; cells were detached with PBS/EDTA solution (1 mM, pH 7.4 NaOH) then, after 5 min 500 g centrifugation, Dounce-homogenized (30 strokes) in cold homogenization buffer (TRIS 5 mM, EGTA 1 mM, DTT 1 mM, pH 7.4 HCl) in the presence of sucrose (0.32 M). Three following centrifugation steps were performed at 10 min 1000 g (4 °C) and the supernatants kept. Two 20 min 24,000 g (4 °C) subsequent centrifugation steps (the second in the absence of sucrose) were performed for separating enriched membranes that after discarding the supernatant were kept in ultrapure water at −80 °C (Vachon et al., 1987). Membrane protein was determined using the QPRO-BCA kit (Cyanagen Srl, Bologna, IT) and the multimode Ensight plate reader (Perkin Elmer, Waltham, US). Luminescence in membranes and cells was recorded in 96-well white opaque microplates (Perkin Elmer, Waltham, MA, USA) using the Victor 2030 luminometer (PerkinElmer, Waltham, MA, USA). For the determination of receptor/G-protein interaction, membranes (3 µg of protein) prepared from cells co-expressing mu-RLuc/Gβ1-RGFP were added to wells in Dulbecco's phosphate-buffered saline(DPBS). For the determination of receptor/β-arrestin 2 interaction, whole cells co-expressing mu-R-Luc/β-arrestin 2-RGFP were plated 24 h before the experiment (100,000 cells/well). The cells were prepared for the experiment by substituting the medium with PBS with MgCl2 (0.5 mM) and CaCl2 (0.9 mM). Coelenterazine at a final concentration of 5 µM was injected 15 min prior reading the cell plate. Different concentrations of ligands in 20 µL of PBS - BSA 0.01% were added and incubated 5 min before reading luminescence. All experiments were performed at room temperature.

2.1.4. Data analysis and terminology

Pharmacological terminology adopted in this report is consistent with IUPHAR recommendations (Neubig et al., 2003). All data are expressed as the mean ± standard error of the mean (s.e.m.) of n experiments. For potency values 95% confidence limits (CL95%) were indicated. In calcium mobilization studies, agonist effects were expressed as maximum change in percent over the baseline fluorescence. Baseline fluorescence was measured in wells treated with saline. In BRET studies agonist effects were calculated as BRET ratio between CPS

3

measured for the RGFP and RLuc light emitted using 510(10) and 460 (25) filters (PerkinElmer, Waltham, MA, USA), respectively. Maximal agonist effects were expressed as fraction of the dermorphin maximal effects which was determined in every assay plate (dermorphin = 1). Concentration response curve to agonists were fitted with the four parameter logistic nonlinear regression model:

$$Effect = Baseline + \frac{(E_{max} - Baseline)}{(1 + 10^{logEC_{50} - Log_{[compound]}Hillslope})}$$

For all assays, agonist potencies are given as pEC_{50} i.e. the negative logarithm to base 10 of the molar concentration of an agonist that produces 50% of the maximal effect of that agonist. The potency of antagonists was expressed as pA_2 derived from the following equation: $pA_2 = -log[(CR-1)/[A]]$, assuming a slope value equal to unity, where CR indicates the ratio between agonist potency in the presence and absence of antagonist and [A] is the molar concentration of the antagonist (Kenakin, 2004).

2.2. In vivo studies

2.2.1. Animals

Four hundred thirty-two Male ICR (CD-1®) mice weighing 30–35 g (Centralized Preclinical Research Laboratory, University of Ferrara, Italy) were group housed (5 mice per cage; floor area per animal was 80 cm²; minimum enclosure height was 12 cm), exposed to a 12:12-h light-dark cycle (light period from 6:30 a.m. to 6:30 p.m.) at a temperature of 20–22 °C and humidity of 45–55% and were provided ad libitum access to food (Diet 4RF25 GLP; Mucedola, Settimo Milanese, Milan, Italy) and water. The experimental protocols performed in the present study were in accordance with the U.K. Animals (Scientific Procedures) Act of 1986 and associated guidelines and the new European Communities Council Directive of September 2010 (2010/63/EU). Experimental protocols were approved by the Italian Ministry of Health (license n. 335/2016-PR) and by the Animal Welfare Body of the University of Ferrara. According to the ARRIVE guidelines, all possible efforts were made to minimise the number of animals used, to minimise the animals' pain and discomfort.

2.2.2. Drug preparation and dose selection

Drugs were dissolved in saline solution (0.9% NaCl) that was also used as the vehicle. The opioid receptor antagonist NLX (6 mg/kg) was administered 15 min before FENT, ACRYLF, OCF and FUF injections. The dose of 6 mg/kg of NLX was used in our previous study (Bilel et al., 2020) and proved its efficacy in blocking the actions of morphine without having any effect per se. Higher doses of NLX (> 6 mg/kg) were tested in our preliminary data. In particular, the dose of 10 mg/kg induced sensorimotor alterations, increased slightly analgesia and also increased heart and breath rates in our animal model. Indeed, the dose of 6 mg/kg is selected for this study.The protocol set in the present study for naloxone injections is aimed to mimic clinical evidence: in fact, it has been reported the need of naloxone redosing to revert fentanyl's toxicity (in particular respiratory depression; Klebacher et al., 2017; Rzasa Lynn and Galinkin, 2018). Thus, a second full dose of naloxone (6 mg/kg) was injected 55 min after the first one in order to better antagonize FENS effects and counteract their reappearance. Drugs were administered by intraperitoneal (i.p.) injection at a volume of 4 μl/g. The range of doses of FENS tested (0.01–15 mg/kg i.p.) was chosen based on our previous studies (Bilel et al., 2019; Bilel et al., 2020).

2.2.3. Behavioural studies

The effects of the four FENS were investigated using a battery of behavioural tests widely used in pharmacology safety studies for the preclinical characterization of new psychoactive substances in rodents (Vigolo et al., 2015; Ossato et al., 2015; Canazza et al., 2016; Fantinati et al., 2017; Ossato et al., 2018; Marti et al., 2019; Bilel et al., 2020; Bilel

et al., 2021). All experiments were performed between 8:30 a.m. and 2:00 p.m. Experiments were conducted blindly by trained observers working in pairs (Ossato et al., 2016). Mouse behaviour (motor responses) was videotaped and analysed offline by a different trained operator who gives test scores.

2.2.3.1. Evaluation of pain induced by a mechanical and a thermal stimulus. Acute mechanical nociception was evaluated using the tail pinch test (Vigolo et al., 2015). A special rigid probe connected to a digital dynamometer (ZP-50N, IMADA, Japan) was gently placed on the tail of the mouse (in the distal portion), and progressive pressure was applied. When the mouse flicked its tail, the pressure was stopped and the digital instrument recorded the maximum peak of weight supported (g/force). A cut off (500 g/force) was set to avoid tissue damage. The test was repeated three times and the final value was calculated by averaging the three obtained scores. Acute thermal nociception was evaluated using the tail withdrawal test (Vigolo et al., 2015). The mouse was restrained in a dark plastic cylinder and half of its tail was dipped in 48 °C water. Then, the length of time (in s) the tail was left in the water was recorded. A cut off (15 s) was set to avoid tissue damage. Acute mechanical and thermal nociception was measured at 0, 35, 55, 90, 145, 205, 265 and 325 min post injection.

2.2.3.2. Motor activity assessment. Alterations of motor activity induced by FENS were measured using the drag and the accelerod tests (Bilel et al., 2020). In the *drag test*, the mouse was lifted by the tail, leaving the front paws on the table, and was dragged backward at a constant speed of about 20 cm/s for a fixed distance (100 cm). The number of steps performed by each paw was recorded by two different observers. For each animal, five to seven measurements were collected. The drag test was performed at 0, 45, 70, 105, 160, 220, 280 and 340 min post injection. In the *accelerod test*, the animals were placed on a rotating cylinder that automatically increases in velocity in a constant manner (0–60 rotations/min in 5 min). The time spent on the cylinder was measured. The accelerod test was performed at 0, 40, 60, 95, 150, 210, 270 and 330 min post injection.

2.2.3.3. Evaluation of skeletal muscle strength (grip strength). This test was used to evaluate the skeletal muscle strength of the mice (Bilel et al., 2020).The grip-strength apparatus (ZP-50N, IMADA) is comprised of a wire grid (5 × 5 cm) connected to an isometric force transducer (dynamometer). In the grip-strength test, mice were held by their tails and allowed to grasp the grid with their forepaws. The mice were then gently pulled backward by the tail until the grid was released. The average force exerted by each mouse before losing its grip was recorded. The mean of three measurements for each animal was calculated, and the mean average force was determined. The skeletal muscle strength is expressed in gram force (gf) and was recorded and processed using IMADA ZP-Recorder software. The grip strength was measured at 0, 15, 35, 70, 125, 185, 245 and 305 min post injection.

2.2.3.4. Cardiorespiratory analysis. The experimental protocol to detect the cardiorespiratory parameters used in this study is designed to monitor awake and freely moving animals with no invasive instruments and with minimal handling (Bilel et al., 2020). A collar was placed around the neck of the animal; this collar has a sensor that continuously detects heart rate, respiratory rate, oxygen saturation and pulse distention with a frequency of 15 Hz. While running the experiment, the mouse moves freely in the cage (with no access to food and water) monitored by the sensor collar using the software MouseOx Plus (STARR Life Sciences® Corp. Oakmont, PA). In the first hour, a collar was placed around the animal's neck to simulate the real one used in the test, thus minimising the possible effects of stress during the experiment. The real collar (with sensor) was then substituted, and baseline parameters were monitored for 60 min. Subsequently, the mice were given FENT,

ACRYLF, OCF and FUF by i.p. injection, and data was recorded for 5 h.

2.2.4. Data and statistical analysis

Antinociceptive effects (tail withdrawal and tail pinch tests) are calculated as the percent of maximal possible effect (EMax% = [(test - control latency)/(cut off time - control)] X 100). Tail withdrawal and tail pinch are expressed as Emax %. Drag and accelerod are expressed in percentage of basal value (%), maximal muscle strength is expressed as gf, heart rate is expressed as heart beats per min (bpm), pulse distention (vessel diameter changes) is expressed as µm, respiratory rate is expressed as respiratory rate per minute (rrpm) and SpO_2 saturation (oxygen blood saturation) is expressed as %.

Statistical analysis of the effects of the substances at different doses over time and of antagonism were performed using a two-way ANOVA followed by a Bonferroni test for multiple comparisons. Statistical analysis was performed using Prism software (GraphPad Prism, USA).

The mean effect values represent the average of the effects induced by each compound at each dose over the time course of the experiment. For Tail pinch, Tail withdrawal, accelerod, drag and grip strength tests, the mean effects were calculated for the 5 h time-course (Figs. 3–7; Panels C and D). However, for the cardiorespiratory curves (Figs. 8–11; Panels C and D), the mean effect values were calculated for the first 2 h of measurements, since after this time point the effects of the drugs disappeared.

The ED_{50} values were calculated (where it was possible) using nonlinear regression which presents the best fit values of log dose of agonist vs. response (GraphPad Prism).

3. Results

3.1. In vitro studies

3.1.1. Calcium mobilisation studies

In CHO cells stably transfected with the human mu opioid receptor, the standard agonist dermorphin evoked a robust concentration-dependent stimulation of calcium release displaying high potency (pEC_{50} of 8.19) and maximal effects ($319 \pm 13\%$ over the basal values). FENT mimicked the stimulatory effect elicited by dermorphin showing similar potency and maximal effects. All FENT derivatives were able to activate the mu opioid receptor in a concentration dependent manner with the following rank order potency: FENT = ACRYLF ≥ FUF = OCF. Regarding ligand efficacy, all compounds were able to elicit maximal effects similar to that of dermorphin, with the exception of FUF that displayed statistically significantly lower maximal effects thus behaving as a partial agonist (Table 1).

In CHO_{delta} cells, the standard agonist DPDPE evoked a robust concentration-dependent stimulation of calcium release with high potency (pEC_{50} of 7.47) and maximal effects ($230 \pm 18\%$ over the basal values). All other compounds were either inactive or displayed an incomplete concentration response curve, stimulating calcium mobilization only at micromolar concentrations.

In CHO_{kappa} cells, the standard agonist dynorphin A evoked a robust concentration-dependent stimulation of calcium release with very high potency (pEC_{50} of 8.81) and maximal effects ($257 \pm 34\%$ over the basal values). All other compounds were either inactive or displayed an incomplete concentration response curve, stimulating calcium mobilization only at micromolar concentrations.

3.1.2. BRET studies

In the BRET G-protein assay, membrane extracts taken from SH-SY5Y cells stably co-expressing the mu/RLuc and Gβ1/RGFP fusoproteins were used in concentration response experiments to evaluate receptor/G-protein interaction. Dermorphin promoted mu/G-protein interaction in a concentration dependent manner with pEC_{50} of 7.71 (7.41–8.01) and maximal effect of 0.96 ± 0.11 stimulated BRET ratio. The intrinsic activities of the compounds under study were computed as fraction of the standard ligand dermorphin maximal-stimulated BRET ratio (dermorphin = 1.00) (Fig. 2-A). All compounds, including FENT, mimicked the maximal effects of dermorphin displaying with following rank order potency: FUF ≥ FENT = OCF ≥ ACRYLF.

Whole SH-SY5Y cells stably expressing the mu/RLuc and the β-arrestin 2/RGFP fusoproteins were used to evaluate mu/β-arrestin 2 interaction. Dermorphin stimulated the interaction of the mu receptor with β-arrestin 2 in a concentration-dependent manner with pEC_{50} 6.96 (6.56–7.37) and maximal effects corresponding to 0.24 ± 0.09 stimulated BRET ratio. As for G protein studies, intrinsic activities of the

Fig. 3. Effect of the systemic administration of FENT (0.01–15 mg/kg i.p; panel A) in the tail pinch test in mice. Interaction of effective dose of FENT (6 mg/kg) with the opioid receptor antagonist NLX (panel B). Comparison of dose-response curves FENT, ACRYLF, OCF and FUF (0.01–15 mg/kg i.p; panel C). Interaction of FENT, ACRYLF, OCF and FUF (6 mg/kg) with NLX (6 mg/kg, i.p.; panel D). Data are expressed as percentage of maximum effect (see materials and methods) and represents the mean ± SEM of 8 determinations for each treatment. Statistical analysis was performed by two-way ANOVA followed by the Bonferroni's test for multiple comparisons for the dose response curve of FENT at different times (panel A and B), while the statistical analysis of panel D was performed with one-way ANOVA followed by Bonferroni test for multiple comparisons. **p < 0.01, ***p < 0.001 versus saline; #p < 0.05,###p < 0.001 versus NLX + agonist;°°°p < 0.01 versus NLX.^^^p<0.001versus FENT;°°°p < 0.001 versus ACRYLF;°°°p < 0.001 versus OCF; ^^p < 0.001 versus FUF.

TAIL WITHDRAWAL

Fig. 4. Effect of the systemic administration of FENT (0.01–15 mg/kg i.p; panel A) in the tail withdrawal test in mice. Interaction of effective dose of FENT (6 mg/kg) with the opioid receptor antagonist NLX (panel B). Comparison of dose-response curves FENT, ACRYLF, OCF and FUF (0.01–15 mg/kg i.p; panel C). Interaction of FENT, ACRYLF, OCF and FUF (6 mg/kg) with NLX (6 mg/kg, i.p.; panel D). Data are expressed as percentage of maximum effect (see materials and methods) and represents the mean ± SEM of 8 determinations for each treatment. Statistical analysis was performed by two-way ANOVA followed by the Bonferroni's test for multiple comparisons for the dose response curve of FENT at different times (panel A and B) and for the comparison of the mean effects (panel C), while the statistical analysis of panel D was performed with one-way ANOVA followed by Bonferroni test for multiple comparisons. **$p < 0.01$, ***$p < 0.001$ versus saline; #$p < 0.05$,###$p < 0.001$ versus NLX + agonist.^^^$p < 0.001$ versus NLX,△△△$p < 0.001$ versus FENT;$^{\circ\circ}$p < 0.001 versus ACRYLF;$^{\natural\natural\natural}$p < 0.001 versus OCF; $^{\Delta\Delta}$p < 0.001 versus FUF.

ACCELEROD TEST

Fig. 5. Effect of the systemic administration of FENT (0.01–15 mg/kg i.p; panel A) in the Accelerod test in mice. Interaction of effective dose of FENT (6 mg/kg) with the opioid receptor antagonist NLX (panel B). Comparison of the mean effect of FENT, ACRYLF, OCF and FUF (0.01–15 mg/kg i.p) observed in 5 h (panel C). Interaction of FENT, ACRYLF, OCF and FUF (6 mg/kg) with NLX (6 mg/kg, i.p.; panel D). Data are expressed as percentage of baseline (see material and methods) and represent the mean ± SEM of 8 determinations for each treatment. Statistical analysis was performed by two-way ANOVA followed by the Bonferroni's test for multiple comparisons for the dose response curve of FENT at different times (panel A and B) and for the comparison of the mean effects (panel C), while the statistical analysis of panel D was performed with one-way ANOVA followed by Bonferroni test for multiple comparisons. *$p < 0.05$, **$p < 0.01$,***$p < 0.001$ versus saline; ###$p < 0.001$ versus NLX + agonist; §p < 0.001 versus OCF.§§p < 0.01,§§§p < 0.001 versus FUF,$^{\circ\circ\circ}$p<0.001 versus ACRYLF;$^{\natural\natural}$p < 0.001,$^{\natural\natural\natural}$p < 0.001 versus NLX; △△△$p<0.001$ versus FENT;†p < 0.05 versus OCF; ‡‡p < 0.001 versus FUF.

compounds were computed as fraction of the standard agonist dermorphin (dermorphin = 1.00) (Fig. 2-A). All compounds displayed similar potency in recruiting the β-arrestin 2 pathway (Table 2). Regarding their efficacy, all compounds behaved as partial agonists for the β-arrestin 2 pathway in comparison with dermorphin whereas FUF was completely inactive (Fig. 2-B; Table 2). Thus FUF was further

investigated as an antagonist of FENT induced β-arrestin 2 recruitment. At the concentration of 0.1 μM, this compound was able to shift the concentration response curve to FENT to the right with no modification of the agonist maximal effect (See Supplementary Fig. 2); a pA$_2$ of 8.53 was derived from these experiments for FUF.

DRAG TEST

GRIP STRENGTH TEST

3.2. Behavioural studies

3.2.1. Evaluation of pain induced by mechanical and thermal stimuli

Acute mechanical and thermal pain stimuli were not affected in mice treated with saline (Figs. 3 and 4). Systemic administration of FENT (0.01–15 mg/kg i.p) increased the threshold to acute mechanical pain stimulus in the tail pinch test (Fig. 3-A). Mechanical analgesia was significantly affected by treatment [F6, 343 = 94.02, p < 0.0001], time [F6,343 = 42.48, p < 0.0001] and time × treatment interaction

[F36,343 = 3.684, p < 0.0001]. Similar to FENT, ACRYLF, OCF and FUF increased the threshold to acute mechanical pain stimulus in a dose-dependent manner that reached the maximum at higher doses (3–15 mg/kg; see Supplementary Fig. 3)Comparison of the dose response curves to FENT in the tail pinch test (Fig. 3-C) revealed the following rank order potencies: ACRYLF ED50 0.97 mg/kg = FUF ED50 1.1 mg/kg = FENT ED50 1.4 mg/kg > OCF ED50 4.54 mg/kg.

Pre-treatment with NLX (6 mg/kg i.p; Fig 3-B) partially prevented the analgesic effect of FENT. The injection of a second dose of NLX (6
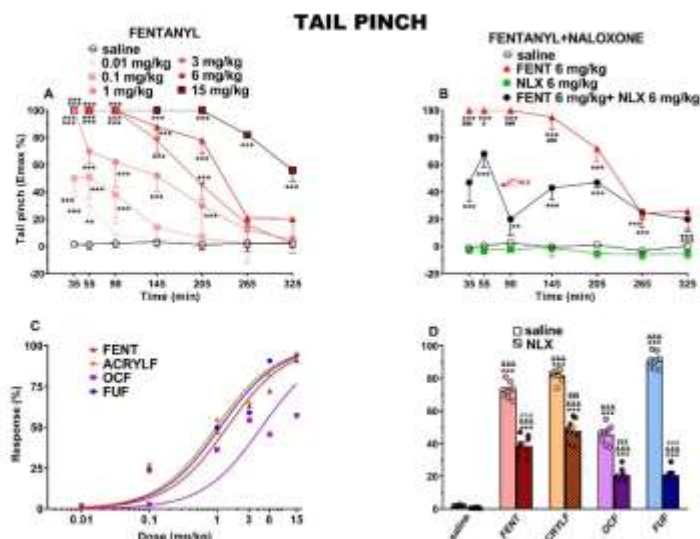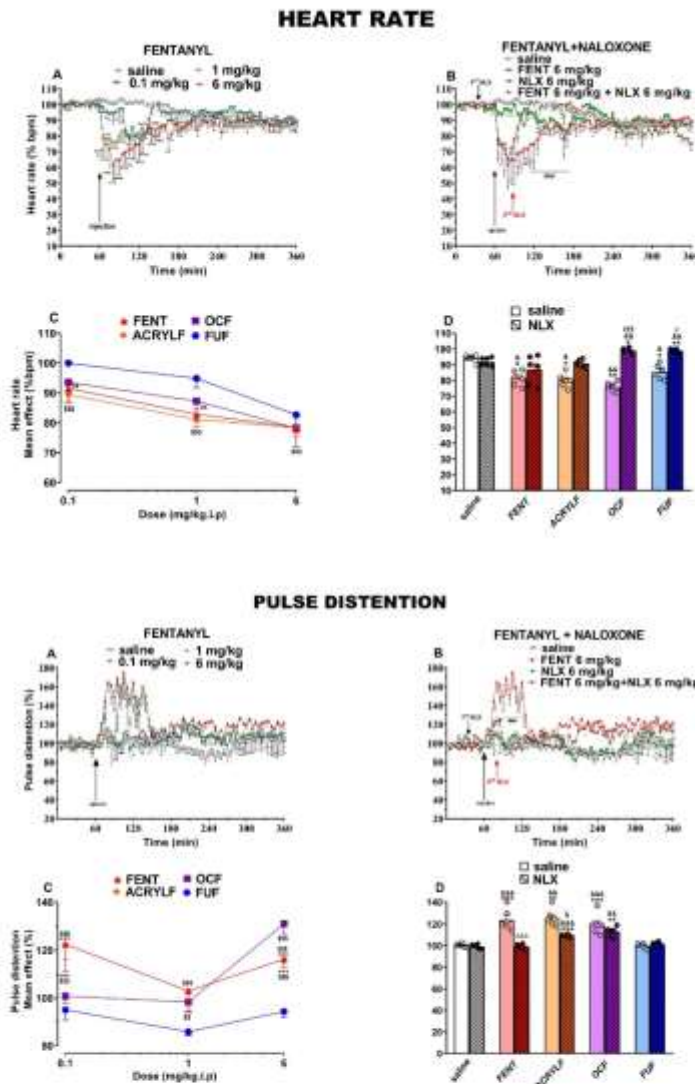
HEART RATE
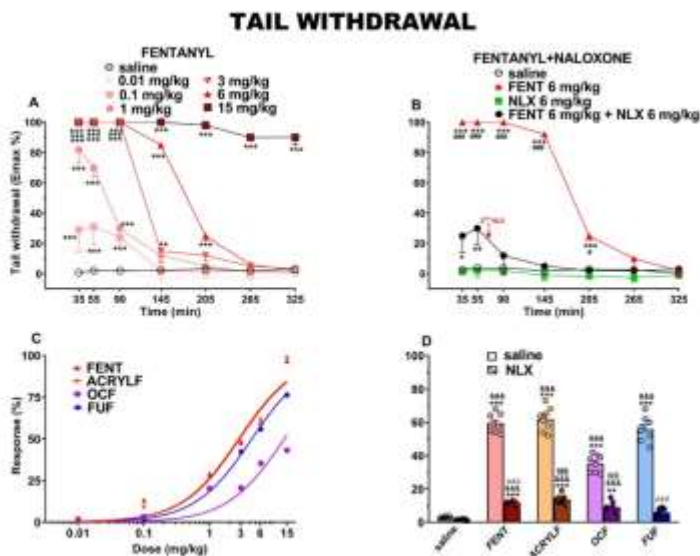
Fig. 8. Effect of the systemic administration of FENT (0.01–15 mg/kg i.p; panel A) on the heart rate in mice. Interaction of effective dose of FENT (6 mg/kg) with the opioid receptor antagonist NLX (panel B). Comparison of the mean effect of FENT, ACRYLF, OCF and FUF (0.01–15 mg/kg i.p) observed in 2 h (panel C). Interaction of FENT, ACRYLF, OCF and FUF (6 mg/kg i.p) with NLX in 5 h (6 mg/kg, i.p; panel D). Data are expressed as percentage of basal value (see material and methods) and represent the mean ± SEM of 6 determinations for each treatment. Statistical analysis was performed by two-way ANOVA followed by the Bonferroni's test for multiple comparisons for the dose response curve of FENT at different times (panel A and B) and for the comparison of the mean effects (panel C), while the statistical analysis of panel D was performed with one-way ANOVA followed by Bonferroni test for multiple comparisons. $^*p < 0.05, ^{**}p < 0.01$ $^{***}p < 0.001$ versus saline; $^{\#\#\#}p < 0.001$ versus NLX + agonist; $^{\$\$}p < 0.01, ^{\$\$\$}p < 0.001$ versus FUF; $^\&p < 0.05, ^{\&\&}p < 0.01$ versus NLX; $^{\triangle\triangle\triangle}p < 0.001$ versus OCF; $^\delta p < 0.05$ versus FUF.
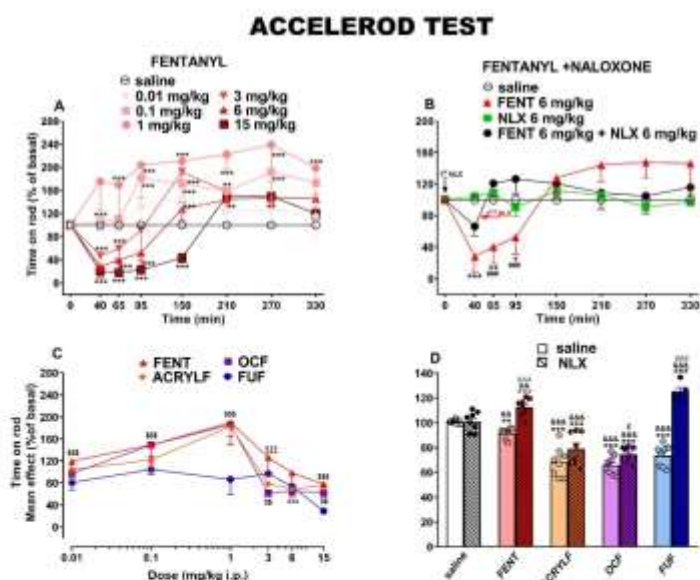
PULSE DISTENTION

Fig. 9. Effect of the systemic administration of FENT (0.01–15 mg/kg i.p; panel A) on Pulse distention in mice. Interaction of effective dose of FENT (6 mg/kg) with the opioid receptor antagonist NLX (panel B). Comparison of the mean effect of FENT, ACRYLF, OCF and FUF (0.01–15 mg/kg i.p) observed in 2 h (panel C). Interaction of FENT, ACRYLF, OCF and FUF (6 mg/kg i.p) with NLX in 5 h (6 mg/kg i.p; panel D). Data are expressed as percentage of basal value (see material and methods) and represent the mean ± SEM of 6 determinations for each treatment. Statistical analysis was performed by two-way ANOVA followed by the Bonferroni's test for multiple comparisons for the dose response curve of FENT at different times (panel A and B) and for the comparison of the mean effects (panel C), while the statistical analysis of panel D was performed with one-way ANOVA followed by Bonferroni test for multiple comparisons. $^{**}p < 0.01$ $^{***}p < 0.001$ versus saline; $^{\#\#\#}p < 0.001$ versus NLX + agonist; $^*p < 0.001$ versus OCF; $^{\$\$}p < 0.01, ^{\$\$\$}p < 0.001$ versus FUF; $^{\&\&}p < 0.01, ^{\&\&\&}p < 0.001$ versus NLX; $^{\triangle\triangle\triangle}p < 0.001$ versus FENT; $^\delta p < 0.05$ versus ACRYLF.

mg/kg i.p; Fig 3-B) at 55 min did not totally block the analgesia induced by the agonist and the effect persisted until the end of the test [F3,196 = 214.1, p < 0.0001], time [F6,196 = 14.02, p < 0.0001] and time × treatment interaction [F18,196 = 7.054, p < 0.0001]. Similar to FENT, the second injection with NLX (6 mg/kg; Fig. 3-D) did not fully block the analgesic effect induced ACRYLF, OCF and FUF (for time-course curves see Supplementary Fig. 3).

Systemic administration of FENT (0.01–15 mg/kg i.p; Fig. 4-A) increased the threshold to acute thermal pain stimulus in the tail withdrawal test. In particular, after the administration of FENT thermal analgesia was significantly affected by treatment [F6,343 = 444.5, p < 0.0001], time [F6,343 = 153.0, p < 0.0001] and time × treatment

interaction [F36, 343 = 26.34, p < 0.0001]. Similar to FENT, ACRYLF, OCF and FUF increased the threshold to acute thermal pain stimulus in a dose-dependent manner that reached the maximum at higher doses (3–15 mg/kg; see supplementary Fig. 4). Comparison of the dose-response curves to FENT in the tail withdrawal test (Fig. 4-C) revealed the following rank order potencies: ACRYLF ED50 = 2.74 mg/kg = FENT ED50 = 2.86 mg/kg > FUF ED50 = 4.39 mg/kg > OCF ED50 = 13.66 mg/kg.

Pre-treatment with NLX (6 mg/kgi.p; Fig. 4-B) partially prevented the analgesic effect of all compounds. The injection of a second dose of NLX (6 mg/kg i.p; Fig. 4-B) at 55 min did not totally block the analgesia induced by FENT [F3, 196 = 251.1, p < 0.0001], time [F6, 196 = 36.45,
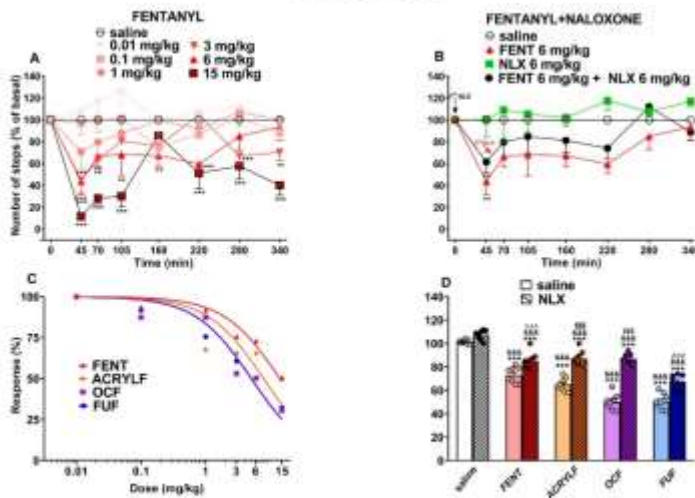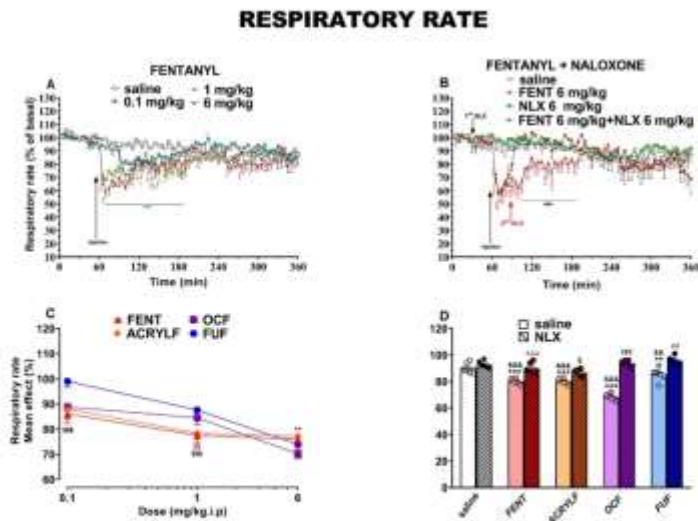
RESPIRATORY RATE

Fig. 10. Effect of the systemic administration of FENT (0.01–15 mg/kg i.p; panel A) on the Respiratory rate in mice. Interaction of effective dose of FENT (6 mg/kg) with the opioid receptor antagonist NLX (panel B). Comparison of the mean effect of FENT, ACRYLF, OCF and FUF (0.01–15 mg/kg i.p) observed in 2 h (panel C). Interaction of FENT, ACRYLF, OCF and FUF (6 mg/kg i.p) with NLX in 5 h (6 mg/kg, i.p; panel D). Data are expressed as percentage of basal value (see material and methods) and represent the mean ± SEM of 6 determinations for each treatment. Statistical analysis was performed by two-way ANOVA followed by the Bonferroni's test for multiple comparisons for the dose response curve of FENT at different times (panel A and B) and for the comparison of the mean effects (panel C), while the statistical analysis of panel D was performed with one-way ANOVA followed by Bonferroni test for multiple comparisons. $^*p < 0.05$, $^{**}p < 0.01$ $^{***}p < 0.001$versus saline; $^{\#\#\#}p < 0.001$versus NLX + agonist; $^\circ p < 0.01$versus OCF $^{\$\$\$}p < 0.001$versus FUF; $^{\wedge\wedge\wedge}p < 0.001$versus NLX; $^{\triangle\triangle\triangle}p<0.001$versus FENT; $^{\S}p < 0.05$versus ACRYLF;$^{\perp\perp\perp}p < 0.001$ versus OCF; $^{\Theta\Theta}p < 0.01$ versus FUF.
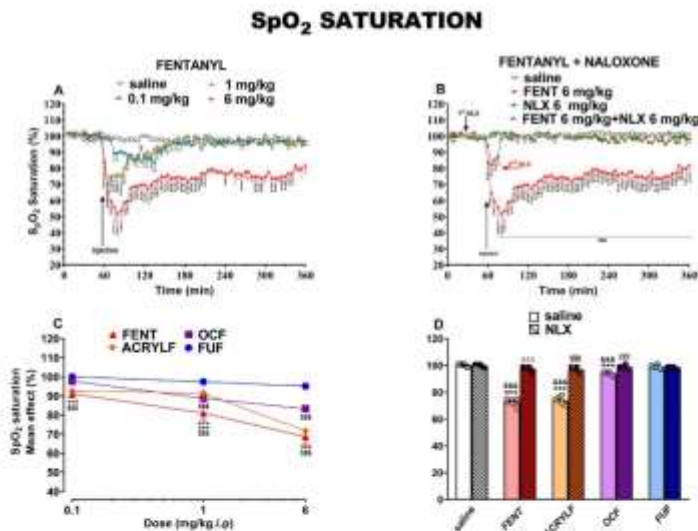
SpO₂ SATURATION

Fig. 11. Effect of the systemic administration of FENT (0.01–15 mg/kg i.p; panel A) on Oxygen saturation (SpO₂) in mice. Interaction of effective dose of FENT (6 mg/kg) with the opioid receptor antagonist NLX (panel B). Comparison of the mean effect of FENT, ACRYLF, OCF and FUF (0.01–15 mg/kg i.p) observed in 2 h (panel C). Interaction of FENT, ACRYLF, OCF and FUF (6 mg/kg i.p) with NLX in 5 h (6 mg/kg, i.p; panel D). Data are expressed as percentage of absolute value (see material and methods) and represent the mean ± SEM of 6 determinations for each treatment. Statistical analysis was performed by two-way ANOVA followed by the Bonferroni's test for multiple comparisons for the dose response curve of FENT at different times (panel A and B) and for the comparison of the mean effects (panel C), while the statistical analysis of panel D was performed with one-way ANOVA followed by Bonferroni test for multiple comparisons.$^{**}p < 0.01$ $^{***}p < 0.001$versus saline; $^{\#\#\#}p < 0.001$versus NLX + agonist; $^\circ p < 0.01$versus OCF $^{\$\$\$}p < 0.001$versus FUF;$^{\wedge\wedge\wedge}p < 0.001$versus NLX; $^{\triangle\triangle\triangle}p<0.001$versus FENT; $^{\S}p < 0.001$versus ACRYLF;$^{\perp\perp\perp}p < 0.001$ versus OCF.

$p < 0.0001$] and time × treatment interaction [F18, 196 = 20.99, $p < 0.0001$] and the effect persisted until the end of the test. As presented in Fig. 4-D, the injection of second dose of NLX (6 mg/kg) was not effective at totally blocking the analgesic effects induced by FENT, ACRYLF, OCF and FUF (for time-course curves see Supplementary Fig. 4).

3.2.2. Evaluation of motor activity

3.2.2.1. Accelerod test.
There was no change in accelerod test performance in mice treated with saline (Fig. 5). Systemic administration of FENT (0.01–15 mg/kg i.p) significantly impaired mouse performance in the accelerod test. Similar to FENT, ACRYLF, OCF and FUF impaired performance in the accelerod test (see Supplementary Fig. 5). After administration of FENT (Fig. 5-A), the performance of mice in the accelerod was affected by the treatment [F₆, ₃₄₃ = 12.79], time [F₇, ₃₄₃ = 8.031, P < 0.0001] and time × treatment interaction [F₄₂, ₃₄₃ = 1.146, P = 0.2533]. In particular, FENT induced a biphasic effect with a facilitatory action at low doses (0.1–1 mg/kg) and an inhibitory action at higher doses (3–15 mg/kg). Comparison of the mean effect among FENT, ACRYLF, OCF and FUF (Fig. 5-C) revealed significant differences in the action of each substance at different doses [significant effect of

Table 1

Effects of dermorphin, fentanyl and its derivatives in calcium mobilization experiments performed in CHO cells coexpressing opioid receptors and the chimeric G-proteins. *p < 0.05 vs dermorphin according to ANOVA followed by the Dunnett test. Data are mean of at least 3 separate experiments made in duplicate.

	mu		Delta		kappa	
	pEC50 (CI.95%)	Emax ± sem %	pEC50 (CI.95%)	Emax ± sem %	pEC50 (CI.95%)	Emax ± sem %
Standard agonists	8.19 (8.02-8.36)	319 ± 13	7.47 (7.09-7.85)	230 ± 18	8.81 (8.22-9.40)	257 ± 34
FENT	8.13 (7.73-8.52)	326 ± 13	CRC incomplete		CRC incomplete	
ACRYLF	8.20 (7.05-9.35)	308 ± 12	CRC incomplete		CRC incomplete	
OCF	7.78 (7.50-8.07)	305 ± 16	CRC incomplete		CRC incomplete	
FUF	7.93 (7.57-8.29)	226 ± 7*	Inactive		Inactive	

Standard agonists were dermorphin, DPDPE and dynorphin A for mu, delta and kappa opioid receptors, respectively.

Table 2

Effects of dermorphin, fentanyl and its derivatives in BRET experiments investigating mu/G protein and mu/β-arrestin 2 interaction.

	mu/G protein		mu/β-arrestin2	
	pEC50 (CI.95%)	α±SEM	pEC50 (CI.95%)	α±SEM
Dermorphin	7.71 (7.41-8.01)	1.00	6.96 (6.56-7.37)	1.00
FENT	8.28 (8.06-8.49)	1.11 ± 0.07	6.86 (6.54-7.18)	0.67 ± 0.02*
ACRYLF	7.87 (7.49-8.25)	1.18 ± 0.10	6.76 (6.48-7.03)	0.68 ± 0.05*
OCF	8.09 (7.63-8.55)	1.03 ± 0.07	7.28 (6.65-7.92)	
FUF	8.66 (8.15-9.16)	1.04 ± 0.09	Inactive	

treatment $F_{3, 166} = 48.49$, p < 0.0001], dose [$F_{5, 166} = 111.7$, P < 0.0001] and dose × treatment interaction [$F_{15, 166} = 9.547$, P < 0.0001]. Surprisingly, FUF induced only inhibition of motor performance at the range dose tested. Moreover, FUF resulted to be the most effective (P < 0.001) compared with the other compounds (for time-course curves of ACRYLF, OCF and FUF see Supplementary Fig. 5). Pre-treatment with NLX (6 mg/kg i.p; Fig. 5-B) partially reduced motor impairment induced at the dose of 6 mg/kg of FENT. Injection of a second dose of NLX (6 mg/kg i.p; Fig. 5-B) totally blocked motor impairment induced by the agonist at the dose of 6 mg/kg: FENT [$F_{3, 196} = 1.006$, P = 0.3915], time [$F_{7, 196} = 6.346$, P < 0.0001] and time × treatment interaction [$F_{21, 196} = 4.263$, P < 0.0001].The injection of a second dose of NLX at 55 min (Fig. 5-D) prevented the inhibition of motor performance in mice treated with FENT and FUF at the dose of 6 mg/kg but not in those treated with ACRYLF and OCF.

3.2.2.2. Drag test. Systemic administration of FENT (0.01–15 mg/kg i.p) reduced the number of steps performed by the front legs (Fig. 6-A). After administration of FENT, the number of steps performed was significantly affected by treatment [$F_{6, 343} = 31.39$, p < 0.0001], time [$F_{7, 343} = 6.703$, P < 0.0001] and time × treatment interaction [$F_{42, 343} = 2.395$, P < 0.0001]. Similar to FENT, ACRYLF, OCF and FUF reduced the number of the steps on the drag test (see Supplementary Fig. 6 for time-course curves). . Comparison of dose-response curves to FENT in the Drag test (Fig 6-C) revealed the following rank order of potencies: FUF ED50 = 5.07 = OCF ED50 = 5.11 mg/kg > ACRYLF ED50 = 7.82 mg/kg > FENT ED50 = 13.93 mg/kg.

The pre-treatment with NLX (6 mg/kg i.p; Fig. 6-B) partially prevented the inhibition of steps at the dose of 6 mg/kg of FENT. The injection of a second dose of NLX (6 mg/kg i.p; Fig. 6-B) at 55 min did not totally prevent the inhibitory effect induced by FENT [$F_{3, 196} = 14.14$, P < 0.0001], time [$F_{7, 196} = 2.319$, P = 0.0275] and time × treatment interaction [$F_{21, 196} = 0.9279$, P = 0.5557]. Similar to FENT, the injection of a second dose of NLX (6 mg/kg i.p; Fig. 6-D) partially prevented the inhibitory effects in mice treated with ACRYLF, OCF and FUF.

3.2.3. Evaluation of skeletal muscle strength

Muscle strength was not affected in mice treated with saline (Fig. 7). Systemic administration of FENT (0.01–15 mg/kg i.p) decreased pulling force in a dose-dependent manner (Fig. 7-A). In particular, after the administration of FENT, skeletal muscle strength was significantly affected by treatment [$F_{6, 343} = 20.55$, P < 0.0001 time [$F_{7, 343} = 7.630$, P < 0.0001] and time × treatment interaction [$F_{42, 343} = 2.311$, P < 0.0001]. Similar to FENT, ACRYLF, OCF and FUF reduced the pulling force in a dose-dependent manner (see Supplementary Fig. 7 for time-course curves). Comparison of dose-response curves to FENT (Fig. 7-C) revealed significant differences in the action of each substance at different doses [significant effect of treatment $F_{3, 166} = 13.34$, p < 0.0001], dose [$F_{5, 166} = 78.45$, P < 0.0001] and dose × treatment interaction [$F_{15, 166} = 8.292$, P = 0.0008]. ACRYLF was more effective than FENT and OCF at inhibiting the number of steps at the dose of 1 mg/kg. OCF was more effective than FENT and ACRYLF and FUF at the doses of 3 and 6 mg/kg and FUF was more effective than FENT and ACRYLF at the highest dose tested (15 mg/kg). Pre-treatment with NLX (6 mg/kg i.p; Fig. 7-B) partially prevented the changes in skeletal muscle force caused by FENT (6 mg/kg). The injection of a second dose of NLX (6 mg/kg i.p) totally blocked the inhibitory effect induced by FENT [$F_{3,196} = 32.86$, P < 0.0001), time [$F_{7, 176} = 5.713$, P < 0.0001] and time × treatment interaction [$F_{21, 196} = 4.578$, P < 0.0001]. Injection of a second dose of NLX (6 mg/kg i.p; Fig. 7-D) totally prevented the inhibitory effects in mice treated with ACRYLF, OCF and FUF.

3.2.4. Cardiorespiratory analysis

The effect of FENT on cardiorespiratory changes has been widely investigated. Using the non-invasive instrument "the MouseOX" (see Materials and Methods) we compared the effects of ACRYLF, OCF and FUF to FENT. The saline used in this experiment showed a stable profile during the 6 h of cardiorespiratory parameter measurement (heart rate, respiratory rate, oxygen saturation and pulse distention; Figs. 8–11). Systemic administration of FENT and its derivatives (0.1–6 mg/kg i.p) induced important dose-dependent variations in cardiorespiratory parameters.

Heart rate (Fig. 8) was rapidly (5 min post injection) and significantly affected by FENT (Fig. 8-A) treatment [$F_{3, 1584} = 70.73$, P < 0.0001], time [$F_{71, 1584} = 6.524$, P < 0.0001] and time × treatment interaction [$F_{213, 1584} = 2.985$, P < 0.0001]. Similar to FENT, ACRYLF, OCF and FUF reduced heart rate in a dose-dependent manner (see Supplementary Fig. 8 for time-course curves). Comparison of the mean effect among FENT, ACRYLF, OCF and FUF (Fig. 8-C), revealed significant differences in the action of each substance at different doses [significant effect of treatment $F_{3, 60} = 28.99$, p < 0.0001], dose [$F_{2, 60} = 109.1$, P < 0.0001] and dose × treatment interaction [$F_{6, 60} = 2.628$, P = 0.0250]. FUF was less effective than FENT, ACRYLF and OCF in decreasing the heart rate over the dose range tested (0.1–6 mg/kg; Fig. 8-C). Pre-treatment with NLX (6 mg/kg.i.p; Fig. 8-B) partially prevented FENT bradycardia. Injection of a second dose of NLX (6 mg/kg i.p; Fig. 8-B) totally blocked the inhibitory effect induced by FENT [significant effect of the treatment ($F_{3, 1440} = 76.66$, P < 0.0001), time ($F_{71,}$

$_{1440}$ = 8.303, P < 0.0001) and time × treatment interaction (F$_{213, 1440}$ = 4.103, P < 0.0001). Similar to FENT, injection of second dose of NLX (6 mg/kg i.p; Fig. 8-D) totally prevented bradycardia induced by ACRYLF, OCF and FUF.

Pulse distention (Fig. 9) in the group of mice treated with FENT (Fig. 9-A) was significantly affected by treatment [F$_{3, 1584}$ = 91,14, P < 0,0001], time [F$_{71, 1584}$ = 4.870, P < 0.0001] and time × treatment interaction [F$_{213, 1584}$ = 2.427, P < 0.0001]. Comparison of mean effect among FENT, ACRYLF, OCF and FUF (Fig. 9-C), revealed significant differences in the action of each substance at different doses [significant effect of treatment F$_{3, 60}$ = 57.41, p < 0.0001], dose [F$_{2, 60}$ = 53.41, P < 0.0001] and dose × treatment interaction [F$_{6, 60}$ = 14.06, P < 0.0001]. FUF did not affect pulse distention. FENT and ACRYLF are more effective than OCF at the dose of 0.1 mg/kg, while OCF was more effective than FENT and ACRYLF at the dose of 6 mg/kg.

Pre-treatment with NLX (6 mg/kg i.p; Fig. 9-B) partially prevented the increase in pulse distention caused by FENT, ACRYLF and OCF. Injection of a second dose of NLX (6 mg/kg i.p; Fig. 9-B) totally blocked the changes in pulse distention induced by: FENT [F$_{3, 1440}$ = 130,0, P < 0,0001], time [F$_{71, 1440}$ = 3,193, P < 0,0001] and time × treatment interaction [F$_{213, 1440}$ = 2,239, P < 0,0001]. Similar to FENT, the injection of second dose of NLX (6 mg/kg i.p; Fig. 9-D) totally prevented the increase in Pulse distention induced by ACRYLF and OCF.

After the administration of FENT, respiratory rate (Fig. 10-A) was also significantly affected by treatment: [F$_{3, 1584}$ = 91.01, P < 0.0001], time [F$_{71, 1584}$ = 12.86, P < 0.0001] and time × treatment interaction [F$_{213, 1584}$ = 3.614, P < 0.0001]. Comparison of the mean effect among FENT, ACRYLF, OCF and FUF (Fig. 10-C) revealed significant differences in the action of each substance at different doses [significant effect of treatment F$_{3, 60}$ = 13.89, p < 0.0001], dose [F$_{2, 60}$ = 124.1, P < 0.0001] and dose × treatment interaction [F$_{6, 60}$ = 9.041, P < 0.0001]. FUF was less effective than FENT, ACRYLF at the dose of 0.1 and 1 mg/kg. OCF was less effective than FENT, ACRYLF at the dose of 1 mg/kg, while OCF was more effective than ACRYLF at the dose of 6 mg/kg. Pre-treatment with NLX (6 mg/kg i.p; Fig. 10-B) partially prevented the bradypnea caused by FENT. Injection of a second dose of NLX (6 mg/kg i.p; Fig. 10-B) totally blocked the inhibitory effect induced by FENT [F$_{3, 1440}$ = 57.67, P < 0.0001], time [F$_{71, 1440}$ = 6.925, P < 0.0001] and time × treatment interaction [F$_{213, 1440}$ = 2.241, P < 0.0001]. Similar to FENT, the injection of a second dose of NLX (6 mg/kg.i.p; Fig. 10-D) totally prevented bradpnea induced by ACRYLF, OCF and FUF.

After administration of FENT (Fig. 11-A), oxygen saturation was significantly affected by treatment [F$_{3, 1584}$ = 1246, P < 0,0001], time [F$_{71, 1584}$ = 22.63, P < 0.0001] and time × treatment interaction [F$_{213, 1584}$ = 6.819, P < 0.0001]. Comparison of the mean effect among FENT, ACRYLF, OCF and FUF (Fig. 11-C) revealed significant differences in the action of each substance at different doses [significant effect of treatment F3, 60 = 176.9, p < 0.0001], dose [F 2, 60 = 277.9, P < 0.0001] and dose × treatment interaction [F6, 60 = 26.51, P < 0.0001]. In contrast to FENT, ACRLF and OCF, FUF did not affect the oxygen saturation over the dose range 0.1–6 mg/kg. FENT and ACRLF were more effective than OCF at the doses of 0.1 and 6 mg/kg while FENT was more effective than ACRYLF and OCF at the dose of 1 mg/kg.

Pre-treatment with NLX (6 mg/kg i.p; Fig. 11-B) partially prevented by FENT (6 mg/kg) SpO$_2$ changes. Injection of a second dose of NLX (6 mg/kg i.p; Fig. 11-B) totally blocked the inhibitory effects induced by FENT [treatment [F$_{3, 1440}$ = 2508, P < 0.0001], time [F$_{71, 1440}$ = 11.58, P < 0,0001] and time × treatment interaction [F$_{213, 1440}$ = 9.521, P < 0.0001]. Similar to FENT, injection of a second dose of NLX (6 mg/kg i.p; Fig. 11-D) totally prevented the inhibitory effects induced by ACRYLF, OCF and FUF.

4. Discussion

Our study presents novel results regarding the in vitro and in vivo characterization of ACRYLF, OCF and FUF, three FENT analogues that have recently emerged as NPS. In vitro, in the calcium mobilization assay the three FENS were able to activate the mu opioid receptor in a concentration dependent manner and all compounds were able to elicit maximal effects similar to that of dermorphin, with the exception of FUF that behaved as a partial agonist. In the BRET G-protein assay, all compounds, including FENT, mimicked the maximal effects of dermorphin. FENT, ACRYLF and OCF behaved as partial agonists for the β-arrestin 2 pathway in comparison to dermorphin whereas FUF was inactive in promoting β-arrestin 2 recruitment. In vivo, all compounds increased mechanical and thermal analgesia, altered motor performance (facilitation at low and inhibition at higher doses) and impaired cardiorespiratory parameters in mice. Of note, FUF showed lower potency for inhibiting cardiorespiratory function and exerted only a monophasic inhibitory action on motor activity. NLX sensitivity of the actions of FENT and its derivatives was variable depending on both the biological function examined and substance used.

4.1. Analgesic effects

The efficacy of FENT as a potent analgesic has been extensively documented in preclinical and clinical studies. The new FENS have also been investigated for their analgesic properties. Our study demonstrates that FENT and its derivatives induce a dose-dependent increase in the threshold to acute mechanical and thermal pain stimulus. Comparison of the dose response curves in the tail pinch (Fig. 2) and withdrawal (Fig. 4) tests demonstrated no major differences in term of analgesic potency between FENT, ACRYLF and FUF. OCF showed the highest ED$_{50}$ value and shorter duration of action. This is in line with previous findings since OCF has been reported to have a shorter duration of action in the mouse hot-plate test compared to FENT (Bagley et al., 1991). However, contrary to our findings, Bagley et al. showed a higher potency of OCF in comparison to FENT in this test. The difference in potency could be related to differences in experimental protocols and the species used (Baumann et al., 2018). Moreover, our data demonstrated analgesic efficacy of FUF corroborating previous findings that suggested high analgesic potency after i.v. administration in the mouse hot plate test (Huang et al., 1986). Pre-treatment for 15 min with 6 mg/kg NLX did not prevent the antinociceptive effect of 6 mg/kg of FENT, ACRYLF, OCF and FUF (Fig. 3-B and D). In the tail pinch test, the pre-treatment seemed to significantly reduce the analgesic effect of FUF but not the other compounds. Neither the second injection of 6 mg/kg of NLX at 55 min of treatment blocked the threshold to mechanical analgesia in mice (Fig. 3-D). The antagonist profile of NLX is somewhat different in the tail withdrawal test (Fig. 4). In fact, the pre-treatment with 6 mg/kg with NLX fully prevented the thermal analgesia induced by FUF and significantly reduced the analgesic effect with the other compounds, the second dose of NLX totally blocked thermal analgesia induced by FENT, ACRYLF and OCF (Fig. 4-B and D). These results confirm the involvement of mu opioid receptors in the analgesia induced by FENT and its analogues. Indeed, a recent study using genetically-engineered mice lacking specific splice variants of MOR-1(E1/E11 KO mice) revealed that butyrylfentanyl and other opioids failed to promote analgesic effects in the radiant heat tail flick test when compared to the wild type mice (Baumann et al., 2018).

A difference in pharmacokinetics of these molecules has been noticed in both tests, where OCF showed a short analgesic action in respect to other molecules and these differences could be related to their chemical structures (Wilde et al., 2019; Varshneya et al., 2022). Moreover, the higher efficacy of NLX in blocking the analgesic effects of the FENT, ACRYLF and OCF in the tail withdrawal test compared to the tail pinch test could be related to differences in the intensity of the nociceptive stimuli that results in differences in NLX efficacy for blocking pain sensitivity in the two tests (Le Bars et al., 2001). The mechanisms by which opioids induce analgesia have been widely studied in animal models (Lazorthes et al., 1986; Besson et al., 1992; Stein et al., 2003; Aoki et al., 2014) and have confirmed that mu agonists produce

analgesia through both pre- and postsynaptic mechanisms at multiple CNS sites (Torrecilla et al., 2002). Moreover, it has been well documented that opioids can directly block pain transmission at the spinal cord level, acting on primary afferents (Wall, 1967; Zollner et al., 2003; Sun et al., 2020) and nociceptive relay neurons in the dorsal horn (Glaum et al., 1994).

4.2. Motor effects

Systemic administration of FENT, ACRYLF, OCF and FUF dose-dependently affects the motor performance in mice (Fig. 5). The data obtained in the accelerod test show a biphasic effect of all FENS but not for FUF (Supplementary Fig. 5). However, in the drag test (Fig. 6-C), the effect of all compounds was only inhibitory with the following rank of ED_{50}: FUF ($ED_{50} = 5.07$ mg/kg) = OCF ($ED_{50} = 5.11$ mg/kg) > ACRYLF ($ED_{50} = 7.82$ mg/kg) $\geq$ FENT ($ED_{50} = 13.93$ mg/kg). As reported in our previous study opioid agonists elicited variable effects in the accelerod and drag test (Bilel et al., 2020). Hence, the data obtained in the accelerod test are in accordance with a recent study by Varshneya and colleagues. It has been reported in the spontaneous locomotion test that FENT at the dose of 1 mg/kg induces hyperlocomotion which is inverted at higher doses (Varshneya et al., 2019). In rodents, opioids can induce a biphasic effect depending on the dose, the time after injection and the test used (Esrawi, 1998; Rodriguez-Arias et al., 2000; Bilel et al., 2020; Pesavento et al., 2022). The interaction of the opioidergic system with other systems like the dopaminergic and serotonergic systems are still under investigation. Yet, one of the mechanisms related to the facilitation of locomotion by opioid agonists is triggered by the activation of the mesolimbic dopaminergic system which is regulated by the endogenous opioid system, controlling the release of dopamine in the nucleus accumbens (Di Chiara & Imperato, 1988; Matsui et al., 2014). Indeed, a recent elegant study revealed that the highly potent FENT interacts with dopamine (D_1 and D_4) receptors in the low micromolar range (Torralva et al., 2020). Moreover, FENT activates serotonin receptors (5-HT1A) at low concentrations (Martin et al., 1991; Torralva et al., 2020). Yet, FENT, ACRYLF and OCF could increase locomotion involving the opioid-serotonin system (Gurtu et al., 1990). The pre-treatment with NLX did not block the inhibitory effects induced by all FENS on the motor performance of mice. The injection of the second dose at 55 min prevented the inhibitory effects induced by FENT and FUF but not that induced by ACRYLF and OCF (Fig. 5-D). These data suggest that the chemical substituent of FENT analogues could play an important role on their opioid receptor occupancy in response to various tests (Wikle et al., 2019; Varshneya et al., 2019, 2022).

The results obtained in the drag test (Fig. 6) revealed a dose-dependent reduction in the number of steps of all compounds. The drag test evaluates the ability of the mouse to balance its body posture using its forelimbs in response to a dynamic stimulation imposed by "tail dragging". Pre-treatment with NLX did not block the inhibitory effects induced by all FENS in the drag test. The injection of the second dose at 55 min did not prevent the inhibitory effects induced by all compounds (Fig. 6-D). In addition to the pharmacokinetic differences of these molecules, the results obtained with NLX antagonism in the drag test suggest a non-opioid mechanism that could be activated by these FENS in the test of motor coordination (Hustveit, 1994; Kitamura et al., 2016; Torralva et al., 2020).

We also hypothesized that the number of steps were reduced due to the muscle rigidity as previously reported with other opioids (Bilel et al., 2020). Muscle rigidity has been majorly reported in cases with respiratory depression after FENT use (Torralva and Janowsky, 2019). Indeed, FENS may produce a rigidity in the diaphragm, chest wall, and upper airway, known as wooden chest syndrome (WCS) (Çoruh et al., 2013; Torralva and Janowsky, 2019). Unexpectedly, the grip strength test (Fig. 7) revealed an inhibition of the muscle strength after the injection of all the compounds in a dose-dependent manner and the effect persisted with higher doses (6 and 15 mg/kg) for the whole observation

period. The analysis of our results by all the operators shows that the animals were not able to grip the grid and this could be related to hypo-tonicity of the muscles (Chaillet et al., 1983; Weinger et al., 1988; Lui et al., 1989). Indeed, as discussed below, the three opioids induced very important impairment of cardiovascular parameters that could potentially elicit a decrease of muscle strength. On this basis we speculate that the grip strength test is not predictive for muscle rigidity in case of FENS and could lead to false interpretations. Pre-treatment with NLX totally prevented inhibitory effects in the grip strength test and this data reveals that mu opioid receptors are responsible of the hypotonic tone in mice. Opioids and in particular FENS could induce hypotonic immobility in mice through the mu receptors located in the nucleus raphe pontis and the caudate nucleus (Blasco et al., 1966). Moreover, it has been demonstrated that supraspinal delta-1 and kappa-1 play an important role in inducing muscle rigidity after FENT administration (Vankova et al., 1996). Fentanyl's interacts with cholinergic system by blocking the acetylcholine release. This mechanism could be blocked by mu antagonists like NLX (Sakai et al., 2002). Indeed, the cholinergic system could also be involved in the alterations of the muscles activity of mice after FENS injections (Sakai et al., 2002; Sohn et al., 2004).

4.3. Cardio-respiratory effects

Cardiorespiratory alterations in preclinical studies following the administration of opioids, particularly FENT's have been well established (Yadav et al., 2018; Hill et al., 2020). We have demonstrated using the MouseOX instrument that FENT, ACRYLF, OCF and FUF significantly and dose-dependently altered the cardiorespiratory parameters (Figs. 8–11) when administered to mice in the range doses 0.1–6 mg/kg. FUF did not alter pulse distention (data not shown). Pre-treatment with a single dose of NLX did not fully prevent bradycardia (Fig. 8-D) and vasodilatation (PD; Fig. 9-D) induced by these opioids, while the second dose of NLX reversed these alterations. Our data demonstrate the role of mu receptors in cardiovascular function (Varshneya et al., 2022). Many clinical studies have reported cardiovascular symptoms after FENT injection, including bradycardia and hypotension, QTc interval prolongation myocardial ischemia (Doshi et al., 2019; Helander et al., 2017). A recent study in USA revealed that of 430 patients hospitalized with opioid overdose found an association with ischemic events, heart failure, and arrhythmias (reviewed in Frisoni et al., 2018; Krantz et al., 2021). The mechanism by which opioids induce bradycardia have been reported in our previous study (Bilel et al., 2020). Moreover, all the opioids reduced respiratory rate and Oxygen saturation (Figs. 10 and 11). FUF showed lower efficacy in respect to the other molecules in the BR (Fig. 10-C) and no effect on the SpO2 saturation. In accordance with our data, Varshneya et al. demonstrated that 3-FUF induced hypoventilation with an efficacy ($ED_{50} = 2.6$ mg/kg) lower than Fentanyl ($ED_{50}..0.96$; Varshneya et al., 2022). These data reveal the role of the furan structure in changing the activity of FENT (Eshleman et al., 2020). A second dose of NLX was also needed to reverse respiratory depression by FENS confirming preclinical studies (Yadav et al., 2018; Hill et al., 2020) and clinical reports from studies showing that high NLX doses may be required to reverse FENT overdose (Rzasa Lynn and Galinkin, 2018; Somerville et al., 2017). One of the mechanical mechanisms by which opioids induce respiratory depression is the chest wall rigidity (Çoruh et al., 2013). The mechanism has shown that it is mediated by activation of mu receptors (Vankova et al., 1996; Soares et al., 2014; Varshneya et al., 2022).

FUF seemed to be the FENT derivative with lower cardiovascular toxicity in respect to ACRYLF and OCF. Various mechanisms have been suggested to understand how FENT alters cardio-respiratory function. A recent study revealed a role of β–arrestin 2 in heterologous desensitization of cardiac-β-adrenergic receptors (βAR) that could impair cardiac function and demonstrated that the ablation of β-arrestin 2 gene rescues β -adrenergic stimuli-induced myocyte contractile function (Shi et al., 2017). Moreover, it is well established that hypoxemia induced

vasodilatation in humans is attributed by β adrenergic receptors (Blauw et al., 1995). Thus the alterations of pulse distention and Oxygen saturation induced by FENT, ACRYLF and OCF but not FUF could be attributed to a crosstalk between β adrenergic receptors and mu opioid receptors via β arrestin 2 signaling in the cardiovascular system (Shi et al., 2017; Gill et al., 2019; Torralva et al., 2020).

4.4. Comparison of the profile of action of FENS

Our in vivo experiments revealed differences in the pharmacotoxicological profile of the compounds tested (Fig. 12). In particular, ACRYLF behaved more similarly to FENT than the other compounds. It has been suggested that the acrylamide moiety of ACRYLF could lead to irreversible receptor binding and higher toxicity (Essawi, 1999). However, our in vitro results demonstrate full agonism for ACRYLF with a similar potency to FENT at mu receptors. Moreover, in vivo, ACRYLF induced the same effects to FENT in analgesia, motor and cardiorespiratory changes. These results suggest that the addition of acrylamide moiety to FENT may not induce significant changes in the FENT pharmacodynamics (Watanabe et al., 2017). In contrast, OCF showed a lower potency in vitro while in vivo the effects of OCF were different in the physiological and behavioural tests. Interestingly the analgesic effect of OCF was relatively short lasting while its actions on motor and cardiorespiratory functions were persistent. The differences in toxic effects of OCF compared to FENT in animals and humans are still under debate. Preclinical studies suggested lower toxicity of OCF (Huang et al., 1986; Bagley et al., 1991) while clinical studies did not (Fletcher et al., 1991). Ocfentanyl has two modifications compared to FENT: replacement of the propionamide group with a methoxyacetamide and the addition of ortho-fluorine to the N-phenyl ring. Our data suggest that these modifications could be responsible for the changes in the pharmacodynamics of OCF especially in cardiorespiratory function which suggests high respiratory and cardiac toxicities that could induce major fatalities (Coopman et al., 2016; EMCDDA, 2017).

Furanylfentanyl is the compound displaying the most divergent pharmacological profile compared to FENT and the other analogues. In fact, in vivo FUF was the only compound with no motor stimulatory effects and the only compound that did not alter pulse distention and oxygen saturation in cardiorespiratory measurements. Moreover, FUF displayed a distinct pharmacological profile also in vitro acting as

partial agonist in calcium mobilization studies and as a mu agonist strongly biased toward G protein in BRET studies. This profile for FUF is worthy of further discussion. Classical studies of the Bohn research group performed using β-arrestin 2 gene knockout mice (βarr2(−/−)) suggested that the analgesic properties of mu agonists depend on G protein signaling while side effects such as respiratory depression and constipation on βarr2 signaling (Bohn et al., 1999; Raehal et al., 2005). The logical consequence of this hypothesis is that mu receptor agonists biased toward G protein may act as safer opioid analgesics. This has been corroborated through the identification of novel mu ligands including oliceridine (TRV130) (DeWire et al., 2013), PZM21 (Manglik et al., 2016) and SR-17018 (Schmid et al., 2017) that behaved in vitro as G protein biased agonists and displayed in vivo a larger therapeutic index compared to classical opioid drugs such as morphine or FENT. Importantly oliceridine has recently been approved by the FDA for intravenous use in moderate to severe pain in adults (Lambert and Calò, 2020). However, recent data questioned the above mentioned hypothesis. In fact, the higher therapeutic index of morphine in βarr2(−/−) mice has not been confirmed by a consortium of three laboratories (Kliewer et al., 2020). Moreover, a very elegant study demonstrated that mice genetically engineered with G-protein-biased mu receptors display increased sensitivity to both the analgesic actions and side effects of opioid drugs (Kliewer et al., 2019). In addition, a very rigorous pharmacological study comparing the in vitro and in vivo actions of opioid drugs including oliceridine, PZM21, and SR-17018 demonstrated a robust correlation between their therapeutic indices and their efficacies, but not their bias factors (Gillis et al., 2020a). Therefore, the importance of biased vs partial agonism in the search for safer opioid analgesics is still an open question (Azevedo Neto et al., 2020, 2021; Gillis et al., 2020b; Vandeputte et al., 2020). We propose that FUF should be added to the panel of mu receptor ligands useful for performing further studies in this very important field of research.

Tolerance is an important factor that is highly implicated on opioid abuse. Indeed, it is well documented that FENT induces tolerance and physical dependence in a rapid and robust manner compared to morphine and other opioids (Bohn et al., 2004; Raehal and Bohn, 2011). Moreover, it has been reported in a recent elegant study the role of β-arrestin 2 in the severity of antinociceptive tolerance and physical dependence (Raehal and Bohn, 2011). Yet, FENT analogues in particular ACRYLF and OCF can induce tolerance and dependence in abusers like
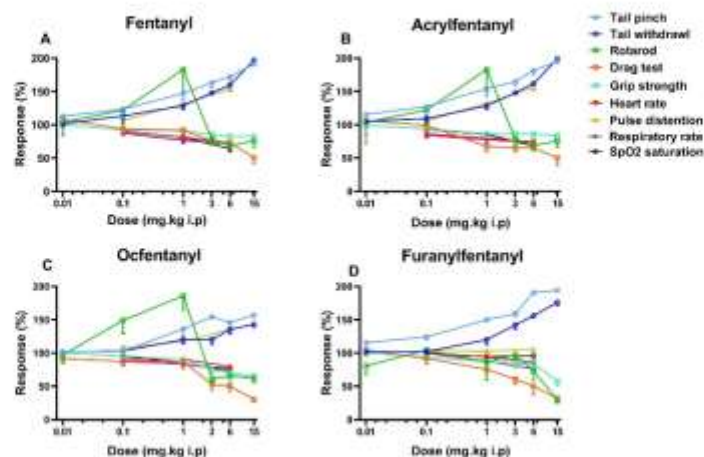

Fig. 12. Dose response curves to FENT (panel A), ACRYLF (panel B), OCF (panel C) and FUF (panel D) on the tail pinch test, tail withdrawal test, accelerod, drag test, grip strength and cardiorespiratory parameters (heart rate, pulse distention, respiratory rate and oxygen saturation) in mice.

13

82

FENT via intracellular mechanisms that involves β-arrestins signaling (Bohn et al., 2004; Raehal& Bohn, 2011) and thus increasing their risk of abuse toxicity and death with overdose (Helmiler et al., 2017; Kuczyńska et al., 2018; Frisoni et al., 2018). Future studies on tolerance of FENS are needed to better understand their abuse liability.

4.5. Naloxone antagonism

The present findings demonstrate that the analgesic, motor and cardiorespiratory actions of FENT as well as of FENS are sensitive to NLX; this suggest the involvement of opioid receptors, particularly the mu receptor, in these actions. However, NLX efficacy in blocking the effects of FENS was variable in the different assays. At this regard it should be underlined that NLX behaves as a competitive opioid receptor antagonist therefore its final effect depends on the relative antagonist/ agonist ratio of concentrations in the brain areas controlling the different functions (Nakamura et al., 2020; Walker et al., 2021). Indeed, many factors are involved in FENT 's affinity for and the kinetics of its association and dissociation with the opioid receptor which greatly impact its reversal by naloxone (Yassen et al., 2007; Varshneya et al., 2022). Naloxone transfers and equilibrates rapidly between the plasma and the brain, and has a blood effect-site equilibration half-life of 5 min comparable to that of FENT. Yet, in rats, the brain mu receptors occupancy by intravenous (IV) NLX was greater than 90% at 5 min for clinically relevant doses of IV administered NLX (0.035 mg/kg, Human Equivalent Dose (HED) 0.4 mg; 0.17 mg/kg, HED 2 mg). Only 50% occupancy remained at 27.3 min and at 85 min after 0.035 mg/kg and 0.17 mg/kg NLX, respectively (Research report by Kang et al., 2022). In humans a dose of 1 mg in an 80 kg individual of NLX will occupy 50% of available receptor sites in the human brain and since NLX is a competitive antagonist at the mu-opioid receptor, this dose may be insufficient to reverse toxicity (respiratory depression) due to very large doses of FENS and their higher affinity for the mu-opioid receptor, in which very few opioid binding sites remain unoccupied (Yassen et al., 2007). Moreover, it is suggested in clinical cases of FENT overdose to use a repeat NLX dosing in order to avoid the reappearance of the effects (Klebacher et al., 2017). Thus the above mentioned evidences may likely explain the different effects of NLX in blocking FENS actions in comparison with other opioids e.g. morphine (Bilel et al., 2020). On the other hand, our findings do not rule out that non-opioid mechanisms might be involved into the in vivo actions of FENS as suggested by recent studies (Baumann et al., 2018; Varshneya et al., 2022). This issue can be eventually addressed in future studies by comparing the in vivo actions of FENT and FENS in wild type and in mice knockout for the mu receptor gene.

5. Conclusions

The present study demonstrates that ACRYLF, OCF and FUF, behave similarly to FENT as mu opioid agonists. In contrast to FENT and the other analogues, FUF acts as a partial agonist in vitro at mu opioid receptors, and as G protein biased mu agonist; this is associated with lower potency in vivo in cardiorespiratory depression. Collectively our data reveal the high risk associated with the use of these compounds and the strong relationship between the chemical structure and the pharmacotoxicology of fentanyl analogues, a drug class playing an important role in the current opioid epidemic.

Credit author statement

Matteo Marti, Sabrine Bilel, Girolamo Calò contributed conception and design of the study. Sabrine Bilel, Micaela Tirri, Raffaella Arfè, Tatiana Bernardi, Federica Boccuto, Beatrice Marchetti, Giorgia Corli performed in vivo experimental section. Joaquim Azevedo Neto, Davide Malfacini performed in vitro experimental section. Matteo Marti, Sabrine Bilel, Girolamo Calò wrote the manuscript. Giovanni Serpelloni, Fabio De-Giorgio, Rosa Maria Gaudio, edited sections of the manuscript. Sabrine Bilel, Matteo Marti, Micaela Tirri, Raffaella Arfè, Tatiana Bernardi, Federica Boccuto performed statistical analysis. Matteo Marti, Sabrine Bilel, Girolamo Calò and Davide Malfacini contributed to manuscript revision, read and approved the submitted version.

Ethical statements

All applicable international, national and/or institutional guidelines for the care and use of animals were followed. All procedures performed in the studies involving animals were in accordance with the ethical standards of the institution or practice at which the studies were conducted. Project activated in collaboration with the Presidency of the Council of Ministers-DPA Anti-Drug Policies (Italy).

Declaration of competing interest

The Authors declare no conflict of interest.

Appendix A. Supplementary data

Supplementary data to this article can be found online at https://doi.org/10.1016/j.neuropharm.2022.109020.

References

EMCDDA, 2016. European Drug Report 2016: Trends and Developments. Publications Office of the European Union, Luxembourg.

EMCDDA, 2017. European Drug Report 2017: Trends and Developments. Publications Office of the European Union, Luxembourg.

EMCDDA, 2019. European Drug Report 2019: Trends and Developments. Publications Office of the European Union, Luxembourg.

Aoki, Y., Mizoguchi, H., Watanabe, C., Takeda, K., Sakurada, T., Sakurada, S., 2014. Potential involvement of mu opioid receptor dysregulation on the reduced antinociception of morphine in the inflammatory pain state in mice. J. Pharmacol. Sci. 124 (2), 258–266. https://doi.org/10.1254/jphs.13242fp.

Azevedo Neto, J., Costanzini, A., De Giorgio, R., Lambert, D.G., Ruzza, C., Calò, G., 2020 Aug 25. Biased versus partial agonism in the search for safer opioid analgesics. Molecules 25 (17), 3870. https://doi.org/10.3390/molecules25173870.PMID: 32854452;PMCID:PMC7504468.

Azevedo Neto, J., Ruzza, C., Sturaro, C., Malfacini, D., Pacifico, S., Zaveri Nurulain, T., Calò, G., 2021 March. Functional selectivity does not predict antinociceptive/ locomotor impairing potencies of NOP receptor agonists. Front. Neurosci. https://doi.org/10.3389/fnins.2021.657153.

Begley, J.R., Kudrna, I.V., Lalinde, N.L., Calogent, J.A., Huang, B. S., Lin, B. S., Jennni, T.P., Bennenga, M.J., Dunlay, B.M., Ouijon, M.H., Spaulding, T.C., Spencer, H.K., 1991. Evolution of the 4-anilidopiperidine class of opioid analgesics. Med. Res. Rev. 11 (4), 403–436.

Baumann, M.H., Majumdar, S., Le Rouzic, V., Hunkele, A., Uprety, R., Huang, X.P., Xu, J., Roth, B.L., Pan, Y.X., Pasternak, G.W., 2018. Pharmacological characterization of novel synthetic opioids (NSO) found in the recreational drug marketplace. Neuropharmacology 134 (Pt A), 101–107. https://doi.org/10.1016/j.neuropharm.2017.08.016.

14

83

Besson, J.M., Besse, D., Lombard, M.C., 1992. Opioid peptides and pain regulation studied in animal models. Clin. Neuropharmacol. 15 (Suppl. 1 Pt A), 52aS3a. https://doi.org/10.1097/00002082t.19920100100029.

Bilel, S., Azevedo, N.J., Arfè, R., Tirri, M., Gregori, A., Serpelloni, G., De Giorgio, F., Frisoni, P., Neri, M., Calò, G., Marti, M., 2020 Jul. In vitro and in vivo pharmacological characterization of the synthetic opioid MT-45. Neuropharmacology 171, 108110. https://doi.org/10.1016/j. neuropharm.2020.108110. Epub 2020 Apr 25. PMID: 32344007.

Bilel, S., Tirri, M., Arfè, R., Stimson, C., Fantinati, A., Cristofori, V., Bernardi, T., Boccuto, F., Cavallo, M., Cavalli, A., De-Giorgio, F., Calò, G., Marti, M., 2021. In vitro and in vivo pharmaco-toxicological characterization of 1-Cyclohexyl-x-methoxy-benzene derivatives in mice: comparison with tramadol and PCP. Int. J. Mol. Sci. 22 (14), 7659. https://doi.org/10.3390/ijms22147659.

Blasco, T.A., Lee, D., Amalric, M., Swerdlow, N.R., Smith, N.T., Koob, G.F., 1986. The role of the nucleus raphe pontis and the caudate nucleus in alfentanil rigidity in the rat. Brain Res. Oct 29;386 (1-2), 280-286. https://doi.org/10.1016/0006-8993(86)90164-2.PMID:3006494.

Blaszo, G.J., Westendorp, R.G., Simons, M., Chang, P.C., Frölich, M., Meinders, A.E., 1995. beta-Adrenergic receptors contribute to hyponatremia induced vasodilation in man. Br. J. Clin. Pharmacol. 40 (5), 453-458.

Bohn, L.M., Lefkowitz, R.J., Gainetdinov, R.R., Peppel, K., Caron, M.G., Lin, F.T., 1999. Enhanced morphine analgesia in mice lacking beta-arrestin 2. Science (New York, N. Y.) 286 (5449), 2495-2498. https://doi.org/10.1126/science.286.5449.2495.

Bohn, L.M., Dykstra, L.A., Lefkowitz, R.J., Caron, M.G., Barak, L.S., 2004. Relative opioid efficacy is determined by the complements of the G protein coupled receptor desensitization machinery. Mol. Pharmacol. 66 (1), 106-112. https://doi.org/10.1124/mol.66.1.106.

Camarda, V., Calo, G., 2013. Chimeric G proteins in fluorimetric calcium assays: experience with opioid receptors. Methods Mol. Biol. 937, 293-306. https://doi.org/10.1007/978-1-62703-086-1_18.

Canazza, I., Ossato, A., Trapella, C., Fantinati, A., De Luca, M.A., Margiani, G., Marti, M., 2016. Effect of the novel synthetic cannabinoids AKB48 and 5F-AKB48 on "tetrad", sensorimotor, neurological and neurochemical responses in mice. In vitro and in vivo pharmacological studies. Psychopharmacology (Berlin) 233 (21-22), 3685-3709. https://doi.org/10.1007/s00213-016-4402-y.

Chaillet, P., Marquis-Collado, H., Costentin, J., 1983 Nov 21. Catatonie or hypotonic immobility induced in mice by intracerebroventricular injection of mu or kappa opioid receptor agonists as well as enkephalins or inhibitors of their degradation. Life Sci. 33 (21), 2105-2111. https://doi.org/10.1016/0024-3205(83)90334-x.

Coopman, V., Cordonnier, J., De Leeuw, M., Cirimele, V., 2016. Ocfentanil overdose fatality in the recreational drug scene. Forensic Sci. Int. 266 (Suppl. C), 469-473. https://doi.org/10.1016/j.forsciint.2016.07.005.

Coruh, B., Tonelli, M.R., Park, D.R., 2013 Apr. Fentanyl-induced chest wall rigidity. Chest 143 (4), 1145-1146. https://doi.org/10.1378/chest.12-2131.

DeWire, S.M., Yamashita, D.S., Rominger, D.H., Liu, G., Cowan, C.L., Graczyk, T.M., Chen, X.T., Pitis, P.M., Gotchev, D., Yuan, C., Koblish, M., Lark, M.W., Violin, J.D., 2013. A G protein-biased ligand at the μ-opioid receptor is potently analgesic with reduced gastrointestinal and respiratory dysfunction compared with morphine. J. Pharmacol. Exp. Therapeut. 344 (3), 708-717. https://doi.org/10.1124/jpet.112.201616.

Di Chiara, G., Imperato, A., 1988. Opposite effects of mu and kappa opiate agonists on dopamine release in the nucleus accumbens and in the dorsal caudate of freely moving rats. J. Pharmacol. Exp. Therapeut. 244 (3), 1067-1080.

Dodd, S., Malhotra, M., Kanneganti, T., et al., 2019. Frequency of cardiovascular events and in hospital mortality with opioid overdose hospitalizations. Am. J. Cardiol. 124, 1528-1533.

Eshleman, A.J., Nagarajan, S., Wolfrum, K.M., Reed, J.F., Nilsen, A., Torralva, R., Janowsky, A., 2020 Dec. Affinity, potency, efficacy, selectivity, and molecular modeling of substituted fentanyls at opioid receptors. Biochem. Pharmacol. 182, 114293. https://doi.org/10.1016/j.bcp.2020.114293. Epub 2020 Oct 20. PMID: 33091380.

Essawi, M.Y.H., 1998. Synthesis of fentanyl analogues as nonequilibrium irreversible ligands for opioid receptors. Bull Fac Pharmacy (Cairo Univ) 36 (3), 39-45.

Essawi, M.Y.H., 1999. Fentanyl analogues with a modified propanamido group as potential affinity labels: synthesis and in vivo activity. Pharmazie 54, 307.

Fantinati, A., Ossato, A., Bianco, S., Canazza, I., De Giorgio, F., Trapella, C., Marti, M., 2017. 1-cyclohexyl-x-methoxybenzene derivatives, novel psychoactive substances seized on the internet market. Synthesis and in vivo pharmacological studies in mice. Hum. Psychopharmacol. 32 (3) https://doi.org/10.1002/hup.2560.

Fleicher, J.E., Sebel, P.S., Murphy, M.R., Mick, S.A., Fein, S., 1991. Comparison of ocfentanil and fentanyl as supplements to general anesthesia. Anesth. Analg. 73, 622-626. https://doi.org/10.1213/00000539.199111000.00019.

Frisoni, P., Bacchio, E., Bilel, S., Talarico, A., Gaudio, R.M., Barbieri, M., et al., 2018. Novel synthetic opioids: the pathologist's point of view. Brain Sci. 8 (9) https://doi.org/10.3390/brainsci8090170.

Gill, H., Kelly, E., Henderson, G., 2019. How the complex pharmacology of the fentanyls contributes to their lethality. Addiction 114 (9), 1524-1525. https://doi.org/10.1111/add.14614.

Gillis, A., Gondin, A.B., Kliewer, A., Sanchez, J., Lim, H.D., Alamein, C., Mananohar, P., Santiago, M., Fritzwanker, S., Schmiedel, F., Katte, T.A., Reekie, T., Grimsey, N.L., Kassiou, M., Kellam, B., Krasel, C., Halls, M.L., Connor, M., Lane, J.R., Schulz, S., Canals, M., 2020 a. Low intrinsic efficacy for G protein activation can explain improved side effect profiles of new opioid agonists. Sci. Signal. 13 (625) https://doi.org/10.1126/scisignal.aaz3140 eaaz3140.

Gillis, A., Kliewer, A., Kelly, E., Henderson, G., Christie, M.J., Schulz, S., Canals, M., 2020 b. Critical assessment of G protein-biased agonism at the μ opioid receptor. Trends Pharmacol. Sci. 41 (12), 947-959. https://doi.org/10.1016/j.tips.2020.09.009.

Glaum, S.R., Miller, R.J., Hammond, D.L., 1994. Inhibitory actions of delta 1-, delta 2-, and mu-opioid receptor agonists on excitatory transmission in lamina II neurons of adult rat spinal cord. J. Neurosci. 14 (8), 4965-4971.

Gurtu, S., 1990. Mu receptor serotonin link in opioid induced hyperactivity in mice. Life Sci. 46 (21), 1539-1544. https://doi.org/10.1016/0024-3205(90)90427-u.

Helander, A., Bradley, M., Hasselblad, A., Norlén, L., Vassilaki, I., Backberg, M., Lapins, J., 2017a. Acute skin and hair symptoms followed by severe, delayed eye complications in subjects using the synthetic opioid MT-45. Br. J. Dermatol. 176 (4), 1021-1027. https://doi.org/10.1111/bjd.15174.

Helander, A., Backberg, M., Signell, P., Beck, O., 2017 Jul. Intoxications involving acrylfentanyl and other novel designer fentanyls - results from the Swedish STRIDA project. Clin. Toxicol. 55 (6), 589-599. https://doi.org/10.1080/15563650.2017.1303141.

Hill, R., Santhakumar, R., Dewey, W., Kelly, E., Henderson, G., 2020 Jan. Fentanyl depression of respiration: comparison with heroin and morphine. Br. J. Pharmacol. 177 (2), 254-266. https://doi.org/10.1111/bph.14860. Epub 2019 Dec 23. PMID: 31499594; PMCID: PMC6989952.

Huang, B. S., Terrell, R.C., Deutsche, K.H., Kudzma, L.V., Lalinde, N.L., 1986. N-aryl-N-(4-piperidinyl) Amides and Pharmaceutical Compositions and Method Employing Such Compounds. U.S. Patent, New Providence, NJ, p. 4584393A. Assigned for.

Hustveit, O., 1994. Binding of fentanyl and pethidine to muscarinic receptors in rat brain. Jpn. J. Pharmacol. 64 (1), 57-59. https://doi.org/10.1254/jjp.64.57.

Kang, Yoma, Kelly, A., 24 January 2022. O'Omon, Andrew Kelleher et al. Naloxone's displacement of [11C]carfentanil and duration of receptor occupancy in the rat brain: implications. for opioid overdose reversal. https://doi.org/10.21203/rs.3.rs-1236438/v1. PREPRINT (Version 1) available at: Research Square.

Kenakin, T., 2004 Jan. Efficacy as a vector: the relative prevalence and paucity of inverse agonism. Mol. Pharmacol. 65 (1), 2-11. https://doi.org/10.1124/mol.65.1.2.PMID:14722230.

Kitanaka, S., Kawana, T., Kaniraga, S., Yamanaka, D., Teterra, H., Locordi, F.M., Yokoyama, M., 2016. Effects of fentanyl on serotonin syndrome like behaviors in rats. J. Anesth. 30 (1), 178-182. https://doi.org/10.1007/s00540-015-2092-y.

Klebacher, R., Harris, M.I., Artyapraksai, N., Tagore, A., Robbins, V., Dudley, L.S., Banter, R., Koners, S., Hill, R.D., Wasserman, E., Slanes, A., Merlin, M.A., 2017. Incidence of naloxone redosing in the age of the new opioid epidemic. Prehosp. Emerg. Care: official journal of the National Association of EMS Physicians and the National Association of State EMS Directors 21 (6), 682-687. https://doi.org/10.1080/10903127.2017.1335818.

Kliewer, A., Schmiedel, F., Sianati, S., Bailey, A., Bateman, J.T., Levitt, E.S., Williams, J. T., Christie, M.J., Schulz, S., 2019 Jan 21. Phosphorylation-deficient G-protein-biased μ-opioid receptors improve analgesia and diminish tolerance but worsen opioid side effects. Nat. Commun. 10 (1), 367. https://doi.org/10.1038/s41467-018-08162-1.PMID:30664663;PMCID:PMC6341117.

Kliewer, A., Gillis, A., Hill, R., Schmiedel, F., Bailey, C., Kelly, E., Henderson, G., Christie, M.J., Schulz, S., 2020. Morphine-induced respiratory depression is independent of β-arrestin2 signalling. Br. J. Pharmacol. 177 (13), 2923-2931. https://doi.org/10.1111/bph.15004.

Krantz, M.J., Palmer, R.B., Haigney, M.C.P., 2021 Jan 19. Cardiovascular complications of opioid use: JACC state-of-the-art review. J. Am. Coll. Cardiol. 77 (2), 205-223. https://doi.org/10.1016/j.jacc.2020.11.002. PMID: 33446314.

Kuczyńska, K., Grzonkowski, P., Kacprzak, L., Zawilska, J.B., 2018. Abuse of fentanyl: an emerging problem to face. Forensic Sci. Int. 289, 207-214. https://doi.org/10.1016/j.forsciint.2018.05.042.

Lambert, D., Calo, G., 2020. Approval of oliceridine (TRV130) for intravenous use in moderate to severe pain in adults. Br. J. Anaesth. 125 (6), e473-e474. https://doi.org/10.1016/j.bja.2020.09.021.

Lazorthes, Y., Verdie, J.C., Caute, B., Maranhao, R., Tafani, M., 1988. Intracerebroventricular morphinotherapy for control of chronic cancer pain. Prog. Brain Res. 77, 395-405. https://doi.org/10.1016/s0079-6123(08)62804-6.

Le Bars, D., Gozariu, M., Cadden, S.W., 2001 Dec. Animal models of nociception. Pharmacol. Rev. 53 (4), 597-652. PMID: 11734620.

Lemmens, H.J., 1995. Pharmacokinetic-pharmacodynamic relationships for opioids in balanced anaesthesia. Clin. Pharmacokinet. 29 (4), 231-242. https://doi.org/10.2165/00003088-199529040-00003.

Lai, P.W., Lee, T.Y., Chan, S.H., 1989 Jan 2. Involvement of locus coeruleus and noradrenergic neurotransmission in fentanyl-induced muscular rigidity in the rat. Neurosci. Lett. 96 (1), 114-119. https://doi.org/10.1016/0304-3940(89)90252-8.PMID:2564649.

Malfacini, D., Ambrosio, C., Grò, M.C., Sbraccia, M., Trapella, C., Guerrini, R., et al., 2015. Pharmacological profile of nociceptin/orphanin FQ receptors interacting with G-proteins and b-arrestins 2. PLoS One 10, e132865. https://doi.org/10.1371/journal.pone.0132865.

Manglik, A., Lin, H., Aryal, D.K., McCorvy, J.D., Dengler, D., Corder, G., Levit, A., Kling, R.C., Bernat, V., Hübner, H., Huang, X.P., Sassano, M.F., Giguère, P.M., Löber, S., Duan, Da, Scherrer, G., Kobilka, B.K., Gmeiner, P., Roth, B.L., Shoichet, B. K., 2016. Structure based discovery of opioid analgesics with reduced side effects. Nature 537 (7619), 185-190. https://doi.org/10.1038/nature19112.

Marti, M., Neri, M., Bilel, S., Di Paolo, M., La Russa, R., Ossato, A., Turillazzi, E., 2019. MDMA alone affects sensorimotor and prepulse inhibition responses in mice and rats: tips in the debate on potential MDMA unsafety in human activity. Forensic Toxicol. 37 (1), 132-144. https://doi.org/10.1007/s11419-018-0444-7.

Martin, D.C., Introna, R.P., Aronstam, R.S., 1991 Apr. Fentanyl and sufentanil inhibit agonist binding to 5-HT1A receptors in membranes from the rat brain.

84

Graphical Abstract to: Sensorimotor Alterations Induced by Novel Fentanyl Analogs in Mice: Possible Impact on Human Driving Performances
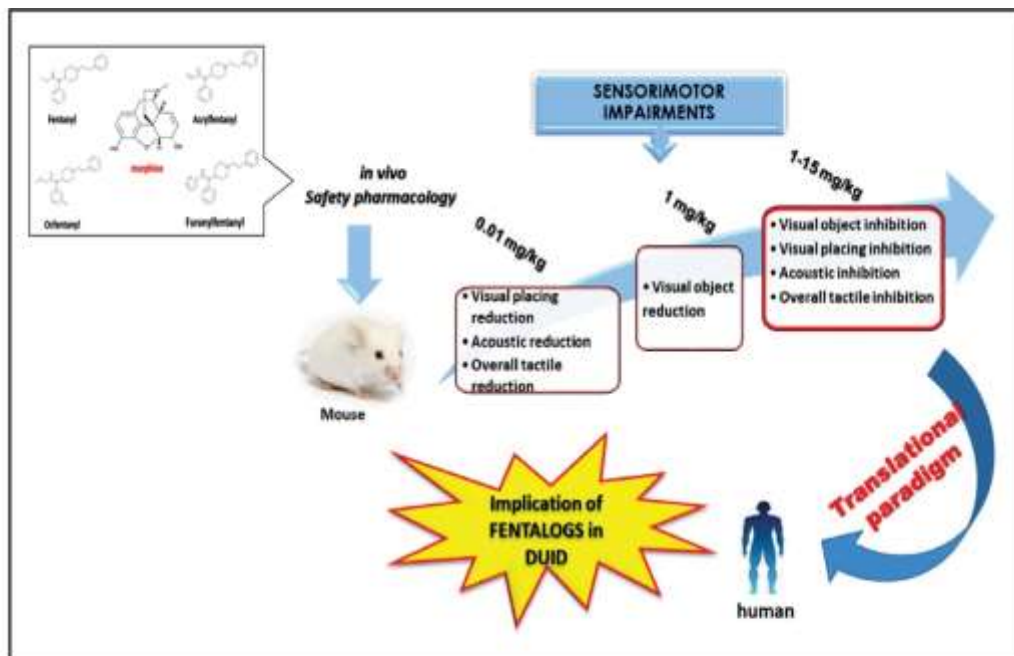
Acute systemic administration of Fentanyl analogs (0.01-15 mg/kg i.p.) induced a progressive impairment of the sensorimotor functions of mice. This preclinical data is in accordance with the data that emerged from the revision of the literature regarding experimental data on humans, driving under the influence of drugs and intoxication cases, suggesting that novel synthetic opioids might affect the psychomotor performances involved in driving.

REVIEW ARTICLE

Sensorimotor Alterations Induced by Novel Fentanyl Analogs in Mice: Possible Impact on Human Driving Performances

Sabrine Bilel[1,#], Arianna Giorgetti[2,#], Micaela Tirri[1], Raffaella Arfè[1], Virginia Cristofori[3], Beatrice Marchetti[1], Giorgia Corli[1], Lorenzo Caruso[4], Giorgio Zauli[5], Raffaele Giorgetti[6,•] and Matteo Marti[1,7,*,•]

[1]*Department of Translational Medicine, Section of Legal Medicine and LTTA Center, University of Ferrara, 44121 Ferrara, Italy;* [2]*Department of Medical and Surgical Sciences, Unit of Legal Medicine, University of Bologna, Via Irnerio 49, 40126 Bologna, Italy;* [3]*Department of Chemistry and Pharmaceutical Sciences, University of Ferrara, Italy;* [4]*Department of Environment and Prevention Sciences, University of Ferrara, Ferrara, Italy;* [5]*Research Department, King Khaled Eye Specialistic Hospital, Riyadh, Saudi Arabia;* [6]*Department of Excellence of Biomedical Science and Public Health, Faculty of Medicine, Polytechnic University of Marche, Ancona, Italy;* [7]*Collaborative Center of the National Early Warning System, Department for Anti-Drug Policies, Presidency of the Council of Ministers, Ferrara, Italy*

Abstract: Operating a vehicle is a complex task that requires multiple cognitive functions and psychomotor skills to cooperate. Driving might be impaired by licit or illicit drugs, including novel psychoactive substances (NPS) and novel synthetic opioids (NSO), the effects of which are still yet to be elucidated in humans. In the present work, a revision of the literature regarding the psychomotor impairing effects of Fentanyl (FENT) and three analogues (Acrylfentanyl, Ocfentanil and Furanylfentanyl) is presented, as emerged by experimental studies on humans, driving under the influence of a drug (DUID) and intoxication cases. An experimental study on a mouse model evaluated the sensorimotor alterations induced by FENT and the three fentalogs. Acute systemic administration of the four opioids (0.01-15 mg/kg i.p.) dose-dependently decreased the visual object and placing tests, the acoustic and the tactile responses of mice. The preclinical data are in accordance with the data that emerged from the revision of the literature regarding experimental data on humans, driving under the influence of drugs and intoxication cases, suggesting that novel synthetic opioids might affect the psychomotor performances on daily human tasks with a particular focus on driving.

1. INTRODUCTION

Driving under the influence of drugs (DUID) refers to the act of operating a vehicle following ingestion, inhalation, absorption, or injection of drugs or medications other than alcohol, that could interfere with the capacity to drive an automobile safely [1]. Driving is a complex task, where the driver continuously elaborates and responds to information received from the external surroundings, and requires several cognitive and psychomotor functions to cooperate [2]. Many substances, both licit and illicit, may cause impairment of driving performance, affecting the body and the behavior in

different ways. The most reported effects in cases of DUID consist of impairments of psychomotor skills and cognitive functions critical to driving, including vigilance, time and distance perception and monitoring, visual acuity, cognition, judgement and risk-taking behavior, reaction time, divided attention, keeping co-ordination and balance [2, 3]. A great alarm has been raised recently by the increase of DUID and traffic accidents due to the use of drugs. Cannabis was the illicit drug most frequently detected in cases of DUID, followed by cocaine while amphetamines and illicit opioids were less frequently detected. In addition to traditional substances, novel psychoactive substances (NPS) have also been related to DUID cases. Over the period from January 2019 to April 2020, 670 toxicology cases involving 46 individual NPS were reported to the UNODC. Of these cases, 62% were classified as DUID [4]. Synthetic cathinones are the most frequently detected NPS in Europe together with synthetic cannabinoids. However, the reports regarding the involvement

*Address correspondence to this author at the Department of Translational Medicine, Section of Legal Medicine and LTTA Center, University of Ferrara, 44121 Ferrara, Italy; Tel: +39 0532 455781; Fax: +39 0532 455777; E-mail: matteo.marti@unife.it
#These authors contributed equally to the work and can be all considered first authors.
•These authors share the seniorship.*

of other NPS in DUID cases are very limited. Many NPS cannot be detected in road and toxicological tests and that could be a good reason for a driver to consume NPS rather than traditional compounds [5].

Novel Synthetic Opioids (NSO) is a growing class of NPS that consists of 67 compounds monitored by the European Monitoring Centre for Drug and Drug Addiction (EMCDDA) from 2009 and 2020, including 10 molecules that emerged just in 2020 [6]. Opioids, particularly in the setting of non-therapeutic consumption, have been reported to impair cognitive function, induce drowsiness, and increase crash risk [7]; however, little is known regarding the effects of NSO on drivers and psychomotor performances relevant for operating a vehicle. The highly potent synthetic fentanyl have also been reported in cases of DUID [3]. These substances are structurally and pharmacologically related to fentanyl (FENT) with some substitutions. Fentanyl derivatives (FENS) are sold as fentanyl substitutes, as heroin, and as contaminants in counterfeit prescription drugs. Among them, Acrylfentanyl (ACRYLF), Ocfentanil (OCF), and Furanylfentanyl (FUF; Fig. 1) have been found in cases of DUID in Europe [3].

The present study showcases a literature review regarding the psychomotor effects connected to ACRYLF, OCF, FUF and FENT, together with experimental data on animals administered the same compounds.
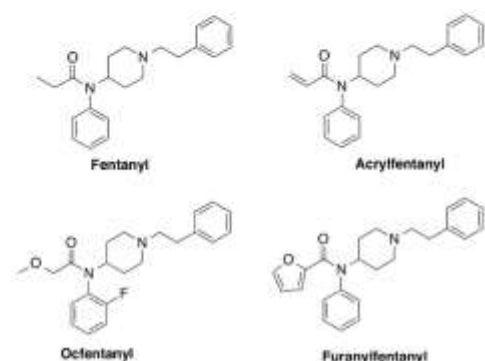
Fig. (1). Chemical structures of Fentanyl; Acrylfentanyl; Ocfentanyl and Furanylfentanyl.

2. PSYCHOMOTOR PERFORMANCES IN HUMANS - LITERATURE REVIEW

The study of psychomotor performances in humans is strongly affected on one side by ethical limitations in conducting experiments and on the other side by the biases connected to the interpretation of case reports, case studies and questionnaires. Due to the limited sample, experimental data are mostly lacking, and it is difficult to draw some scientific conclusions from case studies and case reports. Questionnaires and emergency departments evaluation might be only based on self-reported doses and symptoms, in the absence of forensic proof or analytical confirmation of consumption [8]. Some data might be obtained by postmortem examina-

tions and reports. However, the number of cases and deaths involving NSO is likely underestimated due to the limited availability of updated and validated methods capable of detecting them. The interpretation is further hampered by the low concentrations in biological samples and by the co-consumption of other drugs [9]. According to these limitations, the following information was extracted.

2.1. Experimental Studies in Human

No experimental studies on the human psychomotor performances after consumption of ACRYLF, OCF and FUF were available, although it is expected that their effect is similar to other narcotic-type analgesics [10]. Only experimental studies involving the administration of FENT, either transdermal or intravenous, were retrieved and are shown in Table 1.

Two studies tested psychomotor performances using driving simulators or driving tests. The study of Menefee *et al.*, by a driving simulator, demonstrated no difference before and after the administration of slowly increasing doses of FENT (over a period of 4 weeks). However, the study was conducted on patients who were administered a chronic opioid treatment for non-cancer pain, with doses of up to 15 mg of oxycodone [11]. Also, mental flexibility, memory recall and attentiveness were shown by testing patients with psychomotor performances [11]. Similar results were obtained when testing patients enrolled in long-term non-cancer pain treatment: a non-inferiority was demonstrated with respect to controls, once those patients taking additional unreported drugs were excluded. No significant effect was seen on attention, reaction, visual orientation, motor co-ordination and vigilance [3, 12]. This is expected, given the well-described mechanisms of tolerance in opioids and FENT users [13, 14]. As shown for prescription opioids, it is likely that the recreational use of NSO, alternating high doses and abstinence periods, might result in a lower tolerance development and in a higher risk for driving [2].

Another driving simulator performance study only involved FENT in co-administration with ketamine. Due to this co-consumption and to the difficulties in relating results with other studies, this was not included in our Table [15].

A tracometer (steering task) was used on healthy volunteers administered 100 µg of intravenous FENT, and showed an impact of FENT, especially on the correct reaction time, *i.e.* the length of time to make a cognitive decision of which way to move the target. Motor impairment was seen until 120 minutes, with heavier effects than after the administration of diazepam [16]. With the same concentration and administration route, another study showed that the eye-hand co-ordination test was hampered 15 minutes after the administration of 0-100 µg/70 kg of FENT, though the eye-hand co-ordination returned to normal levels after 60 minutes [17].

An association between plasma levels and psychomotor performances was shown by Veselis *et al.*, who demonstrated impairment in all the tested psychomotor performances starting from a plasma concentration of 2.5 ng/mL, with effects on memory and visual processing even at lower concentrations [18]. On the contrary, the previous work of Ghoneim *et al.*, with the administration of FENT at 200 µg,

Table 1.   Experimental studies.

Author	Substance	Study	Sample	Dose, Duration, Levels	Performance Tested	Results
Ghoneim et al., 1975 [19]	FENT iv	Placebo- and diazepam-controlled, pretest-posttest	10 healthy volunteers (M)	0.1-0.2 mg at weekly intervals	Backward Digit Span, Tapping Board, Serial Learning, Short-Term Memory, Delayed Recall, Simple Reaction Time, Choice Reaction Time, Visual Retention Test at 2, 6 and 8 h	0.2 mg of FENT affected Digit Span and Tapping board at 2h
Stevenson et al., 1986 [16]	FENT iv	Placebo- and diazepam-controlled, double-blind, crossover design	9 healthy volunteers (5M, 4F)	0.1 mg	Tracometer (steering task) measuring reaction time, nonovershoot movement time, total response time, overshoot movement time, frequency of errors, frequency of overshoots	Effect of both drugs in all tests, with slower reaction times with FENT, compared to diazepam
Veselis et al., 1994 [18]	FENT iv	Placebo-controlled, randomized, pretest-posttest	9 healthy volunteers (5M, 4F)	1, 1.5, 2.5 ng/mL	Memory by Rey Auditory-Verbal Recall Task (Rey AVLT), Picture Recall. Psychomotor by Critical Flicker Fusion Task (CFFT), Choice Reaction Time (CRT), Digit Symbol Substitution Test (DSST), Serial Numbers (SN)	Dose-dependent effects on memory. Below 2.5 ng/mL, only alteration of CFFT. Over 2.5 ng/mL, all performances were altered, with a decrement of 15-30%
Zacny et al., 1992 [17]	FENT iv	Placebo-controlled, randomized, double-blind, crossover design	13 healthy volunteers (10 M, 3 F)	0-0.1 mg/70 kg	Maddox Wing (MW), auditory reaction time (ART), eye-hand co-ordination. Tests at 15 and 60 min post-injection	Altered eye-hand co-ordination 15 min post-injection. No other effect
Schneider et al., 1999 [20]	FENT	Placebo-controlled	24 healthy volunteers (M)	0.2 μg/kg, with plasma level of 1.91 ± 1.17 ng/mL after 15 min and 0.67 ng/mL ± 0.23 after 30 min	Divided attention, reaction time measurement (Vienna Reaction Time), signal detection, sustained attention (Pauli test), memory (WIT)	Significant differences in reaction time in response to auditory input, signal detection hit, sustained attention and memory by using a distractor
Jamison et al., 2003 [21]	FENT td	Prospective, oxycodone-controlled, pretest-posttest	144 patients with low back pain (39.6% F)	Average 42.6 μg± 19.0 and 43.7 μg ± 21.7	DSST and Trail Making Test-B 90 and 180 days after administration	Improvement of psychomotor performances
Sabatowski et al., 2003 [12]	FENT td	Prospective, case-control, randomized	30 patients with chronic non-cancer pain (18 M, 12 F) vs. 90 healthy subjects	Median 50 μg/hour, 44 days, 1.35 ng/mL	Attention test (COG), test for reaction time under pressure or determination test (DT), test for visual orientation (TAVT), test for motor co-ordination (2-Hand), vigilance test (VIG)	Non-inferiority with respect to control
Menefee et al., 2004 [11]	FENT td	Prospective, single group pretest-posttest	23 patients (17 M, 6 F) on short-acting opioids (up to 15 mg oral oxycodone) for chronic non-cancer pain	Increase of 25 μg/h per week for 4 weeks (maximum dose 125 μg/h)	Driving task for simple braking reaction time, cue recognition reaction time, destination driving, and evasive action, visual motor tracking/mental flexibility by the Trail Making test A and B, memory by Rey Complex figure test and recognition trial and WMS-III. Attention by d2 Test of Attention and CPT-II. Balance by Berg Balance Test	No difference pre-post FENT for driving tasks. No decrease in performance, but improvement in mental flexibility, immediate and 20-minute memory recall, focus and attentiveness

Abbreviations: FENT: fentanyl. M: males. F: females. iv: intravenous. td: transdermal. h: hours. min: minutes. Wilde intelligence test (WIT) Weschler Memory Scale-III Spatial Span test (WMS-III) Conner's Continuous Performance Test II [CPT-II].

found little effect on memory, only with the Backward Digit Span and Tapping Board task [19]. However, in this study, the administration took place at weekly intervals, likely giving time for the central nervous system (CNS) to adapt to the administration of the drug.

In volunteers, FENT produced significant impairing effects on auditory reaction time, signal detection, sustained attention and some memory task performances even at doses of 0.2 μg/kg (thus, approximately 14 μg in 70-kg males). Despite the very low concentrations measured, around 1.91 ng/mL, these effects on psychomotor performances were seen in the absence of marked sedation [20].

Overall, the data obtained from the experimental studies seems to point to a severe impairing effect when FENT is

consumed by naïve users, while lower risk is expected in the context of a therapeutical administration. The effect of sex/gender was rarely evaluated in the revised articles. The study of Jamison *et al.*, [21] found no relationship between gender and outcome of the neuropsychological tests, although the evaluation was performed on patients and not on healthy volunteers. Although demographic data was available in some studies [11, 12] the effect of sex/gender was not assessed.

Ocfentanyl was selected for a clinical evaluation for its anesthetic effects and studies conducted on humans showed a potency 2.5 times higher than FENT and 200 times higher than morphine, with analgesic effects and sedation of 3 µg/kg of OCF comparable to that of 5 µg/kg of FENT [22]. Analgesic effect and respiratory depression peaked at 6 minutes and lasted approximately 1 hour [22], though this was not confirmed by [23].

Effects were dose-related, with a loss of consciousness described at around 2 µg/kg [22]. Moreover, it showed a lower tendency to accumulate in body tissues and fluids and a separation between hypnotic and analgesic ED_{50} values [24]. These depressant effects on the CNS functions suggest a likely impairing effect on psychomotor performances, despite the lack of experimental data.

2.2. Driving Under the Influence (DUID) of Opioids Cases

Strong opioids, including FENT, tested positive in 17.3% of fatal road crashes in Australia, but the relative contribution of FENT and the concentration of the detected substance were unknown [25]. In the Recommendations for Toxicological investigation of DUID fatalities, due to an increased prevalence of FENT registered by different laboratories, FENT was included in the mandatory substances to test, with a confirmation cut-off in the blood of 0.5 ng/mL [26]. Fentanyl was the most commonly detected drug (around 40%) of pedestrian/bicycle traumas in 2017-2019 [27] and in the USA FENT positive-DUID cases rose from 1% in 2014 to 5% in 2018, being 3% in 2019 [28]. An increase was also reported most recently, by the NMS Lab, that, by reviewing DUID cases over 11 years, revealed that 4.4% were positive for FENT, with a rise from 0.6% in 2010 to 12% in 2020 [29].

Considering also cases in which other drugs were detected, concentrations of FENT in these studies ranged from 0.1 to 157 ng/mL [28], until a maximum of 310 ng/mL [29].

Even though it was reported that the crash risk is not high for opioids, FENT included [30], among 20 cases of impaired driving with FENT-only intake reported by Rohrig *et al.*, 55% of drivers were found unresponsive in their vehicle, 55% left the roadway or lane of travel or showed erratic driving with unsteadiness, un-balance, impairment in walk and turn or one leg stand test, lethargy, and 8% involved a crash. Fentanyl median concentration was 3.7 ng/mL, ranging from 2.0 ng/mL to 16 ng/mL, thus 2 ng/mL was suggested as a starting level of impairment [28]. In the retrospective analysis performed by Hosokawa and Bierly, median FENT concentration tripled from 2010 (1.9 ng/mL) to 2020 (5.3 ng/mL) and the observations performed by the Drug Recognition Experts included poor balance (87%), poor coordination (80%), flaccid muscle tone (73%) slow speech and droopy eyelids (67% and 60%, respectively) [29].

It is worthwhile of consideration that in many cases of a road crash, FENT could be administered in the hospital after the road injuries [31], thus making challenging the evaluation of the prevalence of the substance within DUID cases as well as the estimation of its impact on psychomotor performances.

To the best of our knowledge, no real DUID case involving ACRYLF, OCF or FUF was described, although other fentanyl analogues, *e.g.* acetylfentanyl or butyrylfentanyl, were sometimes co-administered with FENT [29].

2.3. Intoxication Cases

Intoxications are another means to understand the effects of substances on those psychomotor performances which are important for driving. Several intoxications and fatal cases connected to FENT have been reported in the literature [32], with sudden collapse after inhalation of patch [33] or evidence of drowsy or altered mental state until coma. Motor weakness with as low as two patches was also reported among intoxication cases [34]. Since more abundant literature for FENT was found regarding experimental studies and cases of impaired driving, the present subsection will mainly focus on the other FENT-related molecules. Cases of intoxication by ACRYLF, OCF or FUF are reported in Table **2**.

Twenty-one intoxications associated with ACRYLF were reported by Sweden to the EMCDDA, even though no analytical confirmation was available [35]. This means that patients might have ingested other substances in addition to the analyte of interest. Reported symptoms included unconsciousness in 10 out 19 cases, while restlessness/anxiety was reported in 3 cases. Blurred vision was described only in 1 case, together with hallucinations, tiredness and muscular symptoms, but the victim also likely consumed stimulants.

This pattern of effects, mainly leading to various grades of CNS depression was confirmed in 8 intoxications (9 considering one involving also chloroisobutyrfentanyl) reported by the STRIDA project [36] and by a number of deaths, in which signs of respiratory depression were noted [37-39]. In both casuistries, ACRYLF was mainly consumed as nasal spray and, according to online and Intern forums, submilligram doses are enough to have psychoactive effects by this route [35, 36].

Particularly, case #1 had dizziness, paresthesia and tremor but no alteration of the reaction level scale (RLS; [42]), while cases #2, #5, #6, #7 and #8 had a certain grade of CNS depression until unconsciousness even with lower serum levels and similar or even higher sampling time. Particularly, case #8 was the only one reporting a female intoxication, showing an unknown grading of CNS depressant effect. Although sampling time and levels in serum were similar to case #1, who was alert, urinary levels were different and the influence of sex/gender cannot be estimated on the basis of a single case.

FUF was involved in one acute intoxication reported by the STRIDA Project [40], with very high concentrations compared to ACRYLF and with no psychomotor impairment observed (case #9 in Table **2**). No sedation was reported by a user in a forum around 250 µg, who also described strong nausea. Other users reported that FUF "worked" with a sedative

Table 2.   Acute non-fatal intoxications.

Substance	Dose (Self-Reported)	Serum	Psychomotor Performaces	Case or Sample	Sampling Time	Author
ACRYLF	-	-	Tiredness, somnolence, unconsciousness, anxiety, hallucinations, blurred vision	N=21 (18 M, 3 F)	-	EMCDDA, 2017 [35]
ACRYLF	20 mg/day x 4 days	1.3 ng/mL	Dizziness, paresthesia, tremor	#1 M	2 h	Helander *et al.*, 2017 [36]
ACRYLF	1 spray	0.6	Drowsy or confused	#2 M	6.5	
ACRYLF	1 spray	ND	-	#3 M	1.5 h	
ACRYLF	-	1.0	Psychotic behavior (agitation and delirium)	#4 M	1.5 h	
ACRYLF	-	2.1	CNS depression	#5 M	-	
ACRYLF		0.7	GCS 3	#6 M	14 h	
ACRYLF	6-8 spray	0.8	Very drowsy or confused	#7 M	-	
ACRYLF	-	1.3	CNS depression	#8 F	2 h	
FUF	-	148	-	#9 M	Promptly	Helander *et al.*, 2016 [40]
OCF	Snorting	-	Immediate loss of consciousness	N=3 (M)	-	Allibe *et al.*, 2019 [41]

Abbreviations: M: male, F: female, ACRYLF: Acrylfentanyl; FUF: Furanylfentanyl; OCF: Ocfentanyl; CNS: central nervous system; GCS: Glasgow coma scale.

effect of around 1-1.2 mg administered by nasal spray. Many users described a short duration of action followed by longer sedation, lasting around 1 hour and a half [43].

Among adverse effects notable for psychomotor performances, paranoia, psychosis and agitation have been reported after the use of OCF, even if this might be due to co-consumed drugs [22, 44]. Users reported a quick onset, in about 3 minutes, a "stimulant" effect and the early appearance of withdrawal symptoms [45]. Even though cases of death due to OCF were reported [9, 22, 32, 46-48], deaths were non-witnessed and cannot provide a picture of the symptoms. The low number of non-fatal intoxications does not speak in favor of low toxicity of the compound, and, given the described sudden loss of consciousness reported after snorting OCF [41], the possibility of fatal collapses while driving has to be considered.

This experimental section is aimed to evaluate the sensorimotor effects of new Fentanyl derivatives (ACRYLF, OCF and FUF) in the mouse model using behavioural tests of the "safety pharmacology protocol", widely used to characterise new molecules. The results of these tests could validate this experimental protocol to predict the effects of opioids on human visual-motor and auditorial functions and their impact on human daily tasks with a particular focus on driving.

3. MATERIALS AND METHODS

3.1. Animals

Male ICR (CD-1®) mice weighing 30-35 g (Centralized Preclinical Research Laboratory, University of Ferrara, Italy) were group housed (5 mice per cage; floor area per animal was 80 cm²; minimum enclosure height was 12 cm), exposed to a 12:12-h light-dark cycle (light period from 6:30 AM to 6:30 PM) at a temperature of 20-22°C and humidity of 45-55% and were provided ad libitum access to food (Diet 4RF25 GLP; Mucedola, Settimo Milanese, Milan, Italy) and water. The experimental protocols performed in the present study were in accordance with the U.K. Animals (Scientific Procedures) Act of 1986 and associated guidelines and the new European Communities Council Directive of September 2010 (2010/63/EU), a revision of Directive 86/609/EEC. Experimental protocols were approved by the Italian Ministry of Health (license n. 335/2016-PR) and by the Animal Welfare Body of the University of Ferrara. According to the ARRIVE guidelines, all possible efforts were made to minimise the number of animals used, minimise the animals' pain and discomfort and reduce the number of experimental subjects.

3.2. Drug Preparation and Dose Selection

FENT, ACRYLF, OCF and FUF were purchased from LGC Standards (Sesto San Giovanni, Milan, Italy). Naloxone (NLX) was purchased from Tocris (Bristol, UK). All the compounds were dissolved in a saline solution (0.9% NaCl) that was also used as the vehicle. Drugs were administered by intraperitoneal (i.p.) injection at a volume of 4 ul/g. The opioid receptor antagonist NLX (6 mg/kg, i.p.) was administered 15 mins before FENT, ACRYLF, FUF and OCF injections. The range of doses of FENS tested (0.01-15 mg/kg i.p.) was chosen based on our previous study [49].

3.3. Sensorimotor Tests

The effects of the three FENS were investigated using a battery of behavioural tests widely used in pharmacology safety studies for the preclinical characterization of new psychoactive substances in rodents [50-55]. All experiments were performed between 8:30 AM and 2:00 PM. Experiments were conducted blindly by trained observers working in pairs [55]. Mouse behavior was videotaped and analysed offline by a different trained operator who gives test scores.

We studied the voluntary and involuntary sensorimotor responses of the mice resulting from different reactions to visual, acoustic and tactile stimuli [51].

3.3.1. Evaluation of the Visual Response

The visual response was verified by two behavioural tests that evaluated the ability of the mice to capture visual information when they are moving (the visual placing response) or when they are stationary (the visual object response). The visual placing response test is performed using a tail suspension modified apparatus able to bring the mouse toward the floor at a constant speed of 10 cm/s [51]. The downward movement of the mouse is videotaped by a camera. A frame-by-frame analysis allows one to evaluate the beginning of a mouse's reaction while it is close to the floor. When the mouse starts to react, an electronic ruler evaluates the perpendicular distance in millimetres from the eyes of the mouse to the floor. The untreated control mouse perceives the floor and prepares to come into contact with it at a distance of 27 ± 4.5 mm. The visual placing response was measured at 0, 15, 35, 70, 125, 185, 245 and 305 min post-injection. A visual object response test was used to evaluate the ability of the mouse to see an object approaching from the front or the side, thus inducing the animal to shift or turn its head or retreat it [51]. For the frontal visual response, a white horizontal bar was moved in front of the mouse's head; the manoeuvre was repeated three times. For the lateral visual response, a small dentist's mirror was moved into the mouse's field of view in a horizontal arc until the stimulus was between the mouse's eyes. The procedure was conducted bilaterally and was repeated three times. A score of 1 was assigned if there was a reflection in the mouse movement; otherwise, a score of 0 was assigned. The total value was calculated by adding the scores obtained for the frontal and lateral visual object responses (overall score 9). The visual object response was measured at 0, 10, 30, 60, 120, 180, 240 and 300 min post-injection.

3.3.2. Evaluation of the Acoustic Response

Acoustic response measures the reflex of the mouse in response to an acoustic stimulus produced behind the animal. In particular, four acoustic stimuli of different intensities and frequencies were tested [51]. Each sound test was repeated three times. A score of 1 was given if there was a response and a score of 0 was given if there was no response, for a total score of 3 for each sound. The total acoustic score was calculated by adding scores obtained in the four tests (overall score 12). The acoustic response was measured at 0, 10, 30, 60, 120, 180, 240 and 300 min post injection.

3.3.3. Evaluation of the Tactile Response

The tactile response of each mouse was verified through vibrissae, pinna and corneal reflex, as previously described [51]. Data is expressed as the sum of the three parameters mentioned above. The vibrissae reflex was evaluated by touching the vibrissae (right and left) with a thin hypodermic needle once per side. A score of 1 was given if there was a response (turning the head to the side of the touch) or a score of 0 was given if there was no response (overall score 2). The pinna reflex was assessed by touching the pavilions (left and right) with a thin hypodermic needle. First the interior pavilions and then the external pavilions were stimulated. This test was repeated twice per side. A score of 1 was given if there was a response and a score of 0 was given if there was no response (overall score 4). The corneal reflex was assessed by gently touching the cornea of the mouse bilaterally with a thin hypodermic needle and evaluating the response. A score of 1 was given if the mouse moved only its head, 2 if it only closed the eyelid and 3 if it both closed the eyelid and moved the head (overall score 6). Each tactile response was measured at 0, 10, 30, 60, 120, 180, 240 and 300 min post-injection.

3.4. Data and Statistical Analysis

Data are expressed in arbitrary units (visual objects response; acoustic response; vibrissae, corneal and pinna reflex) or percentage of baseline (visual placing response). The statistical analysis of the effects of the individual substances in different concentrations over time and that of antagonism studies were performed using a two-way ANOVA followed by a Bonferroni test for multiple comparisons. The statistical analysis was performed using Prism software (GraphPad Prism, USA). All analyses were performed using GraphPad Prism software.

Dose-response curves were used to calculate the ED_{50} in each test, using Prism software (GraphPad Prism, USA)

4. RESULTS

4.1. Evaluation of the Visual Object Response

The visual object response was not affected in mice treated with the vehicle (Fig. **2**).

Acute systemic administration of the four opioids (0.01-15 mg/kg i.p.) dose-dependently decreased the visual object responses of mice. After the administration of FENT, ACRYLF, OCF and FUF the visual object response was significantly affected by treatment: FENT [$F_{6,392} = 359.4$, $P<0.0001$], time [$F_{7,392} = 84.90$, $P<0.0001$] and time × treatment interaction [$F_{42,392} = 14.98$, $P<0.0001$]; ACRYLF [$F_{6,392} = 502.4$, $P<0.0001$], time [$F_{7,392} = 122.9$, $P<0.0001$] and time × treatment interaction [$F_{42,392} = 22.13$, $P<0.0001$]; OCF [$F_{6,392} = 324.5$, $P<0.0001$], time [$F_{7,392} = 84.91$, $P<0.0001$] and time × treatment interaction [$F_{42,392} = 13.39$, $P<0.0001$]; FUF [$F_{6,392} = 418.5$, $P<0.0001$], time [$F_{7,392} = 108.3$, $P<0.0001$] and time × treatment interaction [$F_{42,392} = 18.58$, $P<0.0001$]; (Fig. **2 A-C-E-G**).

The pre-treatment with NLX (6 mg/kg) totally prevented the inhibitory effects of FUF [$F_{1,112} = 1407$, $P<0.0001$], time [$F_{7,112} = 81.97$, $P<0.0001$] and time × treatment interaction [$F_{7,112} = 38.83$, $P<0.0001$] and partially for the other compounds. The injection of a second dose of NLX (6 mg/kg i.p.) did not totally prevent the visual alterations induced by FENT, ACRYLF and OCF: FENT [$F_{1,112} = 63.71$, $P<0.0001$], time [$F_{7,112} = 32.44$, $P<0.0001$] and time × treatment interaction [$F_{7,112} = 3.064$, $P=0.0055$]; ACRYLF [$F_{1,112} = 84.89$, $P<0.0001$], time [$F_{7,112} = 68.27$, $P<0.0001$] and time × treatment interaction [$F_{1,112} = 4.786$, $P<0.0001$]; OCF [$F_{1,112} = 508.8$, $P<0.0001$], time [$F_{7,112} = 34.51$, $P<0.0001$] and time × treatment interaction [$F_{7,112} = 13.53$, $P<0.0001$]; (Fig. **2 B-D-F-H**).

VISUAL OBJECT RESPONSE

Fig. (2). Effect of acute systemic administration (0.01-15 mg/kg i.p.) of FENT (panel **A**); ACRYLF (panel **C**); OCF (panel **E**) and FUF (panel **G**) on the visual object response test of the mouse. Interaction of effective dose of all the compounds (6 mg/kg) with the opioid receptor antagonist NLX (6 mg/kg, i.p.; respectively panels **B-D-F-H**). Data are expressed as arbitrary units (see materials and methods) and represent the mean ± SEM of 8 determinations for each treatment. Statistical analysis was performed by two-way ANOVA followed by Bonferroni's test for multiple comparisons. *$p<0.05$, **$p<0.01$, ***$p<0.001$ *versus* vehicle; #$p<0.05$, ##$p<0.01$, ###$p<0.001$ *versus* NLX+ agonist. (*A higher resolution/colour version of this figure is available in the electronic copy of the article*).

VISUAL PLACING RESPONSE

Fig. (3). Effect of acute systemic administration (0.01-15 mg/kg i.p.) of FENT (panel **A**); ACRYLF (panel **C**); OCF (panel **E**) and FUF (panel **G**) on the visual placing response test of the mouse. Interaction of effective dose of all compounds (6 mg/kg) with the opioid receptor antagonist NLX (6 mg/kg, i.p.; respectively panels **B-D-F-H**). Data are expressed as a percentage of baseline (see material and methods) and represent the mean ± SEM of 8 determinations for each treatment. Statistical analysis was performed by two-way ANOVA followed by the Bonferroni's test for multiple comparisons. *$p<0.05$, **$p<0.01$, ***$p<0.001$ *versus* vehicle; #$p<0.05$, ##$p<0.01$, ###$p<0.001$ *versus* NLX + agonist. (*A higher resolution/colour version of this figure is available in the electronic copy of the article*).

The comparison of the dose-response curves of all compounds in the sensorimotor tests performed in this study are represented in Fig. **6 (A-B-C-D)**. In particular, the comparison of the dose-response curves (Fig. **6A**) of all compounds in the visual object response test revealed the following rank of potency: OCF (ED_{50}= 1.60 mg/kg) ≥ ACRYLF (ED_{50}= 1.97 mg/kg) ≥ FUF (ED_{50}= 2.17 mg/kg) = FENT (ED_{50}= 2.7 mg/kg).

4.2. Evaluation of the Visual Placing Response

The visual placing response was not affected in mice treated with the vehicle (Fig. **3**).

Acute systemic administration of the four opioids (0.01-15 mg/kg i.p.) dose-dependently decreased the visual placing responses of mice. After the administration of FENT, ACRYLF, OCF and FUF the visual placing response was significantly affected by treatment: FENT [$F_{6,392}$ = 85.91, $P<0.0001$], time [$F_{7,392}$ = 73.13, $P<0.0001$] and time × treatment interaction [$F_{42,392}$ = 4.023, $P<0.0001$]; ACRYLF [$F_{6,392}$ = 91.91, $P<0.0001$], time [$F_{7,392}$ = 73,86, $P<0.0001$] and time × treatment interaction [$F_{42,392}$ = 4.079, $P<0.0001$]; OCF [$F_{6,392}$ = 115.3, $P<0.0001$], time [$F_{7,392}$ = 94.78, $P<0,0001$] and time × treatment interaction [$F_{42,392}$ = 6.645, $P<0.0001$]; FUF [$F_{6,388}$ = 184.5, $P<0.0001$], time [$F_{7,388}$ = 123.1, $P<0.0001$] and time × treatment interaction [$F_{42,388}$ = 8.587, $P<0.0001$]; (Fig. **3A-C-E-G**).

The pre-treatment with NLX (6 mg/kg) partially prevented the inhibitory effect of all the compounds. The injection of a second dose of NLX (6 mg/kg i.p.) did not totally prevent the visual alteration induced by the agonists however it reduced it slightly in the last hours of measurements: FENT [$F_{3,224}$ = 66.85, $P<0.0001$], time [$F_{7,224}$ = 11.50, $P<0.0001$] and time × treatment interaction [$F_{21,224}$ = 3.636, $P<0.0001$]; ACRYLF [$F_{3,224}$ = 106.0, $P<0.0001$], time [$F_{7,224}$ = 15.31, $P<0.0001$] and time × treatment interaction [$F_{21,224}$ = 5.137, $P<0.0001$]; OCF [$F_{3,224}$ = 212.6, $P<0.0001$], time [$F_{7,224}$ = 42.81, $P<0.0001$] and time × treatment interaction [$F_{21,224}$ = 16.56, $P<0.0001$] FUF [$F_{3,224}$ = 277.6, $P<0.0001$], time [$F_{7,224}$ = 41.65, $P<0.0001$] and time × treatment interaction [$F_{21,224}$ = 18.88, $P<0,0001$]; (Fig. **3 B-D-F-H**)].

The comparison of the dose-response curves (Fig. **6B**) of all compounds in the visual placing response test revealed the following rank of potency: OCF (ED_{50}= 0.88 mg/kg) > ACRYLF (ED_{50}= 1.38 mg/kg) ≥ FENT (ED_{50}= 1.87 mg/kg) > FUF (ED_{50}= 2.51 mg/kg).

4.3. Evaluation of the Acoustic Response

The acoustic responses did not change in vehicle-treated mice over the 5-h observation (Fig. **4**). Acute systemic administration of FENT and its derivatives (0.01-15 mg/kg) decreased the acoustic responses in mice. In particular, the administration of FENT and ACRYLF decreased the acoustic response only at the highest dose tested and the effect disappeared after 60 min of treatments at the highest dose tested; with OCF and FUF the acoustic response was significantly affected by treatment: FENT [$F_{6,392}$ = 7.932, $P<0.0001$], time [$F_{7,392}$ = 1.442, $P=0.1871$] and time × treatment interaction [$F_{42,392}$ = 0.8902, $P=0.6685$]; ACRYLF [$F_{6,392}$ = 11.08, P < 0.0001], time [$F_{7,392}$ = 2.461, P = 0.0176] and time × treatment interaction [$F_{42,392}$ = 1.289, P = 0.1144]. In difference to FENT

and ACRYLF, OCF and FUF induced a dose-dependent inhibition of the acoustic reflexes and the effect persisted up to 5 hours of measurements: OCF [$F_{6,392}$ = 177.0, $P<0.0001$], time [$F_{7,392}$ = 29.51, $P<0.0001$] and time × treatment interaction [$F_{42,392}$ = 5.545, $P<0.0001$]; FUF [$F_{6,392}$ = 264.8, $P<0.0001$], time [$F_{7,392}$ = 79.92, $P<0.0001$] and time × treatment interaction [$F_{42,392}$ = 8.625, $P<0.0001$]; (Fig. **4 A-C-E-G**).

The pre-treatment with NLX (6 mg/kg) prevented the inhibitory effects of FENT, ACRYLF and FUF while partially with OCF. The injection of a second dose of NLX (6 mg/kg i.p.) reverted the effect of OCF: FENT [$F_{3,224}$ = 5.802, $P=0.0008$], time [$F_{7,224}$ = 0.9575, $P=0,4632$] and time × treatment interaction [$F_{21,224}$ = 0.5618, $P=0.9402$]; ACRYLF [$F_{3,224}$ = 12.22, $P<0.0001$], time [$F_{7,224}$ = 1.716, $P=0.1063$] and time × treatment interaction [$F_{21,224}$ = 1.027, $P=0.4315$] and OCF [$F_{3,224}$ = 461.2, $P<0.0001$], time [$F_{7,224}$ = 14.23, $P<0.0001$] and time × treatment interaction [$F_{21,224}$ = 10.47, $P<0.0001$]; FUF [$F_{3,224}$ = 628.8, $P<0.0001$], time [$F_{7,224}$ = 30.34, $P<0.0001$] and time × treatment interaction [$F_{21,224}$ = 21.74, $P<0.0001$]; (Fig. **4B-D-F-H**)].

The comparison of the dose-response curves (Fig. **6C**) between OCF and FUF revealed a major potency for FUF (ED_{50}= 2.40 mg/kg) in comparison to OCF (ED_{50}= 4.36 mg/kg). The ED_{50} was not determined for the rest of the compounds.

4.4. Evaluation of the Tactile Response

The overall tactile responses (pinna, vibrissae, cornea) did not change in vehicle-treated mice over the 5-h observation (Fig. **5**). Acute systemic administration of FENT and its derivatives (0.01-15 mg/kg) decreased in a dose-dependent manner the overall tactile responses in mice. In particular, after the administration of FENT, ACRYLF, OCF and FUF the tactile response was significantly affected by treatment FENT [$F_{6,392}$ = 82.00, $P<0.0001$], time [$F_{7,392}$ = 56.06, $P<0.0001$] and time × treatment interaction [$F_{42,392}$ = 19.30, $P<0.0001$]; ACRYLF [$F_{6,392}$ = 88.29, $P<0.0001$], time [$F_{7,392}$ = 57.88, $P<0.0001$] and time × treatment interaction [$F_{42,392}$ = 18.74, $P<0.0001$]; OCF [$F_{6,392}$ = 116.5, $P<0.0001$], time [$F_{7,392}$ = 22.42, $P<0.0001$] and time × treatment interaction [$F_{42,392}$ = 4.863, $P<0.0001$]; FUF [$F_{6,392}$ = 231.4, $P<0.0001$], time [$F_{7,392}$ = 48.47, $P<0,0001$] and time × treatment interaction [$F_{42,392}$ = 11.52, $P<0.0001$]; (Fig. **5 A-C-E-G**).

The pre-treatment with NLX (6 mg/kg) totally prevented the inhibitory effects induced by FUF [$F_{3,224}$ = 324.6, $P<0.0001$], time [$F_{7,224}$ = 31,34, $P<0,0001$] and time × treatment interaction [$F_{21,224}$ = 30.30, $P<0.0001$] and partially with the other compounds. The injection of a second dose of NLX (6 mg/kg i.p.) reverted totally the tactile responses inhibition induced by the three agonists: FENT [$F_{3,224}$ = 251.6, $P<0.0001$], time [$F_{7,224}$ = 169.9, $P<0,0001$] and time × treatment interaction [$F_{21,224}$ = 74.62, $P<0.0001$]; ACRYLF [$F_{3,224}$ = 735.8, $P<0.0001$], time [$F_{7,224}$ = 451.3, $P<0.0001$] and time × treatment interaction [$F_{21,224}$ = 171.7, $P<0,0001$]; OCF [$F_{3,224}$ = 209.2, $P<0.0001$], time [$F_{7,224}$ = 13.50, $P<0,0001$] and time × treatment interaction [$F_{21,224}$ = 9.328, $P<0.0001$]; (Fig. **5 B-D-F-H**).
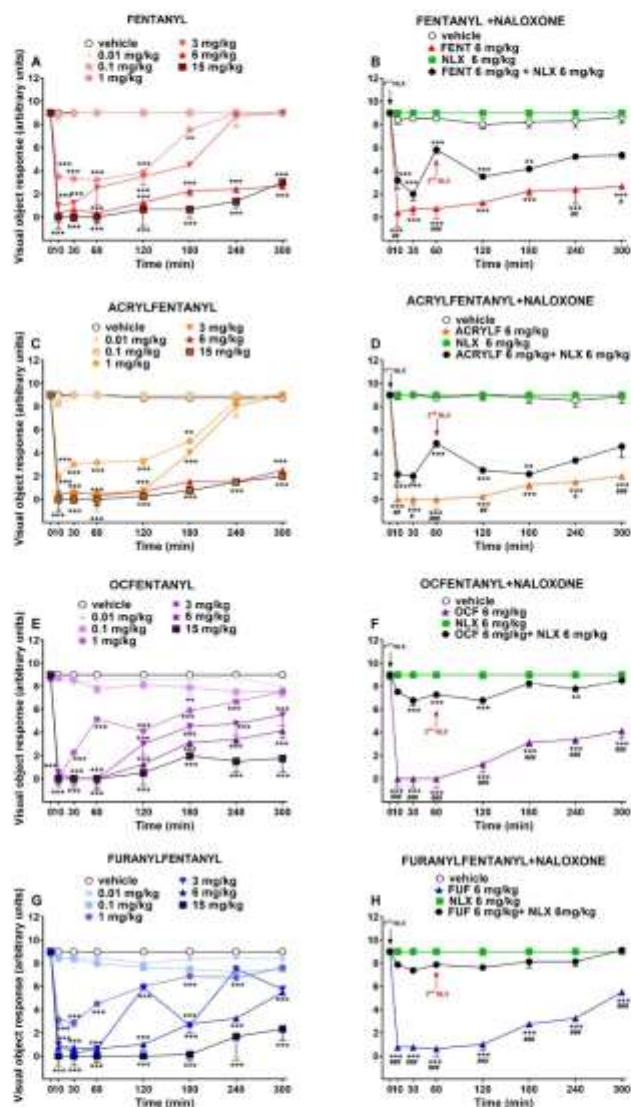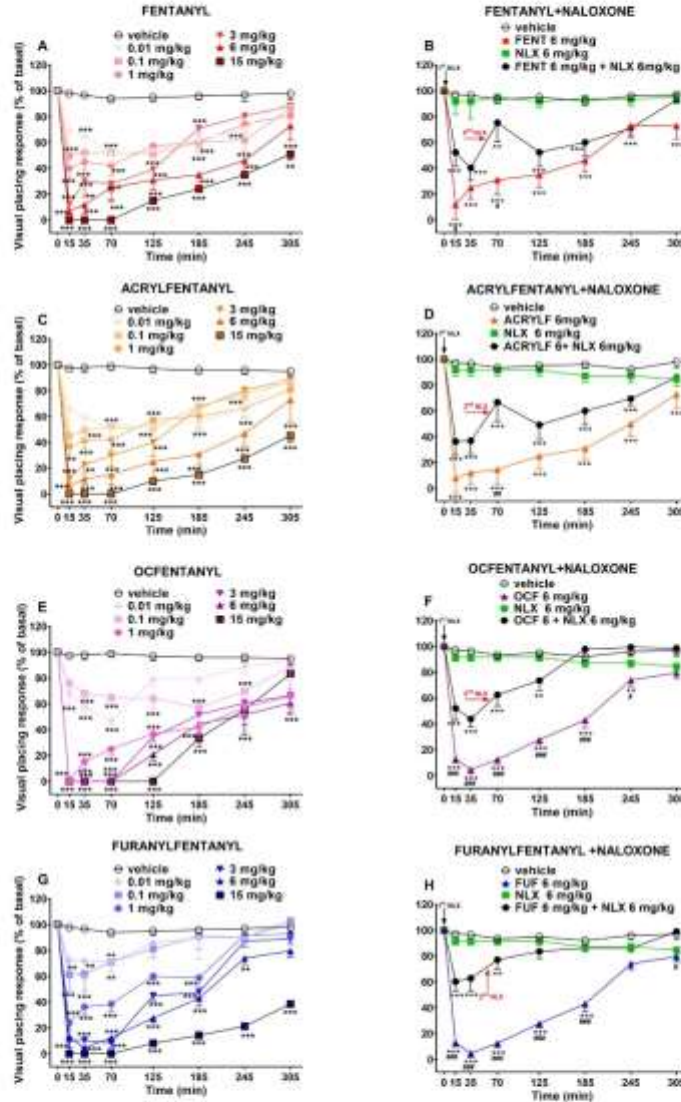
ACOUSTIC RESPONSE
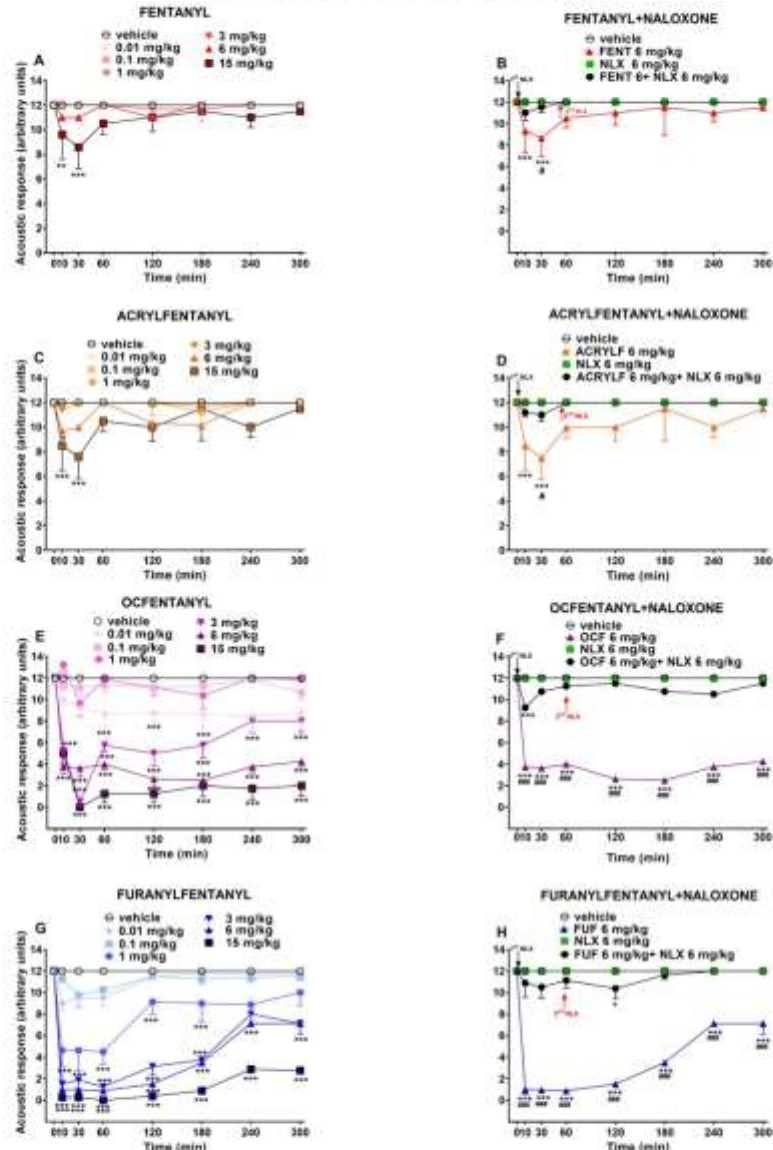
Fig. (4). Effect of acute systemic administration (0.01-15 mg/kg i.p.) of FENT (panel **A**); ACRYLF (panel **C**); OCF (panel **E**) and FUF (panel **G**) on the acoustic response test of the mouse. Interaction of effective dose of all compounds (6 mg/kg) with the opioid receptor antagonist NLX (6 mg/kg, i.p.; respectively panels **B-D-F-H**). Data are expressed as arbitrary units (see material and methods) and represent the mean ± SEM of 8 determinations for each treatment. Statistical analysis was performed by two-way ANOVA followed by the Bonferroni's test for multiple comparisons for both the dose response curve of each compounds at different times. *$p<0.05$, **$p<0.01$, ***$p<0.001$ *versus* vehicle; #$p<0.05$, ###$p<0.001$ *versus* NLX+ agonist. (*A higher resolution/colour version of this figure is available in the electronic copy of the article*).

OVERALL TACTILE RESPONSE
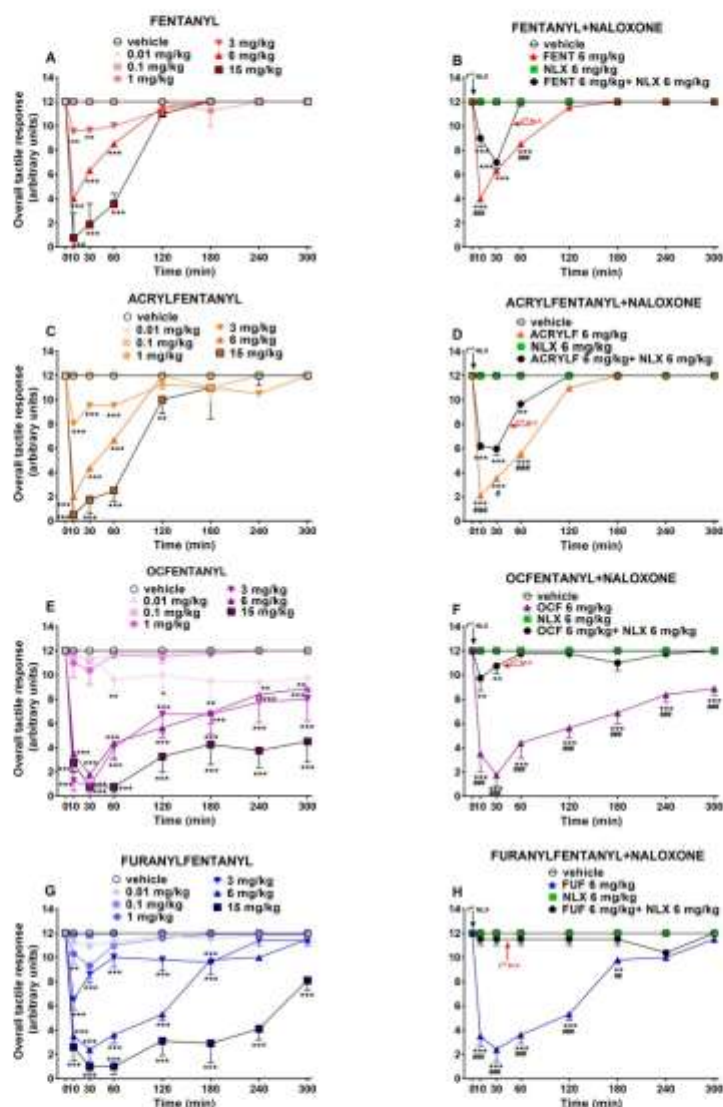
Fig. (5). Effect of acute systemic administration (0.01-15 mg/kg i.p.) of FENT (panel **A**); ACRYLF (panel **C**); OCF (panel **E**) and FUF (panel **G**) on the overall tactile response. Interaction of effective dose of all compounds (6 mg/kg) with the opioid receptor antagonist NLX (6 mg/kg, i.p.; respectively panels **B-D-F-H**). Data are expressed as arbitrary units (see material and methods) and represent the mean ± SEM of 8 determinations for each treatment. Statistical analysis was performed by two-way ANOVA followed by Bonferroni's test for multiple comparisons. *$p<0.05$, **$p<0.01$, ***$p<0.001$ *versus* vehicle; #$p<0.05$, ##$p<0.01$, ###$p<0.001$ *versus* NLX+ agonist. (*A higher resolution/ colour version of this figure is available in the electronic copy of the article*).

DOSE RESPONSE CURVES
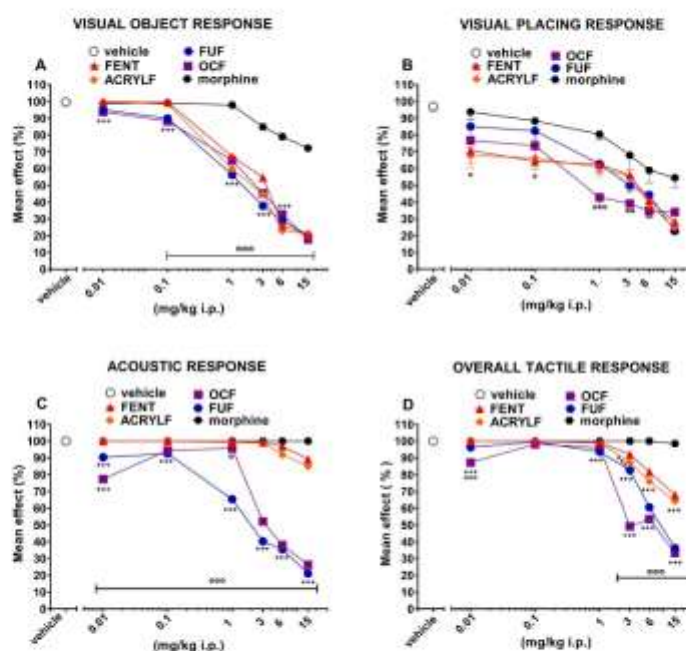
Fig. (6). Dose-response curves of FENT, ACRYLF, OCF and FUF on the visual object response (panel **A**); the visual placing response (panel **B**); the acoustic response (panel **C**); the tactile response (panel **D**). Data of morphine were elaborated in [59]. Data are expressed in percent (%) and represent the mean ± SEM of 8 determinations for each treatment. Statistical analysis was performed by two-way ANOVA followed by Bonferroni's test for multiple comparisons. +++$p < 0.001$ *versus* FENT; *$p < 0.05$, **$p < 0.01$, ***$p < 0.001$ *versus* morphine. (*A higher resolution/colour version of this figure is available in the electronic copy of the article*).

The comparison of the dose-response curves (Fig. **6D**) between OCF and FUF in the tactile response test revealed a major potency for OCF (ED_{50}= 5.85 mg/kg) in comparison to FUF (ED_{50}= 9.20 mg/kg). The ED_{50} was not determined for the rest of the compounds.

5. DISCUSSION

5.1. Visual Object and Visual Placing Responses

The results of the acute systemic administration of FENT, ACRYLF, OCF and FUF on the startle response to visual stimuli demonstrate that opioid receptors, in particular mu receptors, play an important role in modulating the visual responses of mice after opioid injections [57-59]. Indeed, we have demonstrated in our previous study that the inhibitory effects of morphine and its analogue (MT-45) on the visual object and placing tests were totally prevented by the pre-treatment with NLX [59]. In this case, the pre-treatment with NLX partially prevented the inhibitory effects induced by all the opioids in visual objects and visual placing tests. The administration of the second dose of NLX (6 mg/kg at 55 min after treatment) was not effective at blocking the inhibi-

tory effects on visual reflexes induced by FENT, ACRYLF, OCF and FUF. The effect of FENS on the visual placing seemed to be more profound than those in the object test. In contrast to the latter, the visual placing test links the movement of the mouse to its visual perception. In particular, to perform the visual placing test the mouse needs to integrate the visual and tactile stimulus with the vestibular information to correctly extend the muscles of the neck and forelegs to land on the ground [60]. Moreover, studies in freely moving mice [61] and also rats [62] have found that eye movement patterns in these animals are often non-conjugate and these movements were systematically coupled to changes in orientation of the animal's head with respect to the horizontal plane (head tilt). Eye movements in response to static tilt changes are associated with the otolith organs, which sense head acceleration, including gravity, and are referred to as "ocular countertilt" reflexes [63]. It is suggested by Meyer and coworkers, that these eyehead coupling movements in rodents could serve to stabilize the visual field with respect to the ground [64]. Thus, the involvement of the vestibular inputs and the spinal motoneurons in controlling posture and body movement in the face of gravity has been established

97

[65, 66]. Eye movements in freely moving mice constantly stabilize the animal's visual field by counteracting head rotations through the vestibulo-ocular reflex (VOR; [64, 67]), maintaining the large panoramic overhead view [63]. In mice administered fentalogs, this mechanism appears to be hampered and that could reveal the role of fentanyl in impairing the vestibule-ocular reflex.

Other studies on the mechanism of action of opioids in the medial vestibular nucleus have proved that opioids can induce direct excitatory actions after GABAergic inhibition [68] and this could explain the results of our study. Mu-opioid receptors have been detected in the retina of rodents [69, 70]. The acute systemic administration of opioids induced pupil constriction and reduced Pupillary Light Reflexes in mice. These effects were blocked by mu antagonist [71]. These findings also reveal that opioids can act directly with mu-opioid receptors of the retina and alter vision in mice [71, 72].

5.2. Acoustic Response

Our data shows that FENT, ACRYLF, OCF and FUF reduced acoustic response in mice in a dose-dependent manner. The effect of OCF and FUF was more potent and persistent compared to FENT and ACRYLF, and these differences could be related to their chemical structures [73, 74]. The pre-treatment with NLX prevented the acoustic alterations induced by all the opioids, revealing the involvement of mu-opioid receptors in the acoustic inhibitory effects induced by FENS [59]. It is important to highlight that in our previous study, morphine at the range dose of 0.01-15 mg/kg did not affect the acoustic reflexes of mice. However, the effect of FENS was robust and dose-dependent. The mechanism by which FENS could alter the acoustic responses is not yet elucidated. However, there is evidence in the literature demonstrating the expression of opioid peptides in the inner ear. In particular, mRNA for the mu-opioid receptor, delta-opioid receptor, and kappa-opioid receptor was detected in rat and guinea pig cochlea by RT-PCR [75, 76]. In the mouse spiral ganglia neurons most of the neurons were immunoreactive to mu-opioid receptors. In the organ of Corti, mu-opioid receptors were expressed in inner hair cells (IHC) and outer hair cells (OHC), and the fibers underneath the IHC were also detected [77]. It has been reported that intoxication with opioids such as MT-45 and hydrocodone might cause gradual sensory deafness requiring a cochlear implant for the recovery of hearing [78, 79]. The temporary loss of hearing produced by methadone has also been reported [80, 81]. The fact that opioid receptors, in particular, mu ones are expressed in the inner ear of mice confirms their involvement in the acoustic alterations produced in mice after acute systemic administration of FENS and that could be related to temporary dysfunction of the cochlea, which was prevented by NLX pre-treatment in our test [82].

5.3. Tactile Response

Our data demonstrate that FENT, ACRYLF, OCF and FUF significantly reduced the tactile response of mice. Also, in this test, the effect of OCF and FUF is more potent and persistent in comparison to FENT and ACRYLF. Again these differences could be related to their chemical structures

[49, 73, 74]. The pre-treatment with NLX did not totally block the inhibitory effects of FENT, ACRYLF and OCF. While the second dose of NLX totally blocked these effects. Our data revealed the role of mu-opioid receptors in inhibiting the tactile response in mice after opioid injections. Indeed, we demonstrated in our previous study that MT45 (synthetic substitute of morphine) but not morphine reduced the tactile response at the dose of 15 mg/kg and the effect was prevented by a pre-treatment with 6 mg/kg of NLX [59]. The tactile experience through the mystacial vibrissae (whiskers) is the main way to collect information from the outside environment for rodents. The mechanism by which opioids reduce the tactile response in mice is not yet defined. However, a recent elegant study demonstrated that FENT inhibits the Air Puff-Evoked sensory information of mice, acting *via* mu receptors on cerebellar neurons, by reducing GABAergic responses in molecular layer interneurons (MLIs) and Purkinje cells (PCs), through the cAMP-PKA signaling pathway [83]. These findings reveal the role of mu-opioid receptors distributed in the cerebellum area in controlling the sensory responses of rodents.

5.4. Translational Paradigm from Animal to Human in Cases of DUID

Our study is aimed to evaluate the effects of FENS on sensorimotor functions in mouse model and to validate our behavioral tests to predict the possible impact of FENS on human psychomotor performances, particularly in those involved in driving abilities.

Clearly, the inference of data obtained from animal models to humans presents several limitations and should be performed with caution. Keeping in mind the possible biases connected to this operation and the general difficulty in predicting the effects of drugs on the ability to drive on the basis of psychomotor tests, our study revealed substantial accordance between experimental and human data. Our experimental data reveals that FENS impairs sensorimotor functions in mice and that the effects were blocked by a repeated administration of a high dose of the mu-opioid receptor antagonist NLX. The visual placing test performed in mice allows to evaluate functions such as vision, co-ordination and proprioception, which are critical in the fitness and ability to drive. The response to visual stimuli and visual/motor tracking are at the basis of several psychomotor tests and driving measures, such as the simple braking reaction time, cue recognition reaction time, visual retention test and trail-making test, the impairment of which could be considered predictive of an inability to drive and was therefore tested by several authors [11]. FENT impaired eye-hand coordination in humans [17] and the Critical Flicker Fusion Task [18], which tests visual processing and visual-motor skills. Data retrieved from intoxication cases accordingly showed some impairing in the visual functions, with hallucinations and blurred visions reported in cases of ACRYLF intoxications [35]. It appears obvious that when the visual acuity is impaired, the proprioception and the motor response might not be adequate to the external stimuli.

Acoustic perception, as well as a visual one, has been shown to influence the driving speed and motion perception [84], which is in turn connected to braking responses and

driving performances [85]. A reduction in in-car noises of 5dB has been shown to lead to a speed underestimation, with potential effect on the risk of crashing [84]. Hearing impairment is associated with road accidents [86], while auditory advisory information seems to be linked to quicker driver responses [87], suggesting that acoustic cues are fundamental for drivers. Touch is less stimulated, compared to vision during driving and, for this reason, it has been targeted as a sense through which is possible to vehicolate feedback to the driver [88]. However, tactile sensations are fundamental for proprioception, as in the berg balance test, in which the patient has to stand with an eye closed on one foot [11]. Considering experimental cases on humans, low doses of FENT impair auditory, reaction time, signal detection, sustained attention and some memory task performances even in the absence of marked sedation [20]. Accordingly, in our animals, some FENS impaired auditory and tactile responses of mice at low doses (0.01 and 0.1 mg/kg) that did not impair or facilitate spontaneous [89] and stimulated motor activity [49] of mice.

Moreover, our study demonstrated that a single dose of NLX did not block the effects of FENS on sensorimotor functions. While a second dose prevented most of these effects. This is in line with preclinical [49] and clinical reports that suggest repeated administration of NLX dosing in cases of FENT intoxications, in order to avoid the reappearance of its effects [90]. It is worth speculating that the human and the mouse mu-opioid receptors, share a high (94%) level of protein similarity [91]. Yet, a direct comparison of the pharmacological profile of a panel of mu-opioid ligands on the rat *vs.* human [92] and on the rhesus *vs.* human [93] mu opioid receptors, demonstrated very high levels of correlation. In addition, affinity values of a series of N-alkyl benzomorphans were obtained in cells expressing the mouse mu opioid receptor and compared to that of rat and monkey cortex showing again high levels of correlation [94]. Collectively, these findings prove the validity of the mouse model to predict the effects of opioids on humans, particularly, on sensorimotor impairments, and to improve the possible therapeutic interventions in the case of DUID.

CONCLUSION

In the present work, the experimental study performed on a mouse model has shown sensorimotor alterations, including visual, acoustic and tactile responses, induced by fentanyl and by three fentalogs, acrylfentanyl, ocfentanyl and furanylfentanyl. The results are in accordance with the data that emerged from the revision of the literature regarding experimental data on humans, driving under the influence of drugs and intoxication cases, suggesting that novel synthetic opioids might affect the psychomotor performances involved in driving.

AUTHORS' CONTRIBUTIONS

MM, SB, AG and RG contributed conception and design of the study. SB, MT, RA, BM, GC, VC performed *in vivo* experimental section. MM, SB, AG and RG, wrote the manuscript. MT, RA, BM, GC, VC, GZ edited sections of the manuscript. MT, RA, BM, GC, LC performed the statistical analysis.

LIST OF ABBREVIATIONS

FENS	=	Fentanyl Derivatives
Fentalogs	=	Fentanyl Analogs
Fentanyl	=	N-(1-(2-feniletil)-4-piperidinil)-N-fenil-propanammide
Acrylfentanyl	=	N-Phenyl-N-[1-(2-phenylethyl) piperidin-4-yl]prop-2-enamide
Furanylfentanyl	=	N-Phenyl-N-[1-(2-phenylethyl) piperidin-4-yl]furan-2-carboxamide
Ocfentanyl	=	N-(2-Fluorophenyl)-2-methoxy-N-[1-(2-phenylethyl)piperidin-4-yl]acetamide
Naloxone	=	(4R,4aS,7aR,12bS)-4a,9-dihydroxy-3-prop-2-enyl-2,4,5,6,7a,13-hexahydro-1H-4,12-methanobenzofuro[3,2-e]isoquinolin-7-one

ETHICS APPROVAL AND CONSENT TO PARTICIPATE

All applicable international, national and institutional guidelines for the care and use of animals were followed. All procedures performed in the studies involving animals were in accordance with the ethical standards of the institution or practice at which the studies were conducted. The authors certify that they were carried out in accordance with the National Institute of Health Guide for the Care and Use of Laboratory Animals (NIH Publications No. 80-23) revised 1996 or the UK Animals (Scientific Procedures) Act 1986 and associated guidelines, or the European Communities Council Directive of 24 November 1986 (86/609/EEC).

Project was activated in collaboration with the Presidency of the Council of Ministers-DPA Anti-Drug Policies (Italy).

CONSENT FOR PUBLICATION

Not applicable.

FUNDING

CONFLICT OF INTEREST

The authors declare no conflict of interest, financial or otherwise.

ACKNOWLEDGEMENTS

REFERENCES

[1]   Wilhelmi, B.; Cohen, S.P. A framework for "driving under the influence of drugs" policy for the opioid using driver. *Pain Physician*, 2012, 3S(15)(Suppl.), ES215-ES230.

http://dx.doi.org/10.36076/ppj.2012/15/ES215 PMID: 22786459

[2]   Marillier, M.; Verstraete, A.G. Driving under the influence of drugs. WIREs Forensic Sci., 2019, 1(3), e1326.
http://dx.doi.org/10.1002/wfs2.1326

[3]   Busardo, F.P.; Pichini, S.; Pellegrini, M.; Montana, A.; Lo Faro, A.F.; Zaami, S.; Graziano, S. Correlation between blood and oral fluid psychoactive drug concentrations and cognitive impairment in driving under the influence of drugs. Curr. Neuropharmacol., 2017, 16(1), 84-96.
http://dx.doi.org/10.2174/1570159X15666170828162057 PMID: 28847293

[4]   United Nations Office on Drugs and Crime (UNDOC). World Drug report, 2019. Available from: https://wdr.unodc.org/wdr2019/

[5]   Soria, M.L. Driving under the influence of new psychoactive substances. Span. J. Leg. Med. 2018, 44(4), 169-175.
http://dx.doi.org/10.1016/j.remle.2017.11.008

[6]   European Monitoring Centre for Drugs and Drug Addiction (EMCDDA). European Drug Report. 2021. Available from: https://www.emcdda.europa.eu/publications/edr/trends-developments/2021_en

[7]   Fishbain, D.A.; Cutler, R.B.; Rosomoff, H.L.; Rosomoff, R.S. Are opioid-dependent/tolerant patients impaired in driving-related skills? A structured evidence-based review. J. Pain Symptom Manage., 2003, 25(6), 559-577.
http://dx.doi.org/10.1016/S0885-3924(03)00176-3 PMID: 12782437

[8]   Centola, C.; Giorgetti, A.; Zaami, S.; Giorgetti, R. Effects of GHB on psychomotor and driving performance. Curr. Drug Metab., 2018, 19(13), 1065-1072.
http://dx.doi.org/10.2174/1389200219666180124113802 PMID: 29366411

[9]   Brunetti, P.; Pirani, F.; Carlier, J.; Giorgetti, R.; Busardò, F.P.; Lo Faro, A.F. A 2017-2019 update on acute intoxications and fatalities from illicit fentanyl and analogs. J. Anal. Toxicol., 2021, 45(6), 537-554.
http://dx.doi.org/10.1093/jat/bkaa115 PMID: 32860688

[10]   10. European Monitoring Centre for Drugs and Drug Addiction. EMCDDA_Europol Joint Report on a new psychoactive substance: N-(1-phenethylpiperidin-4-yl) Nphenylacetamide (acryloylfentanyl Joint Reports, Publications Office of the European Union, Luxembourg, 2017. Available from: https:// www.emcdda.europa.eu/ system/ files/ publications/ 3873/ TI_PUBPDF_TDAS17001ENN_PDFWEB_20170221105322.pdf

[11]   Menefee, L.A.; Frank, E.D.; Crerand, C.; Jalali, S.; Park, J.; Sanschagrin, K.; Besser, M. The effects of transdermal fentanyl on driving, cognitive performance, and balance in patients with chronic nonmalignant pain conditions. Pain Med., 2004, 5(1), 42-49.
http://dx.doi.org/10.1111/j.1526-4637.2004.04005.x PMID: 14996236

[12]   Sabatowski, R.; Schwalen, S.; Rettig, K.; Herberg, K.W.; Kasper, S.M.; Radbruch, L. Driving ability under long-term treatment with transdermal fentanyl. J. Pain Symptom Manage., 2003, 25(1), 38-47.
http://dx.doi.org/10.1016/S0885-3924(02)00539-0 PMID: 12565187

[13]   Wilson, V.; Lim, R. Patient with very high opioid tolerance enrolled in opioid agonist treatment: A Case Report. J. Addict. Med., 2022, 16(2), 246-248.
http://dx.doi.org/10.1097/ADM.0000000000000868 PMID: 33973925

[14]   Dumas, E.O.; Pollack, G.M. Opioid tolerance development: A pharmacokinetic/pharmacodynamic perspective. AAPS J., 2008, 10(4), 537-551.
http://dx.doi.org/10.1208/s12248-008-9056-1 PMID: 18989788

[15]   Hayley, A.C.; Downey, L.A.; Green, M.; Shiferaw, B.; Kenneally, M.; Keane, M.; Adams, M.; Shehabi, Y. Driving Simulator performance after administration of analgesic doses of ketamine with dexmedetomidine or fentanyl. J. Clin. Psychopharmacol., 2019, 39(5), 446-454.
http://dx.doi.org/10.1097/JCP.0000000000001101 PMID: 31433347

[16]   Stevenson, G.W.; Pathria, M.N.; Lamping, D.L.; Buck, L.; Rosenbloom, D. Driving ability after intravenous fentanyl or diazepam. A controlled double-blind study. Invest. Radiol., 1986, 21(9), 717-719.
http://dx.doi.org/10.1097/00004424-198609000-00008 PMID: 3533834

[17]   Zacny, J.P.; Lance Lichtor, J.; Zaragoza, J.G.; de Wit, H. Subjective and behavioral responses to intravenous fentanyl in healthy volunteers. Psychopharmacology (Berl.), 1992, 107(2-3), 319-326.
http://dx.doi.org/10.1007/BF02245155 PMID: 1615132

[18]   Veselis, R.A.; Reinsel, R.A.; Feshchenko, V.A.; Wronski, M.; Dnistrian, A.; Dutcher, S.; Wilson, R. Impaired memory and behavioral performance with fentanyl at low plasma concentrations. Anesth. Analg., 1994, 79(5), 952-960.
http://dx.doi.org/10.1213/00000539-199411000-00023 PMID: 7978415

[19]   Ghoneim, M.M.; Mewaldt, S.P.; Thatcher, J.W. The effect of diazepam and fentanyl on mental, psychomotor and electroencephalographic functions and their rate of recovery. Psychopharmacology (Berl.), 1975, 44(1), 61-66.
http://dx.doi.org/10.1007/BF00421185 PMID: 1105627

[20]   Schneider, U.; Bevilacqua, C.; Jacobs, R.; Karst, M.; Dietrich, D.E.; Becker, H.; Müller-Vahl, K.R.; Seeland, I.; Gielsdorf, D.; Schedlowski, M.; Emrich, H.M. Effects of fentanyl and low doses of alcohol on neuropsychological performance in healthy subjects. Neuropsychobiology, 1999, 39(1), 38-43.
http://dx.doi.org/10.1159/000026558 PMID: 9892858

[21]   Jamison, R.N.; Schein, J.R.; Vallow, S.; Ascher, S.; Vorsanger, G.J.; Katz, N.P. Neuropsychological effects of long-term opioid use in chronic pain patients. J. Pain Symptom Manage., 2003, 26(4), 913-921.
http://dx.doi.org/10.1016/S0885-3924(03)00310-5 PMID: 14527760

[22]   WHO. Ocfentanil. Critical Review report. 2017. Available from: https://www.who.int/medicines/access/controlledsubstances/CriticalReview_Ocfentanil.pdf?ua=1

[23]   Ebrahim, Z.; Shoenwald, P.; Grimes-Rice, M.; Damask, M.C.; Khairallah, P.A. Multiple dose evaluation of the efficacy of ocfentanil HCl (A-3217) to produce postoperative analgesia. Anesth. Analg., 1991, 72, S63-S64.

[24]   Misailidi, N.; Papoutsis, I.; Nikolaou, P.; Dona, A.; Spiliopoulou, C.; Athanaselis, S. Fentanyls continue to replace heroin in the drug arena: the cases of ocfentanil and carfentanil. Forensic Toxicol., 2018, 36(1), 12-32.
http://dx.doi.org/10.1007/s11419-017-0379-4 PMID: 29367860

[25]   Schumann, J.; Perkins, M.; Dietze, P.; Nambiar, D.; Mitra, B.; Gerostamoulos, D.; Drummer, O.H.; Cameron, P.; Smith, K.; Beck, B. The prevalence of alcohol and other drugs in fatal road crashes in Victoria, Australia. Accid. Anal. Prev., 2021, 153, 105905.
http://dx.doi.org/10.1016/j.aap.2020.105905 PMID: 33631704

[26]   Logan, B.K.; D'Orazio, A.L.; Mohr, A.L.A.; Limoges, J.F.; Miles, A.K.; Scarneo, C.E.; Kerrigan, S.; Liddicoat, L.J.; Scott, K.S.; Huestis, M.A. Recommendations for toxicological investigation of drug-impaired driving and motor vehicle fatalities—2017 update. J. Anal. Toxicol., 2018, 42(2), 63-68.
http://dx.doi.org/10.1093/jat/bkx082 PMID: 29186455

[27]   Tonellato, DJ; Ransohoff, JR; Nash, C; Melamson, SEF; Petrides, AK; Tolan, NV; Goldberg, SA; Boyer, EW; Chai, PR; Erickson, TB Traumatic pedestrian and bicyclist injuries associated with intoxication. Am J Emerg Med. 2020, S0735-6757(20), 30710-5.
http://dx.doi.org/10.1016/j.ajem.2020.08.024

[28]   Rohrig, T.P.; Nash, E.; Osawa, K.A.; Shan, X.; Scarneo, C.; Youso, K.B.; Miller, R.; Tiscione, N.B. Fentanyl and driving impairment. J. Anal. Toxicol., 2021, 45(4), 389-396.
http://dx.doi.org/10.1093/jat/bkaa105 PMID: 32797153

[29]   Chan-Hosokawa, A.; Bierly, J.J. 11-year study of fentanyl in driving under the influence of drugs casework. J. Anal. Toxicol., 2022, 46(3), 337-341.
http://dx.doi.org/10.1093/jat/bkab049 PMID: 34002762

[30]   Drummer, O.H.; Yap, S. The involvement of prescribed drugs in road trauma. Forensic Sci. Int., 2016, 265, 17-21.
http://dx.doi.org/10.1016/j.forsciint.2015.12.050 PMID: 26826848

[31]   Berecki-Gisolf, J.; Hassani-Mahmooei, B.; Collie, A.; McClure, R. Prescription opioid and benzodiazepine use after road traffic injury. Pain Med., 2015, 17(2).

http://dx.doi.org/10.1111/pme.12890 PMID: 26271354

[32]   Giorgetti, A.; Centola, C.; Giorgetti, R. Fentanyl novel derivative-related deaths. *Hum. Psychopharmacol.*, **2017**, *32*(3), e2605.
http://dx.doi.org/10.1002/hup.2605 PMID: 28635020

[33]   Marquardt, K.A.; Steven Tharratt, R. Inhalation abuse of fentanyl patch. *J. Toxicol. Clin. Toxicol.*, **1994**, *32*(1), 75-78.
http://dx.doi.org/10.3109/15563659409000433 PMID: 8308952

[34]   Moon, J.M.; Chun, B.J. Fentanyl intoxication caused by abuse of transdermal fentanyl. *J. Emerg. Med.*, **2011**, *40*(1), 37-40.
http://dx.doi.org/10.1016/j.jemermed.2007.10.075 PMID: 18455903

[35]   European Monitoring Centre for Drugs and Drug Addiction (EMCDDA). Trends and Developments. *European Drug Report*; Publications Office of the European Union: Luxembourg, **2017**.

[36]   Helander, A.; Bäckberg, M.; Signell, P.; Beck, O. Intoxications involving acrylfentanyl and other novel designer fentanyls – results from the Swedish STRIDA project. *Clin. Toxicol. (Phila.)*, **2017**, *55*(6), 589-599.
http://dx.doi.org/10.1080/15563650.2017.1303141 PMID: 28349714

[37]   Guerrieri, D.; Rapp, E.; Roman, M.; Thelander, G.; Kronstrand, R. Acrylfentanyl: Another new psychoactive drug with fatal consequences. *Forensic Sci. Int.*, **2017**, *277*, e21-e29.
http://dx.doi.org/10.1016/j.forsciint.2017.05.010 PMID: 28587915

[38]   Butler, D.C.; Shanks, K.; Behonick, G.S.; Smith, D.; Presnell, S.E.; Tormos, L.M. Three cases of fatal acrylfentanyl toxicity in the united states and a review of literature. *J. Anal. Toxicol.*, **2018**, *42*(1), e6-e11.
http://dx.doi.org/10.1093/jat/bkx083 PMID: 29036502

[39]   Fogarty, M.F.; Papsun, D.M.; Logan, B.K. Analysis of fentanyl and 18 novel fentanyl analogs and metabolites by LC–MS-MS, and report of fatalities associated with methoxyacetylfentanyl and cyclopropylfentanyl. *J. Anal. Toxicol.*, **2018**, *42*(9), 592-604.
http://dx.doi.org/10.1093/jat/bky035 PMID: 29750250

[40]   Helander, A.; Bäckberg, M.; Beck, O. Intoxications involving the fentanyl analogs acetylfentanyl, 4-methoxybutyrfentanyl and furanylfentanyl: Results from the Swedish STRIDA project. *Clin. Toxicol. (Phila.)*, **2016**, *54*(4), 324-332.
http://dx.doi.org/10.3109/15563650.2016.1139715 PMID: 26850293

[41]   Allibe, N.; Billault, F.; Moreau, C.; Marchard, A.; Gaillard, Y.; Hoizey, G.; Eysseric-Guerin, H.; Milan, N. Ocfentanil in France: Seven case reports (2016–2018). *Toxicologie Analytique et Clinique*, **2019**, *31*(4), 317-322.
http://dx.doi.org/10.1016/j.toxac.2018.12.003

[42]   Starmark, J.E.; Stålhammar, D.; Holmgren, E. The Reaction Level Scale (RLS85). Manual and guidelines. *Acta Neurochir. (Wien)*, **1988**, *91*(1-2), 12-20.
http://dx.doi.org/10.1007/BF01400521 PMID: 3394542

[43]   Bluelight.org. Novel opioid; Furanylfentanyl Available from: http://www.bluelight.org/vb/threads/755118- [Accessed on: 2015 Nov].

[44]   Wedinos Quarterly Newsletter.Synthetic opioids. PHILTRE Bull 6: 3. Available from: http://www.wedinos.org/resources/down loads/Philtre_Issue_6.pdf Available from: https://www.wedinos.org/resources/downloads/WN_Annual_Report_1415_final.pdf [Accessed 09 Nov 2016].

[45]   Quintana, P.; Ventura, M.; Grifell, M.; Palma, A.; Galindo, L.; Fornís, I.; Gil, C.; Carbón, X.; Caudevilla, F.; Farré, M.; Torrens, M. The hidden web and the fentanyl problem: Detection of ocfentanil as an adulterant in heroin. *Int. J. Drug Policy*, **2017**, *40*, 78-83.
http://dx.doi.org/10.1016/j.drugpo.2016.10.006 PMID: 27889114

[46]   Coopman, V.; Cordonnier, J.; De Leeuw, M.; Cirimele, V. Ocfentanil overdose fatality in the recreational drug scene. *Forensic Sci. Int.*, **2016**, *266*(Suppl. C), 469-473.
http://dx.doi.org/10.1016/j.forsciint.2016.07.005 PMID: 27471990

[47]   Dussy, F.E.; Hangartner, S.; Hamberg, C.; Berchtold, C.; Scherer, U.; Schlotterbeck, G.; Wyler, D.; Briellmann, T.A. An acute ocfentanil fatality: A case report with post-mortem concentrations. *J. Anal. Toxicol.*, **2016**, *40*(9), 761-766.
http://dx.doi.org/10.1093/jat/bkw096 PMID: 27650310

[48]   Casati, S.; Minoli, M.; Angeli, I.; Ravelli, A.; Crudele, G.D.L.; Orioli, M. An ocfentanil-related death case: UHPLC-MS/MS analysis of the drug. *Drug Test. Anal.*, **2019**, *11*(1), 173-177.
http://dx.doi.org/10.1002/dta.2473 PMID: 30091284

[49]   Bilel, S.; Azevedo Neto, J.; Arfè, R.; Tirri, M.; Gaudio, R.M.; Fantinati, A.; Bernardi, T.; Boccuto, F.; Marchetti, B.; Corli, G.; Serpelloni, G.; De-Giorgio, F.; Malfacini, D.; Trapella, C.; Calo', G.; Marti, M. *In vitro* and *in vivo* pharmaco-dynamic study of the novel fentanyl derivatives: Acrylfentanyl, Ocfentanil and Furanylfentanyl. *Neuropharmacology*, **2022**, *209*, 109020.
http://dx.doi.org/10.1016/j.neuropharm.2022.109020 PMID: 35247453

[50]   Vigolo, A.; Ossato, A.; Trapella, C.; Vincenzi, F.; Rimondo, C.; Seri, C.; Varani, K.; Serpelloni, G.; Marti, M. Novel halogenated derivates of JWH-018: Behavioral and binding studies in mice. *Neuropharmacology*, **2015**, *95*, 68-82.
http://dx.doi.org/10.1016/j.neuropharm.2015.02.008 PMID: 25769232

[51]   Ossato, A.; Vigolo, A.; Trapella, C.; Seri, C.; Rimondo, C.; Serpelloni, G.; Marti, M. JWH-018 impairs sensorimotor functions in mice. *Neuroscience*, **2015**, *300*, 174-188.
http://dx.doi.org/10.1016/j.neuroscience.2015.05.021 PMID: 25987201

[52]   Canazza, I.; Ossato, A.; Trapella, C.; Fantinati, A.; De Luca, M.A.; Margiani, G.; Vincenzi, F.; Rimondo, C.; Di Rosa, F.; Gregori, A.; Varani, K.; Borea, P.A.; Serpelloni, G.; Marti, M. Effect of the novel synthetic cannabinoids AKB48 and 5F-AKB48 on "tetrad", sensorimotor, neurological and neurochemical responses in mice. *In vitro* and *in vivo* pharmacological studies. *Psychopharmacology (Berl.)*, **2016**, *233*(21-22), 3685-3709.
http://dx.doi.org/10.1007/s00213-016-4402-y PMID: 27527584

[53]   Fantinati, A.; Ossato, A.; Bianco, S.; Canazza, I.; De Giorgio, F.; Trapella, C.; Marti, M. 1-cyclohexyl-x-methoxybenzene derivatives, novel psychoactive substances seized on the internet market. Synthesis and *in vivo* pharmacological studies in mice. *Hum. Psychopharmacol.*, **2017**, *32*(3), e2560.
http://dx.doi.org/10.1002/hup.2560 PMID: 28657178

[54]   Ossato, A.; Bilel, S.; Gregori, A.; Talarico, A.; Trapella, C.; Gaudio, R.M.; De-Giorgio, F.; Tagliaro, F.; Neri, M.; Fattore, L.; Marti, M. Neurological, sensorimotor and cardiorespiratory alterations induced by methoxetamine, ketamine and phencyclidine in mice. *Neuropharmacology*, **2018**, *141*, 167-180.
http://dx.doi.org/10.1016/j.neuropharm.2018.08.017 PMID: 30165078

[55]   Ossato, A.; Canazza, I.; Trapella, C.; Vincenzi, F.; De Luca, M.A.; Rimondo, C.; Varani, K.; Borea, P.A.; Serpelloni, G.; Marti, M. Effect of JWH-250, JWH-073 and their interaction on "tetrad", sensorimotor, neurological and neurochemical responses in mice. *Prog. Neuropsychopharmacol. Biol. Psychiatry*, **2016**, *67*, 31-50.
http://dx.doi.org/10.1016/j.pnpbp.2016.01.007 PMID: 26780169

[56]   Marti, M.; Neri, M.; Bilel, S.; Di Paolo, M.; La Russa, R.; Ossato, A.; Turillazzi, E. MDMA alone affects sensorimotor and prepulse inhibition responses in mice and rats: tips in the debate on potential MDMA unsafety in human activity. *Forensic Toxicol.*, **2019**, *37*(1), 132-144.
http://dx.doi.org/10.1007/s11419-018-0444-7

[57]   Howells, R.D.; Groth, J.; Hiller, J.M.; Simon, E.J. Opiate binding sites in the retina: Properties and distribution. *J. Pharmacol. Exp. Ther.*, **1980**, *215*(1), 60-64.
PMID: 6256520

[58]   Zhu, Y.; Hsu, M.S.; Pintar, J.E. Developmental expression of the μ, κ, and δ opioid receptor mRNAs in mouse. *J. Neurosci.*, **1998**, *18*(7), 2538-2549.
http://dx.doi.org/10.1523/JNEUROSCI.18-07-02538.1998 PMID: 9502813

[59]   Bilel, S.; Azevedo, N.J.; Arfè, R.; Tirri, M.; Gregori, A.; Serpelloni, G.; De-Giorgio, F.; Frisoni, P.; Neri, M.; Calò, G.; Marti, M. *In vitro* and *in vivo* pharmacological characterization of the synthetic opioid MT-45. *Neuropharmacology*, **2020**, *171*, 108110.
http://dx.doi.org/10.1016/j.neuropharm.2020.108110 PMID: 32344007

[60]   Lambert, F.M.; Bras, H.; Cardoit, L.; Vinay, L.; Coulon, P.; Glover, J.C. Early postnatal maturation in vestibulospinal pathways in-

volved in neck and forelimb motor control. *Dev. Neurobiol.*, **2016**, 76(10), 1061-1077.
http://dx.doi.org/10.1002/dneu.22375 PMID: 26724676

[61] Meyer, A.F.; Poort, J.; O'Keefe, J.; Sahani, M.; Linden, J.F. A head-mounted camera system integrates detailed behavioral monitoring with multichannel electrophysiology in freely moving mice. *Neuron*, **2018**, 100(1), 46-60.e7.
http://dx.doi.org/10.1016/j.neuron.2018.09.020 PMID: 30308171

[62] Wallace, D.J.; Greenberg, D.S.; Sawinski, J.; Rulla, S.; Notaro, G.; Kerr, J.N.D. Rats maintain an overhead binocular field at the expense of constant fusion. *Nature*, **2013**, 498(7452), 65-69.
http://dx.doi.org/10.1038/nature12153 PMID: 23708965

[63] Khan, S.I.; Della Santina, C.C.; Migliaccio, A.A. Angular vestibuloocular reflex responses in Otop1 mice. I. Otolith sensor input is essential for gravity context-specific adaptation. *J. Neurophysiol.*, **2019**, 121(6), 2291-2299.
http://dx.doi.org/10.1152/jn.00811.2018 PMID: 30969887

[64] Meyer, A.F.; O'Keefe, J.; Poort, J. Two distinct types of eye-head coupling in freely moving mice. *Curr. Biol.*, **2020**, 30(11), 2116-2130.e6.
http://dx.doi.org/10.1016/j.cub.2020.04.042 PMID: 32413309

[65] Tosolini, A.P.; Morris, R. Spatial characterization of the motor neuron columns supplying the rat forelimb. *Neuroscience*, **2012**, 200, 19-30.
http://dx.doi.org/10.1016/j.neuroscience.2011.10.054 PMID: 22100785

[66] Tosolini, A.P.; Mohan, R.; Morris, R. Targeting the full length of the motor end plate regions in the mouse forelimb increases the uptake of fluoro-gold into corresponding spinal cord motor neurons. *Front. Neurol.*, **2013**, 4, 58.
http://dx.doi.org/10.3389/fneur.2013.00058 PMID: 23730296

[67] Payne, H.L.; Raymond, J.L. Magnetic eye tracking in mice. *eLife*, **2017**, 6, e29222.
http://dx.doi.org/10.7554/eLife.29222 PMID: 28872455

[68] Lin, Y.; Carpenter, D.O. Direct excitatory opiate effects mediated by non-synaptic actions on rat medial vestibular neurons. *Eur. J. Pharmacol.*, **1994**, 262(1-2), 99-106.
http://dx.doi.org/10.1016/0014-2999(94)90032-9 PMID: 7813583

[69] Drago, F.; Gorgone, G.; Spina, F.; Panissidi, G.; Bello, A.D.; Moro, F.; Scapagnini, U. Opiate receptors in the rabbit iris. *Naunyn Schmiedebergs Arch. Pharmacol.*, **1980**, 315(1), 1-4.
http://dx.doi.org/10.1007/BF00504223 PMID: 6264328

[70] Selbach, J.M.; Buschnack, S.H.; Steuhl, K.P.; Kremmer, S.; Muth-Selbach, U. Substance P and opioid peptidergic innervation of the anterior eye segment of the rat: an immunohistochemical study. *J. Anat.*, **2005**, 206(3), 237-242.
http://dx.doi.org/10.1111/j.1469-7580.2005.00379.x PMID: 15733295

[71] Cleymaet, A.M.; Berezin, C.T.; Vigh, J. Endogenous opioid signaling in the mouse retina modulates pupillary light reflex. *Int. J. Mol. Sci.*, **2021**, 22(2), 554.
http://dx.doi.org/10.3390/ijms22020554 PMID: 33429857

[72] Cleymaet, A.M.; Gallagher, S.K.; Tooker, R.E.; Lipin, M.Y.; Renna, J.M.; Sodhi, P.; Berg, D.; Hartwick, A.T.E.; Berson, D.M.; Vigh, J. μ-opioid receptor activation directly modulates intrinsically photosensitive retinal ganglion cells. *Neuroscience*, **2019**, 408, 400-417.
http://dx.doi.org/10.1016/j.neuroscience.2019.04.005 PMID: 30981862

[73] Wilde, M.; Pichini, S.; Pacifici, R.; Tagliabracci, A.; Busardò, F.P.; Auwärter, V.; Solimini, R. Metabolic pathways and potencies of new fentanyl analogs. *Front. Pharmacol.*, **2019**, 10, 238.
http://dx.doi.org/10.3389/fphar.2019.00238 PMID: 31024296

[74] Varshneya, N.B.; Hassanien, S.H.; Holt, M.C.; Stevens, D.L.; Layle, N.K.; Bassman, J.R.; Iula, D.M.; Beardsley, P.M. Respiratory depressant effects of fentanyl analogs are opioid receptor-mediated. *Biochem. Pharmacol.*, **2022**, 195, 114805.
http://dx.doi.org/10.1016/j.bcp.2021.114805 PMID: 34673011

[75] Jongkamonwiwat, N.; Phansuwan-Pujito, P.; Sarapoke, P.; Chetsawang, B.; Casalotti, S.O.; Forge, A.; Dodson, H.; Govitrapong, P. The presence of opioid receptors in rat inner ear. *Hear. Res.*, **2003**, 181(1-2), 85-93.

http://dx.doi.org/10.1016/S0378-5955(03)00175-8 PMID: 12855366

[76] Jongkamonwiwat, N.; Phansuwan-Pujito, P.; Casalotti, S.O.; Forge, A.; Dodson, H.; Govitrapong, P. The existence of opioid receptors in the cochlea of guinea pigs. *Eur. J. Neurosci.*, **2006**, 23(10), 2701-2711.
http://dx.doi.org/10.1111/j.1460-9568.2006.04810.x PMID: 16817873

[77] Nguyen, K.D.; Mowlds, D.; Lopez, I.A.; Hosokawa, S.; Ishiyama, A.; Ishiyama, G. Mu-opioid receptor (MOR) expression in the human spiral ganglia. *Brain Res.*, **2014**, 1590, 10-19.
http://dx.doi.org/10.1016/j.brainres.2014.09.051 PMID: 25278190

[78] Helander, A.; Bäckberg, M.; Beck, O. MT-45, a new psychoactive substance associated with hearing loss and unconsciousness. *Clin. Toxicol. (Phila.)*, **2014**, 52(8), 901-904.
http://dx.doi.org/10.3109/15563650.2014.943908 PMID: 25175898

[79] Lopez, I.; Ishiyama, A.; Ishiyama, G. Sudden sensorineural hearing loss due to drug abuse. *Semin. Hear.*, **2012**, 33(3), 251-260.
http://dx.doi.org/10.1055/s-0032-1315724

[80] Christenson, B.J.; Marjala, A.R.P. Two cases of sudden sensorineural hearing loss after methadone overdose. *Ann. Pharmacother.*, **2010**, 44(1), 207-210.
http://dx.doi.org/10.1345/aph.1M250 PMID: 20028962

[81] Saifan, C.; Glass, D.; Barakat, I.; El-Sayegh, S. Methadone induced sensorineural hearing loss. *Case Rep. Med.*, **2013**, 2013, 1-5.
http://dx.doi.org/10.1155/2013/242730 PMID: 23983704

[82] Ramirez, T.; Soto, E.; Vega, R. Opioid modulation of cochlear auditory responses in the rat inner ear. *Synapse*, **2020**, 74(1), e22128.
http://dx.doi.org/10.1002/syn.22128 PMID: 31403743

[83] Yang, H.M.; Zhan, L.J.; Lin, X.Q.; Chu, C.P.; Qiu, D.L.; Lan, Y. Fentanyl inhibits air puff-evoked sensory information processing in mouse cerebellar neurons recorded *in vivo*. *Front. Syst. Neurosci.*, **2020**, 14, 51.
http://dx.doi.org/10.3389/fnsys.2020.00051 PMID: 32848643

[84] Horswill, M.S.; Plooy, A.M. Auditory feedback influences perceived driving speeds. *Perception*, **2008**, 37(7), 1037-1043.
http://dx.doi.org/10.1068/p5736 PMID: 18773726

[85] Wilkins, L.; Gray, R.; Gaska, J.; Winterbottom, M. Motion perception and driving: Predicting performance through testing and shortening braking reaction times through training. *Invest. Ophthalmol. Vis. Sci.*, **2013**, 54(13), 8364-8374.
http://dx.doi.org/10.1167/iovs.13-12774 PMID: 24282222

[86] Ivers, R.Q.; Mitchell, P.; Cumming, R.G. Sensory impairment and driving: The blue mountains eye study. *Am. J. Public Health*, **1999**, 89(1), 85-87.
http://dx.doi.org/10.2105/AJPH.89.1.85 PMID: 9987472

[87] Wang, M.; Liao, Y.; Lyckvi, S.L.; Chen, F. How drivers respond to visual *vs.* auditory information in advisory traffic information systems. *Behav. Inf. Technol.*, **2020**, 39(12), 1308-1319.
http://dx.doi.org/10.1080/0144929X.2019.1667439

[88] Gaffary, Y.; Lécuyer, A. The use of haptic and tactile information in the car to improve driving safety: A review of current technologies. *Front. ICT*, **2018**, 5, 5.
http://dx.doi.org/10.3389/fict.2018.00005

[89] Pesavento, S.; Bilel, S.; Murari, M.; Gottardo, R.; Arfè, R.; Tirri, M.; Panato, A.; Tagliaro, F.; Marti, M. Zebrafish larvae: A new model to study behavioural effects and metabolism of fentanyl, in comparison to a traditional mice model. *Med. Sci. Law*, **2022**, 62(3), 188-198.
http://dx.doi.org/10.1177/00258024221074568 PMID: 35040690

[90] Klebacher, R.; Harris, M.I.; Ariyaprakai, N.; Tagore, A.; Robbins, V.; Dudley, L.S.; Bauter, R.; Koneru, S.; Hill, R.D.; Wasserman, E.; Shanes, A.; Merlin, M.A. Incidence of naloxone redosing in the age of the new opioid epidemic. *Prehosp. Emerg. Care*, **2017**, 21(6), 682-687.
http://dx.doi.org/10.1080/10903127.2017.1335818 PMID: 28686547

[91] Available from: https://www.ebi.ac.uk/interpro/entry/InterPro/IPR000105/

[92] Rothman, R.B.; Xu, H.; Wang, J.B.; Partilla, J.S.; Kayakiri, H.; Rice, K.C.; Uhl, G.R. Ligand selectivity of cloned human and rat opioid mu receptors. *Synapse*, **1995**, 21(1), 60-64.

http://dx.doi.org/10.1002/syn.890210109 PMID: 8525463

[93]   Zhang, X.; Hutchins, S.D.; Blough, B.E.; Vallender, E.J. *In vitro* effects of ligand bias on primate mu opioid receptor downstream signaling. *Int. J. Mol. Sci.*, **2020**, *21*(11), 3999.
http://dx.doi.org/10.3390/ijms21113999 PMID: 32503269

[94]   Abood, M.E.; Noel, M.A.; Carter, R.C.; Harris, L.S. Evaluation of a series of N-alkyl benzomorphans in cell lines expressing transfected δ - and μ-opioid receptors. *Biochem. Pharmacol.*, **1995**, *50*(6), 851-859.
http://dx.doi.org/10.1016/0006-2952(95)02007-Y PMID: 7575648

Article

The Genotoxicity of Acrylfentanyl, Ocfentanyl and Furanylfentanyl Raises the Concern of Long-Term Consequences

Sofia Gasperini [1], Sabrine Bilel [2], Veronica Cocchi [1], Matteo Marti [2,3], Monia Lenzi [1,*] and Patrizia Hrelia [1]

[1] Department of Pharmacy and Biotechnology, Alma Mater Studiorum University of Bologna, 40126 Bologna, Italy

[2] LTTA Center and University Center of Gender Medicine, Department of Translational Medicine, Section of Legal Medicine, University of Ferrara, 44121 Ferrara, Italy

[3] Collaborative Center of the National Early Warning System, Department for Anti-Drug Policies, Presidency of the Council of Ministers, 00186 Rome, Italy

* Correspondence: m.lenzi@unibo.it

Abstract: Three fentanyl analogues Acrylfentanyl, Ocfentanyl and Furanylfentanyl are potent, rapid-acting synthetic analgesics that recently appeared on the illicit market of new psychoactive substances (NPS) under the class of new synthetic opioids (NSO). Pharmacotoxicological data on these three non-pharmaceutical fentanyl analogues are limited and studies on their genotoxicity are not yet available. Therefore, the aim of the present study was to investigate this property. The ability to induce structural and numerical chromosomal aberrations in human lymphoblastoid TK6 cells was evaluated by employing the flow cytometric protocol of the in vitro mammalian cell micronucleus test. Our study demonstrated the non-genotoxicity of Fentanyl, i.e., the pharmaceutical progenitor of the class, while its illicit non-pharmaceutical analogues were found to be genotoxic. In particular, Acrylfentanyl led to a statistically significant increase in the MNi frequency at the highest concentration tested (75 µM), while Ocfentanyl and Furanylfentnyl each did so at both concentrations tested (150, 200 µM and 25, 50 µM, respectively). The study ended by investigating reactive oxygen species (ROS) induction as a possible mechanism linked to the proved genotoxic effect. The results showed a non-statistically significant increase in ROS levels in the cultures treated with all molecules under study. Overall, the proved genotoxicity raises concern about the possibility of serious long-term consequences.

Keywords: Acrylfentanyl; Ocfentanyl; Furanylfentanyl; Fentanyl; new psychoactive substances; new synthetic opioids; genotoxicity; in vitro mammalian cell micronucleus test; flow cytometry

1. Introduction

Fentanyl is a potent, rapid-acting synthetic analgesic, first developed in 1960 by Dr. Paul Janssen and the Janssen Company [1]. Due to its high potency, efficacy and rapid action, Fentanyl has become one of the world's most important opioids and is frequently used to manage acute and chronic pain conditions. Indeed, Fentanyl is about 50–100 times more potent than the well-known natural opioid morphine [2]. Similarly to other opioids, Fentanyl acts as a stimulant of the μ-opioid receptors and typically induces central nervous system effects including euphoria, sedation, fatigue, nausea, vomiting, dizziness, respiratory depression, bradycardia and anesthesia at high dosage [3]. Following Fentanyl's discovery, several structural analogues have been designed by various pharmaceutical companies to enhance the pharmacological action of these drugs [3]. A few years after Fentanyl and its analogues' approval as medicines, clinical misuse and illicit use were reported [2]. Deaths from Fentanyl overdose have been due to inappropriate prescriptions by clinicians, patients' misuse and increased illicit use and abuse [3]. More recently, Fentanyl appeared on the illicit market of new psychoactive substances (NPS) under the class of novel synthetic opioids (NSO) [4]. Fentanyl and its non-pharmaceutical analogues are easily produced in clandestine laboratories and are sold in different forms such as

104

powder or tablets to be injected, ingested, snorted or smoked, often sold as an alternative or adulterant to heroin [4,5]. To date, about one thousand Fentanyl analogues have been reported to the European Monitoring Centre for Drugs and Drugs Abuse (EMCDDA) [6]. In 2017, 940 seizures of Fentanyl derivatives were reported for a total of 14,3 tons in 13 countries of the European Union [5].

Fentanyl analogues contribute to the current epidemic of opioid overdose deaths in many countries [4–6]. Overdose death related to Fentanyl analogues is mainly due to the unpredictability of their potency. Moreover, in some cases of Fentanyl-related deaths involving Acrylfentanyl, Ocfentanyl and Furanylfentanyl (Figure 1), no heroin was detected [7].
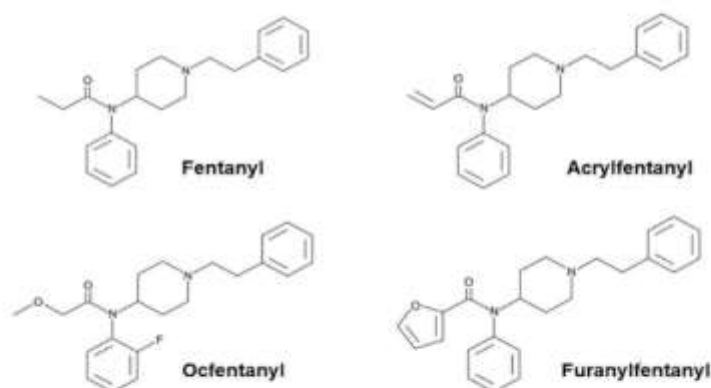
Figure 1. Molecular structures of Fenatnyl, Acrylfentanyl, Ocfentanyl and Furanylfentanyl.

Acrylfentanyl, N-phenyl-N-[1-(2-phenethyl)piperidin-4-yl]prop-2-enamide, was first developed in 1981 as an unsaturated fentanyl analogue [8]. It is an acrylamide derivative of 4-anilinopiperidine. In the last few years, it has appeared on the Surface Web as a research chemical. In 2016, the EMCDDA reported a total of 130 deaths caused by Acrylfentanyl in the United States and Europe [9].

Ocfentanyl, N-(2-fluorophenyl)-2-methoxy-N-[1-(2-phenylethyl)piperidin-4-yl]acetamide, is a fentanyl analogue which has an extra fluorine atom on the o-position of the aniline moiety and a methoxy group instead of a methyl group. It had been studied clinically for its analgesic activity during the early 1990s and was found to have a relative potency 200 times greater than that of morphine and 2.5 times more potent than Fentanyl, with lower cardio-respiratory toxicity. However, it has never been approved for medical use [10]. Ocfentanyl was among the 14 Fentanyl derivatives that were reported in Europe's illicit market between 2012 and 2016. It has been associated with cases of intoxication and death in Belgium and Switzerland [11].

Furanylfentanyl, N-phenyl-N-[1-(2-phenylethyl)piperidin-4-yl]furan-2-carboxamide, is another Fentanyl analogue, first described in 1958, which differs from Fentanyl by the presence of a furanyl ring in place of the methyl group adjacent to the carbonyl bridge. Furanylfentanyl showed a seven-fold higher potency compared with fentanyl, but it has not been approved for any medical use [10]. Since 2015, Furanylfentanyl has been identified in the United States and in 16 member states of the European Union. In 2016, a total of 494 forensic cases regarding Furanylfentanyl, including 128 confirmed fatalities, were reported to the DEA. In 2017, the EMCDDA reported 10 acute intoxications and 19 deaths associated with Furanylfentanyl in Europe and Norway [12].

In general, pharmacotoxicological data on these compounds is limited, but a recent study on the pharmacodynamics of Fentanyl and its three analogues revealed that Acrylfentanyl, Ocfentanyl and Furanylfentanyl behave similarly to Fentanyl as μ opioid agonists.

105

In particular, Acrylfentanyl, Ocfentanyl and Furanylfentanyl acted as partial agonists on µ opioid receptors in vitro. Moreover, in the BRET G-protein assay, Fentanyl, Acrylfentanyl and Ocfentanyl behaved as partial agonists for the β-arrestin 2 pathway, whereas Furanylfentanyl did not promote β-arrestin 2 recruitment. In the same study, Fentanyl, Acrylfentanyl and Ocfentanyl increased mechanical and thermal analgesia and impaired motor and cardiorespiratory parameters in vivo, while Furanylfentanyl showed lower potency for cardiorespiratory and motor effects [13].

Moreover, another study demonstrated that larvae fish exposed for 24 h to fentanyl at different concentrations of 1, 10, 50, 100 µM survived, although they manifested several morphological malformations [14].

Regarding the genotoxicological hazards of fentanyls, to our knowledge, only one study has been published concerning Fentanyl and two of its pharmaceutical analogues (Alfentantil and Remifentanil) [15], while studies on the genotoxicity of non-pharmaceutical fentanyl analogues, including Acrylfentanyl, Ocfentanyl and Furanylfentanyl, are not yet available.

Therefore, in order to fill this gap, the aim of the present study was to evaluate the genotoxicity of these three fentanyl analogues and their progenitor Fentanyl in human lymphoblastoid TK6 cells, particularly in terms of the ability to induce structural and numerical chromosomal aberrations. For this purpose, we evaluated the frequency of micronuclei (MNi) by employing a flow cytometric (FCM) protocol developed in our laboratory and published [16,17] as the in vitro mammalian cell micronucleus test (MNvit), correspondent to OECD guideline n°487. We selected the concentrations to be tested based on cytotoxicity thresholds established by OECD and on apoptosis induction, checked as an alternative cell death mechanism to necrosis [18].

2. Results

2.1. Cytotoxicity Evaluation

According to OECD guideline n°487, the highest concentration to be tested for MNi frequency evaluation should not produce cytotoxicity levels greater than $55 \pm 5\%$, and consequently it is recommended to proceed only if the treated populations display cell viability and cell proliferation of at least $45 \pm 5\%$ when compared with concurrent negative control cultures [18]. Figure 2 shows the compliance with the OECD guideline threshold (represented by the red line) of the cytotoxicity induced by all fentanyls at all the concentrations tested.

Table 1. RPD of TK6 cells after 26 h treatment with Fentanyl, Acrylfentanyl, Ocfentanyl or Furanylfentanyl at the indicated concentrations compared to the concurrent negative control [0 µM]. Each value represents the mean ± SEM of three independent experiments. Data were analyzed using one-way repeated measures ANOVA followed by Dunnet as post-test. * $p < 0.05$ vs. [0 µM]; *** $p < 0.001$ vs. [0 µM]. The red lines separate the RPDs complying or not with the OECD threshold for cell replication $(45 \pm 5\%)$.

Concentration	RPD Fentanyl	RPD Acrylfentanyl	RPD Ocfentanyl	RPD Furanylfentanyl
0 µM	100.0%	100.0%	100.0%	100.0%
25 µM	$95.2 \pm 1.1\%$	$96.8 \pm 0.3\%$	$99.7 \pm 0.2\%$	$98.8 \pm 1.3\%$
50 µM	$89.9 \pm 1.5\%$ *	$91.8 \pm 2.3\%$ *	$97.1 \pm 1.6\%$	$78.4 \pm 1.9\%$ ***
75 µM	$90.0 \pm 2.6\%$	$78.75 \pm 2.8\%$ ***	$95.5 \pm 2.7\%$	$38.3 \pm 1.6\%$
100 µM	$91.2 \pm 2.9\%$ *	$64.1 \pm 1.2\%$ ***	$94.4 \pm 4.1\%$	$20.5 \pm 0.5\%$ ***
150 µM	$85.5 \pm 1.6\%$ ***	$40.9 \pm 1.1\%$ ***	$97.2 \pm 1.7\%$	0.0% ***
200 µM	$80.6 \pm 1.3\%$ ***	$1.5 \pm 2.4\%$ ***	$93.1 \pm 2.4\%$ *	0.0% ***
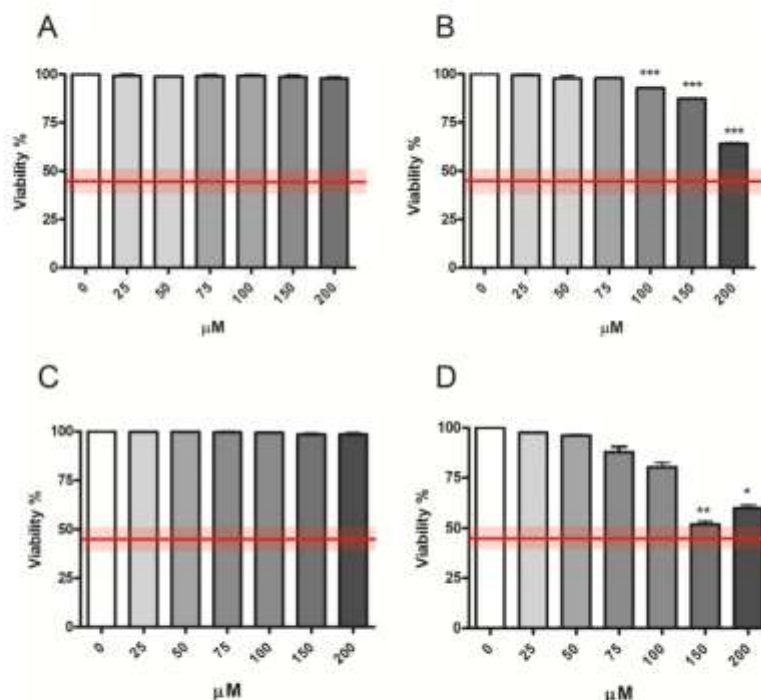
Figure 2. Cell viability of TK6 cells after 26 h treatment with (**A**) Fentanyl, (**B**) Acrylfentanyl, (**C**) Ocfentanyl or (**D**) Furanylfentanylat the indicated concentrations compared to the concurrent negative controls [0 μM]. Each bar represents the mean ± SEM of three independent experiments. Data were analyzed using one-way repeated measures ANOVA followed by Dunnet as post-test. * $p < 0.05$ vs. [0 μM]; ** $p < 0.01$ vs. [0 μM]; *** $p < 0.001$ vs. [0 μM]. The red line represents the OECD threshold for viability (45 ± 5%).

Meanwhile, correct cell replication was also checked by calculating the relative population doubling (RPD), whose formula is reported in Materials and Methods Section 4.4.1 [18].

RPDs were above the OECD guideline threshold (equal to 45 ± 5%) for Fentanyl and Ocfentanyl at all the concentrations tested, for Acrylfentanyl up to 100 μM and for Furanylfentanyl up to 50 μM (Table 1).

2.2. Apoptosis Evaluation

Apoptosis induction was measured to analyze an alternative cell death mechanism to necrosis and to check if apoptosis levels in treated cultures were comparable or up to twice the values measured in the concurrent negative cultures. In particular, the two or three highest concentrations that complied with the OECD cytotoxicity thresholds were evaluated for each substance: 100, 150 and 200 μM for Fentanyl, 50, 75 and 100 μM for Acrylfentanyl, 100, 150 and 200 μM for Ocfentanyl and 25 and 50 μM for Furanylfentanyl. Etoposide (ETP) 5 μg/mL was used as positive control.

Apoptosis never doubled compared to that measured in the concurrent negative control for all fentanyls tested, except for Acrylfentanyl 100 μM (2.5 vs. 1.0, but not statistically significant) (Figure 3).
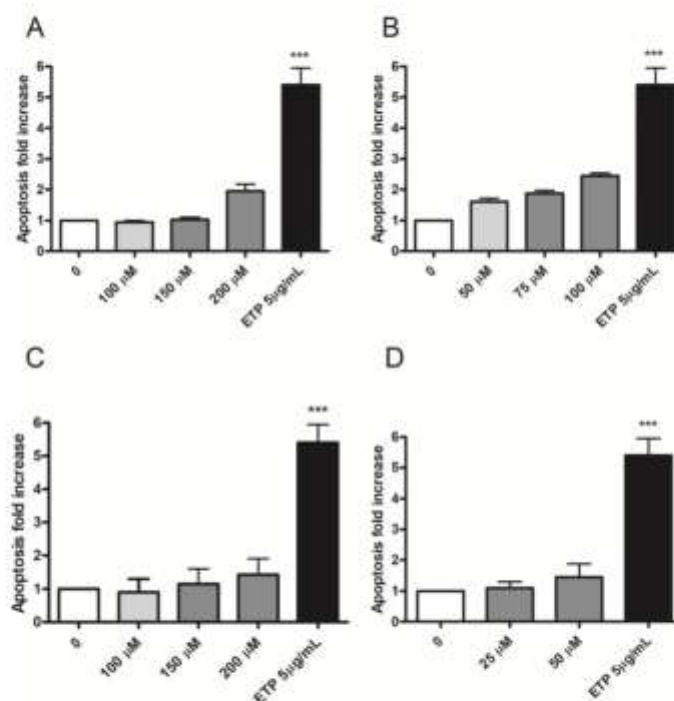
Figure 3. Apoptosis fold increase in TK6 cells after 26 h treatment with (**A**) Fentanyl, (**B**) Acrylfentanyl, (**C**) Ocfentanyl or (**D**) Furanylfentanyl or the positive control ETP at the indicated concentrations, compared to the concurrent negative control [0 μM]. Each bar represents the mean $\pm$ SEM of three independent experiments. Data were analyzed using one-way repeated measures ANOVA followed by Bonferroni as post-test. *** $p < 0.001$ vs. [0 μM].

2.3. MNi Frequency Evaluation

Based on the results obtained from viability, RPD and apoptosis, two concentrations to be tested for MNi frequency evaluation were selected for each compound: 150 and 200 μM for Fentanyl, 75 and 100 μM for Acrylfentanyl, 150 and 200 μM for Ocfentanyl and 25 and 50 μM for Furanylfentanyl.

To evaluate the potential genotoxic effect associated with these fentanyls, the number of MNi was measured in untreated negative control cultures, fentanyls-treated cultures and positive control-treated cultures, i.e., treated with Mytomicin C (MMC) or Vinblastine (VINB).

Fentanyl was the only molecule that did not cause a statistically significant increase in the MNi frequency fold increase at any of the concentrations tested. On the contrary, Acrylfentanyl determined a statistically significant increase only at the highest concentration tested, while Ocfentanyl and Furanylfentnyl did so at both the concentrations tested (Figure 4A,D,G,J).

In Figure 3, representative FCM dot plots are reported to support the results obtained. In particular, they show how the numbers of MNi were much higher in Acrylfentanyl, Ocfentanyl or Furanylfentanyl-treated cultures (Figure 4F,I,L) than in the concurrent negative control cultures (Figure 4E,H,K), while in Fentanyl-treated cultures (Figure 4C) they were comparable to the concurrent negative control cultures (Figure 4B).
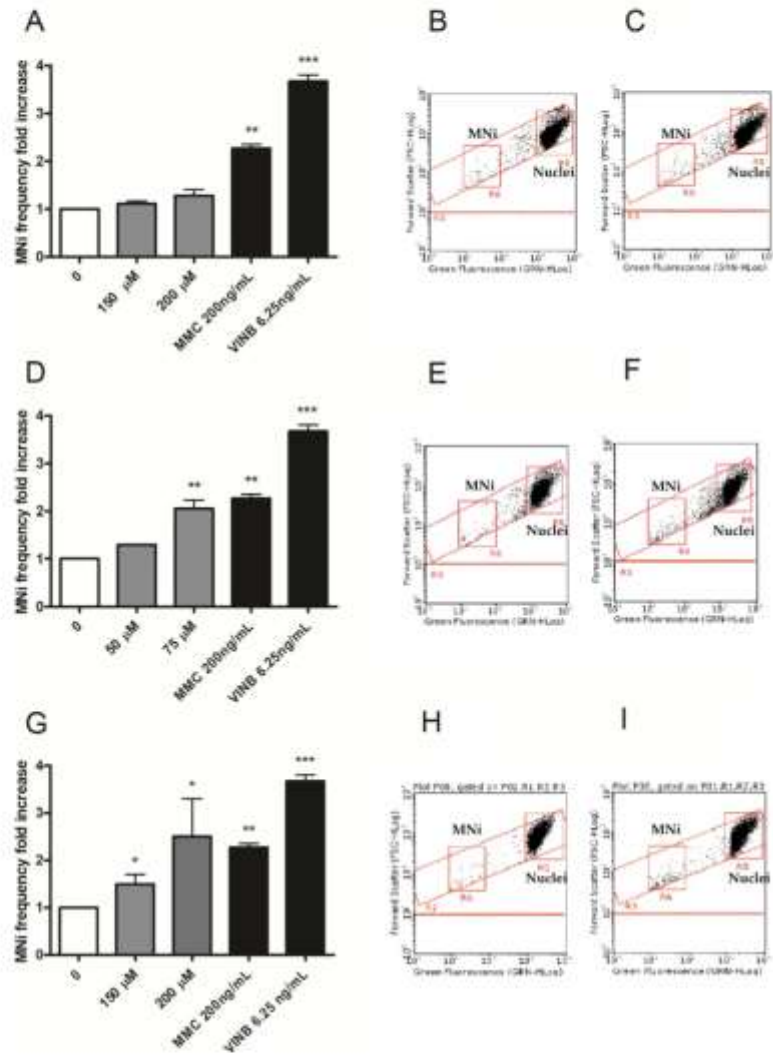
Figure 4. *Cont.*
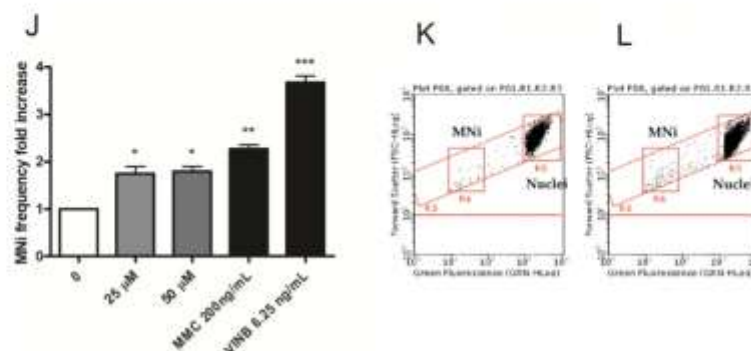
Figure 4. MNi fold increase in TK6 cells after 26 h treatment with (**A**) Fentanyl, (**D**) Acrylfentanyl, (**G**) Ocfentanyl or (**J**) Furanylfentanyl or positive controls (MMC, VINB) at the indicated concentrations compared to the concurrent negative control [0 μM]. Each bar represents the mean ± SEM of three independent experiments. Data were analyzed using one-way repeated measures ANOVA followed by Bonferroni as post-test. * $p < 0.05$ vs. [0 μM]; ** $p < 0.01$ vs. [0 μM]; *** $p < 0.001$ vs. [0 μM]. Dot plots obtained by FCM in (**B,E,H,K**) negative controls, (**C**) Fentanyl 200 μM, (**F**) Acrylfentanyl 75 μM, (**I**) Ocfentanyl 200 μM and (**L**) Furanylfentanyl 50 μM. "MNi" and "Nuclei" indicate the regions of the dot plot where MNi and nuclei can be found.

2.4. ROS Evaluation

In order to identify a possible mechanism linked to the proved genotoxic effect, TK6 cells were treated with all fentanyls under study for 1 h, and then possible ROS induction was measured.

For each substance, the highest concentration tested for the MN frequency evaluation was selected for ROS evaluation: 200 μM for Fentanyl, 100 μM for Acrylfentanyl, 200 μM for Ocfentanyl and 50 μM for Furanylfentanyl. For all fentanyls-treated cultures, the results did not show a statistically significant increase of the mean fluorescence intensity compared with the concurrent negative controls (Figure 5).
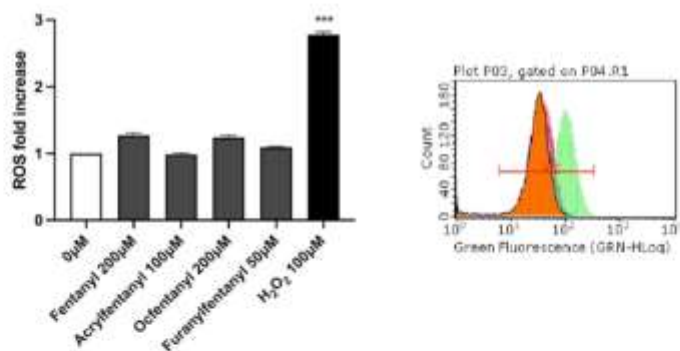
Figure 5. ROS fold increase in TK6 cells after 1 h treatment with Fentanyl, Acrylfentanyl, Ocfentanyl and Furanylfentanyl or positive control [H_2O_2] at the indicated concentrations, compared to the concurrent negative control [0 μM]. Each bar represents the mean ± SEM of three independent experiments. Data were analyzed using repeated ANOVA followed by Dunnet as post-test. *** $p < 0.001$ vs. [0 mg/mL]. Histograms obtained by FCM for the negative control (orange), H_2O_2 (green) and fentanyls (other colors).

3. Discussion

The protection of public health necessarily includes the risk assessment of any substance to which humans are potentially exposed. The risk assessment, in turn, necessarily includes the evaluation of genotoxicity and carcinogenicity. While this concept is well-known and strictly regulated for pharmaceutical drugs, cosmetics, pesticides and food additives, it has not been so frequently studied for drugs of abuse. In general, and rightly so, careful attention is given to the management of the intoxicated patient and to understanding and containing the acute toxic effects. However, we must also pay close attention to the potential long-term effects of genotoxicity, which can induce permanent transmissible changes in the amount or structure of the genetic material, and can occur as early as a single exposure and with increased likelihood following repeated exposure [19].

The available toxicological data are limited regarding the non-pharmaceutical illicit fentanyl analogues Acrylfentanyl, Ocfentanyl and Furanylfentanyl, and genotoxicological data are totally absent. Therefore, in this work we investigated their genotoxic potential and that of their progenitor Fentanyl.

To assess genotoxicity, first we defined the concentrations to be tested of all fentanyls under study, based on absent or poor cell death and replicative capacity [18]. OECD guideline n°487 established a cytotoxicity threshold equal to $55 \pm 5\%$, which consequently corresponds to a cell viability and proliferation of at least $45 \pm 5\%$ when compared to concurrent negative control cultures [18].

For this purpose, we applied propidium iodide (PI) staining to determine the percentage of viable cells in untreated cultures and cultures treated with Fentanyl, Acrylfentanyl, Ocfentanyl or Furanylfentanyl scalar concentrations from 0 to 200 μM. The results obtained showed that all fentanyls complied with the OECD threshold at all the concentrations tested.

In parallel, by the same assay we measured the number of cells at time zero (time of cellular seeding) and at the end of the treatment time, to check correct cell proliferation. The threshold was met by Fentanyl and Ocfentanyl at all the concentrations tested, while by Acrylfentanyl up to 100 μM and by Furanylfentanyl up to 50 μM.

PI staining makes it possible to discriminate between viable and necrotic cells, but it does not highlight apoptotic cells. The distinction is based solely on the difference in membrane integrity and consequent permeability to PI. For this reason, apoptotic cells, characterized by a still intact membrane, could be misinterpreted by the instrument as viable cells. Therefore, we proceeded with a more specific test to highlight this alternative death mechanism. We performed a double staining 7-AAD/Annexin V-PE assay to measure the percentage of apoptotic cells in untreated cultures as well as in those treated with Fentanyl 100, 150 and 200 μM, Acrylfentanyl 50, 75 and 100 μM, Ocfentanyl 100, 150 and 200 μM and Furanylfentanyl 25 and 50 μM, corresponding to the two or three highest concentrations selected from those meeting the cytotoxicity thresholds. The results obtained demonstrated that apoptosis never as much as doubled compared to that measured in the concurrent negative control, for all compounds except for Acrylfentanyl 100 μM but without statistical significance. This outcome is particularly important from a genotoxicological point of view. The process of apoptosis could be triggered as a consequence of unrepaired genetic damage, induced by genotoxic agents. However, resistance to apoptosis can result in the inability of cells through this selective cell elimination to counteract the transmission of genetic damage from mother cell to daughter cells [20,21].

Having identified suitable concentrations, we evaluated genotoxicity in terms of induction of chromosomal aberrations, selecting the MNvit test for this purpose. The *Overview of the set of OECD genetic toxicology test guidelines* lists the genotoxicity tests validated by OECD [22]. Among them, those especially recommended by most regulatory agencies and international authorities and most frequently used by the scientific community are the bacterial reverse mutation test (Ames test), corresponding to OECD guideline n°471, and the MNvit, corresponding to OECD guideline n°487. The former identifies chemicals that induce gene mutations, the latter allows highlighting of structural chromosomal aberrations induced by clastogenic agents and numerical chromosomal aberrations induced

by aneugenic agents. The MNvit test therefore owes its success to scientific validity, versatility and efficacy. However, the classic method of analysis by optical microscopy is affected by certain critical issues, such as the subjectivity of interpretation, long sample preparation and analysis times, and the number of events examined which is extremely low for the purpose of robust statistical analysis. To overcome these limits, we developed and published in 2018 an innovative protocol to score MNi by flow cytometry. Since then, our protocol has been successfully used to prove the genotoxicity of different NPS [23–26] and the lack of genotoxic capacity of other types of substances [17,27].

In the present study our protocol permitted us to demonstrate the inability of Fentanyl to increase statistically significantly the frequency of MNi.

To our knowledge, only one study is available in the literature regarding the genotoxicological evaluation of this drug in vitro and in vivo, reporting a positive outcome only in the in vitro L5178Y $tk^{+/-}$ mouse lymphoma assay (MLA) in the presence of rat liver metabolic activation (S9), and negative outcomes in other genotoxicity tests such as the Ames test, the unscheduled DNA synthesis (UDS) assay on primary rat hepatocytes and the in vitro chromosomal aberration (CA) assay on human lymphocytes and CHO cells. Moreover, the same authors also reported that Fentanyl did not cause a positive response in the in vitro carcinogenicity BALB/c-3T3 transformation test. These results substantially agree with our results, except for the MLA findings.

Regarding the three non-pharmaceutical illicit fentanyl analogues tested in the present work, contrary to their progenitor, our results demonstrated the genotoxic ability of Ocfentanyl and Furanylfentanyl at both the concentrations tested, and that of Acrylfentanyl at the highest concentration tested.

These results may seem to conflict partially with what was demonstrated regarding two other pharmaceutical Fentanyl analogues, Alfentanil and Remifentanil [15]. In particular, Alfentanil determined a non-genotoxic response in the Ames test and in an in vivo MN test [15]. The pharmaceutical analogue Remifentanil was revealed to be non-genotoxic according to the Ames test, an in vitro CA assay in CHO cells, an in vivo MN assay in rat erythrocytes and in vivo/in vitro UDS assay in rat hepatocytes. However, similarly to Fentanyl, Remifentanil also produced a weak genotoxic response only in the in vitro L5178Y $tk^{+/-}$ MLA in the presence of rat liver S9 metabolic activation [15]. All these outcomes are summarized in Table 2.

These contrasting results for Fentanyl analogues are an indication of molecules characterized by structural differences.

In light of this, it would be interesting to investigate the relationship between fentanyls' structures and their genotoxic potential. However, this is not an easy task considering the scarcity of data on this specific aspect of fentanyls.

More generally, regarding the prediction of chemicals' genotoxicity, in silico studies reported aniline and substituted anilines present in all fentanyls, among the representative structural alerts which are present in MN-positive chemicals [28,29]. Furthermore, another innovative in silico study predicting in vitro MN induction individuated tertiary aliphatic and aromatic amines, other functional groups present in all fentanyls, as genotoxic-related structural alerts. Moreover, the same study revealed among these structures α,β-unsaturated compounds, including the acrylamide group, present in acrylfentanyl [29]. Given the different genotoxicological outcomes obtained in our experiments for the four fentanyls, it could be hypothesized that they can be attributed to the chemical reactivity and/or steric hindrance of the different functional groups added to the basic structure of fentanyl. This hypothesis should be demonstrated through specific studies of the structure–activity relationship, but it reminds us of a well-known pharmacological concept, i.e., a small structural change can lead to very different biological effects or even none at all. This fact highlights the importance of testing the genotoxic potential not only of a few representative molecules of a class, but of every single molecule belonging to it, including even slight differences in structure or conformation, as previously demonstrated for other NPS classes [24,26]. Indeed, there is the possibility of different biological effects within the

same structural class, as already observed, for example, in our previous study on synthetic cathinones [25].

Table 2. Available genotoxicological studies on fentanyls.

Fentanyls	Genotoxicity Tests	Reference
Fentanyl	Negative in: • Ames test (on *S. typhimurium* and *E. coli*) • in vivo/in vitro UDS assay (in primary rat hepatocytes) • in vitro CA assay (in human lymphocytes and Chinese hamster ovary (CHO) cells) Positive in: • MLA, only in the presence of S9	[15]
Alfentanyl	Negative in: • Ames test (on *S. typhimurium*) • in vivo MN test (in female rats)	[15]
Remifentanil	Negative in: • Ames test (on *S. typhimurium*) • in vivo/in vitro UDS assay (in primary rat hepatocytes) • in vitro CA assay (in CHO cells) • in vivo MN test (in rat erythrocytes) Positive in: • MLA, only in the presence of S9	[15]

The genotoxic effect observed lead us to investigate the possible mechanism underlying genotoxicity. For this purpose, the study continued by analyzing ROS induction. It is indeed well recognized how ROS, such as singlet oxygen $^1O_2$, superoxide radicals $\cdot O_2{}^-$, hydrogen peroxide H_2O_2 and hydroxyl radical $\cdot OH$, are involved in genetic damage.

After 1 h treatment with the highest doses of the fentanyls tested for MNi frequency evaluation, intracellular ROS levels were measured by means of DCF assay. Our results revealed no statistically significant increase in ROS levels for any of the fentanyls analyzed and, albeit preliminary, suggest the involvement of other mechanisms underlying the proven genetic damage.

4. Materials and Methods

4.1. Reagents

2′,7′-dichlorodihydrofluorescin diacetate (DCFH$_2$-DA), Ethylenediaminetetraacetic acid (EDTA), Etoposide (ETP), fetal bovine serum (FBS), L-Glutamine (L-GLU), Hydrogen peroxide (H$_2$O$_2$), Mitomycin C (MMC), Nonidet, Penicillin-Streptomycin solution (PS), Phosphate-Buffered Saline (PBS), Potassium Chloride, Potassium Dihydrogen Phosphate, Roswell Park Memorial Institute (RPMI) 1640 medium, Sodium Chloride, Sodium Hydrogen Phosphate, Vinblastine (VINB), water bpc grade (all purchased from Merck, Darmstadt, Germany), Guava Nexin reagent (containing 7-aminoactinomycin (7-AAD) and Annexin-V-PE), Guava ViaCount reagent (containing PI) (all purchased from Luminex Corporation, Austin, Texas, USA), RNase A, SYTOX Green (purchased from Thermo Fisher Scientific, Waltham, MA, USA).

4.2. Fentanyls

Fentanyl, Acrylfentanyl, Ocfentanyl and Furanylfentanyl were purchased from LGC Standards (LGC Standards S.r.L., Sesto San Giovanni, Milan, Italy) and www.chemicalservices.net (accessed on 5 October 2022). The test compounds were dissolved in absolute ethanol up to 20 mM stock solution and stored at −20 °C. Absolute ethanol concentration was maintained in the range 0–1% in all experimental conditions, to avoid potential solvent toxicity.

113

4.3. Cell Culture and Treatments

TK6 Human lymphoblastoid cells were purchased from Merck (Darmstadt, Germany) and were grown at 37 °C and 5% CO_2 in RPMI-1640 supplemented with 10% FBS, 1% L-GLU and 1% PS. To maintain exponential growth and considering that the time required to complete the cell cycle is 13–14 h, the cultures were divided every three days in fresh medium and the cell density did not exceed the critical value of 9×10^5 cells/mL.

In all the experiments, aliquots of 2.5×10^5 of TK6 cells were treated with increasing concentrations of Fentanyl, Acrylfentanyl, Ocfentanyl and Furanylfentanyl included in the range 0–200 μM and incubated for 26 h, corresponding to 1.5–2 replication cycles of the TK6 cells.

Cytotoxicity, apoptosis and MNi frequency evaluation were measured at the end of the 26 h treatment time.

4.4. Flow Cytometry

All FCM analysis reported below were performed using a Guava easyCyte 5HT flow cytometer equipped with a class IIIb laser operating at 488 nm (Luminex Corporation, Austin, TX, USA).

4.4.1. Cytotoxicity Analysis

Cytotoxicity assay was performed as previously described by Lenzi et al. [30,31]. Briefly, cells were stained with PI and 1000 cells per sample were analyzed.

The viability percentage recorded in the treated cultures was normalized with that recorded in the concurrent negative control cultures, considered equal to 100%. These results made it possible to confirm that the cell viability percentage respected the OECD threshold (equal to $45 \pm 5\%$) under all experimental conditions [18].

In parallel, always using PI reagent, the number of cells seeded at time zero and that measured at the end of the treatment time were evaluated, to check the correct replication in the negative control cultures and to compare it using RPD with that measured in the treated cultures. Population doubling (PD) and RPD were calculated with the following formulas:

$$PD = log\left(\frac{post - treatment\ cell\ number}{initial\ cell\ number} \right) \div log\ 2$$

$$RPD = \frac{PD\ in\ treated\ cultures}{PD\ in\ control\ cutures} \times 100$$

Similarly to cytotoxicity, cytostasis was checked in order to verify that cell proliferation respected the threshold established by the OECD guideline (equal to $45 \pm 5\%$) [18].

4.4.2. Apoptosis Analysis

The percentage of apoptotic cells was evaluated according to the procedure used by Lenzi et al. [30,31].

Briefly, the percentage of apoptotic cells was assessed by means of a double-staining protocol with 7-AAD and Annexin-V-PE, analyzing 2000 cells per sample.

The percentage of apoptotic cells recorded in the treated cultures was normalized with that recorded in the concurrent negative cultures, considered equal to 1, and expressed as the apoptotic fold increase. These results were checked to ensure that the apoptosis induction was similar to at most double that recorded in the concurrent negative cultures. A concentration of 5 μg/mL of ETP was used as positive control.

4.4.3. MNi Frequency Evaluation

The analysis of MNi frequency was performed using an automated protocol developed in our laboratory [16] and already successfully employed [17,23–27].

114

Briefly, at the end of the treatment time cells were collected, lysed and stained with SYTOX Green. The discrimination between nuclei and MNi was performed based on size difference analyzed by forward scatter (FSC) and the intensity of green fluorescence.

The MNi frequency, calculated as the number of MNi per 10,000 nuclei deriving from living and proliferating cells for every sample, and recorded in treated cultures at all the concentrations tested, was normalized with those recorded in the concurrent negative control cultures.

We used the clastogen Mitomycin C (MMC) and the aneugen Vinblastine (VINB) as positive controls [18].

4.4.4. ROS Evaluation

The analysis of ROS levels was performed using the 2′,7′-dichlorofluorescin (DCF) assay as previously described by Cocchi et al. [24,27].

Briefly, at the end of the treatment time (1 h) 2×10^5 cells were stained at 37 °C in the dark for 20 min with 2′,7′-dichlorodihydrofluorescin diacetate (DCFH$_2$-DA). A total of 5000 events, derived from viable cells, were acquired and analyzed by Guava Incyte software.

The mean fluorescence intensity values of DCF (which is formed in cells in presence of ROS) recorded in the treated cultures were normalized with that recorded in the untreated control culture, accounted equal to 1 and expressed as ROS fold increase.

We used H$_2$O$_2$ 100 μM as positive control.

4.5. Statistical Analysis

Each concentration of fentanyls was tested in triplicate at all the experimental conditions. All analyses were repeated three times. Viability percentage, RPD, apoptosis fold increase and MNi frequency fold increase were expressed as mean ± SEM. For all experimental conditions, more than three groups of matched data were compared, so statistical significance was analyzed by one-way repeated measures ANOVA, followed by Dunnett or Bonferroni post-testing to compare all treated groups with the control. We considered the difference between means as statistically significant if p value < 0.05.

We used Prism Software 4 to carry out the calculations.

5. Conclusions

Our study demonstrated for the first time that Acrylfentanyl, Ocfentanyl and Furanylfentanyl are genotoxic, in terms of their ability to induce chromosomal aberrations. A completely exhaustive evaluation of their genotoxic capacity could suggest proceeding by analyzing their ability to induce point mutations, e.g., by means of the Ames test. However, although this could provide additional genotoxicological information, the positive outcome of the MNvit analysis has already highlighted the important aspect of the research, i.e., it has identified an additional alarming toxicological concern related to these three fentanyl derivatives.

Indeed, the demonstrated genotoxic effect advocates raising awareness about the possibility of serious long-term consequences, given the well-known key role played by genotoxicity in the development of numerous neuro- and chronic-degenerative diseases [20,32].

References

1. Stanley, T.H.; Philbin, D.M.; Coggins, C.H. Fentanyl-oxygen anaesthesia for coronary artery surgery: Cardiovascular and antidiuretic hormone responses. *Can. Anaesth. Soc. J.* **1979**, 26, 168–172. [CrossRef] [PubMed]
2. Stanley, T.H. The Fentanyl Story. *J. Pain* **2014**, 15, 1215–1226. [CrossRef] [PubMed]
3. Di Trana, A.; Del Rio, A. Fentanyl analogues potency: What should be known. *Clin. Ter.* **2020**, 171, e412–e413. [CrossRef] [PubMed]
4. European Monitoring Centre for Drugs and Drug Addiction. *European Drug Report 2019: Trends and Developments*; Publications Office of the European Union: Luxembourg, 2019.
5. UN Office on Drugs and Crime. *World Drug Report 2021 (United Nations Publication, Sales No. E.21.XI.8), Booklet 3: Drug market trends: Cannabis Opioids*; United Nations Publication: New York, NY, USA, 2021.
6. European Monitoring Centre for Drugs and Drug Addiction. *European Drug Report 2021: Trends and Developments*; Publications Office of the European Union: Luxembourg, 2021.
7. Solimini, R.; Pichini, S.; Pacifici, R.; Busardò, F.P.; Giorgetti, R. Pharmacotoxicology of Non-fentanyl Derived New Synthetic Opioids. *Front. Pharmacol.* **2018**, 9, 654. [CrossRef]
8. Zhu, Y.Q.; Ge, G.L.; Fang, S.N.; Zhu, Y.C.; Dai, Q.Y.; Tan, Z.Y.; Huang, Z.M.; Chen, X.J. Studies on potent analgesics. I. Synthesis and analgesic activity of derivatives of fentanyl. *Yao Xue Xue Bao* **1981**, 16, 199–210. (In Chinese)
9. European Monitoring Centre for Drugs and Drug Addiction. *European Drug Report 2016: Trends and Developments*; Publications Office of the European Union: Luxembourg, 2016.
10. Huang, B.-S.; Terrell, R.C.; Deutsche, K.; Kudzma, L.; Lalinde, N.L. N-aryl-n-(4-piperidinyl)amides and pharmaceutical compositions and method employing such compounds. *Gen. Pharmacol. Vasc. Syst.* **1987**, 18, 71–72. [CrossRef]
11. Zawilska, J.B. An Expanding World of Novel Psychoactive Substances: Opioids. *Front. Psychiatry* **2017**, 8, 110. [CrossRef]
12. European Monitoring Centre for Drugs and Drug Addiction. *European Drug Report 2017: Trends and Developments*; Publications Office of the European Union: Luxembourg, 2017.
13. Bilel, S.; Azevedo Neto, J.; Arfè, R.; Tirri, M.; Gaudio, R.M.; Fantinati, A.; Bernardi, T.; Boccuto, F.; Marchetti, B.; Corli, G.; et al. In vitro and in vivo pharmaco-dynamic study of the novel fentanyl derivatives: Acrylfentanyl, Ocfentanil and Furanylfentanyl. *Neuropharmacology* **2022**, 209, 109020. [CrossRef]
14. Pesavento, S.; Bilel, S.; Murari, M.; Gottardo, R.; Arfè, R.; Tirri, M.; Panato, A.; Tagliaro, F.; Marti, M. Zebrafish larvae: A new model to study behavioural effects and metabolism of fentanyl, in comparison to a traditional mice model. *Med. Sci. Law* **2022**, 62, 188–198. [CrossRef]
15. Allen, J.S.; Campbell, J.A.; Cariello, N.F.; Kutz, S.A.; Thilagar, A.; Xu, J.; Ham, A.L.; Mitchell, A.D. Genetic toxicology of remifentanil, an opiate analgesic. *Teratog. Carcinog. Mutagen.* **2003**, 23, 137–149. [CrossRef]
16. Lenzi, M.; Cocchi, V.; Hrelia, P. Flow cytometry vs. optical microscopy in the evaluation of the genotoxic potential of xenobiotic compounds. *Cytom. B Clin. Cytom.* **2018**, 94, 852–862. [CrossRef]
17. Cocchi, V.; Hrelia, P.; Lenzi, M. Antimutagenic and Chemopreventive Properties of 6-(Methylsulfinyl) Hexyl Isothiocyanate on TK6 Human Cells by Flow Cytometry. *Front. Pharmacol.* **2018**, 11, 1242. [CrossRef] [PubMed]
18. Test No. 487: In Vitro Mammalian Cell Micronucleus Test. Available online: https://read.oecd-ilibrary.org/environment/test-no-487-in-vitro-mammalian-cell-micronucleus-test_9789264264861-en (accessed on 19 April 2021).
19. Phillips, D.H.; Arlt, V.M. Genotoxicity: Damage to DNA and its consequences. *EXS* **2009**, 99, 87–110. [CrossRef]
20. Basu, A.K. DNA Damage, Mutagenesis and Cancer. *Int. J. Mol. Sci.* **2018**, 19, 970. [CrossRef]
21. Attaallah, A.; Lenzi, M.; Marchionni, S.; Bincoletto, G.; Cocchi, V.; Croco, E.; Hrelia, P.; Hrelia, S.; Sell, C.; Lorenzini, A. A pro longevity role for cellular senescence. *GeroScience* **2020**, 42, 867–879. [CrossRef] [PubMed]
22. OECD. *Overview of the Set of OECD Genetic Toxicology Test Guidelines and Updates Performed in 2014-2015*; Organisation for Economic Co-Operation and Development: Paris, France, 2017.
23. Lenzi, M.; Cocchi, V.; Cavazza, L.; Bilel, S.; Hrelia, P.; Marti, M. Genotoxic Properties of Synthetic Cannabinoids on TK6 Human Cells by Flow Cytometry. *Int. J. Mol. Sci.* **2020**, 21, 1150. [CrossRef] [PubMed]
24. Cocchi, V.; Gasperini, S.; Hrelia, P.; Tirri, M.; Marti, M.; Lenzi, M. Novel Psychoactive Phenethylamines: Impact on Genetic Material. *Int. J. Mol. Sci.* **2020**, 21, 9616. [CrossRef]
25. Lenzi, M.; Cocchi, V.; Gasperini, S.; Arfè, R.; Marti, M.; Hrelia, P. Evaluation of Cytotoxic and Mutagenic Effects of the Synthetic Cathinones Mexedrone, α-PVP and α-PHP. *Int. J. Mol. Sci.* **2021**, 22, 6320. [CrossRef] [PubMed]

26. Lenzi, M.; Gasperini, S.; Cocchi, V.; Tirri, M.; Marti, M.; Hrelia, P. Genotoxicological Characterization of (±)cis-4,4'-DMAR and (±)trans-4,4'-DMAR and Their Association. *Int. J. Mol. Sci.* **2022**, 23, 5849. [CrossRef]

27. Cocchi, V.; Gasperini, S.; Lenzi, M. Anthraquinones: Genotoxic until Proven Otherwise? A Study on a Substance-Based Medical Device to Implement Available Data for a Correct Risk Assessment. *Toxics* **2022**, 10, 142. [CrossRef]

28. Fan, D.; Yang, H.; Li, F.; Sun, L.; Di, P.; Li, W.; Tang, Y.; Liu, G. In silico prediction of chemical genotoxicity using machine learning methods and structural alerts. *Toxicol. Res.* **2018**, 7, 211–220. [CrossRef]

29. Baderna, D.; Gadaleta, D.; Lostaglio, E.; Selvestrel, G.; Raitano, G.; Golbamaki, A.; Lombardo, A.; Benfenati, E. New in silico models to predict in vitro micronucleus induction as marker of genotoxicity. *J. Hazard. Mater.* **2020**, 385, 121638. [CrossRef]

30. Lenzi, M.; Malaguti, M.; Cocchi, V.; Hrelia, S.; Hrelia, P. Castanea sativa Mill. bark extract exhibits chemopreventive properties triggering extrinsic apoptotic pathway in Jurkat cells. *BMC Complement. Altern. Med.* **2017**, 17, 251. [CrossRef] [PubMed]

31. Lenzi, M.; Cocchi, V.; Malaguti, M.; Barbalace, M.C.; Marchionni, S.; Hrelia, S.; Hrelia, P. 6-(Methylsulfonyl) hexyl isothiocyanate as potential chemopreventive agent: Molecular and cellular profile in leukaemia cell lines. *Oncotarget* **2017**, 8, 111697–111714. [CrossRef] [PubMed]

32. Ribezzo, F.; Shiloh, Y.; Schumacher, B. Systemic DNA damage responses in aging and diseases. *Semin. Cancer Biol.* **2016**, 37–38, 26–35. [CrossRef] [PubMed]

Original article

Zebrafish larvae: A new model to study behavioural effects and metabolism of fentanyl, in comparison to a traditional mice model

S. Pesavento[1], S. Bilel[2], M. Murari[1], R. Gottardo[1] ⓘ, R. Arfè[2],
M. Tirri[2], A. Panato[1], F. Tagliaro[1,3] ⓘ and M. Marti[2,4]

Abstract

In an effort to find alternatives to study *in vivo* the so-called New Psychoactive Substances (NPS), the present work was undertaken to investigate the use of zebrafish larvae as animal model in pharmaco-toxicology, providing behavioural and metabolism information. For this purpose, fentanyl, the progenitor of an extremely dangerous group of NPS, was administered at different doses to zebrafish larvae (1, 10, 50, 100 µM) in comparison to mice (0.1, 1, 6, 15 mg/kg), as a well-established animal model. A behavioural assay was performed at the time of the peak effect of fentanyl, showing that the results in larvae are consistent with those observed in mice. On the other hand, several morphological abnormalities (namely yolk sac edema, abnormal pericardial edema, jaw defect and spinal curvature) were found in larvae mostly at high fentanyl doses (50, 100 µM). Larva extract and mice urine were analyzed by using liquid chromatography coupled to high resolution mass spectrometry to identify the metabolic pathways of fentanyl. The main metabolites detected were norfentanyl and hydroxyfentanyl in both the tested models. In conclusion, the present study provides evidence that fentanyl effects on zebrafish larvae and metabolism are similar to rodents and consequently support the hypothesis of using zebrafish larvae as a suitable rapid screening tool to investigate new drugs, and particularly NPS.

1. Introduction

Even though rodents represent a well-established *in vivo* animal model in pharmaco-toxicology, in modern times, they show problems hindering their practical use in relation to the policies limiting the use of laboratory animals (mammals in particular) and the related complex, time consuming and expensive procedures needed for authorization.[1] On these grounds, alternative animal species have been tested as possible representatives for higher vertebrates, looking for high conservation of genes, receptors and molecular processes.[2]

In the latest decade, zebrafish (*Danio rerio*) have emerged as an attractive species alternative to classical mammalian models because of their unique properties, such as small size, high prolificacy (200–300 eggs per day) and rapid maturation (complete organogenesis at 5 days post fertilization, dpf). Moreover, embryos are transparent allowing the use of noninvasive observation under optical microscope to monitor organogenesis and morphological defects during the developmental stages.[3,4]

Moreover, in contrast with larger species, the small size of larvae (~4 mm long) and adult zebrafish (~40 mm) considerably reduces not only housing space and breeding costs, but also the needed amount of experimental dosing

[1]Unit of Forensic Medicine, Department of Diagnostics and Public Health, University of Verona, Verona, Italy
[2]Department of Translational Medicine, Section of Legal Medicine and LTTA Centre, University of Ferrara, Italy
[3]"World-Class Research Center" Digital biodesign and personalized healthcare", Sechenov First Moscow State Medical University, Moscow, Russia
[4]Collaborative Center of the National Early Warning System, Department for Anti-Drug Policies, Presidency of the Council of Ministers, Italy

Corresponding author:
R. Gottardo, Unit of Forensic Medicine, Department of Diagnostics and Public Health, University of Verona, Ple Scuro, 10-37134 Verona, Italy.
Email: rossella.gottardo@univr.it

solutions (i.e. chemicals or drugs, both for treatment and maintenance).[5] Thanks to the great prolificacy and the prompt development, it is possible to obtain a large number of individuals per spawning, offering the possibility of many experimental replicates in a short time. In the light of these considerations, zebrafish meet the need of a high-throughput animal model that gives rapid and significant results at a low cost[4] Furthermore, it is important to point out that in Europe zebrafish embryos are not considered laboratory animals until the 5 dpf, i.e. the independent feeding stage.[6] This point is particularly relevant in the context of animal studies on the so-called novel psycho-active substances (NPS), which are hardly approved by the Ethics committees, in compliance with the auspices to reduce to a minimum the sacrifice of animals, because of the limited value in the clinical field of these compounds.

Despite divergences related to its adaptation to aquatic life, zebrafish has revealed behaviour and physiological characteristics similar to mammals and particularly to humans. As a matter of fact, *Danio rerio* genome has been sequenced showing approximately 70% of gene homology with humans.[7] Like rodents, zebrafish are capable of performing both phase 1 (oxidation, N-methylation, O-demethylation, N-dealkylation) and phase 2 (sulfation and glucuronidation) reactions.[5] In fact, the great majority of human metabolic enzymes have a direct orthologue in zebrafish, suggesting a strong correlation between the two metabolic profiles.[8]

Fentanyl was synthesized in 1960 by Paul Janssen with the intention to produce a drug with higher receptor specificity than morphine. Fentanyl indeed showed several advantages compared to morphine in terms of potency, short onset and duration of action. Initially, the clinical use was limited to induction of anesthesia by injectable formulations.[9] Then, a large demand prompted the development of different formulations (i.e. tablets, sprays, patches) for the treatment of chronic cancer pain and/or the onset of acute ache. This led to easier availability of the drug, creating a clandestine market, where fentanyl is sometimes used alone, but frequently mixed with cocaine, heroin, alprazolam or other sedative substances. In these cases, unintentional intake of a potent opioid such as fentanyl could lead to severe and potentially fatal consequences, particularly in subjects with a low tolerance to opioids.[10]

In this context, and considering the well-known ongoing "fentanyl emergency" (for reference, see at the link: https://www.unodc.org/documents/scientific/Global_SMART_21_web_new.pdf), our research group has carried out a comparative study between the zebrafish larvae (ZL) and mice using fentanyl as test drug considering both behavioural effects and metabolism. The final aim was to test the usefulness of ZL as a rapid, cheap and easy-to-use screening tool to face the problem of monitoring the emerging NPS with effective tools to investigate not simply the chemical structure but also their *in vivo* impact.

2. Methods

2.1 Reagents And chemicals

Fentanyl was purchased from LGC Standards (LGC Standards, Milan, Italy). Methanol and acetonitrile were obtained from *VWR Chemicals* (Fontenay-Sous-Bois, France). Formic acid 98% for LC-MS, sodium bicarbonate and calcium sulphate were purchased from *Merck KGaA* (Darmstadt, Germany). In *in vivo* studies on mice, ethanol (BioUltra, for molecular biology, ≥99.8%; Sigma-Aldrich), TWEEN® 80 (Sigma-Aldrich) and saline (0.9% NaCl; Eurospital, S.p.A, Italy) were used as vehicles. Instant Ocean was acquired from Tecniplast (Varese, Italy). Ultrapure water was obtained from a model PureLab Chorus 1 Complete (*Elga Veolia* Lane End, High Wycombe, UK) water purification system.

2.2 Animals

2.2.1 Ethics Statement. In the present study, the experimental protocols performed in mice were compliant with the UK Animals (Scientific Procedures) Act of 1986 and relative guidelines and with the new European Communities Council Directive of September 2010 (2010/63/EU), a revision of the Directive 86/609/EEC. Protocols were approved by the Italian Ministry of Health (license n. 335/2016-PR) and by the Animal Welfare Body of the University of Ferrara. According to the ARRIVE guidelines, all possible efforts were made to minimize the number of animals used and animals' pain and discomfort. The experimental protocols applied on ZL were approved by the Ethics Committee of the University of Verona. All zebrafish experiments performed were compliant with the European Directive 2010/63/EU and Italian Legislation (D. Lgs 26/2014).

2.2.2 Animal Husbandry. Zebrafish embryos were obtained from natural spawning of AB-strain wild-type adults raised according to standard protocols[13] at a constant temperature of 28°C. Fluorescent lamps provided illumination with a 14:10-h light-dark cycle. Adult zebrafish were fed four times a day, twice with *Artemia nauplii* and twice with dry food (*Zmsystems*, Winchester, UK). Fish were kept at a maximum density of 17 exemplars in 3.5-lt tanks.

Fifty-six-male ICR (CD-1®) mice weighing 25–30 g (Centralized Preclinical Research Laboratory, University of Ferrara, Italy) were group housed (5 mice per cage; floor area per animal was 80 cm²; minimum enclosure height was 12 cm), exposed to a 12:12 light dark cycle (light period from 6:30 AM to 6:30 PM) at a temperature

of 20–22 °C and humidity of 45–55% and were provided *ad libitum* access to food (Diet 4RF25 GLP; Mucedola, Settimo Milanese, Milan, Italy) and water.

2.3 Maximum-Tolerated Concentration (MTC) study in zebrafish

Zebrafish embryos were raised in fish water medium, consisting of 1 mM calcium sulphate, 1.2 mM sodium bicarbonate and 0.02% *(w/v)* Instant Ocean. MTC studies were performed by placing 4 dpf zebrafish larvae in 48-well plates under waterborne exposure for 24 h at 28°C. ZL were exposed to fentanyl concentrations of 1, 10, 50, 100 μM; a blank solution was prepared to exclude any effect induced by methanol used for the dissolution of fentanyl standard. To assess the morphological defects, a total of 164 larvae were tested. Larvae were monitored using a model DM2500 microscope connected with a ICC50W camera (Leica Microsystem Vertrieb GmbH, Wetzlar, German). Larvae were evaluated for several developmental malformations, including yolk sac edema (YSE) and pericardial edema (PE), body axis (AXIS), trunk length (TRUN), caudal fin (CFIN), pectoral fin (PFIN), pigmentation (PIG), jaw (J) and somite (SOMI) deformities according to the abnormalities highlighted by Noyes.[12]

2.4 Behavioural Assay

2.4.1 Drug Preparation and dose selection

2.4.1.1 Zebrafish Larvae. Fentanyl powder was dissolved in methanol and then diluted in FW: final tested doses were 1 and 10 μM. A solution of 0.34% methanol was used as vehicle. These concentrations were selected based on MTC assay results (Section 3.1). Fishes were exposed to these solutions ten minutes before the beginning of the experiment.

2.4.1.2 Mice. Fentanyl was initially dissolved in 2% absolute ethanol and Tween 80 (2%) and then diluted in a saline solution. The same solution of ethanol, Tween 80 and saline was also used as the vehicle. Drugs were administered by intraperitoneal injection at a volume of 4 μl/g. The doses of fentanyl (0.1–15 mg/kg) were chosen on the basis of a previous preliminary study in mice.[13]

2.4.2 Zebrafish Larvae locomotor activity. ZL locomotor activity was recorded by an automatic tracking system, DanioVision (Noldus, Wageningen, Netherlands). The DanioVision system consists of an observation chamber, the EthoVision 17 XT video tracking software and a Temperature Control Unit. The multi-well plate was placed in the observation chamber, where larvae were exposed to artificial light controlled by the instrument for

120 min acclimation. Then larvae underwent a series of three 10-min dark periods separated by a 10-min period of light. Overall, the behavioural test consisted of a 180 min recording for each experimental replicate. The temperature was set at 28°C controlled with thermostatic unit. The EthoVision software calculated each subject's activity as the distance covered in each minute of the test. The assays were conducted by arraying 5 dpf larvae in a 48-multiwell plate (1 larva/well). Overall, for behavioural tests 32 larvae were used in each of the following conditions: fish water medium, vehicle, fentanyl 1 μM and 10 μM.

2.4.3 Mice Locomotor activity. Changes of the spontaneous motor activity induced by fentanyl were measured using the ANY-maze video-tracking system (Ugo Basile, application version 4.99g Beta). A single mouse was placed in a square plastic cage (60 × 60 cm) located in a sound- and light-attenuated room and the motor activity was evaluated for 310 min.[14,15] Four mice were monitored at the same time in each experiment. The distance travelled (m) was measured every 15 min for a maximum of 310 min. Since typically the spontaneous motor activity of the animal progressively reduces over time, posing problems to distinguish whether the immobility of the mouse is due to the action of opioid agonist or to the normal resting behaviour of the animal in the open field test, the mice were mechanically stimulated when they were completely stationary in both the vehicle group and the fentanyl group. The mechanical stimulus was applied at minute 225, gently touching the back of the mouse with a plastic stick with a rounded tip three consecutive times. For the overall study 56 mice were used. In the open field test for each treatment (vehicle or 4 different fentanyl doses, 0.1, 1, 6 and 15 mg/kg) were used 8 mice (total mice used: 40). In the urine collection studies for each treatment (vehicle and 15 mg/kg fentanyl) were used 8 mice (total mice used: 16).

2.5 Identification And analysis of metabolites

2.5.1 Liquid chromatography-high resolution mass spectrometry (LC-HRMS). The analytical instrumentation used in the present study was a model 1260 Infinity LC coupled to a 6540 Accurate-Mass QTOF spectrometer (Agilent Technologies, Palo Alto, CA, USA). A gradient chromatographic separation was performed using a C18 Zorbax Eclipse XDB column (2.1 × 150 mm, 5 μm particle size, Agilent Technologies), thermostated at 20°C. The flow rate was set at 200 μL/min. A sample volume of 5 μL was injected. The composition of the mobile phase was as follows: formic acid 0.1% as phase A and acetonitrile added with 0.1% formic acid as phase B. The gradient elution profile was: 0–2 min 2% B, 2–13 min linear gradient from 2 to 95% B, 13–16 95% B, 16 min 2% B. The QTOF-MS was fitted with a Jet

Stream electrospray ion source (Agilent Technologies) operating in positive ionization mode. The ion source parameters were heater temperature, 325°C; gas flow, 8 L/min; nebulizer gas pressure, 30 psi; sheath gas temperature, 360°C; sheath gas flow, 12 L/min; VCap, 3750 V; fragmentor voltage, 150 V. Data were acquired in full-scan mode, within a range of 100–1000 m/z. Fragmentation was obtained on the ions of interest by applying a collision energy of 20 eV.

2.5.2 Zebrafish Larvae: In vivo identification of metabolites.

Larvae were incubated for 24 h at 28°C with fentanyl at the final concentrations of 1 and 10 µM. Subsequently, medium and larvae were collected separately: the former was frozen at −20° C while the latter were euthanized with ice water. Afterwards, larvae were snap-frozen by placing them at −80°C. The method developed by Gampfer's[16] was followed for the extraction of larvae. Briefly, larvae were lyophilized using a Savant™ DNA SpeedVac™Concentrator Kits (Thermo Scientific, Waltham, Massachusetts, USA) for 60 min. Thirty-two larvae (one tube) were then extracted by adding 50 µL of methanol, under shaking for 2 min. After centrifugation at 12,054 g for 5 min with Microfuge Lite centrifuge (Beckman Coulter, Ca, USA), the supernatant was transferred in an autosampler vial. The extraction procedure described above was performed on treated larvae, as well as on control larvae in order to exclude the presence of potentially interfering endogenous compounds.

2.5.2 Mice: In vivo identification of metabolites.

Mice were individually placed inside metabolic cages (Ugo Basile SRL, Gemonio, Varese, Italy) with free access to water and food. Total urine samples were collected in the time interval 0–5 h after the injection of vehicle or fentanyl at 15 mg/kg then stocked at −80 °C until analysis. Urine samples were then simply diluted (1:1000) with ultrapure water and directly injected into the LC-QTOF.

2.6 Statistical Analysis

The statistical analysis was performed with using GraphPad Prism software (Version 8). As regards ZL, the influence of fentanyl over the time was assessed by means of a two-way Firedmman test The Dunnet's multiple comparison test was used as a post-hoc test to compare the effect of different doses to the vehicle. Furthermore, Kruskall-Wallis and Dunn's multiple comparison tests were performed to evaluate the significant differences between the two experimental phases (*basal* and *stimulation*). Data were represented as mean ± SEM and significance was set at $p < 0.05$.

Concerning mice, a two-way ANOVA followed by a Bonferroni test for multiple comparisons was performed to analyze the effects of vehicle and fentanyl in different concentrations over the time. Additionally, the comparison

of the effects induced by fentanyl on the response to mechanical stimulation was conducted using a two-way ANOVA followed by a Bonferroni test for multiple comparisons. A Student's t-test was used to determine statistical significance between the two groups (see motor changes after mechanical stimulation). Data were represented as mean ± SEM and significance was set at $p < 0.05$. Data and statistical analysis comply with the recommendations on experimental design and analysis in pharmacology.[17]

3. Results

3.1 Maximum-Tolerated Concentrations (MTC) in zebrafish larvae: morphological and histological considerations

Due to lack of information in literature regarding the concentration levels of fentanyl capable of producing an effect on ZL, it was decided to test a wide range of doses, in order to evaluate the maximum tolerated one. The larvae were exposed for 24 h to fentanyl at concentrations of 1, 10, 50, 100 µM and morphological alterations were monitored using an optical microscope. Although all the treated larvae survived 24h after the exposure, larvae treated with the highest concentrations manifested several morphological malformations. In particular, 100% of larvae exposed to fentanyl 50 and 100 µM showed an abnormal pericardial edema (PE), yolk sac edema (YSE), jaw defect (J) and spinal curvature (SC), as shown in Figure 1. These malformations have already been highlighted for fentanyl,[18,19] other fentanyl analogs,[16] cannabinoids[20] and environmental toxins.[21] Furthermore, at those concentrations, larvae seemed to be sedated and suffering, consequently it was decided to reduce the drug concentrations to 10 µM (which induces malformations only in 1/3 of cases) and 1 µM (that caused no malformations) for further experiments. In the control groups of larvae, no malformations were observed, thus excluding a toxic effect of methanol in the vehicle (0.34%).

3.2 Behavioural Tests

3.2.1 Zebrafish Larvae.

In the present study, a previously validated paradigm[22] was used to test the acute effect of fentanyl on ZL. The assay measured the basal locomotor activity and the response to a light-to-dark transition, consisting of a stereotyped avoidance response (scototaxis), i.e. an increase in activity.[23,24]

Ethovision XT software quantified the total distance travelled by each subject per minute of recording, as a measure of larvae locomotor activity. Firstly, data were analyzed as a whole (Figure 2A) to evaluate the influence of fentanyl. As shown in Figure 2A, fentanyl significantly impairs ZL locomotor activity ($p < 0.05$) and at the
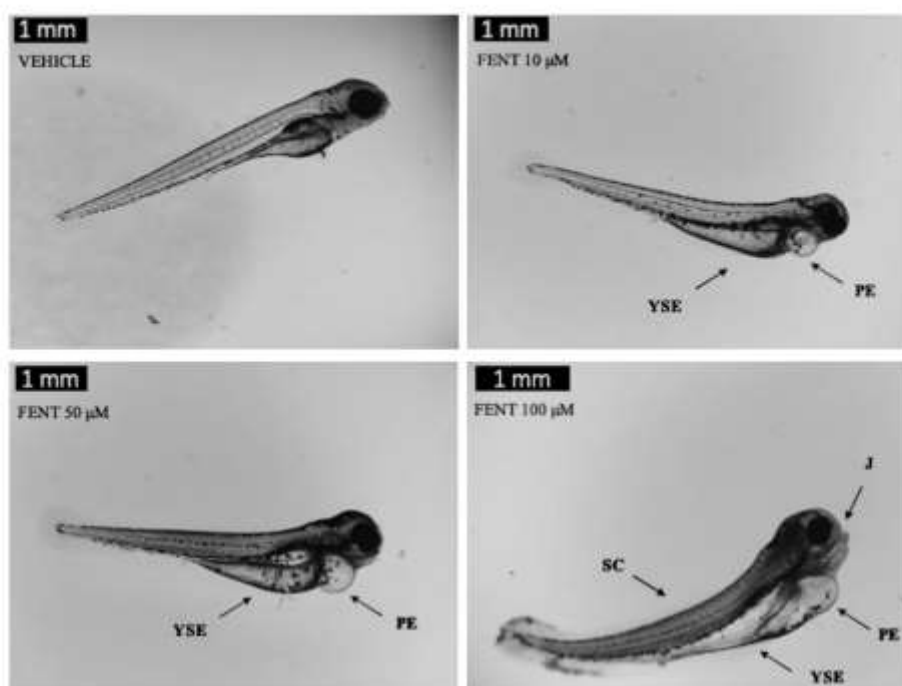
Figure 1. Morphological deformities in zebrafish larvae exposed to fentanyl 10, 50 and 100 μM for 24 h. The observed deformities were pericardial edema, PE; yolk sac edema, YSE; spinal curvature, SC and jaw, J.

highest dose (10 μM) consistently reduced the total distance travelled. Since this initial analysis showed variability between treatments and experimental phases, data were split into two main phases, namely *basal* (1–120 min) and *stimulation*, represented by the mean of 3 replicates of a stimulus (120–180 min) (Figure 2B). In the *basal* phase fentanyl decreased larvae basal activity in a dose-dependent manner ($p < 0.05$), while in the *stimulation* phase only the highest dose (10 μM) caused a decline in locomotion ($p < 0.05$).

3.2.2 Mice.
As Shown in Figure 2 (panel C and D), spontaneous locomotion in mice was significantly affected by systemic administration of fentanyl (0.1–15 mg/kg i.p.; $p < 0.05$). Fentanyl at 1 mg/kg promptly increased the total distance travelled in mice, and the effect was persistent up to 105 min. Increasing the doses, fentanyl (6 and 15 mg/kg) transiently reduced spontaneous locomotion up to 15 min, while it enhanced the motor activity in mice from about 45 to 165 min. The effects of fentanyl on spontaneous locomotion were no longer evident after 180 min and the mice motor activity was similar in fentanyl and

vehicle-treated animals at 225 min (Figure 2C). To reveal a potential effect of fentanyl under these experimental conditions, we stimulated the motor activity of the mouse by means of a mechanical stimulus. Mechanical stimulation of the mouse promotes a transient but significant increase in the motor activity of the vehicle-treated animal at 225 min (Figure 2D) while the groups of animals treated with fentanyl showed a persistence of the inhibitory effect of the opioid on motor activation. In fact, mechanically stimulated motor activity was partially reduced in the group treated with fentanyl 1 mg/kg and totally prevented in those treated with fentanyl at 6 and 15 mg/kg ($p < 0.05$; Figure 2D).

3.3 Identification And analysis of metabolites

In the present study, a tentative identification of fentanyl metabolites was also performed. The analysis was conducted using LC-HRMS acquiring in full-scan mode. An untargeted metabolomic method was used as a first screening approach, followed by a data-dependent MS/MS analysis of the most abundant peaks. Analytes were identified
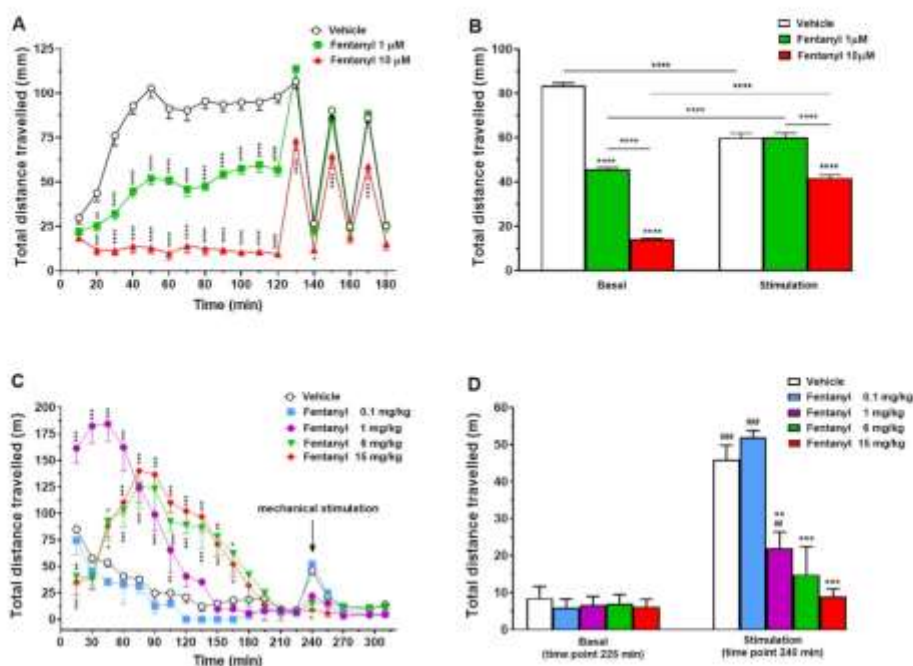
Figure 2. (A) behavioral response to fentanyl (10, 1 μM) in ZL. Data are expressed as the mean ± SEM of total distance travelled (mm) in the unit of time (10 min) for the 32 tested larvae, for each treatment. Statistical analysis was performed by two-way Friedmman test and a Dunnet's multiple comparison test was used as a post-hoc test to compare the effect of different doses to the vehicle. *p = 0.0103, **p = 0.0011, ***p < 0.01 ****p < 0.0001 (B) Data expressed as mean ± SEM of the distance travelled. The bar chart was divided in the two experimental phases *basal* and *stimulation*. A Kruskall-Wallis and a Dunn's multiple comparison tests were performed to evaluate significant differences within groups and experimental phases *p = 0.0259, **p = 0.0043, ***p = 0.0002, ****p < 0.0001. (C-D) Effect of the systemic administration (0.1–15 mg/kg i.p.) of fentanyl on the total distance travelled of the mouse. Data are expressed as metres travelled (total distance travelled) and represent the mean ± SEM of 10 determinations for each treatment. Statistical analysis was performed by two-way ANOVA followed by the Bonferroni's test for multiple comparisons for both the dose response curve of each compound at different times (panel C and D). *p < 0.05, **p < 0.01, ***p < 0.001 versus vehicle.

on the bases of accurate mass (±5 ppm), retention times and MS/MS spectra. Subsequently, the proposed metabolic pathway was drawn taking in consideration the most common metabolic routes in zebrafish larvae or in mice. A list of the identified compounds and their identification data is summarized in Table 1.

The treatment with fentanyl produced in ZL and mice phase I and phase II metabolites, but the parent drug was still present in both models. The observed biotransformations included hydroxylation, N-oxidation and N-dealkylation with the loss of phenethyl moiety. Neither in ZL nor in mice urine despropionylfentanyl was detected.

As depicted in Figure 3, the major route of metabolism in ZL and mice is the N-dealkylation to norfentanyl, which represents the main metabolite detected in both the animal models. The second most represented

metabolite in ZL was M2 obtained from the hydroxylation on the phenyl ring of the phenethyl moiety, whereas the other hydroxylated metabolite, β-hydroxyfentanyl (M3), was less abundant. Another minor metabolite detected was M5, obtained from the N-oxidation on the piperidine ring. As per phase II metabolites, only two conjugated forms of hydroxyfentanyl were detected in ZL (M2' and M3').

In mice urine, only norfentanyl and ω-1-hydroxyfentanyl (M4) and its conjugated form were found.

4. Discussion

The behavioral effects of fentanyl and its derivatives on zebrafish are not fully established. However, it has been reported in two recent studies that acute administration of

Table 1. List of metabolites tentative identified in zebrafish larvae and mice with the proposed fragmentation spectra. The metabolites are rated from + to + + + + according to their peak areas. (n.d.: not detected).

Compounds			Zebrafish Larvae (Extract)			Mice (Urine)		
Name	Chemical formula	Precursor ion	RT	Product ions		RT	Productions	
Fentanyl	$C_{22}H_{28}N_2O$	337.2269	8.4	188.1430 216.1384 281.1989 105.0702	+ + + +	8.4	188.1431 216.1386 281.1996 105.0704	+ + +
M1	$C_{14}H_{20}N_2O$	233.1648	6.8	84.0844 177.1425 150.0949 216.1382	+ + +	6.8	84.0845 177.1425 150.0945 216.1432	+ + + +
M2	$C_{22}H_{28}N_2O_2$	353.2223	7.8	204.1373 121.0643 150.0906 162.0905	+ + +	n.d.		
M3	$C_{22}H_{28}N_2O_2$	353.2223	8.8	186.1318 245.1698 105.0721 279.1819	+	n.d.		
M4	$C_{22}H_{28}N_2O_2$	353.2223	n.d.			7.6	188.1495 105.0762 232.1417 271.8863	+ +
M5	$C_{22}H_{28}N_2O_2$	353.2223	8.6	245.1634 189.1372 146.0951 105.0691	+	n.d.		
M2'	$C_{28}H_{36}N_2O_8$	529.2544	7.2	353.2256 204.1397 121.0666 77.0385	+	n.d.		
M3'	$C_{28}H_{36}N_2O_8$	529.2544	7.5	335.2177 353.2283 279.1893 186.1354	+	n.d.		
M4'	$C_{28}H_{36}N_2O_8$	529.2544	n.d.			7.4	353.2513 188.1580 105.0780 233.1810	+ + +

fentanyl to zebrafish larvae (12–14 dpf) at the concentration of 1 μM did not affect the swimming velocity.[25] Similar findings were observed in locomotion of adult zebrafish (4 weeks of age) at 0.3 μM.[26] At a first glance, these data do not fit with the present findings, but this could be justified with differences in fish age, concentrations of the drug used and applied methodologies. Moreover, the hypolocomotion observed in the basal phase (120 min) could be related to the sedative effect induced by fentanyl at 1 μM, considering that during the stimulated phase treated and untreated fish showed a similar travelled distance. Some previous studies have reported that opioids can increase locomotion[27] or induce biphasic effects.[28] Since respiratory depression in zebrafish has been reported at the concentration of 1 μM, it could be hypothesized that respiratory alterations could affect the swimming activity of zebrafish and thus reduce locomotion.[25] The zebrafish opioid system is more complex than that of vertebrates and humans due to the evolutionary differentiation of receptor sequences. Nevertheless, it shows similar pharmacological properties and conserved functions in respect to the mammalians.[29]

In the present study, in contrast to zebrafish, the rodent model showed hyperlocomotion induced by low doses (1 mg/kg) of fentanyl. These findings are in agreement with several studies, confirming that in rodents the facilitation of locomotion is triggered by the activation of the mesolimbic dopaminergic system, which is regulated by
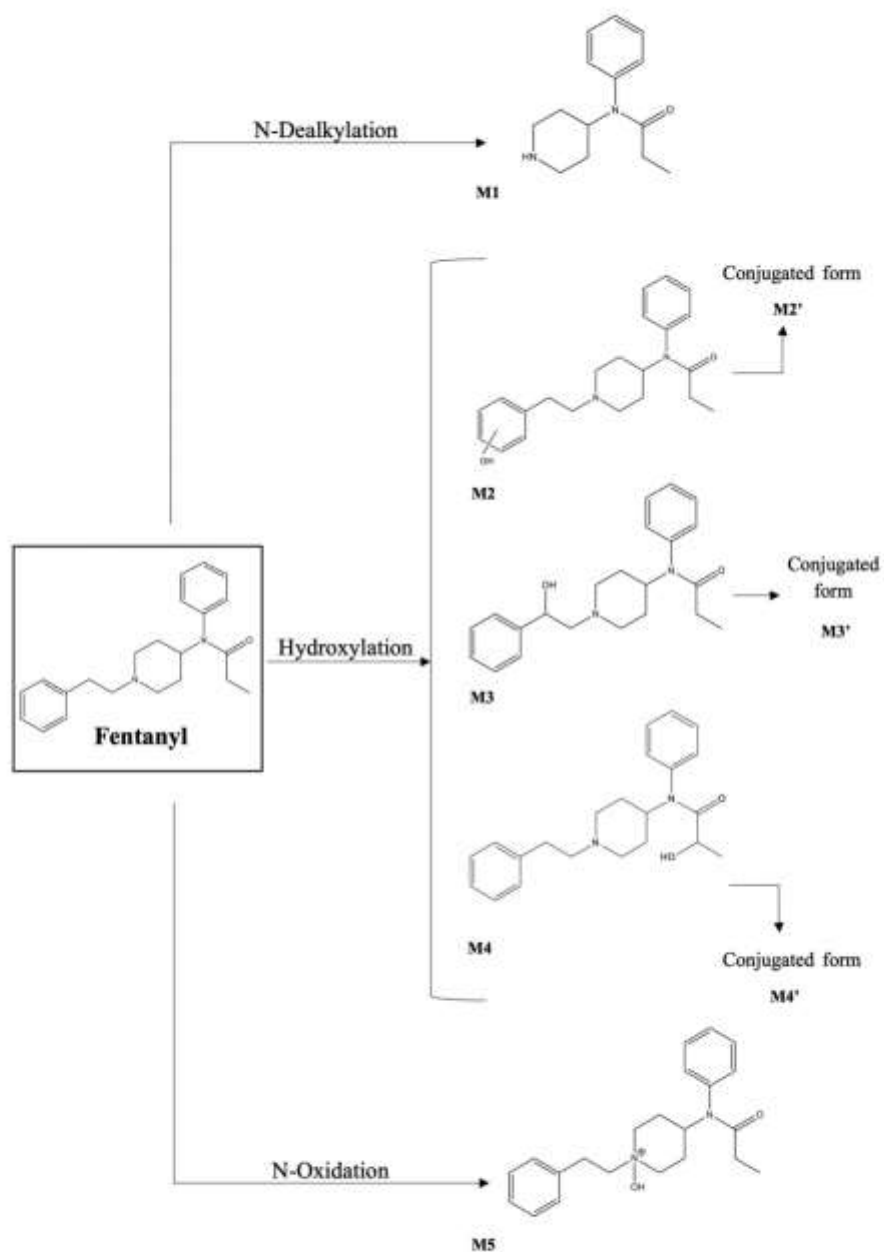
Figure 3. Schematic representation of proposed metabolic pathway of fentanyl, in mice (m) and zebrafish larvae (ZL).

the endogenous opioid system, controlling the release of dopamine in the *nucleus accumbens*.[30–32] Moreover, due to the affinity to serotonin receptors (5-HT1A)[33] fentanyl could increase locomotion involving the opioid-serotonin system.[34] The mechanical stimulation did not affect animals treated with the range dose 1–15 mg/kg at 245 min (Figure 2 C and D). This effect could be related to the respiratory depression seen in mice[15,35] and/or the muscle rigidity as reported in rats[36] and in cases of fentanyl users.[37]

Previous studies carried out both *in vivo* and *in vitro* models[38,39] showed that fentanyl is mainly metabolized to norfentanyl by *N*-dealkylation at the piperidine ring; only less than 1% is converted by alkyl hydroxylation or combined *N*-dealkylation and hydroxylation to hydroxyfentanyl and hydroxynorfentanyl. Fentanyl hydroxylation can occur on different positions, mostly on the 2nd or 3rd position of the piperidine ring, at the ethyl linker of the phenethyl moiety, at the phenyl ring of the anilino moiety or the phenyl ring of the phenethyl moiety, or along the amide alkyl chain. Another minor metabolite described is despropionylfentanyl (4-ANPP), resulting from carboxamide hydrolysis of the fentanyl scaffold. Our data in ZL were consistent with the results in mice urine. As a matter of fact, several metabolic pathways including N-dealkylation, hydroxylation at different positions and glucuronidation were observed in zebrafish. Generally speaking, considering that fentanyl and fentanyl analogs metabolism in human involves reactions like hydroxylation, N or O- dealkylation or O-methylation, the identified metabolic profile is consistent also with previously published studies on fentanyl metabolism in humans.[40,41]

5. Conclusions and future prospective

The results of the present work strongly support the hypothesis that ZL can be used as an experimental model for assessing the effects of a potent opioid, such as fentanyl. Behavioural tests and metabolite production in ZL were consistent with the results in mice. On the grounds of the results of the present study, reasoning by analogy, we can hypothesize that ZL can be regarded as a suitable tool for testing, at least in a preliminary phase, behavioural effects and metabolism not only of other fentanyls but also could be a useful tool for screening effects and metabolism of other drugs, and particularly of the newly synthesized psychoactive compounds known as NPS.

Abbreviations

LC-HRMS	Liquid Chromatography-High Resolution Mass Spectrometry
MTC	Maximum Tolerated Concentration
Dpf	Day Post Fertilization
FENT	Fentanyl
QTOF	Quadrupole-Time of Flight
ZL	Zebrafish Larvae

ORCID iDs

R. Gottardo https://orcid.org/0000-0001-5997-1723
F. Tagliaro https://orcid.org/0000-0002-2187-9128

References

1. Morbiato E, Bilel S, Tirri M, et al. Potential of the zebrafish model for the forensic toxicology screening of NPS: a comparative study of the effects of APINAC and methiopropamine on the behavior of zebrafish larvae and mice. *Neurotoxicology* 2020; 78: 36–46.
2. Hill AJ, Teraoka H, Heideman W, et al. Zebrafish as a model vertebrate for investigating chemical toxicity. *Toxicol Sci* 2005; 1: 6–19.
3. de Souza Anselmo C, Sardela VF, de Sousa VP, et al. Zebrafish (Danio rerio): a valuable tool for predicting the metabolism of xenobiotics in humans? *Comp Biochem Physiol C Toxicol Pharmacol* 2018; 212: 34–46.

4. Ali S, van Mil HGJ and Richardson MK. Large-scale assessment of the zebrafish embryo as a possible predictive model in toxicity testing. *PLoS One* 2011; 6: e21076.

5. Hill AJ, Howard C V and Cossins AR. Efficient embedding technique for preparing small specimens for stereological volume estimation: Zebrafish larvae. *J Microsc* 2002; 206: 179–181.

6. European Commission. Directive 2010/63/EU.

7. Howe K, Clark MD, Torroja CF, et al. The zebrafish reference genome sequence and its relationship to the human genome. *Nature* 2013; 496: 498–503.

8. Goldstone J V, McArthur AG, Kubota A, et al. Identification and developmental expression of the full complement of Cytochrome P450 genes in Zebrafish. *BMC Genomics* 2010; 11: 643.

9. Stanley TH. The fentanyl story. *J Pain* 2014; 15: 1215–1216.

10. Kuczyńska K, Grzonkowski P, Kacprzak Ł, et al. Abuse of fentanyl: an emerging problem to face. *Forensic Sci Int* 2018; 289: 207–214.

11. Kimmel CB, Ballard WW, Kimmel SR, et al. Stages of embryonic development of the zebrafish. *Dev Dyn* 1995; 203: 253–310.

12. Noyes PD, Haggard DE, Gonnerman GD, et al. Advanced morphological - behavioral test platform reveals neurodevelopmental defects in embryonic zebrafish exposed to comprehensive suite of halogenated and organophosphate flame retardants. *Toxicol Sci* 2015; 145: 177–195.

13. Bilel S, Arfè R, Tirri M, et al. The novel fentanyl-analog "Acrylofentanyl" impairs motor, sensorimotor and cardiovascular functions in mice. *Pharmadvances* 2020; 2(1):postit, DOI: 10.36118/pharmadvances.01.2020.14.

14. Ossato A, Bilel S, Gregori A, et al. Neurological, sensorimotor and cardiorespiratory alterations induced by methoxetamine, ketamine and phencyclidine in mice. *Neuropharmacology* 2018; 141: 167–180.

15. Bilel S, Azevedo NJ, Arfè R, et al. In vitro and in vivo pharmacological characterization of the synthetic opioid MT-45. *Neuropharmacology* 2020; 171: 108110.

16. Gampfer TM, Wagmann L, Park YM, et al. Toxicokinetics and toxicodynamics of the fentanyl homologs cyclopropanoyl-1-benzyl-4´-fluoro-4-anilinopiperidine and furanoyl-1-benzyl-4-anilinopiperidine. *Arch Toxicol* 2020; 94: 2009–2025.

17. Curtis MJ, Alexander S, Cirino G, et al. Experimental design and analysis and their reporting II: updated and simplified guidance for authors and peer reviewers. *Br J Pharmacol* 2018; 175: 987–993.

18. Kirla KT, Erhart C, Groh KJ, et al. Zebrafish early life stages as alternative model to study 'designer drugs': concordance with mammals in response to opioids. *Toxicol Appl Pharmacol* 2021; 419: 115483.

19. Cooman T, Bergeron SA, Coltogirone R, et al. Evaluation of fentanyl toxicity and metabolism using a zebrafish model. *J Appl Toxicol* 2022 Epub ahead of print 2021. DOI: 10.1002/jat.4253.

20. Akhtar MT, Ali S, Rashidi H, et al. Developmental effects of cannabinoids on zebrafish larvae. *Zebrafish* 2013; 10: 283–293.

21. Antkiewicz DS, Burns CG, Carney SA, et al. Heart malformation is an early response to TCDD in embryonic zebrafish. *Toxicol Sci* 2005; 84: 368–377.

22. Achenbach JC, Hill J, Hui JPM, et al. Analysis of the uptake, metabolism, and behavioral effects of cannabinoids on Zebrafish Larvae. *Zebrafish* 2018; 15: 349–360.

23. MacPhail RC, Brooks J, Hunter DL, et al. Locomotion in larval zebrafish: influence of time of day, lighting and ethanol. *Neurotoxicology* 2009; 289: 207–214.

24. Kalueff AV. *The rights and wrongs of zebrafish: Behavioral phenotyping of zebrafish.* 2017. Epub ahead of print 2017. DOI: 10.1007/978-3-319-33774-6.

25. Zaig S, Scarpellini C and Montandon G. Respiratory depression and analgesia by opioid drugs in freely-behaving larval zebrafish. *Elife* 2021; 10: 1–20.

26. Evans JR, Torres-Pérez J V, Miletto Petrazzini ME, et al. Stress reactivity elicits a tissue-specific reduction in telomere length in aging zebrafish (Danio rerio). *Sci Rep* 2021; 11: 1–11.

27. Stewart AM and Kalueff AV. The behavioral effects of acute Δ9-tetrahydrocannabinol and heroin (diacetylmorphine) exposure in adult zebrafish. *Brain Res* 2014; 1543: 109–119.

28. Stewart A, Wu N, Cachat J, et al. Pharmacological modulation of anxiety-like phenotypes in adult zebrafish behavioral models. *Prog Neuro-Psychopharmacol Biol Psychiatry* 2011; 35: 1421–1431.

29. Bao W, Volgin AD, Alpyshov ET, et al. Opioid neurobiology, neurogenetics and neuropharmacology in zebrafish. *Neuroscience* 2019; 404: 218–232.

30. Di Chiara G and Imperato A. Opposite effects of mu and kappa opiate agonists on dopamine release in the nucleus accumbens and in the dorsal caudate of freely moving rats. *J Pharmacol Exp Ther* 1988; 244: 1067–1080.

31. Rodríguez-Arias M, Broseta I, Aguilar MA, et al. Lack of specific effects of selective D1 and D2 dopamine antagonists vs. risperidone on morphine-induced hyperactivity. *Pharmacol Biochem Behav* 2000; 66: 189–197.

32. Matsui A, Jarvie BC, Robinson BG, et al. Separate GABA afferents to dopamine neurons mediate acute action of opioids, development of tolerance, and expression of withdrawal. *Neuron* 2014; 82: 1346–1356.

33. Martin DC, Introna RP and Aronstam RS. Fentanyl and sufentanil inhibit agonist binding to 5-HT1A receptors in membranes from the rat brain. *Neuropharmacology* 1991; 30: 323–327.

34. Gurtu S. MU receptor-serotonin link in opioid induced hyperactivity in mice. *Life Sci* 1990; 46: 1539–1544.

35. Yadav SK, Kumar D, Kumar P, et al. Biochemical, oxidative, and physiological changes caused by acute exposure of fentanyl and its 3 analogs in rodents. *Int J Toxicol* 2018; 37: 28–37.

36. Lui P-W, Lee T-Y and Chan SHH. Involvement of locus coeruleus and noradrenergic neurotransmission in fentanyl-induced muscular rigidity in the rat. *Neurosci Lett* 1989; 96: 114–119.

37. Kinshella MLW, Gauthier T and Lysyshyn M. Rigidity, dyskinesia and other atypical overdose presentations observed at a supervised injection site, Vancouver, Canada. *Harm Reduct J* 2018; 15: 1–7.

38. Kanamori T, Togawa-Iwata Y, Segawa H, et al. Use of hepatocytes isolated from a liver-humanized mouse for studies on the metabolism of drugs: application to the metabolism of fentanyl and acetylfentanyl. *Forensic Toxicol* 2018; 36: 467–475.

39. Wallgren J, Vikingsson S, Rautio T, et al. Structure elucidation of urinary metabolites of fentanyl and five fentanyl analogs using LC-QTOF-MS, hepatocyte incubations and

synthesized reference standards. *J Anal Toxicol* 2020; 44: 993–1003.

40. Wilde M, Pichini S, Pacifici R, et al. Metabolic pathways and potencies of new fentanyl analogs. *Front Pharmacol.* 2019; 10: 238.

41. Labroo R, Paine M, Thummel K, et al. Fentanyl metabolism by human hepatic and intestinal cytochrome P450 3A4: implications for interindividual variability in disposition, efficacy, and drug interactions. *Drug Metab Dispos* 1997; 25: 1072–1080.

Toxicity and behavioural effects of ocfentanil and 2-furanylfentanyl in zebrafish larvae and mice

S. Bilel [a], M. Murari [b], S. Pesavento [b], R. Arfè [a], M. Tirri [a], L. Torroni [d], M. Marti [a,c], F. Tagliaro [b,e], R. Gottardo [b,*]

[a] Department of Translational Medicine, Section of Legal Medicine and LTTA Centre, University of Ferrara, Italy
[b] Unit of Forensic Medicine, Department of Diagnostics and Public Health, University of Verona, Verona, Italy
[c] Collaborative Center of the National Early Warning System, Department for Anti Drug Policies, Presidency of the Council of Ministers, Italy
[d] Unit of Epidemiology and Medical Statistics, Department of Diagnostics and Public Health, University of Verona, Verona, Italy
[e] "World-Class Research Center 'Digital biodesign and personalized healthcare', Sechenov First Moscow State Medical University, Moscow, Russia

ARTICLE INFO

ABSTRACT

The introduction of the so-called New Psychoactive Substances represents a problem of global concern due to several factors, including multiplicity of structures, poorly known activity, short half-life in the market, lack of pure standards etc. Among these problems, of the highest relevance is also the lack of information about metabolism and adverse effects, which must be faced using simple and low-cost animal models. On these grounds, the present work has been carried out on 5 days post fertilization zebrafish (Danio rerio) larvae in comparison with adult mice (Mus musculus). Ocfentanil and 2-furanylfentanyl were administered at different concentrations to zebrafish larvae (1, 10 μM) and mice (0.1, 1, 6, 15 mg/kg). The behavioural assay showed a decrease in basal locomotor activity in zebrafish, whereas in mice this effect was evident only after the mechanical stimulus. Larva extracts and mice urine were analysed by using liquid chromatography coupled to high resolution mass spectrometry to identify the metabolic pathways of the fentanyl analogs. For 2-furanylfentanyl, the most common biotransformations observed were hydroxylation, hydration and oxidation in zebrafish larvae, whereas mice produced mainly the dihydrodiol metabolite. Hydroxylation was the major route of metabolism for ocfentanil in zebrafish larvae, while in mice the O-demethylated derivative was the main metabolite. In addition, a study was conducted to evaluate morphological effects of the two drugs on zebrafish larvae. Malformations were noticeable only at the highest concentration of 2-furanylfentanyl, whereas no significant damage was observed with ocfentanil. In conclusion, the two animal models show similarities in behavioral response and in metabolism, considering the different biological investigated.

1. Introduction

The emergence of the so-called New Psychoactive Substances (NPS) is a global phenomenon of great concern, also in forensic and clinical toxicology. The vast majority of adverse clinical effects and social hazards linked to the use and diffusion of NPS is still unknown, posing a significant challenge to the policies of contrast, prevention and treatment policies (Baumann et al., 2010; Huestis et al., 2017). In such a complex situation, a major problem hindering a pharmaco-toxicological knowledge of these compounds lies in the difficulty of setting up adequate animal models to study drug effects and metabolism fast enough to cope with the continuous introduction of new products, most of which quickly disappear. This is mainly related to the complex, tedious and time-consuming procedures required to carry out appropriate pharmacodynamics, pharmacokinetics and metabolism studies in the traditional animal models. Among NPS, in the recent time, special awareness is given to the class of Novel Synthetic Opioids (NSO), generally categorized as fentanyl analogs (e.g., 2-furanylfentanyl, ocfentanil, acetylfentanyl), as well as to newly emerging non-fentanyl compounds (e.g., U-47700, AH-7921, mitragynine) (Garneau et al.,

2020). These compounds were initially developed as possible alternatives to fentanyl, to achieve better therapeutic indices and higher potency (Allibe et al., 2018). Although thousands of fentanyl analogs were synthesised, only three of them have been approved for medical use. On the contrary, a number of synthetic opioids have appeared in the illicit market, sold as stand-alone products, as adulterants of heroin or included into counterfeit prescription pills (European Monitoring Centre for Drugs and Drug Addiction (EMCDDA), 2017). As a consequence, since 2012 thousands of fatalities caused by NSO have been reported worldwide (Goggin et al., 2017; Prekupec et al., 2017; United Nations Office on Drugs and Crime (UNODC), 2017).

Ocfentanil (N-(2-fluorophenyl)– 2-methoxy-N-[1-(2-phenylethyl) piperidin-4-yl]acetamide) is a synthetic opioid structurally related to fentanyl, differing from it because of an extra fluorine atom on the o-position of the aniline moiety and a methoxy instead of a methyl group. It was first produced in the early 1990 s with the aim of creating a potent naloxone-reversible opioid with less cardiovascular effects and respiratory depression. Ocfentanil is sold in a white granular or brown powder, which is available either as free base or as hydrochloric acid salt (Misailidi et al., 2018). Ocfentanil potency is approximately 2.5 times higher that of fentanyl (Misailidi et al., 2019). A study regarding dose-dependent pharmacological effects in humans was conducted by Fletcher et al. in 1991, however no conclusion about its benefits over fentanyl was drawn (Fletcher et al., 1991). To date ocfentanil has not been approved for any medical use.

Two-furanylfentanyl (N-phenyl-N-[1-(2-phenylethyl)piperidin-4-yl] furan-2-carboxamide) (or Fu-F) is a synthetic opioid with a structure similar to fentanyl, differing only in the replacement of the propionyl group for a furan ring (Kanamori et al., 2021). The above-mentioned modifications grant sevenfold higher potency over fentanyl (Wilde et al., 2019). Fu-F was first described in 1958 and, to date, it has not been approved for any medical purpose (Goggin et al., 2017; Huang et al., 1987). Fu-F has been available in the European Union since June 2015, having been identified in 16 Member States and in Norway. In the United States this opioid appeared in December 2015. Several acute intoxications have been reported (Slovenian National Forensic Laboratory, 2016; Varshneya et al., 2022) and in 2018 Fu-F was included in schedule I of the Controlled Substances Act (Drug Enforcement Administration, 2018; Kanamori et al., 2021). Fu-F is commonly sold as a powder but other forms such as liquid, tablets, or nasal spray are also available in the market (European Monitoring Centre for Drugs and Drug Addiction (EMCDDA), 2017).

To study in-vivo effects and metabolism of these substances, overcoming the difficulties related to the use of traditional animal models, our research group has recently joined a research trend proposing ZL as particularly suitable for this purpose. Indeed, ZL present several advantages, such as small dimensions (roughly 4 mm long), high production (200–300 eggs per day) and fast development. These unique features are also extremely useful in terms of experimental time, since it is possible to obtain many replicates in a short time. Lastly, it is important to point out that in Europe zebrafish embryos are not considered laboratory animals until 5 dpf, i.e. the independent feeding stage, thus no specific authorizations are required. (Ali et al., 2011; de Souza Anselmo et al., 2018).

In the last decades, zebrafish has been used as a complementary animal model to study behavioural effects and toxicity of drugs, including fentanyl analogs. Indeed, in a study conducted by Varshneya and co-authors, fentanyl analogs showed significant dose-dependent hyperlocomotion in mice (Varshneya et al., 2019, 2021). In contrast, hypoactive behaviour was highlighted by Kirla et al. for zebrafish larvae (Kirla et al., 2021). Moreover, the morphological effect of fentanyl (Cooman et al., 2021) and fentanyl derivatives (Kirla et al., 2021) at different concentration levels has been recently investigated providing evidence of lethal and sublethal malformations in embryos on the 4th day post fertilization (dpf) after 24 h of exposure. However, up to date information regarding the effect and metabolism of 2-furanylfentanyl

and ocfentanil is still limited (Watanabe et al., 2017).

On these grounds, the present work aims at providing new information on the behavioral effect and metabolism of 2-furanylfentanyl and ocfentanil using ZL in comparison with a well-known animal model such as mice. The ZL model was also used to evaluate morphological effects of the two drugs.

2. Materials and methods

2.1. Zebrafish model

2.1.1. Animal husbandry

Zebrafish experiments were performed at the Centre for Experimental Research (CIRSAL) of the University of Verona in accordance with the Italian and European Legislations (Directive 2010/63/EU) with permission of the Animal Welfare Body of the University of Verona. Larvae utilized in the experiments were the offspring of AB-strain wild-type adults, bred according to standard protocols (Kimmel at al, 1995) at a constant temperature of 28 ($\pm$ 1) °C and tanks were kept to a 14:10-h light-dark cycle. Maintenance 3,5-lt tanks housed mixed sex groups with a maximum density of 17 exemplars. Adult zebrafish were fed four times a day, twice with Artemia nauplii and twice with dry food (Znsystems, Winchester, UK). For reproduction, pairs of adult zebrafish were transferred into a breeding cage: the two breeders were divided by a transparent partition until the following day, when the partition was removed allowing spawning. Embryos were collected and raised in a Petri dish in fish water medium (1 mM calcium sulphate, 1.2 mM sodium bicarbonate and 0.02 % (w/v) Instant Ocean).

2.1.2. Reagents and chemicals

Standards of 2-furanylfentanyl and ocfentanil were provided from Comedical (Comedical, Trento, Italy) as methanolic solutions. Appropriate amounts of these solutions were spiked in fish water medium to obtain the final concentration of 1 μM and 10 μM. As a result of the dilution of the pure standard, the 1 μM and 10 μM solutions contained 0.3 % and 3.3 % of methanol, respectively. Thus, two different vehicles were prepared, the first being composed of fish water and 0.3 % methanol (vehicle 1), the second one (vehicle 2) containing 3.3 % of methanol.

Methanol and acetonitrile were purchased from VWR Chemicals (Fontenay-Sous-Bois, France), while formic acid 98 % for LC-MS from Merck KGaA (Darmstadt, Germany). Sodium bicarbonate and calcium sulphate used for fish water were purchased from Merck KGaA (Darmstadt, Germany) and Instant Ocean from Tecniplast (Varese, Italy); 48-well plates were provided by Sarstedt (Numbrecht, Germany). MilliQ water was obtained from a model PureLab Chorus 1 Complete water purification system (Elga Veolia Lane End, High Wycombe, UK).

2.1.3. Morphological effects of 2-furanylfentanyl and ocfentanil in zebrafish larvae

A total of seventy zebrafish larvae (ZL), deriving from different hatchings in two distinct days, underwent a 24 h-incubation at 28 °C on the fourth day post fertilization. ZL were placed in 48-well plates with one larva per well and 1 ml fish water containing the two fentanyl analogs at two concentration levels (1 and 10 μM). Two replicates of each assay were performed on two different days. Overall, for behavioural tests 14 larvae (n = 7 for each replicate) were used for each of the following: vehicle, 2-furanylfentanyl and ocfentanil 1 μM and 10 μM. Afterwards, larvae were anaesthetised by using ice and then monitored using a model DM2500 microscope connected with a model ICC50W camera (Leica Microsystem Vertrieb GmbH, Wetzlar, German). Larvae were evaluated for their morphological defects including yolk sac edema (YSE), pericardial edema (PE), body axis (AXIS), trunk length (TRUN), caudal fin (CFIN), pectoral fin (PFIN), pigmentation (PIG), jaw (J) and somite (SOMI) deformities according to the abnormalities reported by Noyes (Noyes et al., 2015) and also shown in larvae exposed to

increasing concentrations of fentanyl (Pesavento et al., 2022).

2.1.4. Behavioural assay

2-furanylfentanyl and ocfentanil standards utilized for ZL behavioural assay were diluted in a solution of fish water medium; final tested doses were 1 and 10 μM. These concentrations were selected according to our previous study regarding the maximum tolerated concentrations of fentanyl in zebrafish (Pesavento et al., 2022). Moreover, in order to evaluate a potential solvent effect, control larvae were exposed to 0.3 % and 3.3 % methanol solution (vehicle 1 and 2, respectively). On the fifth day after fertilization, larvae were individually placed in 48-well plates filled with 1 ml of fish water (FW) medium and treatment, either 2-furanylfentanyl, ocfentanil or vehicle control, just before behavioural test. The multi-well plate was arrayed into an infrared backlit plate holder in the observation chamber of DanioVision (Noldus, Wageningen, Netherlands), where larvae were exposed to a white light for 120 min of acclimation. The temperature was set at 28 °C. Subsequently, larvae underwent three series of a rapid change of illumination from darkness to a strong illumination (i.e., 10-min light off and 10-min light on). In total the behavioural test consisted of 180 min recording for each experimental replicate. EthoVision 17 XT video tracking software calculated each subject's activity as the total distance moved in each minute of the recording. The number of replicates and of larvae for each treatment was the same as for the morphological assay, with the addition of n = 14 larvae in fish water medium, used as control.

In order to evaluate the acute effect of the studied NSOs in ZL, a previously validated paradigm (Achenboch et al., 2018) was conducted for each drug. Larvae locomotor activity was measured by means of Ethovision XT software, providing the total distance travelled by each subject in every minute of the recording. Firstly, raw data were analysed in total to assess the drug effect over time, then the assay was divided into two main phases, namely habituation (1–120 min) and stimulation (120–180 min). Furthermore, the stimulation phase consisted in three replicates of a 10-minute period of darkness followed by 10 min of light, considering that in normal conditions larvae tend to increase locomotor activity in darkness and to decrease it after a light stimulus (Kalueff, 2017; MacPhail et al., 2009). Lastly, experimental data were split according to the two concentration levels i.e., 1 μM (0.33 % methanol) and 10 μM (3.3 % methanol) with the purpose of assessing the potential influence of the vehicle (water and methanol).

2.2. Mouse model

2.2.1. Animal husbandry

Ninety-six adult Male ICR (CD-1®) mice (about 12 weeks old) weighing 30–35 g (Centralised Preclinical Research Laboratory, University of Ferrara, Italy) were group housed (5 mice per cage; floor area per animal was 80 cm2; minimum enclosure height was 12 cm), exposed to a 12:12-h light-dark cycle (light period from 6:30 AM to 6:30 PM) at a temperature of 20–22 °C and humidity of 45–55 % and were provided ad libitum access to food (Diet 4RF25 GLP; Mucedola, Settimo Milanese, Milan, Italy) and water. The experimental protocols performed in the present study were in accordance with the U.K. Animals (Scientific Procedures) Act of 1986 and associated guidelines and the new European Communities Council Directive of September 2010 (2010/63/EU). Experimental protocols were approved by the Italian Ministry of Health (licence n. 335/2016-PR) and by the Animal Welfare Body of the University of Ferrara. According to the ARRIVE guidelines, all possible efforts were made to minimize the number of animals used and to reduce the animals' pain and discomfort.

2.2.2. Drug preparation and dose selection

Two-furanylfentanyl and ocfentanil were purchased from LGC standards (LGC Standards S.r.l., Sesto San Giovanni, Milan, Italy) and were dissolved in a saline solution (0.9 % NaCl), which was also used as the vehicle. Drugs were administered by intraperitoneal (i.p.) injection of a

volume of 4 μL/g. The range of doses of drugs tested (0.1–15 mg/kg i.p.) was chosen based on our previous studies (Bilel et al., 2022; Pesavento et al., 2022).

2.2.3. Spontaneous locomotion test

A single mouse was placed in a square plastic cage (60 ×60 cm) located in a sound- and light-attenuated room, and changes induced by 2-furanylfentanyl and ocfentanil in motor activity were monitored for 310 min (Bilel et al., 2020; Ossato et al., 2018) by means of an ANY-maze video-tracking system (Ugo Basile, application version 4.99 g Beta). Four mice were monitored at the same time in each experiment. The system calculated the distance travelled (m) every 15 min for a maximum of 310 min. In order to avoid the problem of distinguishing whether the immobility of the mouse was due to the action of opioids agonist or to the normal resting behaviour of the animal in the open field test, mice were mechanically stimulated when they were completely stationary (Pesavento et al., 2022). At minute 225, each mouse was gently touched on its back three consecutive times with a plastic stick with a rounded tip. In the analysis of spontaneous locomotion in the open field test for each treatment (vehicles or 4 different 2-furanylfentanyl or ocfentanil doses, 0.1, 1, 6 and 15 mg/kg) 8 mice were used (total mice used: 80).

2.3. Identification and analysis of metabolites

A series 1260 HPLC (Agilent Technologies, Waldbronn, Germany) in tandem with a 6540 Accurate-Mass QTOF (Agilent Technologies, Palo Alto, CA, USA) was used for the present study. The chromatographic separation was performed on a Zorbax Eclipse XDB (2.1 × 150 mm, 5 μm particle size, Agilent Technologies). The composition of the mobile phases was as follows: formic acid 0.1 % as phase A and acetonitrile with 0.1 % formic acid as phase B. In all experiments the flow rate was set at 500 μL/min and injection volume was 5 μL. Samples were eluted with a linear gradient from 2 % to 95 % B of solvent B lasting 12 min; the final conditions (95 % B) were kept for 3 min and then the starting conditions (2 % B) were restored in 1 min and kept for 7 min, to allow system re-equilibration. The QTOF-MS was performed using a Jet Stream electrospray ion source (Agilent Technologies) operating in positive ionization mode. Source parameters were gas temperature 325 °C, gas flow 8 L/min, nebulizer pressure 30 psi, sheath gas temperature 360 °C, sheath gas flow 12 L/min, VCap 3750 V, nozzle voltage 500 V and fragmentor voltage 150 V. For continuous mass calibration, the following reference ions were used: purine 121.0508 [M + H] + and HP-921 = hexakis(1 H,1 H,3 H-tetrafluoropropoxy) phosphazine 922.0097 [M + H] + . Data acquisition was performed in full scan mode in the mass range of 100–1000 m/z. Fragmentations were obtained applying a collision energy of 20 or 10 eV on selected ions. MassHunter Acquisition software and the Qualitative Analysis version B.04.00 (Agilent Technologies) were used for data handling.

2.3.1. Zebrafish larvae: in vivo identification of metabolites

After the behavioural assay, the larvae were euthanized with ice. Afterwards, treated and control larvae were collected separately and snap-frozen at − 80 °C and stored until the extraction. ZL on the fifth day post fertilization were lyophilized using Savant™ DNA SpeedVac™ Concentrator Kits (Thermo Scientific, Waltham, Massachusetts, USA) for 60 min and then extracted with 50 μL of methanol, shaken for 2 min and centrifuged at 12,054 g for 5 min with Microfuge Lite centrifuge (Beckman Coulter, Ca, USA). Lastly, the supernatant obtained was transferred in an autosampler vial and injected into the instrument (Gampfer et al., 2020).

2.3.2. Mice: in vivo identification of metabolites

Mice were individually placed inside metabolic cages (Ugo Basile SRL, Gemonio, Varese, Italy) with free access to water and food. Overall, in the urine collection studies for each treatment (vehicle and 15 mg/kg

2-furanylfentanyl or ocfentanil) 8 mice were used (total mice used: 24).

For the identification of metabolites, urines were collected after the injection of vehicle, 2-furanylfentanyl or ocfentanil at 15 mg/kg doses in a time interval of 0–5 h. Urine samples were kept at – 80 °C until analysis. After dilution (1:1000) in autosampler vials with ultrapure water, samples were directly injected into the LC-QTOF.

2.4. Statistics

The statistical analysis was performed using GraphPad Prism software (Version 8). Normal response distributions were verified using Shapiro-Wilk normality test. Afterwards for ZL a two-way ANOVA test followed by a Dunnett's multiple comparison test were conducted to evaluate the effect over time of the two drugs at the lowest concentrations (1 µM). However, for the highest concentrations (10 µM) a two-way ANOVA and a Tukey post-hoc test were used. Moreover, Kruskall-Wallis and Dunn's tests were assessed to measure significant differences ($p < 0.0001$) between the three phases of the behavioural test compared to the vehicle (habituation, light off, light on). To evaluate the effects of 2-furanylfentanyl or ocfentanil in mice at different doses over time compared to the vehicle, a two-way ANOVA followed by a Bonferroni test for multiple comparisons was performed. Furthermore, the comparison of the effects induced by 2-furanylfentanyl or ocfentanil on the response to mechanical stimulation of locomotion was conducted using a two-way ANOVA followed by a Bonferroni test for multiple comparisons. Finally, a Student's t-test was used to determine statistical significance ($p < 0.05$) between the different groups (see motor changes after mechanical stimulation).

3. Results

3.1. Morphological effects on ZL of 2-furanylfentanyl and ocfentanil

A specific study was conducted to test acute morphological effects of 2-furanylfentanyl and ocfentanil on ZL. In 2-furanylfentanyl-treated larvae, the concentration of 1 µM did not induce morphological changes in ZL. On the other hand, the highest concentration (10 µM) caused a yolk sac edema in 62.5 % of cases, which is noticeable as a swollen abdomen in Fig. 1. In addition, skin pigmentation in larvae treated with 2-furanylfentanyl was darker than the control larvae. On the contrary, ZL treated with ocfentanil at the two concentrations tested (1 and 10 µM) did not show any malformations.

3.2. Behavioral assay in ZL

As depicted in Fig. 2 Panel A, the statistical analysis showed a significant effect of treatment ($F_{2739} = 444$, $p < 0.0001$), time ($F_{17,738} = 292.6$, $p < 0.0001$) and time x treatment interaction ($F_{34,738} = 34.38$, $p < 0.0001$). Indeed, there was a significant decrement in larvae locomotion under the effect of the two synthetic opioids in the habituation phase (time point 120), whereas only 2-furanylfentanyl declined the movement during the stimulation phase (120–180 min). The above-mentioned effect was more pronounced at the highest concentration for 2-furanylfentanyl: in Fig. 2 Panel B, the two-way ANOVA showed a significant effect of treatment ($F_{2684} = 5086$, $p < 0.0001$), time ($F_{17,684} = 40.23$, $p < 0.0001$) and time x treatment interaction ($F_{34,684} = 71.91$, $p < 0.0001$). Overall, 2-furanylfentanyl dramatically inhibited the activity of ZL.

As per the lowest drug concentration (1 µM), in the habituation phase both fentanyl analogs reduced the total distance travelled when compared to the vehicle. There was a significant increase in activity in the light off- phase compared to habituation, whereas movement in the light on-phase declined equally in treated and control larvae (Fig. 2; Panel C). Conversely, 2-furanylfentanyl at the highest concentrations (10 µM), reduced and flattened the total distance travelled overall, while ocfentanil 10 µM showed a decrease in locomotion compared to the vehicle only in the habituation phase (Fig. 2; Panel D).

3.2.1. Behavioural assay in mice

Spontaneous locomotion in mice was significantly affected by systemic administration of 2-furanylfentanyl (Fig. 3; Panel A: significant effect of treatment ($F_{4700} = 31.27$, $p < 0.0001$), time ($F_{19,700} = 42.22$, $p < 0.0001$) and time x treatment interaction ($F_{76,700} = 7.118$, $p < 0.0001$)) and ocfentanil (Fig. 3; Panel C: significant effect of treatment ($F_{4700} = 58.98$, $p < 0.0001$), time ($F_{19,700} = 47.80$, $p < 0.0001$) and time x treatment interaction ($F_{76,700} = 9.917$, $p < 0.0001$)) in the 0.1–15 mg/kg range of doses. 2-furanylfentanyl and ocfentanil at 1 mg/kg rapidly increased the total distance travelled in mice, and the effect lasted up to 90 min. By increasing the dose, both compounds at 6 mg/kg transiently reduced spontaneous locomotion at 30 min minutes after injection, while they enhanced locomotion from about 60 to 150–180 min. The opioid agonists at the highest dose (15 mg/kg) significantly inhibited the total distance travelled in the first 30 min, while they facilitated locomotion up to 150 min (Fig. 3; Panel A and C). The effects of 2-furanylfentanyl and ocfentanil were no longer evident
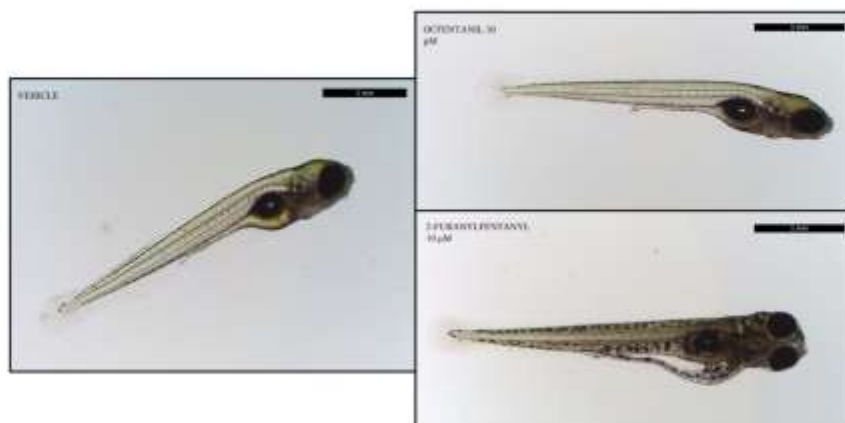

Fig. 1. Morphological effects on zebrafish larvae. ZL treated with ocfentanil 10 µM did not show any malformations. 62.5 % of larvae treated with 10 µM 2-furanylfentanyl have two distinct signs of morphological modifications, i.e. hyperpigmentation and a swollen abdomen.
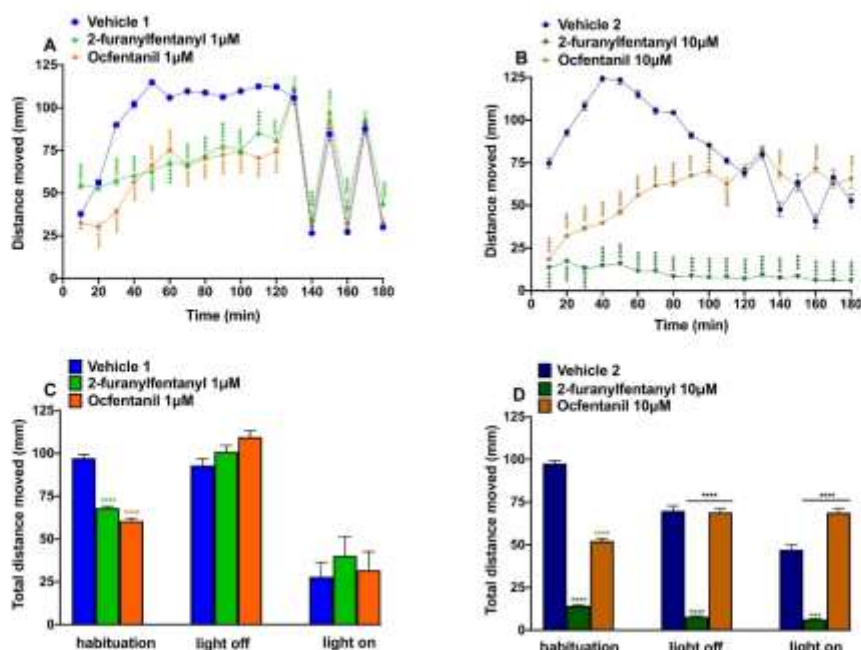
Fig. 2. Behavioural assay on zebrafish larvae. Behavioral response to 2-furanylfentanyl and ocfentanil at the two-concentration level of 1 μM (Panel A, C) and 10 μM (Panel B, D) in ZL. Vehicle 1 and 2 consisted of fish water containing 0.3 % and 3.3 % of methanol, respectively. (A-B) *Light on* time interval: minute 0–120,130–140,150–160,170–180; light off time interval: minute 120–130,140–150,160–170. Number of larvae treated: vehicle 1 n = 14, vehicle 2 n = 14, 2-furanylfentanyl 10 μM n = 14, 2-furanylfentanyl 1 μM n = 14, ocfentanil 10 μM n = 14, ocfentanil 10 μM n = 14. Data are expressed as the mean ± SEM of total distance travelled (mm) in the unit of time (10 min). Statistical analysis was performed by two-way ANOVA test followed by a Dunnett's multiple comparison test in Panel A, while in Panel B a two-way ANOVA followed by Tukey's multiple comparison test were performed. (C-D) Data are expressed as the mean ± SEM of the total distance travelled. The bar chart was split in three different conditions namely *habituation, light off and light on*. Kruskal-Wallis and Dunn's multiple comparison tests were performed to evaluate significant differences within groups and experimental phases. * **p < 0.001, * ** *p < 0.0001.

after 180 min and the spontaneous locomotion of mice was similar in 2-furanylfentanyl- ocfentanil- and vehicle-treated animals at 225 min (Fig. 3; Panel A and C). To reveal a potential effect of 2-furanylfentanyl and ocfentanil under these experimental conditions, the motor activity of the mouse was stimulated mechanically (as described in materials and methods).

Mechanical stimulation of the mouse promoted a transient but significant increase in the motor activity of the vehicle-treated animal at 225 min (Fig. 3; Panel B and D) while the groups of animals treated with 2-furanylfentanyl and ocfentanil showed a persistence of the inhibitory effect of the opioid on motor activation.

In fact, mechanically stimulated motor activity was completely reduced in the group treated with 1–15 mg/kg 2-furanylfentanyl ($F_{0, 70}$ = 11.73; P < 0.0001; Fig. 3; Panel B). Ocfentanil partially prevented (at 1 mg/kg) and completely reduced (at 6 and 15 mg/kg) the mechanically stimulated motor activity in mice ($F_{0, 70}$ = 19.22; P < 0.0001; Fig. 3; Panel D). The observed discrepancies between the two compounds at the dose of 1 mg/kg could be related to differences in their pharmacokinetics in response to various motor tests (Bilel et al., 2022).

3.3. Identification and analysis of metabolites

The analysis of 2-furanylfentanyl and ocfentanil metabolites was conducted using LC-HRMS acquiring data in full-scan mode. The identification of metabolites was performed by considering accurate mass (± 5 ppm), retention times and MS/MS spectra.

The current study identified a total of six metabolites of 2-furanylfentanyl (Table 1). The corresponding metabolic pathway is shown in Fig. 4. On the bases of the relative amount of peak area, in larvae extracts the main metabolites were nor-furanylfentanyl (M1) and hydroxy-furanylfentanyl (M2), resulting from the hydroxylation on the phenethyl group and the corresponding conjugated form (M2'). Other minor metabolites detected were M3, obtained from N-oxidation on the piperidine ring, hydroxy-methoxyfuranylfentanyl (M4) and dihydrodiol metabolite (M5), resulting from hydration on the furan ring. In contrast with ZL, only dihydrodiol metabolite and M2' were identified in mice urine.

On the other hand, seven ocfentanil metabolites were detected in the two animal models, resulting from hydroxylation or/and demethylation of the parent drug (Table 2). The mono-hydroxylation occurred in three different positions in larvae, i.e., at the phenyl ring of the phenethyl moiety (M1), in β-position of the ethyl linker (M2) and at the piperidine ring (M3). On the contrary, in mice urine only M4, resulting from hydroxylation in ω-position, was detected. O-desmethyl ocfentanil (M5), corresponding to the loss of methyl of the methoxy group, was also identified in zebrafish larvae as well as in mice urine, representing in the latter the most abundant metabolite along with its conjugated form (M5'). Another hydroxylation occurred in ZL at the fluorophenyl moiety of M5, forming M6 (hydroxy-O-desmethyl-ocfentanil) (Fig. 5). Strangely enough, two of the most common biotransformations described in fentanyl and in fentanyl analogs, namely N-dealkylation and the formation of 4-ANPP (flouro-despropionylfentanyl), were not detected in the two *in vivo* models tested.
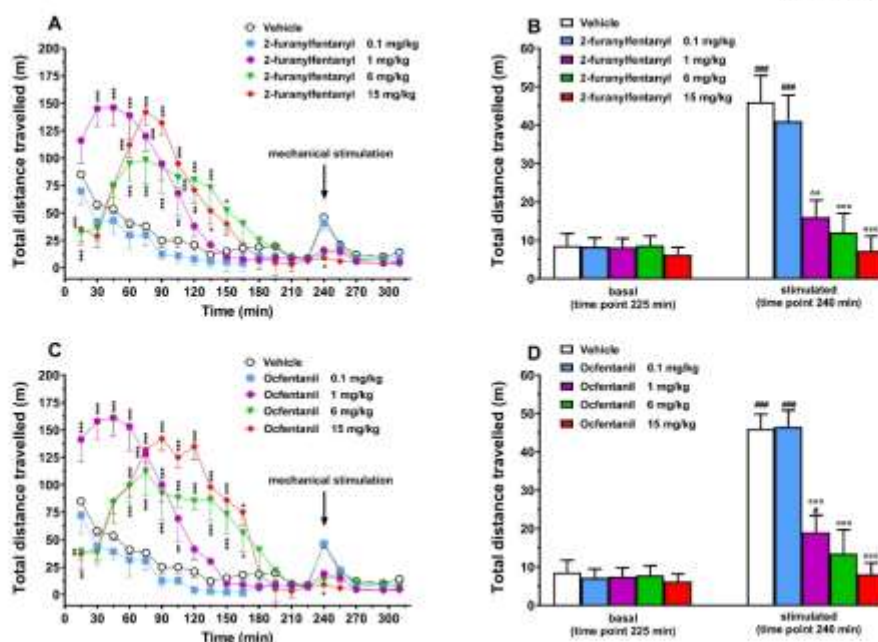
Fig. 3. Behavioural effects on mice. Effect of the systemic administration of 2-furanylfentanyl (0.1–15 mg/kg i.p.; Panel A, B) and ocfentanil (0.1–15 mg/kg i.p.; Panel C, D) on the total distance travelled by the mouse. Data are expressed as metres travelled and represent the mean ± SEM of 8 determinations for each treatment. Statistical analysis was performed by two-way ANOVA followed by Bonferroni's test for multiple comparisons for the dose response curve of each time point (Panel A, C) and by one-way ANOVA followed by Tukey's test for multiple comparisons for the dose response curve of basal (225 min) versus stimulated responses (240 min; Panel B, D). *$p < 0.05$, * *$p < 0.01$, * * *$p < 0.001$ versus vehicle; #$p < 0.05$, # # #$p < 0.001$ versus basal; °°$p < 0.01$, °°°$p < 0.001$ versus stimulated responses.

Table 1

List of 2-furanylfentanyl metabolites tentatively identified in zebrafish larvae and mice with the proposed fragmentation spectra. The metabolites are rated from + to + + + + according to their peak areas (n.d.: not detected).

Compounds			Zebrafish Larvae (Extract)			Mice (Urine)		
Name	Chemical formula	Precursor ion	RT	Major products	%	RT	Major products	%
2-furanylfentanyl	$C_{24}H_{25}N_2O_2$	375.2068	8.6	188.1558 105.0703	+ + +	8.6	188.1467 105.0722	+ + +
M1	$C_{20}H_{18}N_2O_2$	271.1384	7.0	188.0633 170.1110	+ +	n.d.		
M2	$C_{24}H_{26}N_2O_3$	391.2016	7.9	204.1391 121.0653	+ +	n.d.		
M3	$C_{24}H_{26}N_2O_3$	391.2016	8.7	105.0681 283.1390	+	n.d.		
M4	$C_{25}H_{28}N_2O_4$	421.2122	7.9	234.1485 151.0754	+	n.d.		
M5	$C_{24}H_{28}N_2O_4$	409.2124	7.9	188.1380 105.0653	+	8.0	188.1438 105.0701	+ + +
M2'	$C_{30}H_{34}N_2O_3$	567.2337	7.4	391.1900 204.1320	+ +	7.5	391.1649 204.1181	+ +

4. Discussion

The present study reports for the first time a comparison of the effect of two potent fentanyl analogs, i.e. 2-furanylfentanyl and ocfentanil, on the locomotor activity and metabolism in two different animal models, namely ZL and mice. The results are discussed taking also into consideration those previously obtained with fentanyl in similar studies (Kirla et al., 2021; Pesavento et al., 2022).

4.1. Locomotor activity and morphology in ZL

Overall, larvae locomotor activity was impaired after the treatment with the two opioids in both habituation and stimulation phase. In particular, at the lowest concentration (1μM), both 2-furanylfentanyl and ocfentanil decreased the locomotor activity of ZL. A significant dose-dependent reduction in activity due to fentanyl and fentanyl analogs at a comparable concentration was also recently reported in a similar behavioural study in ZL (Kirla et al., 2021; Pesavento et al., 2022).

In this study, it was also demonstrated that a high concentration (10 μM) of 2-furanylfentanyl and ocfentanil induced an inhibitory locomotor effect in ZL in habituation, light on and light off phases. Moreover, the vehicle used for higher concentration induced a slight increase of the locomotion in ZL. This effect could be related to an enhancement of the direct toxicity exerted by the two compounds (Fu et al., 2017) or may also be caused by the synergic effect of methanol present in the vehicle. To investigate the possible role of methanol, a specific study was performed. The influence of methanol on the locomotor activity in ZL was
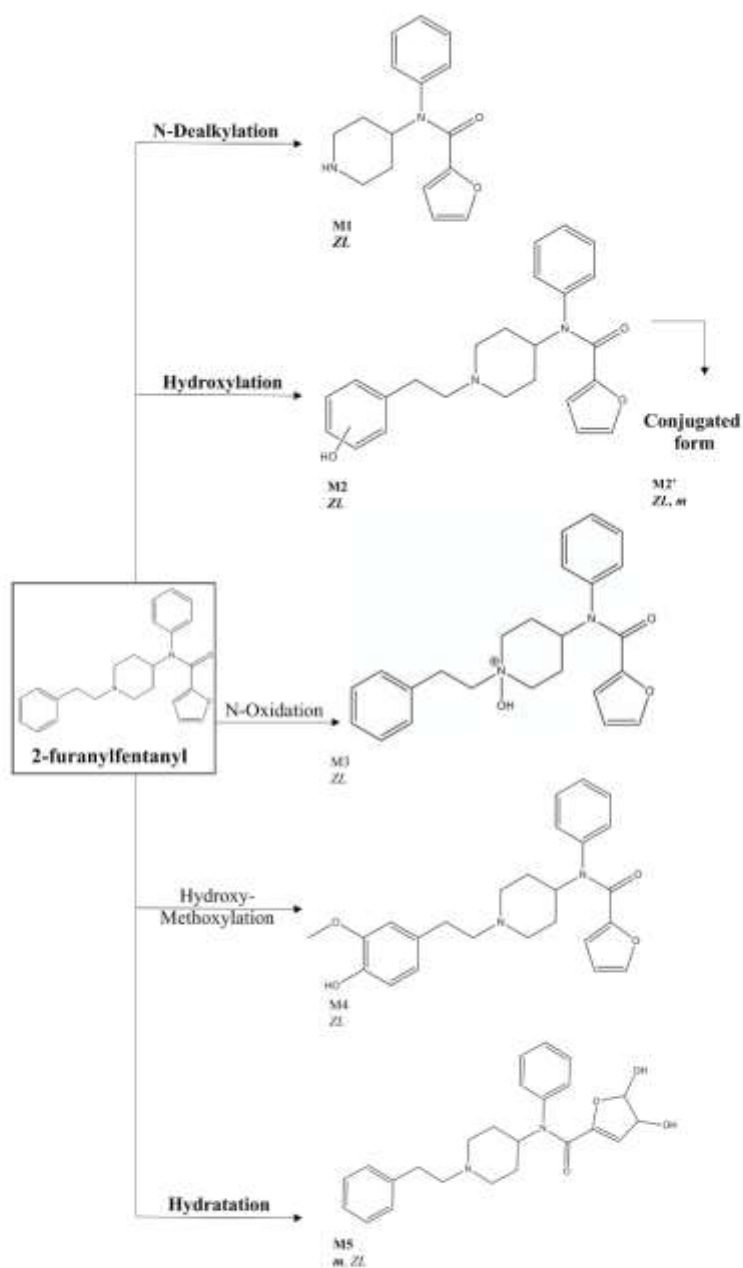
Fig. 4. . 2-furanylfentanyl metabolism. Schematic representation of proposed metabolic pathway of 2-furanylfentanyl, in mice (m) and zebrafish larvae (ZL). The main metabolic reactions and the resulting metabolites are highlighted in bold.

135

Table 2
List of ocfentanil metabolites tentatively identified in zebrafish larvae and mice with the proposed fragmentation spectra. The metabolites are rated from + to + ++ + according to their peak areas (n.d.: not detected).

| Compounds			Zebrafish Larvae (Extract)			Mice (Urine)		
Name	Chemical formula	Precursor ion	RT	Major products	%	RT	Major products	%
Ocfentanil	$C_{22}H_{27}FN_2O_2$	371.2135	7.9	188.1504 105.0697	+++	7.9	188.1426 105.0694	+++
M1	$C_{22}H_{27}FN_2O_3$	387.2084	7.2	204.1470 121.0700	++	n.d.		
M2	$C_{22}H_{27}FN_2O_3$	387.2084	8.2	279.1510 105.0697	++	n.d.		
M3	$C_{22}H_{27}FN_2O_3$	387.2084	7.5	204.1294 186.1181	+	n.d.		
M4	$C_{22}H_{27}FN_2O_3$	387.2084	n.d.			8.7	371.2512 89.0641	+
M5	$C_{21}H_{26}FN_2O_2$	357.1978	7.6	188.1459 105.0703	++	7.6	188.1443 105.0706	+++
M6	$C_{21}H_{26}FN_2O_2$	373.21020	7.9	189.1416 105.0672	+++	n.d.		
M5'	$C_{29}H_{34}FN_3O_6$	533.2299	n.d.			7.2	357.2093 188.1499	++++

evaluated by incubating larvae with fish water containing 0, 0.3 % and 3.3 % methanol (Fig. S1). As shown in the figure, larvae seem not to be sensitive to methanol, except for a slight effect observed with methanol at 3.3 %. However, the inhibition of locomotor activity exerted by ocfentanil and 2-furanylfentanyl at the concentration of 10 μM observed in Fig. 2 is clearly higher than that related to the presence of methanol.

In ZL the effect of 2-furanylfentanyl was more significant than that induced by ocfentanil, but similar to the effect of fentanyl at the same concentration (Pesavento et al., 2022). These differences could be related to a higher toxicity of 2-furanylfentanyl compared to ocfentanil, at least at high doses. In fact, in the morphological test, 2-furanylfentanyl induced malformation in ZL at the dose of 10 μM. In particular, the administration of this drug produced abdominal swelling, which has been reported as a common sign of acute toxicity in zebrafish (Coonan et al., 2021). Moreover, it is known that the yolk sac lipophilicity provides an ideal compartment for the accumulation of hydrophobic toxicants (Sant and Timme-Laragy, 2018). Therefore, the higher hydrophobicity of 2-furanylfentanyl could increase the accumulation of this drug in the yolk sac, causing the observed morphological toxicity. On the contrary, no alterations were observed after incubation with ocfentanil or in fish water containing methanol. A further explanation could be that the malformations occurring after the administration of 2-furanylfentanyl 10 μM, could create by itselves create a motor impairment, hence creating hypolocomotion in the behaviour assay.

4.2. Locomotor activity in mice

The administration of 2-furanylfentanyl and ocfentanil in mice (0.1–15 mg/kg) induced a significant impairment in motor activity, in particular at the dose of 1 mg/kg. These data are in accordance with the recent study of Varahneya et al. (2023) reporting the effect of ocfentanil, and also with our previous studies (Pesavento et al., 2022; Bilel et al., 2022). In our previous study, 2-furanylfentanyl did not induce a stimulation of motor activity in mice at the dose of 1 mg/kg in the accelerod test. However, in the open field test the effect of 2-furanylfentanyl is facilitator. This contradiction could be related to a difference in the efficacy of the two compounds on the mu opioid receptors in response to the motor test used (Bilel et al., 2022). Indeed, a recent study by Santos et al. (2022) revealed that the hyper-locomotor effect of opioids, and in particular of fentanyl, depends on their efficacy on the mu opioid receptors (Santos et al., 2022). In addition, it was suggested that the facilitation of locomotion by opioid agonists is triggered by the activation of the mesolimbic dopaminergic system, which is regulated by the endogenous opioid system, controlling the release of dopamine in the nucleus accumbens (Di Chiara and Imperato, 1988; Matsui et al., 2014). Yet, a recent study by Torralva et al. (2020) revealed that highly potent fentanyl interacts with dopamine (D1 and D4) receptors in the low micromolar range. In addition, fentanyl interacts also with serotonin receptors (5-HT1A) at low concentrations (Martin et al., 1991; Torralva et al., 2020). On these grounds, ocfentanil and 2-furanylfentanyl could increase locomotion involving the opioid-serotonin system, as highlighted by Gurtu (1990)). Additionally, we inserted a mechanical

stimulation at 240 min in the open field test to reveal potential persistence or disappearance of motor impairments in mice. Our results revealed that mechanically stimulated motor activity was completely reduced with 2-furanylfentanyl (1–15 mg/kg) while ocfentanil partially prevented (at 1 mg/kg) or completely reduced (at 6 and 15 mg/kg) mechanically stimulated motor activity in mice. As already reported, the effect of ocfentanil and 2-furanylfentanyl on motor activity (Drag test) persisted up to 5 h (Bilel et al., 2022). The differences seen between the two compounds at the dose of 1 mg/kg could be related to differences in their pharmacodynamics in response to various motor tests (Bilel et al., 2022; Santos et al., 2022). Moreover, the differences in responses to mechanically induced locomotor output could be related to a difference in the action of the two fentanyl analogs on tactile stimulation of the dorsal root ganglia system (Zhang et al., 2015) as demonstrated in the tail pinch test (Bilel et al., 2022).

4.3. Comparison of opioids locomotor effects in ZL and mice

Opioid receptor expression and activation in zebrafish have been demonstrated to be both biologically and pharmacologically comparable to that of rodents and humans (Sanchez-Simon and Rodriguez, 2008; Gonzalez-Nunez and Rodriguez, 2009). Furthermore, zebrafish opioid receptor transcripts could be detected in early development stages (before 3 h post fertilization). In a previous study, we demonstrated that, in contrast to zebrafish, the rodent model showed hyperlocomotion induced by low doses (1 mg/kg) of fentanyl (Pesavento et al., 2022). Our results confirm previous findings concerning differences in locomotor effects induced by opioids between the two models. In ZL the effect seems to be mediated by the activation of the mu opioid receptor, as highlighted by Zaig et al., (2021). Different factors can account for these differences. For instance, an important element to be considered in the comparison between behavioural effects in ZL and mice is developmental stage. Indeed, reduced swimming activity in ZL treated with fentanyl analogues could be related to a higher sensitivity of embryos to toxicants compared with adult mice (Ducharme et al., 2015). In addition, zebrafish hypomotility could be related to earlier respiratory depression compared to mice at low concentrations of fentanyl and its analogs. In particular, differently from mammalians, ZL have a complex respiratory system, which they use to move water through their gills for oxygen absorption and carbon dioxide elimination (Zaig et al., 2021). Furthermore, differences in locomotor effects induced by 2-furanylfentanyl and ocfentanil between the two animal models could be related to differences in metabolism, as discussed below.

Moreover, Kaig and his colleagues revealed that fentanyl induced respiratory depression in ZL and this effect was reversed by a high concentration (20 μM) of the mu opioid receptor antagonist naloxone (Zaig et al., 2021).

4.4. Metabolism of 2-furanylfentanyl and ocfentanil in ZL and mice

According to the metabolic assay performed with the same animal models for fentanyl (Pesavento et al., 2022), ZL and mice showed
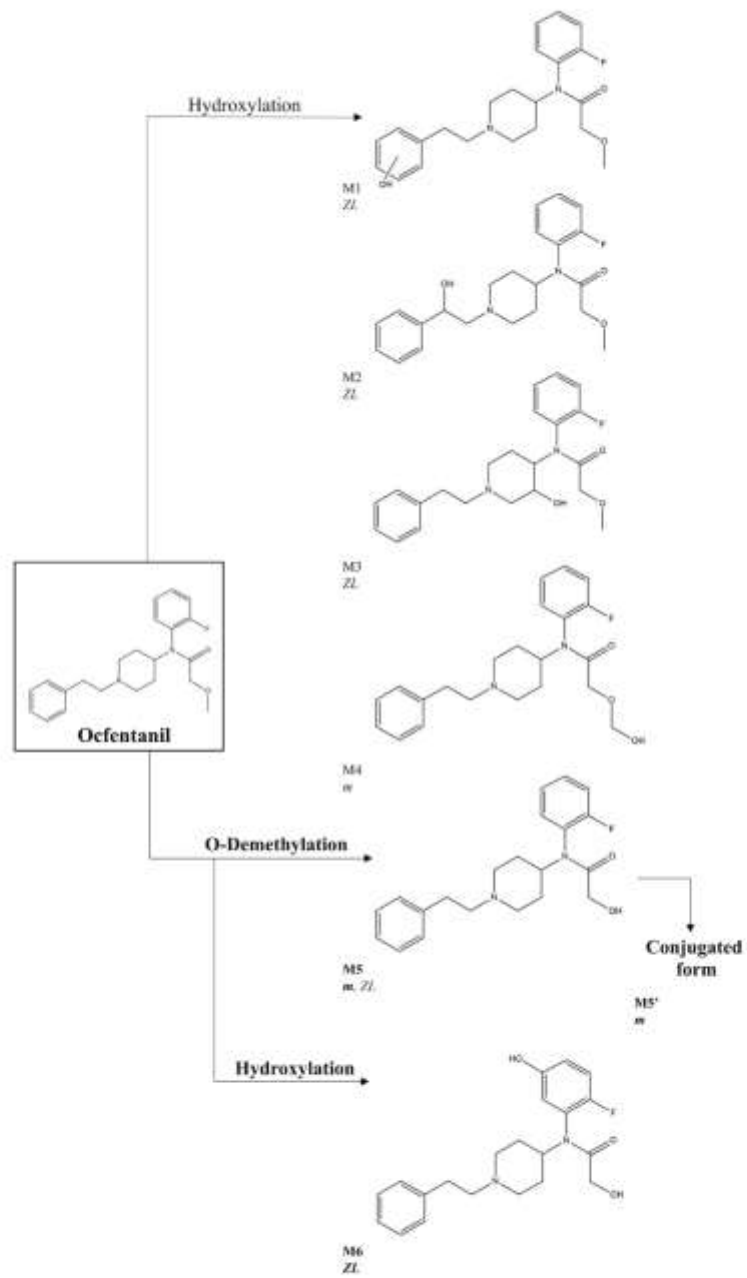
Fig. 5. Ocfentanil metabolism. Schematic representation of proposed metabolic pathway of ocfentanil, in mice (m) and zebrafish larvae (ZL). The main metabolic reactions and the resulting metabolites are highlighted in bold.

137

relatively similar metabolic pathways. In particular, the analysis of larvae extracts identified a large number of phase I metabolites, mostly due to hydroxylation, hydration and oxidation, for 2-furanylfentanyl. On the contrary, mice mainly seemed to produce the dihydrodiol metabolite. The major route of metabolism for ocfentanil in ZL was hydroxylation, while in mice it was o-demethylation. The two models produced phase II metabolites, i.e., glucuronide metabolites. These results are partially consistent with previous studies on 2-furanylfentanyl metabolism in different experimental models (i.e. microsomes and human urine), where the major route of metabolism was represented by hydroxylation and formation of dihydrodiol metabolite (Gaulier et al., 2017; Goggin et al., 2017; Kanamori et al., 2021; Watanabe et al., 2017). However, no 4-anilino-N-phenethylpiperidine (4-ANPP) was observed, pointing out that this common metabolite of fentanyl is not present in its analog. This difference might be due to a lack of the amidase enzyme involved in the production of 4-ANPP in ZL and in mice (Watanabe et al., 2017). On the contrary, ocfentanil results in mice and ZL are consistent with the metabolic pathway proposed by Allibe et al. (2016), in which the major route of metabolism in vitro and in biological samples was represented by hydroxylation, demethylation and glucuronidation, whereas 4-ANPP was not described and nor-ocfentanil was elucidated only in human liver microsomes, but not in biological samples. Our results confirm the validity of ZL for the identification of NSOs metabolites, even though they showed small differences in metabolism when compared to mice, which could be related to the different route of exposure as suggested for other opioids (Kirla et al., 2021).

5. Conclusions

The present study evaluates behavioural effects, toxicity and metabolism of 2-furanylfentanyl and ocfentanil, in ZL and mice. Consequently, in our opinion, the results prove that ZL can provide, at least in a preliminary phase, useful information on different pharmacotoxicological aspects of NSO and consequently can be regarded as a suitable animal model for large-scale screening of the newly introduced clandestine drugs (tentatively also non-opioid), to be performed before the completion of more formal studies in mammals.

Fundings

CRediT authorship contribution statement

Bilel and Murari: data acquisition, Investigation, original draft preparation. Pesavento: Investigation, Methodology, original draft preparation. Arfè and Tirri: investigation. Torroni: Formal analysis. Marti and Tagliaro: Supervision, Funding acquisition. Rossella Gottardo: Conceptualization, original draft preparation, final editing.

Declaration of Competing Interest

The authors declare that they have no known competing financial interests or personal relationships that could have appeared to influence the work reported in this paper.

Data availability

Data will be made available on request.

Acknowledgements

Appendix A. Supporting information

Supplementary data associated with this article can be found in the online version at doi:10.1016/j.neuro.2023.01.003.

References

Achenbach, J.C., Hill, J., Hui, J.P.M., Morash, M.G., Berrue, F., Ellis, L.D., 2018. Analysis of the uptake, metabolism, and behavioral effects of cannabinoids on zebrafish larvae. Zebrafish 15 (4), 349–360. https://doi.org/10.1089/zeb.2017.1541.

Ali, S., van Mil, H.G.J., Richardson, M.K., 2011. Large Scale assessment of the zebrafish embryo as a possible predictive model in toxicity testing. PLoS One 6 (6). https://doi.org/10.1371/journal.pone.0021076.

Allibe, N., Richeval, C., Phanithavong, M., Faure, A., Allorge, D., Paysant, F., Gaulier, J. M., 2018. Fatality involving ocfentanil documented by identification of metabolites. Drug Test. Anal. 10 (6), 995–1000. https://doi.org/10.1002/dta.2326.

Baumann, M.H., Majumdar, S., Le Rouzic, V., Hunkele, A., Uprety, R., Huang, X.P., Pasternak, G.W., 2018. Pharmacological characterization of novel synthetic opioids (NSO) found in the recreational drug marketplace. Neuropharmacology. https://doi.org/10.1016/j.neuropharm.2017.08.016.

Bilel, S., Arfè, R., Tirri, M., Trapella, C., Frisoni, P., Neri, M., Marti, M., 2020. The novel fentanyl analog "Acrylfentanyl" impairs motor, sensorimotor and cardiovascular functions in mice. Pharmadvances 2 (1).

Bilel, S., Azevedo Neto, J., Arfè, R., Tirri, M., Gaudio, R., Fantinati, A., Marti, M., 2022. In vitro and in vivo pharmaco-dynamic study of the novel fentanyl derivatives: acrylfentanyl, ocfentanyl and furanylfentanyl. Neuropharmacology 209, 109020. https://doi.org/10.1016/j.neuropharm.2022.109020.

Cooman, T., Bergeron, S.A., Coltogirone, R., Horstick, E., Arroyo, L., 2021. Evaluation of fentanyl toxicity and metabolism using a zebrafish model. J. Appl. Toxicol. https://doi.org/10.1002/jat.4253.

Di Chiara, G., Imperato, A., 1988. Opposite effects of mu and kappa opiate agonists on dopamine release in the nucleus accumbens and in the dorsal caudate of freely moving rats. J. Pharmacol. Exp. Ther. 244 (3), 1067–1080.

Drug Enforcement Administration, D. of J., 2018. Schedules of controlled substances: placement of furanyl fentanyl, 4 fluoroisobutyryl fentanyl, acryl fentanyl, tetrahydrofuranyl fentanyl, and ocfentanil in schedule I. Final order. Federal Register.

Duchanne, N.A., Reif, D.M., Gustafson, J.A., Bundesen, M., 2015. Comparison of toxicity values across zebrafish early life stages and mammalian studies: implications for chemical testing. Reprod. Toxicol. 55, 3–10.

European Monitoring Centre for Drugs and Drug Addiction (EMCDDA), 2017. Europol Joint Report on a new psychoactive substance: N-phenyl-N-[1 (2 phenylethyl) piperidin-4-yl]- furan-2-carboxamide (furanylfentanyl).

Fletcher, J.E., Sebel, P.S., Murphy, M.R., Mick, S.A., Fein, S., 1991. Comparison of ocfentanil and fentanyl as supplements to general anesthesia. Anesth. Analg. https://doi.org/10.1213/00000539-199111000-00019.

Fu, J., Jiao, J., Weng, K., Yu, D., Li, R., 2017. Zebrafish methanol exposure causes patterning defects and suppressive cell proliferation in retina. Am. J. Transl. Res. 9 (6), 2975–2983.

Gerrent, B., Desbarnats, B., Beauchamp-Doré, A., Lavallée, C., Mireault, P., Lajeunesse, A., 2020. Challenges related to three cases of fatal intoxications to multiple novel synthetic opioids. J. Anal. Toxicol. https://doi.org/10.1093/jat/bkz028.

Gaulier, J., Richeval, C., Gicquel, T., Hugbart, C., Le Dare, B., Allorge, D., Morel, I., 2017. In vitro characterization of NPS metabolites produced by human liver microsomes and the HepaRG cell line using liquid chromatography-high resolution mass spectrometry (LC-HRMS) analysis: application to furanyl fentanyl. Curr. Pharm. Biotechnol. https://doi.org/10.2174/1389201018666171122124401.

Goggin, M.M., Nguyen, A., Janis, G.C., 2017. Identification of unique metabolites of the designer opioid furanyl fentanyl. J. Anal. Toxicol. 41 (5), 367–375. https://doi.org/10.1093/jat/bkx022.

Gonzalez-Nunez, V., Rodriguez, R.E., 2009. The zebrafish: a model to study the endogenous mechanisms of pain. ILAR J. 50 (4), 373–386. https://doi.org/10.1093/ilar.50.4.373.

Gerin, S., 1990. MU receptor-serotonin link in opioid induced hyperactivity in mice. Life Sci. 46 (21), 1539–1544. https://doi.org/10.1016/0024-3205(90)90427-S.

Huang, B.-S., Terrell, R.C., Deutsche, K.H., Kudzma, L.V., Lalinde, L.N., 1987. N-aryl-a-(4-piperidinyl)amides and pharmaceutical compositions and method employing

such compounds. Gen. Pharmacol. Vasc. Syst. https://doi.org/10.1016/0306-3623(07)90295-3.

Iburmis, M.A., Brandt, S.D., Rasa, S., Auwärter, V., Baumann, M.H., 2017. Impact of novel psychoactive substances on clinical and forensic toxicology and global public health. Clin. Chem. https://doi.org/10.1373/clinchem.2017.274662.

Kalueff, A.V., 2017. The rights and wrongs of zebrafish: Behavioral phenotyping of zebrafish. The Rights and Wrongs of Zebrafish: Behavioral Phenotyping of Zebrafish. doi: 10.1007/978-3-319-33774-6.

Kanamori, T., Okada, Y., Segawa, H., Yamamuro, T., Kuwayama, K., Tsujikawa, K., Togawa-Iwata, Y., 2021. Detection and confirmation of the ring-opened carboxylic acid metabolite of a new synthetic opioid furanylfentanyl. Forensic Toxicol. https://doi.org/10.1007/s11419-020-00546-7.

Kimmel, C.B., Ballard, W.W., Kimmel, S.R., Ullmann, B., Schilling, T.F., 1995. Stages of embryonic development of the zebrafish. Dev. Dyn. 203 (3), 253–310. https://doi.org/10.1002/aja.1002030302.

Kirla, K.T., Erhart, C., Groh, K.J., Stadnicka Michalak, J., Eggen, R.I.L., Schirmer, K., Kraemer, T., 2021. Zebrafish early life stages as alternative model to study 'designer drugs': concordance with mammals in response to opioids. Toxicol. Appl. Pharmacol. 419, 115483 https://doi.org/10.1016/j.taap.2021.115483.

MacPhail, R.C., Brooks, J., Hunter, D.L., Padnos, B., Irons, T.D., Padilla, S., 2009. Locomotion in larval zebrafish: Influence of time of day, lighting and ethanol. NeuroToxicology 289, 207–214. https://doi.org/10.1016/j.neuro.2008.09.011.

Martin, D.C., Introna, R.P., Aronstam, R.S., 1991. Fentanyl and sufentanil inhibit agonist binding to 5-HT1A receptors in membranes from the rat brain. Neuropharmacology 30 (4), 323–327. https://doi.org/10.1016/0028-3908(91)90056-H.

Matsui, A., Jarvie, B.C., Robinson, B.G., Hentges, S.T., Williams, J.T., 2014. Separate GABA afferents to dopamine neurons mediate acute action of opioids, development of tolerance, and expression of withdrawal. Neuron 82 (6), 1346–1356. https://doi.org/10.1016/j.neuron.2014.04.030.

Misailidi, N., Papoutsis, I., Nikolaou, P., Dona, A., Spiliopoulou, C., Athanaselis, S., 2018. Fentanyls continue to replace heroin in the drug arena: the cases of ocfentanil and carfentanil. Forensic Toxicol. https://doi.org/10.1007/s11419-017-0379-4.

Misailidi, N., Athanaselis, S., Nikolaou, P., Katselou, M., Dotsikas, Y., Spiliopoulou, C., Papoutsis, I., 2019. A GC-MS method for the determination of furanylfentanyl and ocfentanil in whole blood with full validation. Forensic Toxicol. https://doi.org/10.1007/s11419-018-0449-2.

Ossato, A., Bilel, S., Gregori, A., Talarico, A., Trapella, C., Gaudio, R.M., Marti, M., 2018. Neurological, sensorimotor and cardiorespiratory alterations induced by methoxetamine, ketamine and phencyclidine in mice. Neuropharmacology 141, 167–180. https://doi.org/10.1016/j.neuropharm.2018.08.017.

Pesavento, S., Bilel, S., Murari, M., Gottardo, R., Arfè, R., Tirri, M., Marti, M., 2022. Zebrafish larvae: a new model to study behavioural effects and metabolism of fentanyl, in comparison to a traditional mice model. Med. Sci. Law 62 (3), 188–198. https://doi.org/10.1177/00258024221074568.

Prekupec, M.P., Mansky, P.A., Baumann, M.H., 2017. Misuse of novel synthetic opioids: a deadly new trend. J. Addict Med. 11 (4), 256–265. https://doi.org/10.1097/ADM.0000000000000324.

Sánchez Simon, F.M., Rodríguez, R.E., 2008. Developmental expression and distribution of opioid receptors in zebrafish. Neuroscience 151 (1), 129–137.

Sant, K.E., Timme Laragy, A.R., 2018. Zebrafish as a model for toxicological perturbation of yolk and nutrition in the early embryo. Curr. Environ. Health Rep. https://doi.org/10.1007/s40572-018-0183-2.

Santos, E.J., Banks, M.L., Stevens Negus, S., 2022. Role of efficacy as a determinant of locomotor activation by mu opioid receptor ligands in female and male mice. J. Pharmacol. Exp. Ther. 382 (1), 44–53. https://doi.org/10.1124/jpet.121.001045.

Slovenian National Forensic Laboratory, 2016. NPS and related compounds. Analytical Reports.

de Souza Anselmo, C., Sardela, V.F., de Sousa, V.P., Pereira, H.M.G., 2018. Zebrafish (Danio rerio): a valuable tool for predicting the metabolism of xenobiotics in humans? Comp. Biochem. Physiol. Part C Toxicol. Pharmacol. https://doi.org/10.1016/j.cbpc.2018.06.005.

Torralva, R., Eshleman, A.J., Swanson, T.L., Schmachtenberg, J.L., Schutzer, W.E., Bloom, S.H., Janowsky, A., 2020. Fentanyl but not morphine interacts with nonopioid recombinant human neurotransmitter receptors and transporters. J. Pharmacol. Exp. Ther. 374 (3), 376–391. https://doi.org/10.1124/jpet.120.265561.

United Nations Office on Drugs and Crime (UNODC), 2017. World Drug Report 2019.

Varshneya, N.B., Walentiny, D.M., Moisa, L.T., Walker, T.D., Akinfiresoye, L.R., Beardsley, P.M., 2019. Opioid like antinociceptive and locomotor effects of emerging fentanyl-related substances. Neuropharmacology 151, 171–179. https://doi.org/10.1016/j.neuropharm.2019.03.023.

Varshneya, N.B., Walentiny, D.M., Moisa, L.T., Walker, T.D., Akinfiresoye, L.R., Beardsley, P.M., 2021. Fentanyl related substances elicit antinociception and hyperlocomotion in mice via opioid receptors. Pharmacol. Biochem. Behav. 208, 173242 https://doi.org/10.1016/j.pbb.2021.173242.

Varshneya, N.B., Walentiny, D.M., Stevens, D.L., Walker, T.D., Akinfiresoye, L.R., Beardsley, P.M., 2023. Structurally diverse fentanyl analogs yield differential locomotor activities in mice. Pharmacol. Biochem. Behav. 173496.

Varshneya, N.B., Hassanien, S.H., Holt, M.C., Stevens, D.L., Layle, N.K., Bassman, J.R., Beardsley, P.M., 2022. Respiratory depressant effects of fentanyl analogs are opioid receptor-mediated. Biochem. Pharmacol. 195, 114805 https://doi.org/10.1016/j.bcp.2021.114805.

Watanabe, S., Vikingsson, S., Roman, M., Green, H., Kronstrand, R., Wohlfarth, A., 2017. In vitro and in vivo metabolite identification studies for the new synthetic opioids acetylfentanyl, acrylfentanyl, furanylfentanyl, and 4-fluoro-isobutyrylfentanyl. AAPS J. https://doi.org/10.1208/s12248-017-0070-x.

Wilde, M., Pichini, S., Pacifici, R., Tagliabracci, A., Busardò, F.P., Auwärter, V., Solimini, R., 2019. Metabolic pathways and potencies of new fentanyl analogs. Front. Pharmacol. https://doi.org/10.3389/fphar.2019.00238.

Zaig, S., da Silveira Scarpellini, C., Montandon, G., 2021. Respiratory depression and analgesia by opioid drugs in freely behaving larval zebrafish. eLife 10, e63407.

Zhang, X., Bao, L., Li, S., 2015. Opioid receptor trafficking and interaction in nociceptors. Br. J. Pharmacol. 172 (2), 364–374. https://doi.org/10.1111/bph.12653.

139

Chapter 4 Submitted articles

4.1 Elucidating the harm potential of brorphine analogues as new synthetic opioids: Synthesis, *in vitro*, and *in vivo* characterization

Marthe M. Vandeputte[1,*], Sabrine Bilel[2,*], Micaela Tirri[2], Giorgia Corli[2], Marta Bassi[2], Nathan K. Layle[3], Anna Fantinati[4], Donna Walther[5], Donna M. Iula[3], Michael H. Baumann[5], Christophe P. Stove[1,+], Matteo Marti[2,6,+]

[1]*Laboratory of Toxicology, Department of Bioanalysis, Faculty of Pharmaceutical Sciences, Ghent University, Ghent, Belgium*
[2]*Department of Translational Medicine, Section of Legal Medicine and LTTA Centre, University of Ferrara, Ferrara, Italy*
[3]*Forensic Chemistry Division, Cayman Chemical Company, Ann Arbor, MI 48108, USA*
[4]*Department of Environmental and Prevention Sciences, University of Ferrara, Via Fossato di Mortara, Ferrara, Italy*
[5]*Designer Drug Research Unit (DDRU), Intramural Research Program, National Institute on Drug Abuse, National Institutes of Health, Baltimore, MD 21224, USA*
[6]*Collaborative Center of the National Early Warning System, Department for Anti-Drug Policies, Presidency of the Council of Ministers, Italy*

[*,+] *Contributed equally.*

Corresponding Authors:

Prof. Dr. Matteo Marti

Department of Translational Medicine, Section of Legal Medicine, University of Ferrara, Ferrara, Italy.

Phone +39 0532 455781, fax +39 0532 455777

matteo.marti@unife.it

Prof. Dr. Christophe Stove

Laboratory of Toxicology, Department of Bioanalysis, Faculty of Pharmaceutical Sciences, Ghent University, Ghent, Belgium.

Phone +32 (0) 9 264 81 35

Christophe.Stove@ugent.be

4.1.1 Abstract

The emergence of new synthetic opioids (NSOs) has added complexity to recreational opioid markets worldwide. While NSOs with diverse chemical structures have emerged, brorphine currently remains the only NSO with a piperidine benzimidazolone scaffold. However, the emergence of new generations of NSOs, including brorphine analogues, can be anticipated. This study explored the pharmaco-toxicological effect profile of brorphine and four newly synthesized analogues with differing *para*-ring substituents (orphine, fluorphine, chlorphine, iodorphine) as potential NSOs. *In vitro*, radioligand binding assays in rat brain tissue indicated that all analogues bind to the μ-opioid receptor (MOR) with nM affinity. While analogues with smaller-sized substituents showed the highest MOR affinity, further *in vitro* characterization *via* two MOR activation (β-arrestin 2 and mini-$G_{\alpha i}$ recruitment) assays indicated that chlorphine, brorphine, and iodorphine were generally the most active MOR agonists. None of the compounds showed significant biased agonism. *In vivo*, we investigated the effects of intraperitoneal (IP) administration of the benzimidazolones (0.01-15 mg/kg) on mechanical and thermal antinociception in male CD-1 mice. Chlorphine, and brorphine induced the highest levels of antinociception. Furthermore, the effects on respiratory changes induced by a high dose (15 mg/kg IP) of the compounds were investigated using non-invasive plethysmography. Fluorphine-, chlorphine-, and brorphine-induced respiratory depressant effects were the most pronounced. Pretreatment with naloxone (6 mg/kg IP) suggested non-opioid mechanisms of action for some compounds. Taken together, brorphine-like piperidine benzimidazolones are opioid agonists that have the potential to cause substantial harm to users should they emerge as NSOs.

4.1.2 Introduction

The number of new psychoactive substances (NPS) monitored in Europe continues to grow [1]. While new synthetic opioids (NSOs) represent a relatively small share of the NPS market, they are often considered the most dangerous subclass due to the high risk of overdose [1]. Since 2019, a growing number of structurally diverse, non-fentanyl-related NSOs have emerged [2].

Brorphine is a synthetic piperidine benzimidazolone opioid that was first identified on the NPS market in 2019 [3,4]. While piperidine benzimidazolone derivatives were included in a Janssen patent from 1967 [5], brorphine itself was not studied at the time, and it is commonly assumed that the emergence of brorphine as an NSO is based on its inclusion in a study by Kennedy *et al*. from 2018 [3,4,6]. That study evaluated structure-activity relationships (SARs) of a panel of μ-opioid receptor (MOR) agonists with a specific focus on the determination of MOR signaling bias. Brorphine was among the analogues with a moderately high level of G protein bias [6]. Notably, brorphine appeared on recreational drug markets around the globe from 2019 onwards [3,4,7,8] and was also identified in (postmortem) toxicology samples [4,9,10]. Considering its high abuse potential, brorphine was internationally scheduled in 2022 [11]. By now, its popularity seems to have decreased, with only two identifications in the US in the third quarter of 2023 [3,12,13].

To date, brorphine remains the only NSO with a benzimidazolone scaffold. While the NSO market is currently largely dominated by benzimidazole 'nitazene' opioids [7], growing awareness of the dangers related to nitazenes (including the increased implementation of legislative measures [14]), may fuel a shift towards newer generations of NSOs, as previously observed for fentanyl analogues [15]. In this context, the emergence of other benzimidazolone opioids related to brorphine can be anticipated. Therefore, the aim of this work was to pharmacologically characterize brorphine and four brorphine-like benzimidazolone compounds (orphine, fluorphine, chlorphine, iodorphine) (**Fig.3.1**) that are structurally included in the 1967 patent [5,16]. Limited pharmacological information is available in the scientific literature for orphine, fluorphine, and chlorphine [6,16,17]; to date, there have been no studies on iodorphine. Here, extensive *in vitro* (MOR binding affinity and activation) and *in vivo* (antinociception and respiratory depression) characterization was performed.
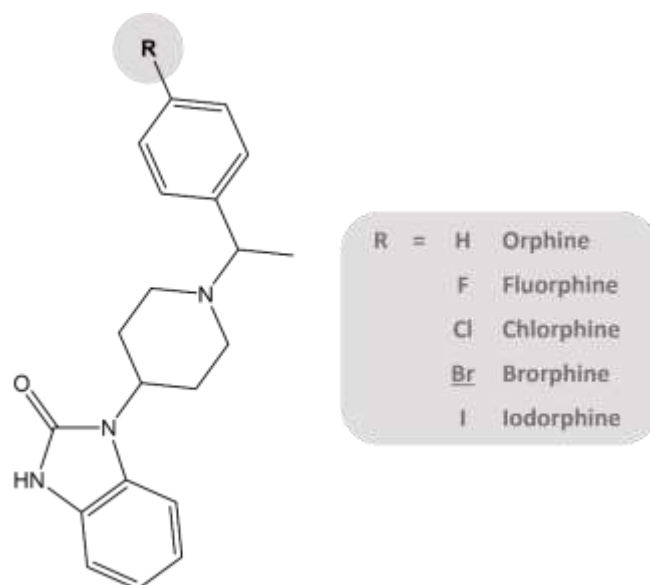
Figure 4.1 *Chemical structure of the studied piperidine benzimidazolone compounds.*

4.1.3 Materials and Methods

4.1.3.1 Chemicals and reagents

Tritiated DAMGO ([^{3}H]DAMGO) was from Perkin Elmer (Waltham, MA, USA). Hydromorphone HCl (hydromorphone) was supplied by Fagron (Nazareth, Belgium). Morphine and fentanyl were from Cayman Chemical (Ann Arbor, MI, USA). Thermo Fisher Scientific (Waltham, MA, USA) supplied Dulbecco's Modified Eagle's Medium (DMEM) (GlutaMAX™), Opti-MEM® I Reduced Serum Medium, penicillin-streptomycin (10,000 U/mL and 10,000 µg/mL) and amphotericin B (250 µg/mL). Fetal bovine serum (FBS) and poly-D-lysine were from Sigma-Aldrich (Darmstadt, Germany). The Nano-Glo® Live Cell Assay System was from Promega (Madison, WI, USA).

Synthesis

The piperidine benzimidazolones were synthesized in one step from commercially available 4-(2-keto-1-benzimidazolinyl)piperidine (**1**) and a corresponding phenylacetone (where R=H, F, Cl, Br, or I) using standard reductive amination conditions (**Fig.A.1**) [6]. Except for brorphine (which was converted to its corresponding hydrochloride using 2M HCl in diethyl ether and tested as such), all analogues were isolated and purified as free bases prior to testing. Details can be found in the **Supplementary Materials (Appendix A)**.

4.1.3.2 *In vitro* experiments

4.1.3.2.1 Radioligand binding assays

Competition binding assays were conducted in rat brain tissue as previously described [18–20]. Details can be found in the **Supplementary Materials (Appendix A)**.

4.1.3.2.2 MOR activation assays

MOR activation was monitored by means of two previously described cell-based bioassays monitoring recruitment of either mini-$G_{\alpha i}$ or β-arrestin 2 (βarr2) [21]. Details related to experimental setup and data analysis [22–24] can be found in the **Supplementary Materials (Appendix A)**.

4.1.3.2.3 Evaluation of biased agonism

MOR biased agonism was evaluated *via* calculation of the relative intrinsic activity (RA_i) for each compound in each bioassay, as previously described [24–26]. Extended methods are described in the **Supplementary Materials (Appendix A)**.

4.1.3.3 *In vivo* experiments

All applicable international, national, and/or institutional guidelines for the care and use of animals were followed. All procedures involving animals were in accordance with the ethical standards of the institution or practice at which the studies were conducted. This project was activated in collaboration with the Presidency of the Council of Ministers-DPA Anti-Drug Policies (Italy).

4.1.3.3.1 Animals

Three hundred forty-four male ICR (CD-1®) mice weighing 30–35 g (ENVIGO Harlan Italy; bred inside the Laboratory for Preclinical Research (LARP) of the University of Ferrara, Italy) were used – for housing details, we refer to the **Supplementary Materials (Appendix A)**. The experimental protocols were in accordance with the European Council Directive of September 2010 (2010/63/EU); a revision of the Directive 86/609/EEC was approved by the Ethics Committee of the University of Ferrara and by the Italian Ministry of Health (authorization number 335/2016-PR). Moreover, adequate measures were taken to reduce the number of animals used and their pain and discomfort according to the ARRIVE guidelines.

4.1.3.3.2 Drug preparation and dose selection

Drugs were initially dissolved in absolute ethanol (final concentration: 5%) and Tween 80 (2%) and brought to the final volume with saline (0.9% NaCl). Drugs were administered by

intraperitoneal (IP) injection (4 µL/g). The dose range for brorphine and its analogues (0.01-15 mg/kg IP) was chosen based on previous studies [27,28]. In antagonist experiments, naloxone (6 mg/kg IP) was administered 15 min before test compound injections, similar to our previous study [28], with a small modification in the injection timing of the second naloxone dose (60 min after the first injection instead of 55 min [28], when a reappearence of the test compounds' effects was observed). 15 mg/kg was the highest and most effective dose in all tests, and was selected to evaluate the effects of brorphine and its analogues on respiratory parameters using non-invasive plethysmography.

4.1.3.3.3 Evaluation of pain induced by mechanical and a thermal stimuli

A battery of behavioural tests widely used in safety pharmacology studies for the preclinical characterization of NPS in rodents was used [27–30]. All experiments were performed between 8:30 am and 2:00 pm and were conducted blind-coded by trained observers, working in pairs [31]. Only data related to antinociception are shown in this study. *Acute mechanical* and *thermal nociception* were evaluated using the tail pinch and tail withdrawal tests, respectively [32]. A detailed description of the tests can be found in the **Supplementary Materials (Appendix A)**.

4.1.3.3.4 Plethysmography analysis

As previously reported by Marchetti *et al.* [33], plethysmography was performed in conscious animals using a non-invasive electrocardiogram (ECG) and plethysmography TUNNEL system with an acquisition frequency of 1000 Hz (Emka Technologies, Paris, France). All plethysmography recording sessions were performed during daytime, and data were analyzed using the IOX2 data acquisition analysis software (Emka Technologies). A detailed description of the plethysmography analysis can be found in the **Supplementary Materials (Appendix A).**

4.1.3.3.5 Data and statistical analysis

Antinociceptive effects are calculated as the percent of maximum possible effect (%MPE = [(test - control latency) / (cut-off force or time - control)] X 100). For plethysmography, BL (ms; breath length, sum of the duration of inspiration, and the duration of expiration), RR (bpm; respiratory rate derived from BL), and TV (mL/s; tidal inspiration volume), were expressed as % change of basal value. Statistical analysis of the effects of the substances at different doses over time and of antagonism studies was done *via* two-way ANOVA followed by a Bonferroni test for multiple comparisons (GraphPad Prism 9, San Diego, CA, USA). The mean effect

values represent the average of the effects induced by each compound at each dose over the time course of the experiment (5 h for nociception assays; 60 min for plethysmography). For all tests, a p value < 0.05 was considered statistically significant.

4.1.4 Results

4.1.4.1 *In vitro* characterization

Radioligand binding studies showed that the piperidine benzimidazolones bind to MOR with nM affinities (K_i range 1.92-133 nM) (**Fig.4.2-A/Table 1**). Chlorphine had the highest affinity (K_i=1.92 nM), followed by orphine (K_i=6.91 nM) and fluorphine (K_i=12.5 nM). The MOR affinity of these drugs was comparable to those of the structurally unrelated morphine (K_i=2.77 nM) and fentanyl (K_i=6.29 nM), but lower than that of hydromorphone (K_i=0.518 nM). Brorphine (K_i=53.7 nM) and iodorphine (K_i=133 nM) showed a lower affinity. Interestingly, different trends were observed in the MOR activation assays (**Fig.4.2-B,C/Table 1**). Chlorphine (EC_{50}=16.1 nM; E_{max}=161%), brorphine (EC_{50}=16.3 nM; E_{max}=169%), and iodorphine (EC_{50}=18.3 nM; E_{max}=49%) showed comparable potencies for βarr2 recruitment. Fluorphine (EC_{50}=32.0 nM; E_{max}=147%) and orphine (EC_{50}=28.4 nM; E_{max}=132%) appeared somewhat less potent, but confidence intervals were overlapping. Efficacies were largely comparable in this assay (E_{max} range 132-169%). In the mini-$G_{\alpha i}$ assay, orphine (EC_{50}=135 nM; E_{max}=184%) and fluorphine (EC_{50}=127 nM; E_{max}=222%) were noticeably less efficacious than the other benzimidazolone opioids (E_{max} range 344-352%). While potency differences were rather limited (EC_{50} range 81.9-301 nM, with mostly overlapping confidence intervals), brorphine (EC_{50}=81.9 nM; E_{max}=344%) appeared to be the most potent. In both assays, piperidine benzimidazolones were generally (somewhat) less potent than fentanyl, and more active than morphine. When evaluating bias (**Table 4.1/Fig.A2**), iodorphine appeared to slightly favour βarr2 over mini-$G_{\alpha i}$ recruitment. However, with the utilized methods, none of the test compounds showed statistically significant biased agonism.
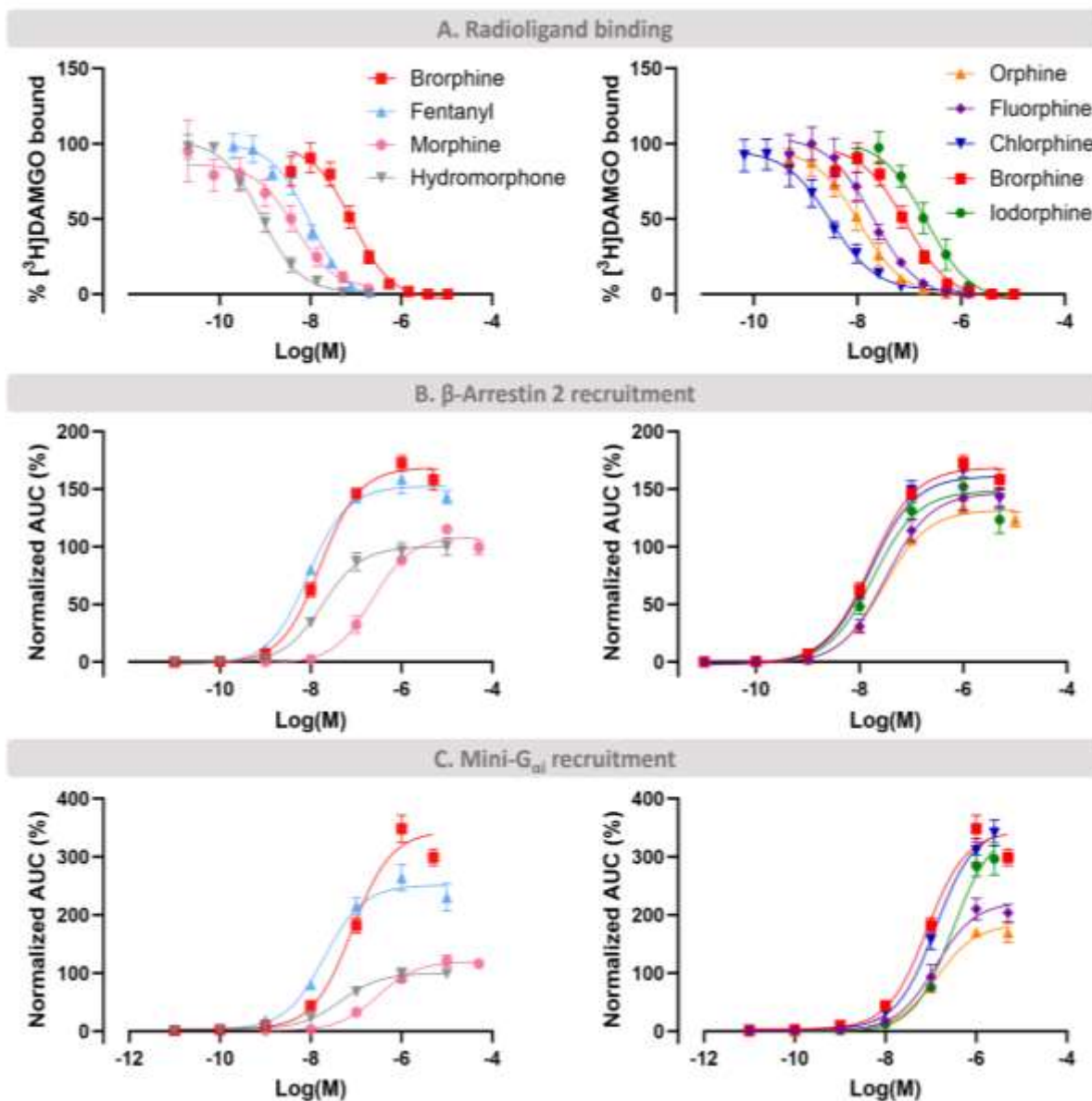
Figure 4.2. *Concentration-response curves as obtained in the different in vitro MOR assays (panel A, radioligand binding assay; panels B-C, MOR activation assays). Radioligand binding data are shown as mean % [³H]DAMGO binding ± standard error of the mean (SEM). MOR activation data are shown as mean MOR activation ± SEM, normalized to the maximum response of hydromorphone (100%). AUC, area under the curve.*

Table 4.1 *Summary of in vitro assay results. Efficacies (E_{max}) are relative to hydromorphone, and 95% confidence intervals are given between parentheses. Bias factors (β_i) are given as mean ± standard error of the mean (SEM). Corresponding bias plots can be found in the Supplementary Materials (Appendix A). N.D. not determined.*

	MOR affinity	MOR-βarr2 recruitment		MOR-mini-$G_{\alpha i}$ recruitment		MOR bias
	K_i *(nM)*	EC_{50} *(nM)*	E_{max} *(%)*	EC_{50} *(nM)*	E_{max} *(%)*	β_i
Orphine	**6.91** (4.08-11.7)	**28.4** (20.6-39.1)	**132** (125-139)	**135** (97.8-187)	**184** (172-196)	**0.09** ± 0.04
Fluorphine	**12.5** (7.51-20.8)	**32.0** (21.7-47.2)	**147** (137-157)	**127** (75.0-217)	**222** (199-246)	**0.01** ± 0.11
Chlorphine	**1.92** (1.20-3.08)	**16.1** (11.5-22.8)	**161** (152-170)	**126** (88.7-180)	**352** (326-380)	**0.10** ± 0.10
Brorphine	**53.7** (33.6-85.9)	**16.3** (12.6-21.3)	**169** (162-176)	**81.9** (55.1-119)	**344** (318-370)	**0.03** ± 0.11
Iodorphine	**133** (76.3-232)	**18.3** (12.8-26.4)	**149** (139-158)	**301** (196-484)	**349** (315-391)	**0.45** ± 0.06
Fentanyl	**6.29** (3.50-11.3)	**8.82** (6.18-12.5)	**153** (145-160)	**20.0** (11.7-34.8)	**251** (231-272)	N.D.
Morphine	**2.77** (0.894-8.31)	**222** (139-361)	**109** (101-116)	**298** (176-508)	**120** (111-129)	N.D.
Hydromorphone	**0.518** (0.356-0.755)	**18.0** (11.5-28.6)	**100** (93.3-107)	**45.2** (23.8-82.1)	**99.7** (90.9-109)	0

.

4.1.4.2 *In vivo* behavioural studies

4.1.4.2.1 Evaluation of pain induced by mechanical and thermal stimuli

Drug effects on acute mechanical and thermal pain stimuli are summarized in **Fig. 4.3**. Systemic administration of brorphine (0.1–15 mg/kg IP) significantly increased the threshold to acute mechanical pain stimuli in the tail pinch test (**Fig. 4.3-A, Appendix A Table A2**) Similar to brorphine, all analogues significantly increased the threshold to acute mechanical pain stimuli at different doses (**Fig. 4.3-B**). However, only chlorphine and brorphine were able to induce maximum antinociception in the tail pinch assay (**Fig. 4.3.-B**). Notably, orphine, fluorphine, and iodorphine all failed to induce antinociception above 50% MPE, suggesting partial agonist effects in this assay. While the effects of chlorphine were generally somewhat more sustained than those of brorphine (**Appendix A Fig. A3-E/Fig. 4.3-A**), a sudden drop to vehicle level was observed for the highest dose of chlorphine at 145 min. Overall, the compounds induced different degrees of antinociception, which in some cases lasted up to 5h post-injection (**Fig. 4.3-B/ Appendix A Fig. A3**).

Naloxone pretreatment significantly reduced the antinociceptive effects of brorphine in the tail pinch test (**Fig. 4.3-C, D, Table A1**). Interestingly, naloxone injections increased the maximum level of mechanical antinociception in orphine-treated mice (**Fig. 4.3-D/Fig. A3-B**). While a single injection of naloxone significantly decreased antinociception induced by fluorphine and iodorphine, the effects of both compounds were fully blocked only after the second naloxone injection (**Fig. A3-D, H**). For chlorphine, naloxone pretreatment had no significant impact on its antinociceptive effects (**Fig. A3-F**). The summed findings in the tail pinch test indicate that effects of fluorphine, brorphine, and iodorphine are opioid-mediated, whereas the effects of orphine and chlorphine are not.

In the tail withdrawal test, systemic administration of brorphine (0.1–15 mg/kg IP) increased the threshold to acute thermal pain stimuli (**Fig. 4.3-E, Appendix A Table A1**). Particularly, thermal antinociception was significantly affected by brorphine treatment. Similar to brorphine, orphine and chlorphine also increased the threshold to acute thermal pain stimuli at different doses (**Fig. 4.3-F**). The mean maximum antinociception produced by orphine at the highest dose was comparable to that of chlorphine and brorphine. By contrast, fluorphine and iodorphine produced weak and transient (≤ 55 min) thermal antinociceptive effects, and only at the highest tested dose(s) (**Appendix A Fig. A4-C, G**).

Interestingly, naloxone overall did not significantly reduce the thermal antinociceptive effect induced by brorphine (**Fig. 3.3-G, Appendix A Table A.1**). Moreover, naloxone attenuated the antinociceptive effects of orphine and chlorphine (**Fig.3.3-H**) but was not able to completely block their effects (**Appendix A Fig. A4-B, F**). Only the weak antinociception induced by fluorphine and iodorphine was fully blocked by naloxone (**Fig.4H/ Appendix A Fig. A4-D, H**).
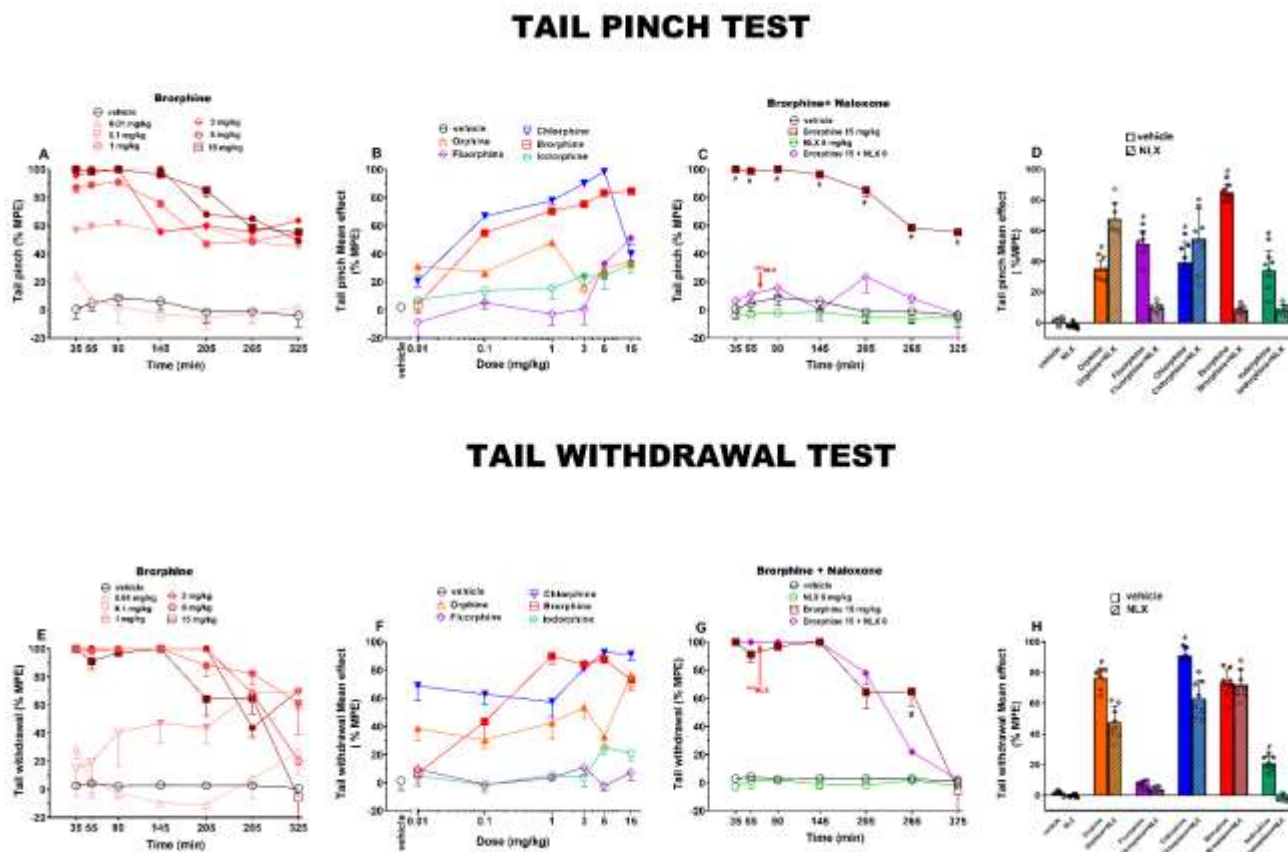
Figure 4.3 Results of the tail pinch and tail withdrawal tests in male mice. Panels A, E: Time-course of the effects induced by different doses of brorphine. Panels B, F: Dose-response curves of brorphine and different brorphine analogues. Panels C, G: Time-course of the observed effects of a high dose of brorphine (15 mg/kg IP) in antagonist experiments with naloxone (6 mg/kg IP). Panels D, H: Impact of naloxone (6 mg/kg IP) on the effects of a high dose of brorphine analogues (15 mg/kg IP). Data are expressed as percentage of maximum possible effect (%MPE) and represent the mean ± SEM as determined in 8 animals (over the whole test session for dose-response curves and bar charts). Statistical analysis was performed by two-way ANOVA followed by the Bonferroni test for multiple comparisons (panels A-C, E-G). Statistical analysis of panels D, H was performed with one-way ANOVA followed by the Bonferroni test for multiple comparisons. Solid symbols indicate significant effects compared to vehicle (p<0.05); Hash symbols indicate significant effects compared to naloxone + agonist treatment (p< 0.05). Significant differences compared to brorphine (for panels B, F) are inserted in the Supplementary Materials (**Appendix Fig. A5**).

4.1.4.2.2 Plethysmography analysis

Systemic administration of brorphine had an important impact on respiratory parameters. Respiratory rate (RR was immediately and significantly affected by brorphine treatment (**Fig. 4.4-A, B**). While fluctuating, a significant decrease in RR persisted until the end of the experiments. Similarly, RR was immediately affected after injection with fluorphine and chlorphine (**Fig. 4.4-A, C**). The effect induced by orphine was less evident throughout the session (**Fig. 4.4-A, C/ Appendix A Fig. A6-A**). Similarly, the effect of iodorphine was comparably less pronounced and somewhat delayed (becoming more sustained around 50 min) (**Fig. 4.4-A, C/ Appendix A Fig. A6-J**). Some significant differences were observed between the respiratory responses induced by brorphine and the different analogues (**Appendix A Fig. A6-A**). Pretreatment with naloxone fully blocked the decrease in RR caused by brorphine (**Fig.4.4-B**, **Appendix A Table A1**), orphine, fluorphine and chlorphine (**Fig. 4.4-C/ Appendix A Fig. A6-A, D, G**). Surprisingly, naloxone injection expedited rather than alleviated the respiratory depressant effects by iodorphine (**Fig. 4.4-C/ Appendix A Fig. A6-J**).

Simultaneously, breath length (BL) increased immediately after administration of brorphine (**Fig. 4.4-D, E**). While some fluctuations could be observed, a significant effect was registered throughout most of the test session (**Fig. 4.4-D, E**). In contrast, BL was not significantly affected by orphine. BL increased significantly after fluorphine and chlorphine administration, and the effect was more sustained with the former (**Fig. 4.4-D/ Appendix A Fig. A6-E, H**). Differing from the other compounds, the effect of iodorphine was delayed (**Fig. 4D/ Appendix A Fig. A6-K**). The comparison of BL responses to brorphine revealed significant differences with those induced by the other analogues (**Appendix A Fig. A7-B**). Naloxone pretreatment fully blocked the BL increase caused by brorphine (**Fig. 4.4E**, **Table A1**), fluorphine and chlorphine (**Fig. 4.4-F/ Appendix A Fig. A6-E, H**). Conversely, as also seen with RR, naloxone pretreatment somewhat expedited the BL increase induced by iodorphine (**Appendix A Fig. A6-K**).

Tidal volume (TV) decreased after the administration of brorphine (**Fig. 4.4-G, H**). The effect was delayed when compared to the effects on RR and BL, but, while fluctuating, overall persisted until the end of the experiments. Different from brorphine, TV decreased immediately after administration of orphine, fluorphine and chlorphine. This decrease was the least pronounced and most transient with orphine (**Fig. 4.4-G/ Appendix A Fig. A6-C, F, I**). Conversely, TV increased significantly with iodorphine treatment (**Fig. 4.4G/ Appendix A Fig. A6-L**).

Comparing TV responses induced by brorphine revealed significant differences with those induced by the other compounds (particularly orphine and iodorphine) (**Appendix A Fig. A6-C**). Naloxone

pretreatment fully blocked the TV decrease caused by brorphine (**Fig. 4.4-H**, **Appendix A Table A1**) [(**Fig. 4.4-I/ Appendix A Fig. A6-C**]. Conversely, compared to the agonist-only situation, pretreatment with naloxone increased the TV after administration of fluorphine (~50%), chlorphine (~70%), and iodorphine (~15%), with the effect appearing within 5 min after agonist injection (**Fig. 4.4-I/ Appendix A Fig. A6-F, I, L**).

PLETHYSMOGRAPHY
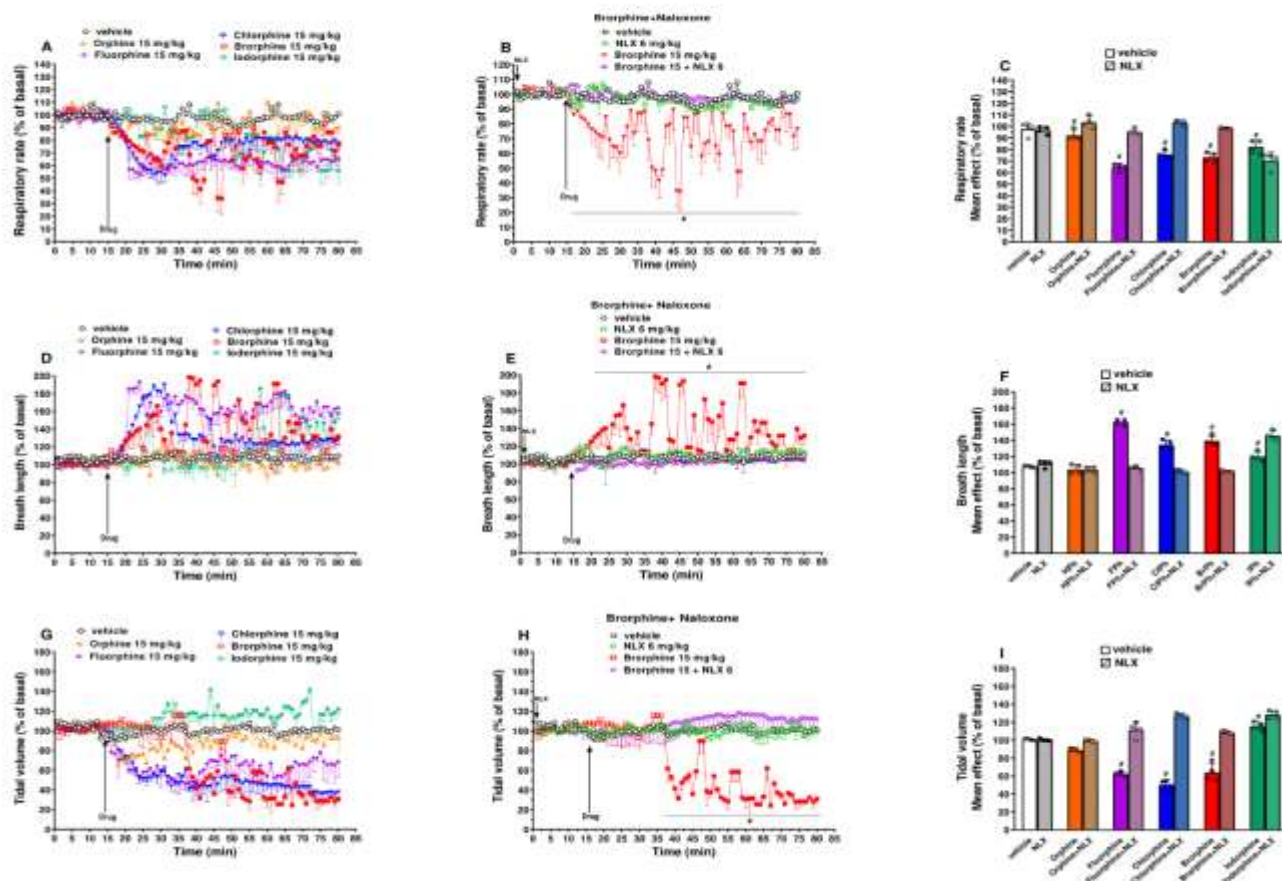
Figure 4.4. *Results of the plethysmography analysis in male mice. Panels A, D, G: Effects of a high dose (15 mg/kg IP) of the different test compounds on respiratory rate (RR), breath length (BL) and tidal volume (TV) over time. Panels B, E, H: Time-course of the observed effects of a high dose of brorphine (15 mg/kg IP) in antagonist experiments with naloxone (6 mg/kg IP). Panels C, F, I: Impact of naloxone (6 mg/kg IP) on the observed effects of a high dose of brorphine analogues (15 mg/kg IP). Data are expressed as percentage change from basal (% change from basal, see 2.4.5) over time and represent the mean ± SEM as determined in 4 animals for each treatment regimen. Statistical analysis was performed by two-way ANOVA followed by the Bonferroni test for multiple comparisons for panels A-B, D-E and G-H, while the statistical analysis of panels C, F and I was performed with one-way ANOVA followed by the Bonferroni test for multiple comparisons. Solid symbols indicate significance compared to vehicle (p<0.05); Hash symbols indicate significant effects compared to naloxone + agonist treatment (p< 0.05). Significant differences compared to brorphine (for panels A, D, G) are inserted in the Supplementary Materials (**Appendix A Fig.A7**).*

153

4.1.5 Discussion

To anticipate the potential emergence of brorphine-related substances as NSOs, this report details the synthesis and extensive pharmacological characterization of brorphine and four closely related analogues with different-sized *para*-phenyl ring substituents (H<F<Cl<Br<I). At the molecular level, MOR can be considered the main target for opioid analgesics [34]. While we previously reported on the MOR binding affinity of brorphine [35,36], binding data for the other piperidine benzimidazolone compounds included in this study are limited or nonexistent. Chlorphine showed the highest MOR affinity, followed by orphine/fluorphine, and brorphine/iodorphine. The higher MOR affinity of chlorphine compared to orphine is in line with a study by Leysen *et al.* [37]. Other studies have also evaluated MOR binding characteristics of orphine [38,39]. Based on our findings, it is tempting to speculate that the MOR binding pocket better accommodates (piperidine benzimidazolone) opioids with a smaller (i.e., fluorine, chlorine) or absent (i.e., orphine) substituent compared to the larger bromine and iodine groups. In addition, electronic contributions to ligand-MOR interactions may differ depending on the substituent [40,41]. However, more research is needed to elucidate at a molecular level the interaction of these compounds with MOR. Notably, while a relatively wide range of K_i values was observed (with an approximately 70-fold difference between the lowest (chlorphine) and highest (iodorphine) K_i values), this translated to a much more narrow range of functional potencies in the MOR activation assays. With the caveat that some confidence intervals are overlapping, the potencies of chlorphine, brorphine, and iodorphine were comparable in the βarr2 assay, whereas orphine and fluorphine were somewhat less potent. These trends are in line with the findings reported by Kennedy *et al.* using a different βarr2 recruitment assay (PathHunter®) [6]. In the mini-$G_{\alpha i}$ assay, the benzimidazolones were similar in terms of potency. This is in contrast to the observations by Kennedy *et al.*, who found a wider range of potencies (with brorphine > chlorphine > fluorphine > orphine) using a [^{35}S]GTPγS assay [6]. Importantly, while efficacy differences were limited in our MOR-βarr2 recruitment assay, the MOR-mini-$G_{\alpha i}$ assay typically results in a broader range of E_{max} values [21]. As a result, more pronounced efficacy differences were revealed in the latter assay, with orphine and fluorphine being less efficacious than the larger-sized analogues. Excluding iodorphine, the same trend was previously reported by Kennedy *et al.* in their βarr2 recruitment assay [6]. Taken together, the functional data reported here and elsewhere [6,17] point towards a higher *in vitro* activity of chlorphine and brorphine (and iodorphine), compared to fluorphine and orphine, across signaling pathways. Hence, while the smaller-sized orphine and fluorphine

may bind to MOR with a higher affinity than the larger-sized and less electronegative brorphine and iodorphine, this does not translate in a higher MOR activation.

Excluding iodorphine, all piperidine benzimidazolones included here have been evaluated in MOR bias-focused SAR studies [6,17]. Schmid *et al.* reported that orphine (SR-8595) showed a modest preference toward recruiting βarr2 (PathHunter®) over G protein ($[^{35}S]GTPγS$) when evaluated using the operational model [17,42]. Chlorphine (SR-11065) showed an improved potency for G protein signaling in this assay platform [17]. In a follow-up study [6], brorphine (compound 21) and chlorphine (compound 18) were reportedly somewhat G protein-biased, whereas orphine (compound 16) and fluorphine (compound 20) showed a slight preference towards the βarr2 pathway. However, other analogues eliciting much more pronounced levels of bias were also discovered in these studies, and none of the herein included compounds were selected by the authors for further research. As such, the current results (where no significant βarr2/mini-$G_{αi}$ bias could be detected using a different assay platform and bias calculation) are not in disagreement with previous work. In addition, the clinical potential of G protein-biased MOR ligands remains a matter of debate [43–45].

The antinociceptive effects of brorphine were previously investigated. Gatch *et al.* showed that brorphine dose-dependently increases thermal antinociception with an ED_{50} of 0.11 mg/kg in mice [46,47], whereas Vandeputte *et al.* found the drug increases tail flick latency with an ED_{50} of 0.08 mg/kg in rats [35]. In the Gatch study, the maximum effect of brorphine lasted for 75 min and returned to baseline within 120 min. In our study, the maximum thermal antinociceptive effect of brorphine (1 mg/kg) lasted for 205 min and had not yet returned to baseline at the end of the session (325 min). These apparent differences in drug time course may be related to varying experimental setups, different mouse strains (Swiss-Webster *versus* CD-1) and routes of administration (subcutaneous *versus* IP) [48]. Our results show that the evaluated analogues all increase the threshold to acute pain stimuli, but with quite different efficacies. Specifically, chlorphine and brorphine were full agonists in the tail pinch test, and orphine induced comparable maximum antinociception in the tail withdrawal test. Maximum antinociception with fluorphine and iodorphine was generally lower. While ED_{50} values could not be calculated, fluorphine and iodorphine were also the least potent analogues, as effects could only be observed at the higher end of the tested dose range (3-15 mg/kg). For orphine, chlorphine, and brorphine, significant antinociceptive effects were observed starting from lower concentrations (≥0.01 mg/kg). Hence, the most efficacious compounds were also the most potent *in vivo*. The high antinociceptive activity of chlorphine was demonstrated in early

pain research [16], where the drug was found to be 130x more potent than meperidine in a mouse hot plate assay. Orphine and fluorphine were less potent in this assay (30x and 40x more potent than meperidine, respectively). Notably, the observed *in vivo* trends were broadly in line with the *in vitro* prediction (with chlorphine and brorphine being more active than fluorphine). Orphine and iodorphine showed a higher and lower *in vivo* antinociceptive activity, respectively, than predicted *in vitro*. This apparent discrepancy may be due to involvement of other receptors and/or signaling pathways, differences in blood-brain barrier penetration, metabolic (in)activation, etc. [4,22,49].

Our data demonstrate possible pharmacokinetic differences between the compounds, which could impact the time course of their antinociceptive effects. Fluorphine-induced maximum effects were generally of shorter duration, and iodorphine-induced effects were transient in the tail withdrawal test. Interestingly, a bell-shaped curve was obtained for chlorphine in the tail pinch assay, with a sudden drop in antinociception around halfway through the session with the highest tested dose. While this could theoretically indicate the involvement of co-activated receptors at high doses (counteracting the antinociceptive effects of chlorphine), it is noteworthy that naloxone pretreatment did not fully eliminate chlorphine-induced antinociception. Yet, the effects were more sustained after naloxone pretreatment. The fact that a bell-shaped curve was not observed in the tail withdrawal test may be related to differences in the intensity of the noxious stimulus [28,50]. While the relatively limited antinociceptive effects produced by fluorphine and iodorphine were fully blocked by naloxone in both assays, this was not consistently the case for the other compounds, indicating the involvement of non-opioid mediated mechanisms. In brorphine-treated mice, naloxone pretreatment largely decreased mechanical, but not thermal antinociceptive effects. While naloxone efficacy may differ depending on the intensity of the pain stimulus [28,51], it is interesting to note that a recent study on the *in vivo* effects of fentanyl analogues consistently observed a larger decrease in thermal (compared to mechanical) antinociception after naloxone pretreatment using an almost identical experimental set up (cfr. *supra*) [28]. In addition, it was previously shown that 1 mg/kg naltrexone reduces brorphine-induced warm water tail flick latency [52]. The antinociceptive effects of chlorphine decreased in both assays after naloxone injection but seemed to reappear approximately halfway through the session. One possibility is that the high dose of chlorphine used in our experiments precluded blockade of MOR by naloxone, even a large dose of 6 mg/kg. As previously proposed for other potent opioids [28,53–55], repeated naloxone dosing may be required to avoid re-narcotization. Orphine-induced thermal

antinociception showed a similar pattern, with effects reappearing after an initial decrease. Surprisingly, however, the level of mechanical antinociception produced by orphine was higher in the presence of naloxone, potentially indicating the involvement of other (subtypes of) (opioid) receptors [56–59].

Respiratory depression is the primary cause of opioid overdose death [60]. More than 60 fatal and non-fatal case reports involving brorphine have been described [4,9,10,61–63], underscoring the risks associated with its use. Here, the respiratory effects induced by a high dose of brorphine and analogues were investigated for the first time using non-invasive plethysmography. Our results generally revealed a decreased respiratory rate, increased breath length, and decreased TV. An interesting exception to the latter is iodorphine, which induced a slight and gradual increase in TV (as also reported for other opioids [64]). The respiratory effects of orphine and iodorphine were generally less pronounced, similar to their partial agonist effects in most antinociception assays. With respect to respiratory effects, fluorphine represents a unique compound which induces weak antinociceptive effects but substantial respiratory depression. The findings with fluorphine demonstrate that measuring antinociceptive effects may not provide information about the potency for inducing other opioid-mediated actions.

Some differences in the time course of respiratory effects were observed. For example, the effects on respiratory rate and breath length induced by chlorphine appeared more transient than those induced by fluorphine and brorphine. In addition, brorphine-induced effects on TV showed a somewhat delayed onset of action compared to the other analogues. With iodorphine, respiratory changes started occurring only after a lag time of approximately 20 min or more, whereas naloxone pretreatment appeared to accelerate the onset of these effects. While the peculiar time course and TV effects of the novel compound iodorphine (alone or with naloxone) warrant further investigation at clinically relevant doses, it is important to note that naloxone may not be effective as an antidote in cases of iodorphine-induced respiratory depression [65]. The effect of naloxone pretreatment further differed between the test compounds. Changes in respiratory rate and breath length were fully blocked after naloxone pretreatment for all analogues (excluding iodorphine), confirming the involvement of opioid receptors (particularly MOR) in these actions [28,55]. However, while naloxone pretreatment blocked orphine- and brorphine-induced TV decreases, a reversal of the effect (i.e., a significant TV increase above baseline) was observed with fluorphine and chlorphine.

Taken together, the evaluated piperidine benzimidazolones are MOR agonists inducing varying degrees of antinociception and respiratory depression in mice. Importantly, although the evaluated compounds are close structural analogues, differences in their time course of actions were observed throughout this work [28,66–68]. Hence, while the current study is limited to male CD-1 mice, similar time course differences can be anticipated in humans, requiring dedicated studies. Brorphine is known to undergo *N*-dealkylation and hydroxylation in humans [9,63], with the *N*-dealkylated metabolite expected to be a common metabolite for the different analogues studied here [9]. While it is currently not known whether any of the brorphine metabolites retain clinically relevant opioid activity [4], metabolic (in)activation may contribute to some of the (unexpected) behavioral findings reported here. In humans, genetic polymorphisms as well as drug-drug interactions may further contribute to interindividual differences in sensitivity to these drugs [68,69]. Pharmacokinetic differences may also explain why, for orphine and iodorphine, the observed *in vivo* effect profile was different from the *in vitro* MOR activation trends [49]. Considering the differences in naloxone sensitivity observed in this study, it is important to note that naloxone is a competitive, non-selective opioid antagonist. Hence, the potency and intrinsic efficacy of MOR agonists may influence the observed effects after naloxone pretreatment [55,65,70–72], as also seen with fentanyl analogues [28,66,70]. However, additional research is needed to explore potential effects of relevant doses of piperidine benzimidazolones at other (non-opioid) receptors. Importantly, such 'off-target' effects may be naloxone-insensitive and may also contribute to the eventual toxicity of the drugs, as has been suggested for brorphine and the serotonin transporter [62]. In this context, it is interesting to note that the *ortho*-chloro analogue of chlorphine has nanomolar affinity for the opioid receptor-like 1 (ORL1) receptor [4,73]. Finally, further *in vivo* studies (including sensorimotor, motor, and cardiovascular tests) would be of interest to allow complete pharmaco-toxicological characterization [70].

With the exception of brorphine [11], all studied analogues are currently non-controlled in most countries. Hence, the dynamic nature of the NSO market bolsters the possibility of brorphine analogues appearing in the future to fill the void left by (newly banned) NSOs [15]. Specifically, from a synthesis point-of-view, the emergence of brorphine analogues differing in the halogen substituent seems feasible, as halogenation is an important tool in drug optimization [41,74,75]. In the context of NPS, this is reminiscent of the identification of halogenated analogues of the synthetic cannabinoid receptor agonist JWH-018 [32,76,77]. However, apart from a relatively straightforward synthesis, other supply- and demand-related

factors are known to influence the emergence of "new" NSOs [15,78], making it hard to predict how the market will evolve. As some of the analogues studied here are currently being offered for sale online, it may be just a matter of time before their formal identification in seized drug material or biological samples. Notably, the expected high *in vivo* potency of certain piperidine benzimidazolones stresses the need for highly sensitive analytical instrumentation for their detection [79].

4.1.6 Conclusions

This study explored the pharmaco-toxicological effect profile of brorphine and a selected set of related piperidine benzimidazolones (orphine, fluorphine, chlorphine, iodorphine) as potential opioid NPS. While analogues with smaller-sized substituents (fluorphine, orphine) showed the highest MOR affinity, chlorphine, brorphine, and iodorphine were generally the most active in terms of *in vitro* MOR activation (βarr2 and mini-$G_{\alpha i}$ recruitment) potential. *In vivo*, the antinociceptive and respiratory effects of the drugs were studied in male CD-1 mice. All analogues generally increased the threshold to acute mechanical and thermal pain stimuli, but only brorphine and chlorphine induced maximal antinociception in both assay procedures. Most of the analogues negatively impacted respiration (respiratory rate, breath length, and tidal volume). Some notable differences in time course and magnitude of naloxone antagonism warrant further investigation into possible non-opioid pharmacological targets and mechanisms of action of the studied opioids. Taken together, brorphine-like piperidine benzimidazolones are opioid agonists that have the potential to cause substantial harm in users should they emerge on recreational drug markets. Hence, careful monitoring of the dynamic NSO market is warranted to rapidly detect and respond to changes in the drug supply.

4.1.7 Author contributions

This work was conceptualized by C.P.S. and M.M.V. M.M.V. conducted *in vitro* receptor activation and radioligand binding experiments, the latter with the help of D.W. **S.B.**, G.C., M.T. and M.B. conducted *in vivo* experiments. A.F. conducted statistical analysis. M.M. and **S.B**. contributed to the final edition of *in vivo* results and discussion. M.M.V. and **S.B**. drafted the manuscript, which was critically revised by C.P.S., M.M., and M.H.B. All authors approved the final version of the manuscript for publication and agree to be held accountable for all aspects of the work related to accuracy or integrity.

4.1.8 Funding

4.1.9 Conflict of interest

The authors have nothing to disclose.

4.1.10 References

1.   European Monitoring Centre for Drugs and Drug Addiction (EMCDDA). European Drug Report 2023: Trends and Developments. LU: Publications Office; 2023.

2.   UNODC. The growing complexity of the opioid crisis. Global SMART Update, Volume 24. Vienna; 2020.

3.   Vandeputte MM, Krotulski AJ, Papsun DM, Logan BK, Stove CP. The rise and fall of isotonitazene and brorphine: two recent stars in the synthetic opioid firmament. Journal of Analytical Toxicology. 2022;2:115–121.

4.   Verougstraete N, Vandeputte MM, Lyphout C, Cannaert A, Hulpia F, Van Calenbergh S, et al. First report on brorphine: the next opioid on the deadly new psychoactive substances' horizon? Journal of Analytical Toxicology. 2020;44:937–946.

5.   Janssen PAJ. Derivatives of benzimidazolinyl piperidine. US3318900A, 1967.

6.   Kennedy NM, Schmid CL, Ross NC, Lovell KM, Yue Z, Chen YT, et al. Optimization of a series of mu opioid receptor (MOR) agonists with high G protein signaling bias. J Med Chem. 2018;61:8895–8907.

7.   Ujváry I, Christie R, Evans-Brown M, Gallegos A, Jorge R, de Morais J, et al. DARK Classics in Chemical Neuroscience: Etonitazene and Related Benzimidazoles. ACS Chem Neurosci. 2021;12:1072–1092.

8.   Krotulski AJ, Papsun DM, Noble C, Kacinko SL, Nelson L, Logan BK. The rise of brorphine - a potent new synthetic opioid identified in the Midwestern United States. 2020.

9.   Krotulski AJ, Papsun DM, Noble C, Kacinko SL, Logan BK. Brorphine—Investigation and quantitation of a new potent synthetic opioid in forensic toxicology casework using liquid chromatography-mass spectrometry. J Forensic Sci. 2020;66:664–676.

10.   Vohra V, King AM, Jacobs E, Aaron C. Death associated with brorphine, an emerging novel synthetic opioid. Clinical Toxicology. 2021;59:851–852.

11.   UNODC. CND Decision on international control of brorphine and metonitazene enters into force. 2022. https://www.unodc.org/LSS/Announcement/Details/a56e0bd9-0da5-4152-a34d-7cff7746bf50. Accessed 10 June 2021.

12.   Krotulski AJ, Walton SE, Mohr ALA, Logan BK. Trend Report Q3 2023: NPS opioids in the United States. NPS Discovery. 2023. https://www.cfsre.org/images/trendreports/2023-Q3-NPS-Opioids-Trend-Report.pdf. Accessed 26 December 2022.

13.   Krotulski AJ, Mohr ALA, Logan BK. Trend Report Q3 2020: NPS opioids in the United States. NPS Discovery. 2020. https://www.cfsre.org/images/trendreports/2020-Q3_NPS-Opioids_Trend-Report.pdf.

14.   Advisory Council on the Misuse of Drugs (ACMD). ACMD advice on 2-benzyl benzimidazole and piperidine benzimidazolone opioids (accessible version). 2023. https://www.gov.uk/government/publications/acmd-advice-on-2-benzyl-benzimidazole-and-piperidine-benzimidazolone-opioids/acmd-advice-on-2-benzyl-benzimidazole-and-

piperidine-benzimidazolone-opioids-accessible-version#introduction. Accessed 9 October 2023.

15. Papsun DM, Krotulski AJ, Logan BK. Proliferation of Novel Synthetic Opioids in Postmortem Investigations After Core-Structure Scheduling for Fentanyl-Related Substances. Am J Forensic Med Pathol. 2022;43:315–327.

16. Janssen PAJ, Van der Eycken CAM. The chemical anatomy of potent morphine-like analgesics. In: Burger A, editor. Drugs affecting the CNS, vol. 2, New York: Dekker; 1968. p. 25–60.

17. Schmid CL, Kennedy NM, Ross NC, Lovell KM, Yue Z, Morgenweck J, et al. Bias factor and therapeutic window correlate to predict safer opioid analgesics. Cell. 2017;171:1165-1175.e13.

18. Vandeputte MM, Krotulski AJ, Walther D, Glatfelter GC, Papsun D, Walton SE, et al. Pharmacological evaluation and forensic case series of *N*-pyrrolidino etonitazene (etonitazepyne), a newly emerging 2-benzylbenzimidazole 'nitazene' synthetic opioid. Arch Toxicol. 2022;96:1845–1863.

19. Truver MT, Smith CR, Garibay N, Kopajtic TA, Swortwood MJ, Baumann MH. Pharmacodynamics and pharmacokinetics of the novel synthetic opioid, U-47700, in male rats. Neuropharmacology. 2020;177:108195.

20. Glatfelter GC, Vandeputte MM, Chen L, Walther D, Tsai M-HM, Shi L, et al. Alkoxy chain length governs the potency of 2-benzylbenzimidazole 'nitazene' opioids associated with human overdose. Psychopharmacology. 2023. 2 September 2023. https://doi.org/10.1007/s00213-023-06451-2.

21. Vasudevan L, Vandeputte MM, Deventer M, Wouters E, Cannaert A, Stove CP. Assessment of structure-activity relationships and biased agonism at the Mu opioid receptor of novel synthetic opioids using a novel, stable bio-assay platform. Biochemical Pharmacology. 2020;177:113910.

22. Vandeputte MM, Vasudevan L, Stove CP. *In vitro* functional assays as a tool to study new synthetic opioids at the μ-opioid receptor: Potential, pitfalls and progress. Pharmacology & Therapeutics. 2022;235:108161.

23. Pottie E, Tosh DK, Gao Z-G, Jacobson KA, Stove CP. Assessment of biased agonism at the A_3 adenosine receptor using β-arrestin and miniG$_{αi}$ recruitment assays. Biochemical Pharmacology. 2020;177:113934.

24. Pottie E, Dedecker P, Stove CP. Identification of psychedelic new psychoactive substances (NPS) showing biased agonism at the 5-HT$_{2A}$R through simultaneous use of β-arrestin 2 and miniG$_{αq}$ bioassays. Biochemical Pharmacology. 2020:114251.

25. Ehlert FJ. On the analysis of ligand-directed signaling at G protein-coupled receptors. Naunyn-Schmiedeberg's Archives of Pharmacology. 2008;377:549–577.

26. Rajagopal S, Ahn S, Rominger DH, Gowen-MacDonald W, Lam CM, DeWire SM, et al. Quantifying ligand bias at seven-transmembrane receptors. Molecular Pharmacology. 2011;80:367–377.

27.   Bilel S, Azevedo N, Arfè R, Tirri M, Gregori A, Serpelloni G, et al. *In vitro* and in vivo pharmacological characterization of the synthetic opioid MT-45. Neuropharmacology. 2020;171:108110.

28.   Bilel S, Neto JA, Arfè R, Tirri M, Gaudio RM, Fantinati A, et al. *In vitro* and in vivo pharmaco-dynamic study of the novel fentanyl derivatives: Acrylfentanyl, Ocfentanyl and Furanylfentanyl. Neuropharmacology. 2022;209:109020.

29.   Ossato A, Bilel S, Gregori A, Talarico A, Trapella C, Gaudio RM, et al. Neurological, sensorimotor and cardiorespiratory alterations induced by methoxetamine, ketamine and phencyclidine in mice. Neuropharmacology. 2018;141:167–180.

30.   Marti M, Neri M, Bilel S, Di Paolo M, La Russa R, Ossato A, et al. MDMA alone affects sensorimotor and prepulse inhibition responses in mice and rats: tips in the debate on potential MDMA unsafety in human activity. Forensic Toxicology. 2019;37:132–144.

31.   Ossato A, Canazza I, Trapella C, Vincenzi F, De Luca MA, Rimondo C, et al. Effect of JWH-250, JWH-073 and their interaction on "tetrad", sensorimotor, neurological and neurochemical responses in mice. Progress in Neuro-Psychopharmacology and Biological Psychiatry. 2016;67:31–50.

32.   Vigolo A, Ossato A, Trapella C, Vincenzi F, Rimondo C, Seri C, et al. Novel halogenated derivates of JWH-018: Behavioral and binding studies in mice. Neuropharmacology. 2015;95:68–82.

33.   Marchetti B, Bilel S, Tirri M, Arfè R, Corli G, Roda E, et al. The Old and the New: Cardiovascular and Respiratory Alterations Induced by Acute JWH-018 Administration Compared to Δ9-THC—A Preclinical Study in Mice. IJMS. 2023;24:1631.

34.   Valentino RJ, Volkow ND. Untangling the complexity of opioid receptor function. Neuropsychopharmacol. 2018;43:2514–2520.

35.   Vandeputte MM, Tsai M-HM, Chen L, Glatfelter GC, Walther D, Stove CP, et al. Comparative neuropharmacology of structurally distinct non-fentanyl opioids that are appearing on recreational drug markets worldwide. Drug and Alcohol Dependence. 2023:109939.

36.   Vandeputte MM, Persson M, Walther D, Vikingsson S, Kronstrand R, Baumann MH, et al. Characterization of recent non-fentanyl synthetic opioids via three different *in vitro* μ-opioid receptor activation assays. Arch Toxicol. 2022;96:877–897.

37.   Leysen JE, Gommeren W, Niemegeers CJE. [³H]sufentanil, a superior ligand for μ-opiate receptors: Binding properties and regional distribution in rat brain and spinal cord. European Journal of Pharmacology. 1983;87:209–225.

38.   Cometta-Morini C, Maguire PA, Loew GH. Molecular determinants of mu receptor recognition for the fentanyl class of compounds. Molecular Pharmacology. 1992;41:185–196.

39.   Leysen J, Tollenaere JP, Koch MH, Laduron P. Differentiation of opiate and neuroleptic receptor binding in rat brain. Eur J Pharmacol. 1977;43:253–267.

40.   Metcalf MD, Coop A. 5′-Halogenated analogs of oxymorphindole. Bioorganic & Medicinal Chemistry Letters. 2007;17:5916–5917.

41.   Hernandes MZ, Cavalcanti SMT, Moreira DRM, de Azevedo Junior WF, Leite ACL. Halogen atoms in the modern medicinal chemistry: hints for the drug design. Current Drug Targets. 2010;11:303–314.

42.   Black JW, Leff P. Operational models of pharmacological agonism. Proceedings of the Royal Society of London - Biological Sciences. 1983;220:141–162.

43.   Gillis A, Kliewer A, Kelly E, Henderson G, Christie MJ, Schulz S, et al. Critical assessment of G protein-biased agonism at the µ-opioid receptor. Trends in Pharmacological Sciences. 2020;41:947–959.

44.   Kelly E, Conibear A, Henderson G. Biased Agonism: Lessons from Studies of Opioid Receptor Agonists. Annu Rev Pharmacol Toxicol. 2023;63:annurev-pharmtox-052120-091058.

45.   Azevedo Neto J, Costanzini A, De Giorgio R, Lambert DG, Ruzza C, Calò G. Biased versus partial agonism in the search for safer opioid analgesics. Molecules. 2020;25:3870.

46.   Gatch MB. Final study report. Evaluation of abuse potential of synthetic opioids using in vivo pharmacological studies. Test of analgesic effects alone and in combination with naltrexone. 'Evaluation of Abuse Potential of Synthetic Opioids Using in Vivo Pharmacological Studies' University of North Texas Health Science Center at Fort Worth. 2020. 2020.

47.   WHO. WHO Expert Committee on Drug Dependence: forty-fourth report. Geneva: World Health Organization; 2022.

48.   Baumann MH, Majumdar S, Le Rouzic V, Hunkele A, Uprety R, Huang XP, et al. Pharmacological characterization of novel synthetic opioids (NSO) found in the recreational drug marketplace. Neuropharm. 2018;134:101–107.

49.   Vandeputte MM, Verougstraete N, Walther D, Glatfelter GC, Malfliet J, Baumann MH, et al. First identification, chemical analysis and pharmacological characterization of *N*-piperidinyl etonitazene (etonitazepipne), a recent addition to the 2-benzylbenzimidazole opioid subclass. Arch Toxicol. 2022;96:1865–1880.

50.   Lutfy K, Eitan S, Bryant CD, Yang YC, Saliminejad N, Walwyn W, et al. Buprenorphine-Induced Antinociception Is Mediated by µ-Opioid Receptors and Compromised by Concomitant Activation of Opioid Receptor-Like Receptors. J Neurosci. 2003;23:10331–10337.

51.   Le Bars D, Gozariu M, Cadden SW. Animal models of nociception. Pharmacol Rev. 2001;53:597–652.

52.   Gatch MB. Evaluation of abuse potential of synthetic opioids using in vivo pharmacological studies: brorphine test of substitution for the discriminative stimulus effects of morphine. 'Evaluation of Abuse Potential of Synthetic Opioids Using in Vivo Pharmacological Studies' University of North Texas Health Science Center at Fort Worth. 2020. 16 November 2020.

53.   Amaducci A, Aldy K, Campleman SL, Li S, Meyn A, Abston S, et al. Naloxone Use in Novel Potent Opioid and Fentanyl Overdoses in Emergency Department Patients. JAMA Netw Open. 2023;6:e2331264.

54.   Klebacher R, Harris MI, Ariyaprakai N, Tagore A, Robbins V, Dudley LS, et al. Incidence of Naloxone Redosing in the Age of the New Opioid Epidemic. Prehospital Emergency Care. 2017;21:682–687.

55.   Dahan A, Aarts L, Smith TW. Incidence, Reversal, and Prevention of Opioid-induced Respiratory Depression. Anesthesiology. 2010;112:226–238.

56.   Hamann SR, Malik H, Sloan JW, Wala EP. Interactions of "Ultra-Low" Doses of Naltrexone and Morphine in Mature and Young Male and Female Rats. Receptors and Channels. 2004;10:73–81.

57.   Hamann, Md, PhD S, Sloan, Md PA, Witt, Md W. Low-dose intrathecal naloxone to enhance intrathecal morphine analgesia: A case report. J of Opioid Management. 2008;4:251–254.

58.   Bianchi M, Panerai AE. Naloxone-induced analgesia: Involvement of κ-opiate receptors. Pharmacology Biochemistry and Behavior. 1993;46:145–148.

59.   Suarez-Roca H, Maixner W. Activation of kappa opioid receptors by U50488H and morphine enhances the release of substance P from rat trigeminal nucleus slices. Journal of Pharmacology and Experimental Therapeutics. 1993;264:648–653.

60.   Baldo BA, Rose MA. Mechanisms of opioid-induced respiratory depression. Arch Toxicol. 2022. 26 April 2022. https://doi.org/10.1007/s00204-022-03300-7.

61.   WHO. 44th ECDD (2021): Critical review report: Brorphine. 2021. https://cdn.who.int/media/docs/default-source/essential-medicines/unedited--advance-copy-44th-ecdd-review-report-brorphine.pdf?sfvrsn=d2f0cc18_3&download=true. Accessed 28 September 2023.

62.   Razinger G, Grenc D, Pezdir T, Kranvogl R, Brvar M. Severe rhabdomyolysis and acute kidney failure due to synthetic opioid brorphine exposure in combination with chronic sertraline therapy. Eur J Clin Pharmacol. 2021;77:1759–1761.

63.   Grafinger KE, Wilde M, Otte L, Auwärter V. Pharmacological and metabolic characterization of the novel synthetic opioid brorphine and its detection in routine casework. Forensic Science International. 2021;327:110989.

64.   Burgraff NJ, Baertsch NA, Ramirez J-M. A comparative examination of morphine and fentanyl: unravelling the differential impacts on breathing and airway stability. The Journal of Physiology. 2023:JP285163.

65.   van Lemmen M, Florian J, Li Z, van Velzen M, Van Dorp E, Niesters M, et al. Opioid Overdose: Limitations in Naloxone Reversal of Respiratory Depression and Prevention of Cardiac Arrest. Anesthesiology. 2023;139:342–353.

66.   Varshneya NB, Hassanien SH, Holt MC, Stevens DL, Layle NK, Bassman JR, et al. Fentanyl analog structure-activity relationships demonstrate determinants of diverging

potencies for antinociception and respiratory depression. Pharmacology Biochemistry and Behavior. 2023;226:173572.

67.   Varshneya NB, Hassanien SH, Holt MC, Stevens DL, Layle NK, Bassman JR, et al. Respiratory depressant effects of fentanyl analogs are opioid receptor-mediated. Biochemical Pharmacology. 2021:114805.

68.   Wilde M, Pichini S, Pacifici R, Tagliabracci A, Busardò FP, Auwärter V, et al. Metabolic Pathways and Potencies of New Fentanyl Analogs. Front Pharmacol. 2019;10:238.

69.   Malcolm NJ, Palkovic B, Sprague DJ, Calkins MM, Lanham JK, Halberstadt AL, et al. Mu-opioid Receptor Selective Superagonists Produce Prolonged Respiratory Depression. iScience. 2023:107121.

70.   Bilel S, Giorgetti A, Tirri M, Arfè R, Cristofori V, Marchetti B, et al. Sensorimotor Alterations Induced by Novel Fentanyl Analogs in Mice: Possible Impact on Human Driving Performances. Curr Neuropharmacol. 2023;21:87–104.

71.   Nakamura A, Yasufuku K, Shimada S, Aritomi H, Furue Y, Chiba H, et al. The antagonistic activity profile of naloxone in μ-opioid receptor agonist-induced psychological dependence. Neuroscience Letters. 2020;735:135177.

72.   Volpe DA, McMahon Tobin GA, Mellon RD, Katki AG, Parker RJ, Colatsky T, et al. Uniform assessment and ranking of opioid μ receptor binding constants for selected opioid drugs. Regul Toxicol Pharmacol. 2011;59:385–390.

73.   Kawamoto H, Ozaki S, Itoh Y, Miyaji M, Arai S, Nakashima H, et al. Discovery of the First Potent and Selective Small Molecule Opioid Receptor-like (ORL1) Antagonist: 1-[(3 *R* ,4 *R*)-1-Cyclooctylmethyl-3-   hydroxymethyl-4-piperidyl]-3-ethyl-   1,3-dihydro-2 *H* - benzimidazol-2-one (J-113397). J Med Chem. 1999;42:5061–5063.

74.   Xu Z, Yang Z, Liu Y, Lu Y, Chen K, Zhu W. Halogen Bond: Its Role beyond Drug–Target Binding Affinity for Drug Discovery and Development. J Chem Inf Model. 2014;54:69–78.

75.   Kurczab R, Kucwaj-Brysz K, Śliwa P. The Significance of Halogen Bonding in Ligand–Receptor Interactions: The Lesson Learned from Molecular Dynamic Simulations of the D_4 Receptor. Molecules. 2019;25:91.

76.   Barbieri M, Ossato A, Canazza I, Trapella C, Borelli AC, Beggiato S, et al. Synthetic cannabinoid JWH-018 and its halogenated derivatives JWH-018-Cl and JWH-018-Br impair Novel Object Recognition in mice: Behavioral, electrophysiological and neurochemical evidence. Neuropharmacology. 2016;109:254–269.

77.   Bilel S, Tirri M, Arfè R, Ossato A, Trapella C, Serpelloni G, et al. Novel halogenated synthetic cannabinoids impair sensorimotor functions in mice. NeuroToxicology. 2020;76:17–32.

78.   Vandeputte MM, Walton SE, Shuda SA, Papsun DM, Krotulski AJ, Stove CP. Detection, chemical analysis, and pharmacological characterization of dipyanone and other new synthetic opioids related to prescription drugs. Anal Bioanal Chem. 2023. 13 May 2023. https://doi.org/10.1007/s00216-023-04722-7.

79.   Walton SE, Krotulski AJ, Logan BK. A Forward-Thinking Approach to Addressing the New Synthetic Opioid 2-Benzylbenzimidazole Nitazene Analogs by Liquid Chromatography–Tandem Quadrupole Mass Spectrometry (LC–QQQ-MS). Journal of Analytical Toxicology. 2021:bkab117.

4.2 *In vitro* and *in vivo* characterization of Butyrylfentanyl and 4-Fluoro-Butyrylfentanyl in female and male mice: role of CRF-1 receptors in respiratory depression

[1]**Bilel Sabrine**, [2]Azevedo Neto Joaquim, [1]Tirri Micaela, [1]Corli Giorgia, [1] Bassi Marta, [3]Fantinati Anna, [4]Serpelloni Giovanni, [5]Malfacini Davide, [3]Trapella Claudio, [5]Calo' Girolamo and [1,6,7]Marti Matteo.

[1]*Department of Translational Medicine, Section of Legal Medicine and LTTA Centre, University of Ferrara, Italy*
[2]*Department of Neuroscience and Rehabilitation, Section of Pharmacology, University of Ferrara Via Fossato di Mortara 17/19, 44121 Ferrara, Italy*
[3]*3Department of Environmental and Prevention Sciences, University of Ferrara, Via Fossato di Mortara, Ferrara, Italy.*
[4]*Neuroscience Clinical Center & TMS Unit Verona, Italy and Department of Psychiatry in the College of Medicine, Drug Policy Institute, University of Florida, Gainesville, FL, United States*
[5]*Department of Pharmaceutical and Pharmacological Sciences, University of Padua, Italy*
[6]*Center of Gender Medicine, University of Ferrara, Italy*
[7]*Collaborative Center of the National Early Warning System, Department for Anti-Drug Policies, Presidency of the Council of Ministers, Italy*

Corresponding Author:

Matteo Marti

Department of Translational Medicine, Section of Legal Medicine, University of Ferrara

via Fossato di Mortara 70, 44121 Ferrara Italy

phone +39 0532 455781, fax +39 0532 455777

email: matteo.marti@unife.it

Abbreviations

|	
NSO	Novel Synthetic Opioids
FENT	Fentanyl;N-(1-(2-phenethyl)-4-piperidinyl-N-phenyl-propanamide
BUF	Butyrylfentanyl;N-phenyl-N-[1-(2-phenylethyl)-4-piperidinyl] butanamide
4F-BUF	4-Fluorobutyrfentanyl or para-fluorobutyrylfentanyl; N-(4-Fluorophenyl)-N-[1-(2-phenylethyl)-4-piperidinyl]-butanamide
NLX	Naloxone; (4R,4aS,7aR,12bS)-4a,9-dihydroxy-3-prop-2-enyl-2,4,5,6,7a,13-hexahydro-1H-4,12methanobenzofuro[3,2e]isoquinolin-7-one
ANT	Antalarmin;N-butyl-N-ethyl-2,5,6-trimethyl-7-(2,4,6-trimethylphenyl) pyrrolo[3,2-e]pyrimidin-4-amine
BRET	Bioluminescence Resonance Energy Transfer assay
ECG	Electrocardiogram
PLETH	Plethysmography

4.2.1 Abstract

Background and purpose: Novel Synthetic Opioids (NSOs), in particulars fentanyl analogs, have been implicated in many cases of intoxication and death with overdose worldwide. The aim of this study is to investigate the pharmaco-toxicology of two fentanyl (FENT) analogues: Butyrylfentanyl (BUF) and 4-Fluoro-Butyrylfentanyl (4-FBUF)

Experimental Approach: *In vitro*, we measured fentanyl (s) opioid receptor efficacy, potency, and selectivity and their capability to promote the interaction of the mu receptor with G protein and β-arrestin 2. *In vivo*, we evaluated the cardio-respiratory changes using the Electrocardiogram (ECG) and plethysmography in female and male mice injected intraperitoneally with BUF or 4F-BUF (0.1-6 mg.kg). Opioid receptor specificity was investigated using naloxone (NLX; 6 mg/kg IP) pre-treatment. Moreover, we investigated the possible role of stress in increasing cardiotoxicity in mice using the CRF-1 antagonist Antalarmin (10 mg/kg)

Key results: *In vitro*, FENT, BUF and 4F-BUF mimicked the maximal effects of dermorphin displaying the following rank of potency: FENT> 4-FBUF> BUF. 4-FBUF displayed lower maximal effects behaving as a partial agonist. FENT and BUF behaved as partial agonists for the β-arrestin 2 pathway, whereas 4-FBUF did not promote β-arrestin 2 recruitment. *In vivo*, our results revealed sex difference in the cardio-respiratory impairments induced by BUF and 4-FBUF. 4F-BUF showed lower potency for inhibiting cardiorespiratory function. NLX sensitivity of the actions of the two compounds was variable in cardiac and respiratory responses. Interestingly the CRF-1 antagonist Antalarmin alone was effective to block the respiratory impairment induced by BUF in both sexes but not 4F-BUF. The combination of NLX and ANT significantly enhanced the action of NLX reversal of the cardiorespiratory impairments induced by BUF and 4F-BUF in female and male CD1 mice.

Conclusion: In this study, we have uncovered a novel mechanism by which synthetic opioids might increase respiratory depression shedding new light on the role of CRF-1 receptors in cardiorespiratory impairments by mu-agonists
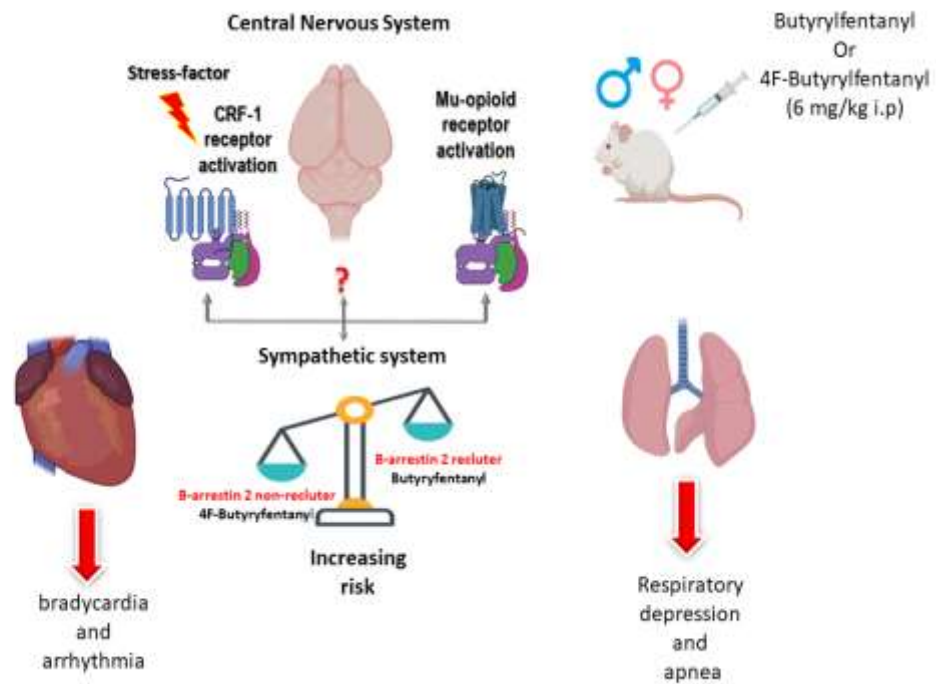
Graphical abstract

Involvement of CRF-1 receptors in the cardiorespiratory effects of fentanyl analogs. The possible mechanism suggested by this study is that fentanyl analogs that possess biased β-arrestin2 recruitment might show higher risk of respiratory depression that increase stress signals activated by corticotropin-releasing factors (CRF-1) resulting in higher adverse effects.

Keywords; Fentanyl; Butyrylfentanyl; 4fluoro-Butyrfentanyl; novel psychoactive substances; mu opioid receptor, β-arrestin 2; naloxone; antalarmin; respiratory depression, CRF-1

4.2.2 Introduction

The European Monitoring Center for Drugs and Drug Addiction (EMCDDA) has been monitoring more than 930 Novel Psychoactive Substances (NPS) since 2009, 41 of which were first reported in Europe in 2022 (EMCDDA. 2022). Novel Synthetic opioids (NSO) is a small class of NPS that includes about 74 new opioids identified on the European drug market since 2009 (EMCDDA. 2022).

Although the number of NSO is low with respect to the other classes such as cathinones, recent signals, mostly from Baltic countries, suggest increased availability and harms (including intoxications and death) linked to fentanyl derivatives and benzimidazole opioids. Recent reports from Estonia and Lithuania revealed an increase in deaths with overdose due to the use of NSO, which reveals the risk of life-threatening poisoning of these compounds (EMCDDA. 2022).

Butyrylfentanyl (BUF) is a fentanyl analog, with an *N*-butyryl group replacing the *N*-propionyl group of fentanyl (**Fig. 4.5**). It is sold on the NPS market as a substitute for heroin or prescription opioids. Seven case reports on BUF-intoxications and deaths were reported in 2014 and this number increased to 81 reports in 2015. This compound was designated as a Schedule I substance under the Controlled Substances Act in 2016 (Drug Enforcement Administration. 2016). BUF showed lower pharmacological efficacy respect to fentanyl (Varshneya et al.,2023). Studies on BUF metabolism in human liver microsomes revealed that this compound undergoes hydroxylation at the butanamide side chain and aromatic ring and *N*-dealkylation through CYP3A4 and CYP2D6 (Steuer et al.,2017). Carboxy- and hydroxy-BUF metabolites were majorly found in blood, urine, and organs of a fatal case (Staeheli et al. 2016).

Para-fluoro-butyrylfentanyl (4F-BUF) is a structural chemical analog of BUF. 4F-BUF and BUF share a common basic chemical structure characterized by a phenethylamine core (**Fig 4.5**). While BUF features a butyryl group, 4F-BUF contains a para-fluoro substitution on the phenethylamine backbone (**Fig 4.5**). This structural variance can significantly impact their pharmacodynamic properties (Varshneya et al., 2023). 4F-BUF was first detected in 2015 (Bäckberg et al., 2015).
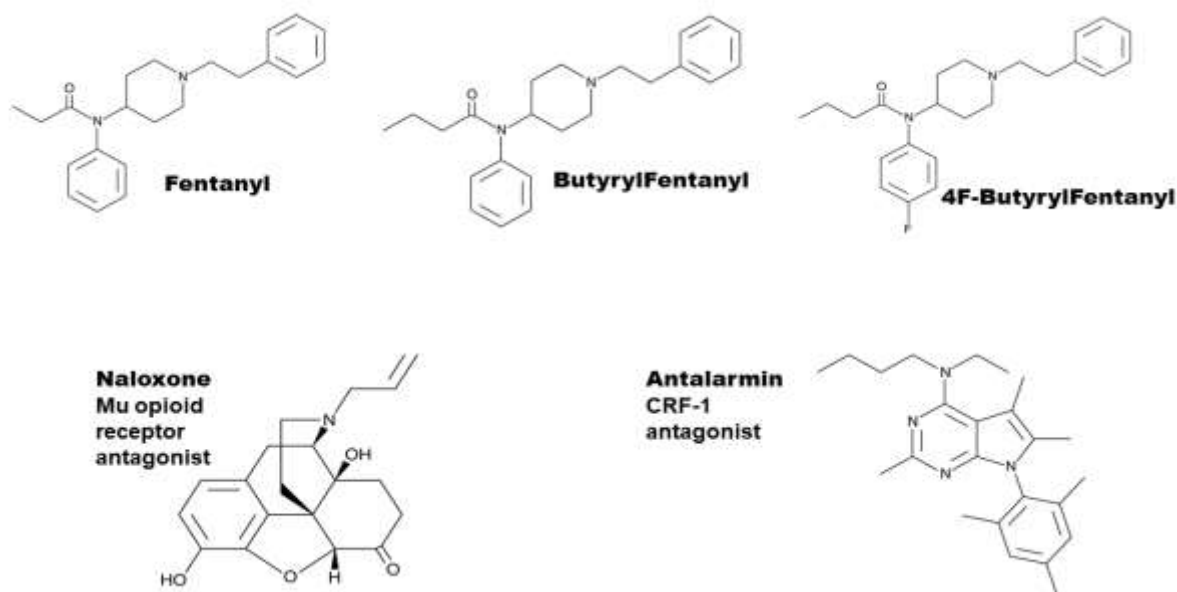
Figure 4.5 *Chemical structures of Fentanyl; Butyrylfentyl; 4F-Butyrlfentanyl; Naloxone and Antalarmin.*

The EMCDDA reported the seizure of this drug in different forms including powders, tablets, electronic cigarette liquid, and nasal spray formulations (EMCDDA. 2015). One case of intoxication by 4F-BUF was reported in Sweden and two death cases were reported from Poland (WHO. 2017). Since September 2017, 4F-BUF has been controlled in Cyprus, Finland, Czech Republic, Sweden, Poland, Denmark and France (WHO. 2017). Functional studies using the [^{35}S]GTPγS binding assay demonstrated that 4F-BUF showed a reduced efficacy for MOR and KOR receptor activation compared with fentanyl (WHO. 2017) and *in vivo* this drug showed a lower analgesic efficacy with respect to fentanyl (WHO. 2017). The metabolic pathway of 4F-BUF was investigated *in vitro*, using human liver microsomes and suggests three major metabolites: nor-4F-BUF, 4F-fentanyl and hydroxyl-4F-BUF (Richeval et al., 2019). Similarly to fentanyl, the most common adverse effects reported with BUF and 4F-BUF were disorientation, miosis, bradycardia, respiratory depression, and apnea which may lead to death in some cases (Bäckberg et al., 2015). Since the appearance of fentanyl analogs in the NPS drug market, the number of cases of intoxication and death due to these substances increased exponentially. The recent world drug report revealed an important increase in female non-medical pharmaceutical opioids users (47%) with respect to opiates users (25%). This may explain the the increasing rate of opioid use disorders in the last few years (UNDOC, Executive summary. 2023).

Sex differences in opioid use, pharmacology, and consequences are an important area of study in medical and scientific research (Fattore et al., 2020). While opioids affect both males and females, there are notable differences in how these drugs impact each gender (Fattore et al., 2020). Indeed, research on sex-based treatment differences in opioids use disorders has increased, however, the studies focusing on sex-dependent differences in the pharmaco-toxicological aspects of these potent synthetic opioids have not yet been discovered.

Therefore, the aim of this study was to investigate the pharmaco-dynamic profile of the BUF and 4F-FUF. To evaluate the *in vitro* basic pharmacological profile of these compounds, a calcium mobilization assay was performed using cells expressing opioid receptors and chimeric G-proteins (Camarda and Calo', 2013). Moreover, a bioluminescence resonance energy transfer (BRET) assay was also used to investigate the ability of the compounds to promote mu receptor interaction with G-protein and β-arrestin 2 (Molinari et al., 2010). We investigated the acute effects of BUF and 4F-BUF, *in vivo,* measuring cardiorespiratory changes using non-invasive Electrocardiogram ECG (Heart rate, RR-interval, and QRS complex) and plethysmography (Breath rate, Breath length, and Minute volume) in CD-1 female and male mice. NLX pre-treatment was applied to investigate receptor specificity in the cardio-respiratory responses of male and female mice. Moreover, many studies revealed the role of the functional antagonism of CRF neurotransmission, in particular CRF-1 receptors in reducing stress and ameliorating negative affective-like states associated with opioids withdrawal and dependence (Heinrichs et al., 1995, Shaham et al., 1998, Stinus et al., 2005). Yet the role of CRF receptors in reducing the acute effects of opioids, especially the cardio-respiratory impairments is lacking in the literature. To fill the gap on this issue we further investigated the possible involvement of the stress-factor in worsening cardio-respiratory impairments related to opioids in female and male animals using the CRF1 receptor antagonist Antalarmin alone and in combination with NLX.

4.2.3 Materials and Methods

4.2.3.1 *In vitro* studies

4.2.3.1.1 Drugs and reagents

All cell culture media and supplements were from Invitrogen (Thermo Fisher Scientific Inc. MA, USA). Dermorphin, DPDPE, and Dynorphin A were synthetized in the laboratory of Prof Remo Guerrini (University of Ferrara). FENT, BUF, 4F-BUF and ANT were purchased from LGC standards (LGC Standards S.r.l., Sesto San Giovanni, Milan, Italy) (authorization SP/141 24/11/2021 to MM) while naloxone was purchased from Sigma Aldrich (St. Louis, MO, USA). Opioid peptides were solubilized in bidistilled water, whereas all other compounds were solubilized in DMSO at a final concentration of 10 mM. Stock solutions of ligands were stored at -20 °C. Serial dilutions were made in each assay buffer.

4.2.3.1.2 Calcium mobilization assay

CHO cells stably coexpressing the human recombinant mu or kappa receptors with the C-terminally modified $G\alpha_{qi5}$ and CHO cells coexpressing the delta receptor and the $G\alpha_{qG66Di5}$ chimeric protein were generated as previously described (Camarda & Calo, 2013). Cells were cultured in medium consisting of Dulbecco's modified Eagle's medium (DMEM) / HAMS F12 (1:1) supplemented with 10% fetal bovine serum (FBS), penicillin (100 IU/ml), streptomycin (100 mg/ml), geneticin (G418; 200 µg/ml) and hygromycin B (100 µg/ml). Cell cultures were kept at 37 °C in 5% CO_2 / humidified air. When confluence was reached (3-4 days), cells were sub-cultured as required using trypsin / EDTA and used for experimentation. Cells were seeded at a density of 50,000 cells / well into 96-well black, clear-bottom plates. After 24 hours incubation the cells were incubated with Hank's Balanced Salt Solution (HBSS) supplemented with 2.5 mM probenecid, 3 µM of the calcium sensitive fluorescent dye Fluo-4 AM, 0.01% pluronic acid and 20 mM HEPES (pH 7.4) for 30 min at 37 °C. Afterwards the loading solution was aspirated followed by a washing step with 100 µl / well of HBSS, HEPES (20 mM, pH 7.4), 2.5 mM probenecid and 500 µM Brilliant Black. Subsequently 100 µl / well of the same buffer was added. After placing cell culture and compound plates into the FlexStation II (Molecular Devices, Sunnyvale, CA, USA), the changes in fluorescence of the cell-loaded calcium sensitive dye Fluor-4 AM were measured.

4.2.3.1.3 BRET assay

SH-SY5Y Cells stably co-expressing different pairs of fusion proteins i.e. mu-RLuc/Gβ1-RGFP or mu-RLuc/β-arrestin 2-RGFP were prepared using a pantropic retroviral expression system as described previously (Molinari et al., 2010; Malfacini et al., 2015). Cells were grown in Dulbecco's modified Eagle's medium (DMEM) / HAMS F12 (1:1) supplemented with 10% fetal bovine serum, penicillin G (100 units/ml), streptomycin (100 µg/ml), L-glutamine (2 mM), fungizone (1 µg/ml), geneticin (G418; 400 µg/ml) and hygromycin B (100 µg/ml) in a humidified atmosphere of 5% CO_2 at 37 °C. For G-protein experiments, enriched plasma membrane aliquots from mu-RLuc/Gβ1-RGFP cells were prepared by differential centrifugation; cells were detached with PBS/EDTA solution (1 mM, pH 7.4 NaOH) then, after 5 min 500 g centrifugation, Dounce-homogenized (30 strokes) in cold homogenization buffer (TRIS 5 mM, EGTA 1 mM, DTT 1 mM, pH 7.4 HCl) in the presence of sucrose (0.32 M). Three following centrifugation steps were performed at 10 min 1000 g (4 °C) and the supernatants kept. Two 20 min 24,000 g (4 °C) subsequent centrifugation steps (the second in the absence of sucrose) were performed for separating enriched membranes that after discarding the supernatant were kept in ultrapure water at -80 °C (Vachon et al., 1987). Membrane protein was determined using the QPRO-BCA kit (Cyanagen Srl, Bologna, IT) and the multimode Ensight plate reader (Perkin Elmer, Waltham, US). Luminescence in membranes and cells was recorded in 96-well white opaque microplates (Perkin Elmer, Waltham, MA, USA) using the Victor 2030 luminometer (PerkinElmer, Waltham, MA, USA). For the determination of receptor/G-protein interaction, membranes (3 µg of protein) prepared from cells co-expressing mu-RLuc/Gβ1-RGFP were added to wells in Dulbecco's phosphate-buffered saline (DPBS). For the determination of receptor/β-arrestin 2 interaction, whole cells co-expressing mu-RLuc/β-arrestin 2-RGFP were plated 24 h before the experiment (100,000 cells/well). The cells were prepared for the experiment by substituting the medium with PBS with $MgCl_2$ (0.5 mM) and $CaCl_2$ (0.9 mM). Coelenterazine at a final concentration of 5 µM was injected 15 minutes prior reading the cell plate. Different concentrations of ligands in 20 µL of PBS - BSA 0.01 % were added and incubated 5 min before reading luminescence. All experiments were performed at room temperature.

4.2.3.1.4 Data analysis and terminology

Pharmacological terminology adopted in this report is consistent with IUPHAR recommendations (Neubig et al., 2003). All data are expressed as the mean ± standard error of the mean (s.e.m.) of *n* experiments. For potency values 95% confidence limits (CL$_{95\%}$) were indicated. In calcium mobilization studies, agonist effects were expressed as maximum change in percent over the baseline fluorescence. Baseline fluorescence was measured in wells treated with saline. In BRET studies agonist effects were calculated as BRET ratio between CPS measured for the RGFP and RLuc light emitted using 510(10) and 460(25) filters (PerkinElmer, Waltham, MA, USA), respectively. Maximal agonist effects were expressed as fraction of the dermorphin maximal effect which was determined in every assay plate (dermorphin=1). Concentration response curve to agonists were fitted with the four-parameter logistic nonlinear regression model:

$$\text{Effect} = \text{Baseline} + \frac{(E_{max} - \text{Baseline})}{(1 + 10^{(LogEC_{50} - Log_{[compound]})Hillslope})}$$

For all assays, agonist potencies are given as pEC$_{50}$ i.e., the negative logarithm to base 10 of the molar concentration of an agonist that produces 50% of the maximal effect of that agonist. The potency of antagonists was expressed as pA$_2$ derived from the following equation: pA$_2$=-log[(CR−1)/[A]], assuming a slope value equal to unity, where CR indicates the ratio between agonist potency in the presence and absence of antagonist and [A] is the molar concentration of the antagonist (Kenakin, 2004). The intrinsic activities of the compounds under study were computed as fraction of the standard ligand dermorphin maximal-stimulated BRET ratio (dermorphin= 1.00)

4.2.3.2 *In vivo* studies

4.2.3.2.1 Animals

Hundred ninety-two female and male ICR (CD-1[®]) adult mice weighing 30–35 g (Centralized Preclinical Research Laboratory, University of Ferrara, Italy) were group housed (5 mice per cage; floor area per animal was 80 cm^2; minimum enclosure height was 12 cm), exposed to a 12:12-h light-dark cycle (light period from 6:30 AM to 6:30 PM) at a temperature of 20–22 °C and humidity of 45–55% and were provided ad libitum access to food (Diet 4RF25 GLP; Mucedola, Settimo Milanese, Milan, Italy) and water. The experimental protocols performed in the present study were in accordance with the U.K. Animals (Scientific Procedures) Act of

1986 and associated guidelines and the new European Communities Council Directive of September 2010 (2010/63/EU). Experimental protocols were approved by the Italian Ministry of Health (license n. 223/2021-PR, CBCC2.46.EXT.21) and by the Animal Welfare Body of the University of Ferrara. According to the ARRIVE guidelines, all possible efforts were made to minimise the number of animals used, to minimise the animals' pain and discomfort.

4.2.3.2.2 Drug preparation and dose selection

Drugs were initially dissolved in absolute ethanol (final concentration: 5%) and Tween 80 (2%) and brought to the final volume with saline (0.9% NaCl). Drugs were administered by intraperitoneal (IP) injection at a volume of 4 μL/g. The dose range of BUF and 4F-BUF (0.1-6 mg/kg IP) was chosen based on our previous studies (Bilel et al., 2022). In antagonist experiments, the opioid receptor antagonist naloxone (6 mg/kg IP) was administered 15 min before test compound injections, similar to our previous study (Bilel et al., 2022). The dose of Antalarmin was chosen based on a previous study (Ducottet et al., 2003t). Also, Antalarmin was given intraperitoneally 15 min before the administration of the agonists (Brodabear et al., 2004). Animals were also injected with the combination ANT (10 mg/kg) and NLX (6mg/kg) 15 min before the administration of the tested agonists. Female and male mice treated with NLX alone (6 mg/kg), Antalarmin alone (10 mg/kg) or their combination didn't show any cardiorespiratory alterations during the 60 min of measurements (data not shown).

4.2.3.2.3 Cardiorespiratory analysis

As previously reported by *Marchetti et al., 2023* (Marchetti et al., 2023), electrocardiogram (ECG) and plethysmography (PLETH) were performed in conscious animals using a non-invasive ECG and PLETH-TUNNEL system with an acquisition frequency of 1000 Hz (Emka Technologies, Paris, France). All plethysmography recording sessions were performed during daytime, and data were analyzed using the iox2 data acquisition analysis software (Emka Technologies). A cylinder-shaped tube (i.e., restraining tunnel) restrains the animal firmly but gently, without causing trauma. To minimize the effects of stress, animals were allowed to stay in the restraining system for 1 min before starting recordings. Indeed, upon observation of the animals after 1 min, plethysmography traces proved that they were calm, and that breathing was stable. The experiment provides baseline recording lasting for 15 min, followed by a recording session of 65 min immediately after vehicle or drug administration (Marchetti et al., 2023).

4.2.3.2.4 Data and statistical analysis

Emka ECG and plethysmography analyzer software were used to analyze tracings recorded during data acquisition. Six leads of ECG were recorded using specific software (iox®, EMKA technologies): three leads were measured (L1, L2, L3), and three were calculated (aVR, aVL, aVF). The parameters reported in this work were obtained from L1 and L2.

For the ECG analysis, HR (bpm; heart rate), RR (ms; time between two consecutive peaks), QRS (ms; is the time from the start to the end of the QRS complex) were expressed as % change of basal value.

For plethysmography, BB_ie (ms; breath length, sum of the duration of inspiration and the duration of expiration), FR_ie (bpm; breathing frequency derived from BB_ie), and MV (F/min; computed from tidal volume and breathing frequency FR_ie), were expressed as % change of basal value.

Statistical analysis of the effects of the substances at different doses over time and of antagonism studies was done via two-way ANOVA followed by a Bonferroni test for multiple comparisons (GraphPad Prism, version 8, San Diego, CA, USA).

The mean effect values represent the average of the effects induced by each compound at each dose over the time course of the experiment (histograms).

4.2.4 Results

4.2.4.1 *In vitro* studies

4.2.4.1.1 Calcium mobilization studies

In CHO cells stably transfected with the human mu opioid receptor, the standard agonist dermorphin evoked a robust concentration-dependent stimulation of calcium release displaying high potency (pEC$_{50}$ of 8.19) and maximal effects (319 ± 13% over the basal values). FENT and its derivatives were able to activate the mu opioid receptor in a concentration dependent manner with the following rank order of similar potency: FENT > 4F-BUF $\geq$ BUF. Regarding ligand efficacy, FENT and BUF were able to elicit maximal effects similar to that of dermorphin, while 4F-BUF displayed statistically significantly lower maximal effects thus behaving as a partial agonist (**Table 4.2**).

Table 4.2 *Effects of dermorphin, FENT, BUF and 4F-BUF in calcium mobilization experiments performed in CHO cells coexpressing opioid receptors and the chimeric G-proteins. *p<0.05 vs dermorphin according to ANOVA followed by the Dunnett test. Data are mean of at least 3 separate experiments made in duplicate.*

	mu		delta		kappa	
	pEC_{50} $(CL_{95\%})$	$E_{max} \pm$ sem %	pEC_{50} $(CL_{95\%})$	$E_{max} \pm$ sem %	pEC_{50} $(CL_{95\%})$	$E_{max} \pm$ sem %
Standard agonists	8.19 (8.02 – 8.36)	319 ± 13	7.47 (7.09-7.85)	230 ± 18	8.81 (8.22-9.40)	257 ± 34
FENT	8.13 (7.73-8.52)	326 ± 13	CRC incomplete		CRC incomplete	
BUF	7.32 (6.70-7.93)	283 ± 18	CRC incomplete		CRC incomplete	
4F-BUF	7.50 (6.92-8.09)	258 ± 8*	Inactive		Inactive	

Standard agonists were dermorphin, DPDPE, and dynorphin A for mu, delta, and kappa opioid receptors, respectively (Data on standard agonists and FENT were reported in Bilel et al., 2022).

In CHO$_{delta}$ cells, the standard agonist DPDPE evoked a robust concentration-dependent stimulation of calcium release with high potency (pEC$_{50}$ of 7.47) and maximal effects (230 ± 18% over the basal values). FENT, BUF and 4F-BUF were inactive or displayed an incomplete concentration response curve, stimulating calcium mobilization only at micromolar concentrations.

In CHO$_{kappa}$ cells, the standard agonist dynorphin A evoked a robust concentration-dependent stimulation of calcium release with very high potency (pEC$_{50}$ of 8.81) and maximal effects (257 ± 34% over the basal values). FENT, BUF and 4F-BUF were either inactive or displayed an incomplete concentration response curve, stimulating calcium mobilization only at micromolar concentrations.

4.2.4.1.1 BRET studies

In the BRET G-protein assay, dermorphin promoted mu/G-protein interaction in a concentration dependent manner with pEC$_{50}$ of 7.71 (7.41-8.01) and maximal effect of 0.96 ± 0.11 stimulated BRET ratio FENT, BUF and 4F-BUF mimicked stimulatory effects elicited by dermorphin showing similar maximal effects and slightly higher potency (**Fig. 4.5** and **Table 4.2**)

In the BRET β-arrestin assay, dermorphin stimulated the interaction of the mu receptor with β-arrestin 2 in a concentration-dependent manner with pEC_{50} 6.96 (6.56-7.37) and maximal effects corresponding to 0.24 ± 0.09 stimulated BRET ratio. FENT and BUF were able to promote the interaction of the mu receptor with β-arrestin 2 showing similar potency but significantly reduced efficacy; in fact, the two compounds behaved as partial agonists. In the BRET β-arrestin assay 4F-BUF was completely inactive as agonist (**Fig. 4.6-D**). Thus, 4F-BUF was further investigated as an antagonist of FENT induced β-arrestin 2 recruitment. At 0.1 μM, 4F-BUF was able to shift the concentration response curve to FENT to the right with no modifications of the agonist maximal effect (**See Appendix B, Fig B1**); a pA_2 of 7.81 was derived from these experiments for 4F-BUF.
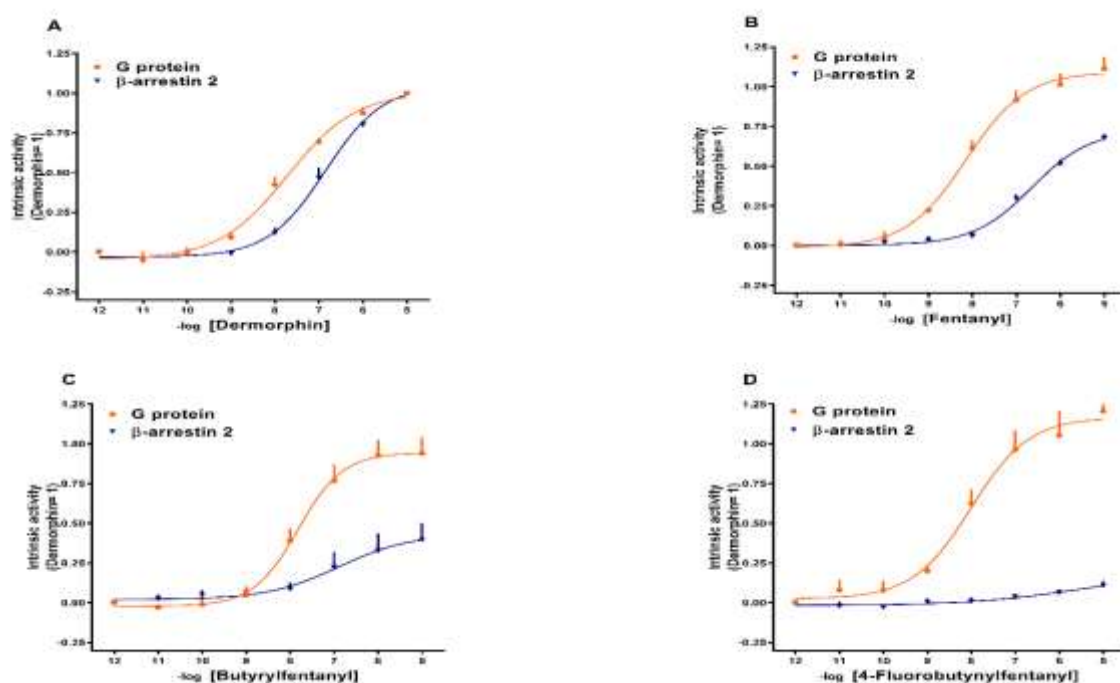
Figure 4.6 *BRET assay. Concentration-response curve to dermorphin, FENT, BUF, 4F-BUF for mu/G protein and mu/β-arrestin 2 (panel A-D) interaction. Data are the mean ± s.e.m. of 5 separate experiments made in duplicate.*

4.2.4.2 *In vivo* studies

4.2.4.2.1 *Cardio-respiratory Analysis*

The vehicle used in this experiment showed a stable profile during the 80 min of ECG (Heart rate, RR and QRS) and plethysmography (FR_ie, BB_ie and MV) parameter measurement in both sex (**Figs. 4.7-4.17**). Systemic administration of BUF and 4F-BUF (0.1-6 mg/kg IP),

induced important variations in cardiorespiratory parameters in female and male mice especially at the highest dose tested (see **Appendix B Fig. B2**).

ECG BUF:

Female ECG measurements:

Heart rate (**Fig. 4.7**) was immediately and significantly affected by BUF treatment [**Fig. 4.7-A**: $F_{3, 1600} = 689.8$, P<0.0001], time [$F_{79, 1600} = 3.539$, P<0.0001] and time × treatment interaction [$F_{237, 1600} = 2.968$, P<0.0001]. In addition, RR_interval increased immediately and significantly in female-BUF treated mice ([**Fig. 4.7-C**: $F_{3, 1600} = 1200$, P<0.0001], time [$F_{79, 1600} = 4.914$, P<0.0001] and time × treatment interaction [$F_{237, 1600} = 4.179$, P<0.0001]). The QRS complex increased immediately and significantly with the dose of 6 mg/kg of BUF [**Fig. 4.7-E**: $F_{3, 1600} = 433.8$, P<0.0001], time [$F_{79, 1600} = 2.819$, P<0.0001] and time × treatment interaction [$F_{237, 1600} = 3.248$, P<0.0001].
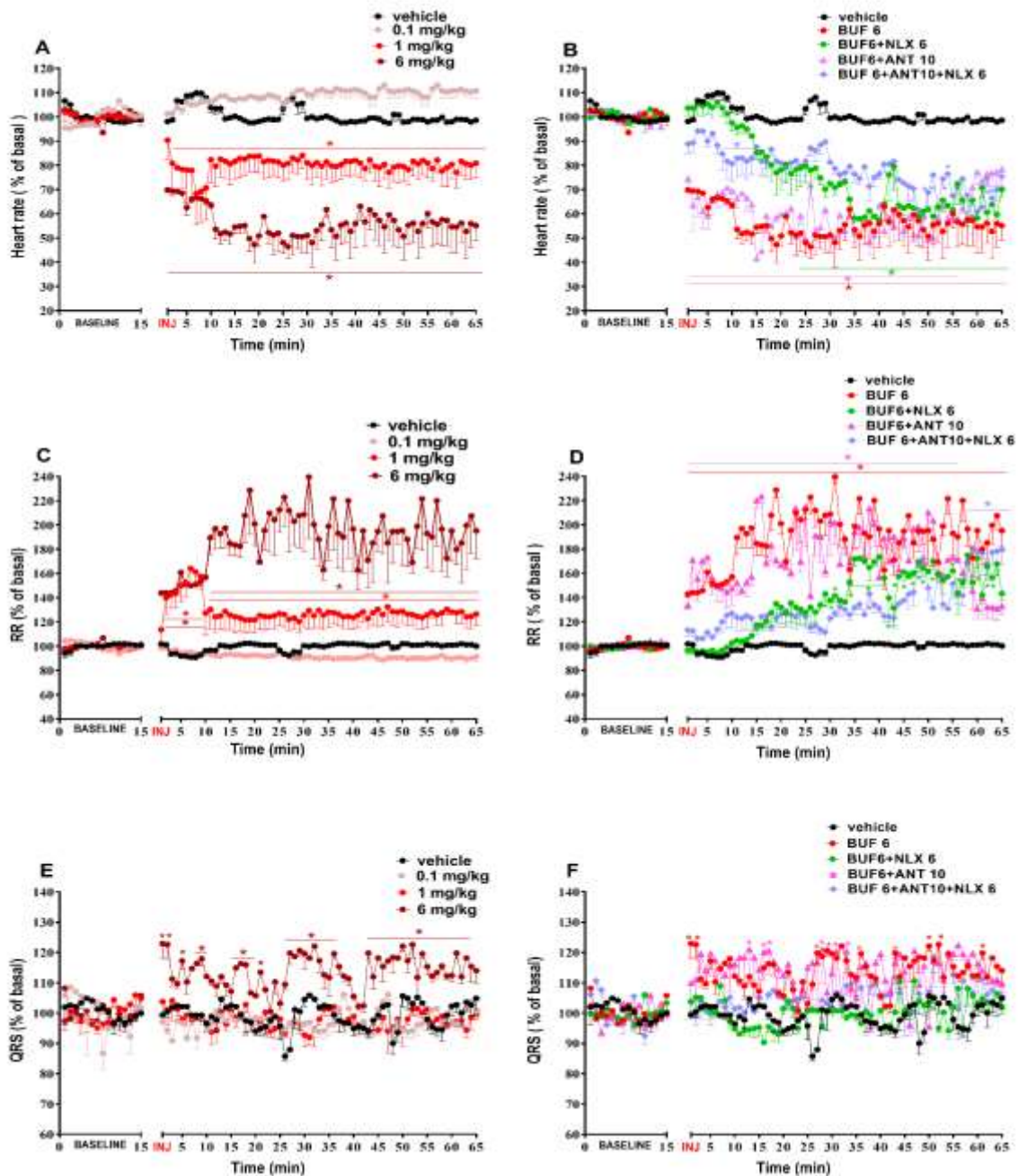
BUTYRLFENTANYL female

Figure 4.7. ECG measurements: Systemic administration of BUF (0.1-6 mg/kg IP;) in Heart rate (panel A); RR_interval (panel C) and QRS complex (panel E) in female mice. Interaction of effective dose of BUF (6 mg/kg) with the opioid receptor antagonist NLX (6 mg/kg) or the CRF-1 antagonist ANT (10 mg/kg) or their combination (ANT 10 mg/kg+NLX 6 mg/kg); (Panel B, D, F). Data are expressed as percentage of baseline (see materials and methods) and represents the mean ± SEM of 6 determinations for each treatment. Statistical analysis was performed by two-way ANOVA followed by Bonferroni's test for multiple comparisons for the dose-response curve of the compounds at different times (panel A-F). *p<0.05 versus vehicle.

Pre-treatment with NLX alone (6 mg/kg IP) or ANT (10 mg/kg.IP) in combination with NLX (6 mg/kg IP); **Fig. 4.7-B**) partially prevented female-BUF bradycardia. The pretreatment with

ANT (10 mg/kg IP) alone was not effective on preventing the effects of BUF on heart rate [**Fig 4.7-B**: $F_{4,\,2000} = 802.5$, P<0.0001], time [$F_{79,\,2000} = 33.49$, P<0.0001] and time × treatment interaction [$F_{316,\,2000} = 4.791$, P<0.0001]; RR_interval [**Fig. 4.7-D**: $F_{4,\,2000} = 805.6$, P<0.0001], time [$F_{79,\,2000} = 29.24$, P<0.0001] and time × treatment interaction [$F_{316,\,2000} = 5.723$, P<0.0001] and QRS complex [**Fig. 4.7-F**: $F_{4,\,2000} = 166.7$, P<0.0001], time [$F_{79,\,2000} = 3.737$, P<0.0001] and time × treatment interaction [$F_{316,\,2000} = 1.827$, P<0.0001].

Male ECG measurements

Heart rate (**Fig. 4.8**) was immediately and significantly affected by BUF treatment [**Fig. 4.8-A**: $F_{3,\,1600} = 1973$, P<0.0001], time [$F_{79,\,1600} = 9.014$, P<0.0001] and time × treatment interaction [$F_{237,\,1600} = 7.697$, P<0.0001]. In addition, RR_interval increased immediately and significantly in male-BUF treated mice ([**Fig. 4.8-C**: $F_{3,\,1600} = 1603$, P<0.0001], time [$F_{79,\,1600} = 8.412$, P<0.0001] and time × treatment interaction [$F_{237,\,1600} = 7.392$, P<0.0001]). The QRS complex increased immediately and significantly with the dose of 1 and 6 mg/kg of BUF [**Fig. 4.8-E**: $F_{3,\,1600} = 242.1$, P<0.0001], time [$F_{79,\,1600} = 1.647$, P=0.0004] and time × treatment interaction [$F_{237,\,1600} = 2.370$, P<0.0001].

BUTYRYLFENTANYL Male
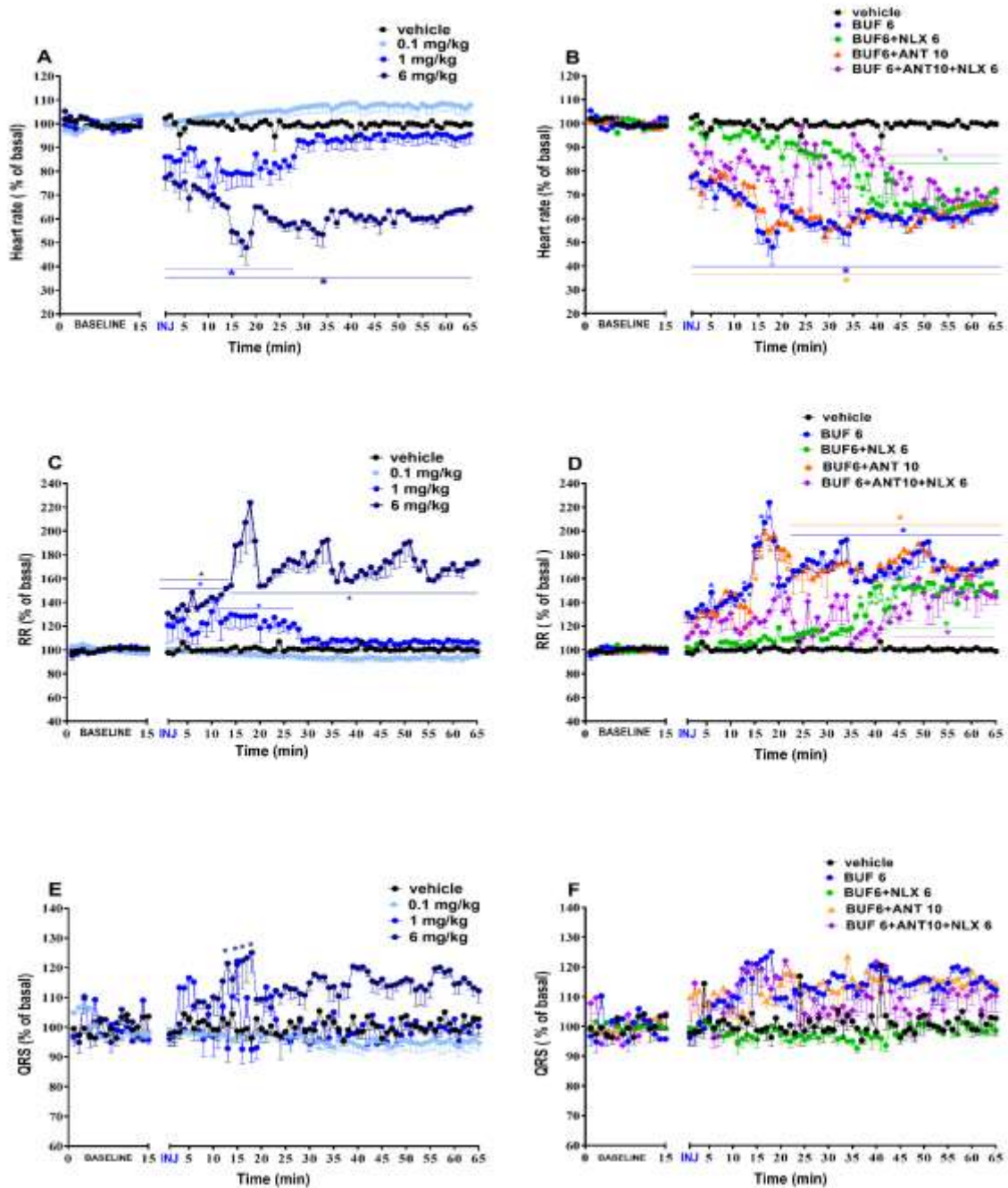
Figure 4.8. *ECG measurements: Systemic administration of BUF (0.1-6 mg/kg IP) in Heart rate (panel A); RR_interval (panel C) and QRS complex (panel E) in male mice. Interaction of effective dose of BUF (6 mg/kg) with the opioid receptor antagonist NLX (6 mg/kg) or the CRF-1 antagonist ANT (10 mg/kg) or their combination (ANT 10 mg/kg+NLX 6 mg/kg); (Panel B, D, F). Data are expressed as percentage of baseline (see materials and methods) and represents the mean ± SEM of 6 determinations for each treatment. Statistical analysis was performed by two-way ANOVA followed by Bonferroni's test for multiple comparisons for the dose-response curve of the compounds at different times (panel A-F). *p<0.05 versus vehicle.*

185

Pre-treatment with NLX alone (6 mg/kg IP) and ANT(10 mg/kg.IP) in combination with NLX (6 mg/kg IP); **Fig. 4.8-B**) partially prevented female-BUF bradycardia while ANT (10 mg/kg IP) alone was not effective on preventing the effects of BUF on heart rate [**Fig. 4.8-B**: $F_{4,\,2000}$ = 1368, P<0.0001], time [$F_{79,\,2000}$ = 58.64, P<0.0001] and time × treatment interaction [$F_{316,\,2000}$ = 8.302, P<0.0001]; RR_interval [**Fig. 4.8-D**: $F_{4,\,2000}$ = 903.8, P<0.0001], time [$F_{79,\,2000}$ = 36.53, P<0.0001] and time × treatment interaction [$F_{316,\,2000}$ = 5.780, P<0.0001] and QRS complex [**Fig. 4.8-F**: $F_{4,\,2000}$ = 151.7, P<0.0001], time [$F_{79,\,2000}$ = 3.408, P<0.0001] and time × treatment interaction [$F_{316,\,2000}$ = 1.526, P<0.0001].

Plethysmography BUF

Female plethysmography measurements

Respiratory rate (**Fig. 4.9**) was immediately and significantly affected by BUF treatment [**Fig. 4.9-A**: $F_{3,\,1600}$ = 440.1, P<0.0001], time [$F_{79,\,1600}$ = 8.146, P<0.0001] and time × treatment interaction [$F_{237,\,1600}$ = 3.655, P<0.0001]. In addition, breath length increased immediately and significantly in female-BUF treated mice ([**Fig. 4.9-C**: $F_{3,\,1600}$ = 1791, P<0.0001], time [$F_{79,\,1600}$ = 44.88, P<0.0001] and time × treatment interaction [$F_{237,\,1600}$ = 11.29, P<0.0001]). Minute volume also decreased immediately and significantly after the administration of BUF [**Fig. 4.9-E**: $F_{3,\,1600}$ = 719.5, P<0.0001], time [$F_{79,\,1600}$ = 8.521, P<0.0001] and time × treatment interaction [$F_{237,\,1600}$ = 4.577, P<0.0001].

BUTYRYLFENTANYL female

Figure 4.9. *Plethysmography measurements: Systemic administration of BUF (0.1-6 mg/kg IP) in Breath rate (panel A); Breath length (panel C) and Minute volume (panel E) in female mice. Interaction of effective dose of BUF (6 mg/kg) with the opioid receptor antagonist NLX (6 mg/kg) or the CRF-1 antagonist ANT (10 mg/kg) or their combination (ANT 10 mg/kg+NLX 6 mg/kg); (Panel B, D, F). Data are expressed as a percentage of baseline (see materials and methods) and represents the mean ± SEM of 6 determinations for each treatment. Statistical analysis was performed by two-way ANOVA followed by Bonferroni's test for multiple comparisons for the dose-response curve of the compounds at different times (panel A-F). *p<0.05 versus vehicle.*

187

Pre-treatment with NLX alone (6 mg/kg IP); **Fig. 4.9-B**) partially prevented BUFbradypnea while MV reduction was potentiated with NLX (**Fig. 4.9-F**). However, ANT (10 mg/kg IP) alone or ANT (10 mg/kg IP) in combination with NLX (6 mg/kg.IP) were effective on preventing the effects of BUF on FR_ie [**Fig. 4.9-B**: $F_{4, 2000} = 506.9$, P<0.0001], time [$F_{79, 2000} = 3.159$, P<0.0001] and time × treatment interaction [$F_{316, 2000} = 4.268$, P<0.0001]; BB_ie [**Fig. 4.9-D**: $F_{4, 2000} = 899.4$, P<0.0001], time [$F_{79, 2000} = 7.576$, P<0.0001] and time × treatment interaction [$F_{316, 2000} = 7.835$, P<0.0001] and MV [**Fig. 4.9-F**: $F_{4, 2000} = 1464$, P<0.0001], time [$F_{79, 2000} = 32.55$, P<0.0001] and time × treatment interaction [$F_{316, 2000} = 8.677$, P<0.0001].

Male plethysmography measurements:

Respiratory rate (**Fig. 4.10**) was immediately and significantly affected by BUF treatment [**Fig 4.10-A**: $F_{3, 1600} = 721$, P<0.0001], time [$F_{79, 1600} = 9.792$, P<0.0001] and time × treatment interaction [$F_{237, 1600} = 3.522$, P<0.0001]. In addition, breath length increased immediately and significantly in BUF treated mice ([**Fig. 4.10-C**: $F_{3, 1600} = 1168$, P<0.0001], time [$F_{79, 1600} = 16.89$, P<0.0001] and time × treatment interaction [$F_{237, 1600} = 7.137$, P<0.0001]). Minute volume also decreased immediately and significantly after the administration of BUF [**Fig. 4.10-E**: $F_{3, 1600} = 884.2$, P<0.0001], time [$F_{79, 1600} = 7.417$, P<0.0001] and time × treatment interaction [$F_{237, 1600} = 4.506$, P<0.0001].
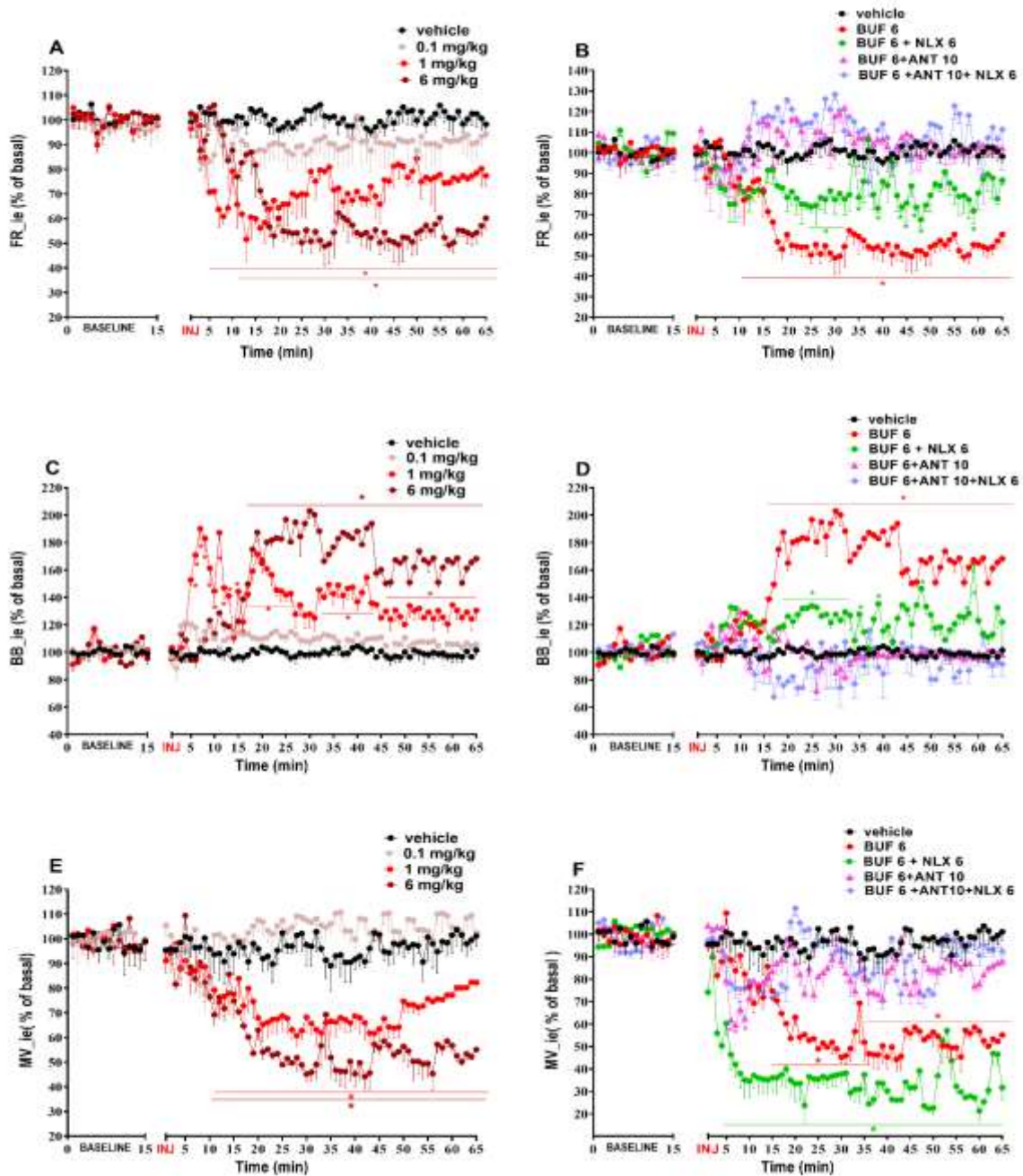
BUTYRYLFENTANYL male
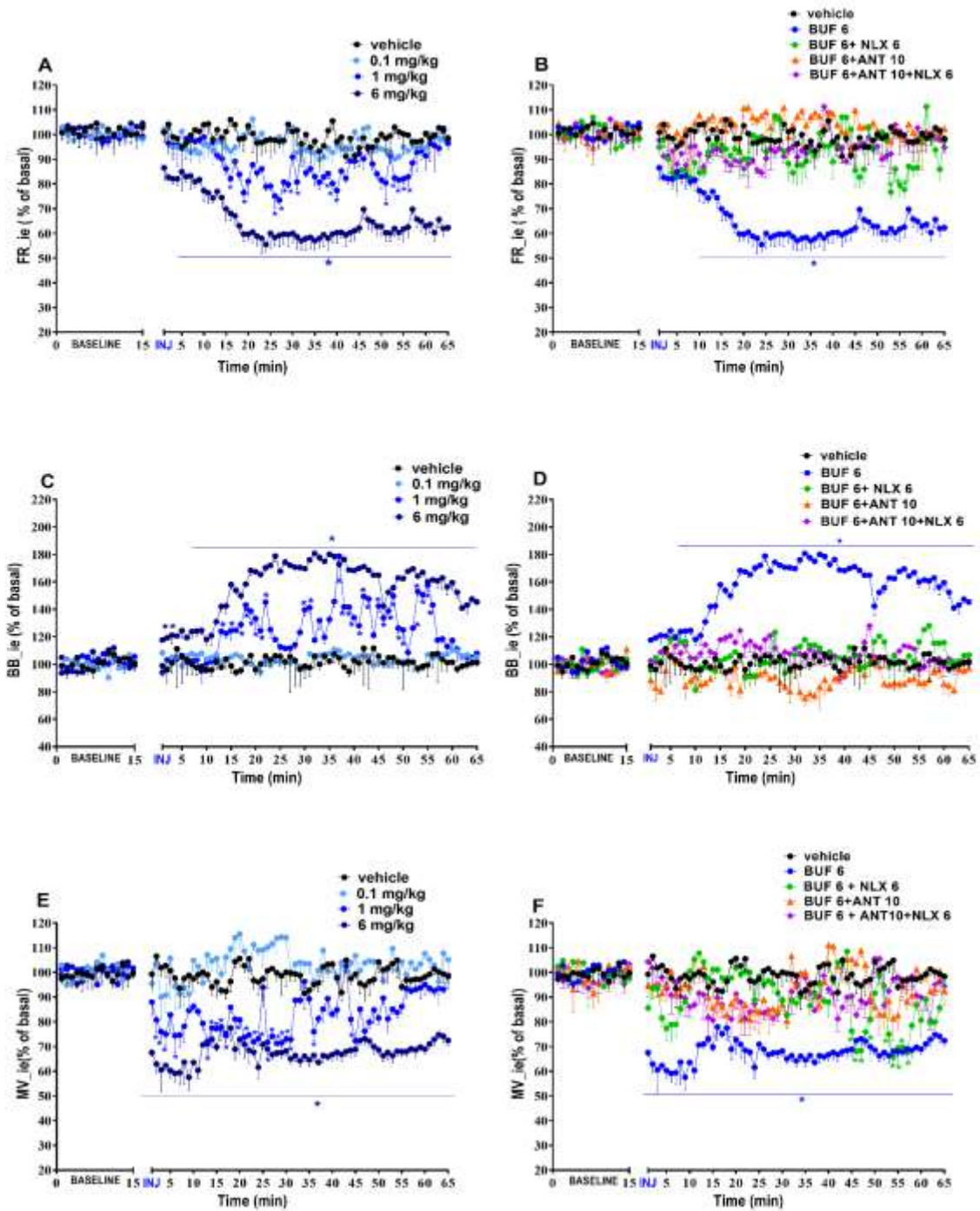
Figure 4.10*. Plethysmography measurements: Systemic administration of BUF (0.1-6 mg/kg IP) in Breath rate (panel A); Breath length (panel C) and Minute volume (panel E) in male mice. Interaction of effective dose of BUF (6 mg/kg) with the opioid receptor antagonist NLX (6 mg/kg) or the CRF-1 antagonist ANT (10 mg/kg) or their combination (ANT 10 mg/kg+NLX 6 mg/kg); (Panel B, D, F). Data are expressed as percentage of baseline (see materials and methods) and represents the mean ± SEM of 6 determinations for each treatment. Statistical analysis was performed by two-way ANOVA followed by Bonferroni's test for multiple comparisons for the dose-response curve of the compounds at different times (panel A-F). *p<0.05 versus vehicle.*

189

Pre-treatment with NLX alone (6 mg/kg IP); **Fig. 4.10-B**) partially prevented female-BUFrespiratory depression while MV reduction was potentiated with NLX (**Fig. 4.10-F**). However, ANT (10 mg/kg IP) alone or ANT (10 mg/kg IP) in combination with NLX (6 mg/kg IP) were effective on preventing the effects of BUF on FR_ie [**Fig 4.10-B**: $F_{3, 2000} = 573.7$, P<0.0001], time [$F_{79, 2000} = 4.971$, P<0.0001] and time × treatment interaction [$F_{316, 2000} = 3.525$, P<0.0001]; BB_ie [**Fig 4.10-D**: $F_{4, 2000} = 1225$, P<0.0001], time [$F_{79, 2000} = 7.187$, P<0.0001] and time × treatment interaction [$F_{316, 2000} = 6.686$, P<0.0001] and MV [**Fig 4.10-F**: $F_{4, 2000} = 384.8$, P<0.0001], time [$F_{79, 2000} = 7.194$, P<0.0001] and time × treatment interaction [$F_{316, 2000} = 3.631$, P<0.0001].

ECG 4F-BUF:

Female ECG measurements:

Heart rate (**Fig. 4.11**) was immediately and significantly affected by 4F-BUF treatment [**Fig 4.11-A**: $F_{3, 1600} = 959.5$, P<0.0001], time [$F_{79, 1600} = 11.72$, P<0.0001] and time × treatment interaction [$F_{237, 1600} = 4.582$, P<0.0001]. In addition, RR_interval increased immediately and significantly in female-BUF treated mice ([**Fig 4.11-C**: $F_{3, 1600} = 1489$, P<0.0001], time [$F_{79, 1600} = 11.44$, P<0.0001] and time × treatment interaction [$F_{237, 1600} = 7.122$, P<0.0001]). The QRS complex increased immediately and significantly with the dose of 6 mg/kg of BUF [**Fig 4.11-E**: $F_{3, 1600} = 104.8$, P<0.0001], time [$F_{79, 1600} = 2.815$, P<0.0001] and time × treatment interaction [$F_{237, 1600} = 1.885$, P<0.0001].

4F-BUTYRYLFENTANYL female

Figure 4.11. *ECG measurements: Systemic administration of 4F-BUF (0.1-6 mg/kg IP) in Heart rate (panel A); RR_interval (panel C) and QRS complex (panel E) in female mice. Interaction of effective dose of 4F-BUF (6 mg/kg) with the opioid receptor antagonist NLX (6 mg/kg) or the CRF-1 antagonist ANT (10 mg/kg) or their combination (ANT 10 mg/kg+NLX 6 mg/kg); (Panel B, D, F). Data are expressed as percentage of baseline (see materials and methods) and represents the mean ± SEM of 6 determinations for each treatment. Statistical analysis was performed by two-way ANOVA followed by Bonferroni's test for multiple comparisons for the dose-response curve of the compounds at different times (panel A-F). *p<0.05 versus vehicle.*

Pre-treatment with NLX alone (6 mg/kg IP), ANT (10 mg/kg IP) in combination with NLX (6 mg/kg IP); **Fig. 4.11-B**) partially prevented female 4F-BUF bradycardia while ANT (10 mg/kg IP) alone was not effective on preventing the effects of BUF on heart rate [**Fig 4.11-B**: $F_{4, 2000}$ = 942.2, P<0.0001], time [$F_{79, 2000}$ = 36.92, P<0.0001] and time × treatment interaction [$F_{316, 2000}$ = 4.539, P<0.0001]; RR_interval [**Fig 4.11-D**: $F_{4, 2000}$ = 805.6, P<0.0001], time [$F_{79, 2000}$ = 29.24, P<0.0001] and time × treatment interaction [$F_{316, 2000}$ = 5.723, P<0.0001] and QRS complex [**Fig 4.11-F**: $F_{4, 2000}$ = 72.02, P<0.0001], time [$F_{79, 2000}$ = 2.073, P<0.0001] and time × treatment interaction [$F_{316, 2000}$ = 1.676, P<0.0001].

Male ECG measurements

Heart rate (**Fig. 4.12**) was immediately and significantly affected by 4F-BUF treatment [**Fig 4.12-A**: $F_{3, 1600}$ = 956.1, P<0.0001], time [$F_{79, 1600}$ = 6.714, P<0.0001] and time × treatment interaction [$F_{237, 1600}$ = 3.436, P<0.0001]. In addition, RR_interval increased immediately and significantly in 4F-BUF treated mice ([**Fig 4.12-C**: $F_{3, 1600}$ = 677.6, P<0.0001], time [$F_{79, 1600}$ = 4.613, P<0.0001] and time × treatment interaction [$F_{237, 1600}$ = 2.563, P<0.0001]). The QRS complex increased immediately and significantly with the dose of 1 and 6 mg/kg of 4F-BUF [**Fig 4.12-E**: $F_{3, 1600}$ = 132.3, P<0.0001], time [$F_{79, 1600}$ = 1.391, P=0.0146] and time × treatment interaction [$F_{237, 1600}$ = 1.579, P<0.0001].
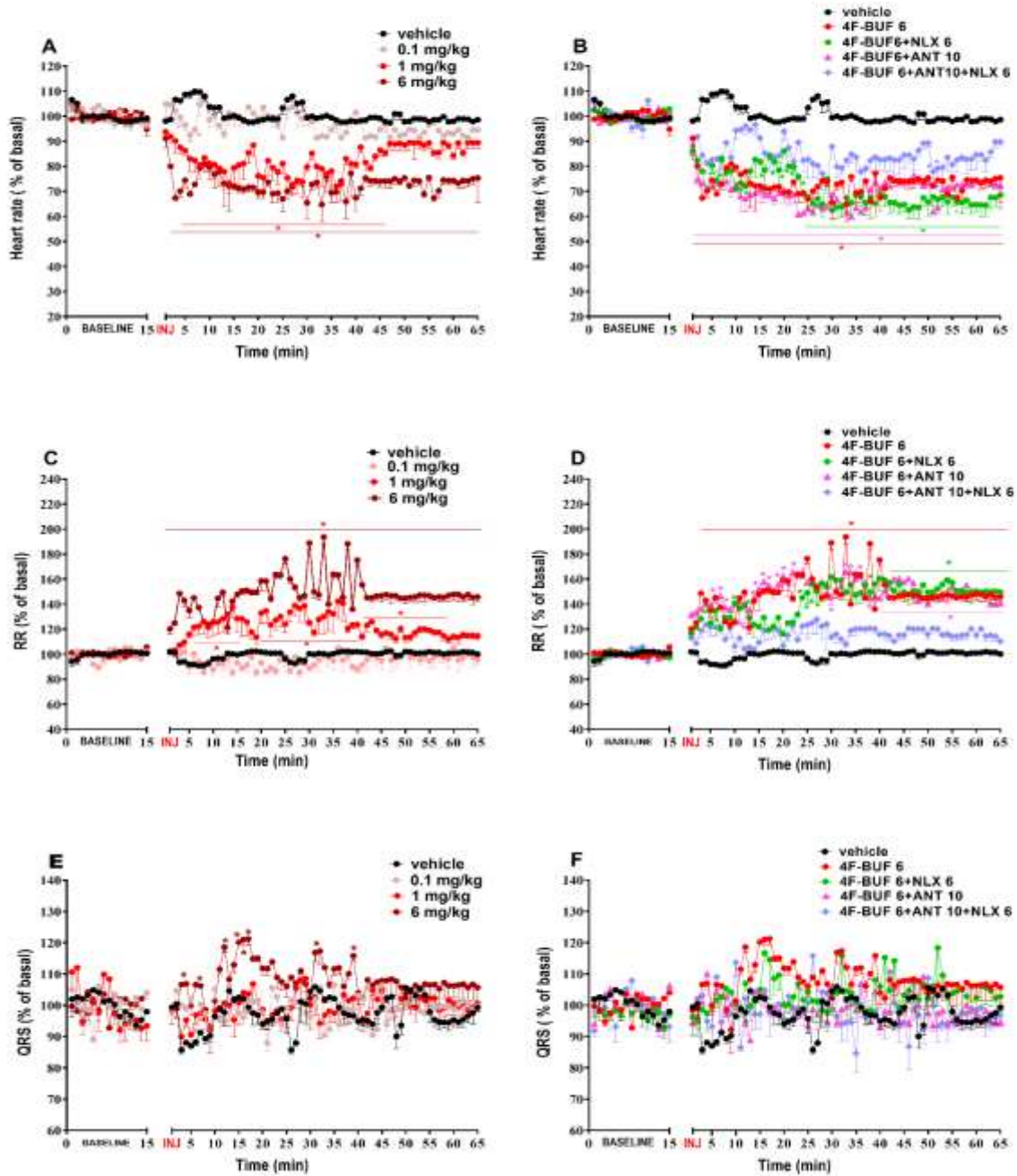
4F-BUTYRYLFENTANYL male
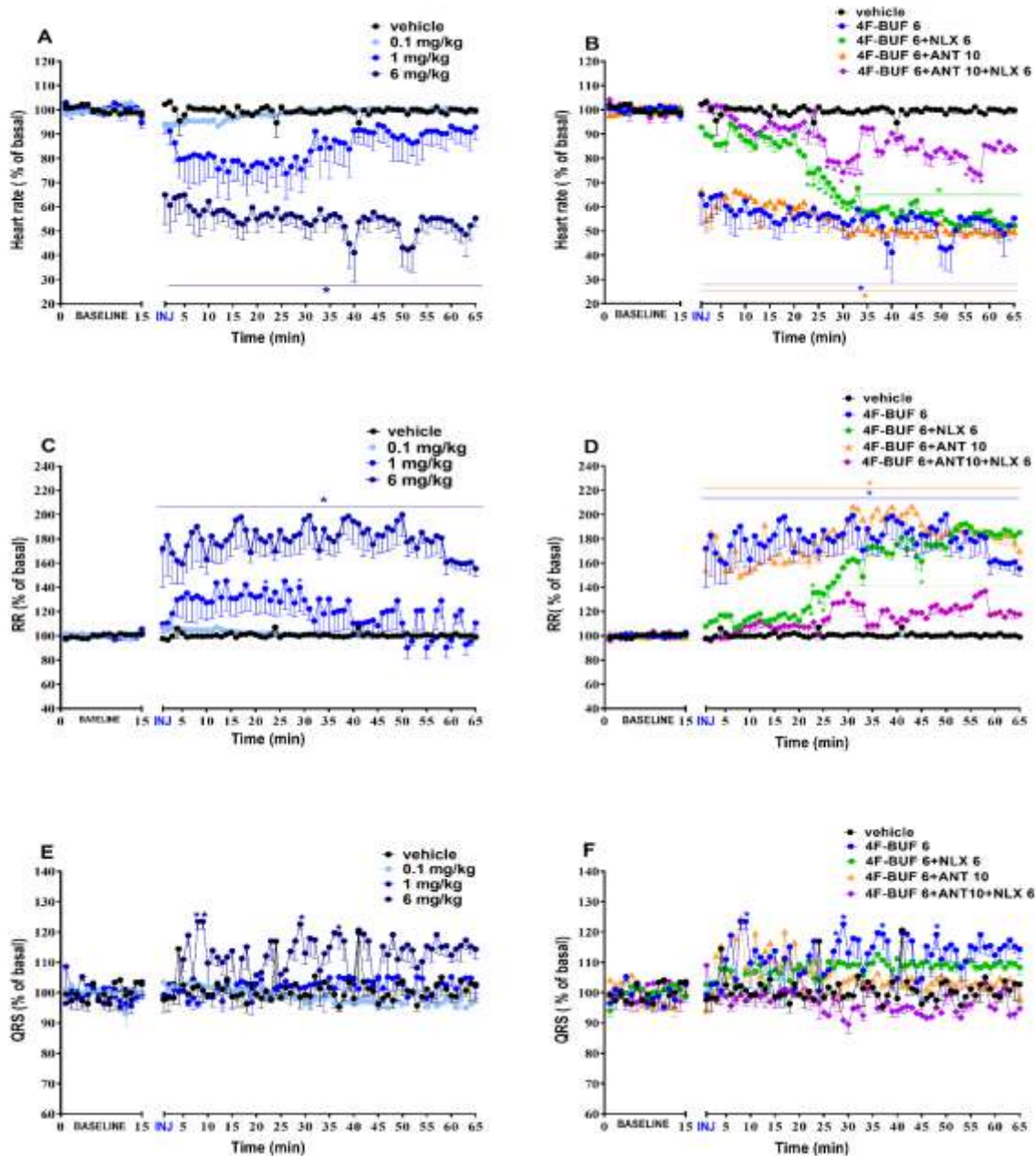
Figure 4.12. *ECG measurements: Systemic administration of 4F-BUF (0.1-6 mg/kg IP) in Heart rate (panel A); RR_interval (panel C) and QRS complex (panel E) in male mice. Interaction of effective dose of 4F-BUF (6 mg/kg) with the opioid receptor antagonist NLX (6 mg/kg) or the CRF-1 antagonist ANT (10 mg/kg) or their combination (ANT 10 mg/kg+NLX 6 mg/kg); (Panel B, D, F). Data are expressed as percentage of baseline (see materials and methods) and represents the mean ± SEM of 6 determinations for each treatment. Statistical analysis was performed by two-way ANOVA followed by Bonferroni's test for multiple comparisons for the dose-response curve of the compounds at different times (panel A-F). *p<0.05 versus vehicle.*

Pre-treatment with NLX alone (6 mg/kg IP) and ANT(10 mg/kg.IP) in combination with NLX (6 mg/kg IP); **Fig. 4.12-B**) partially prevented male 4F-BUF bradycardia while ANT (10 mg/kg IP) alone was not effective on preventing the effects of BUF on heart rate [**Fig 4.12-B**: $F_{4,\,2000}$ = 2141, P<0.0001], time [$F_{79,\,2000}$ = 70.48, P<0.0001] and time × treatment interaction [$F_{316,\,2000}$ = 9.465, P<0.0001]; RR_interval [**Fig 4.12-D**: $F_{4,\,2000}$ = 1102, P<0.0001], time [$F_{79,\,2000}$ = 31.48, P<0.0001] and time × treatment interaction [$F_{316,\,2000}$ = 5.770, P<0.0001] and QRS complex [**Fig 4.12-F**: $F_{4,\,2000}$ = 162.7, P<0.0001], time [$F_{79,\,2000}$ = 3.153, P<0.0001] and time × treatment interaction [$F_{316,\,2000}$ = 2.200, P<0.0001].

Plethysmography 4F-BUF:

Female plethysmography measurements:

Respiratory rate **(Fig. 4.13)** was immediately and significantly affected by 4F-BUF treatment [**Fig 4.13-A**: $F_{3,\,1600}$ = 1174, P<0.0001], time [$F_{79,\,1600}$ = 16.64, P<0.0001] and time × treatment interaction [$F_{237,\,1600}$ = 6.036, P<0.0001].

In addition, breath length increased immediately and significantly in female_-4F-BUF treated mice ([**Fig 4.13-C**: $F_{3,\,1600}$ = 2295, P<0.0001], time [$F_{79,\,1600}$ = 30.62, P<0.0001] and time × treatment interaction [$F_{237,\,1600}$ = 14.11, P<0.0001]). Minute volume also decreased immediately and significantly after the administration of 4F-BUF [**Fig 4.13-E**: $F_{3,\,1600}$ = 888.3, P<0.0001], time [$F_{79,\,1600}$ = 30.42, P<0.0001] and time × treatment interaction [$F_{237,\,1600}$ = 6.161, P<0.0001].

4F-BUTYRYLFENTANYL female

Figure 4.13. *Plethysmography measurements: Systemic administration of 4F-BUF (0.1-6 mg/kg IP) in Breath rate (panel A); Breath length (panel C) and Minute volume (panel E) in female mice. Interaction of effective dose of BUF (6 mg/kg) with the opioid receptor antagonist NLX (6 mg/kg) or the CRF-1 antagonist ANT (10 mg/kg) or their combination (ANT 10 mg/kg+NLX 6 mg/kg); (Panel B, D, F). Data are expressed as a percentage of baseline (see materials and methods) and represents the mean ± SEM of 6 determinations for each treatment. Statistical analysis was performed by two-way ANOVA followed by Bonferroni's test for multiple comparisons for the dose-response curve of the compounds at different times (panel A-F). *p<0.05 versus vehicle.*

195

Pre-treatment with NLX alone (6 mg/kg IP); **Fig. 4.13-B**) partially prevented female-4F-BUF induced bradypnea while MV reduction was potentiated with NLX (**Fig. 4.13-E**). However, ANT (10 mg/kg IP) alone or ANT (10 mg/kg IP) in combination with NLX (6 mg/kg IP) were effective on preventing the effects of BUF on FR_ie [**Fig 4.13-B**: $F_{4,\,2000} = 900.9$, P<0.0001], time [$F_{79,\,2000} = 28.90$, P<0.0001] and time × treatment interaction [$F_{316,\,2000} = 4.632$, P<0.0001]; BB_ie [**Fig 4.13-D**: $F_{4,\,2000} = 1791$, P<0.0001], time [$F_{79,\,2000} = 44.88$, P<0.0001] and time × treatment interaction [$F_{316,\,2000} = 11.29$, P<0.0001] and MV [**Fig 4.13-F**: $F_{4,\,2000} = 1030$, P<0.0001], time [$F_{79,\,2000} = 35.88$, P<0.0001] and time × treatment interaction [$F_{316,\,2000} = 5.347$, P<0.0001].

Male plethysmography measurements

Respiratory rate (**Fig. 4.14**) was immediately and significantly affected by 4F-BUF treatment [**Fig 4.14-A**: $F_{3,\,1600} = 621.2$, P<0.0001], time [$F_{79,\,1600} = 12.02$, P<0.0001] and time × treatment interaction [$F_{237,\,1600} = 4.774$, P<0.0001]. In addition, breath length increased immediately and significantly in male_4F-BUF treated mice ([**Fig 4.14-C**: $F_{3,\,1600} = 1140$, P<0.0001], time [$F_{79,\,1600} = 16.31$, P<0.0001] and time × treatment interaction [$F_{237,\,1600} = 7.737$, P<0.0001]). Minute volume also decreased immediately and significantly after the administration of 4F-BUF [**Fig 4.14-E**: $F_{3,\,1600} = 610.2$, P<0.0001], time [$F_{79,\,1600} = 7.909$, P<0.0001] and time × treatment interaction [$F_{237,\,1600} = 4.588$, P<0.0001].
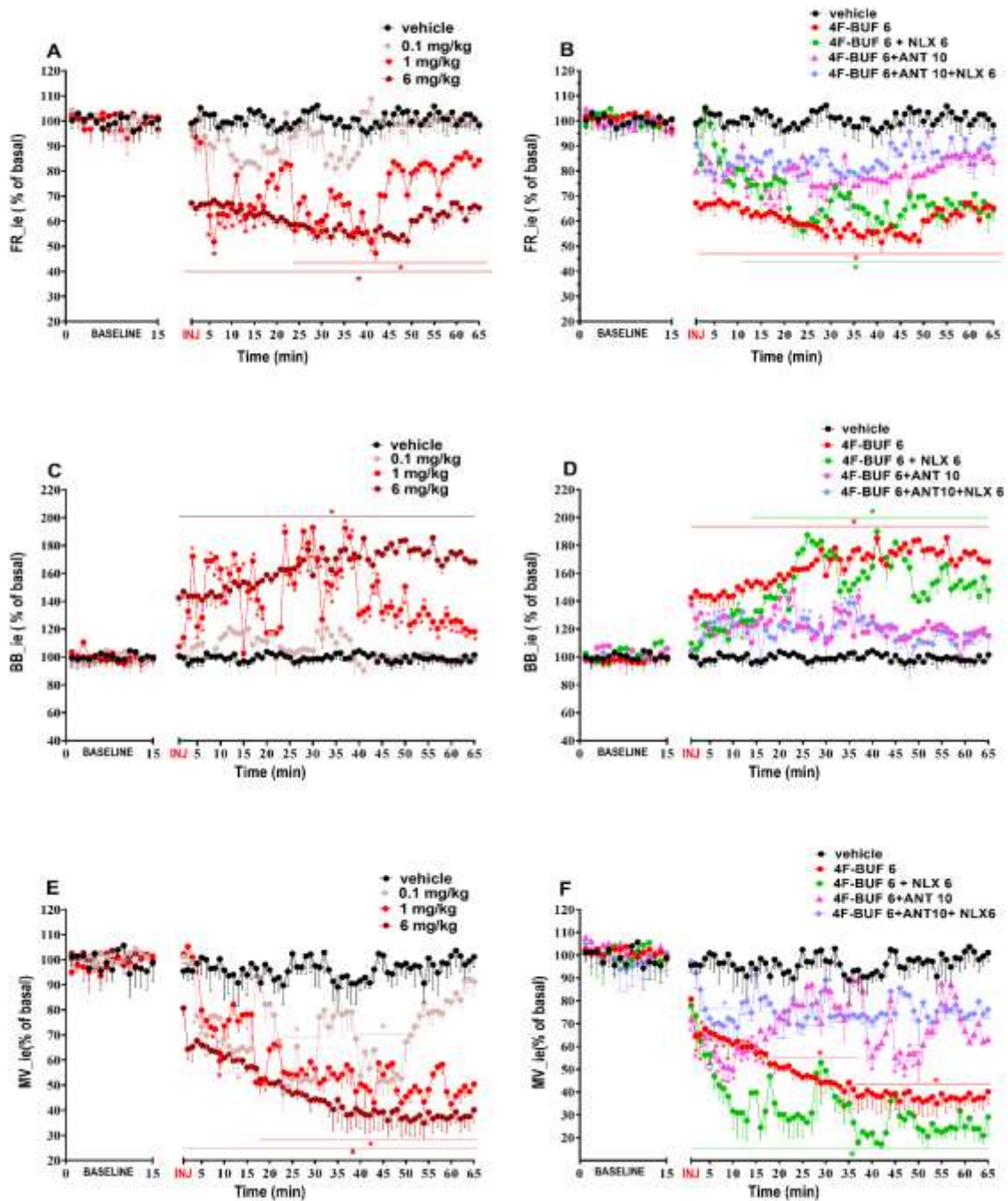
4F-BUTYRYFENTANYL male
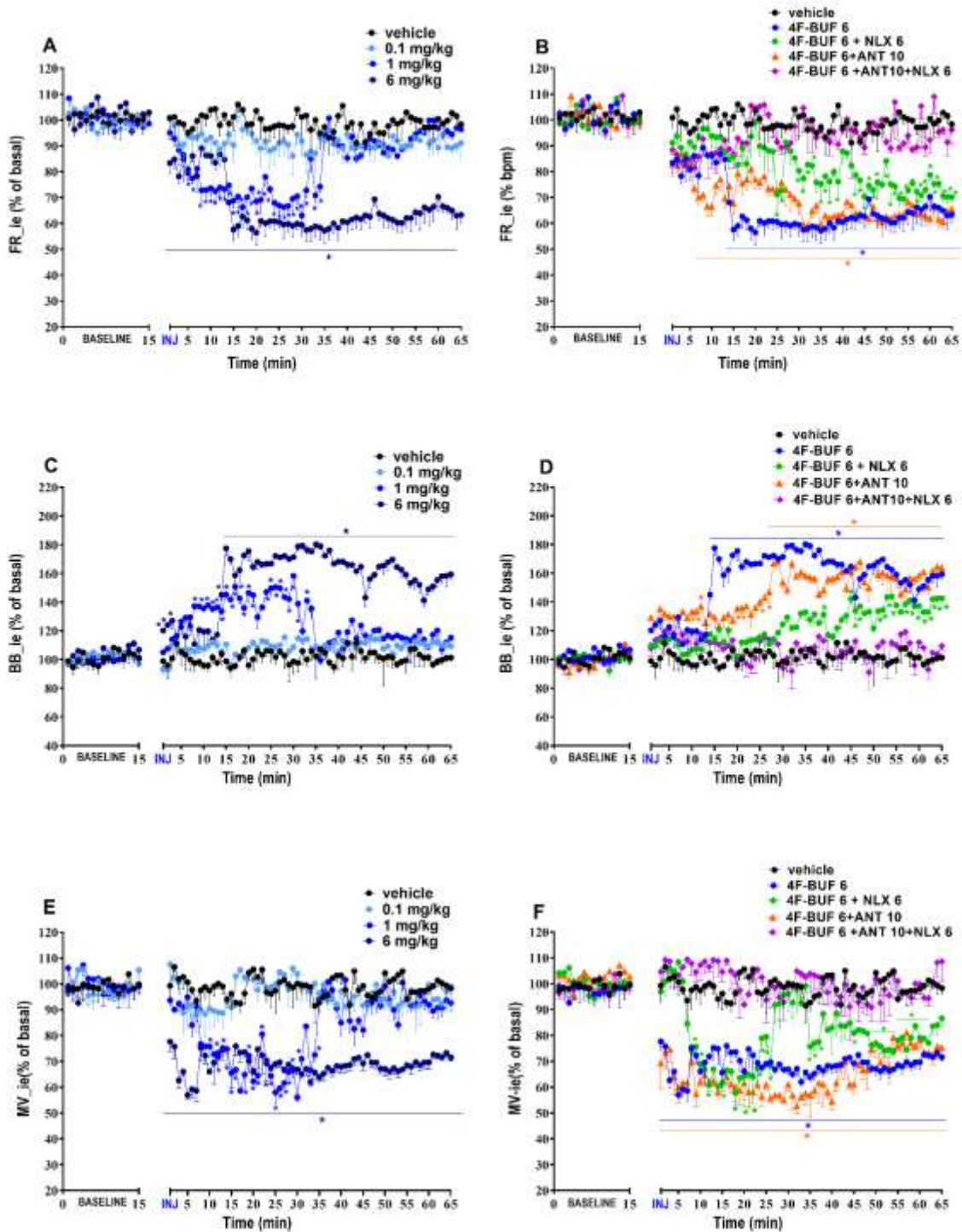
Figure 4.14. *Plethysmography measurements: Systemic administration of 4F-BUF (0.1-6 mg/kg IP) in Breath rate (panel A); Breath length (panel C) and Minute volume (panel E) in male mice. Interaction of effective dose of BUF (6 mg/kg) with the opioid receptor antagonist NLX (6 mg/kg) or the CRF-1 antagonist ANT (10 mg/kg) or their combination (ANT 10 mg/kg+NLX 6 mg/kg); (Panel B, D, F). Data are expressed as percentage of baseline (see materials and methods) and represents the mean ± SEM of 6 determinations for each treatment. Statistical analysis was performed by two-way ANOVA followed by Bonferroni's test for multiple comparisons for the dose-response curve of the compounds at different times (panel A-F). *p<0.05 versus vehicle.*

197

Pre-treatment with NLX alone (6 mg/kg IP); **Fig. 4.14-B**) partially prevented male-4F-BUF respiratory depression while MV reduction was potentiated with NLX (**Fig. 4.14-F**). However, ANT (10 mg/kg IP) alone or ANT (10 mg/kg IP) in combination with NLX (6 mg/kg IP) were effective on preventing the effects of BUF on FR_ie [**Fig 4.14-B**: $F_{3, 2000} = 622.2$, P<0.0001], time [$F_{79, 2000} = 19.15$, P<0.0001] and time × treatment interaction [$F_{316, 2000} = 4.028$, P<0.0001]; BB_ie [**Fig 4.14-D**: $F_{4, 2000} = 952.8$, P<0.0001], time [$F_{79, 2000} = 24.08$, P<0.0001] and time × treatment interaction [$F_{316, 2000} = 6.294$, P<0.0001] and MV [**Fig 4.14-F**: $F_{4, 2000} = 723.2$, P<0.0001], time [$F_{79, 2000} = 13.11$, P<0.0001] and time × treatment interaction [$F_{316, 2000} = 4.592$, P<0.0001].

Comparison of cardiorespiratory response of BUF and 4F-BUF on female and male mice

The comparison of the dose response-curves of BUF and 4F-BUF on female mice revealed significant differences of efficacies between the two compounds on the heart rate (dose of 0.1 mg/kg and 6 mg/kg) and the RR_interval (6 mg/kg) but no differences on the breath rate and the breath length (**see Appendix B Fig. B3**).

The comparison of the dose response-curves of BUF and 4F-BUF on male mice did not show significant differences of the cardiorespiratory parameters with the two compounds acting identically on ECG and PLETH in the dose range examined (**see Appendix B Fig B4**).

Sex differences on the cardiorespiratory responses of BUF

The comparison of the dose response-curves of BUF on female and male mice (**Fig. 4.15**) revealed sex differences in responses to RR_interval [Fig **4.15-B**: $F_{2,60} = 719.4$, P<0.0001], sex [$F_{3, 60} = 381.7$, P<0.0001] and sex × dose interaction [$F_{6, 60} = 483.5$, P<0.0001], respiratory rate [**Fig 4.15-C**: $F_{2, 60} = 124.5$, P<0.0001], sex [$F_{3, 60} = 36.67$, P<0.0001] and sex× dose interaction [$F_{6, 60} = 204,7$, P<0.0001] and breath length [**Fig 4.15-D**: $F_{2, 60} = 1376$, P<0.0001], sex [$F_{3, 60} = 534.6$, P<0.0001] and sex × dose interaction [$F_{6, 60} = 863$, P<0.0001]. However, no sex difference was revealed with BUF on the heart rate.

SEX DIFFERENCES BUTYRYLFENTANYL

*Figure 4.15. Sex differences in the cardiorespiratory response to BUF (0.1-6 mg/kg IP). Panel A: dose-response curves on Heart rate. Panel B: dose-response curves on RR_interval. Panel C: Dose response curves on Breath rate. Panel D: Dose response curves on Breath legth. Data are expressed as percentage of basal value (see material and methods) and represent the mean ± SEM of 6 determinations (female or male) for each treatment. Statistical analysis was performed by two-way ANOVA followed by the Bonferroni's test. *p<0.05 versus vehicle; $p<0.05 versus gender (female/ male).*

Sex differences on the cardiorespiratory responses of 4F-BUF

The comparison of the dose response-curves of 4F-BUF on female and male mice (**Fig 4.16**) revealed sex differences in responses to heart rate [**Fig 4.16-A**: $F_{2, 60}$= 162.8, P<0.0001], sex [$F_{3, 60}$ = 54.22, P<0.0001] and sex × dose interaction [$F_{6, 60}$ = 257, P<0.0001], RR_interval [**Fig 4.16-B**: $F_{2,60}$= 154.4, P<0.0001], dose [$F_{3, 60}$ = 68.39, P<0.0001] and sex × dose interaction [$F_{6, 60}$ = 105.6, P<0.0001], respiratory rate [**Fig 4.16-C**: $F_{2, 60}$ = 189.9, P<0.0001], sex [$F_{3, 60}$ = 57.03, P<0.0001] and sex × dose interaction [$F_{6, 60}$ = 346.4, P<0.0001] and breath length [Fig **4.16-D**: $F_{2, 60}$ = 669.1, P<0.0001], sex [$F_{3, 60}$ = 259.5, P<0.0001] and sex ×dose interaction [$F_{6, 60}$ =424.9, P<0.0001].
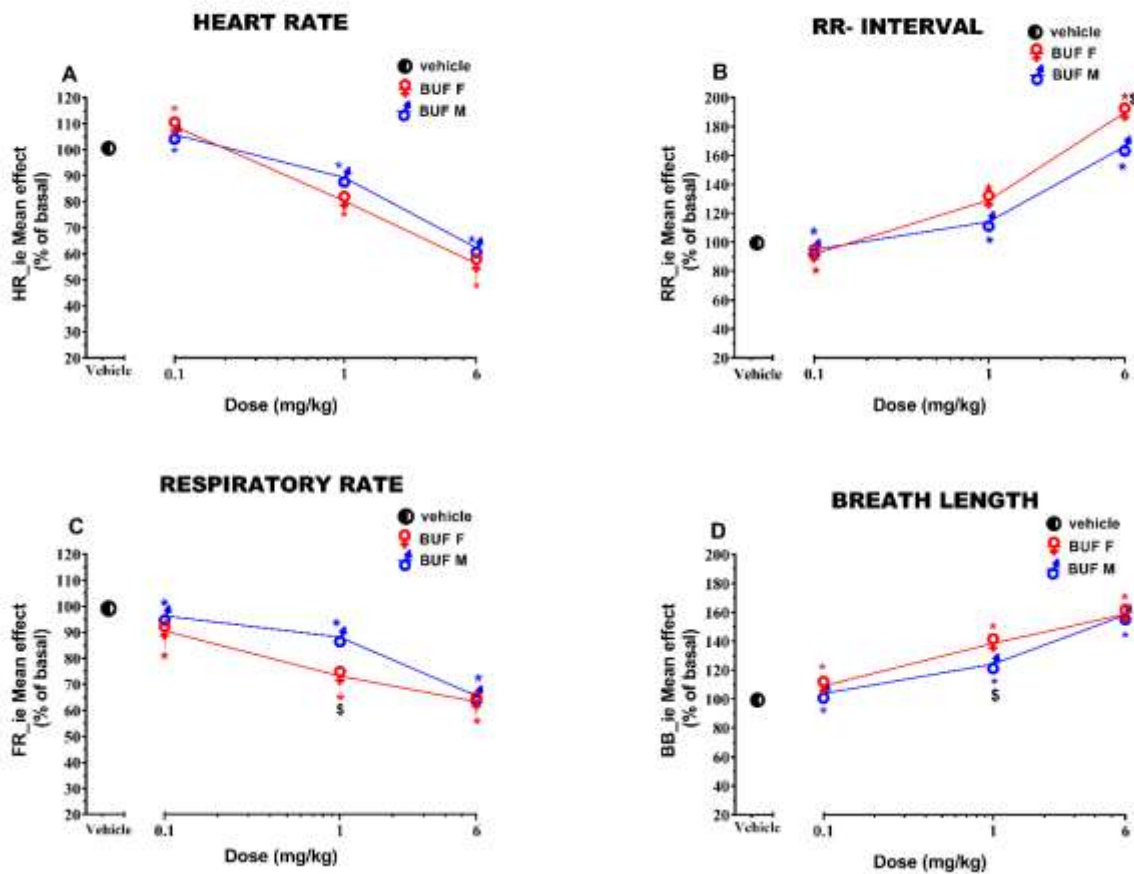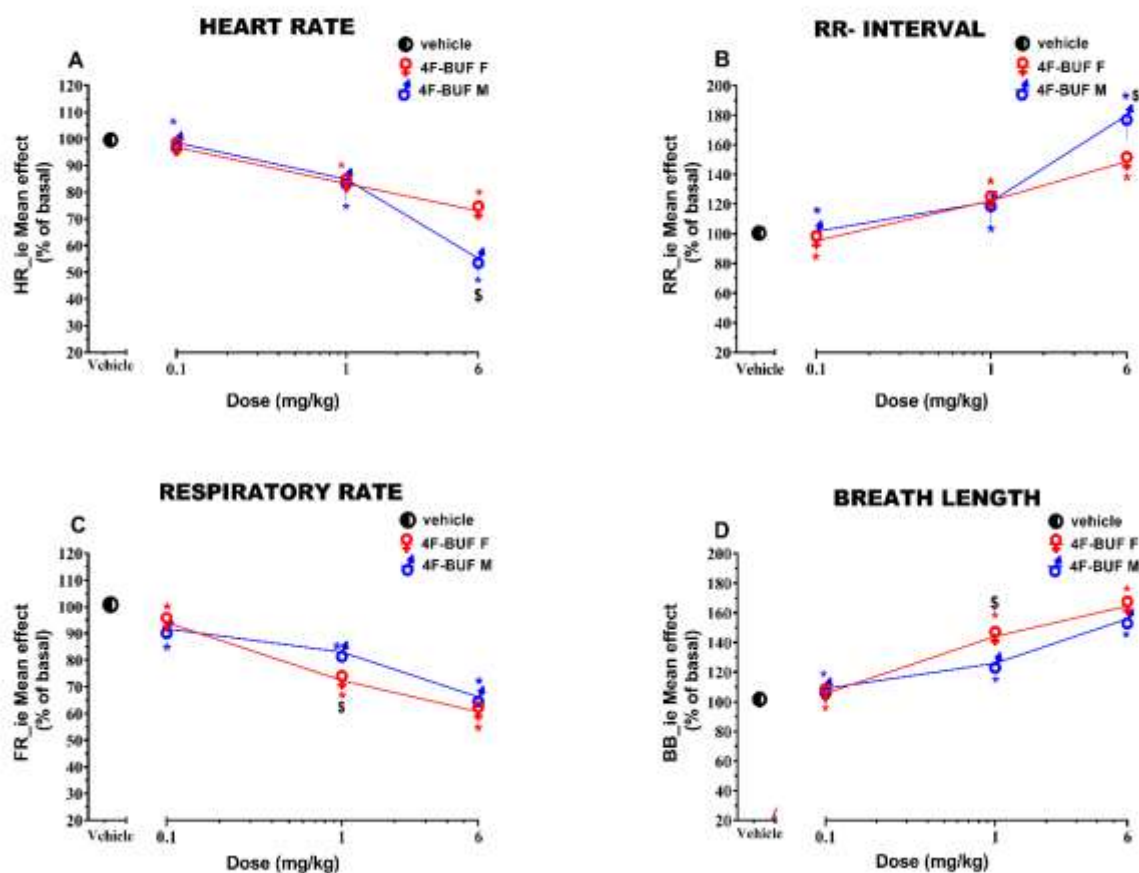
Figure 4.16. *Sex differences in the cardiorespiratory response to 4F-BUF (0.1-6 mg/kg IP). Panel A: dose-response curves on Heart rate. Panel B: dose-response curves on RR_interval. Panel C: Dose response curves on Breath rate. Panel D: Dose response curves on Breath length. Data are expressed as percentage of basal value (see material and methods) and represent the mean ± SEM of 6 determinations (female or male) for each treatment. Statistical analysis was performed by two-way ANOVA followed by the Bonferroni's test. *p<0.05 versus vehicle; $^{\$}$p<0.05 versus gender (female/ male).*

Antagonistic profile of NLX and ANT in cardiorespiratory responses of female and male mice

We illustrated in **Fig. 4.17** the responses of female and male mice to the heart rate and respiratory rate after the pretreatment with NLX and ANT and their combination. In female, Naloxone and the combination of NLX and ANT partially prevented the bradycardia induced by BUF, however with 4F-BUF NLX alone did not have any effect on preventing the bradycardia. and the pretreatment with ANT+NLX increased the reversal effect of NLX (**Fig. 4.17A**). Same effects were seen on the heart rate in male mice. The only difference detected is the higher effect of NLX in reducing the bradycardia induced by 4F-BUF respect to female (**Fig. 4.17-C**).
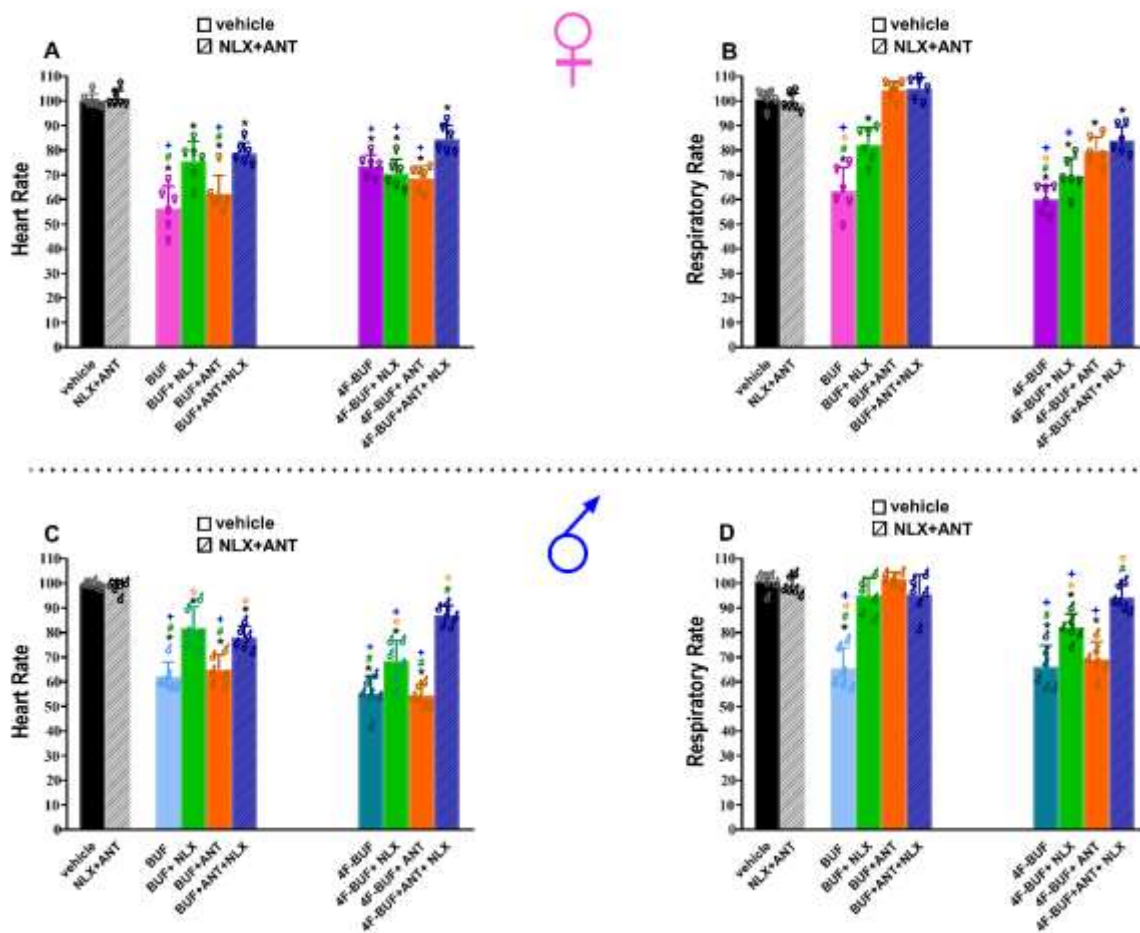
Figure 4.17. *Cardiorespiratory effect of BUF and 4-BUF (6 mg/kg IP) and their interaction with NLX (6 mg/kg), ANT (10 mg/kg) or the combination (ANT 10 mg/kg) + NLX (6 mg/kg) in. Panel A: dose-response curves on Heart rate. Panel B: dose-response curves on RR_interval. Panel C: Dose response curves on Breath rate. Panel D: Dose response curves on Breath length. Data are expressed as percentage of basal value (see material and methods) and represent the mean ± SEM of 6 determinations (female or male) for each treatment. Statistical analysis was performed by two-way ANOVA followed by the Bonferroni's test. *p<0.05 versus vehicle; $^{\$}$p<0.05 versus gender (female/ male).*

The combination of NLX and ANT totally blocked the bradycardia of 4F-BUF in male mice and no significance was detected in comparison to vehicle (**Fig. 4.17-C**). In case of respiratory depression, NLX alone partially blocked the effect of BUF in female and totally in male. ANT alone was more effective than NLX pre-treatment and it prevented totally the respiratory depression induced by BUF in females (**Fig. 4.17-B**). In male mice ANT alone also was effective to prevent the respiratory depression induced by BUF (**Fig. 4.17-B**). This was not the case in animals treated with 4F-BUF. In female NLX blockade was slightly effective in reducing the respiratory reduction induced by 4F-BUF. Also, ANT alone did not block this effect and the combination of NLX and ANT was more effective than the single treatments of

201

the antagonists but kept significant respect to vehicle (**Fig. 4.17-B**). The same effects were seen in case of male mice treated with NLX or ANT alone. However, the combination of ANT+NLX totally prevented the respiratory depression induced by 4F-BUF in males (**Fig. 4.17-D**).

4.2.5 Discussion

Our study presents novel results regarding the *in vitro* and *in vivo* characterization of BUF and 4F-BUF, two fentanyl analogues that have been emerged as NSO. *In vitro*, in the calcium mobilization assay BUF and its fluorinated analogue were able to activate the mu opioid receptor in a concentration dependent manner and BUF was able to elicit maximal effects similar to that of dermorphin and fentanyl while 4F-BUF behaved as a partial agonist. In the BRET G-protein assay, the two compounds mimicked the maximal effects of dermorphin. BUF behaved similarly to fentanyl as partial agonist for the β-arrestin 2 pathway whereas 4F-BUF was inactive in promoting β-arrestin 2 recruitment. *In vivo*, the two compounds impaired cardiorespiratory parameters in mice and sex differences were detected at the highest dose for the cardiac responses and at the lower dose (1 mg/kg) for the respiratory responses. 4F-BUF showed lower potency for inhibiting cardiorespiratory function. NLX sensitivity of the actions of the two compounds was variable in cardiac and respiratory responses. Interestingly the CRF-1 antagonist ANT alone was effective to block the respiratory impairment induced by BUF in both sexes but not 4F-BUF. The combination of NLX and ANT significantly enhanced the action of NLX reversal of the cardiorespiratory impairments induced by BUF and 4F-BUF in female and male CD1 mice.

Comparison of the cardiorespiratory responses between BUF and 4F-BUF

Many preclinical studies have been recently conducted to evaluate the cardiorespiratory effects of fentanyl analogues (Bilel et al., 2022; Varshneya et al., 2023). BUF and 4F-BUF reduced the cardiorespiratory responses at intermediate and high doses (1 and 6 mg/kg). The effect of BUF seemed to be more profound at the highest dose tested in both sexes. Moreover, only with BUF (6 mg/kg) we detected arrythmia and apnea at 10 min after injection in female and male mice (**Appendix B Fig. B3**). 4F-BUF differs from BUF with the para-fluoro substitution on the phenethylamine backbone. Interestingly this chemical modification could change the the potency and efficacy of the compound. Indeed, *Varshneya et al*, (Varshneya et al., 2023) revealed in their recent elegant study that BUF showed higher effectiveness in reducing Minute

volume (Whole body plethysmography) when compared to 4F-BUF (para-fluorobutyrylfentanyl). Our results confirm the findings of *Varshneya et al,* on the higher potency of BUF respect to 4F-BUF and shed light on the role of fluorine substitution on BUF's mu opioid receptors -mediated cardiorespiratory effects (Varshneya et al., 2023). Additionally, our *in vitro* data showed that the two compounds have different ability to promote receptor interaction with arrestin; in fact, BUF behaved as partial agonist while 4F-BUF as an antagonist. Yet, this difference could have an important impact on the intensity of the physiological responses triggered by mu ligands as seen with other fentanyl analogues such as Furanylfentanyl (Bilel et al., 2022) and Carfentanil (Ramoz-Gonzalez et al., 2022).

Sex differences on the cardiorespiratory responses of BUF and 4F-BUF

Many recent clinical reports confirmed that men have higher prevalence of opioid use than women (Walter et al., 2022). In addition, men need higher opioid doses to reach the same pharmacological effects of that reached in women (Lee et al., 2013). These data may explain the increasing rate of death with overdose among young-adult men rather than women (Wilson et al., 2020). Death rate with fentanyl overdose was reported to be two to three times higher for men than women (Butelman et al.,2023), however, the incidence of opioid use disorders and death with overdose by synthetic opioids has increased in woman (Barbosa-Leiker et al., 2021; VanHouten et al., 2019). The primary cause of death from fentanyl and its analogues overdose is respiratory depression and hypoxia.

We evaluated the cardiorespiratory effects of two fentanyl analogs in female and male mice. We found sex difference on the cardiac responses (RR_interval) with BUF, where female showed higher responses at the highest dose tested than male. In addition, also females showed higher sensitivity in the respiratory depression and hypoventilation at the intermediate dose when compared to male (1 mg/kg). Most of the studies on the respiratory effects of opioids are performed in male rodents and the respiratory effects of BUF and 4F-BUF measured in male are very similar to fentanyl (Varshneya et al., 2023). In addition, a recent study in female and male rats injected with increasing doses of fentanyl showed a higher respiratory sensitivity of the female respect to male rats. In particular, female rats showed greater maximum effect on minute ventilation and peak inspiratory flow and longer-lasting respiratory depressing effects than male (Marchette et al., 2023). These results are in accordance with our results on the sex-respiratory differences induced by BUF and 4F-BUF (1 mg/kg). While the respiratory responses clearly demonstrate a higher sensitivity of female than male mice, the results obtain

on the cardiac responses are somewhat different. In fact, in the case of BUF (6 mg/kg), female mice showed higher increase of RR_interval compared to male. Conversely, with 4F-BUF (6 mg/kg) male mice showed slightly higher cardiac sensitivity respect to female. It is noteworthy that difference on cardiac versus respiratory responses between female and male rodents have been also reported with fentanyl. In particular, *Haile et al.*, measured the physiological effects of FEN (0.1 mg/kg) in a set of male and female Sprague-Dawley rats using the pulse oximetry system (Haile et al., 2022). They found out that fentanyl significantly decreased oxygen saturation, heart rate, and general activity in male rats. However, in female rats, only oxygen saturation was significantly decreased by the same dose of fentanyl. Adding to our findings, these results reveal sex-dependent effects of fentanyl and fentanyl analogs (Kaplovitch et al., 2015, Towers et al., 2022). The sex differences observed in our results might be explained by differences on mu distribution between female and male animals (Zhang et al., 2013) and the influence of circulating ovarien hormones and androgens on mu-mediated physiological responses (reviewed in Sharp et al., 2022).

Role of Naloxone and Antalarmin in MOR and CRF-1 mediated cardiorespiratory effects of BUF and 4F-BUF

Following on our previous study on fentanyl analogs (Bilel et al., 2022), we here demonstrated that BUF and 4F-BUF impaired cardiorespiratory activity when administered to female and male mice at the range dose 0.1-6 mg/kg. Both compounds reduced heart rate, increased RR_interval and QRS complex, reduced the breath rate, increased breath length and reduced minute volume. The mechanism by which opioid agonists induce bradycardia, respiratory depression and hypoventilation have been previously detailed (Bilel et al., 2020; Bilel et al 2022, Varshneya et al., 2023). Naloxone pretreatment (6 mg/kg) partially prevented the cardiorespiratory impairment induced by BUF and 4F-BUF. These results are in accordance with several preclinical (Bilel et al., 2022; Haile et al., 2022; Varshneya et al., 2021; Varshneya et al., 2023) and clinical reports (Amaducci 2023; Krantz et al., 2021; Rzasa Lynn & Galinkin, 2018) that proving the necessity of naloxone redosing to reverse cardiorespiratory alterations of fentanyl or its analogs.

In the search of other mechanisms such as stress that might be triggered by the activation of MOR-receptors which results in undesired effects specifically cardiorespiratory depression, we investigate the possible role played by CRF-1 receptors in the physiological responses induced by the opioid agonist as seen with opioids withdrawal and dependance (Papaleo et al., 2007. To the best of our knowledge this is the first study investigating the possible involvement of

the stress-factor in worsening cardio-respiratory impairments related to opioids in female and male animals using Antalarmin in pre-treatment alone or in combination with NLX. Unexpectedly, our results revealed that ANT alone is able to block the respiratory depression induced by BUF (6 mg/kg) in female and male mice but not in case of 4F-BUF. In addition, the pretreatment with ANT and NLX enhanced the reversal action of NLX. While the mechanism by which opioids could activate the CRF-1 receptors is not clearly investigated, it is worth highlighting that CRF receptors and mu are co-localized in the nucleus locus coeruleus (LC) of rodents (Reyes et al., 2006. This may possibly explain the direct interaction of the opioidergic and noradrenergic systems in response to stress stimulus activated by opioids agonists (Guajardo et al., 2021. The effectiveness of ANT alone in blocking respiratory depression in male and female mice treated with BUF but not the fluorinated (4F-BUF) raises several questions that need further investigations, however it is possible to speculate that CRF-1 receptor could be in response to β-arrestin 2 intracellular signaling resulting in deep respiratory depression of mu biased agonists (Ramos-Gonzalez et al., 2022). Adding to that the block of CRF-1 receptors enhances positively the reversal effect of naloxone in cardiac and respiratory responses. These findings corroborate the hypothesis on the role of stress-factor in worsening the acute cardio-respiratory impairment triggered by the potent synthetic opioids and in particular the class of fentanyl analogs (Algera et al., 2018)

4.2.6 Conclusions

The present study revealed that BUF behaves similarly to FENT as mu-agonist. In contrast to BUF, 4F-BUF acts as a partial agonist *in vitro* at mu opioid receptors, and as G protein biased mu agonist. *In vivo* the two compounds induced cardiorespiratory impairments in female and male mice with a higher sensitivity of female in respiratory depression. In this study, we have uncovered a novel mechanism by which synthetic opioids might increase respiratory depression shedding new light on the role of CRF-1 receptors win cardiorespiratory impairments by mu-agonists. This finding increases our understanding of mu-mediated mechanisms and may have implications for antidotal therapies in case of overdose with synthetic opioids.

4.2.7 Funding sources

4.2.8 Conflict of interest:

The Authors declare no conflict of interest.

4.2.9 Ethical statements:

All applicable international, national and/or institutional guidelines for the care and use of animals were followed. All procedures performed in the studies involving animals were in accordance with the ethical standards of the institution or practice at which the studies were conducted. Project activated in collaboration with the Presidency of the Council of Ministers-DPA Anti-Drug Policies (Italy)

4.2.10 Author contributions

This work was conceptualized by M.M and **B.S**. A.N.G and D.M conducted *in vitro* receptor activation and radioligand binding experiments. **B.S**, T.M, C.G, B.M conducted *in vivo* experiments. F.A conducted statistical analysis. M.M. and **B.S** contributed to the final edition of *in vivo* results and discussion. **B.S** drafted the manuscript, which was critically revised by M.M., G.C, T.C and S.G. All authors approved the final version of the manuscript for publication and agree to be held accountable for all aspects of the work related to accuracy or integrity.

4.2.11 References:

1. Algera, M. H., Kamp, J., van der Schrier, R., van Velzen, M., Niesters, M., Aarts, L., Dahan, A., & Olofsen, E. (2019). Opioid-induced respiratory depression in humans: a review of pharmacokinetic-pharmacodynamic modelling of reversal. *British journal of anaesthesia*, *122*(6), e168–e179. https://doi.org/10.1016/j.bja.2018.12.023
2. Bäckberg, M., Beck, O., Jönsson, K. H., & Helander, A. (2015). Opioid intoxications involving butyrfentanyl, 4-fluorobutyrfentanyl, and fentanyl from the Swedish STRIDA project. *Clinical toxicology (Philadelphia, Pa.)*, *53*(7), 609–617. https://doi.org/10.3109/15563650.2015.1054505
3. Barbosa-Leiker, C., Campbell, A. N. C., McHugh, R. K., Guille, C., & Greenfield, S. F. (2021). Opioid Use Disorder in Women and the Implications for Treatment. *Psychiatric research and clinical practice*, *3*(1), 3–11. https://doi.org/10.1176/appi.prcp.2019005
4. Broadbear, J. H., Winger, G., Rivier, J. E., Rice, K. C., & Woods, J. H. (2004). Corticotropin-releasing hormone antagonists, astressin B and antalarmin: differing profiles of activity in rhesus monkeys. *Neuropsychopharmacology : official publication of the American College of Neuropsychopharmacology*, *29*(6), 1112–1121. https://doi.org/10.1038/sj.npp.1300410
5. Camarda, V., Calo, G., 2013. Chimeric G proteins in fluorimetric calcium assays: experience with opioid receptors. Methods Mol. Biol. 937, 293–306. https://doi.org/10.1007/978-1-62703-086-1_18.
6. Drug Enforcement Administration, Department of Justice. Schedules of controlled substances: temporary placement of butyryl fentanyl and beta-hydroxythiofentanyl into Schedule I (2016). Final order.Fed. Regist., 81, 29492–29496.
7. Ducottet, C., Griebel, G., & Belzung, C. (2003). Effects of the selective nonpeptide corticotropin-releasing factor receptor 1 antagonist antalarmin in the chronic mild stress model of depression in mice. *Progress in neuro-psychopharmacology & biological psychiatry*, *27*(4), 625–631. https://doi.org/10.1016/S0278-5846(03)00051-4
8. EMCDDA, 2015. European Drug Report 2015: Trends and Developments. Luxembourg:
9. EMCDDA, 2022. European Drug Report 2022: Trends and Developments. Luxembourg:

10. Fattore, L., Marti, M., Mostallino, R., & Castelli, M. P. (2020). Sex and Gender Differences in the Effects of Novel Psychoactive Substances. *Brain sciences*, *10*(9), 606. https://doi.org/10.3390/brainsci10090606
11. Guajardo, H. M., & Valentino, R. J. (2021). Sex differences in μ-opioid regulation of coerulear-cortical transmission. *Neuroscience letters*, *746*, 135651. https://doi.org/10.1016/j.neulet.2021.135651
12. Haile, C. N., Baker, M. D., Sanchez, S. A., Lopez Arteaga, C. A., Duddupudi, A. L., Cuny, G. D., Norton, E. B., Kosten, T. R., & Kosten, T. A. (2022). An Immunconjugate Vaccine Alters Distribution and Reduces the Antinociceptive, Behavioral and Physiological Effects of Fentanyl in Male and Female Rats. Pharmaceutics, 14(11), 2290. https://doi.org/10.3390/pharmaceutics14112290
13. Heinrichs, S. C., Menzaghi, F., Schulteis, G., Koob, G. F., & Stinus, L. (1995). Suppression of corticotropin-releasing factor in the amygdala attenuates aversive consequences of morphine withdrawal. *Behavioural pharmacology*, *6*(1), 74–80.
14. Kaplovitch, E., Gomes, T., Camacho, X., Dhalla, I. A., Mamdani, M. M., & Juurlink, D. N. (2015). Sex Differences in Dose Escalation and Overdose Death during Chronic

Opioid Therapy: A Population-Based Cohort Study. *PloS one*, *10*(8), e0134550. https://doi.org/10.1371/journal.pone.0134550 \

15. Krantz MJ, Palmer RB, Haigney MCP. Cardiovascular Complications of Opioid Use: JACC State-of-the-Art Review. J Am Coll Cardiol. 2021 Jan 19;77(2):205-223. doi: 10.1016/j.jacc.2020.11.002. PMID: 33446314

16. Kenakin, T. (2004). *A Pharmacology Primer*. Elsevier Academic Press, San Diego.

17. Lee CW-S, Ho I-K. Sex Differences in Opioid Analgesia and Addiction: Interactions among Opioid Receptors and Estrogen Receptors. Molecular Pain. 2013;9. doi:10.1186/1744-8069-9-45

18. Malfacini, D., Ambrosio, C., Gro', M. C., Sbraccia, M., Trapella, C., Guerrini, R., et al (2015). Pharmacological profile of nociceptin/orphanin FQ receptors interacting with G-proteins and b-arrestins 2. PLoS One 10:e132865. doi: 10.1371/journal.pone.0132865

19. Marchette, R. C. N., Carlson, E. R., Frye, E. V., Hastings, L. E., Vendruscolo, J. C. M., Mejias-Torres, G., Lewis, S. J., Hampson, A., Volkow, N. D., Vendruscolo, L. F., & Koob, G. F. (2023). Heroin- and Fentanyl-Induced Respiratory Depression in a Rat Plethysmography Model: Potency, Tolerance, and Sex Differences. *The Journal of pharmacology and experimental therapeutics*, *385*(2), 117–134. https://doi.org/10.1124/jpet.122.001476

20. Molinari P, Vezzi V, Sbraccia M, Grò C, Riitano D, Ambrosio C, Casella I, Costa T. Morphine-like opiates selectively antagonize receptor-arrestin interactions. J Biol Chem. 2010 Apr 23;285(17):12522-35. doi: 10.1074/jbc.M109.059410. Epub 2010 Feb 26. PMID: 20189994; PMCID: PMC2857100.

21. Neubig, R. R., Spedding, M., Kenakin, T., and Christopoulos, A. (2003). International union of pharmacology committee on receptor nomenclature and drug classification. XXXVIII. Update on terms and symbols in quantitative pharmacology. Pharmacol. Rev. 55, 597–606. doi: 10.1124/pr.55.4.4

22. Papaleo, F., Kitchener, P., & Contarino, A. (2007). Disruption of the CRF/CRF1 receptor stress system exacerbates the somatic signs of opiate withdrawal. *Neuron*, *53*(4), 577–589. https://doi.org/10.1016/j.neuron.2007.01.022

23. Ramos-Gonzalez, N., Groom, S., Sutcliffe, K. J., Bancroft, S., Bailey, C. P., Sessions, R. B., Henderson, G., & Kelly, E. (2023). Carfentanil is a β-arrestin-biased agonist at the μ opioid receptor. British journal of pharmacology, 180(18), 2341–2360. https://doi.org/10.1111/bph.16084

24. Reyes, B. A., Glaser, J. D., & Van Bockstaele, E. J. (2007). Ultrastructural evidence for co-localization of corticotropin-releasing factor receptor and mu-opioid receptor in the rat nucleus locus coeruleus. *Neuroscience letters*, *413*(3), 216–221. https://doi.org/10.1016/j.neulet.2006.11.069

25. Richeval C, Baillieux M, Pawlak G, Phanithavong M, Wiart J-f, Humbert L, Batisse A, Lamoureux C, Pfau G, Nefau T, Allorge D, Gaulier J-M (2019) Benzoylfentanyl and parafluorobutyrfentanyl: some analytical and metabolism data. Toxicol Anal Clin 31:258–267. https://doi.org/10.1016/j.toxac.2019.01.004

26. Rzasa Lynn R, Galinkin JL. Naloxone dosage for opioid reversal: current evidence and clinical implications. Ther Adv Drug Saf. 2018 Jan;9(1):63-88. doi:

27. Shaham, Y., Erb, S., Leung, S., Buczek, Y., & Stewart, J. (1998). CP-154,526, a selective, non-peptide antagonist of the corticotropin-releasing factor1 receptor attenuates stress-induced relapse to drug seeking in cocaine- and heroin-trained rats. *Psychopharmacology*, *137*(2), 184–190. https://doi.org/10.1007/s002130050608

28. Sharp, J. L., Pearson, T., & Smith, M. A. (2022). Sex differences in opioid receptor mediated effects: Role of androgens. *Neuroscience and biobehavioral reviews*, *134*, 104522. https://doi.org/10.1016/j.neubiorev.2022.104522

29. Sharp, J. L., Pearson, T., & Smith, M. A. (2022). Sex differences in opioid receptor mediated effects: Role of androgens. *Neuroscience and biobehavioral reviews*, *134*, 104522. https://doi.org/10.1016/j.neubiorev.2022.104522

30. Staeheli, S. N., Baumgartner, M. R., Gauthier, S., Gascho, D., Jarmer, J., Kraemer, T., & Steuer, A. E. (2016). Time-dependent postmortem redistribution of butyrfentanyl and its metabolites in blood and alternative matrices in a case of butyrfentanyl intoxication. *Forensic science international*, *266*, 170–177. https://doi.org/10.1016/j.forsciint.2016.05.034

31. Steuer, A. E., Williner, E., Staeheli, S. N., & Kraemer, T. (2017). Studies on the metabolism of the fentanyl-derived designer drug butyrfentanyl in human in vitro liver preparations and authentic human samples using liquid chromatography-high resolution mass spectrometry (LC-HRMS). *Drug testing and analysis*, *9*(7), 1085–1092. https://doi.org/10.1002/dta.2111

32. Stinus, L., Cador, M., Zorrilla, E. P., & Koob, G. F. (2005). Buprenorphine and a CRF1 antagonist block the acquisition of opiate withdrawal-induced conditioned place aversion in rats. *Neuropsychopharmacology : official publication of the American College of Neuropsychopharmacology*, *30*(1), 90–98. https://doi.org/10.1038/sj.npp.1300487

33. Towers, E. B., Setaro, B., & Lynch, W. J. (2022). Sex- and Dose-Dependent Differences in the Development of an Addiction-Like Phenotype Following Extended-Access Fentanyl Self-Administration. *Frontiers in pharmacology*, *13*, 841873. https://doi.org/10.3389/fphar.2022.841873

34. UNDOC 2023: World drug report: Executive summary

35. Vachon, L., Costa, T., & Herz, A. (1987). Opioid receptor desensitization in NG 108-15 cells. Differential effects of a full and a partial agonist on the opioid-dependent GTPase. *Biochemical pharmacology*, *36*(18), 2889–2897. https://doi.org/10.1016/0006-2952(87)90199-7

36. VanHouten JP, Rudd RA, Ballesteros MF, et al: Drug overdose deaths among women aged 30-64 Years-United States, 1999-2017. *MMWR Morb Mortal Wkly Rep* 2019; 68(1):1–5

37. Varshneya, N. B., Hassanien, S. H., Holt, M. C., Stevens, D. L., Layle, N. K., Bassman, J. R., Iula, D. M., & Beardsley, P. M. (2023). Fentanyl analog structure-activity relationships demonstrate determinants of diverging potencies for antinociception and respiratory depression. Pharmacology, biochemistry, and behavior, 226, 173572. https://doi.org/10.1016/j.pbb.2023.173572

38. Walter, L. A., Bunnell, S., Wiesendanger, K., & McGregor, A. J. (2022). Sex, gender, and the opioid epidemic: Crucial implications for acute care. AEM education and training, 6(Suppl 1), S64–S70. https://doi.org/10.1002/aet2.10756

39. Wilson, N., Kariisa, M., Seth, P., Smith, H., 4th, & Davis, N. L. (2020). Drug and Opioid-Involved Overdose Deaths - United States, 2017-2018. *MMWR. Morbidity and mortality weekly report*, *69*(11), 290–297. https://doi.org/10.15585/mmwr.mm6911a4

40. Zhang, X., Zhang, Y., Asgar, J., Niu, K. Y., Lee, J., Lee, K. S., Schneider, M., & Ro, J. Y. (2014). Sex differences in μ-opioid receptor expression in trigeminal ganglia under a myositis condition in rats. *European journal of pain (London, England)*, *18*(2), 151–161. https://doi.org/10.1002/j.1532-2149.2013.00352.x

Chapter 5 Ongoing Results

5.1 Effect of high dose of fentanyl and fentanyl analogs in cardiorespiratory function of mice: physiological and histological analyses

[1]**Bilel Sabrine**, [1]Tirri Micaela, [1]Corli Giorgia, [1]Marta Bassi, [2]Frisoni Paolo, [3]Neri Margherita [1]Marti Matteo.

[1]*Department of Translational Medicine, Section of Legal Medicine and LTTA Centre, University of Ferrara, Italy*
[2]*Unit of Legal Medicine, AUSL of Ferrara, Italy*
[3]*Department of Medical Sciences, Section of Legal Medicine, University of Ferrara, Italy*

5.1.1 Background

In continuation to my study (Bilel et al., 2022), I have been focusing on the evaluation of the effects of a high dose (15 mg/kg) of Fentanyl and its analogs (Acrylfentanyl, Furanylfentanyl and Furanylfentanyl) on the cardiorespiratory function of mice (heart rate, pulse distention, breath rate and oxygen saturation). Additionally, I have evaluated histological changes on brain, heart, and lungs using immunohistochemistry to better understand the pathology of these drugs in forensic cases.

5.1.2 Materials and methods

5.1.2.1 Animals

Male ICR (CD-1®) mice weighing 30–35 g (Centralized Preclinical Research Laboratory, University of Ferrara, Italy) were group housed (5 mice per cage; floor area per animal was 80 cm2; minimum enclosure height was 12 cm), exposed to a 12:12-h light-dark cycle (light period from 6:30 AM to 6:30 PM) at a temperature of 20–22 °C and humidity of 45–55% and were provided ad libitum access to food (Diet 4RF25 GLP; Mucedola, Settimo Milanese, Milan, Italy) and water. The experimental protocols performed in the present study were in accordance with the U.K. Animals (Scientific Procedures) Act of 1986 and associated guidelines and the new European Communities Council Directive of September 2010 (2010/63/EU). Experimental protocols were approved by the Italian Ministry of Health (license

n. 223/2021-PR, CBCC2.46. EXT.21) and by the Animal Welfare Body of the University of Ferrara. According to the ARRIVE guidelines, all possible efforts were made to minimise the number of animals used, to minimise the animals' pain and discomfort.

5.1.2.2 Drug preparation

Drugs were dissolved in saline solution (0.9% NaCl) that was also used as vehicle. Animals were injected intraperitoneally (at a volume of 4 μl/g), with a dose of 15 mg/kg of fentanyl or Acrylfentanyl or Furanylfentanyl.

5.1.2.3 Evaluation of core body temperature

The core temperature was evaluated by a probe (1 mm diameter) that was gently inserted, after lubrication with liquid vaseline, into the rectum of the mouse (to about 2 cm) and left in position until the stabilization of the temperature (about 10 sec; Vigolo et al., 2015). The probe was connected to a Cole Parmer digital thermometer, model 8402.

5.1.2.4 Cardiorespiratory analysis

The experimental protocol to detect the cardiorespiratory parameters used in this study is designed to monitor awake and freely moving animals with no invasive instruments and with minimal handling (Bilel et al., 2022). A collar was placed around the neck of the animal; this collar has a sensor that continuously detects heart rate (HR), breath rate (BR), oxygen saturation (SpO_2) and pulse distention (μm) with a frequency of 15 Hz. While running the experiment, the mouse moves freely in the cage (with no access to food and water) monitored by the sensor collar using the software MouseOx Plus (STARRLife Sciences® Corp. Oakmont, PA). In the first hour, a collar was placed around the animal's neck to simulate the real one used in the test, thus minimizing the possible effects of stress during the experiment. The real collar (with sensor) was then substituted, and baseline parameters were monitored for 60 min. Subsequently, the mice were given fentanyl, Acrylfentanyl and Furanylfentanyl by intraperitoneal injection, and data was recorded for 5 h.

5.1.2.5 Statistical analysis

Core temperature values are expressed as the difference between control temperature (before injection) and temperature following drug administration (Δ°C) and calculated as maximal

possible effect: {EMax%= [(test T° - control T°)/ (cut off T° - control T°)] X 100. Data are expressed in percentage of basal value [heart rate (expressed as heart beats per min bpm), breath rate (expressed as breath per minute brpm) pulse distention (vessel diameter changes expressed as μm), respiratory rate (expressed as respiratory rate per minute rpm) and SpO$_2$ saturation (oxygen blood saturation expressed as %)]. Data in both tests are presented as mean effect (% of basal) of 5 h measurement in each test.

5.1.2.6 Histological Analysis

Mice brains, hearts and lungs were removed and fixed in 10% buffered formalin for 48 h. Each fixed organ was then dissected (Corli et al., 2023). Each of the sections was then processed for paraffin inclusion. Paraffin-embedded tissue specimens were sectioned at 5 μm, and then haematoxylin and eosin stain were performed. the sections were then observed under optical microscope (Nikon Eclipse E90i; Nikon, Roma, Italy).

5.1.3 Results and discussion
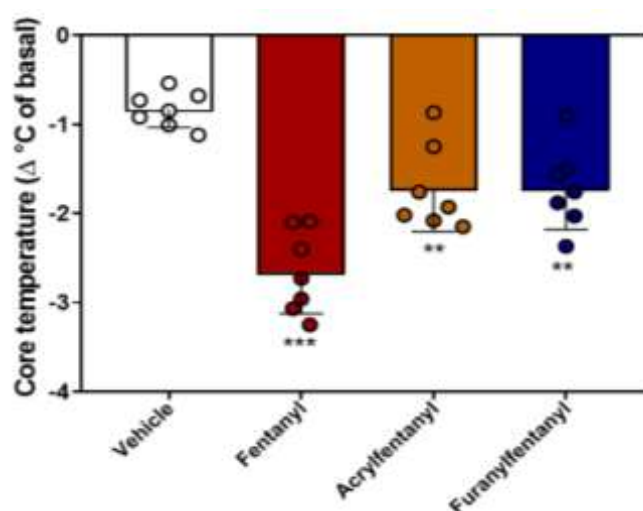
Figure 5.1. *Effect of Fentanyl, Acrylfentanyl and Furanylfentanyl (15 mg/kg. IP) on the core temperature. Data are expressed as mean ± SEM (n = 8/ group). Statistical analysis was performed by One-way ANOVA followed by Bonferroni's test for multiple comparisons. **p<0.01, ***p<0.001 versus vehicle.*

The systemic administration of vehicle induced a slight decrease of core temperature in mice (**Figure 5.1**). The systemic administration of fentanyl, Acrylfentanyl and Furnylfentanyl (15 mg/kg) induced a significant [F $_{(3, 24)}$ = 21.93; P<0.0001] decrease of the core temperature

during the 5 hours of monitoring and this effect was deeper in case of fentanyl with respect to the other tested compounds.

The systemic administration of vehicle did not alter the cardiorespiratory function of mice during the 5 hours of monitoring (**Figure 5.2**). The systemic administration of high dose (15mg/kg IP) of fentanyl and its analogs (Acrylfentanyl and Furanylfentanyl) induced important variation of the cardiorespiratory parameters.
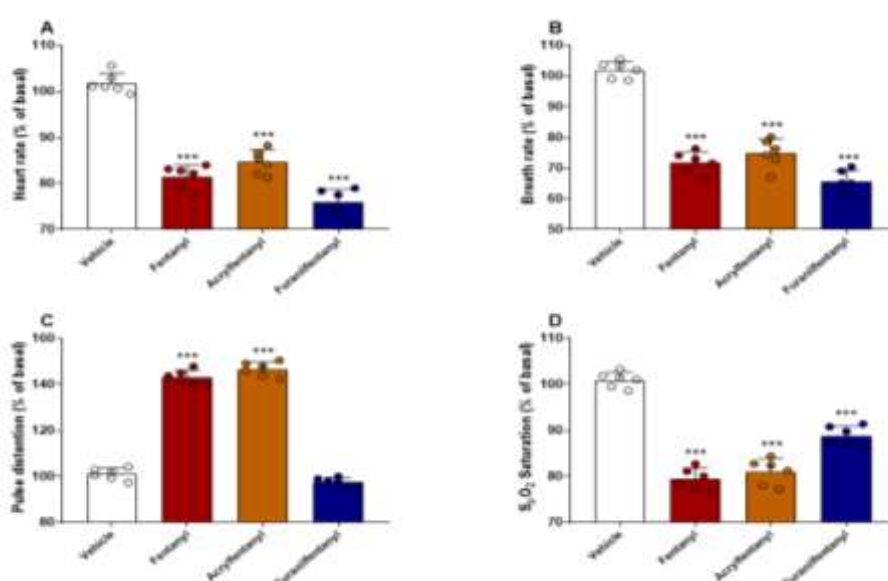
Figure 5.2. *Effect of Fentanyl, Acrylfentanyl and Furanylfentanyl (15 mg/kg IP.) on heart rate (panel A), breath rate (panel B), pulse distention (panel C) and oxygen arterial saturation (panel D). Data are expressed as percentage of basal value (heart rate, breath rate, the pulse distention) as percentage of oxygen blood saturation (%SpO$_2$ saturation) and represent, the mean ± SEM of 6 mice/group. Statistical analysis was performed by one-way ANOVA followed by the Bonferroni's test for multiple comparisons for the dose-response curve of each compound at different times. ***p<0.001 versus vehicle.*

Heart rate decreased significantly after the administration of Fentanyl, Acryfentanyl and Furanylfentanyl treatments [$F_{(3, 20)}$ = 115.2; P<0.0001] and the pulse distance increased significantly with fentanyl and Acrylfentanyl [$F_{(3, 20)}$ = 579.6; P<0.0001] but not with Furanylfentanyl. Similarly, the breath rate decreased significantly after the administration of Fentanyl and its analogs [$F_{(3, 20)}$ = 115.9; P<0.0001] and consequently the SpO$_2$ decreased significantly after the injection of the three compounds [$F_{(3, 20)}$ = 112.6; P<0.0001]. Overall,

the effect of Furanylfentanyl seemed to be less pronounced compared to fentanyl and Acrylfentanyl. Cardiorespiratory effects of Acrylfentanyl are very similar to that induced fentanyl.

The histological analysis of the samples collected from the animals injected with the high dose of Fentanyl, Acrylfentanyl and Furanylfentanyl revealed important pathological aspects in the brain, heart, and lungs. Importantly all the compounds tested induced cerebral edema with almost similar intensities (**Table 5.1**).

Table 5.1. *Histological findings in brain, heart and lungs samples collected from animals treated with high dose (15 mg/kg IP) of Fentanyl, Acrylfentanyl and Furanylfentanyl.*

Animals	Cerebral edema	Heart CBN (contraction band necrosis)	Pulmonary edema	Pulmonary congestion	Acute emphysema
Fentanyl M1	+	CBN+++	+	++	++
Fentanyl M2	+	-	+	+++	++
Fentanyl M3	+	CBN+++	+	+++	++
Fentanyl M4	+	CBN+++	+	+++	++
Acrylfentanyl M1	++	CBN+	+	++	+++
Acrylfentanyl M2	+	CBN+	++	+++	++
Acrylfentanyl M3	+	-	-	+	++
Acrylfentanyl M4	+	-	-	++	+
Furanylfentanyl M1	+	CBN+	+	+++	++
Furanylfentanyl M2	+	-	+	+++	++
Furanylfentanyl M3	+	-	-	-	-
Furanylfentanyl M4	+	-	-	+	++

Fentanyl and its analogs induced important pathological bands in the heart (contraction band necrosis CBN). In this case this marker is evidenced in more animals treated with fentanyl with respect to one animal treated with Furanylfentanyl (**Table 5.1**). Focusing on the respiratory apparatus, the histological aspects of the lungs showed an important pathological finding. In particular, the three compounds induced pulmonary edema, congestion, and acute emphysema in almost all the animals treated with the three compounds (**Table 5.1**). Examples of the pathological findings reported in **Table 5.1** are supported with **Figure 5.3** that clearly shows the differences of the histological aspects between vehicle-treated mice and fentanyl-treated mice.
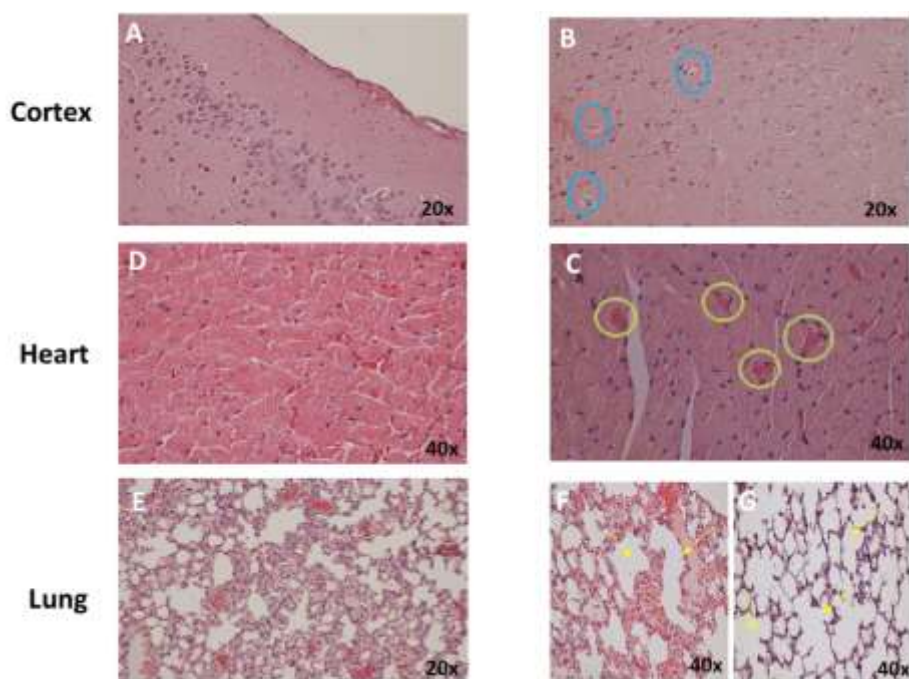
Figure 5.3. Histological aspects of cortex (A, B), heart (C, D) and (E, F and G) in vehicle-treated mice (A, C, E) and 15 mg/kg of fentanyl -treated mice (B, D, F, G). Cortex: slight cerebral edema (blue circles). Heart: areas of contraction bands necrosis (yellow cirles). Lung: Alveolar edema and vascular congestion (yellow arrows in F), acute emphysema (yellow arrows in G).

These results support my published findings regarding the cardiotoxicity of Fentanyl and fentanyl analogs (Bilel et al., 2022). In addition, these data confirm again the differences between the vulnerability of the three compounds. In particular, the administration of a high dose of Furanylfentanyl (15 mg/kg) did not really show important differences respect to the dose of 6 mg/kg (Bilel et al., 2022). Again, Furanylfentanyl did not alter the pulse distention and as shown from **Table 5.1** only one sample among 4 samples showed a slight CBN. These data confirm again the lower potency of Furanylfentanyl respect to Fentanyl and Acrylfentanyl.

The lower *in vivo* potency of Furanylfentanyl could be associated to its partial agonism at mu opioid receptors, and its bias agonism with G protein and not β-arrestin 2 at mu receptors (Bilel et al., 2022).

Due to the high abuse of fentanyl and its analogs many studies have been focusing on the forensic pathology of these compounds. In particular, many autopsy-pathological findings in cases related to fentanyl or analogs (Furanylfentanyl and Acrylfentanyl) overdosing confirm the cerebral edema in the CNS. In addition, cerebral hemorrhage induced by acetylfentanyl was also reported (Frisoni et al., 2019). Regarding the cardiovascular system, pericardial petechiae was reported and that was explained by pathologists to be a generic sign to asphyxia, due to

respiratory failure (Frisoni et al., 2019). In accordance with my preclinical data, autopsy findings confirm the pulmonary congestion and edema in many cases of death with fentanyl and analogs (Concheiro et al., 2018; Frisoni et al., 2019). It is very important to convey that the body temperature is a vital sign that is routinely monitored by medical professionals. I have measured rectal temperature in mice treated with fentanyl and analogs to understand the signs related to cardiorespiratory toxicity. Indeed, I have found an important decrease in the core temperature of mice after the injection of fentanyl and analogs and that could be related to the cardiorespiratory depression induced by these opioids. Indeed, it has been speculated that the decrease of temperature after fentanyl injection is a result of brain hypoxia and respiratory depression (Solis et al., 2017, 2018).

5.1.4 Conclusion

These data are complementary for the study Bilel et al., 2022 and they confirm the *in vitro* and *in vivo* findings on the different pharmacological effects of Fentanyl, Acrylfentanyl and Furanylfentanyl. In addition to the cardiorespiratory depression induced by these compounds, histological findings confirm the tissue damage induced by these potent drugs confirming the increasing inflammation in case of administration of high doses of NSOs and their high risk of death.

5.1.5 Contributions

B.S and M.M designed the study. B.S, T.M, C.G, BM performed *in vivo* experiments. F.P, N.M performed histological analysis. B.S contributed to data curation and the writing of the first draft.

5.2 Differential pharmaco-toxicological and pharmacokinetic responses to 4F-Furanylfentanyl and Isobutyryfentanyl in female and male CD1 Mice

[1]Bilel Sabrine, [1]Tirri Micaela, [1]Corli Giorgia, [1]Bassi Marta, [2]Montesano Camilla, [3]Adolfo Gregori, [2] Sergi Manuel, [1]Marti Matteo.

[1]*Department of Translational Medicine, Section of Legal Medicine and LTTA Centre, University of Ferrara, Italy*
[2]*Faculty of Bioscience and Technology for Food, Agriculture and Environment, University of Teramo, 64100 Teramo, Italy.*
[4]*Carabinieri, Department of Scientific Investigation (RIS), 00191 Rome, Italy.*

5.2.1 Background

4-Fluoro-Furanylfentanyl (4F-FUF) and Isobutyrylfentanyl (IBF) were found for the first time in Italy in 2019. In 2021, in collaboration with Carabinieri (RIS), I have contributed to the *in vivo* experimentation to evaluate the pharmacokinetics of these two compounds in male mice. In continuation to the study (Montesano et al., 2022), I have been focusing on the pharmaco-toxicological characterization of 4F-FUF and IBF considering sex differences using female and male mice and the evaluation of the pharmacokinetics of the two drugs both in female and male mice.

5.2.2 Materials and methods

5.2.2.1 Animals

Female and Male ICR (CD-1®) mice weighing 30–35 g (Centralized Preclinical Research Laboratory, University of Ferrara, Italy) were group housed (5 mice per cage; floor area per animal was 80 cm2; minimum enclosure height was 12 cm), exposed to a 12:12-h light-dark cycle (light period from 6:30 AM to 6:30 PM) at a temperature of 20–22 °C and humidity of 45–55% and were provided ad libitum access to food (Diet 4RF25 GLP; Mucedola, Settimo Milanese, Milan, Italy) and water. The experimental protocols performed in the present study were in accordance with the U.K. Animals (Scientific Procedures) Act of 1986 and associated guidelines and the new European Communities Council Directive of September 2010 (2010/63/EU). Experimental protocols were approved by the Italian Ministry of Health (license n. 223/2021-PR, CBCC2.46. EXT.21) and by the Animal Welfare Body of the University of

Ferrara. According to the ARRIVE guidelines, all possible efforts were made to minimize the number of animals used, to minimize the animals' pain and discomfort. 8 male and 8 female mice were used for behavioural studies (safety pharmacology) and 4 male, and 4 female animals where used the pharmacokinetics studies.

5.2.2.2 Drug preparation

4F-FUF or IBF dissolved in absolute ethanol (final concentration of 2% v/v) and Tween 80 (2% v/v) and brought to its final volume with saline (0.9% NaCl v/v). The solution made with ethanol, Tween 80 and saline was also used as the vehicle (blank control). The drugs were administered by intraperitoneal injection at a volume of 4 μL/g; the final concentration of 4F-FUF or IBF was 5 mg/kg. The control group of female and male mice were administered only with vehicle solution.

5.2.3 Behavioural tests

In the present study, the effect induced by 4F-FUF and IBF on behavioral responses was investigated using a battery of tests widely used in studies of "safety-pharmacology" in rodents (Bilel et al., 2020,2021, 2022). To reduce the number of animals used, mice were evaluated in functional observational tests carried out in a consecutive manner according to the following time scheme: observation of visual object responses (frontal and lateral view), tactile response (vibrissae reflexes), visual placing response, breath rate, mobility time, and tail pinch test. Behavioural tests were conducted in a thermostat-controlled (temperature: 20–22 °C, humidity: 45–55%) and light (150 lux) room with a background noise of 40 ± 4 dB. The apparatus for sensorimotor and physiological test consisted of an experimental chamber (350 × 350 × 350 mm) with black methacrylate walls and a transparent front door. During the week before the experiment, each mouse was placed in the box and handled (once a day) every other day, i.e., 3 times, to get used to both the environment and the experimenter. To avoid mice olfactory cues, cages were carefully cleaned with a dilute (5%) ethanol solution and rinsed with water. All experiments were performed between 8:30 AM to 2:00 PM and conducted blindly by trained observers working in pairs. The behaviour of mice was videotaped by a camera (B/W USB Camera day&night with varifocal lens; Ugo Basile, Italy) placed at the top or on one side of the box and analysed offline by a different trained operator.

5.2.3.1 Evaluation of the Visual Response

Visual response was verified by two behavioural tests which evaluate the ability of the animal to capture visual information when the animal is moving (the visual placing response) or stationary (the visual object response).

Visual object response test was performed to evaluate the ability of the mouse to see an object approaching from the front (frontal view) or the side (lateral view) that typically induces the animal to shift or turn the head or retreat from it. A white horizontal bar was moved frontally to the mouse head, while a small dentist's mirror was moved laterally into the mouse's field of view in a horizontal arc, until the stimulus was between the mouse's eyes. The procedures were conducted bilaterally and repeated 3 times (Bilel et al., 2020). The score assigned to the movement was 1 or 0 if it was not present. The total value was calculated by adding the scores obtained in the frontal with those obtained in the lateral visual object response test (overall score: 9). Tests were measured at 10, 30, 60, 120, 180, 240 and 300 min after the injection.

Visual placing response test is performed using a tail suspension modified apparatus able to bring down the mouse towards the floor at a constant speed of 10 cm/s (Bilel et al., 2020). The downward movement of the mouse was videotaped by a camera (B/W USB Cameraday&night with varifocal lens; Ugo Basile, Italy) placed at the base of the tail suspension apparatus. Movies were analysed off-line by a trained operator who was unaware of the drug treatments performed, to evaluate the beginning of the reaction of the mouse approaching the floor. When the mouse started the reaction, an electronic ruler evaluated the perpendicular distance in millimetres between the eyes of the mice to the floor. Untreated control mice typically perceive the floor and prepare to contact at a distance of about 28 ± 4.3 mm. Tests were measured at 15, 35, 70, 125, 185, 245 and 305 min after the injection.

5.2.3.2 Evaluation of Tactile Response

Tactile responses were verified through vibrissae reflexes induced by the touch of a thin hypodermic needle (Bilel et al., 2020). *Vibrissae reflex* was evaluated by touching vibrissae (right and left) once for side giving a value of 1 if there was a reflex (turning of the head to the side of touch or vibrissae movement) or 0 if not present (overall score: 2).

5.2.3.3 Evaluation of Breath Rate

The experimental protocol for the detection of *respiratory parameter* in this study provides for monitoring of the animal awake, freely moving, with a non-invasive and minimal handling. The animal is leaving free in a cage and the respiration patterns of the mice were videotaped by a camera (B/W USB Camera day & night with varifocal lens; Ugo Basile, Italy) placed above observation's cage (Corli et al., 2023). The analysis frame by frame allows to better evaluate the number of breath rates of the mouse evaluated through the count of about 257 ± 11 breath rates per minutes (brpm). Breath rate was measured at 15, 40, 70, 150, 130, 190, 250 and 310 min after the injection.

5.2.3.4 Evaluation of motor activity

The Mobility time test evaluates spontaneous motor activity of mice (Corli et al., 2023). The mouse is free to move on a square plastic cage (60×60 cm). The observer measures the total time spent moving by the animal (when the mouse walks or moves the front legs) in five minutes. The test was performed at 15, 35, 70, 125, 185, 245 and 305 min after the injection.

5.2.3.5 Evaluation of pain induced by a mechanical stimulus

Acute mechanical nociception was evaluated using the *tail pinch test* (Bilel et al., 2020). A special rigid probe connected to a digital dynamometer (ZP-50N, IMADA, Japan) was gently placed on the tail of the mouse (in the distal portion), and progressive pressure was applied. When the mouse flicked its tail, the pressure was stopped, and the digital instrument recorded the maximum peak of weight supported (g/force). A cut off (500 g/force) was set to avoid tissue damage. The test was repeated three times, and the final value was calculated by averaging the three obtained scores.

5.2.3.6 Statistical Analysis

In sensorimotor response experiments, data are expressed in arbitrary units (visual object response, vibrissae reflexes) and percentage of baseline (visual placing response, breath rate, mobility time). Tail pinch test is expressed as Emax % and is calculated as the percent of maximal possible effect {EMax% = [(test - control latency)/(cut off time - control)] X 100}.

Statistical analysis of the effects of the 4F-FUF and IBF at the dose of 5 mg/ kg over time were performed using a two-way ANOVA followed by a Bonferroni test for multiple comparisons. Statistical analysis was performed using Prism software (GraphPad Prism, USA).

5.2.4 Pharmacokinetic studies

5.2.4.1 Samples collection

Blood samples (total volume: 500 μL) were collected by submandibular blood collection technique into 1 mL vials containing EDTA (4 mg/mL of blood) as preservative and anticoagulant. Then samples were centrifugated at 9000 rpm for 8 min to obtain plasma. After each blood withdrawal, an equal volume of saline solution was subcutaneously injected into mice to maintain volume and osmotic homeostasis. Blood samples were first collected at 30 min then 1h, 2h, 3h, 4h and 5 h. After that animals were sacrificed, and different tissues were collected (brain, heart liver, kidney, spleen and stomach). Plasma and tissues collected from male and female mice were stocked at −20 °C until the analysis (Corli et al., 2022). For blood sample preparation, plasma samples were prepared by adding in each eppendorf: 50 μL plasma (containing the analytes) + 125 μL solution with the internal standards deuterated at 30 ng mL-1 + 25 μL MeOH-ACN 50:50 (v/v) solution 0.1% HCOOH.

For urine samples mice were single-housed (one mouse per metabolic cage, with free access to food and water) in a colony room under constant temperature (23 °C–24 °C) and humidity (45–55%). Urine samples were collected in 2-mL tubes before drug injections (control), and every hour for 6 consecutive hours from the administration of the treatments. After 6 h, urine was collected cumulatively in the 6–12, 12–24 and 24–36 h time interval and stored at −20 °C until analysis. Urine samples were only collected for IBF and not 4F-FUF which have an antidiuretic effect on mice and thus it was not possible collecting a good number of samples to carry out the analysis.

Before LC-HRMS analysis, urine samples were diluted 1:4 with water and filtered with Minisart SRP25 4 mm (0.45 μm) syringe filters (Sartorius, Turin, Italy).

Tissue preparation: About 100 mg of each tissue were weighted in a 2 mL Precellys vial; methanol containing IS (fentanyl-d5 and norfentanyl-d5) was added in order to reach a solvent:tissue ratio of 5:1 (v:w). The homogenate was centrifuged at 12000 rpm for 10 min at

4°C, 100 µL of supernatant were collected and diluted to 300 µL with water before injection into the LC-HRMS system.

5.2.4.2 LC-HRMS analysis

A Thermo Scientific Ultimate 3000 RSLC system coupled with a Thermo Scientific Q-Exactive Mass spectrometer (Thermo Fisher Scientific, Bremen, Germany) was used for analysis. Chromatographic separation was carried out with an Excel 2 C18-PFP (100 × 2.1 mm ID) column from Ace (Aberdeen, Scotland) packed with particles of 2 µm, maintained at 35 °C at a flow rate of 0.5 mL min−1.

Mobile phases consisted of 0.1% (v/v) formic acid + 10 mM ammonium formate in water (Phase A) and 0.1% formic acid in acetonitrile (Phase B). The gradient started with 0% B and these conditions were maintained for one min; phase B was then increased to 25% in two min, to 35% in the following two min and held for three min. Phase B was then ramped to 50% over 1.5 min and to 100% in 0.5 min; it was kept stable for one min and then equilibrated to the initial conditions, yielding a total runtime of 12.5 min. Injection volume was 6 µL.

The Q-Exactive mass spectrometer was equipped with a heated electrospray ionization source (HESI-II) operated in positive mode; mass spectra were acquired in full scan/data dependent in the range 50–800 m/z. The operating parameters of the ion source were set as follows: spray voltage 3.5 kV, capillary temperature 350 °C, heater temperature 300 °C, S-lens RF level 60, sheath gas flow rate 55, auxiliary gas flow rate 20. Nitrogen was used for spray stabilization, for collision-induced dissociation experiments in the high energy collision dissociation (HCD) cell and as the damping gas in the C-trap.

The instrument was calibrated in positive and negative mode every working day. For full scan, resolution was 70,000 (FWHM at m/z 200), whereas automatic gain control (AGC) and maximum injection time were set at 1×10^5 and 100 ms, respectively. In MS/MS mode, resolution was 35,000 (FWHM at m/z 200) and three different collision energies, i.e., 10, 30, 50, were applied. An inclusion list with the masses of the previously identified metabolites was added to the methods (Montesano et al., 2021).

5.2.5 Results and discussion

5.2.5.1 Behavioural effects of 4F-FUF

Systemic administration of 4F-BUF (5 mg/kg IP) induced sensorimotor and motor impairments, increased analgesia and reduced the respiratory rate in female and male treated mice (**Figure 5.4 and 5.5**).

In the visual object test, the visual reflexes to the object were significantly reduced in male [**Fig 5.4-A**: $F_{(1, 112)}$ = 252.5; $P<0.0001$] and female [**Fig 5.4-B**: $F_{(1, 112)}$ = 158.0; $P<0.0001$] mice after the injection with 4FBUF. The effect was more persistent in males (up to 300 min) respect to females (120 min). Sex differences were revealed by ANOVA in 120 min, 240 min and 300 min of measurements [**Fig 5.4-C**: $F_{(2, 112)}$ = 101.3; $P<0.0001$].

In the visual placing test, the visual reflexes to the floor were significantly reduced in male [**Fig 5.4-D**: $F_{(1, 112)}$ = 306.6; $P<0.0001$] and female [**Fig 5.4-E**: $F_{(1, 112)}$ = 752.5; $P<0.0001$] mice after the injection with 4F-BUF. Also in this test, the effect was more persistent in males (up to 305 min) respect to females (245 min). The effect in the visual placing test was deeper than the one observed in the visual object test in both sexes. In this case, sex differences were revealed by ANOVA in 70 min and 305 min of measurement [**Fig 5.4-F**: $F_{(2, 112)}$ = 248.4; $P<0.0001$].

In the vibrissae response test, the administration of 4F-FUF significantly reduced the vibrissae reflexes of male [**Fig 5.4-G**: $F_{(1, 112)}$ = 25.17; $P<0.0001$] and female [**Fig 5.4-H**: $F_{(1, 112)}$ = 15.74; $P=0.0001$] to touches. The effect of 4F-BUF appeared only for 60 min in both sexes and tended to reach basal values after that. No sex differences were detected by ANOVA in this test (**Fig 5.4-I**).
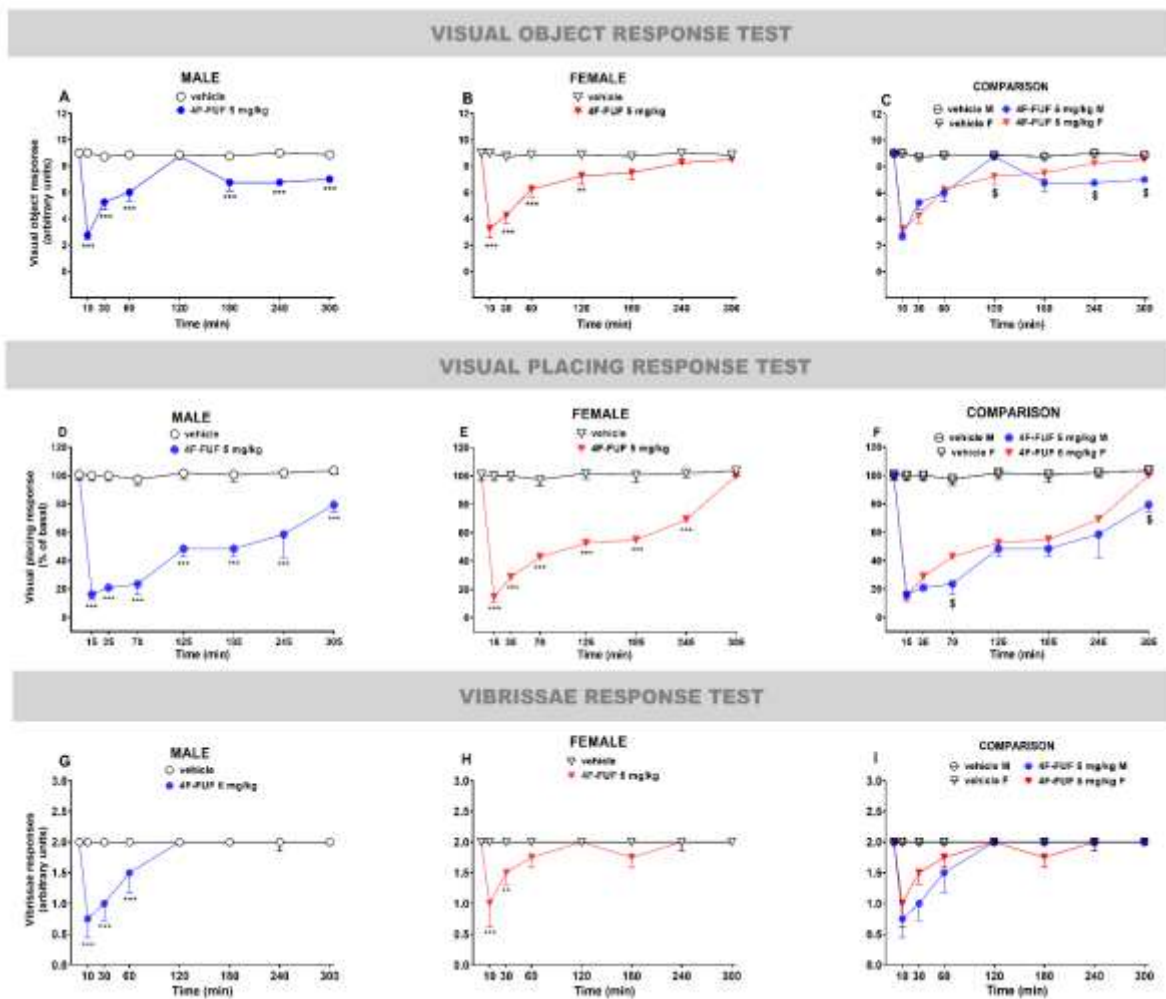
Figure 5.4. *Effects of the systemic administration of 4F-FUF in the visual object test (panels A, B and C), visual placing test (panels D, E and F) and vibrissae response test (panels G, H, and I). Data are expressed as arbitrary units (visual object and vibrissae tests) and percentage of basal value (visual placing test) and represent, the mean ± SEM of 8 female and 8 male mice/group. Statistical analysis was performed by one-way ANOVA followed by the Bonferroni's test for multiple comparisons for the dose-response curve of each compound at different times. **p<0.01, ***p<0.001 versus vehicle. \$p<0.05 versus gender (female/male).*

In the spontaneous locomotion test, the systemic administration of 4F-BUF (5mg/kg IP) induced a significant facilitation of the motor activity of male [**Fig 5.5-A**: $F_{(1, 112)} = 124.1$; P<0.0001] and female [**Fig 5.5-B**: $F_{(1, 112)} = 104.5$; P<0.0001] mice. The effect was more persistent (up to 305 min) in males respect to females (245 min). The effect disappeared in females after 125 min however in males a significant increase was detected at 245 min. In this case, sex differences were revealed by ANOVA at 35, 70 min and 245 min of measurement

[**Fig 5.5-C**: $F_{(2, 112)} = 22.51$; P<0.0001].

In the tail pinch test, the systemic administration of 4F-BUF (5mg/kg IP) induced a significant increase of antinociception in male [**Fig 5.5-D**: $F_{(1, 112)} = 44.1$; P<0.0001] and female [**Fig 5.5-E**: $F_{(1, 112)} = 18.5$; P<0.0001] mice. The effect was more persistent in males (up to 265 min) respect to females (90 min). Sex differences were revealed by ANOVA at 55, 205 min and 265 min of measurements [**Fig 5.5-F**: $F_{(2, 112)} = 1.940$; P=0.1471].

In the breath rate test, the systemic administration of 4F-BUF (5mg/kg IP) induced a significant decrease of breath rate in male [**Fig 5.5-G**: $F_{(1, 112)} = 93.37$; P<0.0001] and female [**Fig 5.5-H**: $F_{(1, 112)} = 123$; P<0.0001] mice. The effect was deeper in male at 10 min than female. The respiratory reduction persisted in male up to 300 min while this effect disappeared in female at this time. Sex differences was revealed by ANOVA at 10 min of measurements [**Fig 4.5-I**: $F_{(2, 112)} = 122$; P=0.1471].
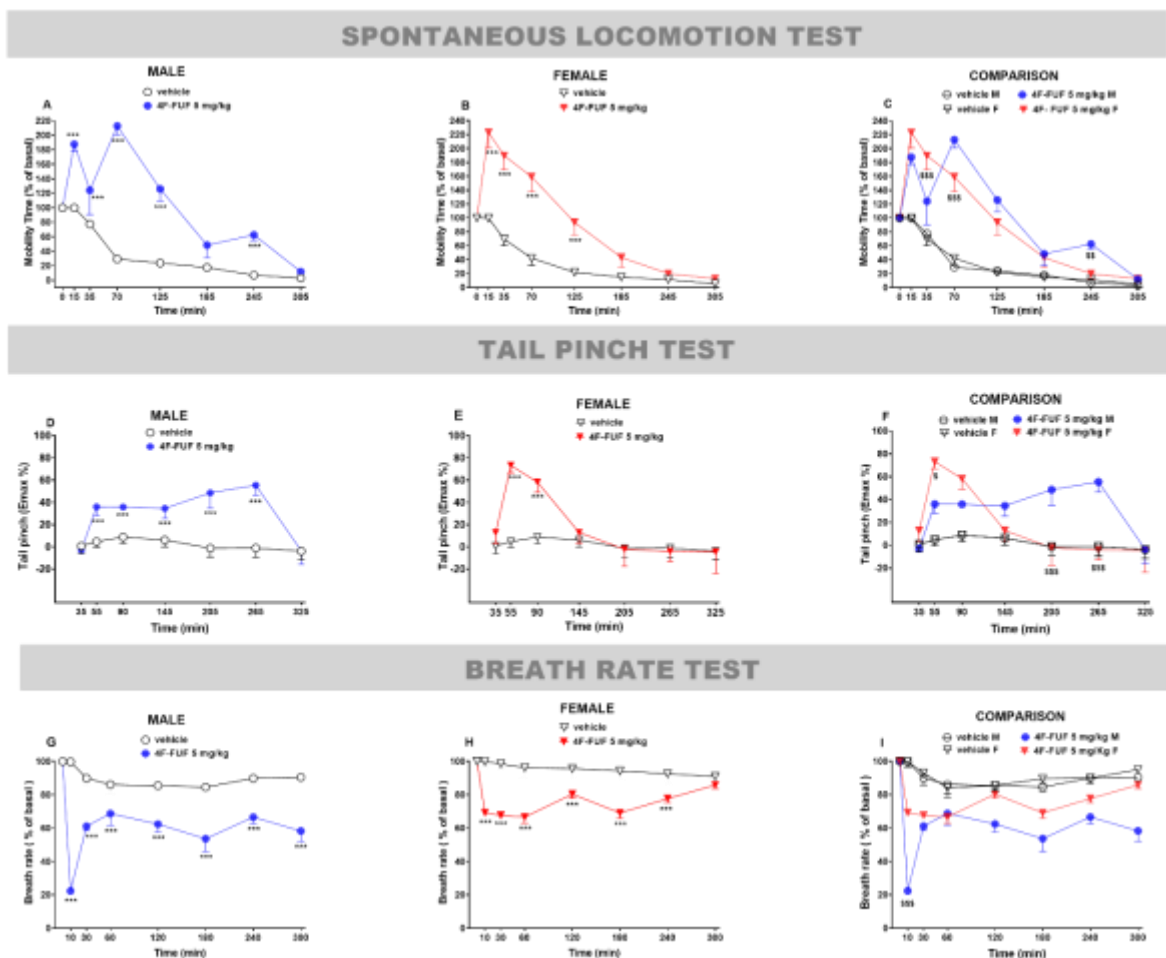
Figure 5.5. *Effects of the systemic administration of 4F-FUF (5m.kg. IP) in the spontaneous locomotion test (panels A, B and C), tail pinch test (panels D, E and F) and breath rate (panels G, H, and I). Data are expressed percentage of basal value (spontaneous locomotion and breath rate tests) and percentage of maximal effect (tail pinch test) and represent, the mean ± SEM of 8 female and 8 male mice/group. Statistical analysis was performed by one-way ANOVA followed by the Bonferroni's test for multiple comparisons for the dose-response curve of each compound at different times. ***p<0.001 versus vehicle. \$\$p<0.01, \$\$\$p<0.001 versus gender (female/male).*

5.2.5.2 Behavioural effects of IBF

Systemic administration of IBF (5 mg/kg IP) induced sensorimotor and motor impairments, increased analgesia and reduced the respiratory rate in female and male treated mice (**Figure 5.6 and 5.7**).

In the visual object test, the visual reflexes to the object were significantly reduced in male [**Fig 4.6-A**: $F_{(1, 100)}$ = 9.287; P=0.0030] and female [**Fig 5.6-B**: $F_{(1, 100)}$ = 94.74; P<0.0001] mice after the injection with 4FBUF. The effect was more profound and persistent (120 min) in females respect to males (10 min). This effect was not detected at 12h and 24h of

measurements. Sex differences were revealed by ANOVA in 10, 30, 60 and 120 min of measurements [**Fig 5.6-C**: $F_{(2, 100)}$ = 58.74; $P<0.0001$].

In the visual placing test, the visual reflexes to the floor were significantly reduced in male [**Fig 5.6-D**: $F_{(1, 100)}$ = 18.09; $P<0.0001$] and female [**Fig 5.6-E**: $F_{(1, 100)}$ = 126.4; $P<0.0001$] mice after the injection with IBF. Also in this test, the effect was more profound and persistent in females (120 min) respect to males (10 min). This effect was not detected at 12h and 24h of measurements. In this case, sex differences were revealed by ANOVA at 15 min, 35 min,70 min 125 min and 185 min of measurement [**Fig 5.6-F**: $F_{(2, 100)}$ = 56.55; $P<0.0001$].

In the vibrissae response test, the administration of IBF significantly reduced the vibrissae reflexes of male [**Fig 5.6-G**: $F_{(1, 100)}$ = 80.86; $P<0.0001$] and slightly of female [**Fig 5.6-H**: $F_{(1, 100)}$ = 1; $P=0.3197$] to touches. The effect of IBF in vibrissae was more profound persistent in males respect to females who showed a moderate effect only at 10 min after injection. Sex differences were detected by ANOVA at 10 min, 30 min, 60 min, 120 min and 180 min in this test (**Fig 5.6-I**).
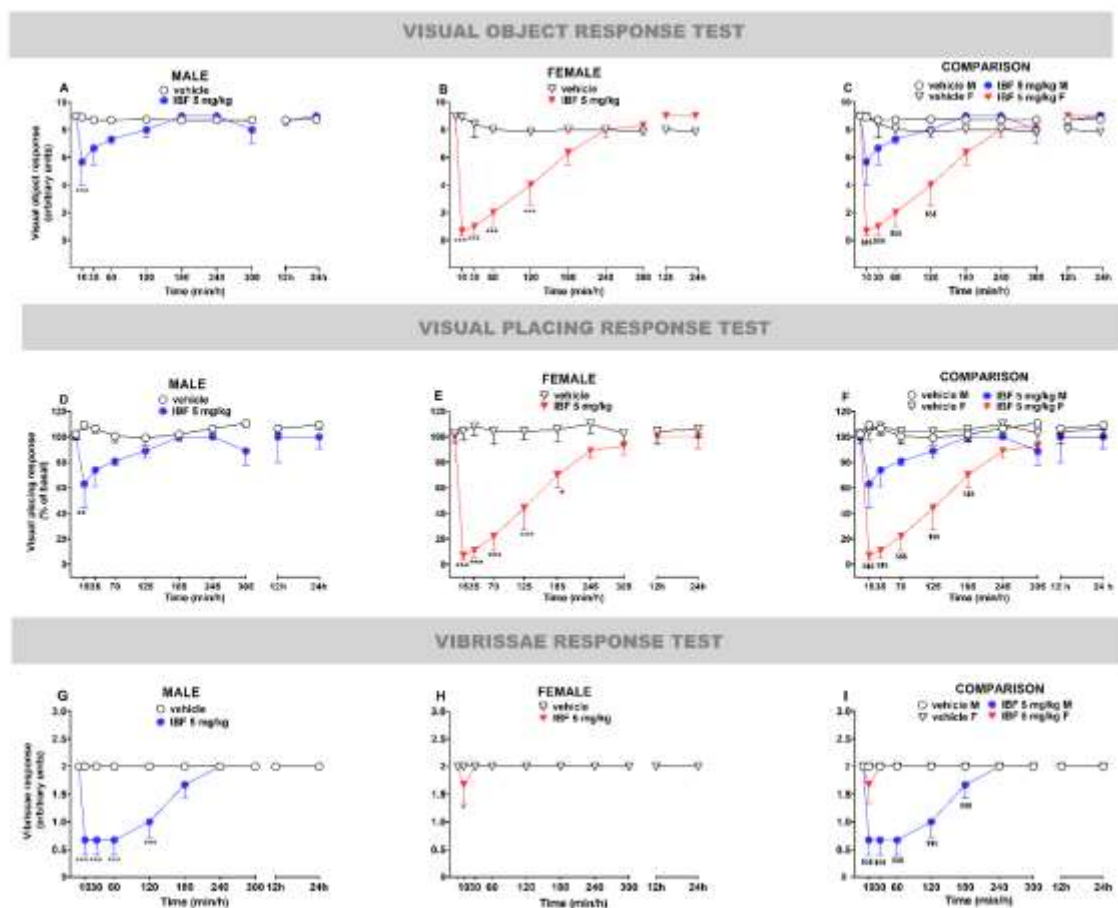
Figure 5.6. *Effects of the systemic administration of IBF (5mg/kg IP) in the visual object test (panels A, B and C), visual placing test (panels D, E and F) and vibrissae response test (panels G, H, and I). Data are expressed as arbitrary units (visual object and vibrissae tests) and percentage of basal value (visual placing test) and represent, the mean ± SEM of 8 female and 8 male mice/group. Statistical analysis was performed by one-way ANOVA followed by the Bonferroni's test for multiple comparisons for the dose-response curve of each compound at different times. **p<0.05, **p<0.01, ***p<0.001 versus vehicle. \$\$\$p<0.001 versus gender (female/male).*

In the spontaneous locomotion test, the systemic administration of IBF (5mg/kg IP) induced a significant effect on the motor activity of male [**Fig 5.7-A**: $F_{(1, 112)} = 1.692$; P=0.1964] and female [**Fig 5.7-B**: $F_{(1, 112)} = 90.57$; P<0.0001] mice. The effect was biphasic in both sexes, however the facilitatory effect was higher and persistent in female. Additionally, significant reduction of locomotion was detected at 12h and 24h of measurements in males and at 24h in females. In this case, sex differences were revealed by ANOVA at 70, 125, 185, 245 and 12h of measurement [**Fig 5.7-C**: $F_{(2, 112)} = 22.51$; P<0.0001].

In the tail pinch test, the systemic administration of IBF (5mg/kg IP) induced a significant increase of antinociception in male [**Fig 5.7-D**: $F_{(1, 112)} = 1506$; P<0.0001] and female [**Fig 5.7-E**: $F_{(1, 112)} = 569.1$; P<0.0001] mice. The antinociceptive effect of IBF was very potent and

228

persistent (significant effect detected at 12h and 24 h). No sex differences were revealed by ANOVA in this test [**Fig 5.7-F**: $F_{(2, 112)} = 0.11$; P=0.7367].

In the breath rate test, the systemic administration of 4F-BUF (5mg/kg IP) induced a significant decrease of breath rate in male [**Fig 5.7-G**: $F_{(1, 112)} = 208.8$; P<0.0001] and female [**Fig 5.7-H**: $F_{(1, 112)} = 119.6$; P<0.0001] mice. The effect was persistent until 300 min of measurement in both sexes, however it disappeared at 12h and 24h of tests. No sex differences were revealed by ANOVA in this test [**Fig 5.7-I**: $F_{(2, 112)} = 0.20$; P=0.6518].
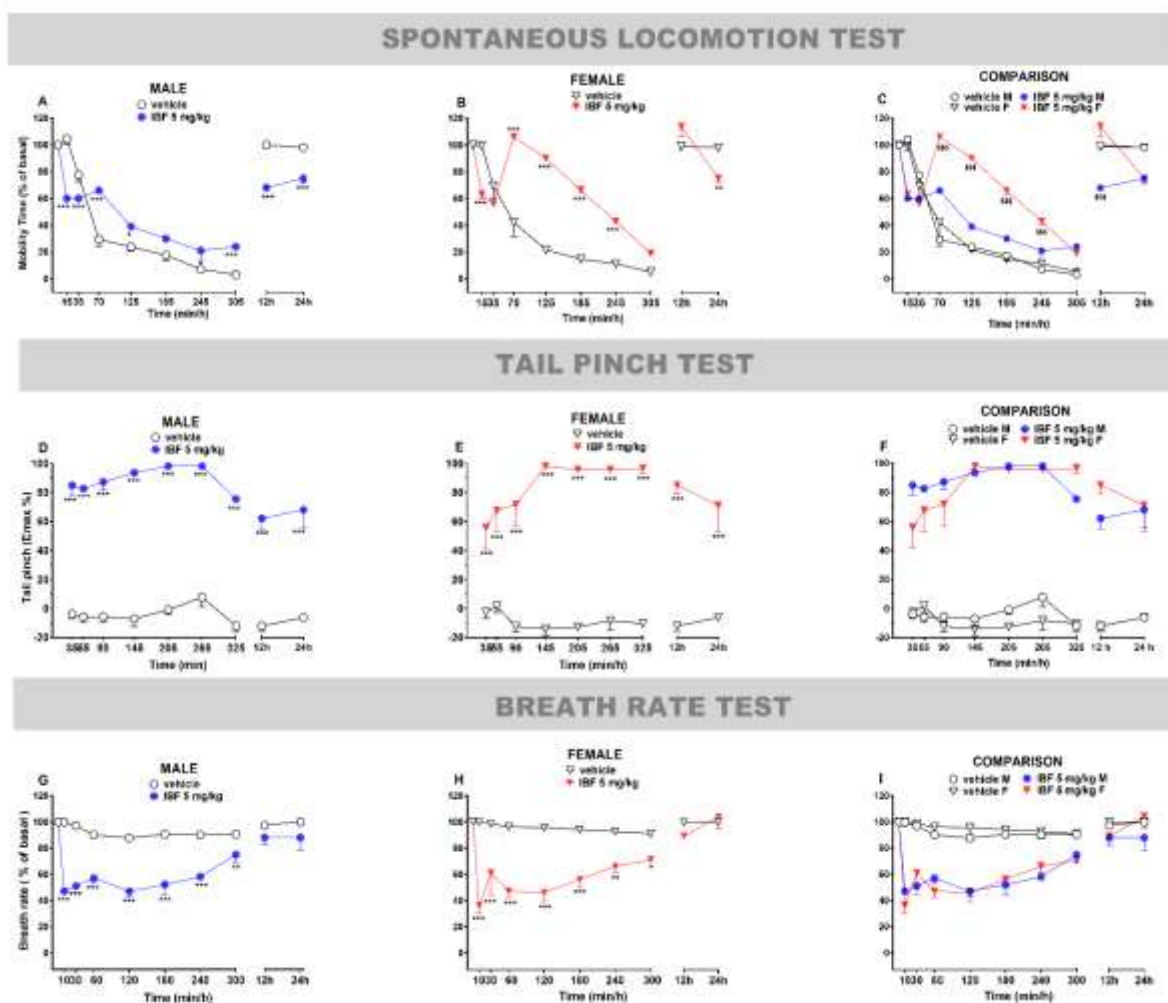

Figure 5.7. *Effects of the systemic administration of IBF (5m.kg. IP) in the spontaneous locomotion test (panels A, B and C), tail pinch test (panels D, E and F) and breath rate (panels G, H, and I). Data are expressed percentage of basal value (spontaneous locomotion and breath rate tests) and percentage of maximal effect (tail pinch test) and represent, the mean ± SEM of 8 female and 8 male mice/group. Statistical analysis was performed by one-way ANOVA followed by the Bonferroni's test for multiple comparisons for the dose-response curve of each compound at different times. *p<0.05, **p<0.01 ***p<0.001 versus vehicle. \$\$\$p<0.001 versus gender (female/male).*

5.2.5.3 Pharmacokinetics of 4F-FUF

5.2.5.3.1 Plasma concentration

Mice did not provide urine samples due to the antidiuretic impact of 4F-FUF. Presently, we conducted an analysis of the pharmacokinetic profile of 4F-FUF only in blood (plasma) and various tissues, including the brain, heart, liver, spleen, lung, kidneys, and stomach.

The plasma concentrations of 4F-FUF remained elevated during the initial hour of analysis for both sexes. In male mice, the concentration of the fentanyl analog exhibited a tendency to decline in the subsequent hours, reaching very low concentrations at 5h. Differently, the plasma concentrations in female mice showed an important drop of 4F-FUF at 2h of analysis and very low concentrations were detected in the following hours (Figure 5.8).
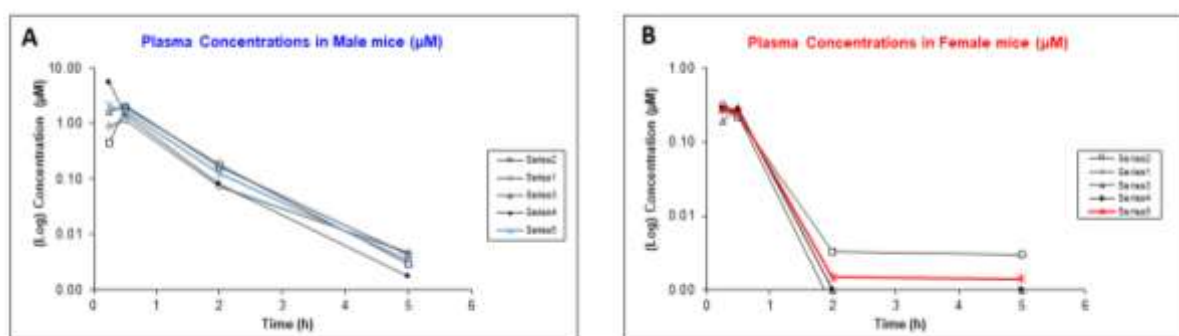

Figure 5.8. *Plasma concentrations of 4F-FUF in male and female mice (μM). 8 mice (4 males and 4 females) were injected with 4F-FUF (5mg/kg IP and plasm samples were used to perform this analysis (5 series indicates that the8analysis was carried out 5 times).*

The pharmacokinetics parameters measured in 4F-FUF of female and male mice are illustrated **Table 5.2**. This table demonstrates higher concentration of 4F-FUF in male mice at 0.25h (25 min) and 0.50h (50 min) respect to female mice. In addition, 4F-FUF is eliminated more rapidly in female than male (clearance female = 826.702 mL/min/kg). The volume of distribution at steady state was higher in female respect to male mice. Overall, these parameters show a different pharmacokinetics between female and male mice with a higher elimination rate of 4F-FUF in females respect to males as shown in **Figure 5.8**.

Table 5.2. *Pharmacokinetic parameters calculated from various plasma samples of female and male mice treated with 4F-FUF (5mg/kg IP).*

Time t[h]	Mean Male Concentration [μM]	Mean Female Concentration [μM]
0,25 h	2.109	0.272
0,50 h	1.659	0.252
2,00 h	0.125	0.001
5,00 h	0.003	0.001
K[h-1]	1.359	1.025
T1/2[h]	0.514	0.687
C(0) [μm]	3.195	0.870
AUC (0-x) [μM·h]	1.996	0.257
AUC (0-¥) [μm]	1.998	0.259
%extr	0.147	0.614
Dose [μmol/Kg]	12.755	12.755
CL (mL/min/Kg)	113.067	826.702
AUMC (last-inf)	1.365	0.131
MRT (min)	40.788	30.355
Vdss (L/kg)	4.592	25.110

K *- Elimination Rate Constant,* ***T1/2*** *- Half-Life,* ***C(0)*** *- Initial Concentration;* ***AUC (0-x)*** *- Area Under the Curve from 0 to x;* ***AUC (0-¥)*** *- Area Under the Curve from 0 to Infinity;* ***%extr*** *- Percent Excreted;* ***AUMC(last-inf)*** *- Area Under the First Moment Curve (AUMC) from the Last Time Point to Infinity;* ***MRT (min)*** *- Mean Residence Time;* ***Vdss*** *- Volume of Distribution at Steady State*

5.2.5.3.2 Tissue distribution

The parent drug (4F-FUF) and four of its major metabolites were detected in female and male tissues (**Figure 5.9**). The distribution of the drug and its metabolites seemed to be quite similar in both sexes. The metabolite M14 which derived from epoxidation and hydrolysis of 4F-FUF was the most abundant followed by M5, M3 and M11. Of note these latter were not detected in the brain.
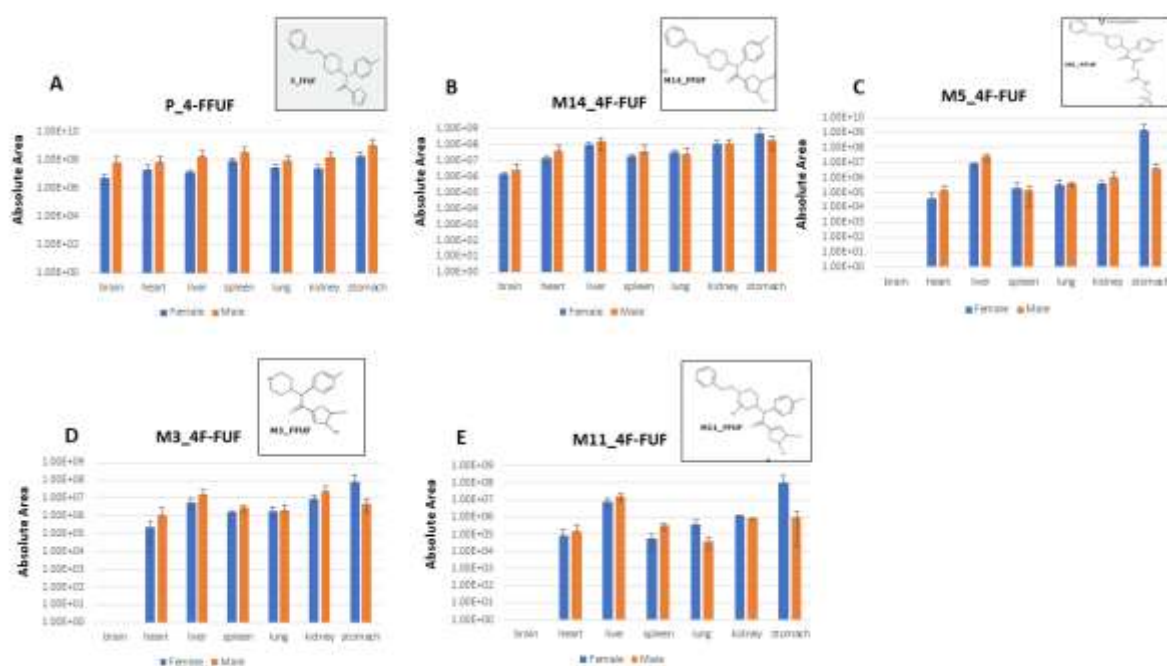

Figure 5.9. *Distribution of 4F-FUF (P) in different tissues (brain, heart, liver, spleen, lung, kidney, and Stomach) of female and male mice after treatment with (4F-FUF 5 mg/kg IP). From panel B to panel E: distribution of the metabolites M14, M5, M3 and M11 in female and male organs. The metabolites were categorized in panels based on their descending order of detection levels.*

5.2.5.4 Pharmacokinetics of IBF

5.2.5.4.1 Plasma concentration

The plasma concentrations of IBF remained elevated during the initial hour of analysis for both sexes. Nevertheless, in male mice, the concentration of the fentanyl analog exhibited a tendency to decline in the subsequent hours, reaching very low concentrations (< Log 0.01µM). In contrast, the plasma concentrations in female mice demonstrated elevated levels of 4F-FUF at the 5-hour mark of the analysis (Figure 5.10).
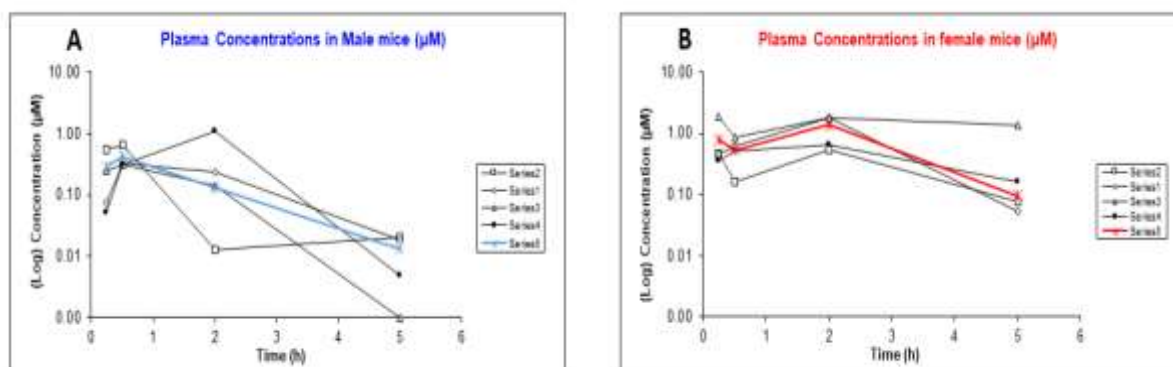

Figure 5.10. *Plasma concentrations of IBF in male and female mice (µM). 8 mice (4 males and 4 females) were injected with IBF (5mg/kg IP) and plasm samples were used to perform this analysis (5 series indicates that the analysis was carried out 5 times).*

The pharmacokinetics parameters measured in IBF of female and male mice are illustrated **Table 5.3**. This table demonstrates higher concentration of IBF in female mice at 0.25h (25 min) respect to male mice. In addition, IBF is eliminated more rapidly in male than female (clearance male = 339 mL/min/kg). The volume of distribution at steady state was also higher in male respect to female. Overall, these parameters show a different pharmacokinetics between female and male mice with a higher elimination rate of IBF in males respect to females as shown in **Figure 5.10**.

Table. 5.3. *Pharmacokinetic parameters calculated from various plasma samples of female and male mice treated with IBF (5mg/kg IP).*

Time t [h]	Mean Male Concentration [μM]	Mean Female Concentration [μM]
0,25 h	0.288	0.795
0,50 h	0.426	0.537
2,00 h	0.132	1.94
5,00 h	0,013	0.096
K [h-1]	0.876	0.454
T1/2 [h]	0.886	1.526
C(0) [μm]	0.605	0.566
AUC (0-x) [μM·h]	0.693	3.610
AUC (0-¥) [μm]	0.713	3.822
%extr	2.756	5.550
Dose [μmol/Kg]	14.286	14.286
CL [mL/min/Kg]	339.015	62.297
AUMC [last-inf]	0.859	7.580
MRT [min]	70.580	118.991
Vdss [L/kg]	23.442	7.413

*K - Elimination Rate Constant, **T1/2** - Half-Life, **C(0)** - Initial Concentration; **AUC (0-x)** - Area Under the Curve from 0 to x; **AUC (0-¥)** - Area Under the Curve from 0 to Infinity; **%extr** - Percent Excreted; **AUMC(last-inf)** - Area Under the First Moment Curve (AUMC) from the Last Time Point to Infinity**; MRT (min)** - Mean Residence Time; **Vdss** - Volume of Distribution at Steady State*

5.2.5.4.2 IBF urinary excretion

The examination of urine samples from female and male mice subjected to IBF treatment (5mg/kg IP) uncovered variations in the excretion patterns of IBF and its metabolites between the two sexes. Notably, **Figure 5.11** illustrates elevated levels of the parent drug IBF and its metabolites in the urine samples of male mice compared to those of female mice. The peak concentrations of IBF and its metabolites were observed during the cumulative 5h urine collection period. Higher levels of metabolites compared to the parent compound are detected between 10h and 15h, however, after 20h a slow amount of the metabolite M10 was detected but not the other metabolites.
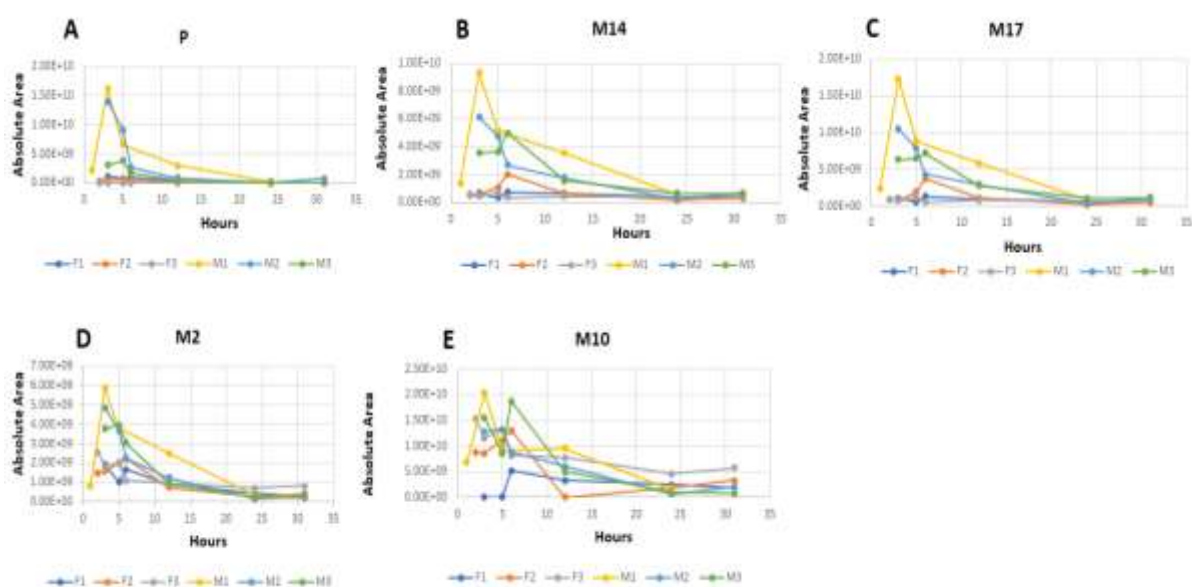

Figure 5. 11. *IBF urinary excretion profile in female and male mice. From panel B to panel E: excretion levels of the metabolites M14, M17, M2 and M10 in female and male urine samples. The metabolites were categorized in panels based on their descending order of detection levels.*

5.2.5.4.3 Tissue distribution

The parent drug (IBF) and five of its major metabolites were detected in female and male mice tissues (**Figure 5.12**). The distribution of the drug and its metabolites seemed to be quite similar in both sexes. The metabolite M10 which derived from epoxidation and N-dealkylation of IBF was the most abundant followed by M14, M17, M2 and M16. In difference to 4F-FUF, the major metabolites were all detected in all the tissues with high concentrations in both sexes.
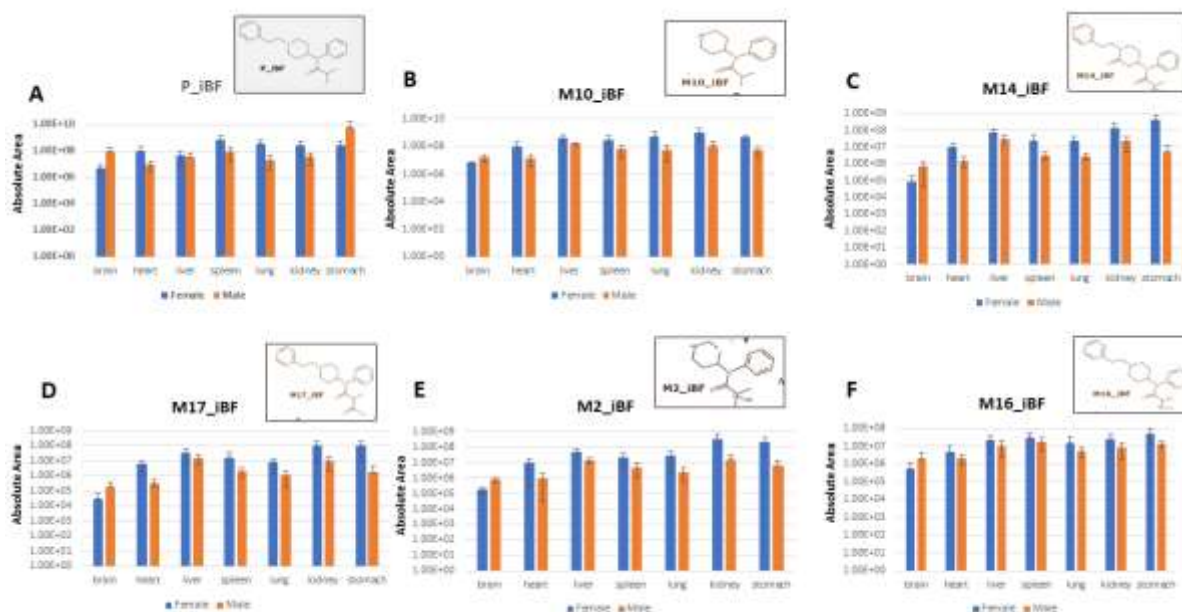

Figure 5.12. *Distribution of IBF (P) in different tissues (brain, heart, liver, spleen, lung, kidney, and Stomach) of female and male mice after treatment with (4F-FUF 5 mg/kg IP). From panel B to panel F: distribution of the metabolites M14, M5, M3 and M11 in female and male organs. The metabolites were categorized in panels based on their descending order of detection levels.*

Briefly, the results obtained in this study are in accordance with previous data on the pharmaco-toxicology and the pharmacokinetics of the two fentanyl analogs 4F-FUF and IBF (Vincenti et al., 2019, Montesano et al., 2021). Expanding upon the existence knowledge, these data reveal that the two compounds impair sensorimotor and motor activities with different degrees of intensity between female and male. The sensorimotor effects of fentanyl and its analogs (Acrylfentanyl, Ocfentanyl and Furanylfentanyl) was investigated in Bilel et al., 2023 in which I have discussed the different mechanisms that could be involved in sensorimotor impairments and the translational paradigm in human shedding light on the contribution of opioids in cases of driving under the influence of drugs as reported recently by the UNDOC (DUID, chapter 1-**Fig 1.3**). Similar to fentanyl and its analogs, these two drugs could have a potential risk on driving and might be involved in cases of DUID (Rohing et al., 2021).

4F-FUF and IBF impaired the motor responses in female and male mice but the effects between the two drugs are different. In particular, the effect of 4F-FUF was facilitatory at 5 mg/kg however in case of IBF the effect was biphasic. These differences might be explained by the difference in efficacy of the two compounds. Indeed, in the case of 4F-FUF, this drug did not induce maximal antinociceptive effects in the tail pinch test. Moreover, IBF induced higher effects on the breath rate test respect to 4F-FUF. 4F-FUF differs from Furanylfentanyl with the substitution of fluorine atom in the furan ring. In the study *Bilel et al., 2022*, I have also revealed lower efficacy of Furanylfentanyl respect to fentanyl and other compounds and that might be related to its partial agonism at mu receptors (Bilel et al., 2022).

These data also revealed that female mice showed a rapid elimination of 4F-FUF respect to male mice. In contrary, in case of IBF the elimination of this latter was more rapid in female mice. These results reveal sex-dependent effects of fentanyl and fentanyl analogs (Kaplovitch et al., 2015, Towers et al., 2022, **section 4.2**). The sex differences observed in these results might be explained by differences on mu distribution between female and male animals (Zhang et al., 2013) and the influence of circulating ovarien hormones and androgens on mu-mediated physiological responses (reviewed in Sharp et al., 2022). Finally adding to the study of *Montesano et al., 2021,* the metabolic pathways of both drugs are confirmed in this study using female mice and different analytical approaches to reveal fentanyl analogs distribution in animal tissues.

5.2.6 Conclusion

These data are complementary for the study *Montesano et al., 2021* and they reveal the sex differences in the pharmaco-toxicological effects of the two compounds. In addition, pharmacokinetic studies reveal sex difference also in the fentanyl analogs concentrations, distribution, and excretion in both sexes. These data shed light on the importance of considering sex differences in preclinical and clinical pharmacological approaches involving fentanyl analogs.

5.2.7 Contributions

B.S and M.M designed the study. **B.S**, T.M, C.G, BM performed *in vivo* experiments. M.C, G.A, M.S performed pharmacokinetic studies and contributed to the data curation. **B.S** is currently writing the first draft.

5.3 Unraveling the sex-specific effects of Brorphine: A comparative Study

[1]Bilel Sabrine, [1]Mantoan Marco, [1]Tirri Micaela, [1]Corli Giorgia, [1] Bassi Marta, [2]Fantinati Anna, [3]Vandeputte Marthe, Stove Christophe,[3]Marti Matteo.

[1]Department of Translational Medicine, Section of Legal Medicine and LTTA Centre, University of Ferrara, Italy
[2]Department of Environmental and Prevention Sciences, University of Ferrara, Via Fossato di Mortara, Ferrara, Italy
[3][2]Laboratory of Toxicology, Department of Bioanalysis, Faculty of Pharmaceutical Sciences, Ghent University, Ghent, Belgium

5.3.1 Background

The lack of data regarding the pharmaco-toxicological impacts of NSOs has hindered the ability to pinpoint doses associated with severe side effects. Additionally, the profound influence of sex on pharmaco-toxicological reactions to drugs is recognized. Distinctions between males and females play a crucial role and can contribute to sex-specific clinical manifestations, as evidenced in the literature for various drugs, including substances of abuse. Consequently, this study is aimed to assess sex-based variations in the effects of the Novel Synthetic Opioid Brorphine in mouse model. Furthermore, Naloxone was administered to reveal the mu opioid receptor's specificity in reversing the pharmaco-toxicological effects of Brorphine in both male and female mice.

5.3.2 Materials and methods

5.3.2.1 Animals

The experiments are conducted on ICR (CD-1®) Male and Female mice weighing 25–35 g (Centralized Preclinical Research Laboratory, University of Ferrara, Italy) were group housed (4 mice per cage; floor area per animal was 80 cm2; minimum enclosure height was 12 cm), exposed to a 12:12-h light-dark cycle (light period from 6:30 a.m. to 6:30 p.m.) at a temperature of 20–22 °C and humidity of 45–55% and were provided ad libitum access to food (Diet 4RF25 GLP; Mucedola, Settimo Milanese, Milan, Italy) and water.

The animal species of choice is that of election for the type of experiments proposed by the study, given the amount of information reported in the literature on the subject, and no animals having a higher neurodevelopment were used (in compliance with art 4, c.2 of D.L. 116/92). The experimental protocols performed in the present study were in accordance with the U.K. Animals (Scientific Procedures) Act of 1986 and associated guidelines and the new European Communities Council Directive of September 2010 (2010/63/EU). Experimental protocols were approved by the Italian Ministry of Health (license n. 335/2016- PR) and by the Animal Welfare Body of the University of Ferrara. According to the ARRIVE guidelines, all possible efforts were made to minimize the number of animals used, to minimize the animals' pain and discomfort.

5.3.2.2 Drug Preparation and Dose Selection

Brorphine was obtained from Cayman chemicals (Ann Arbor, Michigan, USA) while Naloxone (NLX) was purchased from Tocris (Tocris S.r.l. Via Ranzato 12, Milan).

The two compounds were dissolved in absolute ethanol (final concentration of 2% v/v) and Tween 80 (2% v/v) and brought to their final volume with saline (0.9% NaCl v/v). The solution made with ethanol, Tween 80 and saline was also used as the vehicle. The drugs were administered by intraperitoneal injection at a volume of 4 µL/g. The opioid receptor antagonist Naloxone was administered 15 min before the injection of Brorphine.

Given the limited knowledge on cause-and-effect correlation in humans between administered dose and symptomatology, dose selection was based on empirical evidence from previous preclinical studies (Bilel et al., 2022). Based on empirical data and conversion tables between equieffective doses in humans and mice, doses ranged from 0.01 mg/kg to 15 mg/kg, to assess the main effects sought by regular users, such as analgesics and euphoria. In addition, the protocol set in the present study provides administration by intraperitoneal injection of Naloxone, aimed to mimic clinical evidence: in fact, it has been reported the need of Naloxone redosing to revert toxicity (in particular respiratory depression; (Bilel et al., 2022; Klebacher et al., 2017). Indeed, a second full dose of naloxone (6 mg/kg) was injected at 60 min after the first one in order to better antagonize Brorphine effects and counteract their reappearance.

5.3.3 Behavioural studies

The effects of Brorphine were investigated using a battery of behavioral tests widely used in pharmacology safety studies for the preclinical characterization of new psychoactive substances in mice (Bilel et al.,2020 2021, 2022). All experiments were performed between 8:30 a.m. and 2:00 p.m. Experiments were conducted blindly by trained observers working in pairs. Mouse behavior (motor responses) was videotaped and analyzed offline by a different trained operator who gives test scores. The test batteries are performed at 5 minutes after injection and then at 30-60-120-180-240-300 minutes. The results are then compared with a control test performed before administration of Brorphine.

The experimental protocol provides for the successive tests to be performed for each session. Initially, the animal is observed to check the respiratory acts within one minute and the possible manifestation of symptoms related to a neurological or CNS alteration. Subsequently follows the evaluation of sensory functions through different tests that evaluate visual and tactile reactivity. Visual reactivity is assessed by approaching the floor and an object (both frontally and laterally). Analgesia is evaluated by the sensitivity of the animal to the mechanical stimulus (Tail pinch test). A cycle is completed within approximately 35 minutes, so the data collected should be considered around ±10 minutes, especially for 30 and 60 minutes. All behavioural tests are carried out under controlled and constant light, temperature and humidity conditions (150 lux, 20-22 ºC, 45-55% humidity), with a background noise of about 40±4 dB.

Before each test session, each animal is trained once a day (3 days of total training). To avoid altering the responses of the animals during the experiment, the boxes are cleaned with a dilute ethanol solution (5%) and rinsed with water before the beginning of each test. All tests are blindly evaluated, and the behavior of each animal is recorded and analyzed offline by different operators.

5.3.3.1 Evaluation of the Visual Response

Visual object response test was performed to evaluate the ability of the mouse to see an object approaching from the front (frontal view) or the side (lateral view) that typically induces the animal to shift or turn the head or retreat from it. A white horizontal bar was moved frontally to the mouse head, while a small dentist's mirror was moved laterally into the mouse's field of view in a horizontal arc, until the stimulus was between the mouse's eyes. The procedures were conducted bilaterally and repeated 3 times (Bilel et al., 2022). The score assigned to the movement was 1 or 0 if it was not present. The total value was calculated by adding the scores

obtained in the frontal with those obtained in the lateral visual object response test (overall score: 9). Tests were measured at 10, 30, 60, 120, 180, 240 and 300 min after the injection.

5.3.3.2 Evaluation of Breath Rate

The experimental protocol for the detection of *respiratory parameter* in this study provides for monitoring of the animal awake, freely moving, with a non-invasive and minimal handling. The animal is leaving free in a cage and the respiration patterns of the mice were videotaped by a camera (B/W USB Camera day & night with varifocal lens; Ugo Basile, Italy) placed above observation's cage (Corli et al., 2023). The analysis frame by frame allows to better evaluate the number of breath rates of the mouse evaluated through the count of about 257 ± 11 breath rates per minute (brpm). Breath rate was measured at 15, 40, 70, 150, 130, 190, 250 and 310 min after the injection.

5.3.3.3 Evaluation of motor activity

The Mobility time test evaluates spontaneous motor activity of mice (Corli et al., 2023). The mouse is free to move on a square plastic cage (60×60 cm). The observer measures the total time spent moving by the animal (when the mouse walks or moves the front legs) in five minutes. The test was performed at 15, 35, 70, 125, 185, 245 and 305 min after the injection.

5.3.3.4 Evaluation of pain induced by a mechanical stimulus

Acute mechanical nociception was evaluated using the *tail pinch test* (Bilel et al., 2020). A special rigid probe connected to a digital dynamometer (ZP-50N, IMADA, Japan) was gently placed on the tail of the mouse (in the distal portion), and progressive pressure was applied. When the mouse flicked its tail, the pressure was stopped, and the digital instrument recorded the maximum peak of weight supported (g/force). A cut off (500 g/force) was set to avoid tissue damage. The test was repeated three times, and the final value was calculated by averaging the three obtained scores.

5.3.3.5 Data statistical analysis

In sensorimotor response experiment, data are expressed in arbitrary units (visual object response) and percentage of baseline (breath rate, mobility time). Tail pinch test is expressed as Emax % and is calculated as the percent of maximal possible effect {EMax% = [(test - control latency)/(cut off time - control)] X 100}.

Statistical analysis was performed by two-way ANOVA followed by Bonferroni's test for multiple comparisons. *p< 0.05, **p< 0.01, ***p< 0.001 versus vehicle; #p< 0.05, ###p < 0.001 versus Naloxone + Brorphine. \$p< 0.05, \$\$p< 0.01, \$\$\$p< 0.001 versus gender (female/male)

5.3.4 Results and discussion

Systemic administration of Brorphine (0.01-15 mg/kg IP) induced sensorimotor and motor impairments, increased analgesia and reduced the respiratory rate in female and male treated mice (**Figure 5.13-5.16**).

In the visual object test, the visual reflexes to the object were significantly reduced in male [**Fig 5.13-A**: $F_{(6, 280)}$ = 98.62; P<0.0001] and female [**Fig 5.13-C**: $F_{(6, 280)}$ = 589; P<0.0001] mice after the injection with Brorphine at the range dose of 0.01 and 15 mg/kg. The effect of the highest dose of Brorphine (15 mg/kg) revealed a deeper effect in female mice respect to male mice at this dose, however the effect is contradictory with lower doses (0.01 and 0.1 mg/kg). Pre-treatment with Naloxone reduced partially the visual impairments in both sexes and the second full dose of naloxone (6mg/kg) reverted totally the visual impairments in both sexes [**Fig 5.13-B**: $F_{(3, 280)}$ = 42.36; P<0.0001; **Fig 5.13-D**: $F_{(3, 280)}$ = 186.2; P<0.0001]. Sex differences were revealed by ANOVA at all the range dose of Brorphine [**Fig 5.13-E**: $F_{(1, 280)}$ = 37.31; P<0.0001].
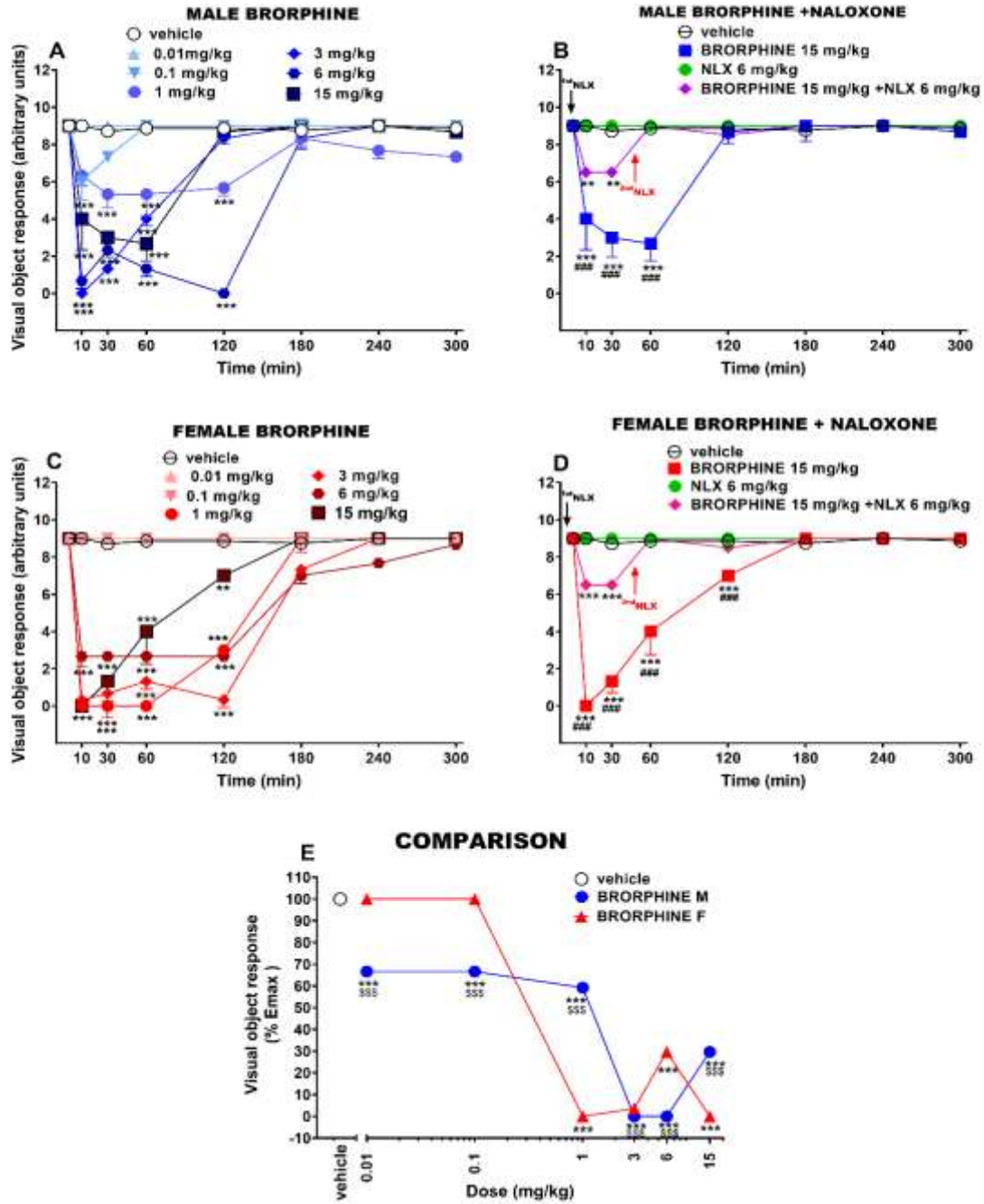
Figure 5.13. *Effects of the systemic administration of Brorphine (0.001-15 mg/kg IP) in the visual object response test, in male mice (panel A) and female mice (panel C). Interaction of effective dose of Brorphine (15 mg/kg) with the opioid receptor antagonist NLX (6 mg/kg) in male mice (panel B) and female mice (Panel C). Comparison of the dose-response curves between males and females in the visual object test. also treated with Naloxone (B), female mice (C) and female mice also treated with Naloxone (D). Data are expressed as arbitrary units (panel A-D) and percentage of maximal effect (Panel E) and represents the mean ± SEM of 8 determinations for each treatment. Statistical analysis was performed by two-way ANOVA followed by Bonferroni's test for multiple comparisons. **p<0.01, ***p<0.001 versus vehicle, ###p<0.001 versus NLX, $$$p<0.001 versus NLX.*

244

In spontaneous locomotion test, Brorphine induce biphasic and significant effects in male [**Fig 5.14-A**: $F_{(6, 280)}$ = 28.4; P<0.0001] and female [**Fig 5.14-C**: $F_{(6, 280)}$ = 47.97; P<0.0001] mice. The most significant level of facilitation was elicited by the 0.01 mg/kg dose of Brorphine in male mice. In contrast, in female mice, the dose of 1 mg/kg induced greater facilitation than both other doses and the same dose in male mice. Overall, the impairment of locomotion by Brorphine was more profound in females than in males. Pre-treatment with Naloxone was not effective in preventing motor impairments in male and the second dose did not revert this effect [**Fig 5.14-B**: $F_{(3, 280)}$ = 85.38; P<0.0001]. Differently, in case of females the second dose of NLX totally prevented the motor impairment induced by Brorphine. [**Fig 5.14-D**: $F_{(3, 280)}$ = 129.5; P<0.0001]. Sex differences were revealed by ANOVA at the doses 0.01, 1 and 15 mg/kg of Brorphine [**Fig 5.14-E**: $F_{(1, 280)}$ = 4.89; P=0.0303].
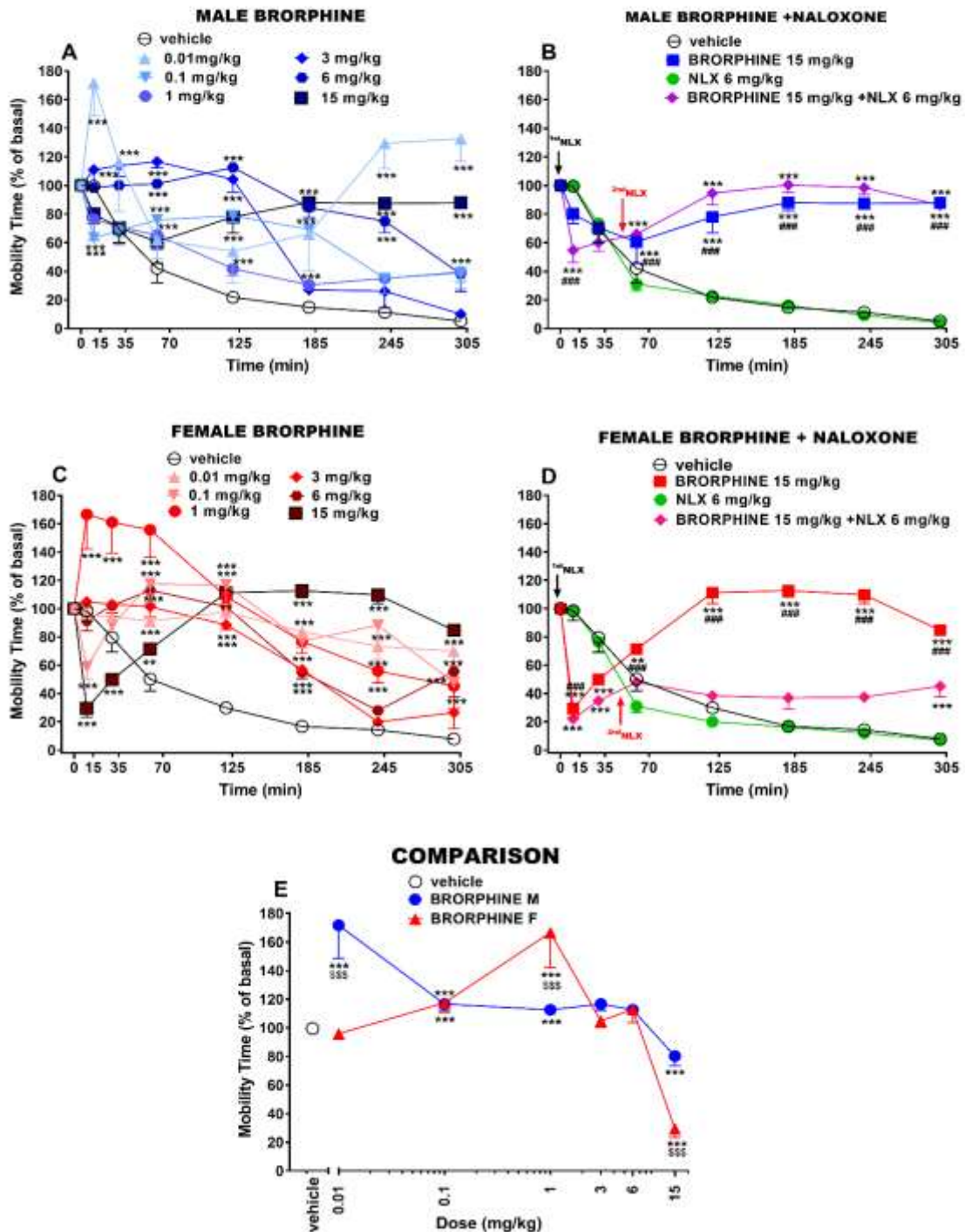
SPONTANEOUS LOCOMOTION TEST

Figure 5.14. *Effects of the systemic administration of Brorphine (0.001-15 mg/kg IP) in the spontaneous locomotion test, in male mice (panel A) and female mice (panel C). Interaction of effective dose of Brorphine (15 mg/kg) with the opioid receptor antagonist NLX (6 mg/kg) in male mice (panel B) and female mice (Panel C). Comparison of the dose-response curves between males and females in the visual object test. also treated with Naloxone (B), female mice (C) and female mice also treated with Naloxone (D). Data are expressed as arbitrary units (panel A-D) and percentage of maximal effect (Panel E) and represents the mean ± SEM of 8 determinations for each treatment. Statistical analysis was performed by two-way ANOVA followed by Bonferroni's test for multiple comparisons. **p<0.01, ***p<0.001 versus vehicle, ###p<0.001 versus NLX, $$$p<0.001 versus NLX.*

In the tail pinch test, the systemic administration of Brorphine (0.01-15 mg/kg IP) induced a dose-dependent and significant increase of antinociception in male [**Fig 5.15-A**: $F_{(6, 280)}$ = 527.7; $P<0.0001$] and female [**Fig 5-15-C**: $F_{(6, 280)}$ = 590.9; $P<0.0001$] mice. In contrast to males, Brorphine exhibited significant effects at the dose of 0.01 mg/kg, while in males, no significant effects were observed at this dose. Pre-treatment with naloxone was effective in preventing the antinociceptive effects of Brorphine (15 mg/kg) in males [**Fig 5-15-B**: $F_{(3, 280)}$ = 282.8; $P<0.0001$] and females [**Fig 5.15-D**: $F_{(3, 280)}$ = 307.7; $P<0.0001$]. Sex differences were revealed by ANOVA at the doses of 0.01, 0.1 and 1 mg/kg of Brorphine [**Fig 5-15-E**: $F_{(1, 280)}$ = 3.80; $P=0.0551$].
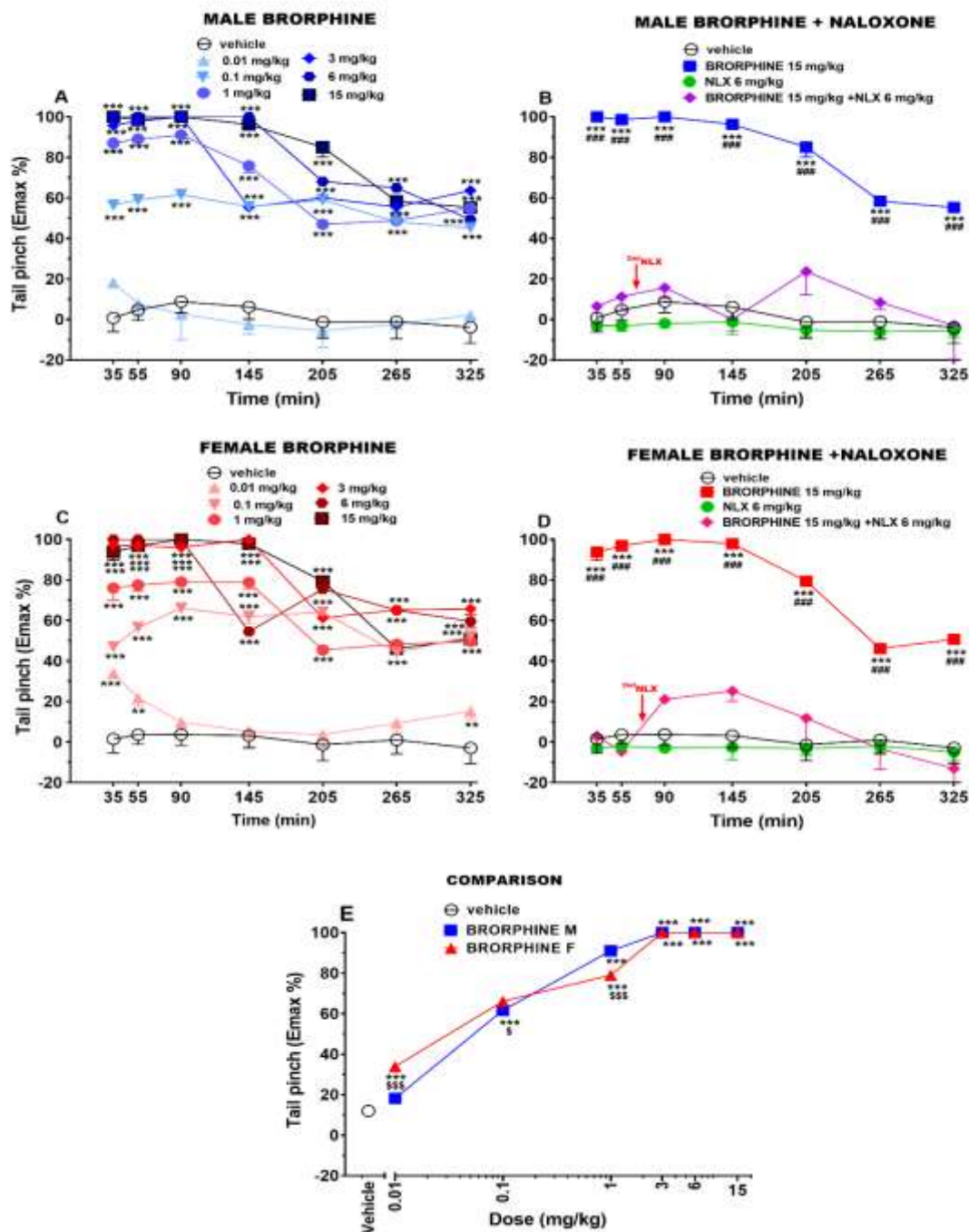
TAIL PINCH TEST

Figure 5.15. *Effects of the systemic administration of Brorphine (0.001-15 mg/kg IP) in the tail pinch test, in male mice (panel A) and female mice (panel C). Interaction of effective dose of Brorphine (15 mg/kg) with the opioid receptor antagonist NLX (6 mg/kg) in male mice (panel B) and female mice (Panel C). Comparison of the dose-response curves between males and females in the visual object test. also treated with Naloxone (B), female mice (C) and female mice also treated with Naloxone (D). Data are expressed as arbitrary units (panel A-D) and percentage of maximal effect (Panel E) and represents the mean ± SEM of 8 determinations for each treatment. Statistical analysis was performed by two-way ANOVA followed by Bonferroni's test for multiple comparisons. **p<0.01, ***p<0.001 versus vehicle, ###p<0.001 versus NLX, \$\$\$p<0.001 versus NLX.*

248

In the breath rate test, the systemic administration of Brorphine (0.01-15 mg/kg IP) induced a dose-dependent and significant decrease of breath rate in male [**Fig 5.16-A**: $F_{(6, 280)}$ = 284.7; P<0.0001] and female [**Fig 5.16-C**: $F_{(6, 280)}$ = 283.7; P<0.0001] mice. In contrast to females, the respiratory reduction persisted with the doses of 3, 6 and 15 mg/kg in males at 300 min of analysis. Neither the pre-treatment, nor the second dose of naloxone were effective to prevent the respiratory depression induced by Brorphine (15 mg/kg) in males [**Fig 5.16-B**: $F_{(3, 280)}$ = 792.3; P<0.0001] and females [**Fig 5.16-D**: $F_{(3, 280)}$ = 304.3; P<0.0001]. However, the effect of naloxone was more effective in females than males in this test. No sex differences revealed by ANOVA in this test [**Fig 5.16-E**: $F_{(1, 280)}$ = 0.021; P=0.8836].
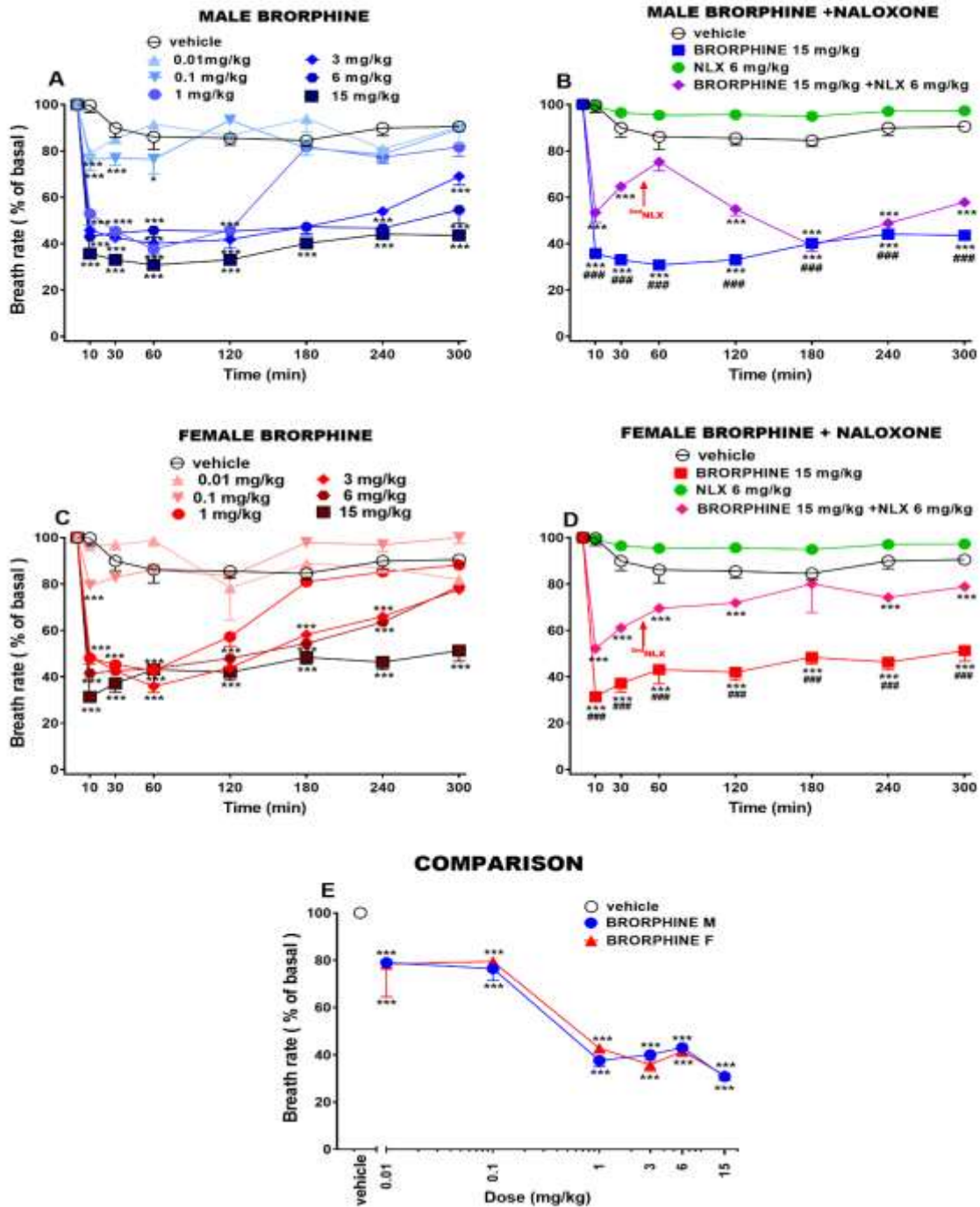
Figure 5.16. *Effects of the systemic administration of Brorphine (0.001-15 mg/kg IP) in the breath rate test, in male mice (panel A) and female mice (panel C). Interaction of effective dose of Brorphine (15 mg/kg) with the opioid receptor antagonist NLX (6 mg/kg) in male mice (panel B) and female mice (Panel C). Comparison of the dose-response curves between males and females in the visual object test. also treated with Naloxone (B), female mice (C) and female mice also treated with Naloxone (D). Data are expressed as arbitrary units (panel A-D) and percentage of maximal effect (Panel E) and represents the mean ± SEM of 8 determinations for each treatment. Statistical analysis was performed by two-way ANOVA followed by Bonferroni's test for multiple comparisons. **p<0.01, ***p<0.001 versus vehicle, ###p<0.001 versus NLX, \$\$\$p<0.001 versus NLX.*

In this research, I explored the pharmacological effects of the NSO Brorphine, a selective mu receptor agonist, in male and female mice. Currently, Brorphine stands as the only emerging NSO featuring a benzimidazolone scaffold. The avaible data on the pharmacology of Brorphine revealed high selectivity of this compound toward mu opioid receptors (Vandeputte et al., 2023). Moreover, the recent *in vivo* data (male rats) on the neuropharmacology of brorphine revealed its high potency in increasing analgesia (tail flick test), inducing catalepsy and reducing body temperature (Vandeputte et al., 2023). The primary effects examined in these experiments revealed important changes in visual object responses, spontaneous locomotor activities, mechanical analgesia, and respiratory rates in female and male mice.

In the visual object test, sex difference was revealed in all the doses tested. Moreover sex-differences were also detected in motor activity and mechanical antinociception. These differences might be related to the difference in the pharmacokinetics between both sexes. Indeed, in my data elaborated above on the two fentanyl analogs (4F-FUF and IBF, **section 5.2**) the two drugs showed sex-differences in the concentrations, distribution, and elimination of these compounds (**Table 5.2 and 5.3**). Interestingly, the effect of NLX was also different in both sexes in motor response and breath rate test. Giving more focus on these important results, these data show a resistance of male mice to NLX in the motor and respiratory tests.

Several recent clinical studies have affirmed a higher prevalence of opioid use in men compared to women (Walter et al., 2022). In addition, the death rate associated with fentanyl overdose has been reported to be two to three times higher in men than in women (Butelman et al., 2023). The current data reveal that NLX treatments differ in males and females where males may show resistance to NLX due to sex-specific expression of cytochromes P450 (Gerger et al., 2023). Moreover, these differences could be associated to differences on mu distribution between both sexes (Zhang et al., 2013) and the influence of circulating ovarien hormones and androgens on mu-mediated physiological responses (reviewed in Sharp et al.,2022).

5.3.5 Conclusion

These data reveal sexual dimorphism in the *in vivo* effects of the NSO Brorphine. In difference to female, male showed more resistance to NLX injections in motor and respiratory tests. These findings highlight the higher risk of respiratory depression among male respect to female sunjects. Consequently, these findings underscore the importance of sex-specific evaluation in studies related to pain management, opioid prescriptions, and opioid misuse.

5.3.6 Contributions

B.S and M.MT designed the study. F.A, V.M, C.S contributed with resources. **B.S**, M.MC, T.M, C.G, BM performed *in vivo experiments*. **B.S** contributed to data curation and the writing of the first draft.

5.4 *In vivo* pharmaco-toxicological characterization of Brorphine and its possible emerging analogues: Orphine, Fluorphine, Chlorphine and Iodorphine

[1]**Bilel Sabrine**, [2]Vandeputte Marthe, [1]Tirri Micaela, [1]Corli Giorgia, [1]Marta Bassi, [2] Stove Christophe,[1]Marti Matteo.

[1]*Department of Translational Medicine, Section of Legal Medicine and LTTA Centre, University of Ferrara, Italy*
[2]*Laboratory of Toxicology, Department of Bioanalysis, Faculty of Pharmaceutical Sciences, Ghent University, Ghent, Belgium*

5.4.1 Background

In continuation to the study reported in **section 4.1** of submitted manuscript (Vandeputte et al., 2023) other *in vivo* data were elaborated using the safety pharmacology, the MouseOX instrument to characterize the cardio-respiratory and the motor effects of these compound.

5.4.2 Materials and methods

All applicable international, national and/or institutional guidelines for the care and use of animals were followed. All procedures performed in the studies involving animals were in accordance with the ethical standards of the institution or practice at which the studies were conducted. This project was activated in collaboration with the Presidency of the Council of Ministers-DPA Anti-Drug Policies (Italy).

5.4.2.1 Animals

Two hundred eighty-four Male ICR (CD-1®) mice weighing 30–35 g (ENVIGO Harlan Italy, Italy; bred inside the Laboratory for Preclinical Research (LARP) of the University of Ferrara, Italy), were group-housed (5 mice per cage; floor area/animal: 80 cm2; minimum enclosure height: 12 cm) on a 12:12-h light–dark cycle (lights on at 6:30 AM), at a temperature of 20–22 °C, humidity of 45–55%, and were provided ad libitum access to food (Diet 4RF25 GLP; Mucedola, Settimo Milanese, Milan, Italy) and water. The experimental protocols were in accordance with the European Communities Council Directive of September 2010 (2010/63/EU), a revision of the Directive 86/609/EEC was approved by the Ethics Committee of the University of Ferrara and by the Italian Ministry of Health (authorization number

335/2016-PR). Moreover, adequate measures were taken to reduce the number of animals used and their pain and discomfort according to the ARRIVE guidelines.

5.4.2.2 Drug preparation and dose selection

Drugs were initially dissolved in absolute ethanol (final concentration: 5%) and Tween 80 (2%) and brought to the final volume with saline (0.9% NaCl). Drugs were administered by intraperitoneal (IP) injection at a volume of 4 µL/g. The dose range of brorphine and its analogues tested (0.01-15 mg/kg IP) was chosen based on our previous studies (Bilel et al., 2022).

In antagonist experiments, the opioid receptor antagonist naloxone (NLX) (6 mg/kg IP) was administered 15 min before test compound injections. The protocol set in the present study for NLX injections is based on our previous study (Bilel et al., 2022) with a small modification in the injection timing of the second NLX dose. The second full dose of NLX (6 mg/kg IP) was injected 60 min after the first one (instead of 55 min) when we noticed a reappearance of the test compounds' effects was observed).

Based on the data obtained *in vivo* after the treatment of the animals with brorphine and analogues at the chosen dose range (0.01-15 mg/kg IP), we selected the dose of 15 mg/kg as the highest and most effective dose in all tests, to evaluate its effects on the cardio-respiratory parameters using the MouseOx instrument.

5.4.3 Behavioural studies

The effects of Brorphine and its analogs were investigated using a battery of behavioural tests widely used in pharmacology safety studies for the preclinical characterization of new psychoactive substances in rodents (Bilel et al., 2020; Bilel et al., 2022). All experiments were performed between 8:30 a.m. and 2:00 p.m. Experiments were conducted blindly by trained observers working in pairs (Bilel et al., 2022). Mouse behaviour (motor responses) was videotaped and analysed offline by a different trained operator who gives test scores.

5.4.3.1 Motor activity assessment

Alterations of motor activity inducedby FENS were measured using the accelerod test (Bilel et al., 2022). In the accelerod test, the animals were placed on a rotating cylinder that automatically increases in velocity in a constant manner (0–60 rotations/min in 5 min). The

time spent on the cylinder was measured. The accelerod test was performed at 0, 40, 60, 95, 150, 210, 270 and 330 min post injection.

5.4.3.2 Evaluation of skeletal muscle strength (grip strength)

This test Evaluation of skeletal muscle strength (grip strength). This test was used to evaluate the skeletal muscle strength of the mice (Bilel et al., 2020). The grip-strength apparatus (ZP-50N, IMADA) is comprised of a wire grid (5 × 5 cm) connected to an isometric force transducer (dynamometer). In the grip-strength test, mice were held by their tails and allowed to grasp the grid with their forepaws. The mice were then gently pulled backward by the tail until the grid was released. The average force exerted by each mouse before losing its grip was recorded. The mean of three measurements for each animal was calculated, and the mean average force was determined. The skeletal muscle strength is expressed in gram force (gf) and was recorded and processed using IMADA ZP-Recorder software. The grip strength was measured at 0, 15, 35, 70, 125, 185, 245 and 305 min post injection.

5.4.3.3 Cardiorespiratory analysis

The experimental protocol to detect the cardiorespiratory parameters used in this study is designed to monitor awake and freely moving animals with no invasive instruments and with minimal handling (Bilel et al., 2022). A collar was placed around the neck of the animal; this collar has a sensor that continuously detects heart rate, respiratory rate, oxygen saturation and pulse distention with a frequency of 15 Hz. While running the experiment, the mouse moves freely in the cage (with no access to food and water) monitored by the sensor collar using the software MouseOx Plus (STARR Life Sciences® Corp. Oakmont, PA). In the first hour, a collar was placed around the animal's neck to simulate the real one used in the test, thus minimising the possible effects of stress during the experiment. The real collar (with sensor) was then substituted, and baseline parameters were monitored for 60 min. Subsequently, the mice were given Orphine, Fluorphine, Chlorphine, Brorphine by IP injection, and data was recorded for 5 h.

5.4.4 Results and discussion

    5.4.4.1 Accelerod test

There was no change in accelerod test performance in mice treated with vehicle (**Figure 5.17**). Systemic administration of Brorphine (0.01–15 mg/kg IP) significantly impaired mouse performance in the accelerod test [**Fig 5.17-A**: $F_{(6, 280)}$ = 284.7; P<0.0001]. In particular, Brorphine induced a biphasic effect with a facilitatory action at the dose of 3mg/kg and an inhibitory action at higher doses (6 and 15 mg/kg). In difference to Brorphine, Orphine and Iodorphine did not induce effects in this test (**Fig 5.17-C, Appendix C Fig.C1**) while Fluorphine and Chlorphine impaired animal performances in the accelerod test. Comparison of the mean effects among the five opioids (**Fig. 5.17-C**) revealed significant differences in the action of each substance at different doses [**Fig 5.17-C**: $F_{(5, 392)}$ = 31.79; P<0.0001].

The pre-treatment with naloxone (6 mg/kg IP) prevented the motor impairments induce by Brorphine [**Fig 5.17-B**: $F_{(3, 392)}$ = 10.29; P<0.0001] and its analogs Fluorphine and Chlorphine (**Fig.5.17-D, Appendix C Fig.C1**).
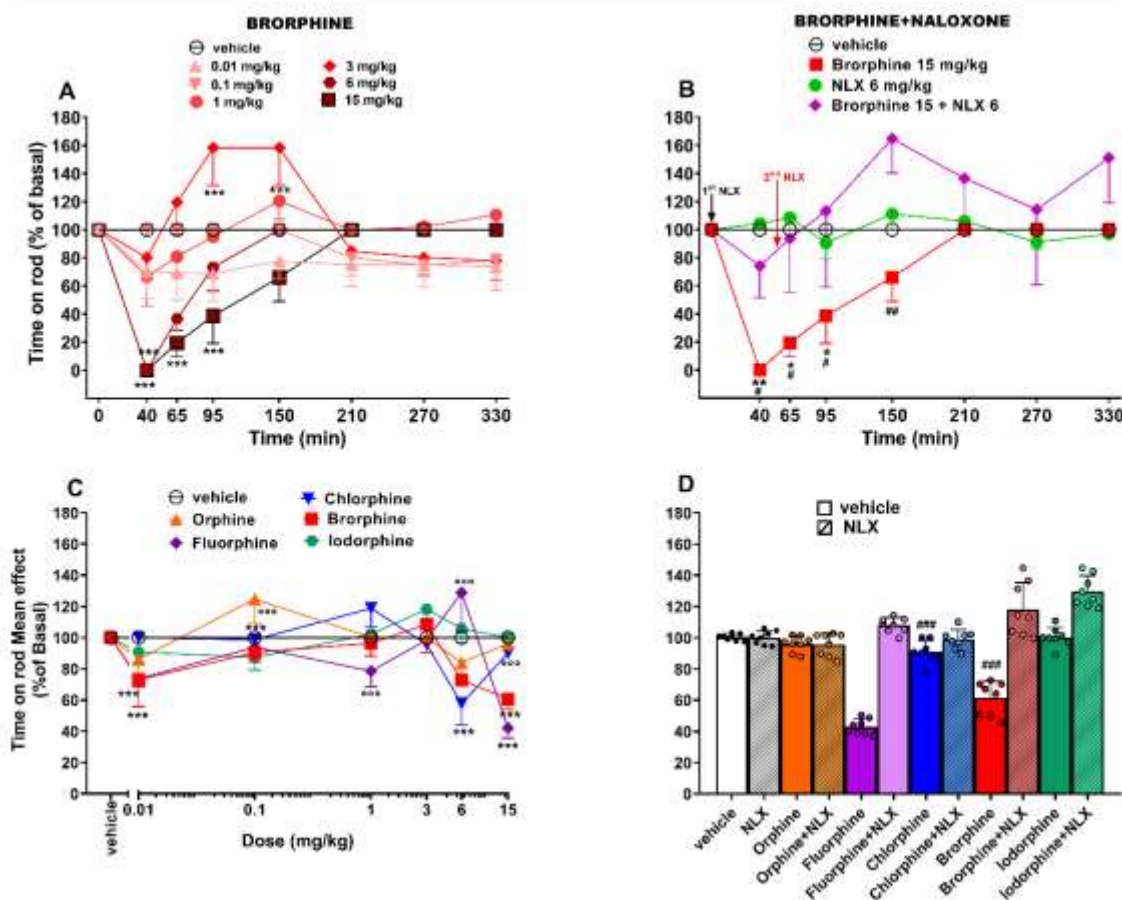
256

Figure 5.17. *Effect of the systemic administration of Brorphine (0.01–15 mg/kg IP; panel A) in the Accelerod test in mice. Interaction of effective dose of Brorphine (15 mg/kg) with the opioid receptor antagonist NLX (panel B). Comparison of the mean effect of Orphine, Fluorphine, Brorphine, Chlorphine and Iodorphine (0.01–15 mg/kg IP) observed in 5 h (panel C). Interaction of Brorphine and its analogs (15 mg/kg) with NLX (6 mg/kg, IP; panel D). Data are expressed as percentage of baseline and represent the mean ± SEM of 8 determinations for each treatment Statistical analysis was performed by two-way ANOVA followed by the Bonferroni's test for multiple comparisons for the dose response curve of Brorphine at different times (panel A and B) and for the comparison of the mean effects (panel C), while the statistical analysis of panel D was performed with one-way ANOVA followed by Bonferroni test for multiple comparisons. *p< 0.05, **p< 0.01, ***p< 0.001 versus vehicle, ##p<0.05, ##p<0.01, ###p < 0.001 versus NLX + agonist; °°°p < 0.001 versus Brorphine.*

5.4.4.2 Evaluation of skeletal muscle strength

Muscle strength was not affected in mice treated with vehicle (**Fig. 5.18**). Systemic administration of Brorphine (0.01–15 mg/kg IP) significantly decreased the pulling force of mice [**Fig. 5.18-A**: $F_{(6, 392)}$ = 54.54; P<0.0001]. In particular, Brorphine induced inhibitory effect at the doses of 0.01. 3 and 6 mg/kg. Interestingly this effect was not significant at the dose of 15 mg/kg. Orphine and Chlorphine also reduced the pulling force of mice and in difference to Brorphine the dose of 15 m/kg showed a significant reduction of grip strength

(**Appendix C Fig.C2; Fig 5.18-C, D)**. Differently, Fluorphine increased muscle strength at the dose of 6 and 15 mg/ kg (**Appendix C Fig.C2; Fig. 5.18-C).** Iodorphine did not show any significant effect at the range dose tested but a slight increase of muscle rigidity was observed in mice treated with 15 mg/kg (Appendix **C Fig.C2; Fig. 5.18-C**). Comparison of the mean effects among the five opioids (**Fig. 5.18-C**) revealed significant differences in the action of each substance at different doses [**Fig. 5.18-C**: $F_{(5, 392)} = 31.79$; $P<0.0001$].
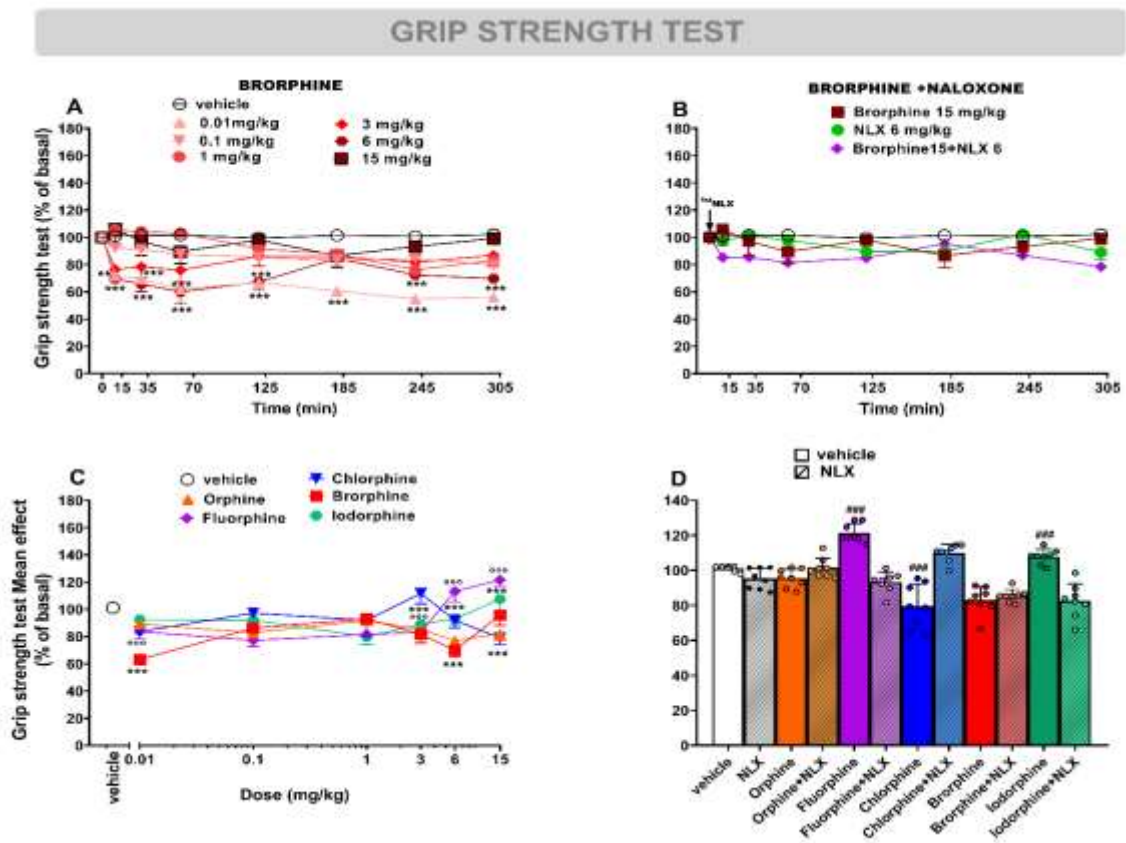

Figure 5.18. *Effect of the systemic administration of Brorphine (0.01–15 mg/kg IP; panel A) in the Grip strength test in mice. Interaction of effective dose of Brorphine (15 mg/kg) with the opioid receptor antagonist NLX (panel B). Comparison of the mean effect of Orphine, Fluorphine, Brorphine, Chlorphine and Iodorphine (0.01–15 mg/kg IP) observed in 5 h (panel C). Interaction of Brorphine and its analogs (15 mg/kg) with NLX (6 mg/kg, IP; panel D). Data are expressed as percentage of baseline and represent the mean ± SEM of 8 determinations for each treatment Statistical analysis was performed by two-way ANOVA followed by the Bonferroni's test for multiple comparisons for the dose response curve of Brorphine at different times (panel A and B) and for the comparison of the mean effects (panel C), while the statistical analysis of panel D was performed with one-way ANOVA followed by Bonferroni test for multiple comparisons. ***p< 0.001 versus vehicle, ###p < 0.001 versus NLX + agonist; ° ° °p < 0.001 versus Brorphine.*

Since naloxone injections belong to a battery of tests in which the grip strength test is included the treatment with naloxone is reported for Brorphine even if the dose of 15 mg/kg was not effective. The pre-treatment with NLX in case of Brorphine didn't affect muscle rigidity in mice treated with 15 mg/kg (**Fig. 5.18-B**). The pre-treatment with naloxone (6 mg/kg IP) prevented the pulling force impairments induce by Fluorphine, Chlorphine and Iodorphine (**Appendix C Fig.C2; Fig. 5.16-D**).

5.4.4.3 Cardiorespiratory analysis

The vehicle used in this experiment showed a stable profile during the 6 h of cardiorespiratory parameter measurement (heart rate, pulse distention respiratory rate and oxygen saturation (**Figure 5.19**). Systemic administration of Brorphine (15mg/kg IP), induced important variations in cardiorespiratory parameters. Heart rate (**Fig. 5.19-A**) was rapidly (5 min post injection) and significantly affected by Brorphine treatment [**Fig. 5.19-A**: $F_{(3, 1460)} = 1284$, $P < 0.0001$]. Similar to Brorphine, Fluorphine, Chlorphine and Iodorphine but not Orphine significantly reduced heart rate at the dose of 15 mg/kg [**Fig. 5.19-B**: $F_{(5, 2190)} = 701.5$, $P < 0.0001$], (**Appendix C Fig.C3**). Pre-treatment with NLX (6 mg/kg.IP; **Fig. 5.19-A**) prevented Brorphine bradycardia. Similar to Brorphine the treatment with NLX prevented the decrease of heart rate in Fluorphine, Chlorphine and Iodorphine treatment (**Appendix C Fig.C3; Fig. .5.19-C**).

Pulse distention (**Figure 5.19**) in the group of mice treated with Brorphine was significantly affected by treatment [**Fig. 5.19-D**: $F_{(3, 1460)} = 130.7$, $P < 0.0001$]. In difference to Brorphine, its four analogs showed a significant decrease in pulse distention [**Fig. 5 .19-E**: $F_{(5, 2190)} = 1047$, $P < 0.0001$], (**Appendix C Fig.C3**). The pre-treatment with NLX prevented the increase in pulse distention induced by Brorphine (**Fig. 5.19-A**). Similarly, NLX treatments prevented the decrease in pulse distention induced by Orphine, Fluorphine and Iodorphine (**Appendix C Fig. C3; Fig. 5.19-F**).
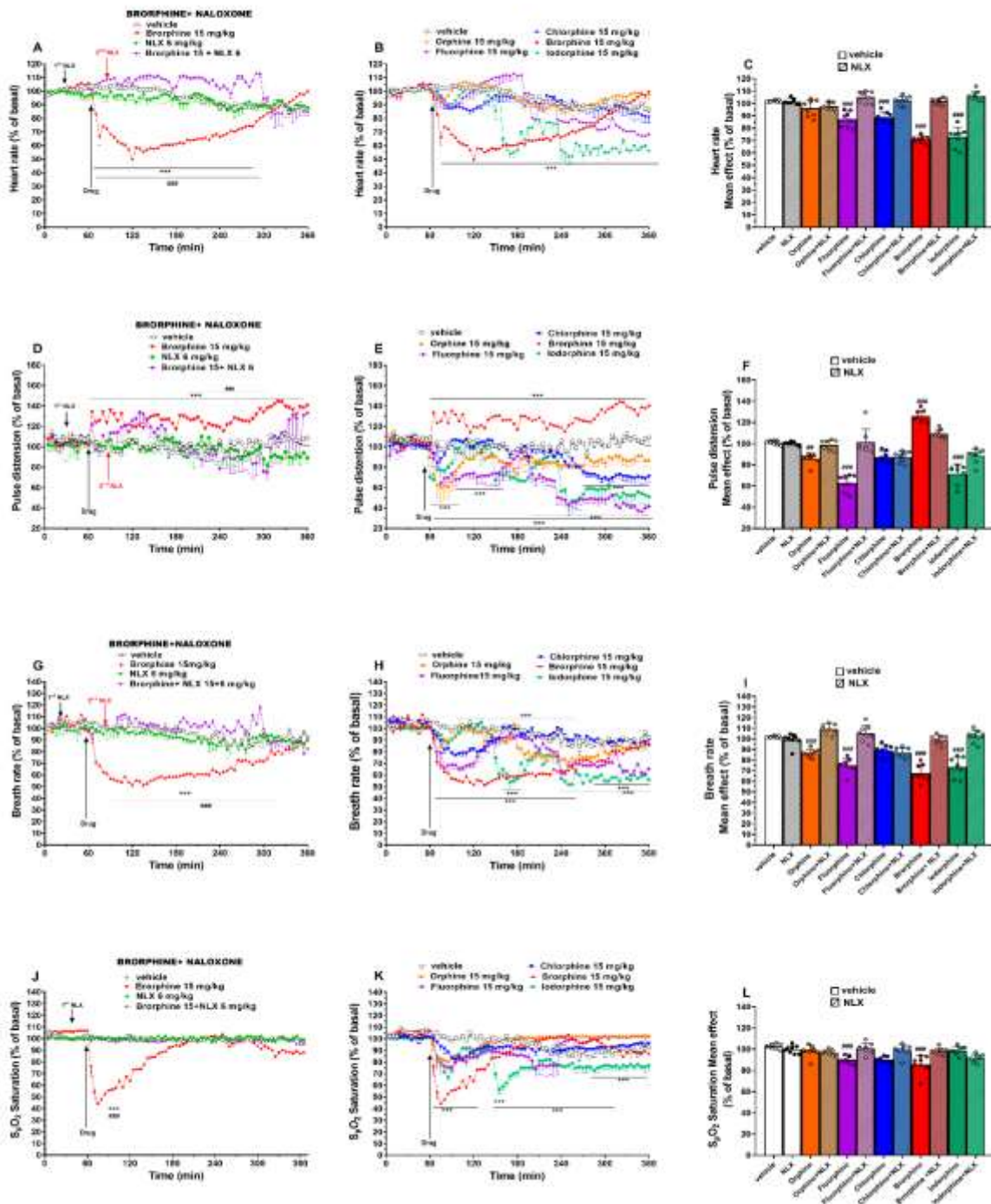
CARDIORESPIRATORY ANALYSIS

Figure 5.19. *Cardiorespiratory effects of the systemic administration of Brorphine (0.01–15 mg/kg IP) and its interaction with the opioid receptor antagonist NLX (Panels A-D-G-J). Effects of a high dose (15 mg/kg IP) of the different test compounds on Heart rate, pulse distention, breath rate and oxygen saturation over time (Panels B-E-H-K). Interaction of Brorphine and its analogs (15 mg/kg) with NLX (6 mg/kg, IP.; panels C-F-I-L). Data are expressed as percentage change from basal (% of basal) over time and represent the mean ± SEM as determined in 8 animals for each treatment regimen. Statistical analysis was performed by two-way ANOVA followed by the Bonferroni test for multiple comparisons for panels A-B, D-E, G-H and J-K, while the statistical analysis of panels C, F, I and L was performed with one-way ANOVA followed by the Bonferroni test for multiple comparisons. ***p< 0.001 versus vehicle, ###p < 0.001 versus NLX + agonist; °°°p < 0.001 versus Brorphine.*

After the administration of Brorphine, breath rate (**Fig. 5.19-G**) was also significantly affected by treatment [**Fig. 5.19-G**: F $_{(3, 1460)}$ = 751.1, P < 0.0001]. Similarly to Brorphine, the five analogs induced a significant decrease in breath rate treatment [**Fig. 5.19-H**: F $_{(5, 2190)}$ = 1035, P < 0.0001], (**Appendix C Fig. C4**). Overall, the effect of Orphine is moderate in this test and the respiratory reduction was delayed with respect to Brorphine (**Appendix C Fig. C4**). In addition, the effect of Iodorphine fluctuates during the different hours of measurements. In particular, initial significant impairments slightly appear in the first hour then tend to be more profound in the last two hours of measurements (**Appendix C Fig.C4; Fig. 5.19-H**). NLX pre-treatment prevented respiratory reductions induced by Brorphine (**Fig.5.19-G**) and its analogs (**Fig. 5.19-I; Appendix C Fig. C4**).

After administration of Brorphine, oxygen saturation (**Fig. 4.19-J**) was also significantly affected by treatment [**Fig. 4.19-J**: F $_{(3, 1460)}$ = 2219, P < 0.0001]. Similarly to Brorphine, the five analogs induced a significant decrease in oxygen saturation [**Fig. 4.19-K**: F $_{(5, 2190)}$ = 522.4, P < 0.0001]. The analogs of Brorphine induced a moderated and transient effect in this parameter (**Appendix C Fig.C4**). Only Iodorphine showed a deep drop of SpO_2 saturation in the second hour of analysis (**Appendix C Fig.C4; Fig.4.19-K**). In addition, the effect of Iodorphine fluctuates during the different hours of measurements. In particular, initial significant impairments appeared in the first hour then the effect tended to be more profound in the last two hours of measurements (**Fig.4.19-K; Appendix C Fig.C4**). NLX pre-treatment prevented the oxygen saturation reductions induced by Brorphine (**Fig.4.19-G**) and its analogs (**Fig. 4.19-I; Appendix C Fig.C4**).

Systemic administration of Orphine, Fluorphine, Chlorphine and Brorphine induced impairment of motor performance in the accelerod test (**Figure 4.17**). The data obtained in the accelerod test show a biphasic effect of all the compounds but not for Iodorphine which did not affect locomotion in this test (**Fig. 4.17-C**). The biphasic effect of opioids agonists was disclosed in my previous studies on NSOs such as MT-45, fentanyl and fentanyl analogs (Bilel et al., 2020; Bilel et al., 2022). In addition, Brorphine and its analogs except Iodorphine impaired muscle strength. It is worth noting that these effects are contradictory. In particular, Orphine and Chlorphine reduced muscle rigidity at the dose of 6 and 15 mg/kg however, in case of Brorphine this dose was not active in this test. Only Fluorphine increased muscle

rigidity at 6 and 15 mg/kg. Based in my previous publications, Fluorphine showed a similar trend of action to morphine (Bilel et al., 2020) which increased muscle rigidity at 15 mg/kg. Differently, Orphine, Chlorphine and Brorphine showed similar effects to fentanyl in this test (Bilel et al., 2022). The pre-treatment with Naloxone prevented the motor and the muscle rigidity impairments revealing a central action of the mu-opioid receptors. The absence of effects of Iodorphine suggest the role of the chemical substituent in NSOs on their opioid receptor occupancy in response to various tests (Bilel et al., 2022, Vandeputte et al, 2023, Varshneya et al., 2022). The mechanisms by which opioids impair motor and muscle rigidity are detailed in (Bilel et al., 2020 and Bilel et al 2022).

In cardiorespiratory analysis, I have demonstrated using the MouseOX instrument that Orphine, Fluorphine, Chlorphine, Brorphine and Iodorphine significantly altered the cardiorespiratory parameters (**Figs. 5.18–5.19**) when administered to mice at the highest dose of 15 mg/kg. The effects observed by Orphine are very moderate with respect to the other compounds. Moreover, the effects of Iodorphine are delayed but persistent with respect to the other opioids. Only Brorphine showed an increase of pulse distention, but all the other compounds showed a decrease of this parameter at the same dose tested. Brorphine showed higher effect in breath rate and oxygen saturation parameters. The effects of Brorphine were the most pronounced and profound in this test. Pretreatment with a single dose of NLX prevented cardiorespiratory impairments induced by the five compounds suggesting again the central role of mu-opioid receptor in cardiorespiratory depression by Brorphine and its analogs (see **section 4.1** for submitted manuscripts, Vandeputte et al., 2023). The results obtained in pulse distention reveal that only Brorphine induces vasodilatation in mice at the dose of 15mg/kg, however, all the analogs induced vasoconstriction. These data suggest the possible involvement of other mechanisms (intermediated by mu opioid receptors) in cardiorespiratory effects of Brorphine and its analogs. Together with the data obtained in antinociception and plethysmography (**section 4.2**) suggest other mechanisms involved in the action of some compounds and to better understand their functional processes, we have submitted Psychoactive Drug Screening Program (PDSP) to request for the analysis of Orphine, Fluorphine, Chlorphine and Iodorphine. We requested determination of binding affinity at the following targets:

Mu opioid receptor (MOR); delta opioid receptor (DOR); kappa opioid receptor (KOR); sigma receptors (Sigma 1, Sigma 2); nociceptin/orphanin FQ peptide receptor (NOR); serotonin

transporter (SERT); subtypes of serotonin receptors (5-HT1A, 5-HT1B, 5-HT1D, 5-HT1E, 5-HT2A, 5-HT2B, 5-HT2C, 5-HT3, 5-HT5A, 5-HT6, 5-HT7A); dopamine receptors (DAT); subtypes of dopamine receptors (D1, D2, D3, D4, D5); norepinephrine transporter (NET); subtypes of muscarinic acetylcholine receptors (M1, M2, M3, M4, M5); subtypes of adrenergic receptors (Alpha1A, Alpha1B, Alpha1D, Alpha2A, Alpha2B, Alpha2C); subtypes of beta-adrenergic receptors Beta1, Beta2, Beta3); subtype of the GABA receptor (GABAA); subtypes of histamine receptors (H1, H2, H3, H4); subtypes of glutamate receptors (AMPA, Kainate-Rat Brain, NMDA, NR2B); benzodiazepines binding site (BZP-Rat Brain Site); peripheral benzodiazepine receptor (PBR), most of these targets are included in the PDSP's standard 'comprehensive screen'.

5.4.5 Conclusion

These data reveal that Brorphine analogs may pose a significant risk of harm to users if they appear in recreational drug markets. Therefore, it is essential to vigilantly monitor the evolving NSO market to promptly identify and address shifts in the drug supply.

5.4.6 Contributions

B.S and M.MT, VM, CS designed the study. VM, CS contributed with resources. **B.S**, T.M, C.G, BM performed *in vivo* experiments. **B.S** contributed to data curation and the writing of the first draft.

5.5 In silico ADMET prediction of emerging NSOs

[1]**Bilel Sabrine**, [2]Alaaldin M. Alkilany, [2]Ousama Rachid, [1]Marti Matteo.

[1]*Department of Translational Medicine, Section of Legal Medicine and LTTA Centre, University of Ferrara, Italy*
[2] *Department of Pharmaceutical Sciences, College of Pharmacy, QU Health, Qatar University, Qatar*

5.5.1 Backgroud

Due to the increasing availability of NSOs and the lack of knowledge of their physicochemical and their toxicological properties, it becomes relevant to develop rapid methodologies to identify the pharmaco-toxicological effects of these compounds and their impact on human health.

During my mobility period at Qatar University, I attended lectures on pharmacokinetics and phramacogenomics and I learned how to use the in silico ADMET (Absorption, Distribution, Metabolism, Excretion and Toxicity) prediction for different classes of NPS. Recently, I have applied this method to predict the toxicity of the NPS γ-valerolactone (GVL) to γ-hydroxybutyric acid (GHB); (Arfè et al, 2023). In this study, I have performed in silico ADMET analysis to evaluate the toxicity of fentanyl and fentanyl analogs (Acrylfentanyl, Ocfentanyl, Furanylfentanyl, Isobutyrylfentanyl, 4F-Furanylfentanyl, Butyrylfentanyl and 4-Fluoro-Butyrylfentanyl) and Brorphine and its analogs (Orphine, Fluorphine, Chlorphine and Iodorphine).

5.5.2 Methods

The *in silico* characterization of the ADMET profile of the different NSOs was conducted through Simulations Plus ADMET Predictor® Version 10.4 (×64) on a Windows 11 operating system. The program allows for prediction of ADMET properties based on the molecular structures of compounds. It uses artificial neural network ensemble (ANNE) models which were trained to ensemble with data sets that share the same "architecture" (i.e., same inputs and number of neurons) from well-defined drugs, using the 2D structure and the atomic descriptors

for data selection. ADMET Predictor® models have been shown to have a similar or better accuracy when compared to other available software (Golbamaki et al., 2014)

5.5.2.1 Evaluation of risks

5.5.2.1.1 ADMET risk

As an initial screening step, the NSOs were screened based on some of their calculated risk scores. The program provides a score, labelled "ADMET_Risk" that is a general score ranging from 0 to 24 which indicates the number of potential ADMET issues that a compound may face. A threshold of concern for each risk is suggested by the program and is calculated by defining the threshold below which 90% of drugs in the World Drug Index (WDI) score. In addition, the compounds were assessed for their conformance to Lipinski's Rule of Five (RO5). According to RO5, a drug can be orally active only if it meets at least three of the following criteria: molecular weight (MW) <500 Daltons, hydrogen bond acceptors (HBA) ≤10, hydrogen bond donors (HBD) ≤5, logP ≤5 (13).

Absorption risk

The absorption risk model (Absn_Risk) includes eight rules based on descriptors and predicted properties licensed as part of the PhysChem model group, each of which contributes one vote to the score. The rules are illustrated in **Table 5.4**.

Table 5.4. *The eight rules based on descriptors and predicted properties used to assess absorption risk.*

Parameter	Rule of absorption risk
Size	MWt > [450,500] or N_Atoms > [30,35] or MolVol > [470,520] or N_Bonds > [35,40]
RotB	N_FrRotB > [8,10] (too flexible)
HBD	HBDH > [3,5] and HBDch > [1.5,2.0] (too many good H-bond donors)
HBA	HBA > [7,10] and HBAch < [-6.0,-5.0] (too many good H-bond acceptors)
Charge	NPA_ABSQ > [19,21] or T_PSA > [120 Å2,140 Å2] (excessive charge)
Kow	S+logP > [4.5,5.0] or S+logD > [3.5,4.0] OR MlogP > [3.5,4.0] (high logPoctanol-water)
Peff	S+Peff < [0.40,0.60] (low permeability)
Sw	S+Sw < [0.005,0.010] (low solubility)

RotB. Rotational bonds; N_FrRotB. number of freely rotatable bonds; HBD hydrogen bond donors; HBDH. hydrogen bond donors hydrogens; HBDch hydrogen bond charge HBA. hydrogen bond acceptors; NPA_ABSQ Sum of absolute values of estimated NPA partial; T_PSA Topological polar surface area; Kow. n-Octanol/Water Partition Coefficient; S+logP. Octanol-water partition coefficient Simulations Plus; S+logD, Octanol-water distribution coefficient Simulations Plus [cm/s×10⁴]; MlogP, Moriguchi octanol-water partition coefficient. Peff, human jejunal permeability; S+Peff. human effective jejunal permeability Simulations Plus; Sw, Water solubility; S+Sw, Native water solubility; Simulations Plus

5.5.2.1.2 Cytochrome risk

The cytochrome risk model is comprised of six rules, each with a weight of one illustrated in

Table 5.5.

Table 5.5. The six rules based on descriptors and predicted properties used to assess cytochrome risk.

Parameter	Rule of cytochrome risk
1A2	CYP1A2_CLint > [20,40]
2C9	CYP2C9_CLint > [10,20]
2C19	CYP2C19_CLint > [20,40]
2D6	CYP2D6_CLint > [10,20]
3A4	CYP3A4_CLint > [20,50] and CYP3A4_HLM_CLint > [30,75]
CLEARANCE	CYP_HLM_CLint > [90,150] or HEP_hCLint > [60,90]

*CYP1A2_CLint, intrinsic clearance constant for CYP 1A2 mediated metabolism [µl/min/mg]; **CYP2C9_CLint**. intrinsic clearance constant for CYP 2C9 mediated metabolism [µl/min/mg]; **CYP_2C19_CLint**. intrinsic clearance constant for CYP 2C19 mediated metabolism [µl/min/mg]; **CYP2D6_CLint**.intrinsic clearance constant for CYP 2D6 mediated metabolism [µl/min/m]; **CYP3A4_CLint**. intrinsic clearance constant for CYP 3A4 mediated metabolism[µl/min/mg]; **CYP_HLM_CLint:** overall in vitro (unbound) intrinsic clearance in Human Liver Microsomes [µ L/min/mg HLM protein]; **HEP_hCLint:** overall in vitro (unbound) intrinsic clearance in human hepatocytes [µ L/min/10^6 cells].*

5.5.2.1.3 Toxicity risk

The toxicity risk model consists of five rules (**Table 5.6**), including one based on mutation risk. Each has an associated weight of one. The rat and mouse toxicity thresholds are based on the distribution of in-scope values in the focused WDI, as is the mutagenicity threshold. The hepatotoxicity rule "HEPX" reflects the way actual blood test results are interpreted, e.g., hepatotoxicity is indicated if aspartic acid transaminase (Ser_AST) and alanine transaminase (Ser_ALT) are both elevated in serum. Liver injury also usually elevates serum levels of lactate dehydrogenase and including Ser_LDH in the rule reduces the number of false positives. Concomitant elevation of the other serum enzyme model predictions, Ser_AlkPhos or Ser_GGT, is indicative of even more severe liver injury.

Table 5.6. *The five rules based on descriptors and predicted properties used to assed toxicity risk.*

Parameter	Rule of toxicity risk
hERG	hERG_FILTER = Yes and hERG_pIC$_{50}$ > [5.5,6.0] (potential hERG liability)
rat	*Rat_Acute* < [200,300] (acute toxicity in rats)
Xm:	*Mouse_TD50* < [25,40] (carcinogenicity in chronic mouse studies)
HEPX	*Ser_AST* = Elevated and *Ser_ALT* = Elevated and *Ser_LDH* = Elevated (liver enzymes elevated in serum)
MUT	*MUT_Risk* > 1

hERG, human Ether-a-go-go Related Gene*; **hERG_FILTER,*** qualitative estimation of the likelihood of the hERG potassium channel inhibition in human **hERG_pIC$_{50}$,** a measure of affinity towards hERG K+channel and potential for cardiac toxicity [mol/L], **Rat_acute**, LD$_{50}$ for lethal rat acute toxicity by any mechanism [mg/kg] **Xm**, carcinogenicity in chronic mouse studies, **Mouse_TD$_{50}$,** the TD$_{50}$ is the dose of a substance given to mice orally throughout their lifetimes resulting in half of the population experiencing tumors [mg/kg/day]; **HEPX**, Hepatotoxicity; **Ser_AST** serum aspartic acid transaminase, **Ser_ALT** serum alanine transaminase; **Ser_LDH** serum lactate dehydrogenase

5.5.2.1.4 Mutation risk

The mutation risk component of toxicity risk and ADMET risk integrates the 10 test predictions from Simulation Plus in silico Ames tests for mutagenicity. It exceeds 1.0 for 15% of the focused WDI subset and exceeds 1.2 for 9% of it. Most of the individual toxicity risk rules are rather conservative, with each individual rule being violated to some extent by 7-16% of in-scope predictions for WDI reference set. Toxicity risk is greater than 2.0 for 6% of the focused WDI after default out-of-scope risk penalties have been factored in; it is equal to 2.0 for 10% of it.

5.5.2.1.5 Summary of ADMET parameters and recommended ranges

The criteria used to set the ADMET scores (**Table 5.7**) are based on predictions for a refined reference subset drawn from the WDI and developed in ADMET modules by Simulation Plus (all the cited criteria and their scores are found in the manual provided by ADMET Predictor®).
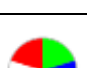
Table 5.7. Overview of ADMET parameters with their recommended ranges.

Parameter	Recommended Range	Comments
ADMET_Risk	**< 7**	Includes components of all risk models as well as fraction unbound to plasma and volume of distribution.
Absn_Risk	**< 4**	Considers size, rotational bonds, hydrogen bonding capacity, polar surface area, permeability, lipophilicity, solubility.
TOX_Risk	**< 2**	Consists of hERG, acute toxicity in rats, carcinogenicity in chronic rat/mouse studies, hepatotoxicity, mutation.
MUT_Risk	**< 2**	Comprises of Ames mutagenicity test, which tests for mutagenic capacity of compounds in bacteria.
CYP_Risk	**< 2**	Includes inhibition of CYPs 1A2, 2C19, 2C9, 2D6, and 3A4, excessive clearance, and inhibition of midazolam or testosterone.

5.5.3 Results and Discussion

The risk scores for fentanyl, fentanyl analogs, Brorphine and Brorphine analogs were calculated (**Table 5.8**). All risk score thresholds are illustrated in **Table 5.8**. The compounds selected were below the ADMET_risk threshold of 7. No mutation risk was predicted for all compounds. Only Ocfentanyl and Orphine were not predicted to have absorption risks. Differently, all the other compounds showed absorption risk. The highest scores detected by ADMET (0.096-1) includes 4F-Furanyfentanyl, Isobutyrylfentayl, Butyrylfentanyl and 4-Fluoro-Butyrylfentanyl.

Table 5.8. *Risk scores of Fentanyl and its analogs, Brorphine and its analogs by ADMET Predictor®. The wedge colors in the star plots correspond to the following: green for ADMET_Risk, blue for Absn_Risk, red for TOX_Risk, purple for CYP_Risk, and yellow for MUT_Risk.*

NSO	Overall Risks	ADMET_Risk	Absn_Risk	MUT_Risk	TOX_Risk	CYP_Risk
Fentanyl		2.377 Kow; hERG; 2D6	0.536 Kow	0	0.842 hERG	1 2D6
Acrylfentanyl		2.132 Kow; hERG; 2D6	0.381 Kow	0	0.751 hERG	1 2D6
Ocfentanyl		1.937 hERG;2D6; 3A4	0	0	0.48 hERG	1.457 2D6; 3A4
Furanylfentanyl		3.13 Kow;hERG; 2D6; 3A4	0.328 Kow	0	0.978 hERG	1.823 2D6; 3A4
4F-Furanylfentanyl		4.01 Kow;fu; hERG; 2D6; 3A4	1 Kow	0	1 hERG	2 2D6; 3A4
Isobutyrylfentanyl		2.872 Kow; hERG; 2D6	0.966 Kow	0	0.90 hERG	1 2D6
Butyrlfentanyl		3.385 Kow; hERG; 2D6; 3A4	1 Kow	0	1 hERG	1.42 2D6; 3A4
4-Fluoro-Butyrylfentanyl		4.106 Kow;Vd; hERG; rat; 2D6; 3A4	0.966 Kow	0	1.014 hERG;rat	2 2D6; 3A4
Brorphine		0.87 Kow; 2D6	0.556 Kow	0	0	0.314 2D6
Orphine		1.009 2D6; 3A4	0	0	0	1.009 2D6; 3A4
Fluorphine		1.315 Kow; 2D6; 3A4	0.114 Kow	0	0	1.2 2D6; 3A4
Chlorphine		0.377 Kow; 2D6	0.336 Kow	0	0	0.041 2D6
Iodorphine		1.676 Kow; 3A4	0.774 Kow	0	0	0.902 3A4

Kow *n-Octanol/Water Partition Coefficient;* **hERG***, human Ether-a-go-go Related Gene, a qualitative estimation of the likelihood of hERG potassium channel inhibition in human;* **rat:** *LD_{50} for lethal rat acute toxicity by any mechanism [mg/kg],* **Vd,** *volume of distribution,* **2D6** *and* **3A4***: cytochrome clearance,* **fu** *fraction unbound.*

The absorption codes indicate that the detected absorption risk is related to high lipophilicity (Kow). In addition, the predicted toxicity risks of all the compounds were below the threshold of 2. However, ADMET predicted risk of cardiotoxicity (code hERG) for all the list of fentanyl(s) but not for Brorphine and analogs. Moreover, only 4-Fluoro-Butyrlfentanyl showed a code risk for rat acute toxicity (code rat). All the opioids were below the cytochrome risk. ADMET prediction showed cytochrome codes related to the cytochromes CYP340 and CYP2D6 (**Table 5.8**). Exceptionally, ADMET predicted a risk of Fu (fraction unbound) only for 4F-Furanylfentanl and a risk of Vd (volume of distribution for 4-Fluoro-Butyrylfentanyl).

The prediction of ADMET parameters is one of the most reliable tools that has increasingly been included in the research of quantitative structure–activity relationship (QSAR) models for early drug discovery (Kar and Leszczynski, 2020). Due to the lack of knowledge of the pharmaco-toxicological effects of many NSOs, I applied *in silico* ADMET prediction to compare the toxicological effects of fentanyl and its structural analogs and Brorphine and its analogs. Fentanyl and Acrylfentanyl were predicted to have very similar toxicological profiles (risk scores and codes are very similar in all risks). This data is in accordance with our *in vitro* and *in vivo* data where we have found a similar pharmacodynamic profile between Fentanyl and Acrylfentanyl (Bilel et al., 2022, data in section **5.1**).

The absorption risk of all the compounds reveals a code related to high lipophilicity (kow) except for Ocfentanyl and Orphine. ADMET simulation can also reveal data for the physicochemical properties of the inserted conpounds. Indeed, only Ocfentanyl and Orphine have a LogP values below the threshold 3.5 reported in **Table 5.4** (3.33 for Ocfentanyl and 3.17 for Orphine; data not shown). In silico ADMET enables the assessment of physicochemical information before certified reference materials become accessible for *in vitro* or *in vivo* studies. Computationally derived data can offer insights into the physicochemical characteristics of upcoming fentanyl analogs and other NSOs that are yet to be introduced like Brorphine analogs (Shakmuth & kerighan 2023).

ADMET prediction allows also to simulate cardiotoxicity risk through the qualitative estimation of the likelihood of human Ether-a-go-go Related Gene (hERG) potassium channel inhibition in human. Fentanyl and its analogs were predicted to have a high affinity to hERG potassium channel in human, this reflect their high cardiotoxic risk as revealed in many case

reports (Frisoni et al., 2019) and preclinical studies (Bilel et al., 2022, current data presented in chapters **4** and **5**). Of note, Brorphine and its analogs did not show toxicity risk and ADMET did not provide hERG code related to these compounds however ADMET predicted, through the estimation of hERG-Filter (**Table 5.4**) a block of the hERG potassium channel by Brorphine, Fluorphine, Chlorphine and Iodorphine but not for Orphine (data not shown). The absence of hERG code with these compounds is that the simulated affinity for all these compounds is below the rule of toxicity risk related to hERG pIC_{50} (<5.5 mol/L) included in descriptors (**Table 5.4**). Taking the exemple of fentanyl and Brorphine the hERG pIC_{50} affinity predicted for fentanyl was 5.9 mol/L (exceeding the toxicity rule in **Table 5.4**), however for Brorphine hERG pIC_{50} affinity was 5.2 mol/L (data not shown). This data demonstrates that there is a very small difference in this predicted parameter. These results confirm the low cardiotoxic effect of Orphine (see section **5.3**) and shed light on the importance of considering different parameters provided by ADMET such as (hERG Filter) to compare the cardiotoxicity of NSOs. The cytochrome risk provided by ADMET for the inserted opioids highlights a code risk related to CYP3A4 and CYP2D6. All the drugs where either substrate of CYP3A4 or CYP2D6 or both (Ocfentanyl, Furnaylfentanyl, 4F-Furanylfentanyl, Orphine and Fluorphine).

Substances that undergo metabolism by cytochrome P450 enzymes, particularly CYP3A4 and CYP2D6, carry inherent risks related to drug interactions and pharmacokinetics. These risks stem from the intricate interplay of these enzymes in drug metabolism and can impact the efficacy and safety of various medications. The polydrug use is common in case of intoxications and death with NSOs including fentanyl analogs (Guerrieri et al., 2017) and Brorphine (Krotulski et al., 2020). Owing to genetic polymorphism in CYP3A4 and CYP2D6 and the potential for drug interactions, these opioids pose substantial risks for considerable variations in serum levels (Smith, 2011).

5.5.4 Conclusion

The ADMET prediction of NSOs confirms the toxic risk related to these drugs and predicts important toxicokinetic parameters related to cardiotoxicity and opioids metabolism. This *in silico* tool should be validated for rapid NPS ADMET screening.

5.5.5 Contributions

B.S, M.M, K.A.M and R.O designed the study. **B.S** performed silico ADMET prediction analysis and contributed to data curation and the writing of the first draft.

Chapter 6 General conclusion

The rapid emergence of novel psychoactive substances (NPS) in the international drug market constitutes a substantial threat to public health and poses a challenge to drug policy. Frequently, there is limited knowledge regarding the adverse health effects and societal harms associated with NPS, creating a considerable obstacle for preventive measures and treatment strategies. The analysis and recognition of a diverse array of chemically distinct substances concurrently present in drug markets presents a challenging task. To address this situation, it is imperative to prioritize monitoring, information dissemination, early warning systems, and raising awareness of the risks associated with NPS. In the last few years, NSOs emergence increased public concerns due to their contribution in intoxications and death worldwide (Edinoff et al., 2023). The multidisciplinary approach developed in this project is aimed at increasing knowledge regarding the pharmaco-toxicological aspects of NSOs.

The pharmaco-toxicological characterization of NSOs belonging to different subclasses of Opioids analogs reported in published articles expands new information regarding the vulnerability of NSOs. In particular, the study of *Bilel et al.,2021* (Bilel et al., 2021), was aimed to characterize a seized mixture containing 1-cyclohexyl-x-methoxybenzene derivatives that share structure similarities with the opioid tramadol and phencyclidine. The results of this study revealed that the effects of these isomers are qualitatively similar to those induced by tramadol and/or phencyclidine and in some tests, effects were partially blocked by naloxone administration suggesting the involvement of the opioid receptor system. The importance of this study lies in the possibility of use of these mixtures as adulterant to other synthetic opioids and that may increase toxicity risk in users. Understanding the effects of unclassified compounds will help their recognition and prohibition on the NPS market (Wong et al., 2023).

The rates of overdose deaths involving synthetic opioids in particular fentanyl and fentanyl analogs, increased over 22% from 2020 to 2021 (CDCP., 2023). Understanding the effects of fentanyl and its analogs is of a great matter to develop strategies of prevention. Indeed, the study of (Montesano et al., 2021) was aimed to characterize *in vitro* and *in vivo* the metabolites of two fentanyl analogs (Isobutyrylfentanyl and 4F-Furanylfentanyl) seized in Italy and were found in cases of intoxication and death in Europe (EMCDDA, 2017). The introduction of an analytical approach aimed at identifying the metabolic profile of many synthetic opioids is

mandatory in the forensic field. In particular, it helps to understand the involvement of specific compounds in cases of polydrug assumption as seen with other classes of NPS (Pichini et al.,2022). Adding to the data published in *Montesano et al., 2021*, the two fentanyl analogs were characterized *in vivo* (**section 5.2**) in male and female animals. In addition, the pharmacokinetic profile was determined in both sexes. The data above reveal the sex differences in the pharmaco-toxicological and pharmacokinetics of Isobutyrylfentanyl and 4F-Furanylfentanyl. This information underscores the significance of incorporating considerations for sex differences in both preclinical and clinical pharmaco-toxicological strategies related to fentanyl analogs (Fattore et al., 2020).

Other structure analogs of fentanyl (Acrylfentanyl, Ocfentanyl, Furanylfentanyl) were also characterized *in vitro* and *in vivo* (Bilel et al., 2022) the results of this study revealed that fentanyl analogs behave differently at the mu opioid receptor component unveiling the role of β-arrestin 2 in the pharmacology of opioids (Azevedo et al., 2020). To confirm this recent evidence the pharmacological effects of two other fentanyl analogs (Butyrylfentanyl and 4F-Butyrylfentanyl) that differ with the bias to β-arrestin 2 (**chapter 4, section 4.2**.) was investigated in female and male mice. Additionally, I introduced to the study an antagonist of CRF-1 receptor to unveil the possible involvement of stress in cardiorespiratory depression of opioids.

Interestingly, the findings of the study uncovered a novel mechanism by which synthetic opioids might increase respiratory depression shedding new light on the role of CRF-1 receptors in cardiorespiratory impairments by (biased β-arrestin 2) mu-agonists. This finding increases our understanding of mu-mediated mechanisms and may have implications for antidotal therapies in case of overdose with synthetic opioids (Ramos-Gonzalez et al., 2022).

In order to understand the long-term effects of fentanyl and its analogs, a new approach lying on the investigation of genotoxicity in human cell line, particularly in terms of the ability to induce structural and numerical chromosomal aberrations (Gasperini et al., 2022). The results of this study reveal a risk of genotoxicity among fentanyl analogs. These data raise concerns on the histopathological and biochemical changes resulting from opioids use (**section 5.1**) and abuse (Frisoni et al., 2019).

The recent increase of Brorphine disponibility in the drug market of NSOs and its involvement in death in US and Europe has led to the necessity of investigating its pharmaco-toxicological effect together with it is possible emerging analogs (Orphine, Fluorphine, Chlorphine and Iodorphine). The data obtained from *in vitro* and *in vivo* studies (**chapter 4 section 4.1** and **chapter 5 sections 5**.**2-5.3**) reveal that Brorphine and the piperidine benzimidazolones with brorphine-like characteristics act as opioid agonists, posing a significant risk to users if they were to emerge as NSOs (Vandeputte et al., 2023). Adding to this data Brorphine was characterized *in vivo* in female and male mice to reveal the effect of sex on its pharmaco-toxicology (**chapter 5 section 5.2**). Importantly, the results obtained reveal sexual dimorphism in the *in vivo* effects of the NSO Brorphine. In particular, male mice showed more resistance to NLX injections in motor and respiratory tests respect to female. These findings highlight the higher risk of respiratory depression among male respect to female and shed light on the importance of sex-specific evaluation in studies involving NSOs (Fattore et al., 2020).

Due to the need to rapidly assess the effects of exponentially emerging NSOs that pose a threat to users, it was essential to develop new, rapid screening methods for this purpose. The study of *Pesavento et al., 2021* (Pesavento et al., 2021) et *Bilel et al, 2023* (Bilel et al., 2023) introduced the use of zebrafish model for rapid screening of NSOs such as fentanyl analogs. Both studies validated these methods due to the similarity of the results to that of the mouse model including metabolites (Wagmann & Meyer, 2022). Appending to the zebrafish models, computational methods such as the in silico ADMET prediction tool have also been incorporated to my research project. The results obtained from in silico ADMET prediction of a series of NSOs opioids (**section 5.5**) are qualitatively similar to the data obtained *in vivo* for these compounds. In support of the data obtained with other NPS, in silico ADMET prediction should be included in the rapid screening tools for NPS (Arfè et al., 2023).

Future studies will be focusing on implementing more analysis *in silico*, *in vitro* and *in vivo* with more recent classes of NSOs such as the class of benzimidazoles "Nitazene". In addition, future studies will be focusing on the characterization of Antalarmin *in vitro* and *in vivo* and studying its pharmacokinetics and interaction with the opioid system to better understand the role of CRF-1 receptors in cardiorespiratory depression with opioids.

In synthesis, the comprehensive outcomes derived from the multidisciplinary approach employed throughout my Ph.D. project have revealed significant pharmacological insights and novel mechanisms related to the toxicity of NSOs. Furthermore, these findings have indicated the potential new tools in rapidly screening NSO. The dissemination of this information will contribute to increasing awareness of the risks associated with NSOs.

References

Arfè, R., Bilel, S., Tirri, M., Corli, G., Bergamin, E., Serpelloni, G., Bassi, M., Borsari, M., Boccuto, F., Bernardi, T., Caruso, L., Alkilany, A. M., Rachid, O., Botrè, F., De-Giorgio, F., & Marti, M. (2023). Comprehensive evaluation of the pharmacological and toxicological effects of γ-valerolactone as compared to γ-hydroxybutyric acid: Insights from in vivo and in silico models. *Drug and alcohol dependence*, *252*, 110951. https://doi.org/10.1016/j.drugalcdep.2023.110951

Armenian, P., Vo, K. T., Barr-Walker, J., & Lynch, K. L. (2018). Fentanyl, fentanyl analogs and novel synthetic opioids: A comprehensive review. *Neuropharmacology, 134(Pt A)*, 121–132. https://doi.org/10.1016/j.neuropharm.2017.10.016

Azevedo Neto, J., Costanzini, A., De Giorgio, R., Lambert, D. G., Ruzza, C., & Calò, G. (2020). Biased versus Partial Agonism in the Search for Safer Opioid Analgesics. *Molecules (Basel, Switzerland), 25*(17), 3870. https://doi.org/10.3390/molecules25173870

Baumann, M. H., Tocco, G., Papsun, D. M., Mohr, A. L., Fogarty, M. F., & Krotulski, A. J. (2020). U-47700 and Its Analogs: Non-Fentanyl Synthetic Opioids Impacting the Recreational Drug Market. *Brain sciences, 10*(11), 895. https://doi.org/10.3390/brainsci10110895

Bilel, S., Azevedo Neto, J., Arfè, R., Tirri, M., Gaudio, R. M., Fantinati, A., Bernardi, T., Boccuto, F., Marchetti, B., Corli, G., Serpelloni, G., De-Giorgio, F., Malfacini, D., Trapella, C., Calo', G., & Marti, M. (2022). In vitro and in vivo pharmaco-dynamic study of the novel fentanyl derivatives: Acrylfentanyl, Ocfentanyl and Furanylfentanyl. Neuropharmacology, 209, 109020. https://doi.org/10.1016/j.neuropharm.2022.109020

Bilel, S., Azevedo, N. J., Arfè, R., Tirri, M., Gregori, A., Serpelloni, G., De-Giorgio, F., Frisoni, P., Neri, M., Calò, G., & Marti, M. (2020). In vitro and in vivo pharmacological characterization of the synthetic opioid MT-45..*Neuropharmacology,171*, 108110. https://doi.org/10.1016/j.neuropharm.2020.108110

Bilel, S., Murari, M., Pesavento, S., Arfè, R., Tirri, M., Torroni, L., Marti, M., Tagliaro, F., & Gottardo, R. (2023). Toxicity and behavioural effects of ocfentanil and 2-furanylfentanyl in zebrafish larvae and mice. *Neurotoxicology,95*,83–93. https://doi.org/10.1016/j.neuro.2023.01.003

Bilel, S., Tirri, M., Arfè, R., Sturaro, C., Fantinati, A., Cristofori, V., Bernardi, T., Boccuto, F., Cavallo, M., Cavalli, A., De-Giorgio, F., Calò, G., & Marti, M. (2021). In Vitro and In Vivo Pharmaco-Toxicological Characterization of 1-Cyclohexyl-x-methoxybenzene Derivatives in Mice: Comparison with Tramadol and PCP. *International journal of molecular sciences, 22*(14), 7659. https://doi.org/10.3390/ijms22147659

Bohn, L. M., Lefkowitz, R. J., Gainetdinov, R. R., Peppel, K., Caron, M. G., & Lin, F. T. (1999). Enhanced morphine analgesia in mice lacking beta-arrestin 2. *Science (New York, N.Y.), 286(*5449), 2495–2498. https://doi.org/10.1126/science.286.5449.2495

Centers for Disease Control and Prevention (CDC) (2008). Nonpharmaceutical fentanyl-related deaths--multiple states, April 2005-March 2007. MMWR. *Morbidity and mortality weekly report,* 57(29), 793–796. https://www.cdc.gov/mmwr/preview/mmwrhtml/mm5729a1.htm

Centers for Disease Control and Prevention (CDC). https://emergency.cdc.gov/han/han00384.asp (Accessed December 2017).

Centers for Disease Control and Prevention (CDCP) Fentanyl. https://www.cdc.gov/opioids/basics/fentanyl.html

Concheiro, M., Chesser, R., Pardi, J., & Cooper, G. (2018). Postmortem Toxicology of New Synthetic Opioids. *Frontiers in pharmacology*, 9, 1210. https://doi.org/10.3389/fphar.2018.01210

Coppola, M., & Mondola, R. (2015). AH-7921: a new synthetic opioid of abuse.*Drug and alcohol review, 34*(1), 109–110. https://doi.org/10.1111/dar.12216

Corli, G., Tirri, M., Arfè, R., Marchetti, B., Bernardi, T., Borsari, M., Odoardi, S., Mestria, S., Strano-Rossi, S., Neri, M., Gaudio, R. M., Bilel, S., & Marti, M. (2023). Pharmaco-Toxicological Effects of Atypical Synthetic Cathinone Mephtetramine (MTTA) in Mice: Possible Reasons for Its Brief Appearance over NPSs Scene. *Brain sciences, 13*(2), 161. https://doi.org/10.3390/brainsci13020161

DECISIONE (UE) 2022/391 DEL CONSIGLIO del 3 marzo 2022. https://eur-lex.europa.eu/legal content/IT/TXT/PDF/?uri=CELEX:32022D0391

Dhaliwal A, Gupta M. Physiology, Opioid Receptor. [Updated 2023 Jul 24]. In: StatPearls [Internet]. Treasure Island (FL): *StatPearls Publishing*; 2023 Jan-. Available from: https://www.ncbi.nlm.nih.gov/books/NBK546642/

Di Trana, A., & Del Rio, A. (2020). Fentanyl analogues potency: what should be known. *La Clinica terapeutica,* 171(5), e412–e413. https://doi.org/10.7417/CT.2020.2250

European Commission. (2021) European Commission "Brorphine" Database Search. https://ec.europa.eu/growth/toolsdatabases/tris/en/search/?trisaction=search.results (accessed Feb 5, 2021).

European Monitoring Center for drugs and Drug Addiction (2020): Looking back on 25 years of annual reporting on the drugs problem in Europe. https://www.emcdda.europa.eu/publications/brochures/25-years-annual-reporting_en#

European Monitoring Center for drugs and Drug Addiction. New psychoactive substances (NPS). https://www.emcdda.europa.eu/topics/nps_en

European monitoring Center for Drugs and Drug Addiction. Risk assessment. assessment report on a new psychoactive substance. *N*-phenyl-*N*-[1-(2-phenylethyl) piperidin-4-yl] furan-2-carboxamide (franylfentanyl) https://www.emcdda.europa.eu/publications/joint-reports/furanylfentanyl_en

European Monitoring Centre for Drugs and Drug Addiction (2012): FENTANYL IN EUROPE EMCDDA TRENDSPOTTER STUDY. Report from an EMCDDA expert meeting 9 to

10 October 2012. https://www.emcdda.europa.eu/publications/scientific-studies/2012/trendspotters-report_en

European Monitoring Centre for Drugs and Drug Addiction (2020). Isotonitazene. Report on the risk assessment of N,N-diethyl-2-[[4-(1-methylethoxy)phenyl]methyl]-5-nitro-1Hbenzimidazole-1-ethanamine (isotonitazene) in accordance with Article 5c of Regulation (EC) No 1920/2006 (as amended)

European Monitoring Centre for Drugs and Drug Addiction (2023), European Drug Report 2023: Trends and Developments, https://www.emcdda.europa.eu/publications/european-drug-report/2023_en

Fattore, L., Marti, M., Mostallino, R., & Castelli, M. P. (2020). Sex and Gender Differences in the Effects of Novel Psychoactive Substances. *Brain sciences, 10*(9), 606. https://doi.org/10.3390/brainsci10090606

Fels, H., Krueger, J., Sachs, H., Musshoff, F., Graw, M., Roider, G., & Stoever, A. (2017). Two fatalities associated with synthetic opioids: AH-7921 and MT-45. *Forensic science international, 277,* e30–e35. https://doi.org/10.1016/j.forsciint.2017.04.003

Frisoni, P., Bacchio, E., Bilel, S., Talarico, A., Gaudio, R. M., Barbieri, M., Neri, M., & Marti, M. (2018). Novel Synthetic Opioids: The Pathologist's Point of View. *Brain sciences, 8*(9), 170. https://doi.org/10.3390/brainsci8090170

Gerges, S. H., & El-Kadi, A. O. S. (2023). Sexual Dimorphism in the Expression of Cytochrome P450 Enzymes in Rat Heart, Liver, Kidney, Lung, Brain, and Small Intestine. *Drug metabolism and disposition: the biological fate of chemicals, 51*(1), 81–94. https://doi.org/10.1124/dmd.122.000915

Golbamaki, A., Cassano, A., Lombardo, A., Moggio, Y., Colafranceschi, M., & Benfenati, E. (2014). Comparison of in silico models for prediction of Daphnia magna acute toxicity. *SAR and QSAR in environmental research, 25*(8), 673–694. https://doi.org/10.1080/1062936X.2014.923041

Grafinger, K. E., Wilde, M., Otte, L., & Auwärter, V. (2021). Pharmacological and metabolic characterization of the novel synthetic opioid brorphine and its detection in routine casework. *Forensic science international,327*, 110989. https://doi.org/10.1016/j.forsciint.2021.110989

Helander, A., Bäckberg, M., & Beck, O. (2014). MT-45, a new psychoactive substance associated with hearing loss and unconsciousness. *Clinical toxicology (Philadelphia, Pa.), 52*(8), 901–904. https://doi.org/10.3109/15563650.2014.943908

Jannetto, P. J., Helander, A., Garg, U., Janis, G. C., Goldberger, B., & Ketha, H. (2019). The Fentanyl Epidemic and Evolution of Fentanyl Analogs in the United States and the European Union. *Clinical chemistry, 65*(2), 242–253. https://doi.org/10.1373/clinchem.2017.281626

Kaplovitch, E., Gomes, T., Camacho, X., Dhalla, I. A., Mamdani, M. M., & Juurlink, D. N. (2015). Sex Differences in Dose Escalation and Overdose Death during Chronic Opioid Therapy: A Population-Based Cohort Study. *PloS one, 10*(8), e0134550. https://doi.org/10.1371/journal.pone.0134550 \

Kar, S., & Leszczynski, J. (2020). Open access in silico tools to predict the ADMET profiling of drug candidates. *Expert opinion on drug discovery, 15*(12), 1473–1487. https://doi.org/10.1080/17460441.2020.1798926

Klebacher, R., Harris, M. I., Ariyaprakai, N., Tagore, A., Robbins, V., Dudley, L. S., Bauter, R., Koneru, S., Hill, R. D., Wasserman, E., Shanes, A., & Merlin, M. A. (2017). Incidence of Naloxone Redosing in the Age of the New Opioid Epidemic. *Prehospital emergency care, 21*(6), 682–687. https://doi.org/10.1080/10903127.2017.1335818

Krotulski AJ, Fogarty MF, Logan BK (2020) Para-methyl-AP-237. April 13, 2020. https://www.npsdiscovery.org/wp-content/uploads/2020a/04/para-Methyl-AP 237_041320_NMSLabs_Report.pdf.. Accessed 14 Apr 2020

Krotulski AJ, Walton SE, Mohr ALA, Logan BK. Trend Report Q1 2023: NPS opioids in the United States. *NPS Discovery. 2023.* https://www.cfsre.org/nps-discovery/trend-reports/nps-opioids/report/49?trend_type_id=2. Accessed 26 December 2022.

Krotulski, A. J., Papsun, D. M., Noble, C., Kacinko, S. L., & Logan, B. K. (2021). Brorphine-Investigation and quantitation of a new potent synthetic opioid in forensic toxicology casework using liquid chromatography-mass spectrometry. *Journal of forensic sciences, 66*(2), 664–676. https://doi.org/10.1111/1556-4029.14623

Krotulski, A. J., Papsun, D. M., Noble, C., Kacinko, S. L., & Logan, B. K. (2021). Brorphine-Investigation and quantitation of a new potent synthetic opioid in forensic toxicology casework using liquid chromatography-mass spectrometry. *Journal of forensic sciences, 66*(2), 664–676. https://doi.org/10.1111/1556-4029.14623

Lopes, G. S., Bielinski, S., Moyer, A. M., Jacobson, D. J., Wang, L., Jiang, R., Larson, N. B., Miller, V. M., Zhu, Y., Cavanaugh, D. C., & St Sauver, J. (2021). Sex differences in type and occurrence of adverse reactions to opioid analgesics: a retrospective cohort study. *BMJ open, 11*(6), e044157. https://doi.org/10.1136/bmjopen-2020-044157

Montesano, C., Vincenti, F., Fanti, F., Marti, M., Bilel, S., Togna, A. R., Gregori, A., Di Rosa, F., & Sergi, M. (2021). Untargeted Metabolic Profiling of 4-Fluoro-Furanylfentanyl and Isobutyrylfentanyl in Mouse Hepatocytes and Urine by Means of LC-HRMS. *Metabolites, 11*(2), 97. https://doi.org/10.3390/metabo11020097

Papsun, D., Krywanczyk, A., Vose, J. C., Bundock, E. A., & Logan, B. K. (2016). Analysis of MT-45, a Novel Synthetic Opioid, in Human Whole Blood by LC-MS-MS and its Identification in a Drug-Related Death. *Journal of analytical toxicology, 40*(4), 313–317. https://doi.org/10.1093/jat/bkw012

Peng, J., Sarkar, S., & Chang, S. L. (2012). Opioid receptor expression in human brain and peripheral tissues using absolute quantitative real-time RT-PCR. *Drug and alcohol dependence, 124*(3), 223–228. https://doi.org/10.1016/j.drugalcdep.2012.01.013

Pérez-Mañá, C., Papaseit, E., Fonseca, F., Farré, A., Torrens, M., & Farré, M. (2018). Drug Interactions With New Synthetic Opioids. *Frontiers in pharmacology, 9*, 1145. https://doi.org/10.3389/fphar.2018.01145

Pergolizzi, J., Jr, Raffa, R., LeQuang, J. A. K., Breve, F., & Varrassi, G. (2023). Old Drugs and New Challenges: A Narrative Review of Nitazenes. *Cureus, 15*(6), e40736. https://doi.org/10.7759/cureus.40736

Pesavento, S., Bilel, S., Murari, M., Gottardo, R., Arfè, R., Tirri, M., Panato, A., Tagliaro, F., & Marti, M. (2022). Zebrafish larvae: A new model to study behavioural effects and metabolism of fentanyl, in comparison to a traditional mice model. *Medicine, science, and the law*, *62*(3), 188–198. https://doi.org/10.1177/00258024221074568

Pichini S., Graziano S, Varì,M.R Pellegrin M, Marchei. E Rotolo M. C, Berretta Paolo Tini A, Di Trana A, Busardò F (2022). The role of analytical pharmacotoxicology in adressing the main functions of the National Early Warning System on NPS. *Toxicologie Analytique et Clinique*, S53, 34, Issue 3, Supplement. https://doi.org/10.1016/j.toxac.2022.06.063

Rohrig, T. P., Nash, E., Osawa, K. A., Shan, X., Scarneo, C., Youso, K. B., Miller, R., & Tiscione, N. B. (2021). Fentanyl and Driving Impairment. *Journal of analytical toxicology, 45*(4), 389–396. https://doi.org/10.1093/jat/bkaa105

Schackmuth, M., & Kerrigan, S. (2023). Lipophilicity of fentalogs: Comparison of experimental and computationally derived data. *Journal of forensic sciences, 68*(5), 1542–1554. https://doi.org/10.1111/1556-4029.15324

Schäfer, M. (2011). Mechanisms of action of opioids. In A. Evers, M. Maze, & E. Kharasch (Eds.), Anesthetic Pharmacology: Basic Principles and Clinical Practice (pp. 493-508). Cambridge: *Cambridge University Press*. https://doi.org/10.1017/CBO9780511781933.032

Sharma, K. K., Hales, T. G., Rao, V. J., NicDaeid, N., & McKenzie, C. (2019). The search for the "next" euphoric non-fentanil novel synthetic opioids on the illicit drugs market: current status and horizon scanning. *Forensic toxicology, 37*(1), 1–16. https://doi.org/10.1007/s11419-018-0454-5

Sharp, J. L., Pearson, T., & Smith, M. A. (2022). Sex differences in opioid receptor mediated effects: Role of androgens. *Neuroscience and biobehavioral reviews, 134*, 104522. https://doi.org/10.1016/j.neubiorev.2022.104522

Smith H. S. (2011). The metabolism of opioid agents and the clinical impact of their active metabolites. *The Clinical journal of pain, 27*(9), 824–838. https://doi.org/10.1097/AJP.0b013e31821d8ac1

Sobczak, M., Sałaga, M., Storr, M. A., & Fichna, J. (2014). Physiology, signaling, and pharmacology of opioid receptors and their ligands in the gastrointestinal tract: current concepts and future perspectives. *Journal of gastroenterology, 49*(1), 24–45. https://doi.org/10.1007/s00535-013-0753-x

Solis, E., Jr, Cameron-Burr, K. T., & Kiyatkin, E. A. (2017). Heroin Contaminated with Fentanyl Dramatically Enhances Brain Hypoxia and Induces. Brain Hypothermia. *eNeuro, 4*(5), ENEURO.0323-17.2017. https://doi.org/10.1523/ENEURO.0323-17.2017

Solis, E., Jr, Cameron-Burr, K. T., Shaham, Y., & Kiyatkin, E. A. (2018). Fentanyl-Induced Brain Hypoxia Triggers Brain Hyperglycemia and Biphasic Changes in Brain Temperature. *Neuropsychopharmacology official publication of the American College of Neuropsychopharmacology, 43*(4), 810–819. https://doi.org/10.1038/npp.2017.181

Tirri, M., Arfè, R., Bilel, S., Corli, G., Marchetti, B., Fantinati, A., Vincenzi, F., De-Giorgio, F., Camuto, C., Mazzarino, M., Barbieri, M., Gaudio, R. M., Varani, K., Borea, P. A., Botrè, F., & Marti, M. (2022). In Vivo Bio-Activation of JWH-175 to JWH-018: Pharmacodynamic and Pharmacokinetic Studies in Mice. *International journal of molecular sciences, 23*(14), 8030. https://doi.org/10.3390/ijms23148030

Toubia, T., & Khalife, T. (2019). The Endogenous Opioid System: Role and Dysfunction Caused by Opioid Therapy. *Clinical obstetrics and gynecology, 62*(1), 3–10. https://doi.org/10.1097/GRF.0000000000000409

Towers, E. B., Setaro, B., & Lynch, W. J. (2022). Sex- and Dose-Dependent Differences in the Development of an Addiction-Like Phenotype Following Extended-Access Fentanyl Self-Administration. *Frontiers in pharmacology, 13*, 841873. https://doi.org/10.3389/fphar.2022.841873

Tuusov, J., Vals, K., Tõnisson, M., Riikoja, A., Denissov, G., & Väli, M. (2013). Fatal poisoning in Estonia 2000-2009. Trends in illegal drug-related deaths. *Journal of forensic and legal medicine, 20*(1), 51–56. https://doi.org/10.1016/j.jflm.2012.04.023Ellis, C. R., Kruhlak, N. L., Kim, M. T., Hawkins, E. G., & Stavitskaya, L. (2018). Predicting opioid receptor binding affinity of pharmacologically unclassified designer substances using molecular docking. *PloS one, 13*(5), e0197734. https://doi.org/10.1371/journal.pone.0197734

Uchiyama, N., Matsuda, S., Kawamura, M. et al (2013). Two new-type cannabimimetic quinolinyl carboxylates, QUPIC and QUCHIC, two new cannabimimetic carboxamide derivatives, ADB-FUBINACA and ADBICA, and five synthetic cannabinoids detected with a thiophene derivative α-PVT and an opioid receptor agonist AH-7921 identified in illegal products. Forensic Toxicol 31, 223–240. https://doi.org/10.1007/s11419-013-0182-9

UNDOC 2022, World Drug Report. https://www.unodc.org/unodc/en/data-and-analysis/world-drug-report-2022.html

UNDOC EWA, https://www.unodc.org/LSS/Page/NPS/DataVisualisations

UNDOC. World drug report 2023. https://www.unodc.org/res/WDR-2023/WDR23_Exsum_fin_SP.pdf

Vandeputte, M. M., Cannaert, A., & Stove, C. P. (2020). In vitro functional characterization of a panel of non-fentanyl opioid new psychoactive substances. *Archives of toxicology, 94*(11), 3819–3830. https://doi.org/10.1007/s00204-020-02855-7

Vandeputte, M. M., Krotulski, A. J., Papsun, D. M., Logan, B. K., & Stove, C. P. (2021). The Rise and Fall of Isotonitazene and Brorphine: Two Recent Stars in the Synthetic Opioid Firmament. *Journal of analytical toxicology*, bkab082. Advance online publication. https://doi.org/10.1093/jat/bkab082\

Vandeputte, M. M., Tsai, M. M., Chen, L., Glatfelter, G. C., Walther, D., Stove, C. P., Shi, L., & Baumann, M. H. (2023). Comparative neuropharmacology of structurally distinct non-fentanyl opioids that are appearing on recreational drug markets worldwide. *Drug and alcohol dependence, 249*, 109939. https://doi.org/10.1016/j.drugalcdep.2023.109939

Vandeputte, M. M., Vasudevan, L., & Stove, C. P. (2022). In vitro functional assays as a tool to study new synthetic opioids at the μ-opioid receptor: Potential, pitfalls and progress. *Pharmacology &therapeutics,235*, 108161. https://doi.org/10.1016/j.pharmthera.2022.108161

VanHouten, J. P., Rudd, R. A., Ballesteros, M. F., & Mack, K. A. (2019). Drug Overdose Deaths Among Women Aged 30-64 Years - United States, 1999-2017. MMWR. *Morbidity and mortality weekly report, 68*(1), 1–5. https://doi.org/10.15585/mmwr.mm6801a1

Vasudevan, L., Vandeputte, M., Deventer, M., Wouters, E., Cannaert, A., & Stove, C. P. (2020). Assessment of structure-activity relationships and biased agonism at the Mu opioid receptor of novel synthetic opioids using a novel, stable bio-assay platform. *Biochemical pharmacology, 177*, 113910. https://doi.org/10.1016/j.bcp.2020.113910

Velagapudi, V., & Sethi, R. (2023). Illicit Non-Pharmaceutical Fentanyl and Its Analogs: A Short Review of Literature. *Kansas journal of medicine, 16*, 25–27. https://doi.org/10.17161/kjm.vol16.18555

Verougstraete, N., Vandeputte, M. M., Lyphout, C., Cannaert, A., Hulpia, F., Van Calenbergh, S., Verstraete, A. G., & Stove, C. (2021). First Report on Brorphine: The Next Opioid on the Deadly New Psychoactive Substance Horizon? *Journal of analytical toxicology, 44*(9), 937–946. https://doi.org/10.1093/jat/bkaa094

Vigolo, A., Ossato, A., Trapella, C., Vincenzi, F., Rimondo, C., Seri, C., Varani, K., Serpelloni, G., & Marti, M. (2015). Novel halogenated derivates of JWH-018: Behavioral and binding studies in mice. *Neuropharmacology, 95*, 68–82. https://doi.org/10.1016/j.neuropharm.2015.02.008

Vincenti F., Pagano F., Montesano C., Sciubba F., Di Cocco M.E., Gregori A., Rosa F.D., Lombardi L., Sergi M., Curini R (2020). Multi-analytical characterization of 4-fluoro-furanyl fentanyl in a drug seizure. *Forensic Chem.* ;21:100283. https://doi.org/10.1016/j.forc.2020.100283

Wagmann, L., & Meyer, M. R. (2022). Reviewing toxicokinetics with a focus on metabolism of new psychoactive substances in the zebrafish (larvae) model. *WIREs Forensic Science, 4*(4), e1454. https://doi.org/10.1002/wfs2.1454

Wightman, R. S., Perrone, J., Scagos, R., Hallowell, B. D., Krieger, M., Li, Y., McGregor, A. J., Nelson, L. S., & Marshall, B. D. L. (2021). Toxicological and pharmacologic sex differences in unintentional or undetermined opioid overdose death. *Drug and alcohol dependence, 227*, 108994. https://doi.org/10.1016/j.drugalcdep.2021.108994

Wong S L, Teng LN, Tan, J, Pan, J (2023) Screening unknown novel psychoactive substances using GC–MS based machine learning, Forensic Chemistry,34, 100499. https://doi.org/10.1016/j.forc.2023.100499

Wood, J. D., & Galligan, J. J. (2004). Function of opioids in the enteric nervous system. *Neurogastroenterology and motility, 16* Suppl 2, 17–28. https://doi.org/10.1111/j.1743-3150.2004.00554.x

Zawilska, J. B., Adamowicz, P., Kurpeta, M., & Wojcieszak, J. (2023). Non-fentanyl new synthetic opioids - An update. *Forensic science international, 349*, 111775. https://doi.org/10.1016/j.forsciint.2023.111775

Appendix A

Supplementary Materials to "Elucidating the harm potential of brorphine analogues as new psychoactive substances: Synthesis, *in vitro,* and *in vivo* characterization"

Marthe M. Vandeputte[1,*], Sabrine Bilel[2,*], Micaela Tirri[2], Giorgia Corli[2], Marta Bassi[2], Nathan K. Layle[3], Anna Fantinati[4], Donna Walther[5], Donna M. Iula[3], Michael H. Baumann[5], Christophe P. Stove[1,+], Matteo Marti[2,6,+]

[1]Laboratory of Toxicology, Department of Bioanalysis, Faculty of Pharmaceutical Sciences, Ghent University, Ghent, Belgium
[2]Department of Translational Medicine, Section of Legal Medicine and LTTA Centre, University of Ferrara, Ferrara, Italy
[3]Forensic Chemistry Division, Cayman Chemical Company, Ann Arbor, MI 48108, USA
[4]Department of Environmental and Prevention Sciences, University of Ferrara, Via Fossato di Mortara, Ferrara, Italy
[5]Designer Drug Research Unit (DDRU), Intramural Research Program, National Institute on Drug Abuse, National Institutes of Health, Baltimore, MD 21224, USA
[6]Collaborative Center of the National Early Warning System, Department for Anti-Drug Policies, Presidency of the Council of Ministers, Italy

[,+] Contributed equally.*

Corresponding Authors:

Matteo Marti

Department of Translational Medicine, Section of Legal Medicine, University of Ferrara, Ferrara, Italy.

Phone +39 0532 455781, fax +39 0532 455777

matteo.marti@unife.it

Christophe Stove

Laboratory of Toxicology, Department of Bioanalysis, Faculty of Pharmaceutical Sciences, Ghent University, Ghent, Belgium.

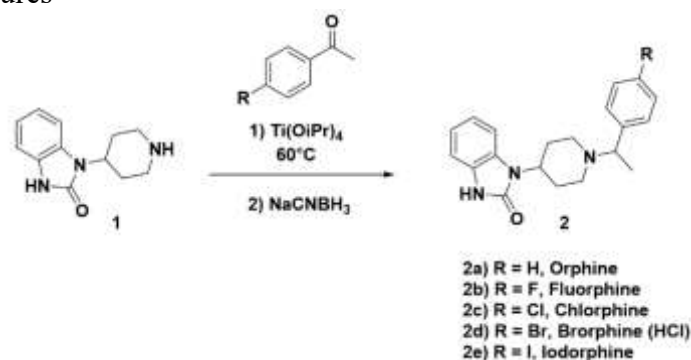Phone +32 (0) 9 264 81 35

Christophe.Stove@ugent.be

Figure A.1. *General synthetic route to compounds 2a-2e. The piperidine benzimidazolones were synthesized in one step from commercially available 4-(2-keto-1-benzimidazolinyl)piperidine (**1**) and a corresponding phenylacetone (where R = H, F, Cl, Br, or I) using standard reductive amination conditions [1]. With the exception of brorphine (which was converted to its corresponding hydrochloride using 2M HCl in diethyl ether and tested as such), all analogues were isolated and purified as free bases prior to testing.*
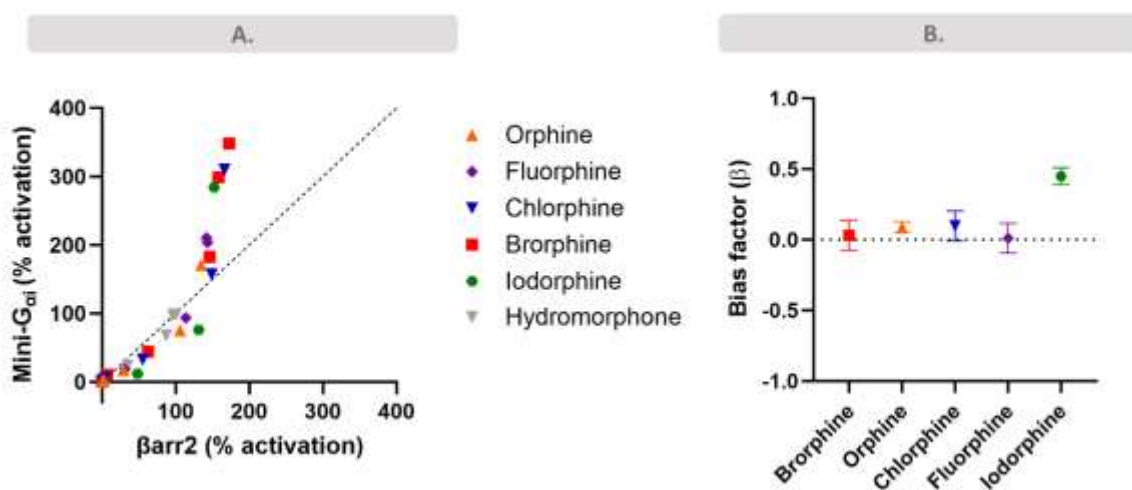

Figure A2. A. Semi-quantitative bias plot. *Comparison of the extent of mini-$G_{\alpha i}$ and βarr2 recruitment for the different compounds as determined in the respective MOR activation assays (% activation is relative to hydromorphone at the different tested concentrations).* ***B. Quantitative bias plot.*** *Bias factors (β) ± standard error of the mean (SEM) (calculated from three independent experiments) are plotted for all compounds. Hydromorphone was used as unbiased reference agonist (β = 0, not shown). A positive (negative) bias factor indicates a preference towards the βarr2 (mini-$G_{\alpha i}$) pathway. No statistically significant biased agonism was detected.*
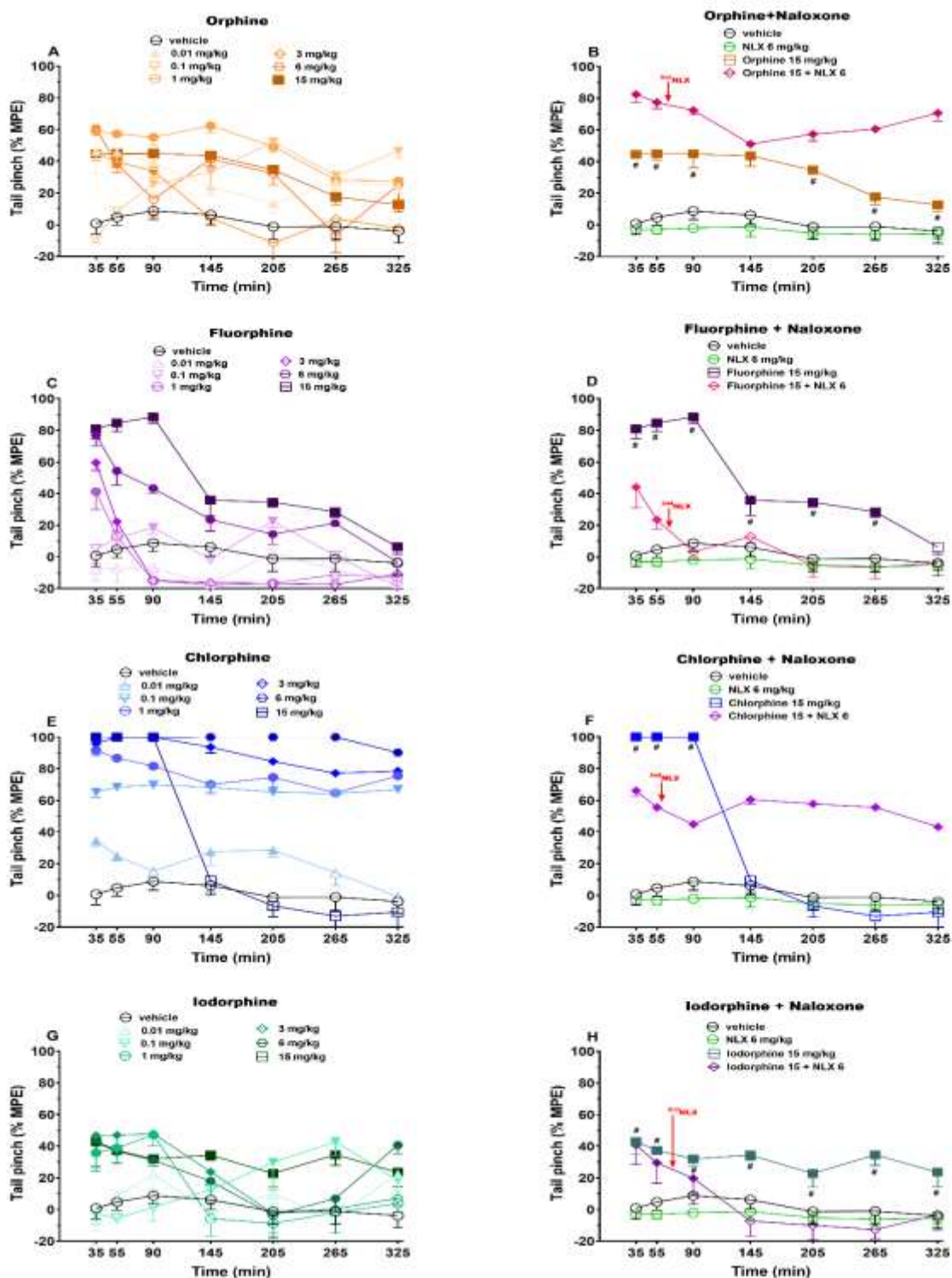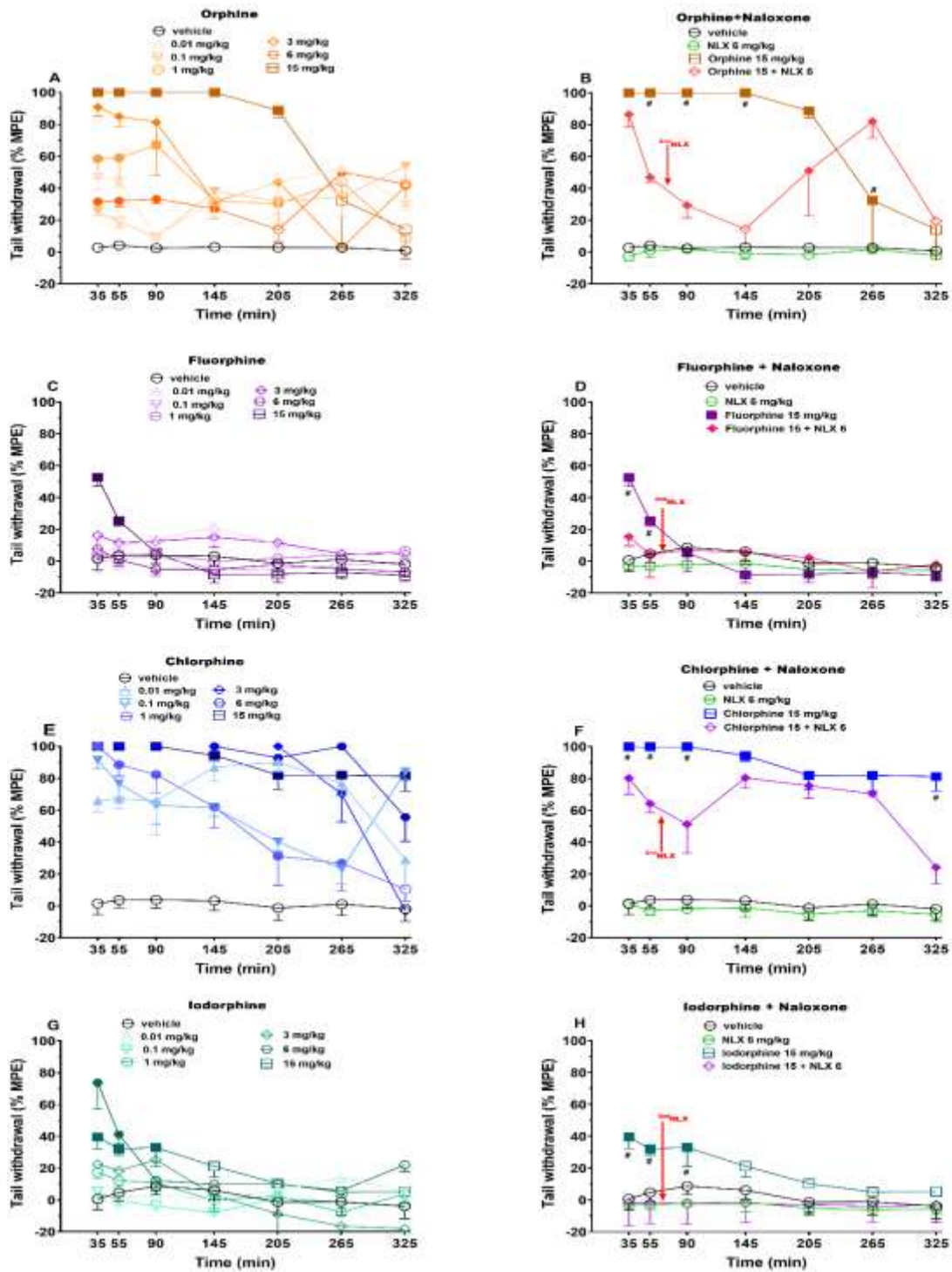
TAIL PINCH TEST

Figure A.3. *Time-course of drug effects after systemic administration of orphine, fluorphine, chlorphine, and iodorphine (0.01–15 mg/kg IP) in the tail pinch test **(panels A, C, E and G)**. **Panels B, D, F and H**: Time-course of the impact of naloxone (6 mg/kg IP) on the effects of a high dose of orphine, fluorphine, chlorphine, and iodorphine (15 mg/kg IP). Data are expressed as percentage of maximum possible effect (%MPE, see materials and methods in the main text) and represent the mean ± SEM as determined in 8 animals for each treatment regimen. Statistical analysis was performed by two-way ANOVA followed by the Bonferroni test for multiple comparisons. Solid symbols indicate significant effects compared to vehicle (p< 0.05); Hash symbols indicate significant effects compared to naloxone + agonist treatment (p< 0.05)*

287

TAIL WITHDRAWAL TEST

Figure A.4. *Time-course of drug effects after systemic administration of orphine, fluorphine, chlorphine, and iodorphine (0.01-15 mg/kg IP) in the tail withdrawal test* **(panels A, C, E, and G)**. **Panels B, D, F, and H**: *Time-course of the impact of naloxone (6 mg/kg IP) on the effects of a high dose of orphine, fluorphine, chlorphine, and iodorphine (15 mg/kg IP). Data are expressed as percentage of maximum possible effect (%MPE, see materials and methods in the main text) and represent the mean ± SEM as determined in 8 animals for each treatment regimen. Statistical analysis was performed by two-way ANOVA followed by the Bonferroni test for multiple comparisons. Solid symbols indicate significant effects compared to vehicle (p<0.05); Hash symbols indicate significant effects compared to naloxone + agonist treatment (p< 0.05).*
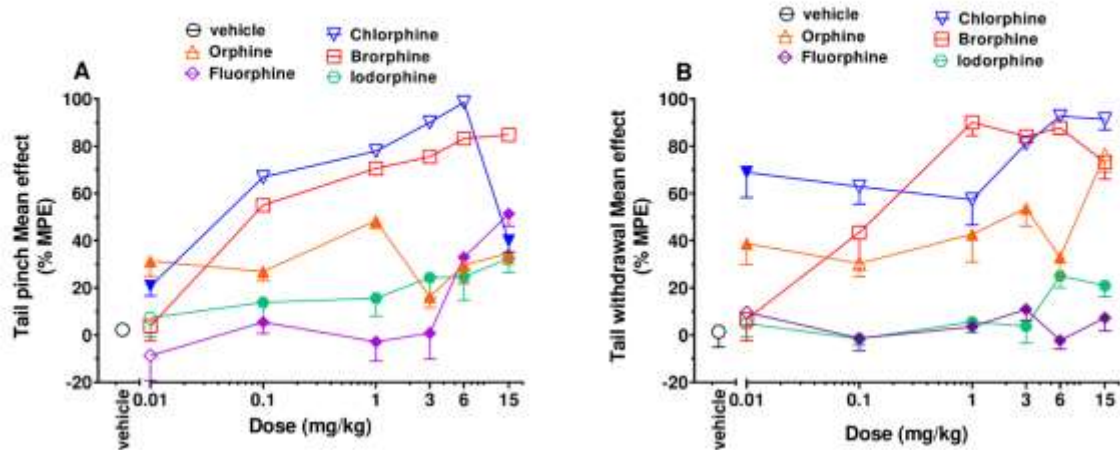
Figure A.5. *Comparison of dose-response curves for orphine, fluorphine, chlorphine, brorphine and iodorphine (0.01–15 mg/kg IP) in the tail pinch test (**panel A**) and tail withdrawal test (**panel B**). Data are expressed as percentage of maximum possible effect (%MPE, see materials and methods in the main text) and represent the mean ± SEM as determined in 8 animals for each treatment regimen. Statistical analysis was performed by two-way ANOVA followed by the Bonferroni test for multiple comparisons. Solid symbols indicate significant effects compared to brorphine (p< 0.05).*
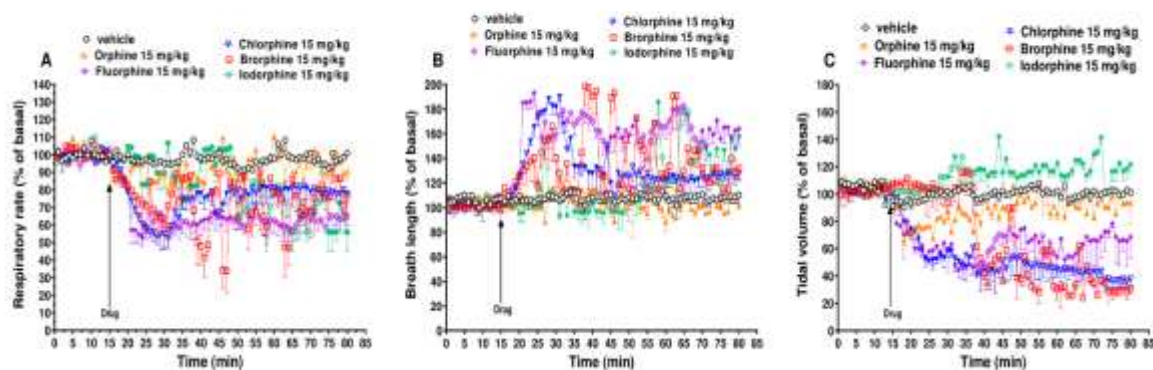
PLETHYSMOGRAPHY
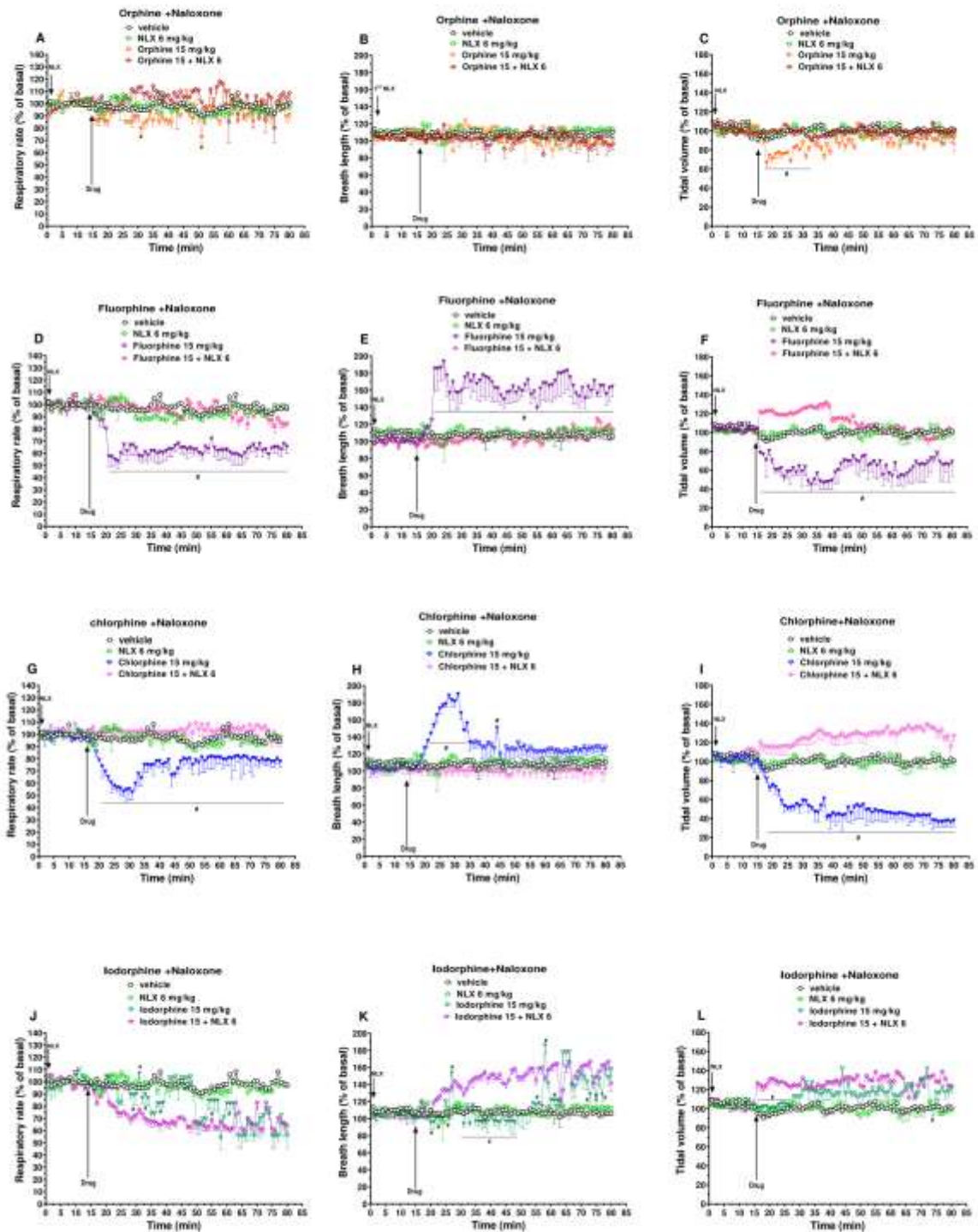
Figure A.6. Time-course of drug effects after systemic administration of orphine, fluorphine, chlorphine, and iodorphine (15 mg/kg IP) on respiratory parameters (respiratory rate RR, breath length BL, and tidal volume TV) with or without naloxone (6 mg/kg IP). Data are expressed as percentage change from basal value (% change from basal, see materials and methods in the main text) and represent the mean ± SEM as determined in 4 animals for each treatment regimen. Statistical analysis was performed by two-way ANOVA followed by the Bonferroni test for multiple comparisons. Solid symbols indicate significant effects compared to vehicle (p< 0.05); Hash symbols indicate significant effects compared to naloxone + agonist treatment (p< 0.05).

Plethysmography: comparison with brorphine

Figure A.7. Time-course of drug effects after systemic administration of orphine, fluorphine, chlorphine, and iodorphine (15 mg/kg IP) on respiratory parameters (respiratory rate RR, breath length BL, and tidal volume TV) with or without naloxone (6 mg/kg IP). Data are expressed as percentage change from basal value (% change from basal, see materials and methods in the main text) and represent the mean ± SEM as determined in 4 animals for each treatment regimen. Statistical analysis was performed by two-way ANOVA followed by the Bonferroni test for multiple comparisons. Solid symbols indicate significant effects compared to brorphine (p< 0.05).

Supplementary Table A1

Table A.1. Descriptive statistics of the different in vivo tests. The statistical analysis was performed by two-way ANOVA followed by the Bonferroni test for multiple comparisons.

	F_{ratio} (DFn-DFd)			p-value
	Treatment	**Time**	**Interaction**	
Tail pinch test (Fig 3.3-A)	$[F_{6,236}=524.1]$	$[F_{6,236}=64.01]$	$[F_{36,236}=6.758]$	p < 0.0001
Tail pinch test Brorphine+Naloxone (Fig 3.3-C)	$[F_{3,176}=282.8]$	$[F_{6,176}=12.44]$	$[F_{18,176}=7.958]$	p < 0.0001
Tail withdrawal test (Fig 3.3-E)	$[F_{6,236}=115.8]$	$[F_{6,236}=8.920]$	$[F_{36,236}=5.732]$	p < 0.0001
Tail withdrawal test Brorphine+Naloxone (Fig 3.3-E)	$[F_{3,176}=411.1]$	$[F_{6,176}=79.51]$	$[F_{18,176}=27.24]$	p < 0.0001
Respiratory rate (Fig 3.4-B)	$[F_{3,960}=273.2]$	$[F_{79,960}=3.831]$	$[F_{237,960}=2.538]$	p < 0.0001
Breath length (Fig 3.4-E)	$[F_{3,960}=223.7]$	$[F_{79,960}=3.374]$	$[F_{237,960}=2.538]$	p < 0.0001
Tidal volume (Fig 3.4-H)	$[F_{3,960}=367.2]$	$[F_{79,960}=3.624]$	$[F_{237,960}=5.892]$	p < 0.0001

Supplementary Materials & Methods

Synthesis

All material/reagents were purchased from commercial vendors and used without purification.

- *1,3-dihydro-1-[1-(1-phenylethyl)-4-piperidinyl]-2H-benzimidazol-2-one (2a/orphine)*
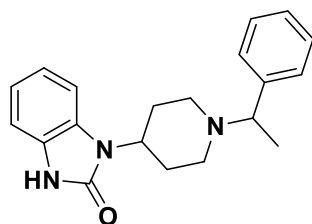

A mixture of 4-(2-keto-1-benzimidazolinyl)piperidine and acetophenone was treated with Ti(OiPr)$_4$ and heated to 60°C under nitrogen. The reaction mixture stirred overnight, cooled to room temperature and then further in an ice bath. The reaction mixture was diluted with dry EtOH. In a separate flask, NaCNBH$_3$ was dissolved in dry EtOH and the resulting solution was slowly added in portions to the reaction mixture. The ice bath was removed, and the reaction was left to stir at room temperature overnight under nitrogen. Reaction progress was monitored by TLC. Upon completion, the reaction mixture was concentrated to remove EtOH and the residue was poured into a mixture of 1:1 EtOAc:H$_2$O, stirred rapidly at room temperature, and then the phases were separated. The aqueous phase was extracted with additional portions of EtOAc and the organics were combined, washed with H$_2$O, brine, and dried over MgSO$_4$. The organics were filtered and concentrated under reduced pressure to afford a crude oil. The crude material was purified by normal phase chromatography, eluting with a gradient of 0-5% MeOH in DCM to afford **2a** (orphine) as an off-white solid (22%). ^{1}H-NMR (400 MHz, DMSO-d$_6$) δ 10.82 (s, 1H), 7.3-7.4 (m, 4H), 7.2-7.3 (m, 2H), 6.9-7.0 (m, 3H), 4.05 (tt, 1H, *J*=4.1, 12.3 Hz), 3.53 (q, 1H, *J*=6.6 Hz), 3.10 (br d, 1H, *J*=11.0 Hz), 2.89 (br d, 1H, *J*=10.8 Hz), 2.2-2.4 (m, 2H), 2.0-2.1 (m, 1H), 1.9-2.0 (m, 1H), 1.66 (br d, 1H, *J*=10.8 Hz), 1.58 (br d, 1H, *J*=11.0 Hz), 1.33 (d, 3H, *J*=6.6 Hz). MS (ESI): 322 MH$^+$.

- *1-[1-[1-(4-fluorophenyl)ethyl]-4-piperidinyl]-1,3-dihydro-2H-benzimidazol-2-one (2b/fluorphine)*
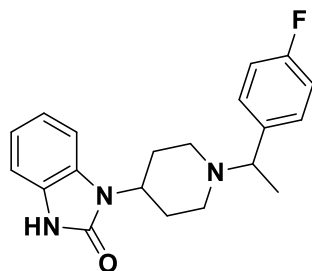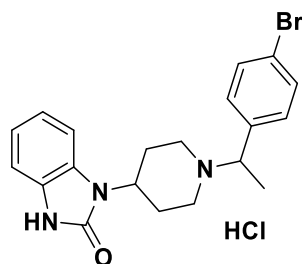

This compound was prepared according to the procedure for **2a** using 4'-fluoroacetophenone to afford **2b** (fluorphine) as an off-white solid (45%). ^{1}H-NMR (400 MHz, DMSO-d$_6$) δ 10.82 (s, 1H), 7.39 (dd, 2H, *J*=5.8, 8.4 Hz), 7.1-7.2 (m, 3H), 6.9-7.0 (m, 3H), 4.05 (tt, 1H, *J*=3.9, 12.1 Hz), 3.56 (q, 1H, *J*=6.6 Hz), 3.06 (br d, 1H, *J*=10.8 Hz), 2.87 (br d, 1H, *J*=10.8 Hz), 2.2-2.4 (m, 2H), 1.9-2.1 (m, 2H), 1.5-1.7 (m, 2H), 1.32 (d, 3H, *J*=6.6 Hz). MS (ESI): 340 MH$^+$.

- *1-[1-[1-(4-chlorophenyl)ethyl]-4-piperidinyl]-1,3-dihydro-2H-benzimidazol-2-one (2c/chlorphine)*
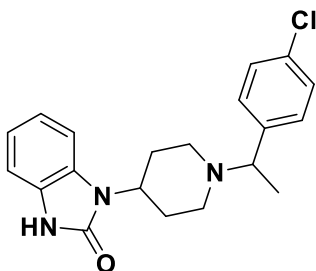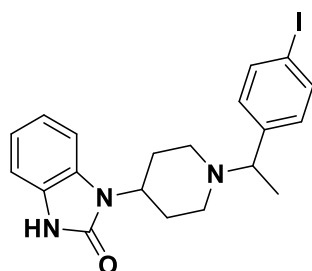

This compound was prepared according to the procedure for **2a** using 4'-chloroacetophenone to afford **2c** (chlorphine) as a pale yellow solid (26%). ^{1}H-NMR (400 MHz, DMSO-d$_6$) δ 10.82 (s, 1H), 7.39 (s, 4H), 7.20 (br d, 1H, *J*=6.4 Hz), 6.9-7.0 (m, 3H), 4.0-4.1 (m, 1H), 3.56 (q, 1H, *J*=6.6 Hz), 3.06 (br d, 1H, *J*=10.8 Hz), 2.87 (br d, 1H, *J*=10.8 Hz), 2.2-2.4 (m, 2H), 1.9-2.1 (m, 2H), 1.5-1.7 (m, 2H), 1.31 (d, 3H, *J*=6.6 Hz). MS (ESI): 356 MH$^+$.

- *1-[1-[1-(4-bromophenyl)ethyl]-4-piperidinyl]-1,3-dihydro-2H-benzimidazol-2-one, monohydrochloride (2d/brorphine)*

This compound was prepared according to the procedure for **2a** using 4'-bromoacetophenone, and the resulting product was treated with 2M HCl in diethyl ether to afford **2d** (brorphine HCl) as an off-white solid (45%). ^{1}H-NMR (400 MHz, DMSO-d$_6$) δ 11.13 (br s, 1H), 10.87 (s, 1H), 7.6-7.7 (m, 5H), 6.9-7.0 (m, 3H), 4.4-4.6 (m, 2H), 3.74 (br d, 1H, J=10.1 Hz), 3.2-3.3 (m, 1H), 2.8-3.0 (m, 3H), 2.74 (dq, 1H, J=3.4, 12.9 Hz), 1.7-1.9 (m, 2H), 1.70 (d, 3H, J=6.9 Hz). MS (ESI): 400 MH$^+$.

- *1-(1-(1-(4-iodophenyl)ethyl)piperidin-4-yl)-1,3-dihydro-2H-benzo[d]imidazol-2-one (2e/iodorphine)*

This compound was prepared according to the procedure for **2a** using 4'-iodoacetophenone to afford **2e** (iodorphine) as a tan solid (37%). ^{1}H-NMR (400 MHz, DMSO-d$_6$) δ 10.82 (s, 1H), 7.69 (d, 2H, J=8.3 Hz), 7.1-7.2 (m, 3H), 6.9-7.0 (m, 3H), 4.0-4.1 (m, 1H), 3.51 (q, 1H, J=6.6 Hz), 2.8-3.1 (m, 2H), 2.2-2.4 (m, 2H), 1.9-2.1 (m, 2H), 1.5-1.7 (m, 2H), 1.30 (d, 3H, J=6.9 Hz). MS (ESI): 448 MH$^+$.

Radioligand binding assays

For radioligand binding assays, 10 mM stock solutions of the reference standards were prepared in dimethyl sulfoxide (DMSO) (or dimethylformamide (DMF) for chlorphine) and stored at -80°C. On the day of an experiment, thawed aliquots were diluted in assay buffer. Competition binding assays were conducted as previously described [2–4]. Briefly, 0.5 g of thawed whole rat brains minus cerebellum (BioIVT, Westbury, NY, US; kept at -80°C) were homogenized in 20 mL of ice-cold Tris HCl buffer (50 mM, pH 7.5). The resulting tissue suspension was centrifuged twice (30,000 g, 15 min, 4°C) and the pellet was resuspended (100 mg/mL). Competition binding experiments were initiated by adding 100 µL of the tissue suspension to polypropylene tubes (or glass tubes for chlorphine due to the incompatibility of DMF with polypropylene) containing 300 µL Tris buffer, 50 µL test drug (final concentration range between 20 pM and 10 µM), and 50 µL [^{3}H]DAMGO (final concentration 1 nM). Every condition was run in triplicate within an experiment. Tubes containing only assay buffer or naloxone instead of test drug were also included. After 1 h incubation, the assay was terminated by rapid filtration over Whatman GF/B filters using a cell harvester (Brandel Instruments, Gaithersburg, MD, USA). Washed filters were transferred to 24-well plates, and Cytoscint (MP Biomedicals, Irvine, CA, USA) was added for radioactivity counting (Microbeta2 counter, Perkin Elmer). Counts per minute (cpms) were corrected for non-specific binding and were normalized to percent of [^{3}H]DAMGO bound in Microsoft Excel (Redmond, WA, USA). Data from at least three independent experiments were combined (n = 3-5) and GraphPad Prism 9 (San Diego, CA, USA) was used to compute K_i values following nonlinear regression analysis (one-site fit K_i).

MOR activation assays

For MOR activation assays, stock solutions were prepared in water (hydromorphone), methanol (fentanyl, morphine, brorphine), DMSO (orphine, fluorphine, iodorphine) or DMF (chlorphine). All solutions were kept at -20°C and diluted in Opti-MEM® prior to the experiments. MOR activation was monitored by means of two previously described, cell-based bioassays monitoring recruitment of either mini-G$_{\alpha i}$ or βarr2 (the latter in the presence of G protein-coupled receptor kinase 2, GRK2) [5]. Human embryonic kidney (HEK) 293T cells stably expressing the MOR-mini-G$_{\alpha i}$ or MOR-βarr2-GRK2 assay system were routinely cultured in supplemented DMEM (GlutaMAX™; including 10% heat-inactivated FBS, 100 IU/mL penicillin, 100 µg/mL streptomycin, and 0.25 mg/L amphotericin) at 37°C in a

humidified atmosphere containing 5% CO_2. One day prior to the assay, cells were seeded (5 x 10^4 cells/well) on white, flat-bottom 96-well plates (pre-coated with poly-D-lysine) and incubated overnight. On the day of the assay, cells were washed twice with Opti-MEM® and 90 µL Opti-MEM® was added to each well followed by addition of 25 µL Nano-Glo® Live Cell Reagent according to manufacturer's instructions. The plate was subsequently placed in a Tristar 5 multimode plate reader (Berthold Technologies GmbH & Co., Bad Wildbad, Germany), allowing continuous monitoring of bioluminescence until stabilization of the signal (~13-30 min). After the equilibration, 20 µL of 6.75x concentrated stock solutions (in-well concentrations ranging from 10 pM to 50 µM) were added to the cells, and luminescence was further monitored for approximately 2 h and 15 min. Appropriate solvent controls were included on each plate. In line with our previous work [6], hydromorphone was used as a reference agonist for normalization, whereas fentanyl and morphine were included as common reference opioids. Each compound was run in both assays in at least 3 independent experiments (*n* = 3-5), with duplicates included for each concentration within an experiment. Using Microsoft Excel, absolute light units were corrected for inter-well variation and solvent controls before calculating areas under the curve (AUCs) [7]. AUC values were normalized to the maximum response of hydromorphone (set at 100%) using GraphPad Prism 9. In line with previous studies using the NanoBiT® system [8], data points associated with the highest concentration were excluded in case of an AUC reduction of ≥ 20% to avoid skewing of the concentration-response curves owing to cell toxicity or solubility issues. The complete data set was screened for outliers (standard Grubbs' test), resulting in exclusion of 12 outliers (1.34%). Normalized data from independent experiments were compiled (log(agonist) *versus* response, three parameters) to obtain final potency (EC_{50}) and efficacy (E_{max}; relative to hydromorphone) values for each test compound.

Evaluation of MOR biased agonism

The tendency of a piperidine benzimidazolone compound to induce preferential recruitment of either mini-$G_{\alpha i}$ or βarr2 was evaluated by calculation of the relative intrinsic activity (RA_i) for each compound in each bioassay (HM = hydromorphone) [8–10]:

$$RA_{i,reference\ agonist}^{pathway} = \frac{\dfrac{E_{max,i}}{EC_{50,i}}}{\dfrac{E_{max,HM}}{EC_{50,HM}}} = \frac{EC_{50,HM} \ x \ E_{max,i}}{E_{max,HM} \ x \ EC_{50,i}}$$

The obtained RA_i values for each compound per pathway were combined into the bias factor (β_i) according to the formula [9,10]:

$$\beta_i = \log\left(\frac{RA_{i,HM}^{\beta arr2}}{RA_{i,HM}^{mini-G_{\alpha i}}}\right)$$

The bias factor was calculated for each compound from three independent experiments. Statistical analysis in GraphPad Prism 9 included non-parametric one-way ANOVA (Kruskal-Wallis), followed by a post-hoc Dunn's multiple comparisons test. Differences compared to the reference agonist hydromorphone ($\beta_{HM} = 0$) were considered statistically significant when $p < 0.05$ [8]. To visualize potential trends in pathway bias, semi-quantitative bias plots were generated by plotting the normalized AUC values obtained in the mini-$G_{\alpha i}$ assay against those obtained in the $\beta arr2$ recruitment assay. Curves were fit in GraphPad Prism 10 by means of a centered second order polynomial (quadratic) equation.

Animals

The animals were group-housed (5 mice per cage; floor area/animal: 80 cm^2; minimum enclosure height: 12 cm) on a 12:12-h light–dark cycle (lights on at 6:30 AM), at a temperature of 20–22°C, humidity of 45–55%, and were provided ad libitum access to food (Diet 4RF25 GLP; Mucedola, Settimo Milanese, Milan, Italy) and water [11]. In the battery of behavioral tests used in the safety pharmacology studies, 8 mice were used for each treatment condition (vehicle, 6 different doses of the test drugs, naloxone, and naloxone + one high dose of the test drugs; total mice used = 296). In the plethysmography studies, 4 mice were used for each treatment condition (vehicle, one high dose of test drugs, naloxone, and naloxone + one high dose of the test drugs; total mice used = 48).

Tail pinch test

A dedicated rigid probe connected to a digital dynamometer (ZP-50N, IMADA, Japan) was gently placed on the tail of the mouse (in the distal portion), and progressive pressure was applied. When the mouse flicked its tail, the pressure was stopped, and the instrument recorded the maximum peak of weight supported (g-force). A cut-off of 500 g-force was set to avoid tissue damage. The measurement was repeated three consecutive times per timepoint, and the

final value was calculated by averaging these three scores [11]. Acute mechanical nociception was measured at 0, 35, 55, 90, 145, 205, 265, and 325 min post-injection [11].

Tail withdrawal test

The mouse was restrained in a dark plastic cylinder and half of its tail was dipped in 48°C water. Then, the length of time (in s) the tail was kept in the water was recorded. The test was repeated three times (final value represents the average), and a cut-off of 15 s was set to avoid tissue damage [11]. Acute thermal nociception was measured at 0, 35, 55, 90, 145, 205, 265, and 325 min post-injection [11].

Plethysmography analysis

A cylinder-shaped tube (i.e., restraining tunnel) restrains the animal firmly but gently, without causing trauma. Animals were put in the restraining system 1 min prior to starting the recordings, to minimize the effects of stress, as supported by the plethysmography traces, showing that they were calm, with stable breathing. The experiment provides baseline recording for 15 min, 5 min for vehicle or drug administration, followed by a recording session of 60 min [12]. The vehicle used in this experiment showed a stable profile of respiratory parameters during the 80 min measurement [12].

References

1.   Kennedy NM, Schmid CL, Ross NC, Lovell KM, Yue Z, Chen YT, et al. Optimization of a series of mu opioid receptor (MOR) agonists with high G protein signaling bias. J Med Chem. 2018;61:8895–8907.

2.   Vandeputte MM, Krotulski AJ, Walther D, Glatfelter GC, Papsun D, Walton SE, et al. Pharmacological evaluation and forensic case series of *N*-pyrrolidino etonitazene (etonitazepyne), a newly emerging 2-benzylbenzimidazole 'nitazene' synthetic opioid. Arch Toxicol. 2022;96:1845–1863.

3.   Truver MT, Smith CR, Garibay N, Kopajtic TA, Swortwood MJ, Baumann MH. Pharmacodynamics and pharmacokinetics of the novel synthetic opioid, U-47700, in male rats. Neuropharmacology. 2020;177:108195.

4.   Glatfelter GC, Vandeputte MM, Chen L, Walther D, Tsai M-HM, Shi L, et al. Alkoxy chain length governs the potency of 2-benzylbenzimidazole 'nitazene' opioids associated with human overdose. Psychopharmacology. 2023. 2 September 2023. https://doi.org/10.1007/s00213-023-06451-2.

5.   Vasudevan L, Vandeputte MM, Deventer M, Wouters E, Cannaert A, Stove CP. Assessment of structure-activity relationships and biased agonism at the Mu opioid receptor of novel synthetic opioids using a novel, stable bio-assay platform. Biochemical Pharmacology. 2020;177:113910.

6.   Vandeputte MM, Vasudevan L, Stove CP. *In vitro* functional assays as a tool to study new synthetic opioids at the μ-opioid receptor: Potential, pitfalls and progress. Pharmacology & Therapeutics. 2022;235:108161.

7.   Pottie E, Tosh DK, Gao Z-G, Jacobson KA, Stove CP. Assessment of biased agonism at the A_3 adenosine receptor using β-arrestin and miniG$_{\alpha i}$ recruitment assays. Biochemical Pharmacology. 2020;177:113934.

8.   Pottie E, Dedecker P, Stove CP. Identification of psychedelic new psychoactive substances (NPS) showing biased agonism at the 5-HT$_{2A}$R through simultaneous use of β-arrestin 2 and miniG$_{\alpha q}$ bioassays. Biochemical Pharmacology. 2020:114251.

9.   Ehlert FJ. On the analysis of ligand-directed signaling at G protein-coupled receptors. Naunyn-Schmiedeberg's Archives of Pharmacology. 2008;377:549–577.

10.   Rajagopal S, Ahn S, Rominger DH, Gowen-MacDonald W, Lam CM, DeWire SM, et al. Quantifying ligand bias at seven-transmembrane receptors. Molecular Pharmacology. 2011;80:367–377.

11.   Bilel S, Azevedo NJ, Arfè R, Tirri M, Gregori A, Serpelloni G, et al. In vitro and in vivo pharmacological characterization of the synthetic opioid MT-45. Neuropharmacology. 2020;171:108110.

12.   Marchetti B, Bilel S, Tirri M, Arfè R, Corli G, Roda E, et al. The Old and the New: Cardiovascular and Respiratory Alterations Induced by Acute JWH-018 Administration Compared to Δ9-THC—A Preclinical Study in Mice. IJMS. 2023;24:1631.

Appendix B

Supplementary Materials to "In vitro and in vivo characterization of Butyrylfentanyl and 4-Fluoro-Butyrylfentanyl in female and male mice: role of CRF-1 receptors in respiratory depression"

[1]Bilel Sabrine, [2]Azevedo Neto Joaquim, [1]Tirri Micaela, [1]Corli Giorgia, [1] Bassi Marta, [3]Fantinati Anna, [4]Serpelloni Giovanni, [5]Malfacini Davide, [3]Trapella Claudio, [5]Calo' Girolamo and [1,6,7]Marti Matteo.

[1]*Department of Translational Medicine, Section of Legal Medicine and LTTA Centre, University of Ferrara, Italy*
[2]*Department of Neuroscience and Rehabilitation, Section of Pharmacology, University of Ferrara Via Fossato di Mortara 17/19, 44121 Ferrara, Italy*
[3]*3Department of Environmental and Prevention Sciences, University of Ferrara, Via Fossato di Mortara, Ferrara, Italy.*
[4]*Neuroscience Clinical Center & TMS Unit Verona, Italy and Department of Psychiatry in the College of Medicine, Drug Policy Institute, University of Florida, Gainesville, FL, United States*
[5]*Department of Pharmaceutical and Pharmacological Sciences, University of Padua, Italy*
[6]*Center of Gender Medicine, University of Ferrara, Italy*
[7]*Collaborative Center of the National Early Warning System, Department for Anti-Drug Policies, Presidency of the Council of Ministers, Italy*
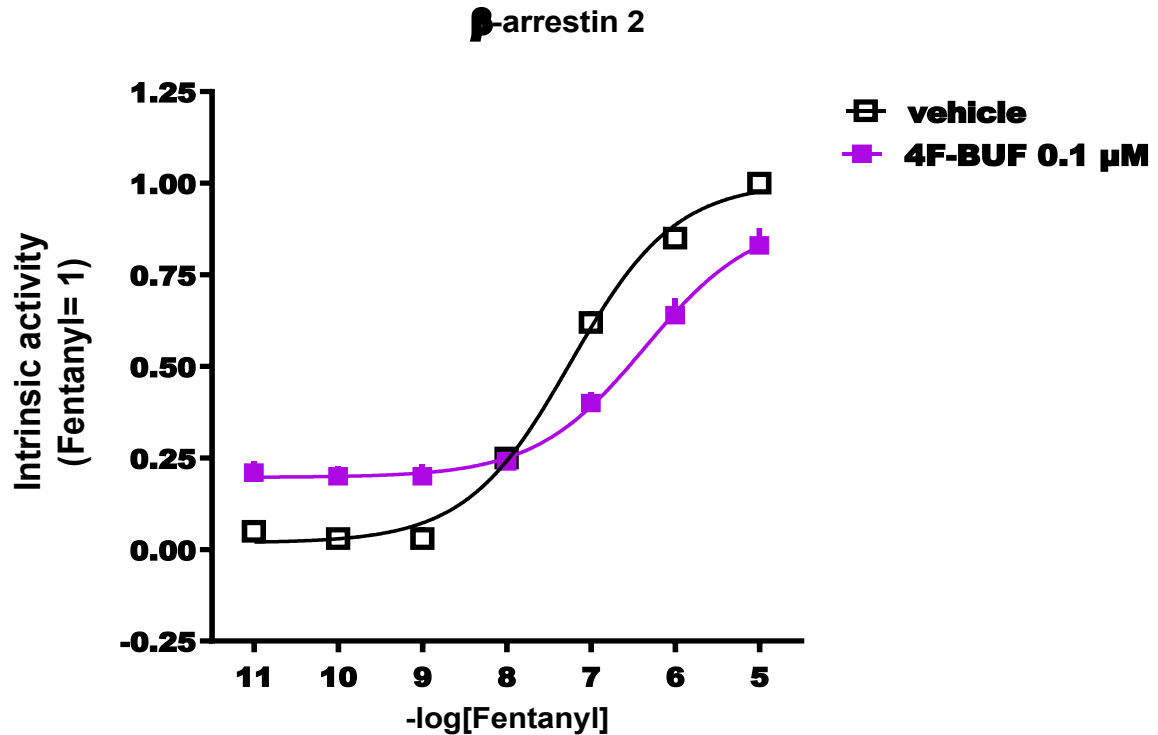
Corresponding Author:

Matteo Marti

Department of Translational Medicine, Section of Legal Medicine, University of Ferrara
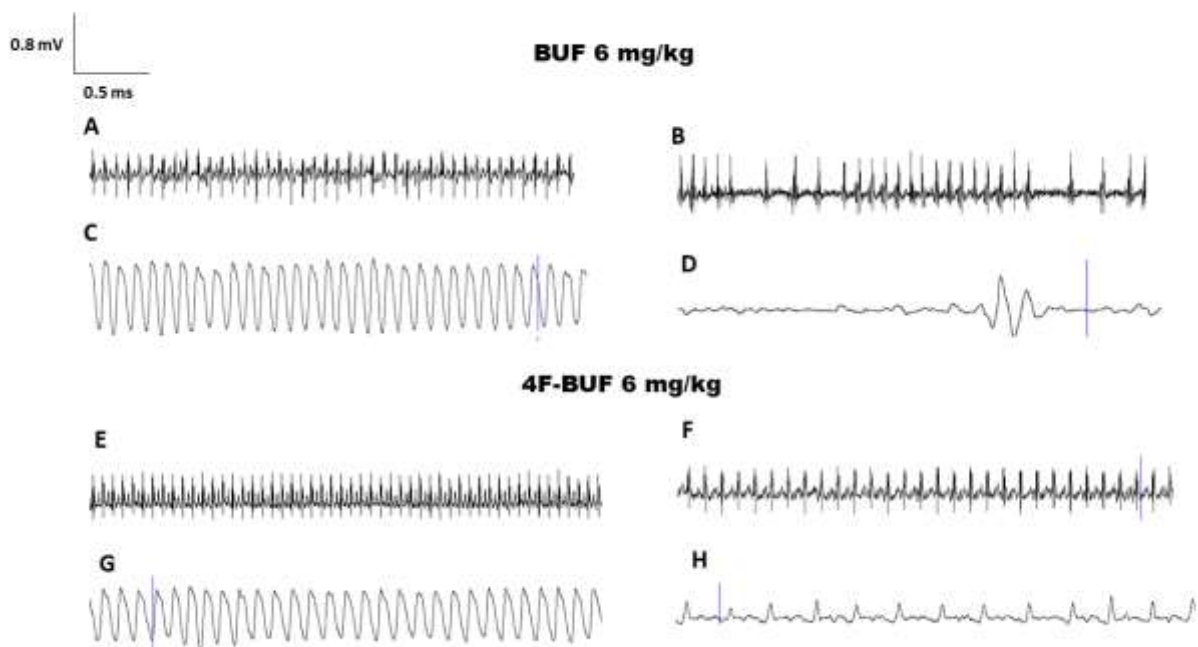
via Fossato di Mortara 70, 44121 Ferrara Italy

phone +39 0532 455781, fax +39 0532 455777

email: matteo.marti@unife.it

β-arrestin 2

Supplementary Figure B.1. BRET assay. Concentration response curve to Fentanyl for mu/β-arrestin 2 interaction measured in absence and in presence of 0.1 μM 4F-BUF. Data are the mean ± s.e.m. of 5 separate experiments in duplicate.


Supplementary Figure B2: ECG and plethysmography track of BUF (6 mg/kg) and 4F-BUF (6 mg/kg) in cardiorespiratory responses in mice. ECG track representing basal from lead 2 (panel A), bradycardia and arrhythmia detected in lead 2 (panel B), basal pleth (panel C), apnea detected in lead 2 (panel D). ECG and plethysmography track of 4F-BUF (6 mg/kg): basal from lead 2 (panel (C), bradycardia from lead 2 (panel F), basal pleth (panel F) and bradypnea (panel H). Recording was performed with ecgTUNNEL system (Emka Technologies), and tracks were exported after analysis with iox2 software.

COMPARISON BUF and 4F-BUF female
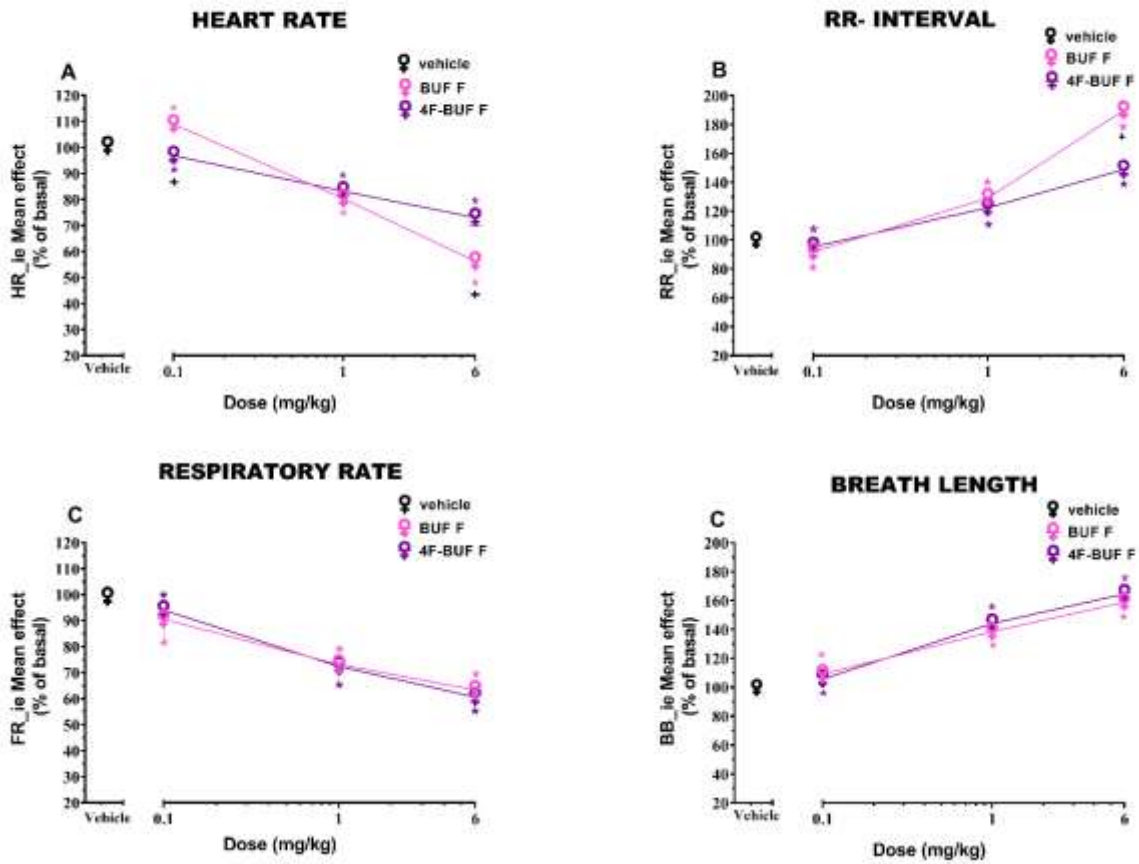
Supplementary Figure B.3. *Comparison of dose response curves to BUF and 4F-BUF in cardiorespiratory responses in female mice. Data are expressed as percentage of basal value (see material and methods) and represent the mean ± SEM of 6 determinations (female) for each treatment. Statistical analysis was performed by two-way ANOVA followed by the Bonferroni's test. *p<0.05 versus vehicle; ⁺p<0.05 versus 4F-BUF.*

COMPARISON BUF and 4F-BUF male
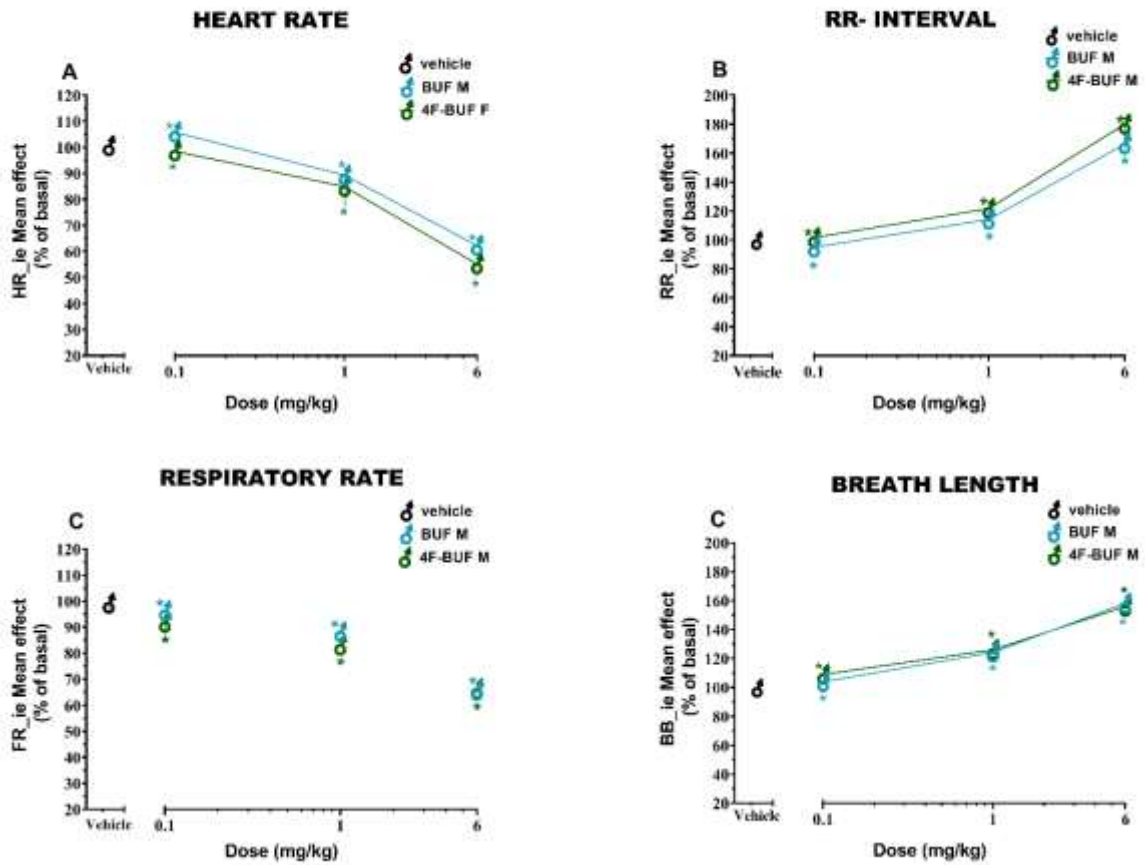
Supplementary Figure B.4. Comparison of dose response curves to BUF and 4F-BUF in cardiorespiratory responses in male mice. Data are expressed as percentage of basal value (see material and methods) and represent the mean ± SEM of 6 determinations (male) for each treatment. Statistical analysis was performed by two-way ANOVA followed by the Bonferroni's test. *p<0.05 versus vehicle.

Appendix C

Supplementary Materials to: In vivo pharmaco-toxicological characterization of Brorphine and its possible emerging analogues: Orphine, Fluorphine, Chlorphine and Iodorphine
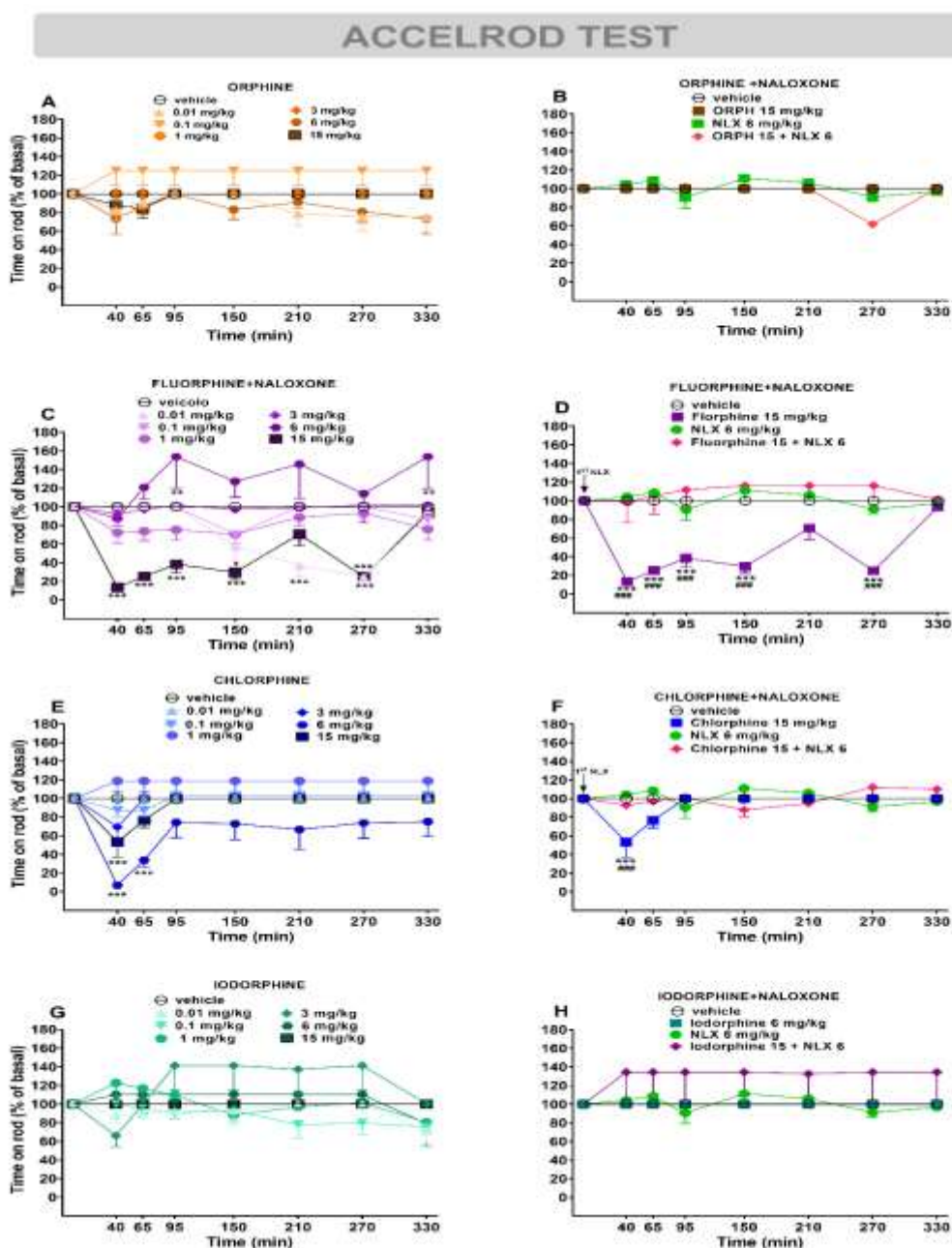

Figure C1 *Effect of the systemic administration of Orrphine, Fluorphine , Chlorphine and Iodorphine (0.01–15 mg/kg IP) on the accelerod test (Panels, A-C-E-G). Interaction of Orrphine, Fluorphine, Chlorphine and Iodorphine (15 mg/kg IP) with NLX (6 mg/kg, IP.; panels B-D-F-H). Data are expressed as percentage change from basal (% of basal) over time and represent the mean ± SEM as determined in 8 animals for each treatment regimen. Statistical analysis was performed by two-way ANOVA followed by the Bonferroni test for multiple comparisons. ***p< 0.001 versus vehicle, ###p < 0.001 versus NLX.*
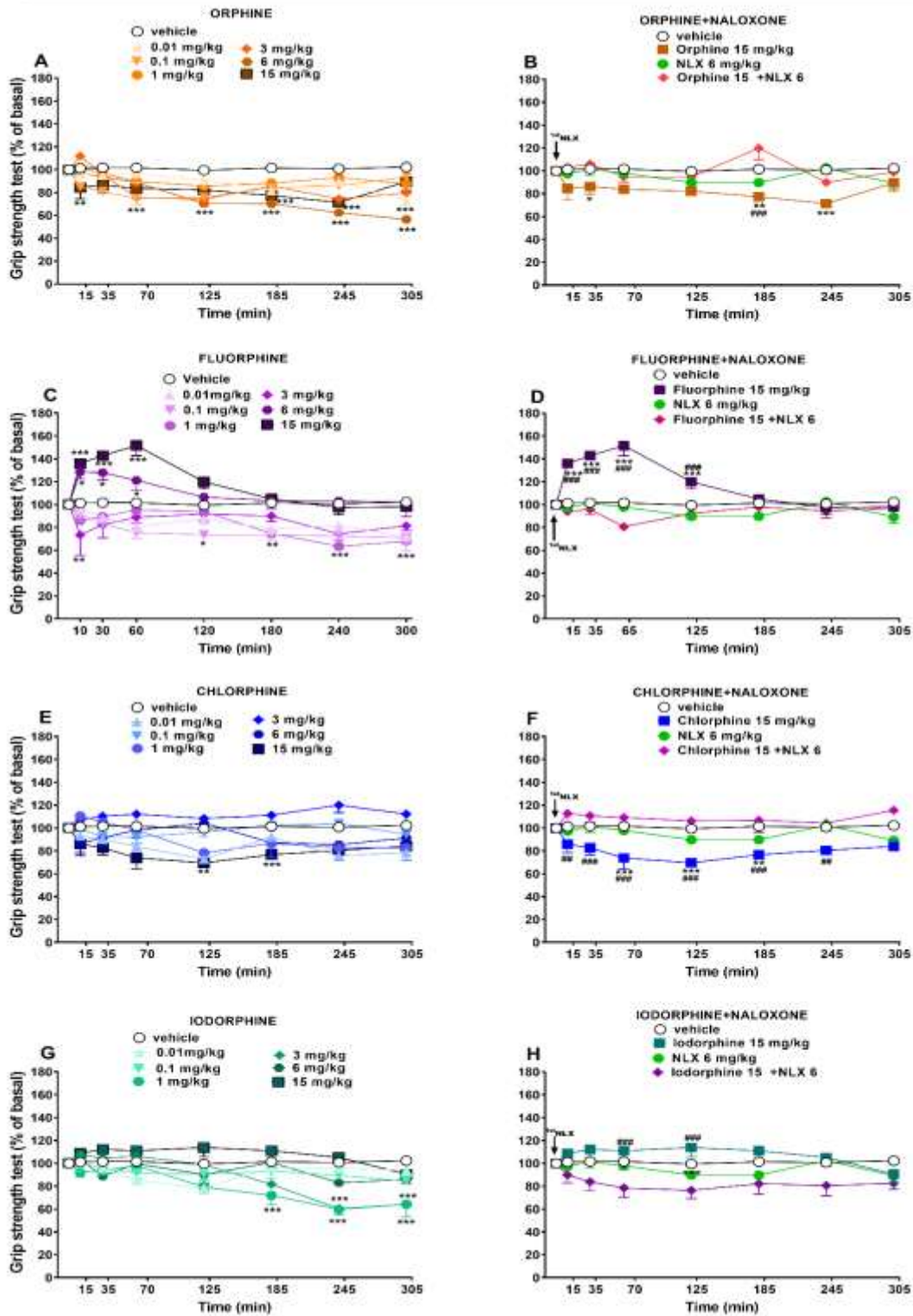
GRIP STRENGTH TEST

Figure C2. *Effect of the systemic administration of Orrphine, Fluorphine , Chlorphine and Iodorphine (0.01–15 mg/kg IP) on the Grip strength test (Panels, A-C-E-G). Interaction of Orrphine, Fluorphine, Chlorphine and Iodorphine (15 mg/kg IP) with NLX (6 mg/kg, IP.; panels B-D-F-H). Data are expressed as percentage change from basal (% of basal) over time and represent the mean ± SEM as determined in 8 animals for each treatment regimen. Statistical analysis was performed by two-way ANOVA followed by the Bonferroni test for multiple comparisons. ***p< 0.001 versus vehicle, ###p < 0.001 versus NLX.*
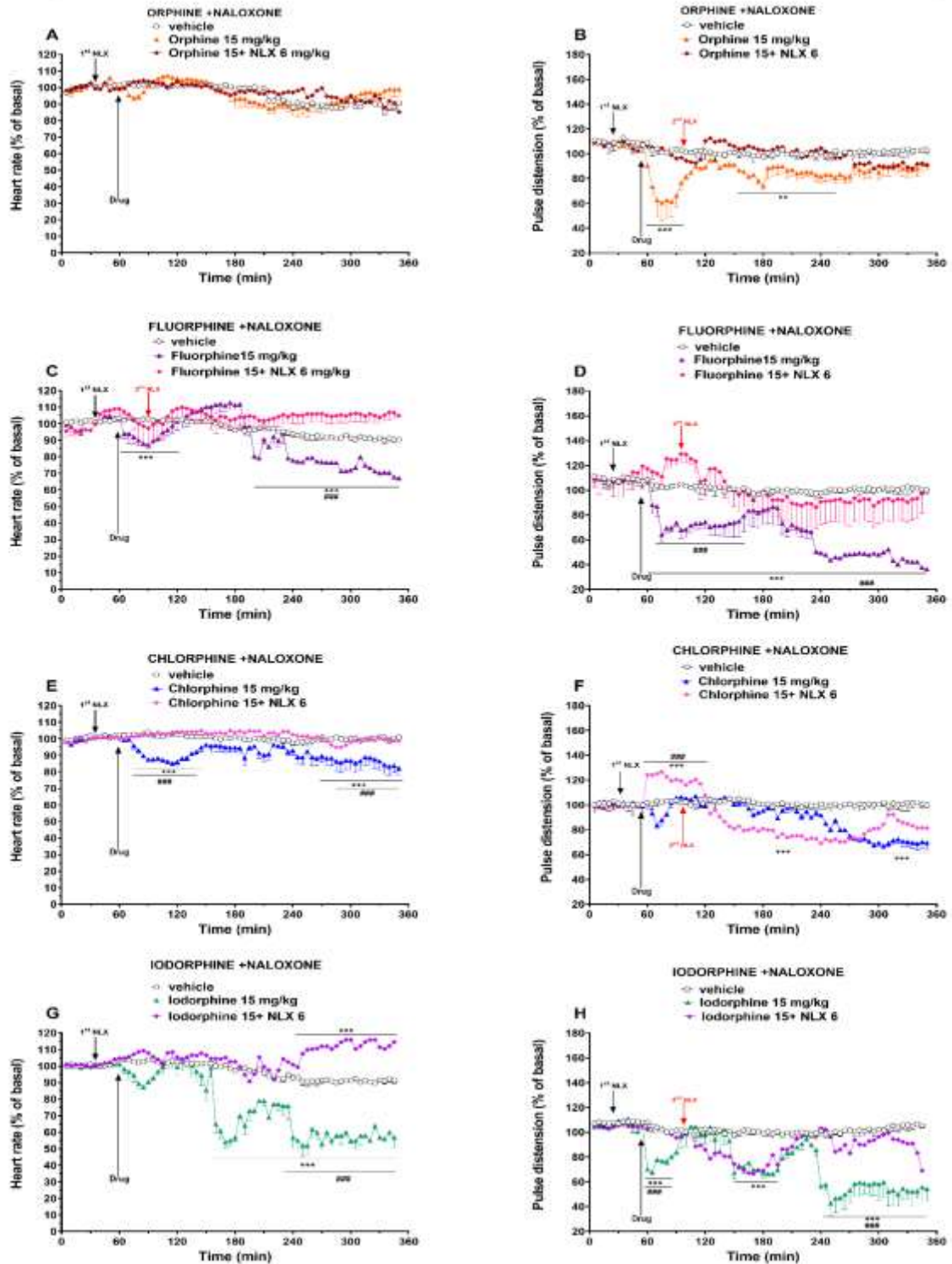
HEART RATE AND PULSE DISTENTION

Figure C3. *Time-course of drug effects after systemic administration of orphine, fluorphine, chlorphine, and iodorphine (15 mg/kg IP) on cardiorespiratory parameters (heart rate panels A-C-E-G, pulse distention panels B-D-F-H) with or without naloxone (6 mg/kg IP). Data are expressed as percentage change from basal value (% of basal) and represent the mean ± SEM as determined in 8 animals for each treatment regimen. Statistical analysis was performed by two-way ANOVA followed by the Bonferroni test for multiple comparisons. ***p< 0.001 versus vehicle, ###p < 0.001 versus NLX.*
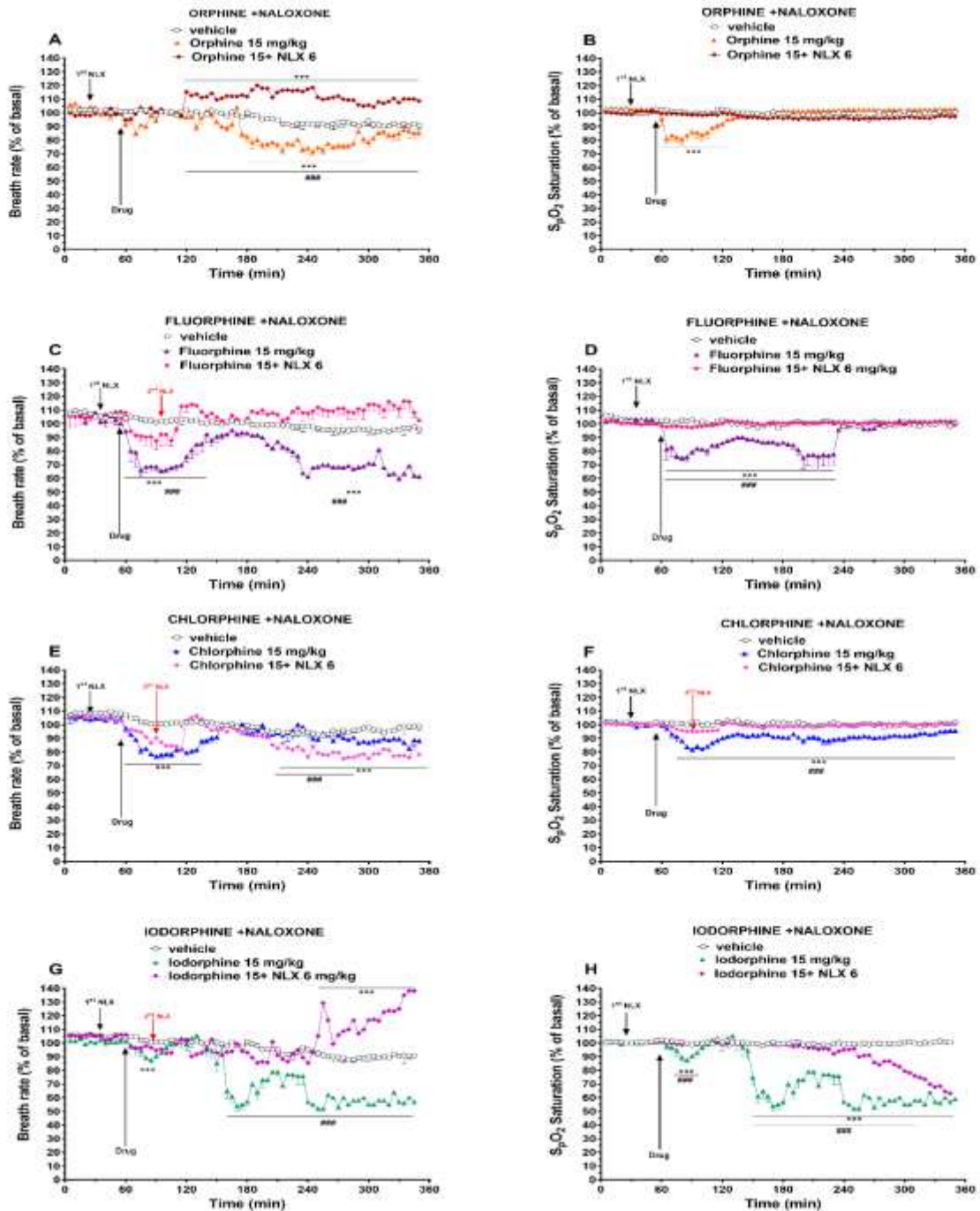
BREATH RATE AND OXYGEN SATURSATION

Figure C4. *Time-course of drug effects after systemic administration of orphine, fluorphine, chlorphine, and iodorphine (15 mg/kg IP) on cardiorespiratory parameters (breath rate panels A-C-E-G, SpO$_2$ saturation panels B-D-F-H) with or without naloxone (6 mg/kg IP). Data are expressed as percentage change from basal value (% of basal) and represent the mean ± SEM as determined in 8 animals for each treatment regimen. Statistical analysis was performed by two-way ANOVA followed by the Bonferroni test for multiple comparisons. ***p< 0.001 versus vehicle, ###p < 0.001 versus NLX.*

Bridging gaps in NPS knowledge: Contributions from 2020 to 2023

My Ph.D. project primarily centers on characterizing NSOs. Yet, as a member of the laboratory team, I've actively contributed to various studies involving the in vivo characterization of diverse classes of NPS, encompassing synthetic cannabinoids, stimulants, hallucinogens, and sedatives. Below, you'll find a list of articles arranged in ascending order based on their respective publication years.

List of publications:

Mestria, S., Odoardi, S., Federici, S., **Bilel, S.,** Tirri, M., Marti, M., & Strano Rossi, S. (2021). Metabolism Study of N-Methyl 2-Aminoindane (NM2AI) and Determination of Metabolites in Biological Samples by LC-HRMS. *Journal of analytical toxicology,45*(5), 475–483. https://doi.org/10.1093/jat/bkaa111

Foti, F., **Bilel, S**., Tirri, M., Arfè, R., Boccuto, F., Bernardi, T., Serpelloni, G., De-Giorgio, F., & Marti, M. (2021). Low-normal doses of methiopropamine induce aggressive behaviour in mice. *Psychopharmacology*, *238*(7), 1847–1856. https://doi.org/10.1007/s00213-021-05813-y

Caffino, L., Mottarlini, F., Bilel, S., Targa, G., Tirri, M., Maggi, C., Marti, M., & Fumagalli, F. (2021). Single Exposure to the Cathinones MDPV and α-PVP Alters Molecular Markers of Neuroplasticity in the Adult Mouse Brain. *International journal of molecular sciences*, *22*(14), 7397. https://doi.org/10.3390/ijms22147397

Arfè, R., **Bilel, S**., Tirri, M., Frisoni, P., Serpelloni, G., Neri, M., Boccuto, F., Bernardi, T., Foti, F., De-Giorgio, F., & Marti, M. (2021). Comparison of N-methyl-2-pyrrolidone (NMP) and the "date rape" drug GHB: behavioral toxicology in the mouse model. *Psychopharmacology, 238*(8), 2275–2295. https://doi.org/10.1007/s00213-021-05852-5

Tirri, M., Frisoni, P., **Bilel, S**., Arfè, R., Trapella, C., Fantinati, A., Corli, G., Marchetti, B., De-Giorgio, F., Camuto, C., Mazzarino, M., Gaudio, R. M., Serpelloni, G., Schifano, F., Botrè, F., & Marti, M. (2021). Worsening of the Toxic Effects of (±)Cis-4,4'-DMAR Following Its Co-Administration with (±)Trans-4,4'-DMAR: Neuro-Behavioural, Physiological, Immunohistochemical and Metabolic Studies in Mice. *International journal of molecular sciences, 22*(16), 8771. https://doi.org/10.3390/ijms22168771

Marti, M., Talani, G., Miliano, C., **Bilel, S.,** Biggio, F., Bratzu, J., Diana, M., De Luca, M. A., & Fattore, L. (2021). New insights into methoxetamine mechanisms of action: Focus on serotonergic 5-HT2 receptors in pharmacological and behavioral effects in the rat.

Experimental neurology, 345, 113836. https://doi.org/10.1016/j.expneurol.2021.113836

De-Giorgio, F., Bergamin, E., **Bilel, S.,** Tirri, M., Arfè, R., Marchetti, B., Corli, G., Serpelloni, G., & Marti, M. (2021). Ethanol enhanced MDPV- and cocaine-induced aggressive behavior in mice: Forensic implications. *Drug and alcohol dependence, 229*(Pt A), 109125.https://doi.org/10.1016/j.drugalcdep.2021.109125

Tirri, M., **Bilel, S.**, Arfè, R., Corli, G., Marchetti, B., Bernardi, T., Boccuto, F., Serpelloni, G., Botrè, F., De-Giorgio, F., Golembiowska, K., & Marti, M. (2022). Effect of -NBOMe Compounds on Sensorimotor, Motor, and Prepulse Inhibition Responses in Mice in Comparison With the 2C Analogs and Lysergic Acid Diethylamide: From Preclinical Evidence to Forensic Implication in Driving Under the Influence of Drugs. *Frontiers in psychiatry, 13*, 875722. https://doi.org/10.3389/fpsyt.2022.875722

Mazdai, L., Fabbri, M., Tirri, M., Corli, G., Arfè, R., Marchetti, B., **Bilel, S**., Bergamin, E., Gaudio, R. M., Rubini, M., De-Giorgio, F., & Marti, M. (2022). Epigenetic Studies for Evaluation of NPS Toxicity: Focus on Synthetic Cannabinoids and Cathinones. *Biomedicines, 10*(6), 1398. https://doi.org/10.3390/biomedicines10061398

Barbieri, M., Tirri, M., **Bilel, S.,** Arfè, R., Corli, G., Marchetti, B., Caruso, L., Soukupova, M., Cristofori, V., Serpelloni, G., & Marti, M. (2022). Synthetic cannabinoid JWH-073 alters both acute behavior and in vivo/vitro electrophysiological responses in mice. *Frontiers in psychiatry, 13*, 953909. https://doi.org/10.3389/fpsyt.2022.953909

Tirri, M., Arfè, R., **Bilel, S**., Corli, G., Marchetti, B., Fantinati, A., Vincenzi, F., De-Giorgio, F., Camuto, C., Mazzarino, M., Barbieri, M., Gaudio, R. M., Varani, K., Borea, P. A., Botrè, F., & Marti, M. (2022). In Vivo Bio-Activation of JWH-175 to JWH-018: Pharmacodynamic and Pharmacokinetic Studies in Mice. *International journal of molecular sciences, 23*(14), 8030. https://doi.org/10.3390/ijms23148030

Corli, G., Tirri, M., **Bilel, S.**, Giorgetti, A., Bernardi, T., Boccuto, F., Borsari, M., Giorgetti, R., & Marti, M. (2023). Ethanol enhances JWH-018-induced impairment of sensorimotor and memory functions in mice: From preclinical evidence to forensic implication in Driving Under the Influence of Drugs. *Drug and alcohol dependence, 247*, 109888. https://doi.org/10.1016/j.drugalcdep.2023.109888

Corli, G., Tirri, M., Arfè, R., Marchetti, B., Bernardi, T., Borsari, M., Odoardi, S., Mestria, S., Strano-Rossi, S., Neri, M., Gaudio, R. M., **Bilel, S.,** & Marti, M. (2023). Pharmaco-Toxicological Effects of Atypical Synthetic Cathinone Mephtetramine (MTTA) in Mice: Possible Reasons for Its Brief Appearance over NPSs Scene. *Brain sciences, 13*(2), 161. https://doi.org/10.3390/brainsci13020161

Marchetti, B., **Bilel, S**., Tirri, M., Corli, G., Roda, E., Locatelli, C. A., Cavarretta, E., De-Giorgio, F., & Marti, M. (2023). Acute Cardiovascular and Cardiorespiratory Effects of JWH-018 in Awake and Freely Moving Mice: Mechanism of Action and Possible Antidotal Interventions?. *International journal of molecular sciences, 24*(8), 7515. https://doi.org/10.3390/ijms24087515

Tirri, M., Corli, G., Arfè, R., Marchetti, B., Bilel, S., Bernardi, T., Boccuto, F., Odoardi, S., Mestria, S., Strano-Rossi, S., & Marti, M. (2023). Behavioral and Pharmacokinetics

Studies of N-Methyl-2-Aminoindane (NM2AI) in Mice: An Aminoindane Briefly Used in the Illicit Drug Market. *International journal of molecular sciences, 24*(3), 1882. https://doi.org/10.3390/ijms24031882

Corli, G., Tirri, M., **Bilel, S.,** Arfè, R., Coccini, T., Roda, E., Marchetti, B., Vincenzi, F., Zauli, G., Borea, P. A., Locatelli, C. A., Varani, K., & Marti, M. (2023). MAM-2201 acute administration impairs motor, sensorimotor, prepulse inhibition, and memory functions in mice: a comparison with its analogue AM-2201. *Psychopharmacology, 240*(7), 1435–1452. https://doi.org/10.1007/s00213-023-06378-8

Marchetti, B., **Bilel, S**., Tirri, M., Arfè, R., Corli, G., Roda, E., Locatelli, C. A., Cavarretta, E., De Giorgio, F., & Marti, M. (2023). The Old and the New: Cardiovascular and Respiratory Alterations Induced by Acute JWH-018 Administration Compared to Δ9-THC-A Preclinical Study in Mice. International journal of molecular sciences, 24(2), 1631. https://doi.org/10.3390/ijms24021631

Bilel, S., Zamberletti, E., Caffino, L., Tirri, M., Mottarlini, F., Arfè, R., Barbieri, M., Beggiato, S., Boccuto, F., Bernardi, T., Casati, S., Brini, A. T., Parolaro, D., Rubino, T., Ferraro, L., Fumagalli, F., & Marti, M. (2023). Cognitive dysfunction and impaired neuroplasticity following repeated exposure to the synthetic cannabinoid JWH-018 in male mice. *British journal of pharmacology,* 10.1111/bph.16164. Advance online publication. https://doi.org/10.1111/bph.16164

Arfè, R., **Bilel, S.,** Tirri, M., Corli, G., Bergamin, E., Serpelloni, G., Bassi, M., Borsari, M., Boccuto, F., Bernardi, T., Caruso, L., Alkilany, A. M., Rachid, O., Botrè, F., De-Giorgio, F., & Marti, M. (2023). Comprehensive evaluation of the pharmacological and toxicological effects of γ-valerolactone as compared to γ-hydroxybutyric acid: Insights from in vivo and in silico models. *Drug and alcohol dependence, 252,* 110951. https://doi.org/10.1016/j.drugalcdep.2023.110951

Frisoni, P., Corli, G., **Bilel, S.,** Tirri, M., Gasparini, L. C., Alfieri, L., Neri, M., De-Giorgio, F., & Marti, M. (2023). Effect of Repeated Administration of γ-Valerolactone (GVL) and GHB in the Mouse: Neuroadaptive Changes of the GHB and GABAergic System. Pharmaceuticals (Basel, Switzerland), 16(9), 1225. https://doi.org/10.3390/ph16091225

Achievements

This section showcases a compilation of titles of three successful experimental theses I supervised for students' graduation in Pharmaceutical Chemistry and Technology Single Cycle Degree (University of Ferrara) and screenshots featuring oral presentations, that I presented throughout my PhD program. I was awarded by Elsevier "Journal Neuroscience Methods" with **Best Paper Award** for the oral communication "***In silico*, *in vitro* and *in vivo* pharmacological characterization of emerging novel synthetic opioids: focus on sex differences"** in the 9th conference of the Mediterranean Neuroscience Society (MNS) 2023. Moreover, it features a certificate received from Elsevier as a recognition of the quality and the relevance of the articles submitted to the journal from 2020-2022.

Supervised experimental thesis in Pharmaceutical Chemistry and Technology Single Cycle Degree (University of Ferrara)

CORSO DI LAUREA IN CHIMICA E TECNOLOGIE FARMACEUTICHE

STUDIO FARMACO-TOSSICOLOGICO DELL' 1- CICLOESIL-X-METOSSIBENZENE: CONFRONTO CON TRAMADOLO E PCP

Relatore: **Laureando:**

Prof. Matteo Marti   *Alessandro Sulpasso*

Correlatrice:

Dott.ssa Sabrine Bilel

Anno Accademico 2021/2022

UNIVERSITA' DEGLI STUDI DI FERRARA

CORSO DI LAUREA IN CHIMICA E TECNOLOGIA FARMACEUTICHE

CARATTERIZZAZIONE DEGLI EFFETTI FARMACOTOSSICOLOGICI INDOTTI DALLA BRORFINA IN TOPI CD-1.

Relatore:
Matteo Marti

Laureando:
Giorgia Galante

Correlatore:
Sabrine Bilel

Anno Accademico
2021/2022

313

UNIVERSITA' DEGLI STUDI DI FERRARA

CORSO DI LAUREA IN CHIMICA E TECNOLOGIA
FARMACEUTICHE

SEX AND GENDER DIFFERENCES IN THE EFFECTS OF NOVEL SYNTHETIC OPPIOID BRORPHINE

Supervisor: Student:
Prof. Matteo Marti   Marco Mantoan

Tutor:
Dr. Sabrine Bilel

Academic year
2021/2022

Oral presentations

MNS CROATIA 2022
May 29 - June 2, 2022 Dubrovnik
8th Conference of the Mediterranean
Neuroscience Society

UNIVERSITÀ DEGLI STUDI DI FERRARA
- EX LABORE FRUCTUS -

In vitro and in vivo pharmaco-dynamic study of the novel fentanyl
derivatives: Acrylfentanyl, Ocfentanyl and Furanylfentanyl

Prof. Matteo Marti   2021-2022   Dr .Sabrine Bilel

MNS2023 Tunisia
Carthage, 14-18 October 2023
9th Conference of the Mediterranean
Neuroscience Society

UNIVERSITÀ DEGLI STUDI DI FERRARA
- EX LABORE FRUCTUS -

In silico, in vitro and in vivo pharmacological
characterization of emerging novel synthetic opioids:
focus on sex differences

Tutor: Speaker:

                                                          Dr. Sabrine Bilel

Prof. Matteo Marti   Preclinical and Forensic Toxicology Laboratory,
              Department of Translational Medicine, LTTA Center, University of Ferrara, Italy
          Collaborative Center for Anti-drug Policies Department, Presidency of the Council of Ministers, Italy

Elsevier certificate of Recognition